frontiers | Research Topics

Multi-omics in studying the mechanisms of anti-cancer drugs resistance and toxicity

Edited by
Jian Zhang, Clare Y. Slaney, Haitao Wang and Rudy Leon De Wilde

Published in
Frontiers in Pharmacology
Frontiers in Oncology

ISSN 1664-8714
ISBN 978-2-83251-649-2
DOI 10.3389/978-2-83251-649-2

About Frontiers

Frontiers is more than just an open access publisher of scholarly articles: it is a pioneering approach to the world of academia, radically improving the way scholarly research is managed. The grand vision of Frontiers is a world where all people have an equal opportunity to seek, share and generate knowledge. Frontiers provides immediate and permanent online open access to all its publications, but this alone is not enough to realize our grand goals.

Frontiers journal series

The Frontiers journal series is a multi-tier and interdisciplinary set of open-access, online journals, promising a paradigm shift from the current review, selection and dissemination processes in academic publishing. All Frontiers journals are driven by researchers for researchers; therefore, they constitute a service to the scholarly community. At the same time, the *Frontiers journal series* operates on a revolutionary invention, the tiered publishing system, initially addressing specific communities of scholars, and gradually climbing up to broader public understanding, thus serving the interests of the lay society, too.

Dedication to quality

Each Frontiers article is a landmark of the highest quality, thanks to genuinely collaborative interactions between authors and review editors, who include some of the world's best academicians. Research must be certified by peers before entering a stream of knowledge that may eventually reach the public - and shape society; therefore, Frontiers only applies the most rigorous and unbiased reviews. Frontiers revolutionizes research publishing by freely delivering the most outstanding research, evaluated with no bias from both the academic and social point of view. By applying the most advanced information technologies, Frontiers is catapulting scholarly publishing into a new generation.

What are Frontiers Research Topics?

Frontiers Research Topics are very popular trademarks of the *Frontiers journals series*: they are collections of at least ten articles, all centered on a particular subject. With their unique mix of varied contributions from Original Research to Review Articles, Frontiers Research Topics unify the most influential researchers, the latest key findings and historical advances in a hot research area.

Find out more on how to host your own Frontiers Research Topic or contribute to one as an author by contacting the Frontiers editorial office: frontiersin.org/about/contact

Multi-omics in studying the mechanisms of anti-cancer drugs resistance and toxicity

Topic editors

Jian Zhang — Southern Medical University, China

Clare Y. Slaney — Peter MacCallum Cancer Centre, Australia

Haitao Wang — Center for Cancer Research, National Cancer Institute (NIH), United States

Rudy Leon De Wilde — University Medicine Oldenburg, Germany

Citation

Zhang, J., Slaney, C. Y., Wang, H., De Wilde, R. L., eds. (2023). *Multi-omics in studying the mechanisms of anti-cancer drugs resistance and toxicity*. Lausanne: Frontiers Media SA. doi: 10.3389/978-2-83251-649-2

Table of contents

frontiers in Pharmacology

ORIGINAL RESEARCH
published: 23 March 2022
doi: 10.3389/fphar.2022.855485

C1QTNF6 is a Prognostic Biomarker and Related to Immune Infiltration and Drug Sensitivity: A Pan-Cancer Analysis

Wei Liu†, Jian Zhang†, Tao Xie†, Xiaoting Huang, Baiyao Wang, Yunhong Tian and Yawei Yuan**

Department of Radiation Oncology, Affiliated Cancer Hospital and Institute of Guangzhou Medical University, Guangzhou, China

OPEN ACCESS

Edited by:
Jian Zhang,
Southern Medical University, China

Reviewed by:
Qichun Wei,
Zhejiang University, China
Md. Nazim Uddin,
China Pharmaceutical University, China
Benhua Xu,
Fujian Medical University Union Hospital, China

***Correspondence:**
Yawei Yuan
yuanyawei@gzhmu.edu.cn
Yunhong Tian
tianyunhong2020@gzhmu.edu.cn

†These authors have contributed equally to this work

Specialty section:
This article was submitted to Pharmacology of Anti-Cancer Drugs, a section of the journal Frontiers in Pharmacology

Received: *15 January 2022*
Accepted: *17 February 2022*
Published: *23 March 2022*

Citation:
Liu W, Zhang J, Xie T, Huang X, Wang B, Tian Y and Yuan Y (2022) C1QTNF6 is a Prognostic Biomarker and Related to Immune Infiltration and Drug Sensitivity: A Pan-Cancer Analysis. Front. Pharmacol. 13:855485. doi: 10.3389/fphar.2022.855485

Background: The discovery of reliable cancer biomarkers could tune a diagnosis and improve the way patients are treated. However, many cancers lack robust biomarkers. *C1QTNF6* has been preliminarily elucidated for its role in some tumors. However, no pan-cancer analysis has been performed to comprehensively explore the value of *C1QTNF6*.

Methods: Data from the TCGA database, GTEx database stored in the USUC Xena were used for analyzing the profiles of *C1QTNF6* expression in normal and tumor tissues in pan-cancer. Subsequently, the gene alteration rates of *C1QTNF6* were acquired on the online web cBioportal. With the aid of the TCGA data, the association between *C1QTNF6* mRNA expression and copy number alterations (CNA) and methylation was determined. Survival analyses of *C1QTNF6* were carried out. Moreover, the tumor biological and immunological characteristics of *C1QTNF6* were clarified in the forms of the correlation between *C1QTNF6* expression and hallmark Pathway scores in MsigDB database, immune cell infiltration, immune-related genes. We conducted a GSEA of *C1QTNF6* to illustrate its potential biological functions. In addition, GDSC2 data with 198 drugs were adopted to explore drug sensitivity with the change of *C1QTNF6* expression.

Result: *C1QTNF6* was overexpressed in many types of cancer, Survival analysis showed that *C1QTNF6* independently served as a prognostic indicator for poor survival in many tumors. Besides, we also identified a positive correlation between *C1QTNF6* and cancer hallmark pathway score, tumor microenvironment related pathways score (TMEp score), and immune characteristic. In terms of drug sensitivity analysis, we found higher expression level of *C1QTNF6* predicts a high IC50 value for most of 198 drugs which predicts drug resistance.

Conclusions: Our study provides a new biological marker for pan-cancer, which is beneficial to the diagnosis and treatment of cancer, which bring a new therapeutic target for tumors.

Keywords: pan-cancer analysis, C1QTNF6, prognosis, immune infiltration, tumor microenvironment, drug sensitivity

INTRODUCTION

At present, cancer remains a hindrance in the field of medicine (Hausman, 2019). Compared to normal cells, cancer cells have several unique hallmarks, including unlimited replication, overactivation of growth signals, resistance to cell death, immune re-editing, and metabolic reprogramming (Hanahan and Weinberg, 2011; Macheret and Halazonetis, 2015). These changes are the result of mutations in a variety of genes, including proto-oncogenes and suppressor genes (Kroemer and Pouyssegur, 2008; Park et al., 2020). We hypothesized that these genes may serve as viable therapeutic targets in cancer treatment. Targeted therapies such as BRAF inhibitors and VEGF inhibitors have achieved initial efficacy in the treatment of diverse solid tumors (Davies et al., 2002; Carmeliet, 2005). Besides, immunotherapy based on *PD-1/PD-L1* or *CTLA-4* mutations offers hope for advanced tumors (Ai et al., 2020; Han et al., 2020). However, unfortunately, a significant proportion of patients are less sensitive to targeted therapy or immunotherapy (Qin et al., 2019). Therefore, there is an urgent need for new biomarkers to guide cancer treatment.

Complement C1q Tumor Necrosis factor-related Protein 6 (*C1QTNF6*) is an inflammation-related gene, which has been preliminarily described to be related to the biological characteristics of tumors (Wang et al., 2020). Zhang et al. found that *C1QTNF6* regulates proliferation and apoptosis of non-small cell lung cancer (NSCLC) (Zhang and Feng, 2021). Takeuchi et al. found that *C1QTNF6* regulates angiogenesis and apoptosis in hepatocellular carcinoma through the Akt pathway (Takeuchi et al., 2011). Therefore, *C1QTNF6* might perform an integral function in tumor progression. Nevertheless, no pan-cancer analysis has been performed to comprehensively demonstrate the value of *C1QTNF6* in multiple cancers.

In recent years, the establishment of several large public databases has greatly promoted the development of bioinformatics. TCGA and GTEx databases are among the most used databases (Blum et al., 2018). By analyzing cancer transcriptome data and clinical data, we can screen for meaningful biomarkers to assess patient prognosis or guide treatment.

Here, bioinformatics analysis was conducted for the purpose of comprehensively examining the significance of *C1QTNF6* in pan-cancer by combining GTEx and TCGA data. Our results can provide a robust prognostic marker for multiple cancers. The expression level of *C1QTNF6*, as well as its prognostic significance in pan-cancer, was explored. We further found the role of *C1QTNF6* in the tumor microenvironment (TME), including the correlation between *C1QTNF6* and the immunosuppressive genes, immune cell infiltration score, chemokines, and chemokine receptors. It is worth noting that increased *C1QTNF6* expression indicates greater drug resistance. Taken together, our research can also provide a reference for the understanding of the cancer-immune microenvironment and cancer therapies.

MATERIALS AND METHODS

Data Download and Expression Analysis

RNA-sequencing samples of the Genotype-Tissue Expression (GTEx) and The Cancer Genome Atlas (TCGA) were acquired through UCSC Xena in TCGA TARGET GTEx columns (https://xena.ucsc.edu). We downloaded the methylation data and DNA copy number data from cBioportal dataset (https://www/cbioportal/org/). The differences in the expression levels between tumors and normal tissues were assessed by means of the T-test, and a p-value of less than 0.05 denoted a significance. The analysis was conducted with the help of R software.

Gene Mutation Analysis and Methylation Analysis

First, mutation analysis was performed on the cBioportal online web. On the website, the gene was selected as *C1QTNF6*, and the object of analysis was set as "TCGAPan-Cancer Atlas". The frequency analysis of *C1QTNF6* alteration in each cancer was obtained. The cBioPortal database was utilized for the purpose of acquiring Copy number alterations (CNA) and methylation data, while methylation data are from the HM450 types, both the association between the *C1QTNF6* expression and the CNA and methylation were calculated the Pearson's correlation coefficients.

Survival Analysis

Next, a univariate Cox regression was performed to explore the prognostic significance of *C1QTNF6* in pan-cancer. We also analyzed the progression-free interval (PFI), disease-free interval (DFI), disease-specific survival (DSS), and overall survival (OS). Meanwhile, univariate cox regression and multivariate Cox regression analysis of *C1QTNF6* and other cliniacal features were carried out in tumors where *C1QTNF6* was an independent prognostic indicator. The R package "Survminer" was used for analysis (Biecek, 2020).

Analysis of C1QTNF6 in Tumor Microenvironment

The MsigDB database contains 50 hallmark Pathway datasets. First, Combining the RNA-seq data of 33 cancers and a single-sample gene set enrichment analysis (ssGSEA) algorithm utilizing GSVA packages (Hänzelmann et al., 2013), we quantified the score of each cancer hallmark. The immune characteristic parameters including ImmuneScore, StromalScore, and ESTIMATEScore of each cancer were calculated by the "ESTIMATE" R package (Verhaak, 2016). We adopted the algorithm that is published in Nature journal and "prcomp" packages to calculate the tumor microenvironment pathways score (TMEp score). The immueCellAI database was utilized for the purpose of acquiring the scores of infiltrating immune cells from the TCGA pan-cancer (http://bioinfo.life.hust.edu.cn). A total of 33 cancers were studied for their gene expression levels of chemokines, chemokine receptors, and immunosuppressive genes. After obtaining the above scores as well as the immune-associated genes expression level (chemokines, chemokine receptors, and immunosuppressive genes) of each tumor, we used the "corrplot" R package (Simko, 2021) to calculate the correlation between *C1QTNF6* and above scores and immune-related genes expression, and used the "ggplot2" package to draw the correlation heat map (Wickham, 2016).

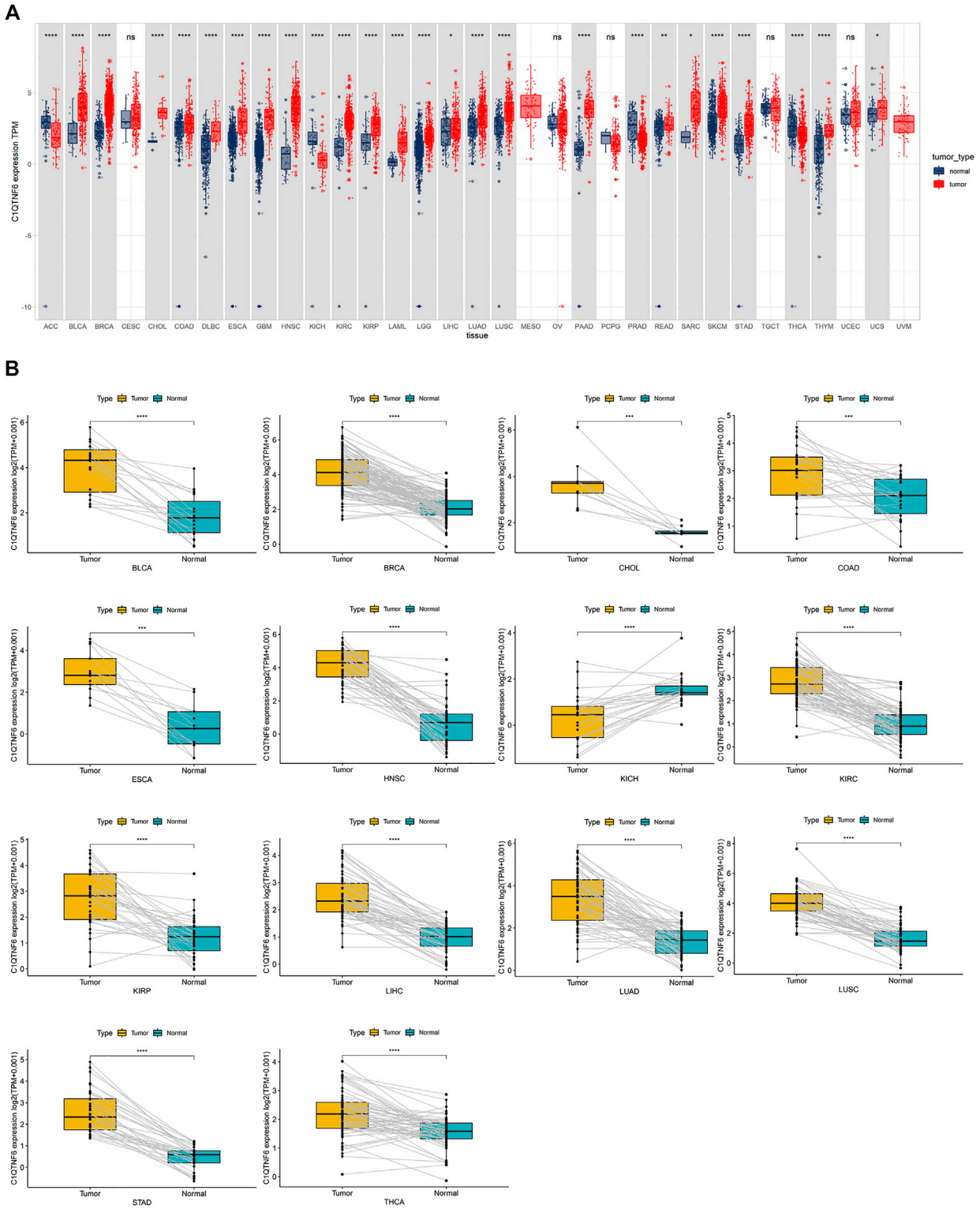

FIGURE 1 | C1QTNF6 profile in pan-cancer. **(A)** Integrated GTEx database and TCGA database revelation of C1QTNF6 expression across normal and tumor tissues. **(B)** According to the TCGA data, the levels of C1QTNF6 in corresponding tumors and normal tissues varied across various cancers. *$p < 0.05$, **$p < 0.01$, ***$p < 0.001$, ****$p < 0.0001$.

Gene Set Enrichment Analysis of C1QTNF6 in Pan-Cancer

GSEA was launched to explore the potential biological functions of *C1QTNF6* in the tumor process by using "clusterProfiler" (Yu et al., 2012), The top 20 significant pathways of *C1QTNF6* were obtained in each cancer, we showed GSEA plots of the 8 cancers with the largest proportion of immune pathways with the help of "ggridges" packages (Wilke, 2021).

Drug Sensitivity Analysis

We explored the relationship between gene expression and drug sensitivity from the GDSC2 database (https://www.cancerrxgene.org/). Subsequently, Spearman- correlation analysis was employed for the purpose of investigating the correlation between drugs and *C1QTNF6* expression level, and the drugs with the top 6 strongest positive correlation and the top 6 strongest (only 6) negative correlation were displayed respectively. Next, we analyzed the difference in sensitivity between the low- and high-expression group (according to the median value of *C1QTNF6*) to 9 commonly used anticancer drugs, we assessed the sensitivity difference by the Kruskal-Wallis rank-sum test ($p < 0.05$).

RESULTS

The Expression of *C1QTNF6* in Pan-Cancer

C1QTNF6 was differentially expressed in 26 cancers in the TCGA cohort. The *C1QTNF6* expression level was remarkably up-regulated in 22 distinct types of tumors, including UCS, CHOL, STAD, DLBC, SARC, GBM, PAAD, HNSC, LUSC, KIRC, LUAD, KIRP, LIHC, LGG, LAML, ESCA, READ, COAD, SKCM, BRCA, THYM, BLCA. *C1QTNF6* was significantly down-regulated in 4 tumors, including ACC, KICH, PRAD, and THCA; The cancers in the gray box had significant differences between tumor and normal tissues, whereas cancers in the white box had no differences (**Figure 1A**) Subsequently, paired expression analysis showed *C1QTNF6* was significantly up-regulated in the 13 kinds of tumors, notably, KIRP, HNSC, LIHC, ESCA, LUAD, COAD, KIRC, LUSC, CHOL, STAD, BRCA, THCA, BLCA. Paired expression analysis showed that *C1QTNF6* was solely significantly down-regulated in KICH (**Figure 1B**).

Gene Mutation Analysis and Methylation Analysis

First, analysis in the cBioportal database showed the alteration frequency of *C1QTNF6* in Pan-cancer. The results showed that the alteration frequency of *C1QTNF6* in uterine carcinosarcoma was the highest, and the main type is the amplification mutation (**Figure 2A**). Subsequently, we explored the association between *C1QTNF6* and copy number mutation (CNA) in pan-cancer. The results showed that *C1QTNF6* had a strong positive correlation with CNA in CHOL, UCS, PCPG (**Figure 2B**). Then, we explored the correlation between *C1QTNF6* and methylation in pan-cancer. The findings demonstrated that *C1QTNF6* exhibited a positive correlation with methylation in LAML, and a strong negative correlation with ACC and UVM, etc. (**Figure 2C**).

Survival Analysis

Subsequently, we investigated the prognostic significance of *C1QTNF6* in pan-cancer. We also evaluated the overall survival (OS, **Figure 3A**), disease-specific survival (DSS, **Figure 3B**), disease-free interval (DFI, **Figure 3C**), and Progression-free interval (PFI, **Figure 3D**), respectively. Univariate Cox regression was used to eliminate the confounding bias. First, in overall survival, *C1QTNF6* was an independent prognostic gene in KIRC, LUAD, LGG, KIRP, ACC, UVM, MESO, LIHC, HNSC, KICH, BLCA, THCA, and UCEC. Then, in the analysis of disease-specific survival, *C1QTNF6* was an independent prognostic gene in KIRC, LGG, LUAD, MESO, KIRP, THCA, UVM, ACC, KICH, HNSC, LUSC, and LIHC. Subsequent analysis of disease-free survival showed that *C1QTNF6* was an independent prognostic gene in UCEC, KIRP, LUAD, PAAD, and PRAD. Finally, PFS analysis showed that *C1QTNF6* was an independent prognostic gene in KIRC, PRAD, LGG, UVM, LUAD, KICH, ACC, MESO, KIRP, UCEC, THCA, HNSC, and CESC. A value of Hazard ratio greater than 1 indicates a risk prognostic factor, it is found that *C1QTNF6* predicts poor survival in most cancers. At the same time, univariate cox regression and multivariate cox regression analysis of *C1QTNF6* and clinical features were carried out in tumors which suggest *C1QTNF6* is independent prognostic factor in OS analysis, the multicox result demonstrate that *C1QTNF6* is an independent factors associated with patients overall survival time in KIRC, LUAD, LGG, KIRP, ACC, UVM, MESO, LIHC, HNSC, which is generally consistent with the unicox results (**Supplementary Figures S1A–M**). For instance, Univariate Cox regression analysis showed that age,stage, *C1QTNF6 were significantely associated with the prognosis of ACC,* Multivariate Cox regression analysis showed that *C1QTNF6* was an independent factor after adjusted for other clinical characteristic in ACC patients.

Correlation Between *C1QTNF6* and Cancer Pathway (Hallmark Pathway Sets)

The correlation between the expression level of *C1QTNF6* and the tumor pathway score was shown in **Figure 4**. We found that *C1QTNF6* is positively correlated with most cancer super-pathways. Among these pathways, oncogenic pathways such as angiogenesis and hypoxia showed a strong correlation with our *C1QTNF6* gene. A few pathways are negatively correlated with *C1QTNF6* expressions, such as Oxidative phosphorylation, fatty acid metabolism, and bile acid metabolism pathways.

Correlation Analysis of *C1QTNF6* and Microenvironment Related Pathways

We found that *C1QTNF6* was strongly correlated with TME related pathways, such as EMT1, base excision, and mismatch

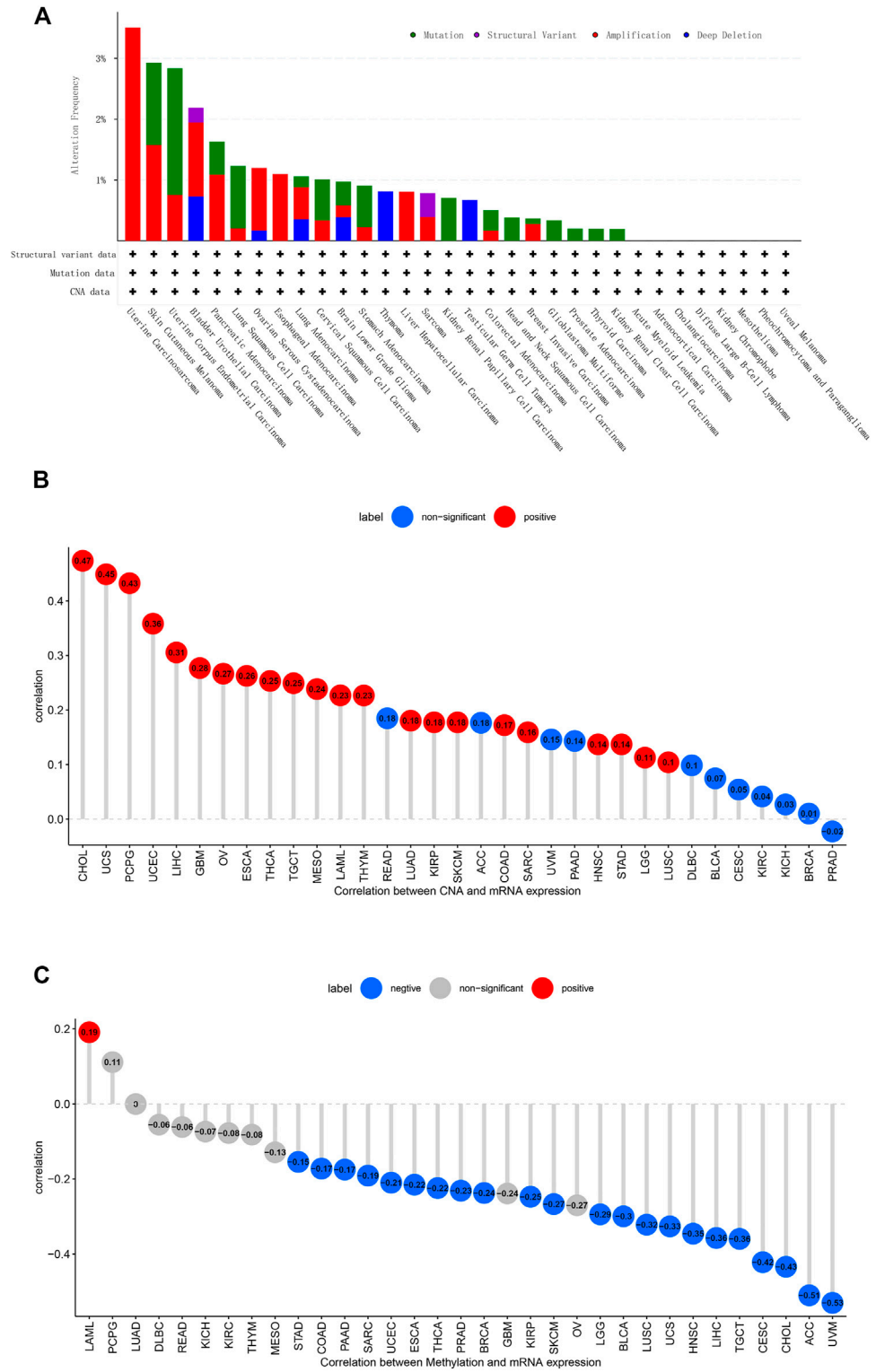

FIGURE 2 | CNA and DNA methylation of C1QTNF6 in pan-cancer. **(A)** alteration frequency of C1QTNF6 in each cancer of TCGA. **(B)** C1QTNF6 expression and DNA copy number correlation profile in each cancer of TCGA. The deeper red color means significant cancer types ($p < 0.05$). **(C)** correlations between C1QTNF6 expression and DNA methylation, the blue represented negatively correlated, and the red represented positively correlated.

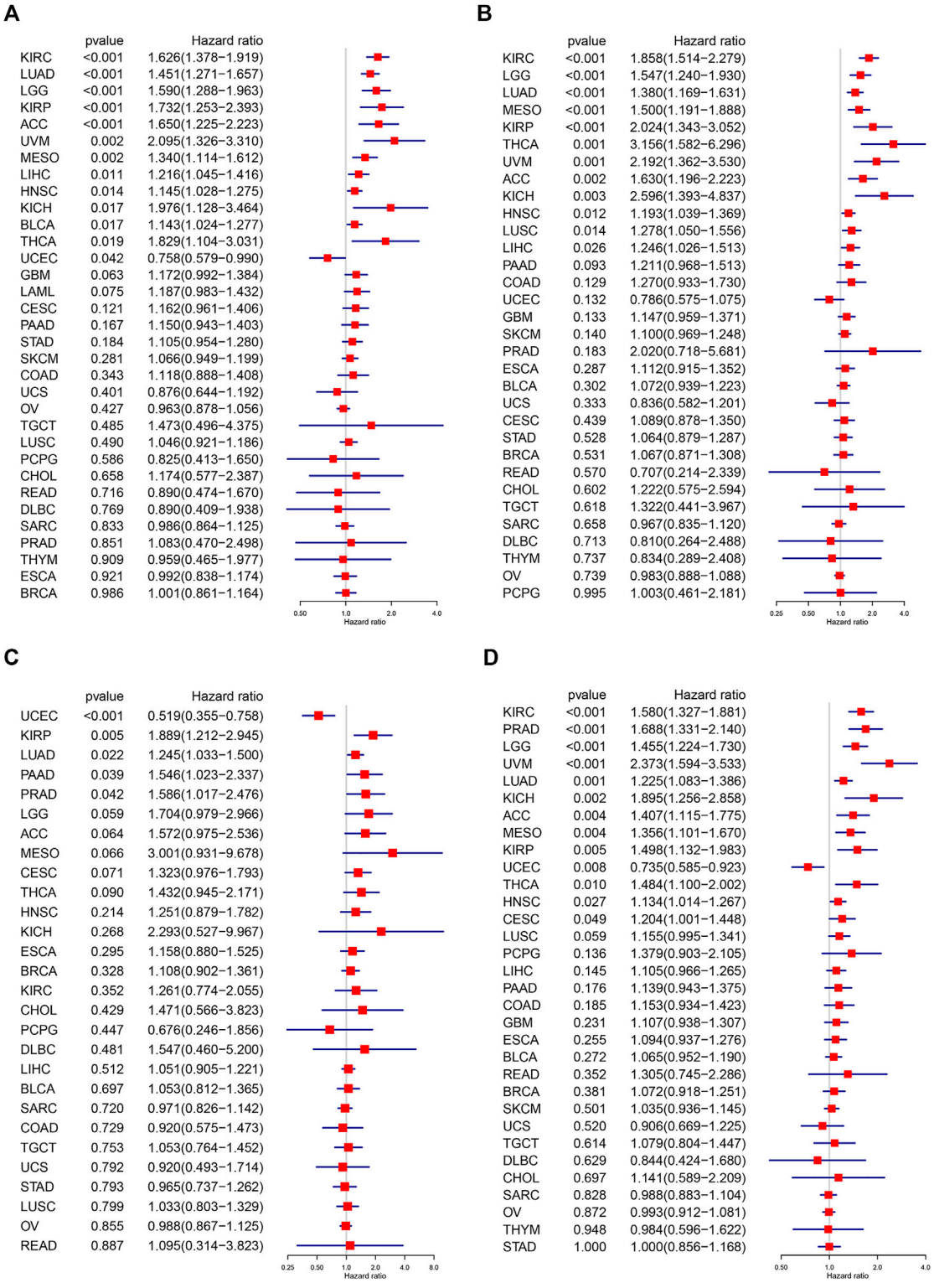

FIGURE 3 | Univariate Cox regression analysis of C1QTNF6. The results were shown with a forest map for **(A)** OS; **(B)** DSS; **(C)** DFI; **(D)** PFI.

repair pathways correlated with the onset and progression of cancer (**Figure 5A**). Additionally, the activation of these pathways was highly correlated with the onset and progression of cancer, and this was highly consistent with our results in **Figure 4**. *C1QTNF6* gene expression was also significantly correlated with the immune checkpoint and CD8 T effector

FIGURE 4 | Heatmap for different hallmark pathway enrichment scores with C1QTNF6 expression level. *$p < 0.05$, **$p < 0.01$, ***$p < 0.001$, ****$p < 0.0001$.

pathways (**Figure 5A**). The correlation between *C1QTNF6* and the immune score is shown in **Figure 5B**. StromalScore, Estimatescore, and immuneScore were all associated with *C1QTNF6*. *C1QTNF6* was found negatively correlated with These findings show that *C1QTNF6* could play a critical function in the control of biological activity in the immune milieu. Meanwhile, we explored the association between the infiltration of immune cells and *C1QTNF6* expression, and the findings were demonstrated in **Supplementary Figure S2**. We found the expression of *C1QTNF6* was negatively correlated with most immune cells, including B cell, Neutrophil, and CD8_T, and positively correlated with Monocyte and Macrophage. Next, GSEA was performed for the purpose of further examining the association of various pathways, especially immune-related

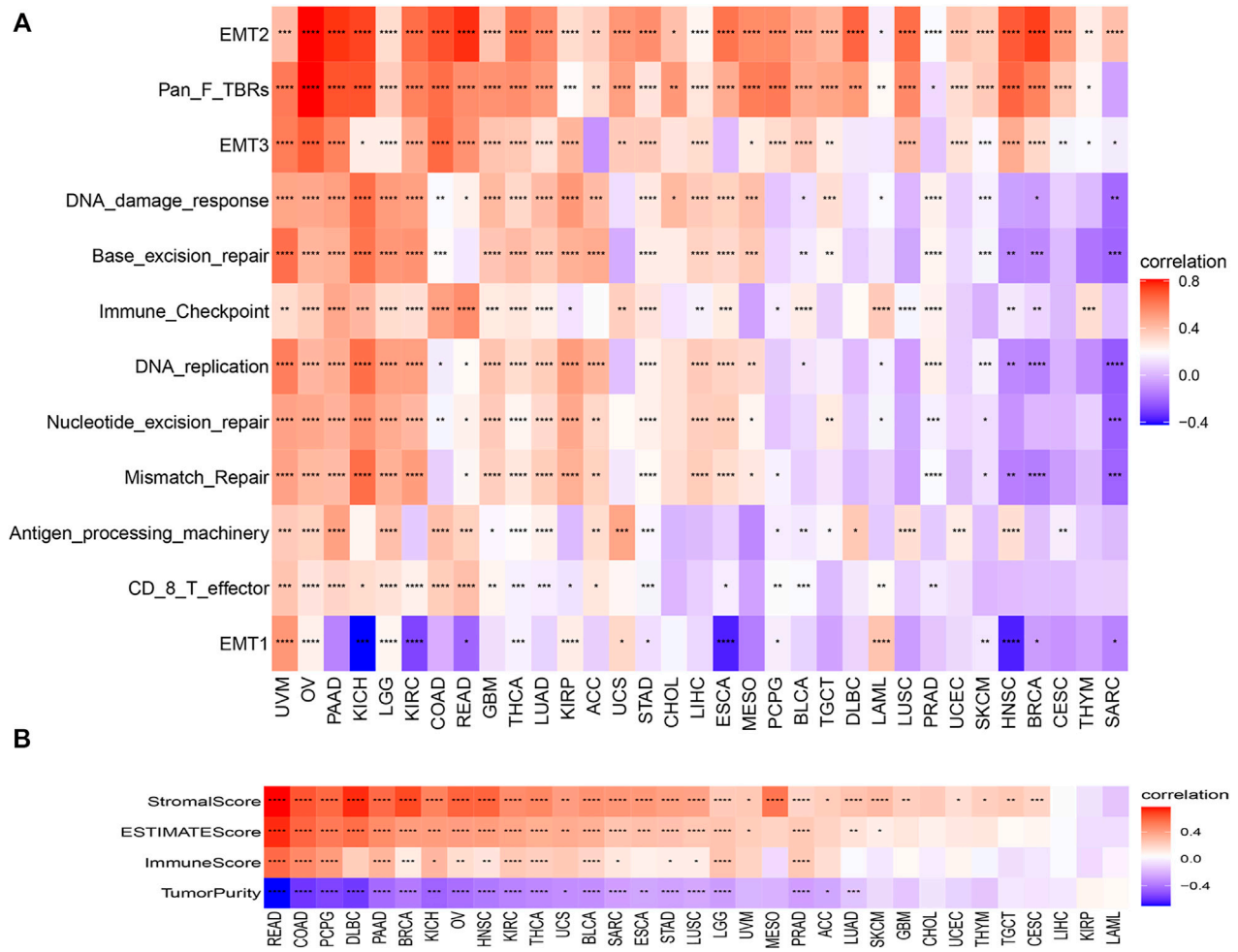

FIGURE 5 | Tumor microenvironment role of C1QTNF6. **(A)** The correlations between the C1QTNF6 expression level and TMEp scores. **(B)** the correlations between the C1QTNF6 express level and ImmuneScore, StromalScore, and ESTIMATEscore. *$p < 0.05$, **$p < 0.01$, ***$p < 0.001$, ****$p < 0.0001$.

pathways, with *C1QTNF6* in pan-cancer. The first 20 related pathways of GSEA are presented in the form of a mountain map, and immune-related pathways are marked in red (**Figures 6A–H**). For instance, in UCS, *C1QTNF6* was associated with the immune system, cytokine pathways, antigen processing-presentation, neutrophil degranulation, and interleukin immunomodulatory responses. These results further illustrate the important role of *C1QTNF6* in immune regulation.

Correlation Between *C1QTNF6* and Immune-Related Genes

We further explored the correlation between the *C1QTNF6* gene and genes associated with immune cells in pan-cancer. The results showed that *C1QTNF6* exhibited a positive association with most immunosuppressive genes, chemokines, and chemokine receptor genes (**Figures 7A–C**). Among the immunosuppressive genes, we found that the immune checkpoints including *LAG3*, *PDCD1*, *CTLA4*, and *TIGIT*, among the chemokines, there are *CXCL12*, *CCL2*, *CCL26*, and in chemokine receptors, we exhibited the *CCR1*, *CCR10*, *CXCR4*, etc.

Drug Sensitivity Analysis

A total of 198 drugs were identified as being associated with *C1QTNF6*. We showed the 6 drugs (**Figure 8A**) with the strongest positive correlation and the 6 drugs with the strongest negative correlation (only 6 negative, **Figure 8B**). The drugs that were identified to have positive correlation with *C1QTNF6* were namely AZD1208 (R = 0.21, p = 5.91E-09), Daprinad (R = 0.21, p = 4.09E-05), crizotinib (R = 0.2, p = 2.38E-08), Vorinostat (R = 0.2, p = 2.17E-08), PD173074 (R = 0.19, p = 1.69E-07), and MK-8776 (R = 0.19, p = 1.30E-07). In addition, six drugs were identified to be negatively correlated with C1QTNF6, namely Sapitinib (R = -0.17, p = 1.85E-06), Dasatinib e-05 (R = -0.15, p = 4.22), Trametinib (R = 0.1, p = 0.0042), Osimertinib (R = -0.09, p = 0.015), AZD8186 (R = -0.09, p = 0.017), and Selumetinib (R = -0.07, p = 0.0495). The results of the complete drug sensitivity analysis were presented in **Supplementary Table S1**. The commonly used anticancer drug in clinical treatment

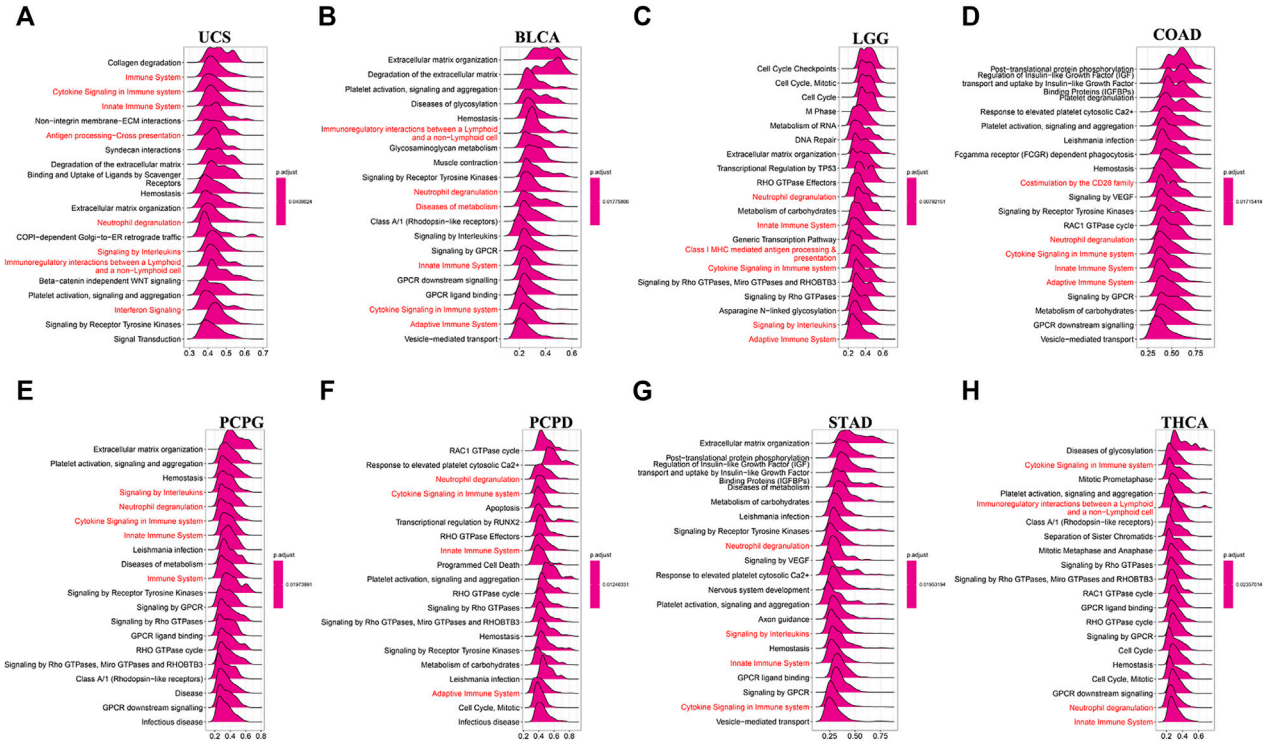

FIGURE 6 | C1QTNF6's GSEA results in TCGA pan-cancer. **(A–H)** The most 20 related pathways of GSEA are presented in the form of a mountain map, and immune-related pathways are marked in red.

including Oxaliplatin, Cyclophosphamide, Cytarabine, Cisplatin, Cytarabine, Vinorelbine, Sorafenib, Docetaxel, and Fluorouracil were all less effective (higher IC50 value) in High expression of *C1QTNF6* groups (**Supplementary Figure S3**).

DISCUSSION

With the development of high-throughput bioinformatics, people's understanding of genes or genomes has reached a new level. Exploration of molecular characterization of disease and individual genetic composition can facilitate clinical scientists to diagnose and treat the disease, which also facilitates the development of drug research and development, especially in cancer research. The discovery of a few genetic biomarkers has limited aid in the diagnosis and treatment of cancer, and identifying more biomarkers or combinations of biomarkers is increasingly important. In this study, we explore the role of *C1QTNF6* with comprehensive means using TCGA pan-cancer data.

Many studies have preliminarily elucidated the role of *C1QTNF6* in cancer. Qu et al. found that *C1QTNF6* is involved in promoting the proliferation and migration of gastric cancer cells and reducing apoptosis of gastric cancer cells (Qu et al., 2019). Han et al. found that *C1QTNF6* may be an independent prognostic factor for lung adenocarcinoma (Han et al., 2019). Song et al. discovered that *C1QTNF6* stimulates proliferation and attenuated apoptosis in oral squamous cell carcinoma (Song et al., 2021). Therefore, *C1QTNF6* might serve an instrumental function in the occurrence and progression of cancer. However, there has not been a comprehensive analysis of the significance of *C1QTNF6* in cancer.

We evaluated the *C1QTNF6* expression level in pan-cancer data and discovered that *C1QTNF6* is overexpressed in many types of cancer, such as LGG, LAML, LIHC, KIRP, LUAD, KIRC, LUSC, HNSC, PAAD, GBM, READ, ESCA, SARC, DLBC, SKCM, COAD, STAD, CHOL, THYM, BRCA, UCS, BLCA. Therefore, monitoring the expression level of *C1QTNF6* may be an effective diagnostic method for these cancers. Subsequently, the mutation analysis found that the alteration frequency of *C1QTNF6* in uterine carcinosarcoma was the highest. *C1QTNF6* had a strong positive correlation with CNA in CHOL, UCS, and PCPG. This enriched our understanding of the functionality of *C1QTNF6*. Survival analysis showed that *C1QTNF6* was an independent prognostic indicator for many tumors. Patient prognosis could be improved to a great extent as a result of this discovery. Analysis of the immune microenvironment revealed the role of *C1QTNF6* in the immune environment including immune-related gene and immune cells infiltration. The final drug sensitivity analysis provided the strongest association with *C1QTNF6*. This provides an idea for targeting *C1QTNF6* therapy.

Our study found that *C1QTNF6* is associated with a variety of classical pathways in many tumors, including epithelial-

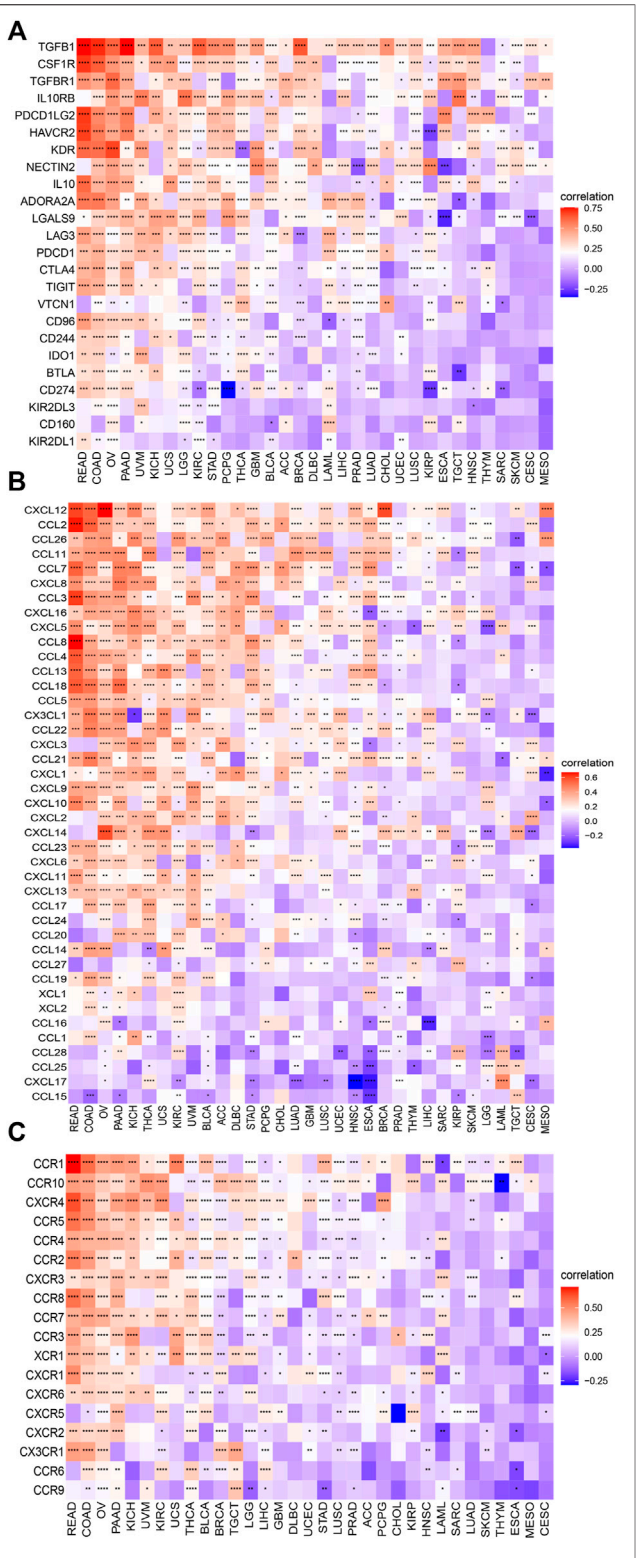

FIGURE 7 | C1QTNF6 is correlated with immune-associated genes. The heatmap demonstrating the correlation between the C1QTNF6 expression level and **(A)** immunosuppressive genes. **(B)** chemokine genes. **(C)** chemokine receptors. *$p < 0.05$, **$p < 0.01$, ***$p < 0.001$, ****$p < 0.0001$.

mesenchymal transformation (EMT), angiogenesis, apical junction, *TGF-β* signaling pathway, hypoxia, and Notch pathway. For instance, *C1QTNF6* had a significant correlation with EMT and angiogenesis. EMT has been widely recognized as a pathway through which cancer cells acquire malignant biological functions (Lamouille et al., 2014; Dongre and Weinberg, 2019). Through EMT, the potential of cancer cells to proliferate, invade and migrate is activated (Owusu-Akyaw et al., 2019; Pastushenko and Blanpain, 2019). In addition, EMT has been linked to drug resistance in many tumors (Du and Shim, 2016). Therefore, our study found a strong correlation between *C1QTNF6* and EMT, which could explain the poor prognosis after overexpression of *C1QTNF6* in many tumors. Angiogenesis which is one of the hallmarks of tumors is also necessary for tumor proliferation and invasion (Ramjiawan et al., 2017; Li et al., 2019). At present, antiangiogenic drugs have achieved preliminary results in the treatment of diverse solid tumors, but a considerable number of patients lack the persistent response of antiangiogenic drugs. Besides, our study found a significant positive correlation between *C1QTNF6* and angiogenesis, which is of reference value for us to further explore the mechanism of tumor angiogenesis and develop new therapeutic methods. In addition, TFN-α SIGNALING VIA NFK-β and *IL2 STAT5* SIGNALING also showed a strong relationship with the *C1QTNF6* gene. The biological activity of *IL2* is related to T cell activation, $CD8^+$ cytotoxicity, B cell activation, and the antitumor effects of enhanced macrophages, which all have been widely reported (Abbas et al., 2018).

Immune reprogramming is one of the hallmarks of cancer. Several therapies based on cancer immunity have been used clinically, such as immune checkpoints (Zhou et al., 2021). For instance, results of the bladder cancer clinical trial BLASST-1 showed that Nivolumab (Opdivo) in combination with gemcitabine and cisplatin neoadjuvant therapy in patients with muscle-infiltrating bladder cancer (MIBC) achieved a significant effect: a pathology complete response rate (pCR) of 49% (Gupta et al., 2020). Therefore, identifying the changes in the cancer-immune microenvironment not only helps us understand the pathogenesis of cancer but also promotes the development of cancer immunotherapy (Huang et al., 2018). According to the findings of the present research, *C1QTNF6* serves a prominent function in the immune milieu of cancer cells. It is significantly linked to diverse immune pathways and immune components. In the TME, stromal and immune cells are the two most crucial kinds of non-tumor constituents, and both have been considered to play a crucial role in the diagnosis and prognostic evaluation of cancers. In tumors, immune and stromal scores can be used to aid in the quantification of immunological and stromal components that are present (Bruni et al., 2020). *C1QTNF6* shows a great correlation with the ESTIMATEscore, StromalScore, and ImmuneScore. Besides, *C1QTNF6* is obviously correlated with many immune checkpoints including *LAG3*, *PDCD1*, *CTLA4*, which suggested that *C1QTNF6* may act as a new immune checkpoint for tumor immunity. Meanwhile, our results show that *C1QTNF6* also have markable relation with chemokines and chemokines receptor such as *CCL22*, *CCL5*, etc. *CCL22* secreted by the M2 macrophages may recruit Treg T cells, which suppressed the immune response (Atri et al., 2018). *CCL5* is a

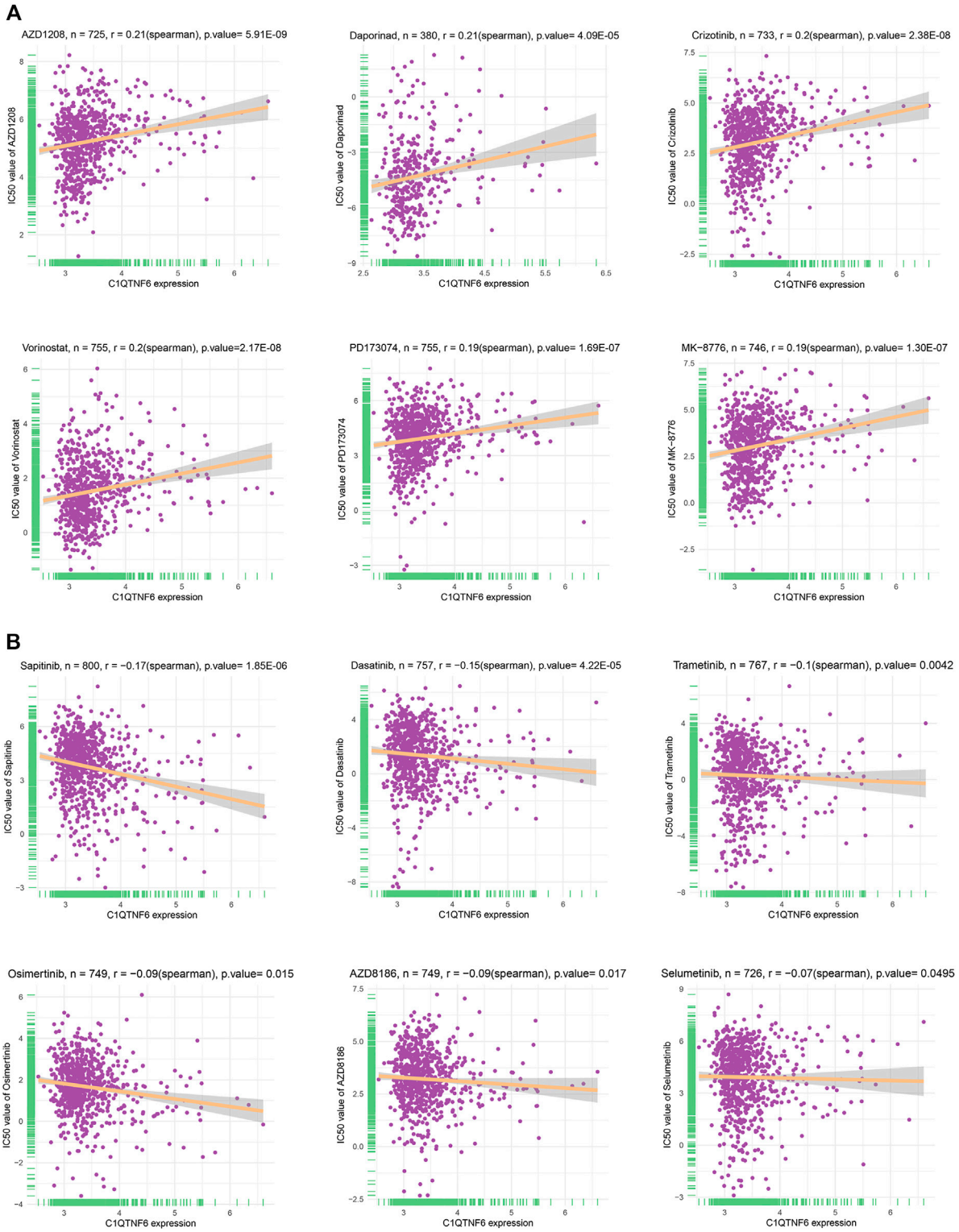

FIGURE 8 | Drug sensitivity analysis in the form of correlation chart calculated by online tool GDSC2. **(A)** The top 6 positively correlated. **(B)** The only 6 negatively correlated.

key chemokine for $CD8^+$ T cells to enter tumor cells (Dangaj et al., 2019). *C1QTNF6* shows a significant association with the infiltration of monocyte, Macrophage, B cells, Monitoring the *C1QTNF6* expression may reflect the degree of infiltration of these immune cells, it is noteworthy that *C1QTNF6* is not manifest a strong correlation to all the immune cells because the activation, chemotaxis, and infiltration of immune cells are regulated by gene networks, especially in pan-cancer analysis. The above results indicate that *C1QTNF6* has significance for further exploration in immune regulation in the tumor microenvironment. These findings were further validated by the GSEA and correlation exploration between *C1QTNF6* and immune cells. In the drug sensitivity analysis, we found higher *C1QTNF6* expression in tumors indicates a higher IC50 value for most drugs in the GDSC2 database, which shows the measurement of *C1QTNF6* expression level may act as a reliable indicator for clinical therapy. P-gp, a well-known multidrug resistance protein, encoded by MDR1, it serve as medicine pump by reverse the concentration of lipophilic drugs with positive charge inside the cell to the outside of the cell, so that the intracellular chemotherapy drugs can not reach the effective concentration and develop drug resistance (Robey et al., 2018). In non-small-cell-lung cancer, MET amplification is thought to be responsible for resistance to targeted drugs in EGFR-mutation-positive patients, which results in malignant biological behavior of tumors, such as invasion, metastasis, escape from apoptosis (Coleman et al., 2021). Combining with the *C1QTNF6* expression and its drug sensitivity analysis (positively correlated and negatively correlated), we may establish risk stratification for cancer patients, which optimize the development and application of anti-cancer drugs. These findings suggest that *C1QTNF6* may be a potential target for cancer therapy, which make contribution to study the mechanisms of anti-cancer drugs resistance.

Cancer immunotherapy has recently been in full swing. Effective identification of potential tumor antigens has contributed to the development of immunotherapy. These tumor antigens are often associated with more copy number mutations or methylation changes. Our study provides the mutation landscape of *C1QTNF6* in pan-cancer and the correlation landscape with copy number variation and methylation. Furthermore, we identified a correlation between *C1QTNF6* and chemokine receptors. All these results provide a reference that *C1QTNF6* can be used not only as an indicator of the TME, but also as a highly effective indicator of immune indicators.

Overall, our study is the first pan-cancer analysis of *C1QTNF6*. Compared with other studies, our study provided a landscape of the prognosis and immunity correlation of *C1QTNF6* in a variety of cancers, which is conducive to the precise treatment of cancer. However, there are also limitations in our study. We lack experiments to verify our conclusions, which we will improve in the future.

CONCLUSION

Overall, we identified the value of *C1QTNF6* in pan-cancer by multiple analyses. *C1QTNF6*, as a promising prognostic biomarker, manifests its promising prospect in immunoregulation and a potential target for tumor therapy.

DATA AVAILABILITY STATEMENT

Publicly available datasets were analyzed in this study. This data can be found here: This study used online resources, which are available from the TCGA database, GTEx through USUC Xena at https://xena.ucsc.edu, the cBioportal database at http://www.cbioportal.org/, and GDSC2 at https://www.cancerrxgene.org/.

AUTHOR CONTRIBUTIONS

WL, JZ, and TX conceived the study. WL wrote the paper and drew the figures. The data were evaluated by BW and XH. YT and YY edited and reviewed the manuscript. YY and XH were in charge of sourcing the necessary funds. All the authors made significant contributions to the present research and gave their approval to the final version of the manuscript submitted for publication.

FUNDING

This work was supported by the Guangzhou Science and Technology Plan Project (grant number 202102020034) and the National Natural Science Foundation of China (grant number 81773354).

ACKNOWLEDGMENTS

We would like to thank the Cancer Genome Atlas (TCGA) working groups for kindly sharing data. We also thank R Development Core Team and the R community (http://www.r-project.org) for the time and effort they put into creating and optimizing R.

SUPPLEMENTARY MATERIAL

The Supplementary Material for this article can be found online at: https://www.frontiersin.org/articles/10.3389/fphar.2022.855485/full#supplementary-material

Supplementary Figure S1 | Univariate cox regression and multivariate cox regression analysis of C1QTNF6 and other clinical features in KIRC, LUAD, LGG, KIRP, ACC, UVM, MESO, LIHC, HNSC, KICH, BLCA, THCA, UCEC.

Supplementary Figure S2 | Correlation between the expression of C1QTNF6 and the infiltrating levels of immune cell. $^*p < 0.05$, $^{**}p < 0.01$, $^{***}p < 0.001$, $^{****}p < 0.0001$.

Supplementary Figure S3 | Drug sensitivity of commonly used anti-cancer drugs in clinical use in the forms of boxplot charts calculated by online tool GDSC2. **(A–I)** Oxaliplatin, Cyclophosphamide, Cytarabine, Cisplatin, Cytarabine, Vinorelbine, Sorafenib, Docetaxel, Fluorouracil.

Supplementary Table S1 | Drug sensitivity differences according to the C1QTNF6 expression of all the 198 drugs in the GDSC2 database.

REFERENCES

Abbas, A. K., Trotta, E., R Simeonov, D., Marson, A., and Bluestone, J. A. (2018). Revisiting IL-2: Biology and Therapeutic Prospects. *Sci. Immunol.* 3, 3. doi:10.1126/sciimmunol.aat1482

Ai, L., Xu, A., and Xu, J. (2020). Roles of PD-1/pd-L1 Pathway: Signaling, Cancer, and beyond. *ADV. EXP. MED. BIOL.* 1248, 33–59. doi:10.1007/978-981-15-3266-5_3

Atri, C., Guerfali, F. Z., and Laouini, D. (2018). Role of Human Macrophage Polarization in Inflammation during Infectious Diseases. *INT. J. MOL. SCI.* 19, 19. doi:10.3390/ijms19061801

Biecek, A. K. A. M. (2020). Survminer: Drawing Survival Curves Using 'ggplot2'. Available at: https://CRAN.R-project.org/package=survminer.

Blum, A., Wang, P., and Zenklusen, J. C. (2018). SnapShot: TCGA-Analyzed Tumors. *CELL* 173, 530. doi:10.1016/j.cell.2018.03.059

Bruni, D., Angell, H. K., and Galon, J. (2020). The Immune Contexture and Immunoscore in Cancer Prognosis and Therapeutic Efficacy. *NAT. REV. CANCER* 20, 662–680. doi:10.1038/s41568-020-0285-7

Carmeliet, P. (2005). VEGF as a Key Mediator of Angiogenesis in Cancer. *Oncology* 69, 4–10. doi:10.1159/000088478

Coleman, N., Hong, L., Zhang, J., Heymach, J., Hong, D., and Le, X. (2021). Beyond Epidermal Growth Factor Receptor: MET Amplification as a General Resistance Driver to Targeted Therapy in Oncogene-Driven Non-small-cell Lung Cancer. *ESMO Open* 6, 100319. doi:10.1016/j.esmoop.2021.100319

Dangaj, D., Bruand, M., Grimm, A. J., Ronet, C., Barras, D., Duttagupta, P. A., et al. (2019). Cooperation between Constitutive and Inducible Chemokines Enables T Cell Engraftment and Immune Attack in Solid Tumors. *CANCER CELL* 35, 885–e10. doi:10.1016/j.ccell.2019.05.004

Davies, H., Bignell, G. R., Cox, C., Stephens, P., Edkins, S., Clegg, S., et al. (2002). Mutations of the BRAF Gene in Human Cancer. *NATURE* 417, 949–954. doi:10.1038/nature00766

Dongre, A., and Weinberg, R. A. (2019). New Insights into the Mechanisms of Epithelial-Mesenchymal Transition and Implications for Cancer. *Nat. Rev. Mol. Cell Biol.* 20, 69–84. doi:10.1038/s41580-018-0080-4

Du, B., and Shim, J. S. (2016). Targeting Epithelial-Mesenchymal Transition (EMT) to Overcome Drug Resistance in Cancer. *MOLECULES* 21, 21. doi:10.3390/molecules21070965

Gupta, S., Sonpavde, G., Christopher, J. W., McGregor, B. A., Gupta, S., and Maughan, B. L. (2020). Results from BLASST-1 (Bladder Cancer Signal Seeking Trial) of Nivolumab, Gemcitabine, and Cisplatin in Muscle Invasive Bladder Cancer Undergoing Cystectomy. *J. Clin. Oncol.* 38. *ASCO GU*.

Han, M., Wang, B., Zhu, M., and Zhang, Y. (2019). C1QTNF6 as a Novel Biomarker Regulates Cellular Behaviors in A549 Cells and Exacerbates the Outcome of Lung Adenocarcinoma Patients. In Vitro *Cell Dev. Biol. Anim.* 55, 614–621. doi:10.1007/s11626-019-00377-w

Han, Y., Liu, D., and Li, L. (2020). PD-1/PD-L1 Pathway: Current Researches in Cancer. *AM. J. CANCER RES.* 10, 727–742.

Hanahan, D., and Weinberg, R. A. (2011). Hallmarks of Cancer: the Next Generation. *CELL* 144, 646–674. doi:10.1016/j.cell.2011.02.013

Hänzelmann, S., Castelo, R., and Guinney, J. (2013). GSVA: Gene Set Variation Analysis for Microarray and RNA-Seq Data. *BMC BIOINFORMATICS* 14, 7. doi:10.1186/1471-2105-14-7

Hausman, D. M. (2019). What Is Cancer? *PERSPECT. BIOL. MED.* 62, 778–784. doi:10.1353/pbm.2019.0046

Huang, Y., Kim, B. Y. S., Chan, C. K., Hahn, S. M., Weissman, I. L., and Jiang, W. (2018). Improving Immune-Vascular Crosstalk for Cancer Immunotherapy. *NAT. REV. IMMUNOL.* 18, 195–203. doi:10.1038/nri.2017.145

Kroemer, G., and Pouyssegur, J. (2008). Tumor Cell Metabolism: Cancer's Achilles' Heel. *CANCER CELL* 13, 472–482. doi:10.1016/j.ccr.2008.05.005

Lamouille, S., Xu, J., and Derynck, R. (2014). Molecular Mechanisms of Epithelial-Mesenchymal Transition. *Nat. Rev. Mol. Cell Biol.* 15, 178–196. doi:10.1038/nrm3758

Li, S., Xu, H. X., Wu, C. T., Wang, W. Q., Jin, W., Gao, H. L., et al. (2019). Angiogenesis in Pancreatic Cancer: Current Research Status and Clinical Implications. *ANGIOGENESIS* 22, 15–36. doi:10.1007/s10456-018-9645-2

Macheret, M., and Halazonetis, T. D. (2015). DNA Replication Stress as a Hallmark of Cancer. *Annu. Rev. Pathol.* 10, 425–448. doi:10.1146/annurev-pathol-012414-040424

Owusu-Akyaw, A., Krishnamoorthy, K., Goldsmith, L. T., and Morelli, S. S. (2019). The Role of Mesenchymal-Epithelial Transition in Endometrial Function. *HUM. REPROD. UPDATE* 25, 114–133. doi:10.1093/humupd/dmy035

Park, J. H., Pyun, W. Y., and Park, H. W. (2020). Cancer Metabolism: Phenotype, Signaling and Therapeutic Targets. *CELLS* 9, 2308. doi:10.3390/cells9102308

Pastushenko, I., and Blanpain, C. (2019). EMT Transition States during Tumor Progression and Metastasis. *Trends. CELL BIOL.* 29, 212–226. doi:10.1016/j.tcb.2018.12.001

Qin, W., Hu, L., Zhang, X., Jiang, S., Li, J., Zhang, Z., et al. (2019). The Diverse Function of PD-1/PD-L Pathway beyond Cancer. *FRONT. IMMUNOL.* 10, 2298. doi:10.3389/fimmu.2019.02298

Qu, H. X., Cui, L., Meng, X. Y., Wang, Z. J., Cui, Y. X., Yu, Y. P., et al. (2019). C1QTNF6 Is Overexpressed in Gastric Carcinoma and Contributes to the Proliferation and Migration of Gastric Carcinoma Cells. *INT. J. MOL. MED.* 43, 621–629. doi:10.3892/ijmm.2018.3978

Ramjiawan, R. R., Griffioen, A. W., and Duda, D. G. (2017). Anti-angiogenesis for Cancer Revisited: Is There a Role for Combinations with Immunotherapy? *ANGIOGENESIS* 20, 185–204. doi:10.1007/s10456-017-9552-y

Robey, R. W., Pluchino, K. M., Hall, M. D., Fojo, A. T., Bates, S. E., and Gottesman, M. M. (2018). Revisiting the Role of ABC Transporters in Multidrug-Resistant Cancer. *NAT. REV. CANCER* 18, 452–464. doi:10.1038/s41568-018-0005-8

Simko, T. W. A. V. (2021). R Package 'corrplot': Visualization of a Correlation Matrix (Version 0.90). Available at: https://github.com/taiyun/corrplot.

Song, X., Li, L., Shi, L., Liu, X., Qu, X., Wei, F., et al. (2021). C1QTNF6 Promotes Oral Squamous Cell Carcinoma by Enhancing Proliferation and Inhibiting Apoptosis. *CANCER CELL INT.* 21, 666. doi:10.1186/s12935-021-02377-x

Takeuchi, T., Adachi, Y., and Nagayama, T. (2011). Expression of a Secretory Protein C1qTNF6, a C1qTNF Family Member, in Hepatocellular Carcinoma. *Anal. Cell Pathol (Amst)* 34, 113–121. doi:10.3233/ACP-2011-009

Verhaak, K. Y. A. H. (2016). Estimate: Estimate of Stromal and Immune Cells in Malignant Tumor Tissue from Expression Data. Available at: https://R-Forge.R-project.org/projects/estimate/.

Wang, J., Zhu, M., Ye, L., Chen, C., She, J., and Song, Y. (2020). MiR-29b-3p Promotes Particulate Matter-Induced Inflammatory Responses by Regulating the C1QTNF6/AMPK Pathway. *Aging (Albany NY)* 12, 1141–1158. doi:10.18632/aging.102672

Wickham, H. (2016). ggplot2: Elegant Graphics for Data Analysis. *Springer-Verlag New York*.

Wilke, C. O. (2021). Ggridges: Ridgeline Plots in 'ggplot2'.

Yu, G., Wang, L. G., Han, Y., and He, Q. Y. (2012). clusterProfiler: an R Package for Comparing Biological Themes Among Gene Clusters. *OMICS* 16, 284–287. doi:10.1089/omi.2011.0118

Zhang, W., and Feng, G. (2021). C1QTNF6 Regulates Cell Proliferation and Apoptosis of NSCLC *In Vitro* and *In Vivo*. *Biosci. Rep.* 41, 41. doi:10.1042/BSR20201541

Zhou, C., Wei, W., Ma, J., Yang, Y., Liang, L., Zhang, Y., et al. (2021). Cancer-secreted Exosomal miR-1468-5p Promotes Tumor Immune Escape via the Immunosuppressive Reprogramming of Lymphatic Vessels. *MOL. THER.* 29, 1512–1528. doi:10.1016/j.ymthe.2020.12.034

Conflict of Interest: The authors declare that the research was conducted in the absence of any commercial or financial relationships that could be construed as a potential conflict of interest.

frontiers in Oncology

ORIGINAL RESEARCH
published: 29 March 2022
doi: 10.3389/fonc.2022.855674

Molecular Biomarker of Drug Resistance Developed From Patient-Derived Organoids Predicts Survival of Colorectal Cancer Patients

Lifeng Chen[1†], *Bo Tian*[2†], *Wen Liu*[1], *Haitao Liang*[3], *Yong You*[1*] *and Weizhen Liu*[4*]

[1] Department of Hematology, Union Hospital, Tongji Medical College, Huazhong University of Science and Technology, Wuhan, China, [2] Department of Orthopaedic Surgery, Zhongshan Hospital, Fudan University, Shanghai, China, [3] Shenzhen Second People's Hospital (The First Hospital Affiliated to Shenzhen University, Health Science Center), Shenzhen, China, [4] Department of Gastrointestinal Surgery, Union Hospital, Tongji Medical College, Huazhong University of Science and Technology, Wuhan, China

OPEN ACCESS

Edited by:
Jian Zhang,
Southern Medical University, China

Reviewed by:
William Gmeiner,
Wake Forest School of Medicine, United States
Ann Zeuner,
National Institute of Health (ISS), Italy

***Correspondence:**
Weizhen Liu
weizhenliu@hust.edu.cn
Yong You
youunion@126.com

[†]These authors have contributed equally to this work

Specialty section:
This article was submitted to Pharmacology of Anti-Cancer Drugs, a section of the journal Frontiers in Oncology

Received: 15 January 2022
Accepted: 10 February 2022
Published: 29 March 2022

Citation:
Chen L, Tian B, Liu W, Liang H, You Y and Liu W (2022) Molecular Biomarker of Drug Resistance Developed From Patient-Derived Organoids Predicts Survival of Colorectal Cancer Patients. Front. Oncol. 12:855674. doi: 10.3389/fonc.2022.855674

The drug 5-fluorouracil (5-Fu) is the critical composition of colorectal cancer (CRC) treatments. Prognostic and predictive molecular biomarkers for CRC patients (CRCpts) treated with 5-Fu-based chemotherapy can provide assistance for tailoring treatment approach. Here, we established a molecular biomarker of 5-Fu resistance derived from colorectal cancer organoids (CRCOs) for predicting the survival of CRCpts. Forty-one CRCO cultures were generated from 50 CRC tumor tissues after surgery (82%). The following experiments revealed a great diversity in drug sensitivity for 10 μM 5-Fu treatment tested by using organoid size change. Fourteen cases (34.1%) were 5-Fu sensitive and the other 27 (65.9%) were resistant. Then, differentially expressed genes (DEGs) associated with 5-Fu resistance were outputted by transcriptome sequencing. In particular, DEGs were generated in two comparison groups: 1) 5-Fu sensitive and resistant untreated CRCOs; 2) CRCOs before 5-Fu treatment and surviving CRCOs after 5-Fu treatment. Some molecules and most of the pathways that have been reported to be involved in 5-Fu resistance were identified in the current research. By using DEGs correlated with 5-Fu resistance and survival of CRCpts, the gene signature and drug-resistant score model (DRSM) containing five molecules were established in The Cancer Genome Atlas (TCGA)-CRC cohort by least absolute shrinkage and selection operator (LASSO) regression analysis and 5-fold cross-validation. Multivariate analysis revealed that drug-resistant score (DRS) was an independent prognostic factor for overall survival (OS) in CRCpts in TCGA-CRC cohort ($P < 0.001$). Further validation results from four Gene Expression Omnibus (GEO) cohorts elucidated that the DRSM based on five genes related to 5-Fu chemosensitivity and developed from patient-derived organoids can

predict survival of CRCpts. Meanwhile, our model could predict the survival of CRCpts in different subgroups. Besides, the difference of molecular pathways, tumor mutational burden (TMB), immune response-related pathways, immune score, stromal score, and immune cell proportion were dissected between DRS-high and DRS-low patients in TCGA-CRC cohort.

Keywords: colorectal cancer, organoids, 5-fluorouracil, drug resistance, molecular biomarker, predict, survival

INTRODUCTION

Colorectal cancer (CRC) is the fourth most common diagnosed cancer and the second leading cause of cancer death worldwide (1). CRC tumors are highly heterogeneous in their intratumor and intertumor characteristics because of microsatellite instability (MSI), chromosomal instability (CIN), DNA repair defects, aberrant DNA methylation, and other factors. These factors determine how colorectal cancer patients (CRCpts) respond to specific therapy (2). In the era of precision oncology, implicit molecular characterization of the tumor is essential in defining the best therapeutic plan. Therefore, the establishment of prognostic and predictive molecular biomarkers is increasingly becoming more valuable in cancer treatment (3, 4).

In clinical practice, although new options have been developed including targeted therapy and immunotherapy, chemotherapy based on 5-fluorouracil (5-Fu) is still the critical composition of CRC treatments (5). However, drug resistance is ubiquitous, resulting in tumor progression and poor outcome in CRCpts. For instance, despite advances in response rate with the advent of various modulation strategies such as monoclonal antibodies combined with chemotherapy, 5-year relative survival rate for metastatic colorectal cancer (mCRC) is only slightly over 12% (6). Approximately half of metastatic CRCs are resistant to 5-Fu-based chemotherapies (7). One of the major culprits for this observation is the appearance of drug resistance. Prognostic and predictive molecular biomarkers for CRCpts receiving 5-Fu-based chemotherapy can provide assistance for tailoring treatment approach.

Organoid is a self-organized three-dimensional (3D) construct and constituted of various cell types that ultimately generated from stem cells. It is capable of mimicking the architecture and functionality of primary organs (8). Patient-derived tumor organoids (PDTOs) have been proven to recapitulate the tumor's pathological morphology, marker expression, chromosomal stability, genomic characterization, and tumor heterogeneity (8, 9). Recently, several studies suggested that PDTOs can predict the response to chemotherapy, chemoradiation, and targeted therapy, suggesting that PDTOs may represent a companion preclinical tool in precision oncology (10–12). However, the success rate of establishing PDTOs from CRCpts still needs to be improved (<90%), and PDTO-based drug assays require at least 1–2 weeks (10–13). These challenges may hamper the implementation of PDTO approach in a clinical setting.

PDTOs can more faithfully represent patient tumors than cell lines that potentially enable more comprehensive insights into mechanisms of drug resistance (8, 9). In this research, we successfully generated a gene signature and score system as molecular biomarkers that can predict the prognosis of CRCpts by using drug sensitivity data (5-Fu) of colorectal cancer organoids (CRCOs). Our model may be helpful in tailoring therapeutic regimens and act as a supplement of PDTO-guided personalized treatment for CRCpts.

MATERIALS AND METHODS

Study Design

Study Objectives

To generate a gene signature of chemosensitivity developed from PDTOs and investigate the potential of the gene signature to predict the survival of CRCpts.

Research Subjects

Surgical specimens from CRCpts were used to establish a biobank of CRCOs. CRC datasets from The Cancer Genome Atlas (TCGA) program and Gene Expression Omnibus (GEO) database were employed to develop and validate the gene signatures for predicting the survival of CRCpts, respectively.

Study Design

The drug sensitivity of CRCOs to 5-Fu were tested, and differentially expressed genes (DEGs) related to 5-Fu resistance were generated by transcriptome sequencing. Gene signature and drug-resistant score model (DRSM) for predicting the survival of CRCpts were developed and validated in TCGA and GEO datasets by using drug-resistant genes (DRGs) associated with 5-Fu resistance, respectively.

The overall flowchart depicting the development and validation of the gene signatures and DRSM was presented in **Figure 1**.

Tumor Samples of Colorectal Cancer Patients

Fifty surgically resected cancer tissues from previously untreated CRCpts were collected in the Department of Gastrointestinal Surgery, Union Hospital, Tongji Medical College, Huazhong University of Science and Technology. The diameters of the CRC tissues for CRCO culture were about 5.00–10.00 mm. The

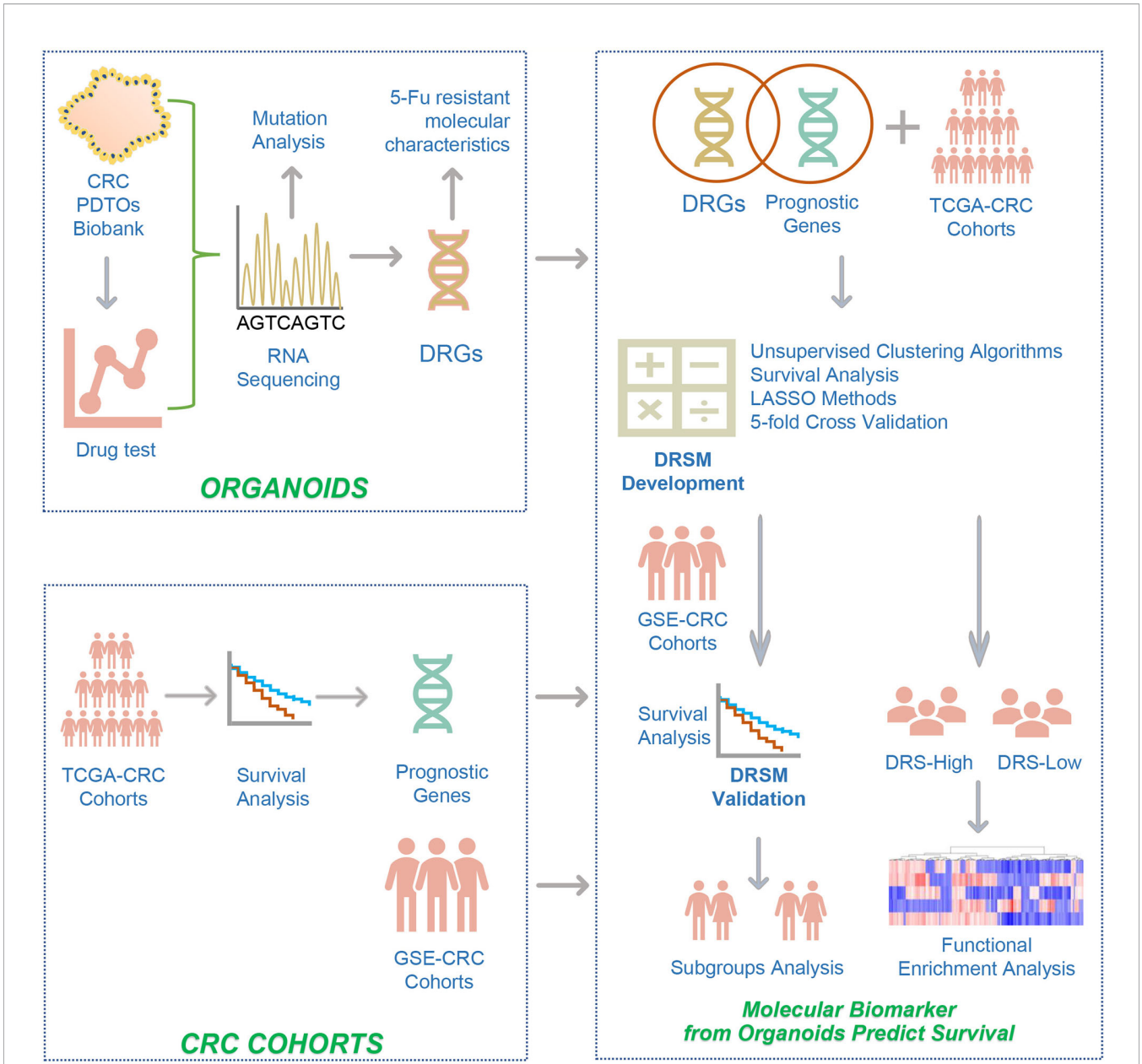

FIGURE 1 | The overall flowchart depicting the development and validation of the gene signatures and drug-resistant score model. The study design was described in detail in the *Methods* (Study design). CRC, colorectal cancer; PDTOs, patient-derived tumor organoids; 5-Fu, 5-fluorouracil; DRGs, drug-resistant genes; TCGA, the cancer genome atlas; GSE, gene expression omnibus series; LASSO, least absolute shrinkage and selection operator; DRSM, drug-resistant score model; DRS, drug resistant score.

tissue collections and experiments were reviewed and approved by the institutional review boards of Union Hospital, Tongji Medical College. Informed consents were obtained from all the patients enrolled in this study.

Processing of Surgical Specimen Tissues

After being harvested, the CRC tissues were transferred into 15-ml centrifuge tubes with cold phosphate buffer saline (PBS) containing gentamicin/amphotericin B (GIBCO, R01510) and normocin (InvivoGen, antnr-1). The tissues were maintained on ice prior to tissue disaggregation and organoid culture.

The Isolation and Primary Culture of Colorectal Cancer Tissues

Primary cancer cells were isolated and cultured using previously described methods (10, 11, 14). Briefly, CRC tissues were washed

in cold PBS containing streptomycin/penicillin (GIBCO, 15140-122) for 5 cycles (5 min per cycle), minced into small pieces, and incubated at 37°C in digestion solution with 10 ml Dulbecco's Modified Eagle Medium (DMEM) (GIBCO, C1199500BT) containing 1.5 mg/ml collagenase II (Solarbio, C8150), 500 U/ml collagenase IV (Sigma-Aldrich, C9407), 0.1 mg/ml dispase type II (Sigma-Aldrich, D4693), 20 mg/ml hyaluronidase (Solarbio, h8030), 10 mM RHOK inhibitor ly27632 (Sigma-Aldrich, Y0503), and 1% fetal bovine serum. Tumor tissues were resuspended every 5 min. For all cases, the digestion was terminated by adding 10 ml cold PBS until no tissue fragments were left. The suspension was filtered with 100 μm cell strainer, and the tumor cells were collected after centrifugation for 5 min at 300–400g.

Finally, the tumor cells were mixed with Matrigel (Corning, 356231) and seeded into a prewarmed 24-multiwell plate. After the Matrigel has solidified, the tumor cells were cultured in CRCO culture medium containing 1× Advanced DMEM/F12 (GIBCO, 12634-010), 1× 4-(2-hydroxyethyl)-1-piperazineethanesulfonic acid (HEPES) (GIBCO, 15630080), 1× Glutamax (GIBCO, 35050061), 1× Normocin (InvivoGen, ant-nr-1), 1× Gentamicin/amphotericin B (GIBCO, R01510), 1× N2 supplement (Invitrogen, 17502-048), 1× B27 supplement (Invitrogen, 17504-044), 500 ng/ml R-spondin 1 (Sino Biological Inc., 11083-HNAS), 100 ng/ml Noggin (Sino Biological Inc., 50688-M02H), 50 ng/ml epidermal growth factor (EGF) (Sino Biological Inc., 50482-MNCH), 1 mM n-Acetylcysteine (Sigma-Aldrich, A9165), 10 mM Niacinamide (Sigma-Aldrich, N0636), 500 nM A8301 (Tocris, 2939), 3 μM SB202190 (Sigma-Aldrich, S7067), 10 nM Gastrin (Sigma-Aldrich, G9145), and 10 nM Prostaglandin E2 (Sigma-Aldrich, P6532) at 37°C, 5% CO_2 incubator.

Colorectal Cancer Organoid Culture

CRCOs were cultured using previously described methods (10, 11, 14). The culture medium of CRCOs was refreshed every 3 days. CRCOs were subcultured every 3–14 days depending on the growth rate of organoids. CRCOs were passaged by mechanical dissociation into small fragments through shearing with 1% Bovine Serum Albumin (BSA)-coated glass pipette tip. For those dense organoids, they were resuspended in prewarmed TrypLE™ Express enzyme (1×) (GIBCO, 12605-010) before mechanical dissociation. After dissociation, CRCOs were washed with cold PBS several times to clear out the Matrigel. Finally, CRCO fragments were resuspended in fresh Matrigel, seeded into a prewarmed 24-multiwell plate, and cultured as described above.

For CRCO cryopreservation, organoids were harvested and mechanically dissociated into small fragments as described above. Then, organoid fragments were mixed with freezing medium (CELLBANKER™ 2, ZENOAQ, 170905) and frozen following standard procedures. As required, the frozen CRCOs were thawed according to standard procedures and cultured as mentioned before. The culture medium was supplemented with 10 μM RHOK inhibitor Y-27632 for the first 3 days of culture after thawing.

Drug Sensitivity Test of Colorectal Cancer Organoids

The assays for drug sensitivity of CRCOs were conducted as described previously (11). Organoid size change at day 24 to day 0 after treatment was used as the indicator for the judgment of drug sensitivity of CRCOs. The optimal validated cutoff value of organoid size change was 36.42% (11).

Briefly, well-grown CRCOs were mechanically dissociated into small fragments, resuspended in 100% Matrigel (≈10 fragments/μl), seeded into 48-well cell culture plate (15 μl, ≈150 fragments/well), and cultured with 300 μl CRCO culture medium. When organoid size reached about 100 μm (day 0), the culture medium was replaced with 300 μl fresh medium containing 10 μM 5-Fu (Selleck, S1209). After 3 days, the 5-Fu-containing medium was refreshed again. Subsequently, the culture medium was replaced by fresh drug-free CRCO culture medium every 3 days in most cases. The medium was refreshed every 1–2 days during the period from day 7 to day 24 for some cases, which have grown much faster than others.

Images of CRCOs were obtained every 3 days after 5-Fu treatment using a ZEISS microscope (ZEISS, Vert.A1). Then, CRCO size was evaluated by using Image-Pro Plus 6.0 (Media Cybernetics, Inc.) software. About 100 organoids were measured per case.

RNA Extraction and Preparation

CRCOs in good condition were collected, homogenized in TRIzol™ Reagent (Invitrogen, 15596026), and frozen at -80°C. Organoid RNA was extracted according to the TRIzol Reagent protocol. RNA contamination and degradation were monitored on 1% agarose gels. RNA integrity was evaluated using the RNA Nano 6000 Assay Kit of the Bioanalyzer 2100 system (Agilent Technologies, CA, USA). RNA purity was examined using the NanoPhotometer® spectrophotometer (IMPLEN, CA, USA).

Transcriptome Sequencing of Colorectal Cancer Organoids

A total amount of 1 μg RNA per sample was used as input material for the RNA sample preparations. Sequencing libraries were generated using NEBNext® Ultra™ RNA Library Prep Kit for Illumina® (NEB, USA) following the manufacturer's recommendations, and index codes were added to attribute sequences to each sample. Detailed information about library preparation for transcriptome sequencing was attached in **Supplementary Methods**. The clustering of the index-coded samples was performed on a cBot Cluster Generation System using TruSeq PE Cluster Kit v3-cBot-HS (Illumina) according to the manufacturer's instructions. After cluster generation, the library preparations were sequenced on an Illumina Novaseq platform, and 150-bp paired-end reads were generated.

Gene Expression and Functional Enrichment Analysis

Fragments per kilobase million (FPKM) was used to evaluate expression levels of individual genes. To identify differentially expressed genes (DEGs), the R package limma was used (15),

which implements an empirical Bayesian approach to estimate gene expression changes. DEGs were determined by significance criteria (P value <0.05) as implemented in the R package limma (15). The Venn diagram was used to visualize common significant DEGs between the different conditions.

The clusterProfiler (16) R package was performed to demonstrate functional enrichment analysis. We identified functional pathways that were upregulated and downregulated by running a gene set enrichment analysis (GSEA) (17) of the adjusted expression data for all transcripts. Enrichment P values were based on 1,000 permutations and subsequently adjusted for multiple testing using the Benjamini–Hochberg procedure to control the false discovery rate (FDR). A developing R package enrichplot (https://github.com/GuangchuangYu/enrichplot) implements several visualization methods to help interpret enrichment results and was adopted to visualize GSEA results.

Datasets of Colorectal Cancer in The Cancer Genome Atlas and Gene Expression Omnibus Databases

CRC datasets from TCGA and GEO databases were used for the development and validation of gene signature and DRSM for predicting the survival of CRCpts, respectively. It was worth noting that only stage II–IV CRCpts were enrolled in the current study because patients with stage I disease underwent surgical resection but did not receive 5-Fu chemotherapy.

The Cancer Genome Atlas Datasets

The clinical and gene expression data (FPKM, fragments per kilobase of exon model per million reads mapped) of CRCpts (TCGA-COAD and TCGA-READ) were obtained from the Genomic Data Commons (GDC) Data Portal (https://portal.gdc.cancer.gov/) by using TCGAbiolinks (18).

Gene Expression Omnibus Datasets

The CRC datasets were preliminarily screened by using the search query as follows: ("colorectal neoplasms"[MeSH Terms] OR colorectal cancer[All Fields]) AND "Homo sapiens"[porgn] AND (("gds"[Filter] OR "gse"[Filter]) AND ("Expression profiling by array"[Filter] OR "Expression profiling by high throughput sequencing"[Filter]) AND ("50"[n_samples]: "10000"[n_samples])) in GEO database. The datasets derived from cell lines and other irrelevant datasets were eliminated manually. In particular, CRC datasets were also enrolled through literature review to avoid missing valuable datasets. Then, the datasets were obtained by using GEOquery. The preliminarily selected GEO datasets were as follows: GSE40967, GSE17538, GSE87211, GSE24551, GSE38832, GSE33113, GSE14333, GSE39084, GSE71187, GSE12945, and GSE29623.

Univariate and Multivariate Survival Analyses

For filtration of the prognosis-related genes, we calculated the prognosis related P value of each gene using univariate and multivariate survival analyses. The Kaplan–Meier method was used to generate survival curves, and the log-rank test was used to determine the statistical significance of differences. The hazard ratios for univariate analysis were calculated using the Cox proportional hazards regression model. A multivariate Cox regression model was used to determine independent prognostic factors using R coxph package. Genes with P values <0.05 were considered significant.

Development of the Drug-Resistant Score Model

Then, the least absolute shrinkage and selection operator (LASSO) regression model implemented in the glmnet (v4.0-2) package was used for the next-step filtration of genes. LASSO regression penalizes the data-fitting standard by eliminating predictive variables. To evaluate the variability and reproducibility of the estimates produced by the LASSO regression model, we repeated the regression fitting process and calculated the best lambda to reduce the error rate by 5-fold cross-validation. Twenty-six genes with non-zero coefficient estimates were retained. The multivariate Cox regression model was used to estimate the coefficient and prognosis-related P value of each gene. Five genes were identified as significant with P value <0.05, for considering as independent prognostic factors. LASSO regression was performed to construct the score model shown as follows: DRS = GEL (gene expression level) (*CACNA1D*) × -0.0563 + GEL (*CIITA*) × -0.0356 + GEL (*PFN2*) × 0.0332 + GEL (*SEZ6L2*) × 0.0378 + GEL (*WDR78*) × -0.0386.

The R package MaxStat (https://CRAN.R-project.org/package=maxstat) was used to test possible cut points and find the one achieving the maximum rank statistic to separate datasets into score-low and score-high groups. R package forestplot was used for presentation of the results of GEO datasets and TCGA dataset.

Statistical Analysis

The P values were two-sided. A value of $P < 0.05$ was considered as statistically significant. CRCO size (day24/d0) was selected as the parameter to evaluate the sensitivity of CRCOs to 5-Fu treatment, and 36.4% was used as the cutoff following the results from previous research (11). Wilcoxon rank-sum test was used for comparison of two groups. Correlation coefficients were computed by Spearman and distance correlation analyses. Two-sided Fisher exact tests were used to analyze contingency tables. To identify significant genes in the differential gene analysis, we applied the Benjamini–Hochberg method to convert the P values to FDRs. All heatmaps, including unsupervised hierarchical clustering, were generated by the function of pheatmap (https://github.com/raivokolde/pheatmap). The statistics of survival analysis, RNA sequencing, gene expression, and functional enrichment analysis were specifically described above.

RESULTS

Establishment of 41 Colorectal Cancer Organoid Lines

From April 2018 to August 2018, we obtained 50 surgically resected cancer tissues from previously untreated CRCpts. All of

them were adenocarcinoma. Cancer cells were isolated and cultured in 3D Matrigel by using the procedures as reported by Hans Clevers group (14, 19). Considering the interpatient tumor heterogeneity, we also specifically referred to the impressive experience from Fujii (20) to improve the success rate of culture. We favorably generated 41 organoid cultures from 50 tumor tissues (82%). For two, we did not observe growth. The complete structures of two were disrupted after several days of swelling. The other five were lost due to bacterial/yeast infection. Additional analysis showed that PTDO generation was not correlated with patients' characteristics (**Table S1**). It has been well confirmed that CRCOs recapitulated characteristics of CRC primary tumor tissues (10, 11, 14). Note that because normal human colon epithelial organoids require Wnt ligand (Wnt 3a) in the culture medium (19), it was considered that organoids cultured in Wnt3a-free media were CRCOs and further characterization relative to the primary tumor was not undertaken. Therefore, the histopathological and genomic (DNA sequencing) features were not characterized in the current study to confirm that organoids derived from cancer patients can recapitulate the features of corresponding tumors.

Sensitivity of Colorectal Cancer Organoids to 5-Fluorouracil

Ex vivo drug sensitivity screen in 3D cancer organoid culture nominates therapeutic candidates (14, 21). Cell viability testing using ATP detection assay was the most common approach for drug sensitivity evaluation of cancer organoids (10, 14, 22, 23). Organoid size change, serving as a measure of organoid survival, is as effective as CellTiter-Glo 3D cell viability assay (11) and is more economical and easier to use. We tested the sensitivity of 41 CRCO lines to 5-Fu by using this method (**Figures 2A–D**). The kinetic size change curves and ratios of CRCO size at day 24 to day 0 [CRCOs size (day24/d0)] after 5-Fu treatment revealed great diversity in drug sensitivity for 10-μm 5-Fu treatment (**Figures 2C, D**), which is consistent with the widely divergent response of CRCpts to 5-Fu-based chemotherapy (24, 25).

We chose CRCO size change (day24/d0) as the parameter to evaluate the sensitivity of CRCOs to 5-Fu treatment and 36.4% as the cutoff according to a previous study (11). CRCO size change (day24/d0) ranged from 0.035 to 4.65 (**Figure 2D**). Fourteen cases (34.1%) were 5-Fu sensitive and the other 27 (65.9%) were resistant (**Figure 2D**). Additional analysis showed that organoid sensitivity to 5-Fu was not correlated with patients' characteristics (**Table S1**). After testing the drug sensitivity of CRCOs to 5-Fu, we continually cultured and expanded the surviving organoids that were resistant for transcriptome sequencing analysis subsequently.

5-Fluorouracil-Resistant Molecular Characteristics of Colorectal Cancer Organoids

Many intrinsic and extrinsic factors involved in 5-Fu resistance in CRC have been well studied (26, 27). Here, CRCOs were employed for the first time to reveal 5-Fu resistance mechanisms of CRC. We utilized transcriptome sequencing to dissect 5-Fu-resistant molecular characteristics of CRCOs (**Figures 3A, B**). DEGs were generated in two comparison groups: 1) 5-Fu sensitive (*group A*) and resistant (*group B*) untreated CRCOs; 2) CRCOs before 5-Fu treatment (*group C*) and surviving CRCOs after 5-Fu treatment (*group D*) (**Figures 3A, B**). Principal component analysis (PCA) showed a high degree of similarity between groups A/B and C/D, respectively (**Figures S1A, B**). Therefore, the criteria of $P < 0.05$ and logFC > 0.58 (fold change >1.5) were used for identification of DEGs (28). Here, 113 and 111 genes were upregulated, and 677 and 2,617 genes were downregulated in groups B and D compared with groups A and C, respectively (**Figures 3C, D**). Only 1 upregulated and 151 downregulated genes were overlapped in the two comparison groups (**Figures 3C, D**), demonstrating that these two different comparison groups (A vs. B, C vs. D) revealed vastly divergent DEGs. The detailed information of DEGs was listed in **Table S2**.

Some of these DEGs have been reported to participate in regulating 5-Fu resistance in CRC. For instance, several genes upregulated in *Group B* or *Group D*, including *ALDOA* (29), *GLUT2 (SLC2A1)* (30, 31), *NACC1* (31), *POLR2A* (32), and *TGFB1* (33), promote 5-Fu resistance in CRC. Besides, some DEGs (*FERMT1* (34), *HEY2* (35, 36), *ITGB4* (37, 38), *PDXP* (39), *TIMP1* (40), TP53I3 (39), et al.) probably have a role in 5-Fu resistance in CRC. Interestingly, the expression levels of most explored enzymes (*TYMS*, *MTHFR*, *TP*, et al.) involved in the resistance of 5-Fu and other fluoropyrimidines (26, 41) had no significant difference in the two comparison groups in the current study.

We also used GSEA to dissect the pathways associated with 5-Fu resistance. Most of the pathways that have been shown to be involved in 5-Fu resistance were identified in the current research (**Figures 3E, F**) (42, 43). Pyrimidine metabolic resistance played a central role in 5-Fu resistance and was also identified here (**Figure S2A**) (42, 43). Additionally, other well-proven pathways regarding 5-Fu resistance discovered in the current analysis included mismatch repair, apoptosis, cell cycle, and mitochondria (oxidative phosphorylation) (**Figures S2B–O**). All enriched pathways were attached as supplementary materials (**Figures S3A–D**; **Tables S3A, B**). **Figures S3A–D** were deposited in the Mendeley Database (DOI: 10.17632/rnrmjkvjjc.2).

Screening of Drug-Resistant Genes Associated With Prognosis in Colorectal Cancer Patients

First, we screened prognostic genes associated with survival of CRCpts in TCGA datasets. PCA showed that the gene expression data of TCGA-COAD and TCGA-READ could be integrated into a TCGA-CRC dataset for subsequent analysis (**Figures 4A, B**). The results showed that the expression levels of 1,784 protein-coding genes were significantly associated with survival of CRCpts by using univariate Cox proportional hazards model analysis (**Figure 4C** and **Table S4**). Then, the DRGs were screened out among the 1,784 genes. There were 77 overlapped genes between 1,784 prognostic protein-coding genes and those DEGs associated with 5-Fu resistance derived from the CRC PDTOs (DRGs) (**Figure 4C** and **Table S5**).

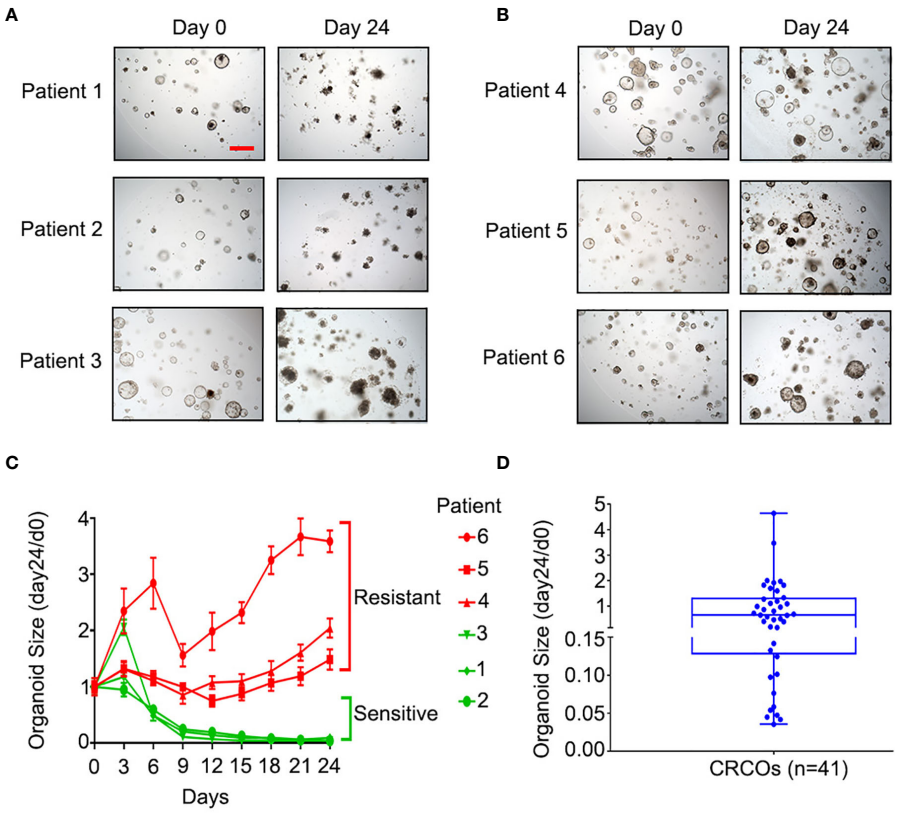

FIGURE 2 | Sensitivity of CRCOs to 5-Fu. **(A)** Representative bright-field images of 5-Fu-sensitive CRCOs at day 0 and day 24 after 10-μM 5-Fu treatment in three selected cases. *The CRCOs with disrupted structures are dead and do not have the ability to repopulate.* **(B)** Representative bright-field images of 5-Fu-resistant CRCOs at day 0 and day 24 after 10-μM 5-Fu treatment in three selected cases. *CRCOs with complete structures are alive and have the ability to repopulate*. Scale bar, 200 μm. **(C)** CRCO size change after 10-μM 5-Fu treatment in six selected cases. The data shown are means with SEM from 8 duplicates. **(D)** Box plot of CRCO size change (day24/d0) in all of the 41 cases. Within the box, the horizontal blue center line denotes the median value (50th percentile), while the box contains the 25th to 75th percentiles of the distribution of values. The blue whiskers mark the minimum and maximum of the values. CRCOs, colorectal cancer organoids; 5-Fu, 5-fluorouracil; SEM, standard error of mean.

Then, multivariate Cox analysis was performed to further screen candidate genes for the construction of DRSM. Variables with *P* value <0.25 in univariate test (44) or reported prognostic value were selected. Age (*P* = 2E-04), prior malignancy (*P* = 0.13), and site of tumor (45) and TNM stage (*P* < 0.0001) were included, but gender (*P* = 0.85) and race (*P* = 0.91) were excluded from the multivariate Cox model (**Figures 4D–I**). Multivariate Cox analysis disclosed that 46 of 77 DRGs' expression levels were significantly correlated with the survival of CRCpts in TCGA-CRC dataset (**Table S6**). Expression data of these 46 genes would be used for the DRSM development next.

Development of the Drug-Resistant Score Model by Using Drug-Resistant Genes Associated With 5-Fluorouracil Resistance

To evaluate the contribution of DRGs to CRCpts' survival, we applied unsupervised clustering algorithms to group the expression data of 46 DRGs in TCGA-CRC dataset, and subsequently, the CRCpts were divided into Group1 (n = 319) and Group2 (n = 190) (**Figure 5A**). Univariate Cox analysis showed that patient survival of Group2 was significantly better than that of Group1 (*P* = 0.00074) (**Figure 5B**).

Then, LASSO regression analysis method and 5-fold cross-validation were used to develop the DRSM for CRCpts in TCGA-CRC dataset. After the best lambda value and coefficient of 46 DRGs were outputted (**Figures 5C, D** and **Table S7**), we obtained 26 genes with non-zero coefficients (**Table S8**). Next, these 26 genes were further filtered using multivariate Cox analysis in TCGA-CRC dataset. Five genes finally remained after the second filter: *CACNA1D* (*P* = 0.0019), *CIITA* (*P* = 0.00503), *PFN2* (*P* = 0.01176), *SEZ6L2* (*P* = 0.02853), and *WDR78* (*P* = 0.0305).

Afterward, the DRSM was established in TCGA-CRC dataset by LASSO regression analysis method and 5-fold cross-validation based on the five genes above (**Figures 5E, F**). The result showed that coefficients of the five genes were all non-zero. The equation of DRS was finally derived: DRS = GEL (gene expression level) (*CACNA1D*) × -0.0563 + GEL (*CIITA*) ×

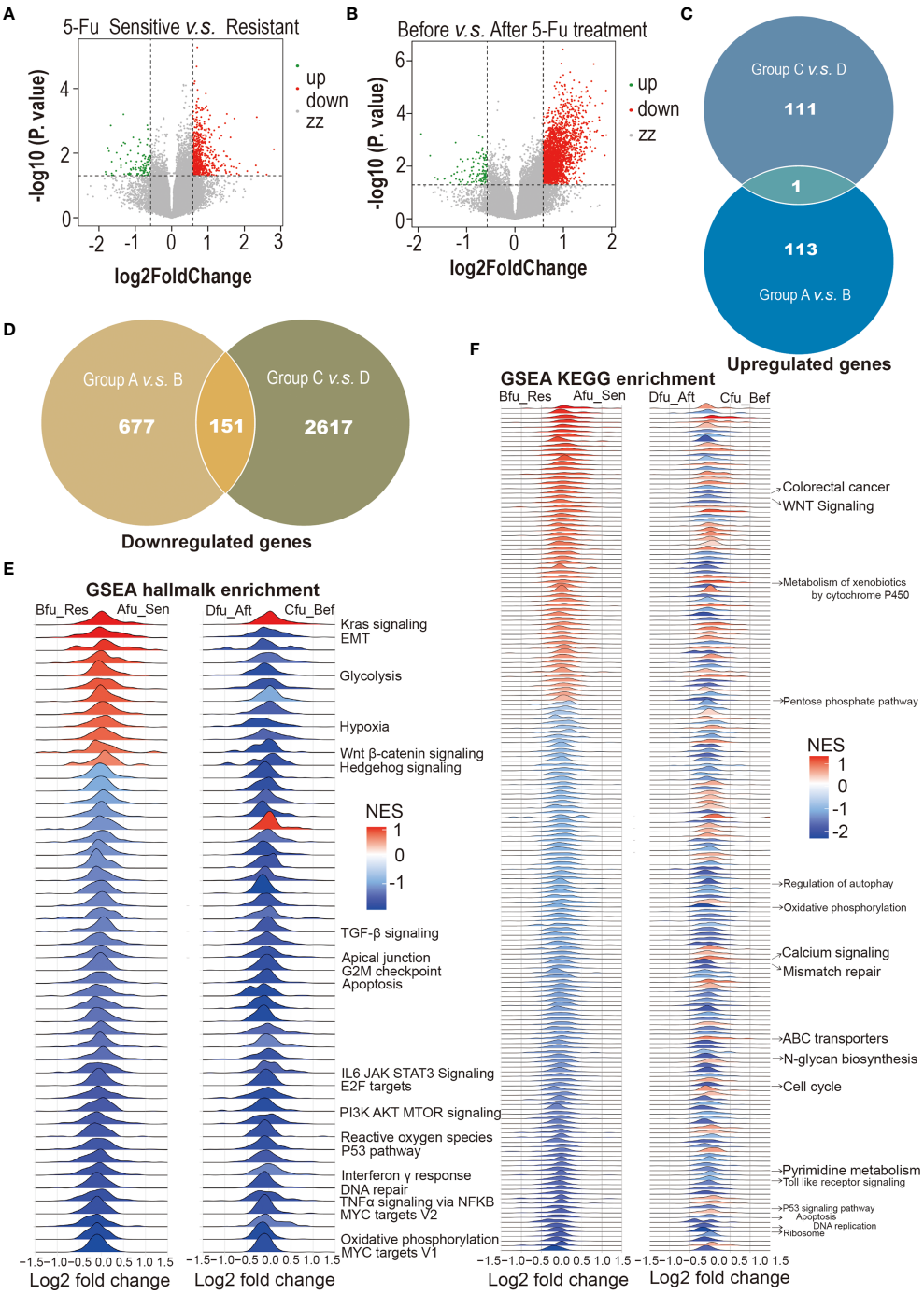

FIGURE 3 | 5-Fu-resistant molecular characteristics of colorectal cancer organoids (CRCOs). **(A)** Volcano plot for differentially expressed genes between 5-Fu-sensitive (group A) and -resistant (group B) untreated CRCOs. **(B)** Volcano plot for differentially expressed genes between CRCOs before 5-Fu treatment (group C) and surviving CRCOs after 5-Fu treatment (group D). **(C)** Venn diagram showed that only 1 upregulated gene was overlapped in the two comparison groups. **(D)** Venn diagram showed that 151 downregulated genes were overlapped in the two comparison groups. **(E, F)** Gene set enrichment analysis (GSEA) using the hallmark and KEGG gene sets to dissect the pathways associated with 5-Fu resistance, respectively. The pathways that have been validated in literature were marked. 5-Fu, 5-fluorouracil; GSEA, gene set enrichment analysis; Res, resistant; Sen, sensitive; Aft, after; Bef, before; NES, normalized enrichment score; KEGG, kyoto encyclopedia of genes and genomes; CRCOs, colorectal cancer organoids.

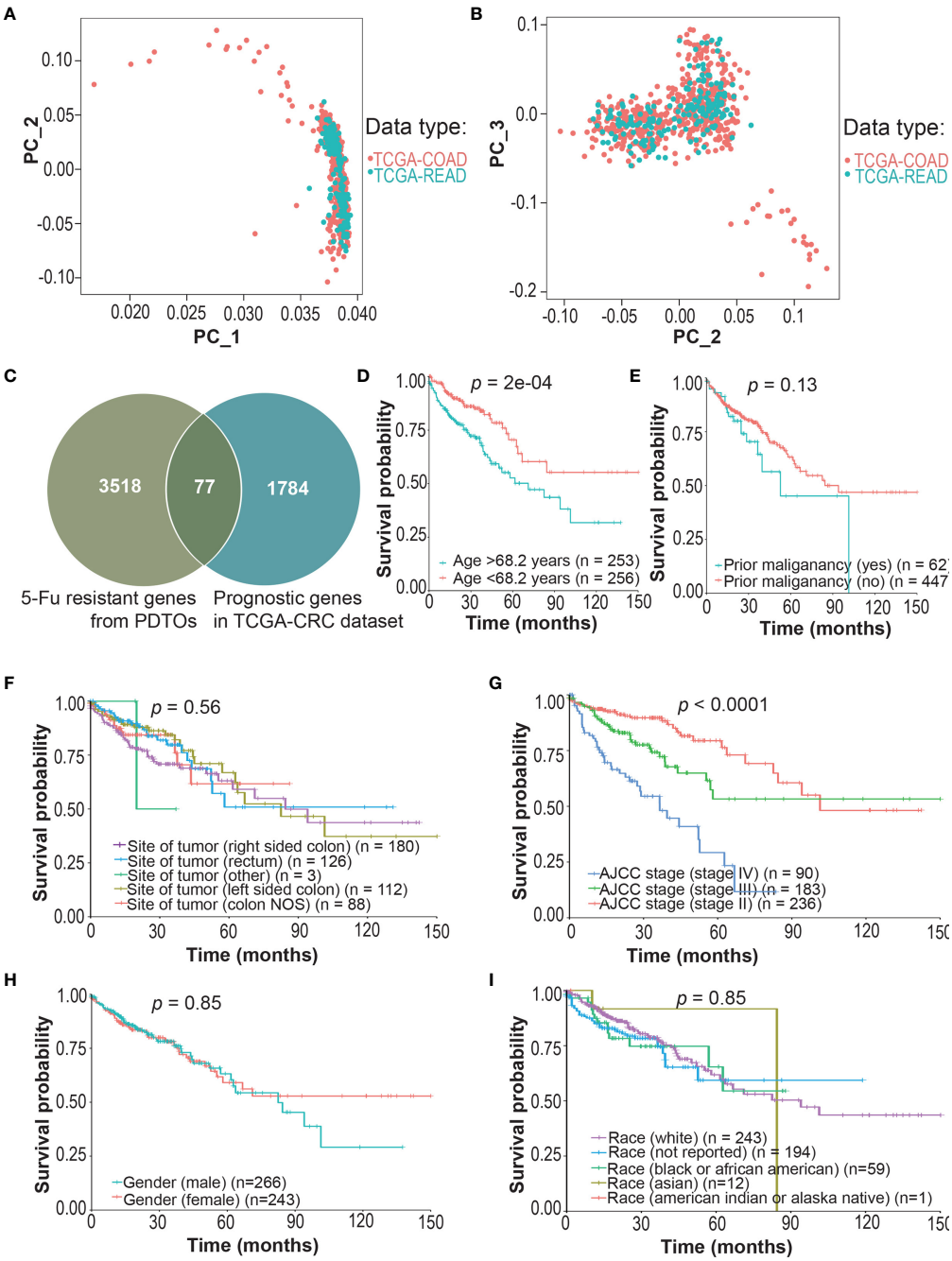

FIGURE 4 | Screening of drug (5-Fu)-resistant genes (DRGs) associated with prognosis in colorectal cancer patients (CRCpts). **(A, B)** PCA for the gene expression data of TCGA-COAD and TCGA-READ cohorts. **(C)** Venn diagram of 5-Fu-resistant genes from patient-derived tumor organoids (PDTOs) and prognostic genes in TCGA-CRC dataset. **(D–I)** Univariate analysis for age/prior maliganancy/site of tumor/AJCC stage/gender/race and their correlation with clinical outcome [overall survival (OS)] in TCGA-CRC cohort. PC, principal components; TCGA, the cancer genome atlas; COAD, colon adenocarcinoma; READ, rectal adenocarcinoma; 5-Fu, 5-fluorouracil; PDTOs, patient-derived tumor organoids; CRC, colorectal cancer; NOS, not otherwise specified; AJCC, American Joint Committee on Cancer; DRGs, drug-resistant genes; CRCpts, colorectal cancer patients; PCA, principal components analysis; OS, overall survival.

-0.0356 + GEL (*PFN2*) × 0.0332 + GEL (*SEZ6L2*) × 0.0378 + GEL (*WDR78*) × -0.0386.

In TCGA-CRC cohort, the univariate Cox regression model revealed that the DRS was associated with prognosis of CRC patients in terms of OS ($P < 0.0001$) (**Figure 6A**). Multivariate analysis after adjustment revealed that DRS ($P < 0.001$), age ($P < 0.001$), and American Joint Committee on Cancer (AJCC) stage ($P < 0.001$) were independent prognostic factors for OS in CRC

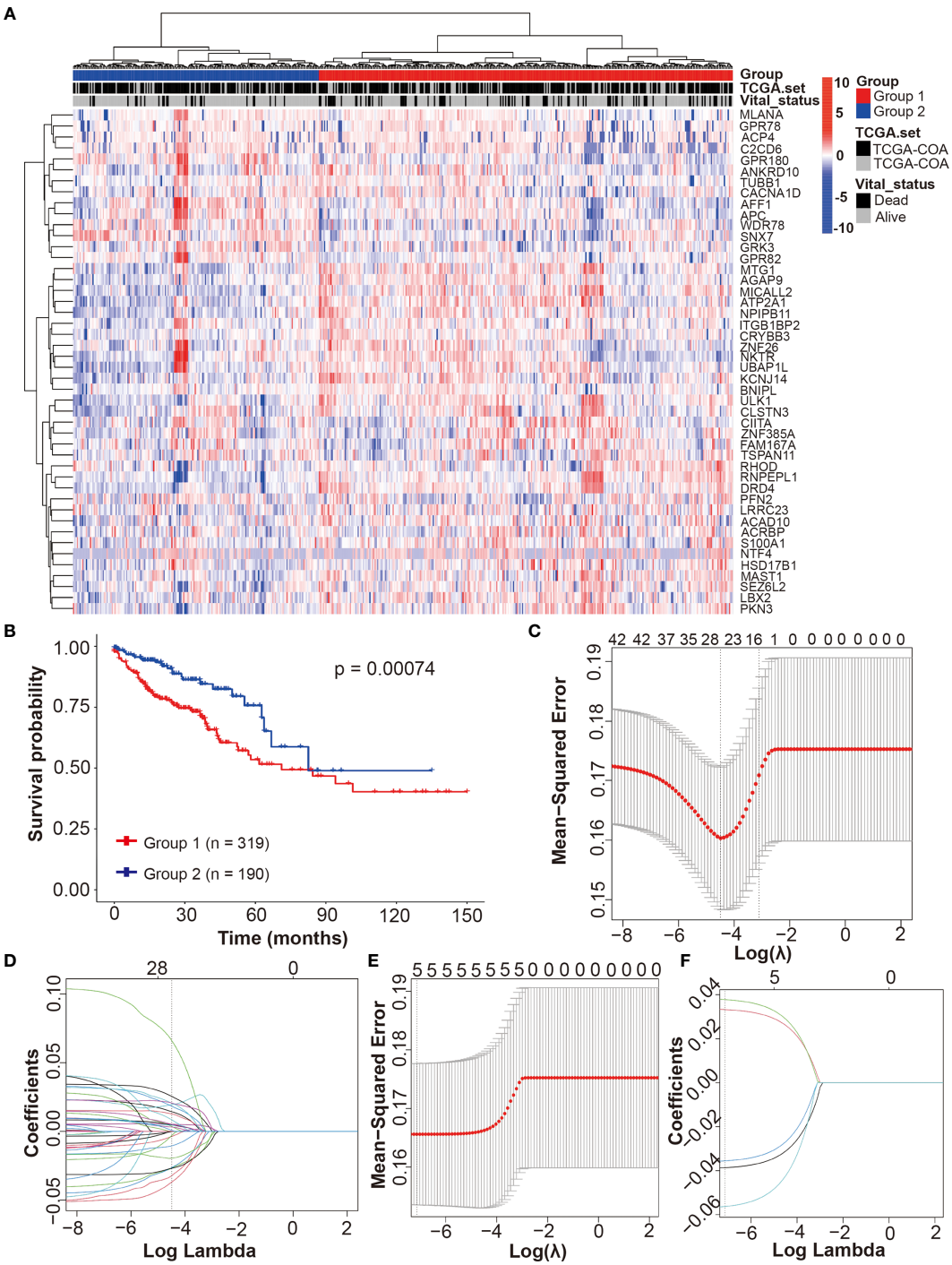

FIGURE 5 | Development of the drug-resistant score model (DRSM) by using DRGs associated with 5-Fu resistance. **(A)** Unsupervised clustering of 698 tumor samples using the expression data of 46 DRGs in TCGA-CRC dataset revealed two molecular subtypes (group1, n = 319; group2, n = 190). **(B)** Univariate analysis for groups (1 or 2) and their correlation with clinical outcome [overall survival (OS)] in TCGA-CRC cohort. **(C)** Optimal parameter (lambda) selection in the LASSO model using 5-fold cross-validation *via* minimum criteria for 46 DRGs. **(D)** LASSO coefficient profiles of the 46 DRGs at the optimal lambda value selected using 5-fold cross-validation. **(E)** Optimal parameter (lambda) selection in the LASSO model using 5-fold cross-validation *via* minimum criteria for 5 DRGs after filtering using multivariate Cox analysis. **(F)** LASSO coefficient profiles of the 5 DRGs at the optimal lambda value selected using 5-fold cross-validation. TCGA, the cancer genome atlas; DRSM, drug-resistant score model; DRGs, drug-resistant genes; 5-Fu, 5-fluorouracil; CRC, colorectal cancer; OS, overall survival; LASSO, least absolute shrinkage and selection operator.

patients, and prior malignancy ($P = 0.883$) and site of tumor ($P > 0.2$) lost their significance (**Figure 6B**). The result of receiver operating characteristic (ROC) curve (AUC = 0.99) indicated that our DRSM had a favorable prognosis predictive performance in TCGA-CRC dataset (**Figure 6C**).

Validation of the Drug-Resistant Score Model

The prognosis predictive value of our DRSM was subsequently validated in four GSE datasets. Four GEO datasets [GSE39084 (n = 61), GSE71187 (n = 52), GSE12945 (n = 49), and GSE29623 (n = 37)] were excluded due to the small sample size. Three GEO datasets [GSE24551 (DFS), GSE33113 (RFS), and GSE14333 (DFS)] were not enrolled for validation because it was rare that endpoints such as disease free survival (DFS) progression free survival (PFS), or recurrence free survival (RFS) have been shown to be true surrogates for OS or disease free survival (DSS). Hence, 4 of 11 GEO datasets were finally selected for the validation of DRSM as follows: GSE40967 (n = 233, OS), GSE17538 (n = 204, OS), GSE87211 (n = 196, OS), and GSE38832 (n = 104, DSS).

Next, we validated the prognosis predictive value of our DRSM in GEO datasets. In all of the four enrolled GEO cohorts, the univariate Cox regression model indicated that the DRS was significantly associated with prognosis of CRC patients in terms of OS or DSS with the *P* values of 8e–04 (GSE40967), 0.0016 (GSE17538), 0.018 (GSE87211), and 0.0044 (GSE38832) (**Figures 6D–G**). Further multivariate analysis in three enrolled GEO cohorts (GSE40967, GSE17538, and GSE38832) also showed that DRS was an independent prognostic factor for OS or DSS in CRCpts (**Table S9**). In the GSE87211 cohort, the multivariate analysis was not performed because the event number was too limited (28 events out of 203 cases) and there were at least seven required variables for Cox regression (age, invasion depth, lymph node metastasis, metastasis, recurrence, KRAS mutations, and score level) (46). In GSE38832, there was no statistically significant difference ($P = 0.093$) between DRS-high and DRS-low CRCpts after multivariate Cox regression analysis probably due to the relatively small sample size (n = 104). Our validation results from the four GSE cohorts above elucidated that the DRSM based on five genes of chemosensitivity to 5-Fu developed from patient-derived organoids can predict the survival of CRCpts.

Predictive Value of Drug-Resistant Score Model in Colorectal Cancer Patient Subgroups

To investigate whether our gene signature can serve as a powerful prognostic indicator in different stages of CRCpts, we performed a subset analysis based on AJCC staging system in TCGA-CRC cohort. The results from univariate and multivariate analyses showed that the DRSM could predict outcomes of stage II, III, and IV CRCpts, respectively (**Figures 7A–C** and **Table S10**). Embryological, biological, anatomical, and molecular features are different among right-sided, left-sided, and rectal CRC. Sidedness has an important role on several aspects of CRC (5). Next, we tested the prognostic value of DRSM according to tumor location in TCGA-CRC datasets. Univariate and multivariate survival analyses revealed that DRS-high CRCpts had worse survival than DRS-low CRCpts in right-sided colon cancer ($P < 0.001$, n = 180) and rectal cancer ($P = 0.006$, n = 126), but there was no statistical difference in left colon cancer due to the relatively small sample size ($P = 0.102$, n = 113) (**Figures 7D–F** and **Table S10**).

TP53 and *KRAS* are second and third most frequently mutated genes among the non-hypermutated CRC tumors and contribute to colorectal carcinogenesis. *KRAS* mutations predict poor prognosis in CRC (47, 48). Univariate and multivariate survival analyses in GSE40967 cohort showed that the DRS-high CRCpts had worse survival than DRS-low CRCpts with *P53* mutations ($P = 0.012$, n = 82) (**Figure 7G** and **Table S11**). There was no statistically significant difference between DRS-high and DRS-low CRCpts with wild-type *P53* probably because of the small sample size ($P = 0.170$, n = 53) (**Figure 7H** and **Table S11**). Univariate and multivariate Cox analyses further exhibited that our DRSM could serve as an independent predictor of both *KRAS*-mutated and wild-type CRCpts' survival in the GSE40967 dataset ($P = 0.008$, n = 94; $P = 0.044$, n = 127) (**Figures 7I, J** and **Table S11**). We did not perform subgroup analysis according to CpG island methylator phenotype (CIMP), CIN, *BRAF* mutation, and subtypes from the French national Cartes d'Identité des Tumeurs (CIT) program in the GSE40967 cohort because of small sample size of subgroups. There were no appropriate additional variables for subgroup analysis in the GSE17538, GSE87211, and GSE38832 cohorts.

Functional Enrichment Analyses Between DRS-High and DRS-Low Patients

Finally, we used DEGs between DRS-high and DRS-low patients in TCGA-CRC cohort to dissect the difference of molecular pathways, tumor mutational burden (TMB), immune response-related pathways, immune score, stromal score, and immune cell proportion (**Figure 8A** and **Table S12**). GSEA method was employed to determine the upregulated and downregulated molecular pathways in DRS-high CRCpts based on the kyoto encyclopedia of genes and genomes (KEGG) and Hallmark gene sets. The MYC targets, reactive oxygen species pathway, base excision repair, citrate cycle, and tricarboxylic acid (TCA) cycle were upregulated, while KRAS signaling, ABC transporters, calcium signaling pathway, and chemokine signaling pathway were downregulated in DRS-high CRCpts (**Figures 8B, C**). Detailed information about upregulated and downregulated molecular pathways was listed in supplementary materials (**Figures S4A, B** and **Table S13**). **Figures S4A, B** were deposited in the Mendeley Database (DOI: 10.17632/rnrmjkvjjc.2).

TMB is a measure of the amount of mutations carried by tumor cells. TMB-low is associated with poor prognosis in CRCpts treated with adjuvant 5-Fu-based chemotherapy (49). However, there was no significant difference in TMB between DRS-high and DRS-low CRCpts (**Figure 8D**). Next, we further explored the differences in immune response-related pathways, immune score, stromal score, and immune cell proportion between DRS-high and DRS-low CRCpts. Our results found that CD8 T effector, antigen processing machinery, and immune

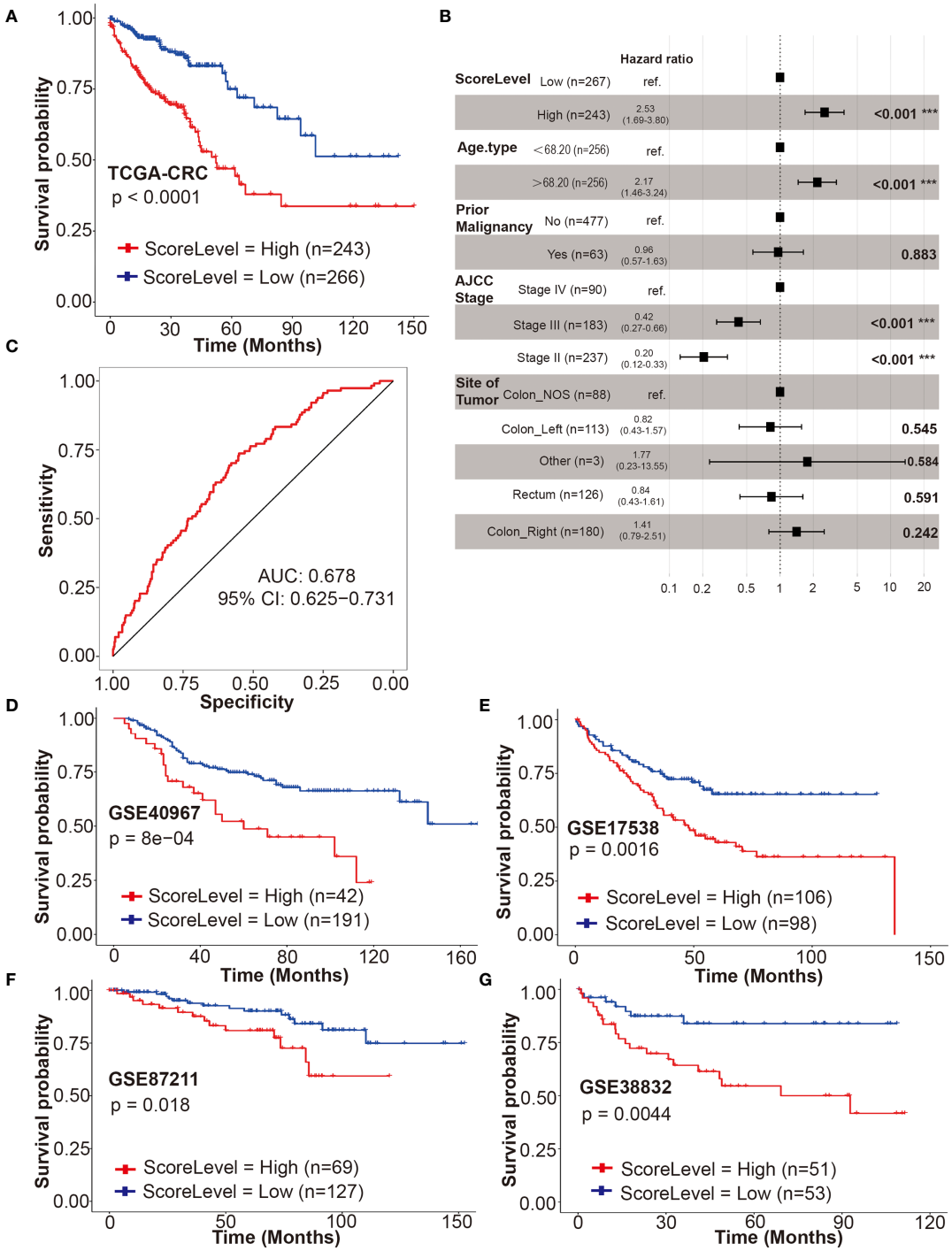

FIGURE 6 | Validation of the DRSM. **(A)** Univariate analysis for drug-resistant score (DRS) (high or low) and its correlation with clinical outcome [overall survival (OS)] in TCGA-CRC cohort. **(B)** Multivariate analysis after adjustment revealed DRS, age, and AJCC stage were independent prognostic factors for OS in TCGA-CRC cohort, and prior malignancy and site of tumor lost their significance. **(C)** Receiver operating characteristic (ROC) curve (AUC = 0.99) indicated that DRSM had favorable prognosis predictive performance in TCGA-CRC dataset. AUC indicates area under the curve. **(D–G)** Univariate analysis for DRS (high or low) and its correlation with clinical outcome (OS or DSS) in GSE40967, GSE17538, GSE87211, and GSE38832 datasets, respectively. ***$P < 0.001$. TCGA, the cancer genome atlas; CRC, colorectal cancer; AJCC, American Joint Committee on Cancer; NOS, not otherwise specified; AUC, area under the curve; CI, confidence interval; GSE, gene expression omnibus series; DRSM, drug-resistant score model; DRS, drug resistant score; OS, overall survival; ROC, receiver operating characteristic; DSS, disease free survival.

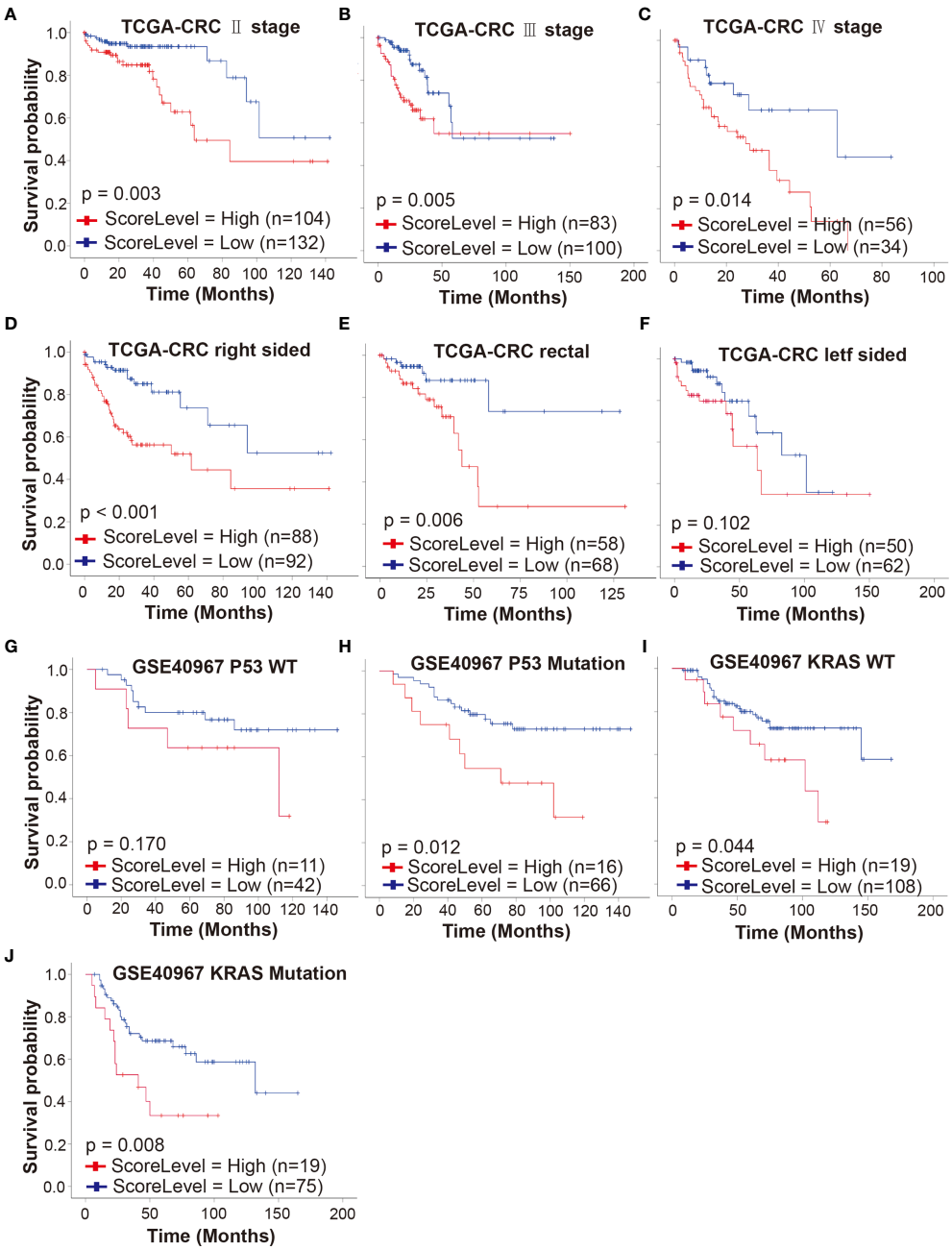

FIGURE 7 | Predictive value of DRSM in CRCpt subgroups. **(A–C)** Univariate analysis for DRS (high or low) and its correlation with clinical outcomes (OS) of stage II, stage III, and stage IV CRCpts in TCGA-CRC cohort, respectively. **(D–F)** Univariate analysis for DRS (high or low) and its correlation with clinical outcomes (OS) of right-sided, rectal, and left-sided CRCpts in TCGA-CRC cohort, respectively. **(G, H)** Univariate analysis for DRS (high or low) and its correlation with clinical outcomes (OS) of CRCpts with wild-type and mutated P53 in GSE40967 cohort, respectively. **(I, J)** Univariate analysis for DRS (high or low) and its correlation with clinical outcomes (OS) of CRCpts with wild-type and mutated KRAS in GSE40967 cohort, respectively. TCGA, the cancer genome atlas; CRC, colorectal cancer; GSE, gene expression omnibus series; WT, wild type; DRSM, drug-resistant score model; CRCpts, colorectal cancer patients; DRS, drug resistant score; OS, overall survival.

checkpoint pathways were significantly downregulated in DRS-high CRCpts (**Figure 8E**). Immune score was significantly lower in DRS-high CRCpts (P = 0.0022) (**Figure 8F**). There was no significant difference in stromal score between DRS-high and DRS-low CRCpts (P = 0.12) (**Figure 8G**). For immune cell proportion, T cell CD4 memory resting, T cell CD4 memory activated, and plasma cells were lower and mast cell activated and monocytes were higher in DRS-high CRCpts (**Figure 8H**).

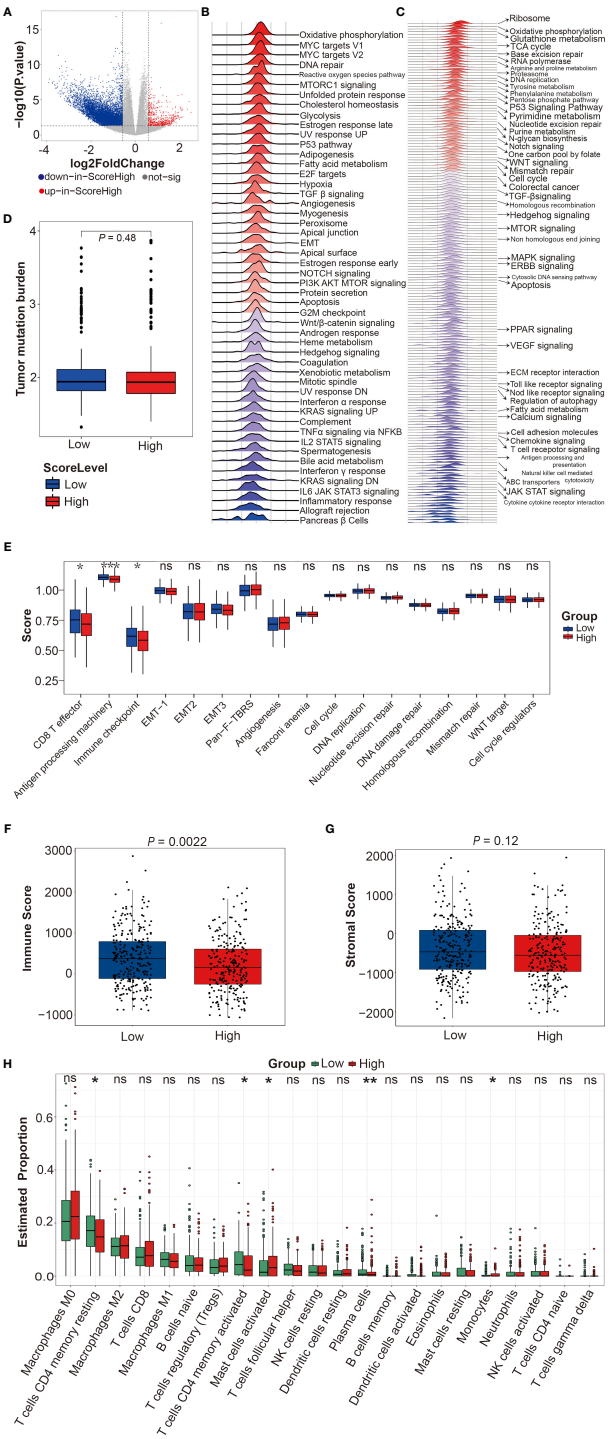

FIGURE 8 | Functional enrichment analyses between DRS-high and DRS-low patients in TCGA-CRC cohort. **(A)** Volcano plot for differentially expressed genes of CRC tumors between DRS-high and DRS-low CRCpts in TCGA-CRC cohort. **(B, C)** Gene set enrichment analysis (GSEA) using the hallmark and KEGG gene sets to dissect the pathways associated with DRS in TCGA-CRC cohort. **(D)** Box plots of tumor mutational burden (TMB) by DRS (low or high). **(E)** Box plots of immune response-related pathways by DRS (low or high). **(F, G)** Box plots of immune score and stromal score by DRS (low or high). **(H)** Box plots of immune cell proportion by DRS (low or high). Within each box, the horizontal black center line denotes the median value (50th percentile), while the box contains the 25th to 75th percentiles of each group's distribution of values. The black whiskers mark the 5th and 95th percentiles, and values beyond these upper and lower bounds are considered outliers. *$P < 0.05$; **$P < 0.01$; ***$P < 0.001$; ns, not significant. sig, significant; DRS, drug resistant score; TCGA, the cancer genome atlas; CRC, colorectal cancer; CRCpts, colorectal cancer patients; GSEA, gene set enrichment analysis; KEGG, kyoto encyclopedia of genes and genomes; TMB, tumor mutational burden.

DISCUSSION

In this study, we investigated whether DRGs developed from PDTOs could be used to faithfully identify robust drug response biomarkers. The 5-Fu-resistant genes were established by analysis of RNA sequencing data from CRCOs and were employed to generate the DRSM using LASSO regression analysis in TCGA and GSE CRC datasets. Indeed, we found that gene signatures of 5-Fu resistance derived from CRCOs could predict the survival of CRCpts. Our results suggested that genetic characteristics of drug resistance in PDTOs could improve the drug response prediction for cancer patients.

Until now, genome-wide mRNA expression levels in CRC have been obtained in lots of studies by using large-scale genomic profiling technology. Many gene expression signatures for survival prediction of CRCpts also have been developed (50–52), but none was routinely used in the clinic. A systematic review including 31 gene signatures concluded that although the published signatures showed significant statistical correlation with prognosis, their capacity to accurately categorize independent samples into low-risk and high-risk subgroups remained limited (52). Consistent with the conclusion above, the results of the current study in validation cohorts (GSE datasets) demonstrated that the prediction power of our gene signatures was moderate, with AUC ranging from 0.557 (95% CI: 0.476–0.639) to 0.672 (95% CI: 0.549–0.794). Strong prediction power is necessary for gene signatures to be used clinically, even when patients' survival differences exist. Thus, further well-designed research with a large sample size is needed for developing gene signatures with higher predictive accuracy in CRCpts.

5-Fu-resistant genes generated from CRC cell lines have been used to construct gene signatures to predict survival of CRCpts (34, 53, 54). Considering the advantage of PDTOs over cell lines (8, 9), gene signatures derived from PDTOs may exhibit better predictive power. Kong et al. recently reported that biomarkers that were identified by network-based machine learning using 5-Fu pharmacogenomic data generated from 19 3D organoid lines accurately predicted the drug responses of 114 CRCpts (14, 55). In the current study, the 5-Fu-resistant genes were obtained from pharmacogenomic and expression data of 41 CRCOs. In addition to comparing 5-Fu-sensitive and -resistant CRCOs, we analyzed the gene expression data of CRCOs before 5-Fu treatment and surviving CRCOs after 5-Fu treatment to generate 5-Fu-resistant genes. It is worth noting that 5-Fu is generally used in combination with oxaliplatin for CRCpts clinically. The treatments of CRCpts, especially the drug information, were often unavailable in TCGA-CRC and GSE datasets used in the current study. Since 5-Fu is the critical composition of CRC treatments and used in a vast majority of CRCpts, we only employed the sensitivity data of CRCOs to 5-Fu for the development of the DRSM.

Of note, we used organoid size change (d24/d0) after a single dose (10 μM) of 5-Fu treatment to evaluate the drug sensitivity of CRCOs in the current study. IC50 after 6 days of drug treatment was regularly employed in other studies about drug sensitivity tests of cancer organoids (10, 14, 22, 23). The former method was selected in our study according to a research about testing the response of rectal cancer organoids (RCOs) to drugs and irradiation (11). Yao et al. (11) tested the response of 80 RCOs to 5-Fu (10 μM), irinotecan (CPT-11), and irradiation by using organoid size change (d24/d0) to evaluate the drug sensitivity of RCOs and found that the organoid data were highly matched to clinical outcomes of rectal cancer patients (RCpts). In that study, outcomes of RCpts were accessed by pathologic tumor regression grade (TRG) of surgical specimens after neoadjuvant chemoradiation (11). Considering the sufficient sample size and reliable evaluation methods of clinical outcomes (11), organoid size change (d24/d0) is a valid parameter for testing the response of cancer organoids to treatments. This method is also as effective as CellTiter-Glo 3D cell viability assay (11) and is more economical and easier to use. In addition, we chose 36.4% as the cutoff of organoid size change (d24/d0) according to a previous study (11). This cutoff was derived based on the fact that the primary tumors of patients with TRG = 0 or 1 were considered to be sensitive to treatments and other patients with TRG = 2 or 3 were resistant (11). The 5-year recurrence-free survival rates were 98% (TRG = 0), 90% (TRG =1), 73% (TRG = 2), and 68% (TRG = 3) (56). By using this cutoff in the current study, more than half of PTDOs are considered to be resistant to 5-Fu. In fact, the patients with TRG = 2 can also benefit from neoadjuvant chemoradiation. Given that we aimed to develop a molecular biomarker of CRCpts' survival, this cutoff was exactly appropriate for the current study.

Our DRSM consisted of five genes, namely, *CACNA1D*, *CIITA*, *PFN2*, *SEZ6L2*, and *WDR78*. CACNA1D encodes the α 1D subunit of the L-type calcium channel and is engaged in various calcium-dependent processes, including neurotransmitter or hormone release, muscle contraction, and gene expression. *CACNA1D* showed significant correlations with chemosensitivity for mitozolamide, cyclodisone, and deoxydoxorubicin (57). *CACNA1D* has been also enrolled in the gene signatures for predicting the benefit of 5-Fu-based chemotherapy (58, 59). *CIITA* is a non-DNA-binding coactivator of major histocompatibility complex (MHC) class II molecules whose high expression is usually associated with enhanced involvement of CD4+ lymphocytes in tumor suppression and a better prognosis (60). *PFN2* is an actin cytoskeleton regulator and serves an important role in cell motility. The results from Kim et al. (61) suggested that *PFN2* promoted the migration, invasion, and stemness of HT29 human CRC stem cells. *SEZ6L2* is a type 1 transmembrane protein and belongs to the seizure-related gene 6 (*SEZ6*) family. Upregulation of *SEZ6L2* correlates with poor prognosis for CRCpts, and *SEZ6L2* knockdown can impair tumor growth by promoting caspase-dependent apoptosis in CRC (62). *WDR78* is essential for ciliary beating and axonemal dyneins. Studies showed that *WDR78* has been enrolled in the molecular signatures for predicting the prognosis of CRCpts (63, 64). In further studies, we will explore the specific roles and mechanisms of the five genes in 5-Fu resistance in CRC.

The current research, however, is subjected to several limitations. The first is the limited sample size of CRCOs. We

tested the response of 41 CRCO lines to 5-Fu to generate 5-Fu-resistant genes. The sample size needs to be expanded in further research. The second limitation concerns that only 5-Fu-resistant genes were derived, while resistant genes of other clinically used drugs (oxaliplatin, CPT-11, et al.) for CRCpts were not. In previous research, 5-Fu-based chemotherapy improves the survival of resected stage III, a subset of stage II and metastatic CRCpts (5, 65). Given the fact that drugs other than 5-Fu used for CRCpts in TCGA and GSE datasets were unable to be confirmed, we just utilized 5-Fu-resistant genes to construct the prediction model. Oxaliplatin- and CPT-11-resistant genes will be incorporated in the model in further study using our own independent CRCpt cohort. In addition, as with majority of similar studies, the design of the current study is retrospective. Our prediction model needed further validation in prospective clinical studies.

In the current era of precision and personalized cancer medicine, molecular biomarkers enabling selection of the appropriate treatments for specific patients are of great importance (66–68). Cancer organoid technology, together with molecular biomarkers, holds promise for individualizing cancer treatment. We here provide suggestions that gene signatures of drug resistance developed from CRC PTDOs have the potential to be possible candidates of such molecular biomarkers.

CONCLUSIONS

Taken together, the DRSM developed in the current study by using 5-Fu-resistant genes derived from CRCOs can predict the survival of CRCpts in TCGA and GSE CRC datasets. This gene signature may be useful in tailoring therapeutic regimens and acts as a supplement of PDTO-guided personalized treatment for CRCpts. Further study with a large sample size and even a prospective design is needed.

DATA AVAILABILITY STATEMENT

The RNA sequencing data (raw data) of colorectal cancer organoids presented in the study are deposited in the Sequence Read Archive (SRA) of National Center for Biotechnology Information (NCBI), accession number PRJNA813221. The **Figures S3** and **S4** presented in the study are deposited in the Mendeley Database, DOI 10.17632/rnrmjkvjjc.2. Additional datasets and materials and associated protocols are available upon request from the corresponding author (YY and WZL) to comply with institutional ethics regulation.

ETHICS STATEMENT

The studies involving human participants were reviewed and approved by Ethics Committee of Tongji Medical College, Huazhong University of Science and Technology. The patients/participants provided their written informed consent to participate in this study.

AUTHOR CONTRIBUTIONS

LFC and WZL designed the current study and supervised the project. YY also supervised the project. LFC and BT executed most of the experiments and bioinformatics analysis. WZL was responsible for CRC tumor sample collection. LFC and BT wrote the article. WZL and YY provided support for research funding. BT, WL, HTL, and WZL revised the article. All authors read and approved the final article.

FUNDING

This work was supported by the National Natural Science Foundation of China (No. 81873440).

ACKNOWLEDGMENTS

We thank all of the patients and their families for participating in the current research. We thank Xiaoying Zhu and Fei Gao for giving help and advice about this research.

SUPPLEMENTARY MATERIAL

The Supplementary Material for this article can be found online at: https://www.frontiersin.org/articles/10.3389/fonc.2022.855674/full#supplementary-material

Figures S3 and S4 are available here: DOI 10.17632/rnrmjkvjjc.2.

REFERENCES

1. Bray F, Ferlay J, Soerjomataram I, Siegel RL, Torre LA, Jemal A. Global Cancer Statistics 2018: GLOBOCAN Estimates of Incidence and Mortality Worldwide for 36 Cancers in 185 Countries. *CA Cancer J Clin* (2018) 68:394–424. doi: 10.3322/caac.21492
2. Turano M, Delrio P, Rega D, Cammarota F, Polverino A, Duraturo F, et al. Promising Colorectal Cancer Biomarkers for Precision Prevention and Therapy. *Cancers (Basel)* (2019) 11(12):1932. doi: 10.3390/cancers11121932
3. De Rosa M, Rega D, Costabile V, Duraturo F, Niglio A, Izzo P, et al. The Biological Complexity of Colorectal Cancer: Insights Into Biomarkers for Early Detection and Personalized Care. *Therap Adv Gastroenterol* (2016) 9:861–86. doi: 10.1177/1756283X16659790
4. De Rosa M, Pace U, Rega D, Costabile V, Duraturo F, Izzo P, et al. Genetics, Diagnosis and Management of Colorectal Cancer (Review). *Oncol Rep* (2015) 34:1087–96. doi: 10.3892/or.2015.4108
5. Dekker E, Tanis PJ, Vleugels JLA, Kasi PM, Wallace MB. Colorectal Cancer. *Lancet* (2019) 394:1467–80. doi: 10.1016/S0140-6736(19)32319-0
6. Siegel RL, Miller KD, Fedewa SA, Ahnen DJ, Meester RGS, Barzi A, et al. Colorectal Cancer Statistics, 2017. *CA Cancer J Clin* (2017) 67:177–93. doi: 10.3322/caac.21395
7. Douillard JY, Cunningham D, Roth AD, Navarro M, James RD, Karasek P, et al. Irinotecan Combined With Fluorouracil Compared With Fluorouracil

Alone as First-Line Treatment for Metastatic Colorectal Cancer: A Multicentre Randomised Trial. *Lancet* (2000) 355:1041–7. doi: 10.1016/S0140-6736(00)02034-1
8. Li M, Izpisua Belmonte JC. Organoids - Preclinical Models of Human Disease. *N Engl J Med* (2019) 380:569–79. doi: 10.1056/NEJMra1806175
9. Drost J, Clevers H. Organoids in Cancer Research. *Nat Rev Cancer* (2018) 18:407–18. doi: 10.1038/s41568-018-0007-6
10. Vlachogiannis G, Hedayat S, Vatsiou A, Jamin Y, Fernández-Mateos J, Khan K, et al. Patient-Derived Organoids Model Treatment Response of Metastatic Gastrointestinal Cancers. *Science* (2018) 359:920–6. doi: 10.1126/science.aao2774
11. Yao Y, Xu X, Yang L, Zhu J, Wan J, Shen L, et al. Patient-Derived Organoids Predict Chemoradiation Responses of Locally Advanced Rectal Cancer. *Cell Stem Cell* (2019) 26(1):17–26.e6. doi: 10.1016/j.stem.2019.10.010
12. Tiriac H, Belleau P, Engle DD, Plenker D, Deschênes A, Somerville TDD, et al. Organoid Profiling Identifies Common Responders to Chemotherapy in Pancreatic Cancer. *Cancer Discovery* (2018) 8:1112–29. doi: 10.1158/2159-8290.CD-18-0349
13. Ganesh K, Wu C, O'Rourke KP, Szeglin BC, Zheng Y, Sauvé CG, et al. A Rectal Cancer Organoid Platform to Study Individual Responses to Chemoradiation. *Nat Med* (2019) 25:1607–14. doi: 10.1038/s41591-019-0584-2
14. van de Wetering M, Francies HE, Francis JM, Bounova G, Iorio F, Pronk A, et al. Prospective Derivation of a Living Organoid Biobank of Colorectal Cancer Patients. *Cell* (2015) 161:933–45. doi: 10.1016/j.cell.2015.03.053
15. Ritchie ME, Phipson B, Wu D, Hu Y, Law CW, Shi W, et al. Limma Powers Differential Expression Analyses for RNA-Sequencing and Microarray Studies. *Nucleic Acids Res* (2015) 43:e47. doi: 10.1093/nar/gkv007
16. Yu G, Wang LG, Han Y, He QY. Clusterprofiler: An R Package for Comparing Biological Themes Among Gene Clusters. *Omics* (2012) 16:284–7. doi: 10.1089/omi.2011.0118
17. Subramanian A, Tamayo P, Mootha VK, Mukherjee S, Ebert BL, Gillette MA, et al. Gene Set Enrichment Analysis: A Knowledge-Based Approach for Interpreting Genome-Wide Expression Profiles. *Proc Natl Acad Sci USA* (2005) 102:15545–50. doi: 10.1073/pnas.0506580102
18. Colaprico A, Silva TC, Olsen C, Garofano L, Cava C, Garolini D, et al. TCGAbiolinks: An R/Bioconductor Package for Integrative Analysis of TCGA Data. *Nucleic Acids Res* (2016) 44:e71. doi: 10.1093/nar/gkv1507
19. Sato T, Stange DE, Ferrante M, Vries RG, Van Es JH, Van den Brink S, et al. Long-Term Expansion of Epithelial Organoids From Human Colon, Adenoma, Adenocarcinoma, and Barrett's Epithelium. *Gastroenterology* (2011) 141:1762–72. doi: 10.1053/j.gastro.2011.07.050
20. Fujii M, Shimokawa M, Date S, Takano A, Matano M, Nanki K, et al. A Colorectal Tumor Organoid Library Demonstrates Progressive Loss of Niche Factor Requirements During Tumorigenesis. *Cell Stem Cell* (2016) 18:827–38. doi: 10.1016/j.stem.2016.04.003
21. Pauli C, Hopkins BD, Prandi D, Shaw R, Fedrizzi T, Sboner A, et al. Personalized *In Vitro* and *In Vivo* Cancer Models to Guide Precision Medicine. *Cancer Discov* (2017) 7:462–77. doi: 10.1158/2159-8290.CD-16-1154
22. Sachs N, de Ligt J, Kopper O, Gogola E, Bounova G, Weeber F, et al. A Living Biobank of Breast Cancer Organoids Captures Disease Heterogeneity. *Cell* (2018) 172:373–386.e310. doi: 10.1016/j.cell.2017.11.010
23. Broutier L, Mastrogiovanni G, Verstegen MM, Francies HE, Gavarró LM, Bradshaw CR, et al. Human Primary Liver Cancer-Derived Organoid Cultures for Disease Modeling and Drug Screening. *Nat Med* (2017) 23:1424–35. doi: 10.1038/nm.4438
24. Sauer R, Becker H, Hohenberger W, Rödel C, Wittekind C, Fietkau R, et al. Preoperative Versus Postoperative Chemoradiotherapy for Rectal Cancer. *N Engl J Med* (2004) 351:1731–40. doi: 10.1056/NEJMoa040694
25. Hofheinz RD, Wenz F, Post S, Matzdorff A, Laechelt S, Hartmann JT, et al. Chemoradiotherapy With Capecitabine Versus Fluorouracil for Locally Advanced Rectal Cancer: A Randomised, Multicentre, non-Inferiority, Phase 3 Trial. *Lancet Oncol* (2012) 13:579–88. doi: 10.1016/S1470-2045(12)70116-X
26. Vodenkova S, Buchler T, Cervena K, Veskrnova V, Vodicka P, Vymetalkova V. 5-Fluorouracil and Other Fluoropyrimidines in Colorectal Cancer: Past, Present and Future. *Pharmacol Ther* (2020) 206:107447. doi: 10.1016/j.pharmthera.2019.107447
27. Xie P, Mo JL, Liu JH, Li X, Tan LM, Zhang W, et al. Pharmacogenomics of 5-Fluorouracil in Colorectal Cancer: Review and Update. *Cell Oncol (Dordr)* (2020) 43(6):989–1001. doi: 10.1007/s13402-020-00529-1
28. Zhao B, Erwin A, Xue B. How Many Differentially Expressed Genes: A Perspective From the Comparison of Genotypic and Phenotypic Distances. *Genomics* (2018) 110:67–73. doi: 10.1016/j.ygeno.2017.08.007
29. Kawai K, Uemura M, Munakata K, Takahashi H, Haraguchi N, Nishimura J, et al. Fructose-Bisphosphate Aldolase A is a Key Regulator of Hypoxic Adaptation in Colorectal Cancer Cells and Involved in Treatment Resistance and Poor Prognosis. *Int J Oncol* (2017) 50:525–34. doi: 10.3892/ijo.2016.3814
30. Wang T, Ning K, Lu TX, Hua D. Elevated Expression of TrpC5 and GLUT1 is Associated With Chemoresistance in Colorectal Cancer. *Oncol Rep* (2017) 37:1059–65. doi: 10.3892/or.2016.5322
31. Liu W, Fang Y, Wang XT, Liu J, Dan X, Sun LL. Overcoming 5-Fu Resistance of Colon Cells Through Inhibition of Glut1 by the Specific Inhibitor WZB117. *Asian Pac J Cancer Prev* (2014) 15:7037–41. doi: 10.7314/APJCP.2014.15.17.7037
32. Liu Y, Zhang X, Han C, Wan G, Huang X, Ivan C, et al. TP53 Loss Creates Therapeutic Vulnerability in Colorectal Cancer. *Nature* (2015) 520:697–701. doi: 10.1038/nature14418
33. Moon JR, Oh SJ, Lee CK, Chi SG, Kim HJ. TGF-β1 Protects Colon Tumor Cells From Apoptosis Through XAF1 Suppression. *Int J Oncol* (2019) 54:2117–26. doi: 10.3892/ijo.2019.4776
34. Zheng Y, Zhou J, Tong Y. Gene Signatures of Drug Resistance Predict Patient Survival in Colorectal Cancer. *Pharmacogenomics J* (2015) 15:135–43. doi: 10.1038/tpj.2014.45
35. Candy PA, Phillips MR, Redfern AD, Colley SM, Davidson JA, Stuart LM, et al. Notch-Induced Transcription Factors are Predictive of Survival and 5-Fluorouracil Response in Colorectal Cancer Patients. *Br J Cancer* (2013) 109:1023–30. doi: 10.1038/bjc.2013.431
36. Heisig J, Weber D, Englberger E, Winkler A, Kneitz S, Sung WK, et al. Target Gene Analysis by Microarrays and Chromatin Immunoprecipitation Identifies HEY Proteins as Highly Redundant bHLH Repressors. *PloS Genet* (2012) 8:e1002728. doi: 10.1371/journal.pgen.1002728
37. Li M, Jiang X, Wang G, Zhai C, Liu Y, Li H, et al. ITGB4 is a Novel Prognostic Factor in Colon Cancer. *J Cancer* (2019) 10:5223–33. doi: 10.7150/jca.29269
38. Zhang W, Ramdas L, Shen W, Song SW, Hu L, Hamilton SR. Apoptotic Response to 5-Fluorouracil Treatment is Mediated by Reduced Polyamines, non-Autocrine Fas Ligand and Induced Tumor Necrosis Factor Receptor 2. *Cancer Biol Ther* (2003) 2:572–8. doi: 10.4161/cbt.2.5.532
39. De Angelis PM, Svendsrud DH, Kravik KL, Stokke T. Cellular Response to 5-Fluorouracil (5-FU) in 5-FU-Resistant Colon Cancer Cell Lines During Treatment and Recovery. *Mol Cancer* (2006) 5:20. doi: 10.1186/1476-4598-5-20
40. Sørensen NM, Byström P, Christensen IJ, Berglund A, Nielsen HJ, Brünner N, et al. TIMP-1 is Significantly Associated With Objective Response and Survival in Metastatic Colorectal Cancer Patients Receiving Combination of Irinotecan, 5-Fluorouracil, and Folinic Acid. *Clin Cancer Res* (2007) 13:4117–22. doi: 10.1158/1078-0432.CCR-07-0186
41. Salonga D, Danenberg KD, Johnson M, Metzger R, Groshen S, Tsao-Wei DD, et al. Colorectal Tumors Responding to 5-Fluorouracil Have Low Gene Expression Levels of Dihydropyrimidine Dehydrogenase, Thymidylate Synthase, and Thymidine Phosphorylase. *Clin Cancer Res* (2000) 6:1322–7.
42. Blondy S, David V, Verdier M, Mathonnet M, Perraud A, Christou N. 5-Fluorouracil Resistance Mechanisms in Colorectal Cancer: From Classical Pathways to Promising Processes. *Cancer Sci* (2020) 111:3142–54. doi: 10.1111/cas.14532
43. Mader RM, Müller M, Steger GG. Resistance to 5-Fluorouracil. *Gen Pharmacol* (1998) 31:661–6. doi: 10.1016/S0306-3623(98)00191-8
44. Bursac Z, Gauss CH, Williams DK, Hosmer DW. Purposeful Selection of Variables in Logistic Regression. *Source Code Biol Med* (2008) 3:17. doi: 10.1186/1751-0473-3-17
45. Phipps AI, Lindor NM, Jenkins MA, Baron JA, Win AK, Gallinger S, et al. Colon and Rectal Cancer Survival by Tumor Location and Microsatellite Instability: The Colon Cancer Family Registry. *Dis Colon Rectum* (2013) 56:937–44. doi: 10.1097/DCR.0b013e31828f9a57
46. Vittinghoff E, McCulloch CE. Relaxing the Rule of Ten Events Per Variable in Logistic and Cox Regression. *Am J Epidemiol* (2007) 165:710–8. doi: 10.1093/aje/kwk052

47. The Cancer Genome Atlas Network. Comprehensive Molecular Characterization of Human Colon and Rectal Cancer. *Nature* (2012) 487:330–7. doi: 10.1038/nature11252
48. Conlin A, Smith G, Carey FA, Wolf CR, Steele RJ. The Prognostic Significance of K-Ras, P53, and APC Mutations in Colorectal Carcinoma. *Gut* (2005) 54:1283–6. doi: 10.1136/gut.2005.066514
49. Lee DW, Han SW, Bae JM, Jang H, Han H, Kim H, et al. Tumor Mutation Burden and Prognosis in Patients With Colorectal Cancer Treated With Adjuvant Fluoropyrimidine and Oxaliplatin. *Clin Cancer Res* (2019) 25:6141–7. doi: 10.1158/1078-0432.CCR-19-1105
50. Salazar R, Roepman P, Capella G, Moreno V, Simon I, Dreezen C, et al. Gene Expression Signature to Improve Prognosis Prediction of Stage II and III Colorectal Cancer. *J Clin Oncol* (2011) 29:17–24. doi: 10.1200/JCO.2010.30.1077
51. Gao S, Tibiche C, Zou J, Zaman N, Trifiro M, O'Connor-McCourt M, et al. Identification and Construction of Combinatory Cancer Hallmark-Based Gene Signature Sets to Predict Recurrence and Chemotherapy Benefit in Stage II Colorectal Cancer. *JAMA Oncol* (2016) 2:37–45. doi: 10.1001/jamaoncol.2015.3413
52. Sanz-Pamplona R, Berenguer A, Cordero D, Riccadonna S, Solé X, Crous-Bou M, et al. Clinical Value of Prognosis Gene Expression Signatures in Colorectal Cancer: A Systematic Review. *PloS One* (2012) 7:e48877. doi: 10.1371/journal.pone.0048877
53. Buhl IK, Gerster S, Delorenzi M, Jensen T, Jensen PB, Bosman F, et al. Cell Line Derived 5-FU and Irinotecan Drug-Sensitivity Profiles Evaluated in Adjuvant Colon Cancer Trial Data. *PloS One* (2016) 11:e0155123. doi: 10.1371/journal.pone.0155123
54. Paquet ER, Cui J, Davidson D, Pietrosemoli N, Hassan HH, Tsofack SP, et al. A 12-Gene Signature to Distinguish Colon Cancer Patients With Better Clinical Outcome Following Treatment With 5-Fluorouracil or FOLFIRI. *J Pathol Clin Res* (2015) 1:160–72. doi: 10.1002/cjp2.17
55. Kong J, Lee H, Kim D, Han SK, Ha D, Shin K, et al. Network-Based Machine Learning in Colorectal and Bladder Organoid Models Predicts Anti-Cancer Drug Efficacy in Patients. *Nat Commun* (2020) 11:5485. doi: 10.1038/s41467-020-19313-8
56. Trakarnsanga A, Gönen M, Shia J, Nash GM, Temple LK, Guillem JG, et al. Et Al: Comparison of Tumor Regression Grade Systems for Locally Advanced Rectal Cancer After Multimodality Treatment. *J Natl Cancer Inst* (2014) 106 (10):dju248. doi: 10.1093/jnci/dju248
57. Huang Y, Anderle P, Bussey KJ, Barbacioru C, Shankavaram U, Dai Z, et al. Membrane Transporters and Channels: Role of the Transportome in Cancer Chemosensitivity and Chemoresistance. *Cancer Res* (2004) 64:4294–301. doi: 10.1158/0008-5472.CAN-03-3884
58. Song K, Zhao W, Wang W, Zhang N, Wang K, Chang Z. Individualized Predictive Signatures for 5-Fluorouracil-Based Chemotherapy in Right- and Left-Sided Colon Cancer. *Cancer Sci* (2018) 109:1939–48. doi: 10.1111/cas.13622
59. Wei X, Zhou X, Zhao Y, He Y, Weng Z, Xu C. A 14-Gene Gemcitabine Resistance Gene Signature is Significantly Associated With the Prognosis of Pancreatic Cancer Patients. *Sci Rep* (2021) 11:6087. doi: 10.1038/s41598-021-85680-x
60. Satoh A, Toyota M, Ikeda H, Morimoto Y, Akino K, Mita H, et al. Epigenetic Inactivation of Class II Transactivator (CIITA) is Associated With the Absence of Interferon-Gamma-Induced HLA-DR Expression in Colorectal and Gastric Cancer Cells. *Oncogene* (2004) 23:8876–86. doi: 10.1038/sj.onc.1208144
61. Kim MJ, Lee YS, Han GY, Lee HN, Ahn C, Kim CW. Profilin 2 Promotes Migration, Invasion, and Stemness of HT29 Human Colorectal Cancer Stem Cells. *Biosci Biotechnol Biochem* (2015) 79:1438–46. doi: 10.1080/09168451.2015.1043118
62. An N, Zhao Y, Lan H, Zhang M, Yin Y, Yi C. SEZ6L2 Knockdown Impairs Tumour Growth by Promoting Caspase-Dependent Apoptosis in Colorectal Cancer. *J Cell Mol Med* (2020) 24:4223–32. doi: 10.1111/jcmm.15082
63. Yang J, Kim H, Shin K, Nam Y, Heo HJ, Kim GH, et al. Et Al: Molecular Insights Into the Development of Hepatic Metastases in Colorectal Cancer: A Metastasis Prediction Study. *Eur Rev Med Pharmacol Sci* (2020) 24:12701–8. doi: 10.26355/eurrev_202012_24168
64. Fang Z, Xu S, Xie Y, Yan W. Identification of a Prognostic Gene Signature of Colon Cancer Using Integrated Bioinformatics Analysis. *World J Surg Oncol* (2021) 19:13. doi: 10.1186/s12957-020-02116-y
65. Sveen A, Kopetz S, Lothe RA. Biomarker-Guided Therapy for Colorectal Cancer: Strength in Complexity. *Nat Rev Clin Oncol* (2020) 17:11–32. doi: 10.1038/s41571-019-0241-1
66. Zeggini E, Gloyn AL, Barton AC, Wain LV. Translational Genomics and Precision Medicine: Moving From the Lab to the Clinic. *Science* (2019) 365:1409–13. doi: 10.1126/science.aax4588
67. Aronson SJ, Rehm HL. Building the Foundation for Genomics in Precision Medicine. *Nature* (2015) 526:336–42. doi: 10.1038/nature15816
68. Voest EE, Bernards R. DNA-Guided Precision Medicine for Cancer: A Case of Irrational Exuberance? *Cancer Discov* (2016) 6:130–2. doi: 10.1158/2159-8290.CD-15-1321

Conflict of Interest: The authors declare that the research was conducted in the absence of any commercial or financial relationships that could be construed as a potential conflict of interest.

Publisher's Note: All claims expressed in this article are solely those of the authors and do not necessarily represent those of their affiliated organizations, or those of the publisher, the editors and the reviewers. Any product that may be evaluated in this article, or claim that may be made by its manufacturer, is not guaranteed or endorsed by the publisher.

frontiers | Frontiers in Pharmacology

ORIGINAL RESEARCH
published: 01 April 2022
doi: 10.3389/fphar.2022.868203

MMP9 Expression Correlates With Cisplatin Resistance in Small Cell Lung Cancer Patients

Longqiu Wu[1†], Xiangcai Wang[1†], Xin He[1†], Qiang Li[1†], Qian Hua[1], Rongrong Liu[2,3] and Zhengang Qiu[1]**

[1]Department of Oncology, The First Affiliated Hospital of Gannan Medical University, Ganzhou, China, [2]Department of Neurology, Ganzhou People's Hospital, Ganzhou, China, [3]Department of Neurology, The First Affiliated Hospital of Gannan Medical University, Ganzhou, China

OPEN ACCESS

Edited by:
Clare Y. Slaney,
Peter MacCallum Cancer Centre, Australia

Reviewed by:
Yonglin Yi,
Southern Medical University, China
Xiaohua Li,
Sixth People's Hospital of Chengdu, China

***Correspondence:**
Rongrong Liu
LRR1026@163.com
Zhengang Qiu
qiuzhengang@gmu.edu.cn

†These authors have contributed equally to this work and share first authorship

Specialty section:
This article was submitted to Pharmacology of Anti-Cancer Drugs, a section of the journal Frontiers in Pharmacology

Received: 02 February 2022
Accepted: 24 February 2022
Published: 01 April 2022

Citation:
Wu L, Wang X, He X, Li Q, Hua Q, Liu R and Qiu Z (2022) MMP9 Expression Correlates With Cisplatin Resistance in Small Cell Lung Cancer Patients. Front. Pharmacol. 13:868203. doi: 10.3389/fphar.2022.868203

Background: Cisplatin is the basis of the primary treatment for SCLC chemotherapy. However, the limited objective response rate and definite drug resistance greatly restrict the clinical potential and therapeutic benefits of cisplatin use. Therefore, it is essential to identify biomarkers that can discern the sensitivity of SCLC patients to cisplatin treatment.

Methods: We collected two SCLC cohorts treated with cisplatin that included mutation data, prognosis data and expression data. The sensitivity of cisplatin was evaluated by the pRRophetic algorithm. MCPcounter, quanTIseq, and xCell algorithms were used to evaluate immune cell score. GSEA and ssGSEA algorithms were used to calculate immune-related pathway scores. Univariate and multivariate Cox regression models were employed, and survival analysis was used to evaluate the prognostic value of the candidate genes.

Results: MMP9-High is related to improved clinical prognoses of patients with SCLC (HR = 0.425, $p = 0.0085$; HR = 0.365, $p = 0.0219$). Multivariate results showed that MMP-High could be used as an independent predictor of the prognosis of SCLC after cisplatin treatment (HR = 0.216, $p = 0.00153$; HR = 0.352; $p = 0.0199$). In addition, MMP9-High displayed a significantly lower IC50 value of cisplatin and higher immunogenicity than MMP9-Low SCLC. Compared with MMP9-Low SCLC, MMP9-High included significantly increased levels of T-cells, cytoxic lymphocytes, B-cells, NK-cells, and dense cells (DCS). Similarly, the activity of cytokine binding, B-cell, NK-cell mediated immune response chemokine binding, and antigen presentation pathways in MMP9-High was significantly higher than that in MMP9-Low.

Conclusion: In this study, we identified that MMP9-High could be potentially considered a novel biomarker used to ascertain the improved prognosis of SCLC patients after cisplatin treatment. Furthermore, we indicated that the tumor immune microenvironment of MMP9-High SCLC is mainly characterized by a large number of infiltrated activated immune cells as well as activated immune-related pathways.

Keywords: small lung cell cancer, cisplatin, MMP9, survival, resistance

INTRODUCTION

Small cell lung cancer (SCLC), which accounts for 13–15% of lung cancer, is a subtype of lung cancer known to exhibit high malignancy and poor prognosis (Sabari et al., 2017; Qiu et al., 2019; Luo et al., 2019). The median survival time of SCLC patients is only 8–13 months, and the 5-year survival rate is 1–5% (de Hoyos and DeCamp, 2014; Carter et al., 2014). Chemotherapy for SCLC is comprised of a combination approach that includes platinum-based antineoplastic drugs commonly used in the treatment of various cancers. Cisplatin a well-known, effective, and widely used first-line drug with an objective response rate (ORR) of 50–60% (Horn et al., 2018). However, almost all patients diagnosed with SCLC will inevitably present with drug resistance and tumor recurrence. Studies have shown that the functional mechanism of cisplatin resistance occurs as a result of structural changes to DNA or cytoplasm, the abnormality of DNA damage repair, the change of signaling triggered by molecular damage caused by cisplatin, and the change of compensatory survival signal (Galluzzi et al., 2014; Inoue et al., 2014; Song et al., 2015). However, the lack of biomarkers used to identify cisplatin sensitivity in SCLC population is a large clinical detriment. Therefore, it is of great importance to find biomarkers that pertain to the sensitivity of SCLC patients undergoing cisplatin treatment.

Evidence has recognized the close relationship between tumor immune microenvironment (TIME) and chemotherapeutic drugs. Tumor-associated macrophages (TAMs), tumor-associated neutrophils (TANs), myeloid-derived suppressor cells (MDSCs), regulatory T-cells, Immunosuppressive cells such as T-regulatory cells (Tregs), and regulatory B-cells (Bregs) can not only directly inhibit killer cells such as CTL and NK, but also interact with each other, enhancing the effect of inhibitory factors and facilitating the recruitment of more immunosuppressive cells. This process enables tumor cells to achieve immune escape (Lin et al., 2019). Additionally, TAMs are known to secrete TGF-β1, which results in the up-regulation of Gfi-1 expression in tumor cells. Gfi-1 expression in the promoter region effectively inhibits the expression of CTGF and HMGB1, which accordingly reduce the sensitivity of tumor cells to gemcitabine (Xian et al., 2017). TAMs expressed IGF act on the IGF1 receptor to promote chemotherapy resistance of gemcitabine and albumin-bound paclitaxel (Ireland et al., 2016). In addition, the study showed that during the chemotherapy of gemcitabine, TAMs, G-MDSCs, Tregs and T-cells decreased, and CTL increased (Mitchem et al., 2013; Eriksson et al., 2016). Gemcitabine promoted the up regulation of HLA-DR, CD40, CCR7 and the down regulation of CD163 and cd206, and induced M1 polarization (Di Caro et al., 2016). In conclusion, chemotherapy drugs can act on TIME, and TIME can also affect the effect of chemotherapy drugs.

Matrix metalloproteinases (MMPs) play an important role in tumorigenesis, development, invasion and metastasis. MMP9 is the largest molecular weighted enzyme in the MMP family. The function of MMP9 is closely related to tumor invasion and metastasis through its functional degradation of type IV and V collagen and gelatin (Mondal et al., 2020). Studies have shown that MMP9 expression is regulated in ovarian cancer, cervical cancer, non-small cell lung cancer and breast cancer, all of which demonstrate a close relationship to cisplatin sensitivity (Rauvala et al., 2006; Braicu et al., 2014; Qiao et al., 2020; Makhoul et al., 2016). In addition, Li et al. found evidence that MMP9 can regulate the biological function of monocytes (Zhou et al., 2012; Li et al., 2021; Xu et al., 2021). Furthermore, Xu et al. found that the high MMP9 group was significantly enriched in the immune response pathway and cytokine production pathway (Xu et al., 2021). However, at present, the expression of MMP9 and cisplatin sensitivity in SCLC patients has not been clarified and the associated relationship with the tumor immune microenvironment is not clear. Therefore, in this study, we aimed to explore the relationship between MMP9 expression and cisplatin sensitivity as well as elucidate the TIME in SCLC, so as to provide a theoretical basis for the precise treatment of SCLC and improve the clinical benefits to patients.

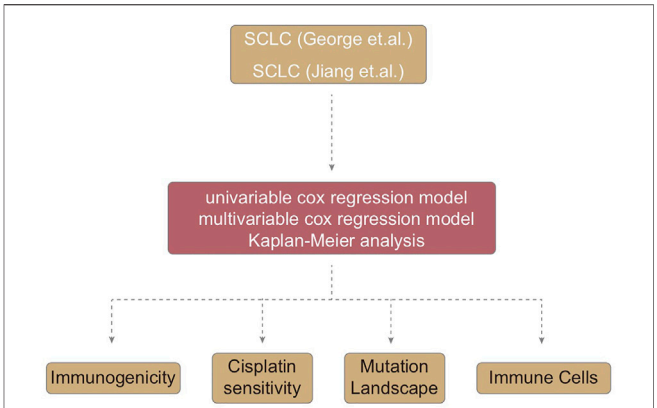

FIGURE 1 | The comprehensive study design.

METHODS

SCLC Cohort

We collected two published SCLC cohorts from the gene expression omnibus (GEO) database (Clough and Barrett, 2016), namely SCLC (George et al., 2015) and SCLC (Jiang et al., 2016). In this study, the inclusion criteria for SCLC patients were that the included SCLC patients must have survival data, expression data, and mutation data. According to the above inclusion criteria, a total of 68 SCLC patients were recorded from paper 1 (**Supplementary Table S1**) and 48 SCLC patients from paper 2 (**Supplementary Table S2**). We filtered the mutation data of the two SCLC cohorts according to the definition and type of non-synonymous mutation in a maftools R package (Mayakonda et al., 2018). The non-synonymous mutation data obtained after filtering was then used for subsequent analyses. The analysis process of this study is detailed in **Figure 1**.

Prediction of Cisplatin Sensitivity

We used the pRRophetic algorithm (Geeleher et al., 2014) to predict the IC50 value of cisplatin by constructing a relevant ridge

regression model with a GDSC cell line expression profile as a training set, and the SCLC cohort as validation set. According to the median value of MMP9 expression, SCLC patients were divided into MMP9-High and MMP9-Low categories. The IC50 values of cisplatin between the two groups were analyzed using the Mann Whitney *U* test. Further, a Spearman correlation test was used to analyze the expression of MMP9 and the related IC50 value of cisplatin.

Analysis of Tumor Immune Microenvironment Infiltration

MCPcounter, quanTIseq and xCell algorithms were used to analyze the expression profile data of SCLC and obtain the overall score of immune cells (Becht et al., 2016; Aran et al., 2017; Plattner et al., 2020). GSEA was used to analyze the difference of signal pathway activity between MMP9-High and MMP9-Low classes (Reimand et al., 2019). ssGSEA (Hänzelmann et al., 2013) was used to evaluate the signal pathway activity of each SCLC patient in the c2 and c5 pathway sets according to the MsigDB database (Liberzon et al., 2011).

The Predictive Value of MMP9 in an Immunotherapy Cohort

We verified the prognostic value of MMP9 expression in the NSCLC cohort receiving ICIs treatment using a CAMOIP webpage tool (Lin et al., 2021a).

Immunogenicity Analysis

The mutation data and expression data of the TCGA cohort were downloaded using the TCGAbiolinks R package. The data of tumor mutation burden (TMB) and neoantigen loads (NALs) of the TCGA cohort were obtained from published literature (Thorsson et al., 2018).

Immunohistochemistry

Tissue samples were deparaffinized and rehydrated. After treatment with endogenous peroxidase blocking solution, they were treated with specific antibodies against MMP9 (ab76003, Abcam), overnight at 4°C. After they were washed with PBS, the samples were treated with horseradish peroxidase-conjugated anti-rabbit IgG (SV0002, Boster, Wuhan, China) and then stained with diaminobenzidine (DAB). All results were assessed by two pathologists. Expression levels were scored by multiplying the percentage of positive cells by the staining intensity. The positivity percentage was scored as 0 if <5% (negative), 1 if 5–30% (sporadic), 2 if 30–70% (focal) and 3 if 70% (diffuse) of the cells were stained; and staining intensity was scored as 0 for no staining, 1 for weak to moderate staining and 2 for strong staining. A score of ≥2 was regarded as 'high' and the score of <2 is regarded as "low" in immunohistochemical staining.

Cell Counting Kit-8 Assay

Cells were cultured at 5×10^3 cells per well in a 96-well plate with cytotoxic drugs for 24 h. Cytotoxic drugs (cisplatin and etoposide) were diluted to obtain different concentration gradients. Absorbance was detected at 450 nm after treatment with 10 μl CCK-8 reagent (Dojindo, Kumamoto) for 4 h. The experiments were performed in five replicate wells per sample and the assays were conducted in triplicate.

Quantitative Real-Time PCR

Total RNA was isolated using Trizol reagent (Invitrogen, United States), according to the manufacturer's instructions. The quantity and purity of the total RNA was measured using the Nanodrop® ND1000 (Thermo Fisher) and the Agilent Bioanalyzer. Reverse transcription was performed with 2 μg of total RNA using M-MLV reverse transcriptase (Accurate Biology, AG11728) according to the manufacturer's recommendations. Quantitative PCR was performed using CFX96 Touch Real-Time PCR Detection Instrument (BioRad, United States). Reactions were performed using SYBR® Green Premix Pro Taq HS qPCR Kit (ROX Plus) (AG11718). Values were normalized to GAPDH via the $2^{-\Delta\Delta Ct}$ method.

Statistical Analysis

The statistical results of KM survival analysis were obtained by a log rank test, and the visual results of KM survival analyses were obtained by survivor and survminer. Univariate COX and multivariate COX models were used to verify whether MMP9 can be used as an independent predictor of the prognosis of SCLC patients treated with cisplatin. The different analysis of continuity variables between MMP9-High and MMP9-Low groups was completed by the Mann Whitney *U* test. In this study, all the analysis is based on R software. The p value is bilateral, and $p < 0.05$ is regarded as statistically significant.

RESULTS

MMP9 is an Independent Predictor of the Prognosis of SCLC Treated With Cisplatin

In order to explore the influence of MMP9 on the prognosis of patients with SCLC treated with cisplatin, we used the univariate COX regression model and multivariate COX regression model to evaluate the SCLC cohort, including SCLC (George et al.) and SCLC (Jiang et al.). In SCLC (George et al.), we found that only MMP9-High was related to an improved clinical prognosis of patients with SCLC, while common clinical factors were not relevant in the prognosis of patients (**Figure 2A**; HR = 0.425; $p = 0.0085$). Multivariate results showed that MMP-High could be used as an independent predictor of prognosis of SCLC after cisplatin treatment (**Figure 2A**; HR = 0.216; $p = 0.00153$). Then, univariate COX and multivariate COX regression models were also applied to SCLC (Jiang et al.), and the results showed that MMP9-High was not only related to significantly prolonged clinical prognosis time (**Figure 2B**; HR = 0.365; $p = 0.0219$) but it can also be used as an independent predictor (**Figure 2B**; HR = 0.352; $p = 0.0199$). The KM curve shows that MMP9-High is related to significantly prolonged OS in patients with SCLC (**Figure 2C**: log-rank $p = 0.007$; HR = 0.44; **Figure 2D**: log-rank $p = 0.017$; HR = 0.39). We used a Sankey diagram to visualize the clinical features of two SCLC cohorts one by one (**Figures 2E,F**).

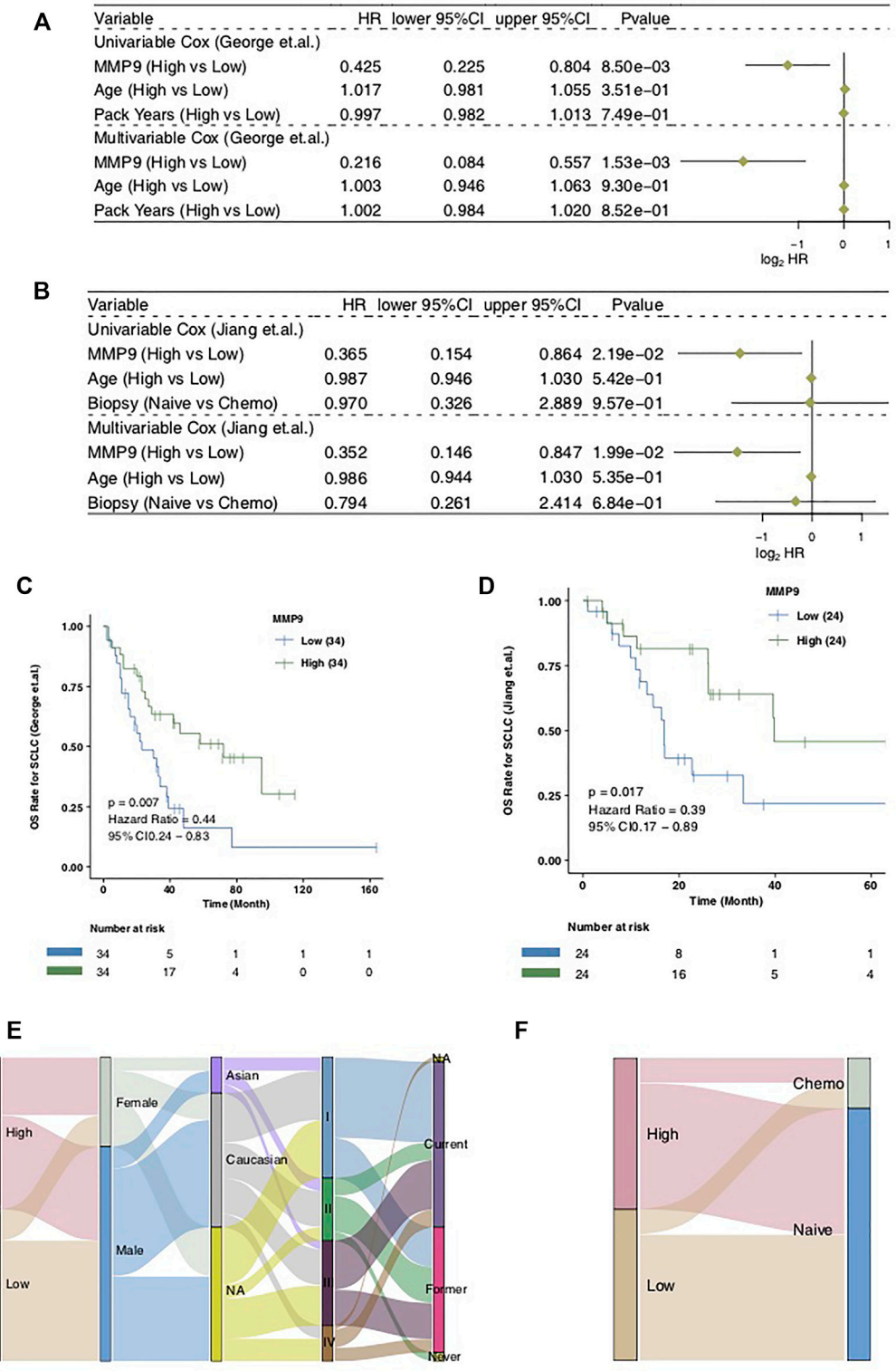

FIGURE 2 | The prognostic value of MMP9. The univariate and multivariate COX regression model of the SCLC (George et al.) **(A)** and the SCLC (Jiang et al.) **(B)**. Kaplan-Meier curves comparing the progress free survival (PFS) of patients with MMP9-High and patients with MMP9-Low in the SCLC (George et al.) **(C)** and the SCLC (Jiang et al.) **(D)**. A Sankey diagram visualizing the clinical characteristics between MMP9-High and MMP9-Low patients in the SCLC (George et al.) **(E)** and the SCLC (Jiang et al.) **(F)**.

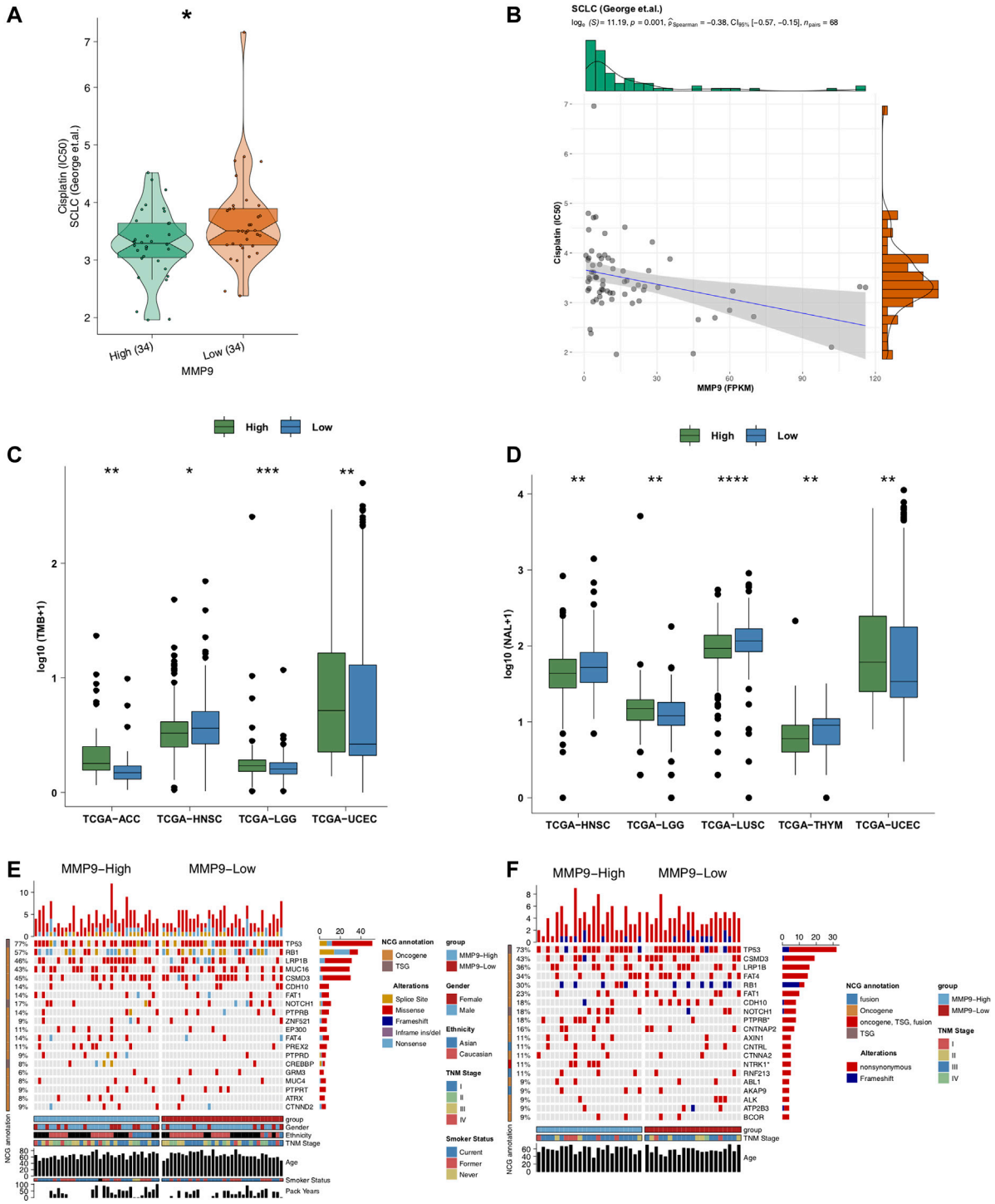

FIGURE 3 | The association between MMP9, immunogenicity, and cisplatin. **(A)** Comparison of IC50 values of cisplatin between MMP9-High and MMP9-Low tumors. **(B)** The association between the IC50 value of cisplatin and the expression of MMP9. **(C)** Comparison of the tumor mutation burden between MMP9-High and MMP9-Low tumors. **(D)** Comparison of neoantigen loads (NALs) between MMP9-High and MMP9-Low tumors. The top 20 mutated driver genes in the SCLC (George et al.) **(E)** and SCLC (Jiang et al.) **(F)**. (*$p < 0.05$; **$p < 0.01$; ***$p < 0.001$; ****$p < 0.0001$; Mann-Whitney *U* test).

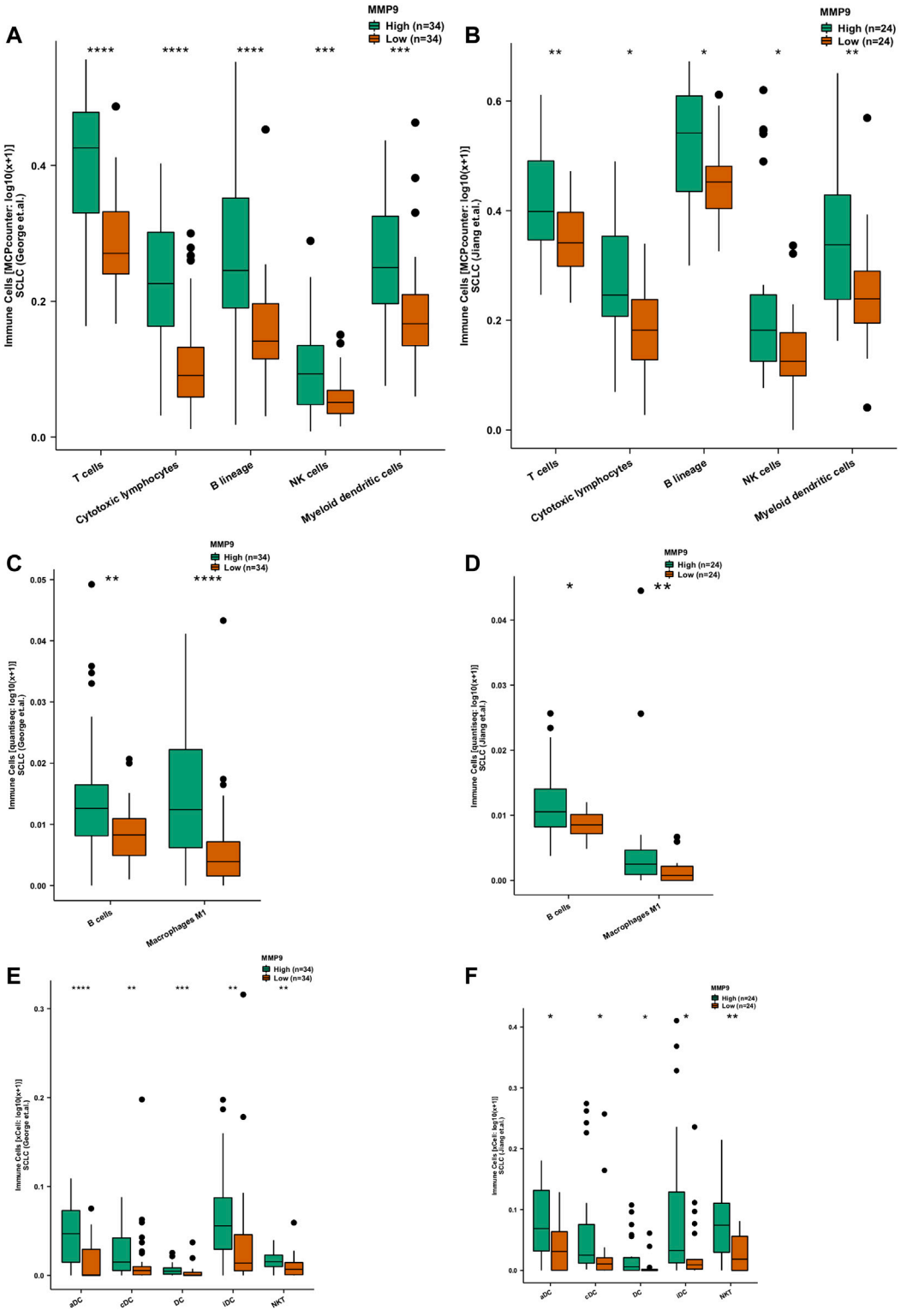

FIGURE 4 | The association between MMP9 and immune cells. Comparison of immune cells estimated according to MCPcounter between MMP9-High and MMP9-Low tumors in the SCLC (George et al.) **(A)** and the SCLC (Jiang et al.) **(B)**. Comparison of immune cells estimated by quanTIseq between MMP9-High and MMP9-Low tumors in the SCLC (George et al.) **(C)** and the SCLC (Jiang et al.) **(D)**. Comparison of immune cells estimated by xCell between MMP9-High and MMP9-Low tumors in the SCLC (George et al.) **(E)** and the SCLC (Jiang et al.) **(F)**. (*$p < 0.05$; **$p < 0.01$; ***$p < 0.001$; ****$p < 0.0001$; Mann-Whitney *U* test).

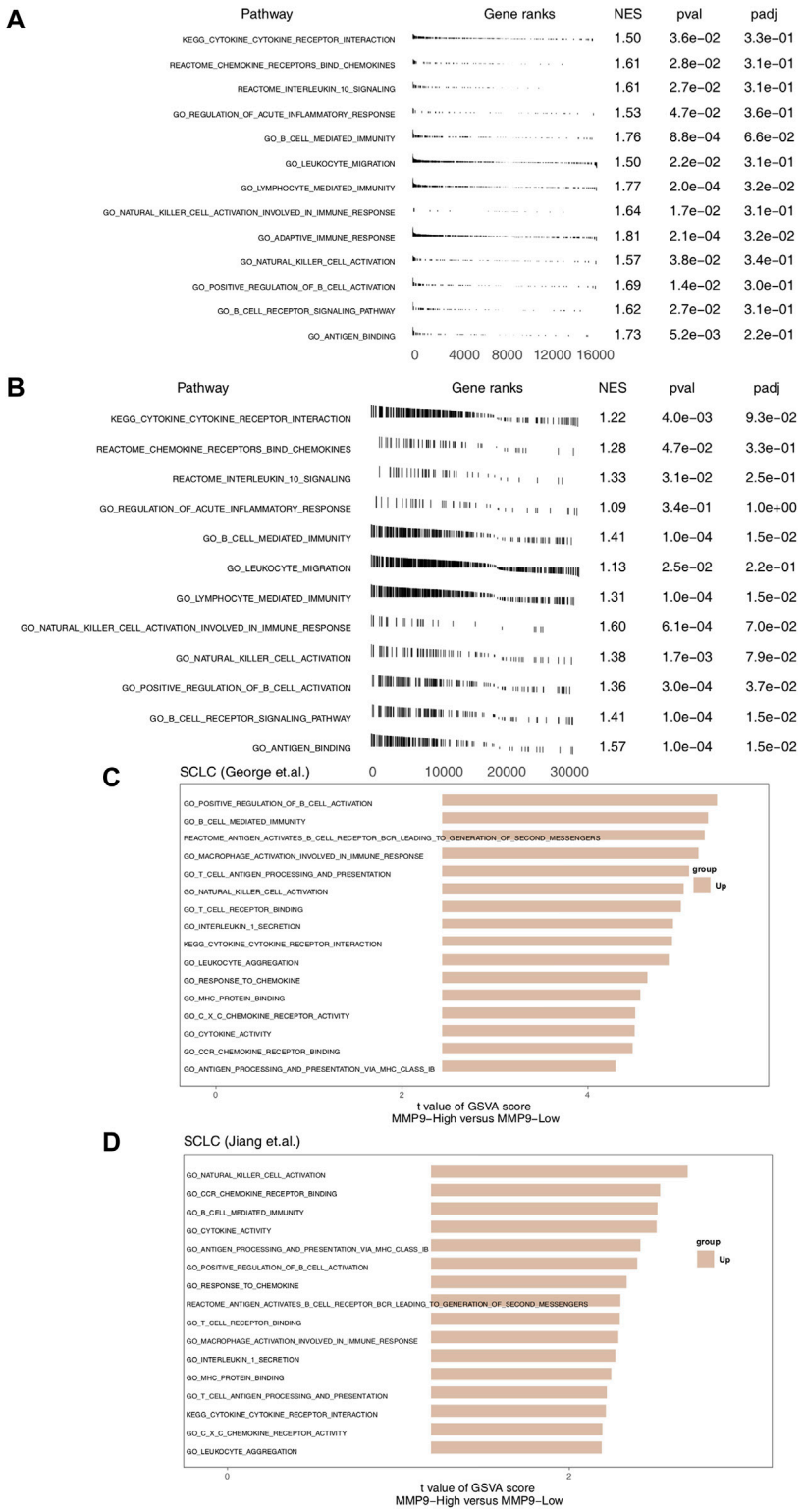

FIGURE 5 | The association between MMP9 and immune-related signaling. **(A)** The results of GSEA in the SCLC (George et al.) relating to immune signaling. **(B)** The results of GSEA in the SCLC (Jiang et al.) relating to immune signaling. The GSEA of hallmark gene sets was downloaded from the MSigDB, and each run was performed with 1000 permutations. Differences in pathway activities scored per cell by MMP9-High and MMP9-Low tumors in the SCLC (George et al.) **(C)** and the SCLC (Jiang et al.) **(D)**. Shown are *t* values from a linear model.

MMP9 is Related to Cisplatin Sensitivity and Immunogenicity

We employed the pRRophetic algorithm to predict the cisplatin sensitivity of each SCLC patient to obtain an IC50 value. We found that MMP9-High had significantly lower IC50 values of cisplatin than MMP9-Low SCLC (**Figure 3A**; $p < 0.05$). Similarly, the expression of MMP9 was negatively correlated with the IC50 value of cisplatin (**Figure 3B**, $p = 0.001$; R = −0.38; method: spearman). We found that MMP9-High had significantly higher TMB than MMP9-Low (**Figure 3C**; All $p < 0.05$) and NALs (**Figure 3D**; all $p < 0.05$). **Figure 3E** shows that for SCLC (George et al.), the type and mutation frequency of the driver genes in the top 20 mutation frequencies in the cohort. The results showed that there was no significant difference between the driver genes in the top 20 mutation frequencies of MMP9-High and MMP9-Low. In SCLC (Jiang et al.), the mutation frequency of MMP9-High is significantly higher than that of MMP9-Low in PTPRB and NTRK (**Figure 3F**). **Supplementary Figures S1A,B** shows the mutual exclusion and co-occurrence of the top 20 driving mutations in MMP9-High and MMP9-Low, respectively.

MMP9 is Related to Activated Immune Cells

Under the MCPcounter algorithm, whether in SCLC (George et al.) or SCLC (Jiang et al.), we found that the TIME when MMP9-High was higher than MMP9-Low was significantly infiltrated with t-cells, cytoxic lymphocytes, B-cells, NK cells, and dense cells (DCS) (**Figures 4A,B**; all $p < 0.05$). Under the quanTIseq algorithm, we found that MMP9-High has significantly increased B cells and m1 macrophages when compared with MMP9-Low (**Figure 4C**: George et al.; **Figure 4D**: Jiang et al.). With the xCell algorithm, we found that, compared with MMP9-Low, MMP9-High has significant DCs and NKT (**Figure 4E**: George et al.; **Figure 4F**: Jiang et al.).

MMP9 is Related to the Up-Regulation of the Immune-Related Signaling Pathway

In order to further explore the difference of signal pathway activity between MMP9-High and MMP9-Low, we used GSEA and ssGSEA to evaluate and calculate the signal pathway activity. **Figures 5A,B** shows that in SCLC (George et al.) and SCLC (Jiang et al.), MMP9-High has significantly increased activity of immune activation related pathways, such as cytokine binding and immune response mediated by B cells and NK cells when compared with MMP9-Low. In addition, the results of ssGSEA analysis showed that the activity of MMP9-High in B-cell, T-cell and NK cell activation, cytokine secretion, chemokine binding, and antigen presentation was significantly higher than that of MMP9-Low (**Figures 5C,D**).

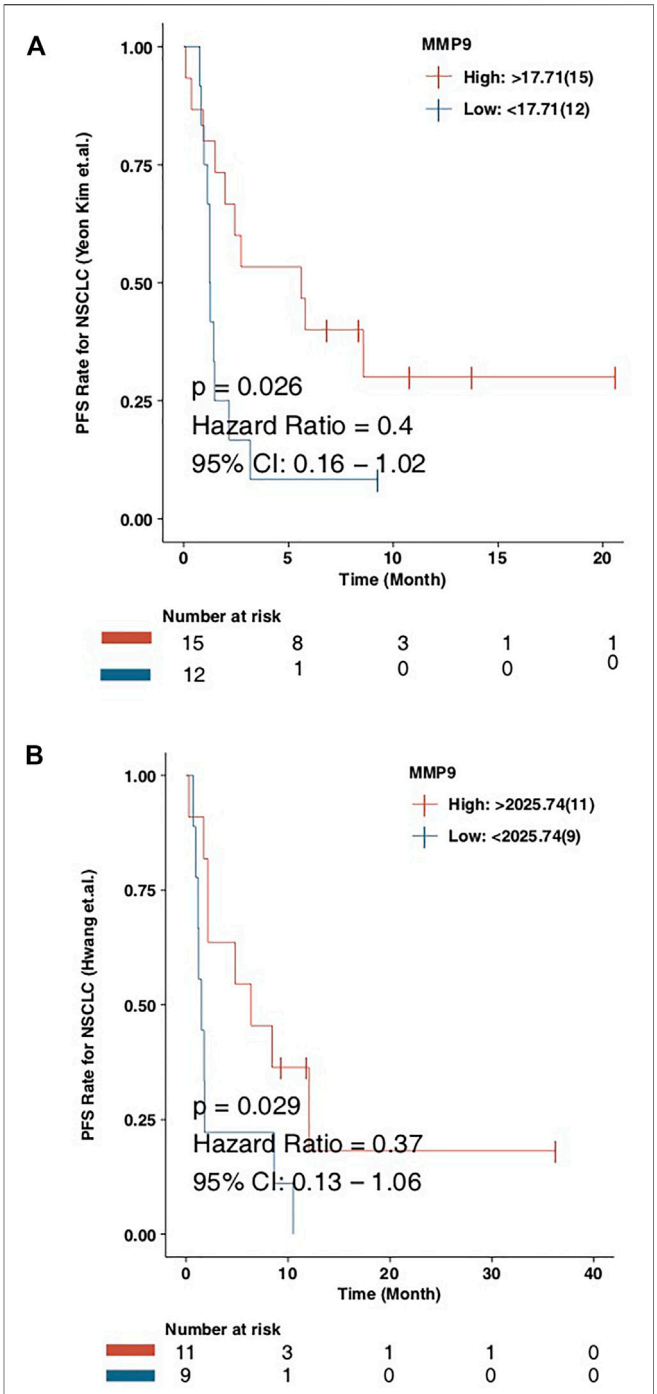

FIGURE 6 | The prognostic value of the MMP9 in immunotherapy. Kaplan-Meier curves comparing the progress free survival (PFS) of patients with MMP9-High and patients with MMP9-Low in the NSCLC (Kim et al.) **(A)** and the NSCLC (Hwang et al.) **(B)**.

MMP9 is Related to the Prognosis of Immunotherapy

In order to explore the role of MMP9 in the prognosis of patients receiving immune checkpoint inhibitors, we used CAMOIP as a web tool to verify the relationship between MMP9 and the prognosis of immunotherapy. We found that in the NSCLC (Kim et al.) cohort, the PFS time of MMP9-High was significantly longer than that of MMP9-Low (**Figure 6A**; log-rank $p = 0.026$; HR = 0.4). In another NSCLC (Hwang et al.) cohort, the PFS time of MMP9-High was significantly longer than

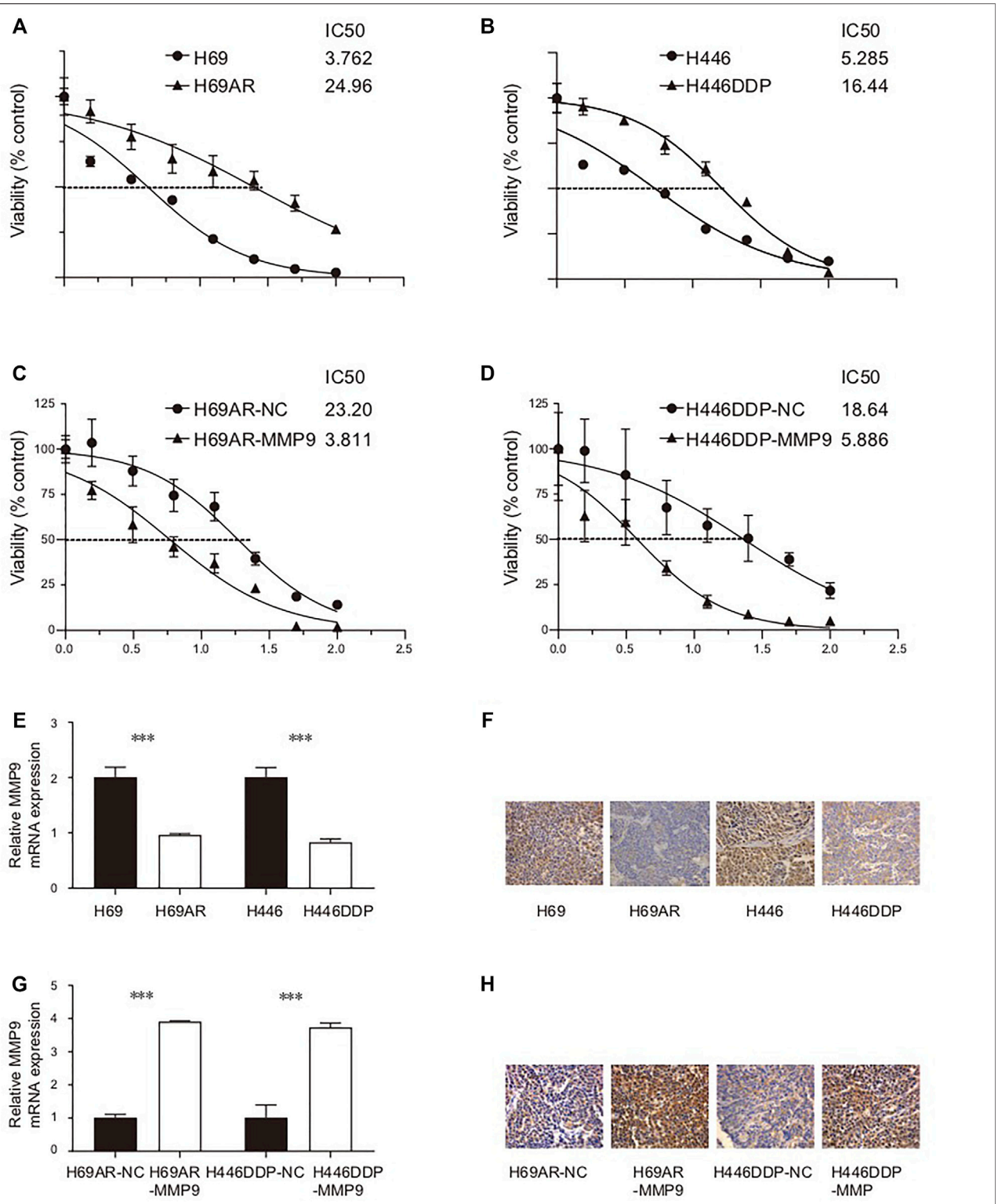

FIGURE 7 | (A) The IC50 of H69/H69AR cells to cisplatin. **(B)** The IC50 of H446/H446DDP to cisplatin. **(C)** The IC50 of H69AR-NC/H69AR-MMP9 to cisplatin. **(D)** The IC50 of H446DDP-NC/H446DDP-MMP9 to cisplatin. **(E)** The expression level of MMP9 mRNA in H69, H69AR, H446 and H446DDP. **(F)** The expression level of CDYL protein in H69, H69AR, H446 and H446DDP. **(G)** The expression level of MMP9 mRNA in H69AR-NC, H69AR-MMP9, H446DDP-NC and H446DDP-MMP9. **(H)** The expression level of CDYL protein in H69AR-NC, H69AR-MMP9, H446DDP-NC and H446DDP-MMP9 (***$p < 0.001$).

that of MMP9-Low (**Figure 6B**; log-rank $p = 0.029$; HR = 0.37). These results suggest that MMP9 may be an important biomarker for the prognosis of immunotherapy.

Small Cell Lung Cancer Model Proves that MMP9 is Related to Cisplatin Sensitivity

In this study, the IC50 values of two pairs of chemotherapy-sensitive and drug-resistant small cell lung cancer cells to the first-line chemotherapy drug (cisplatin) were detected using the CCK8 method. The results showed that the IC50 of chemotherapy-sensitive H69/H446 small cell lung cancer cells to cisplatin was significantly lower than that of the corresponding chemotherapy-resistant cells (H69AR/H446DDP) (**Figures 7A,B**). To detect the effect of MMP9 on the chemotherapy resistance of small cell lung cancer cells, this study used the CCK8 method to detect the IC50 value of chemotherapy-resistant small cell lung cancer cells with upregulated expression of MMP9 to first-line chemotherapy drugs (cisplatin and etoposide). The results showed that upregulating the expression level of MMP9 (H69-MMP9, H446-MMP9) in chemotherapy-resistant small cell lung cancer cells significantly reduced the IC50 value of SCLC cells to chemotherapy drugs (**Figures 7C,D**), and the subsequent chemotherapy resistance of cells decreased.

Firstly, the basic expression levels of MMP9 mRNA and MMP9 protein in small cell lung cancer cells were detected by real-time fluorescence quantitative PCR and immunohistochemistry. The results of the real-time quantitative PCR showed that the expression level of MMP9 mRNA in chemotherapy-resistant H69AR cells and H446DDP cells was significantly lower than that in chemotherapy-sensitive H69 cells and H446 cells (**Figure 7E**) ($p < 0.001$). Immunohistochemically, the results also showed that the expression level of CDYL protein in chemotherapy-resistant H69AR cells and H446DDP cells was lower than that of their parents' chemotherapy-sensitive H69 cells and H446 cells (**Figure 7F**). Based on the basic expression level of MMP9 in the above two pairs of chemotherapy-sensitive and chemotherapy-resistant small cell lung cancer cells, this study further uses lentivirus-mediated LV5-MMP9 to up-regulate the expression level of MMP9 in chemotherapy-resistant H69AR and H446DDP small cell lung cancer cells. The verification results of quantitative PCR, and immunohistochemistry showed that we successfully constructed the small cell lung cancer cell model with an up-regulated expression of CDYL (H69AR-MMP9, H446DDP-MMP9). (**Figures 7G,H**). ($p < 0.001$).

DISCUSSION

The results of the univariate COX regression, multivariate COX regression, and KM analysis demonstrated that MMP9-High may be an independent predictor of improved prognosis in SCLC patients after receiving cisplatin. In addition, the expression of MMP9 was negatively correlated with the IC50 value of cisplatin. Based on the observations pertaining to MMP9, we analyzed the TIME of patients with SCLC. Compared with MMP9-Low, MMP9-High displayed significantly increased activated immune cells and an amplified active immune activation pathway. In addition, according to the immunotherapy cohort, MMP9 may represent a suitable novel biomarker for screening patients undergoing immunotherapy.

Remodeling the immunogenicity of tumor cells may be one of the reasons underlying the improved prognosis of patients with MMP9-High SCLC after cisplatin treatment. After cisplatin induces the death of tumor cells, it will release immunogenic substances originally located in tumor cells, thus activating the APC-mediated antigen presentation process, resulting in an anti-tumor immune response. Evidence from a study investigating the anti-tumor mechanism of cisplatin employed protein omics based on mass spectrometry in order to detect the content of protein in the supernatant of tumor cell culture before and after cisplatin administration. A total of 2,239 varieties of protein were identified, of which 526 types were up-regulated more than 3 times after cisplatin treatment, including tumor-driving genes such as NRAS, heat shock proteins, metabolic enzymes, and other proteins. Furthermore, APC stimulated by antigenic substances in these supernatants can significantly enhance the proliferation and functional level of CD8+T cells, suggesting that antigen release induced by chemotherapeutic drugs can significantly activate anti-tumor immune response through the antigen presentation system (Beyranvand Nejad et al., 2016; Lin et al., 2020).

In this study, we found that MMP9-High has significantly higher TMB and NALs than MMP9-Low. Up-regulation of immunocompetent ligand on the surface of tumor cells may contribute to the possible mechanisms of improved prognosis in patients with MMP9-High SCLC after cisplatin treatment. In addition to the above-mentioned release of immunogenic substances related to cell death, chemotherapeutic drugs can also affect the protein expression of tumor cells. Immunogenic tumor cells remodeling tumor cells can down-regulate the expression of MHCI to avoid the killing effect of CTL cells. It has been found that cisplatin can up-regulate MHCI on the surface of head and neck cancer cells and enhance the presentation of tumor antigens, thus promoting the recognition of tumor cells by CTL and the activation of CD8+T cells (Gameiro et al., 2012; Tran et al., 2017; Lin et al., 2021b). In addition, cisplatin can also lead to the up-regulation of MHCI expression in ovarian cancer cells (Grabosch et al., 2019). After subcutaneous inoculation of tumor cells pretreated with cisplatin *in vitro*, it was found that, when compared with the control group, the tumor cells treated with cisplatin were not likely to form tumors, and the expression of MHCI in grown tumors was higher (Nio et al., 2000). Similar results were obtained with regard to colon cancer cells (Ohtsukasa et al., 2003). We can infer that cisplatin can up-regulate the expression of MHCI *in vitro* and *in vivo*. In addition to tumor cells, chemotherapeutics can up-regulate the expression level of MHCI in antigen presenting cells (APCs) (Jackaman et al., 2012). In addition, studies reveal that cisplatin can improve the antigen presenting ability of APC such as DCs(Shurin et al., 2009; Zitvogel et al., 2013; Lin et al., 2021c). In this study, we found that MMP9-High has significantly infiltrated

DCs, higher MHC, and increased antigen presentation activities compared to that of MMP9-Low.

Inflammatory TIME may be one of the reasons for the improved prognosis of patients with MMP9-High SCLC after cisplatin treatment. Chemotherapy drugs can enhance the sensitivity of tumor cells to immune killing. For example, cisplatin can enhance the sensitivity of tumor cells to the CTL specific killing effect (Ramakrishnan et al., 2012). In addition, active immune effector cells, such as NKs, serve to mediate cytotoxicity (Lichtenstein and Pende, 1986). Furthermore, cisplatin also causes effector cells to produce more cytokines that regulate and promote various immune responses (Kepp et al., 2013; Huang et al., 2021). Moreover, chemotherapy can eliminate immunosuppressive cells such as MDSC and Tregs by inducing apoptosis and through other mechanisms, so that immunotherapy can achieve the maximum efficacy. For example, the use of cisplatin before the injection of DNA vaccine encoding CRT can reduce the level of MDSC in tumor-bearing mice (Tseng et al., 2008; Li et al., 2020). Cisplatin is beneficial in inducing the formation of self-reactive T-cells and anti-tumor immune responses (Tseng et al., 2008). The CTLs and NKs with significant infiltration in MMP9-High, respectively, verified the above results.

However, this research has some limitations. First, the cohorts of SCLC are very limited, and this study only includes two of the SCLC cohorts recorded in the current public data. Secondly, the SCLC cohort lacks data on cisplatin drug sensitivity, and the data on cisplatin drug sensitivity in this study is based on the pRRophetic algorithm.

CONCLUSION

Based on the results obtained in this study, we identified that MMP9-High may be a potential new biomarker that facilitates the improved prognosis of SCLC patients after cisplatin treatment. In addition, the TIME of MMP9-High SCLC is primarily characterized by a large number of infiltrated activated immune cells and activated immune-related pathways.

DATA AVAILABILITY STATEMENT

The original contributions presented in the study are included in the article/**Supplementary Material**, further inquiries can be directed to the corresponding authors.

ETHICS STATEMENT

Ethical review and approval was not required for the study on human participants in accordance with the local legislation and institutional requirements. Written informed consent for participation was not required for this study in accordance with the national legislation and the institutional requirements.

AUTHOR CONTRIBUTIONS

Conceptualization, RL, LW; Formal analysis, ZQ; Visualization, ZQ; Writing–original draft, XH, XW, QH; Writing–review and editing, ZQ, XH, XW, QH, QL, RL, and LW. All authors read and approved the final manuscript.

FUNDING

This work was supported by the Science and Technology Project of Education Department of Jiangxi Province (GJJ211513, 180812,180805), the Science and Technology Project of Health and Family Planning Commission of Jiangxi Province (Number 20195363, 20195361), the Haosen Oncology Research Fund (Y-HS2019/2-015), and the Science and Technology Project of Ganzhou City (GZ2021SF002).

SUPPLEMENTARY MATERIAL

The Supplementary Material for this article can be found online at: https://www.frontiersin.org/articles/10.3389/fphar.2022.868203/full#supplementary-material

REFERENCES

Aran, D., Hu, Z., and Butte, A. J. (2017). xCell: Digitally Portraying the Tissue Cellular Heterogeneity Landscape. *Genome Biol.* 18, 220. doi:10.1186/s13059-017-1349-1

Becht, E., Giraldo, N. A., Lacroix, L., Buttard, B., Elarouci, N., Petitprez, F., et al. (2016). Estimating the Population Abundance of Tissue-Infiltrating Immune and Stromal Cell Populations Using Gene Expression. *Genome Biol.* 17, 218. doi:10.1186/s13059-016-1070-5

Beyranvand Nejad, E., van der Sluis, T. C., van Duikeren, S., Yagita, H., Janssen, G. M., van Veelen, P. A., et al. (2016). Tumor Eradication by Cisplatin Is Sustained by CD80/86-Mediated Costimulation of CD8+ T Cells. *Cancer Res.* 76, 6017–6029. doi:10.1158/0008-5472.CAN-16-0881

Braicu, E. I., Gasimli, K., Richter, R., Nassir, M., Kümmel, S., Blohmer, J. U., et al. (2014). Role of Serum VEGFA, TIMP2, MMP2 and MMP9 in Monitoring Response to Adjuvant Radiochemotherapy in Patients with Primary Cervical Cancer-Rresults of a Companion Protocol of the Randomized NOGGO-AGO Phase III Clinical Trial. *Anticancer Res.* 34, 385–391.

Carter, B. W., Glisson, B. S., Truong, M. T., and Erasmus, J. J. (2014). Small Cell Lung Carcinoma: Staging, Imaging, and Treatment Considerations. *RadioGraphics* 34, 1707–1721. doi:10.1148/rg.346140178

Clough, E., and Barrett, T. (2016). The Gene Expression Omnibus Database. *Methods Mol. Biol.* 1418, 93–110. doi:10.1007/978-1-4939-3578-9_5

de Hoyos, A., and DeCamp, M. M. (2014). Surgery for Small Cell Lung Cancer. *Thorac. Surg. Clin.* 24, 399–409. doi:10.1016/j.thorsurg.2014.07.005

Di Caro, G., Cortese, N., Castino, G. F., Grizzi, F., Gavazzi, F., Ridolfi, C., et al. (2016). Dual Prognostic Significance of Tumour-Associated Macrophages in Human Pancreatic Adenocarcinoma Treated or Untreated with Chemotherapy. *Gut* 65, 1710–1720. doi:10.1136/gutjnl-2015-309193

Eriksson, E., Wenthe, J., Irenaeus, S., Loskog, A., and Ullenhag, G. (2016). Gemcitabine Reduces MDSCs, Tregs and TGFβ-1 while Restoring the Teff/treg Ratio in Patients with Pancreatic Cancer. *J. Transl Med.* 14, 282. doi:10.1186/s12967-016-1037-z

Galluzzi, L., Vitale, I., Michels, J., Brenner, C., Szabadkai, G., Harel-Bellan, A., et al. (2014). Systems Biology of Cisplatin Resistance: Past, Present and Future. *Cell Death Dis* 5, e1257. doi:10.1038/cddis.2013.428

Gameiro, S. R., Caballero, J. A., and Hodge, J. W. (2012). Defining the Molecular Signature of Chemotherapy-Mediated Lung Tumor Phenotype Modulation and Increased Susceptibility to T-Cell Killing. *Cancer Biother. Radiopharm.* 27, 23–35. doi:10.1089/cbr.2012.1203

Geeleher, P., Cox, N., and Huang, R. S. (2014). pRRophetic: an R Package for Prediction of Clinical Chemotherapeutic Response from Tumor Gene Expression Levels. *PLoS One* 9, e107468. doi:10.1371/journal.pone.0107468

George, J., Lim, J. S., Jang, S. J., Cun, Y., Ozretić, L., Kong, G., et al. (2015). Comprehensive Genomic Profiles of Small Cell Lung Cancer. *Nature* 524, 47–53. doi:10.1038/nature14664

Grabosch, S., Bulatovic, M., Zeng, F., Ma, T., Zhang, L., Ross, M., et al. (2019). Cisplatin-induced Immune Modulation in Ovarian Cancer Mouse Models with Distinct Inflammation Profiles. *Oncogene* 38, 2380–2393. doi:10.1038/s41388-018-0581-9

Hänzelmann, S., Castelo, R., and Guinney, J. (2013). GSVA: Gene Set Variation Analysis for Microarray and RNA-Seq Data. *BMC Bioinformatics* 14, 7. doi:10.1186/1471-2105-14-7

Horn, L., Mansfield, A. S., Szczęsna, A., Havel, L., Krzakowski, M., Hochmair, M. J., et al. (2018). First-Line Atezolizumab Plus Chemotherapy in Extensive-Stage Small-Cell Lung Cancer. *N. Engl. J. Med.* 379, 2220–2229. doi:10.1056/NEJMoa1809064

Huang, W., Lin, A., Luo, P., Liu, Y., Xu, W., Zhu, W., et al. (2021). EPHA5 Mutation Predicts the Durable Clinical Benefit of Immune Checkpoint Inhibitors in Patients with Lung Adenocarcinoma. *Cancer Gene Ther.* 28, 864–874. doi:10.1038/s41417-020-0207-6

Inoue, M., Koga, F., Yoshida, S., Tamura, T., Fujii, Y., Ito, E., et al. (2014). Significance of ERBB2 Overexpression in Therapeutic Resistance and Cancer-specific Survival in Muscle-Invasive Bladder Cancer Patients Treated with Chemoradiation-Based Selective Bladder-Sparing Approach. *Int. J. Radiat. Oncol. Biol. Phys.* 90, 303–311. doi:10.1016/j.ijrobp.2014.05.043

Ireland, L., Santos, A., Ahmed, M. S., Rainer, C., Nielsen, S. R., Quaranta, V., et al. (2016). Chemoresistance in Pancreatic Cancer Is Driven by Stroma-Derived Insulin-like Growth Factors. *Cancer Res.* 76, 6851–6863. doi:10.1158/0008-5472.CAN-16-1201

Jackaman, C., Majewski, D., Fox, S. A., Nowak, A. K., and Nelson, D. J. (2012). Chemotherapy Broadens the Range of Tumor Antigens Seen by Cytotoxic CD8(+) T Cells *In Vivo*. *Cancer Immunol. Immunother.* 61, 2343–2356. doi:10.1007/s00262-012-1307-4

Jiang, L., Huang, J., Higgs, B. W., Hu, Z., Xiao, Z., Yao, X., et al. (2016). Genomic Landscape Survey Identifies SRSF1 as a Key Oncodriver in Small Cell Lung Cancer. *Plos Genet.* 12, e1005895. doi:10.1371/journal.pgen.1005895

Kepp, O., Menger, L., Vacchelli, E., Locher, C., Adjemian, S., Yamazaki, T., et al. (2013). Crosstalk between ER Stress and Immunogenic Cell Death. *Cytokine Growth Factor. Rev.* 24, 311–318. doi:10.1016/j.cytogfr.2013.05.001

Li, M., Lin, A., Luo, P., Shen, W., Xiao, D., Gou, L., et al. (2020). DNAH10 Mutation Correlates with Cisplatin Sensitivity and Tumor Mutation burden in Small-Cell Lung Cancer. *Aging (Albany NY)* 12, 1285–1303. doi:10.18632/aging.102683

Li, S., Wang, H., Zhang, Y., Qiao, R., Xia, P., Kong, Z., et al. (2021). COL3A1 and MMP9 Serve as Potential Diagnostic Biomarkers of Osteoarthritis and Are Associated with Immune Cell Infiltration. *Front. Genet.* 12, 721258. doi:10.3389/fgene.2021.721258

Liberzon, A., Subramanian, A., Pinchback, R., Thorvaldsdóttir, H., Tamayo, P., and Mesirov, J. P. (2011). Molecular Signatures Database (MSigDB) 3.0. *Bioinformatics* 27, 1739–1740. doi:10.1093/bioinformatics/btr260

Lichtenstein, A. K., and Pende, D. (1986). Enhancement of Natural Killer Cytotoxicity by Cis-Diamminedichloroplatinum (II) *In Vivo* and *In Vitro*. *Cancer Res.* 46, 639–644.

Lin, A., Wei, T., Meng, H., Luo, P., and Zhang, J. (2019). Role of the Dynamic Tumor Microenvironment in Controversies Regarding Immune Checkpoint Inhibitors for the Treatment of Non-small Cell Lung Cancer (NSCLC) with EGFR Mutations. *Mol. Cancer* 18, 139. doi:10.1186/s12943-019-1062-7

Lin, A., Zhang, J., and Luo, P. (2020). Crosstalk between the MSI Status and Tumor Microenvironment in Colorectal Cancer. *Front. Immunol.* 11, 2039. doi:10.3389/fimmu.2020.02039

Lin, A., Wei, T., Liang, J., Qi, C., Li, M., Luo, P., et al. (2021). *CAMOIP: A Web Server for Comprehensive Analysis on Multi-Omics of Immunotherapy in Pan-Cancer*. China: bioRxiv.

Lin, A., Qiu, Z., Zhang, J., and Luo, P. (2021). Effect of NCOR1 Mutations on Immune Microenvironment and Efficacy of Immune Checkpoint Inhibitors in Patient with Bladder Cancer. *Front. Immunol.* 12, 630773. doi:10.3389/fimmu.2021.630773

Lin, A., Xu, W., Luo, P., and Zhang, J. (2021). Mutations Status of Chemokine Signaling Pathway Predict Prognosis of Immune Checkpoint Inhibitors in Colon Adenocarcinoma. *Front. Pharmacol.* 12, 721181. doi:10.3389/fphar.2021.721181

Luo, P., Lin, A., Li, K., Wei, T., and Zhang, J. (2019). DDR Pathway Alteration, Tumor Mutation Burden, and Cisplatin Sensitivity in Small Cell Lung Cancer: Difference Detected by Whole Exome and Targeted Gene Sequencing. *J. Thorac. Oncol.* 14, e276–e279. doi:10.1016/j.jtho.2019.08.2509

Makhoul, I., Griffin, R. J., Siegel, E., Lee, J., Dhakal, I., Raj, V., et al. (2016). High-circulating Tie2 Is Associated with Pathologic Complete Response to Chemotherapy and Antiangiogenic Therapy in Breast Cancer. *Am. J. Clin. Oncol.* 39, 248–254. doi:10.1097/COC.0000000000000046

Mayakonda, A., Lin, D. C., Assenov, Y., Plass, C., and Koeffler, H. P. (2018). Maftools: Efficient and Comprehensive Analysis of Somatic Variants in Cancer. *Genome Res.* 28, 1747–1756. doi:10.1101/gr.239244.118

Mitchem, J. B., Brennan, D. J., Knolhoff, B. L., Belt, B. A., Zhu, Y., Sanford, D. E., et al. (2013). Targeting Tumor-Infiltrating Macrophages Decreases Tumor-Initiating Cells, Relieves Immunosuppression, and Improves Chemotherapeutic Responses. *Cancer Res.* 73, 1128–1141. doi:10.1158/0008-5472.CAN-12-2731

Mondal, S., Adhikari, N., Banerjee, S., Amin, S. A., and Jha, T. (2020). Matrix Metalloproteinase-9 (MMP-9) and its Inhibitors in Cancer: A Minireview. *Eur. J. Med. Chem.* 194, 112260. doi:10.1016/j.ejmech.2020.112260

Nio, Y., Hirahara, N., Minari, Y., Iguchi, C., Yamasawa, K., Toga, T., et al. (2000). Induction of Tumor-specific Antitumor Immunity after Chemotherapy with Cisplatin in Mice Bearing MOPC-104E Plasmacytoma by Modulation of MHC Expression on Tumor Surface. *Anticancer Res.* 20, 3293–3299.

Ohtsukasa, S., Okabe, S., Yamashita, H., Iwai, T., and Sugihara, K. (2003). Increased Expression of CEA and MHC Class I in Colorectal Cancer Cell Lines Exposed to Chemotherapy Drugs. *J. Cancer Res. Clin. Oncol.* 129, 719–726. doi:10.1007/s00432-003-0492-0

Plattner, C., Finotello, F., and Rieder, D. (2020). Deconvoluting Tumor-Infiltrating Immune Cells From RNA-seq Data Using quanTIseq. *Meth. Enzymol.* 636, 261–285. doi:10.1016/bs.mie.2019.05.056

Qiao, X., Gu, Y., Yu, J., Wang, J., Liu, X., Gu, M., et al. (2020). The Combination of CD147 and MMP-9 Serum Levels Is Identified as Novel Chemotherapy Response Markers of Advanced Non-small-cell Lung Cancer. *Dis. Markers* 2020, 8085053. doi:10.1155/2020/8085053

Qiu, Z., Lin, A., Li, K., Lin, W., Wang, Q., Wei, T., et al. (2019). A Novel Mutation Panel for Predicting Etoposide Resistance in Small-Cell Lung Cancer. *Drug Des. Devel Ther.* 13, 2021–2041. doi:10.2147/DDDT.S205633

Ramakrishnan, R., Huang, C., Cho, H. I., Lloyd, M., Johnson, J., Ren, X., et al. (2012). Autophagy Induced by Conventional Chemotherapy Mediates Tumor Cell Sensitivity to Immunotherapy. *Cancer Res.* 72, 5483–5493. doi:10.1158/0008-5472.CAN-12-2236

Rauvala, M., Turpeenniemi-Hujanen, T., and Puistola, U. (2006). The Value of Sequential Serum Measurements of Gelatinases and Tissue Inhibitors during Chemotherapy in Ovarian Cancer. *Anticancer Res.* 26, 4779–4784.

Reimand, J., Isserlin, R., Voisin, V., Kucera, M., Tannus-Lopes, C., Rostamianfar, A., et al. (2019). Pathway Enrichment Analysis and Visualization of Omics Data Using g:Profiler, GSEA, Cytoscape and EnrichmentMap. *Nat. Protoc.* 14, 482–517. doi:10.1038/s41596-018-0103-9

Sabari, J. K., Lok, B. H., Laird, J. H., Poirier, J. T., and Rudin, C. M. (2017). Unravelling the Biology of SCLC: Implications for Therapy. *Nat. Rev. Clin. Oncol.* 14, 549–561. doi:10.1038/nrclinonc.2017.71

Shurin, G. V., Tourkova, I. L., Kaneno, R., and Shurin, M. R. (2009). Chemotherapeutic Agents in Noncytotoxic Concentrations Increase Antigen

Presentation by Dendritic Cells via an IL-12-dependent Mechanism. *J. Immunol.* 183, 137–144. doi:10.4049/jimmunol.0900734

Song, Y., Zhou, X., Bai, W., and Ma, X. (2015). FBW7 Increases Drug Sensitivity to Cisplatin in Human Nasopharyngeal Carcinoma by Downregulating the Expression of Multidrug Resistance-Associated Protein. *Tumour Biol.* 36, 4197–4202. doi:10.1007/s13277-015-3056-4

Thorsson, V., Gibbs, D. L., Brown, S. D., Wolf, D., Bortone, D. S., Ou Yang, T. H., et al. (2018). The Immune Landscape of Cancer. *Immunity* 48, 812. e14. doi:10.1016/j.immuni.2018.03.023

Tran, L., Allen, C. T., Xiao, R., Moore, E., Davis, R., Park, S. J., et al. (2017). Cisplatin Alters Antitumor Immunity and Synergizes with PD-1/pd-L1 Inhibition in Head and Neck Squamous Cell Carcinoma. *Cancer Immunol. Res.* 5, 1141–1151. doi:10.1158/2326-6066.CIR-17-0235

Tseng, C. W., Hung, C. F., Alvarez, R. D., Trimble, C., Huh, W. K., Kim, D., et al. (2008). Pretreatment with Cisplatin Enhances E7-specific CD8+ T-Cell-Mediated Antitumor Immunity Induced by DNA Vaccination. *Clin. Cancer Res.* 14, 3185–3192. doi:10.1158/1078-0432.CCR-08-0037

Xian, G., Zhao, J., Qin, C., Zhang, Z., Lin, Y., and Su, Z. (2017). Simvastatin Attenuates Macrophage-Mediated Gemcitabine Resistance of Pancreatic Ductal Adenocarcinoma by Regulating the TGF-β1/Gfi-1 axis. *Cancer Lett.* 385, 65–74. doi:10.1016/j.canlet.2016.11.006

Xu, T., Gao, S., Liu, J., Huang, Y., Chen, K., and Zhang, X. (2021). MMP9 and IGFBP1 Regulate Tumor Immune and Drive Tumor Progression in Clear Cell Renal Cell Carcinoma. *J. Cancer* 12, 2243–2257. doi:10.7150/jca.48664

Zhou, J., Zhang, J., and Chao, J. (2012). Porphyromonas Gingivalis Promotes Monocyte Migration by Activating MMP-9. *J. Periodontal Res.* 47, 236–242. doi:10.1111/j.1600-0765.2011.01427.x

Zitvogel, L., Galluzzi, L., Smyth, M. J., and Kroemer, G. (2013). Mechanism of Action of Conventional and Targeted Anticancer Therapies: Reinstating Immunosurveillance. *Immunity* 39, 74–88. doi:10.1016/j.immuni.2013.06.014

Conflict of Interest: The authors declare that the research was conducted in the absence of any commercial or financial relationships that could be construed as a potential conflict of interest.

Publisher's Note: All claims expressed in this article are solely those of the authors and do not necessarily represent those of their affiliated organizations, or those of the publisher, the editors and the reviewers. Any product that may be evaluated in this article, or claim that may be made by its manufacturer, is not guaranteed or endorsed by the publisher.

frontiers | Frontiers in Pharmacology

ORIGINAL RESEARCH
published: 05 April 2022
doi: 10.3389/fphar.2022.857060

Identification of a DNA Damage Response and Repair-Related Gene-Pair Signature for Prognosis Stratification Analysis in Hepatocellular Carcinoma

*Yi Chen, Mengjia Huang, Junkai Zhu, Li Xu, Wenxuan Cheng, Xiaofan Lu† * and Fangrong Yan **

State Key Laboratory of Natural Medicines, Research Center of Biostatistics and Computational Pharmacy, China Pharmaceutical University, Nanjing, China

OPEN ACCESS

Edited by:
Haitao Wang,
National Cancer Institute (NIH), United States

Reviewed by:
Yang Zhao,
Nanjing Medical University, China
Dongqiang Zeng,
Southern Medical University, China

***Correspondence:**
Xiaofan Lu
xlu.cpu@foxmail.com
Fangrong Yan
f.r.yan@163.com

†Present Address:
Xiaofan Lu,
Department of Cancer and Functional Genomics, Institute of Genetics and Molecular and Cellular Biology, CNRS/INSERM/UNISTRA, Illkirch, France

Specialty section:
This article was submitted to Pharmacology of Anti-Cancer Drugs, a section of the journal Frontiers in Pharmacology

Received: *18 January 2022*
Accepted: *24 February 2022*
Published: *05 April 2022*

Citation:
Chen Y, Huang M, Zhu J, Xu L, Cheng W, Lu X and Yan F (2022) Identification of a DNA Damage Response and Repair-Related Gene-Pair Signature for Prognosis Stratification Analysis in Hepatocellular Carcinoma. Front. Pharmacol. 13:857060. doi: 10.3389/fphar.2022.857060

Background: Nowadays, although the cause of hepatocellular carcinoma (HCC) mortality and recurrence remains at a high level, the 5-year survival rate is still very low. The DNA damage response and repair (DDR) pathway may affect HCC patients' survival by influencing tumor development and therapeutic response. It is necessary to identify a prognostic DDR-related gene signature to predict the outcome of patients.

Methods: Level 3 mRNA expression and clinical information were extracted from the TCGA website. The GSE14520 datasets, ICGC-LIRI datasets, and a Chinese HCC cohort were served as validation sets. Univariate Cox regression analysis and LASSO-penalized Cox regression analysis were performed to construct the DDR-related gene pair (DRGP) signature. Kaplan–Meier survival curves and time-dependent receiver operating characteristic (ROC) analysis curves were calculated to determine the predictive ability of this prognostic model. Then, a prognostic nomogram was established to help clinical management. We investigated the difference in biological processes between HRisk and LRisk by conducting several enrichment analyses. The TIDE algorithm and R package "pRRophetic" were applied to estimate the immunotherapeutic and chemotherapeutic response.

Results: We constructed the prognostic signature based on 23 DDR-related gene pairs. The patients in the training datasets were divided into HRisk and LRisk groups at median cut-off. The HRisk group had significantly poorer OS than the LRisk group, and the signature was an independent prognostic indicator in HCC. Furthermore, a nomogram of the riskscore combined with TNM stage was constructed and detected by the calibration curve and decision curve. The LRisk group was associated with higher expression of HBV oncoproteins and metabolism pathways, while DDR-relevant pathways and cell cycle process were enriched in the HRisk group. Moreover, patients in the LRisk group may be more beneficial from immunotherapy. We also found that *TP53* gene was more frequently mutated in the HRisk group. As for chemotherapeutic drugs commonly used in HCC, the HRisk group was highly sensitive to 5-fluorouracil, while the LRisk group presented with a significantly higher response to gefitinib and gemcitabine.

Conclusion: Overall, we developed a novel DDR-related gene pair signature and nomogram to assist in predicting survival outcomes and clinical treatment of HCC patients. It also helps understand the underlying mechanisms of different DDR patterns in HCC.

Keywords: DNA damage response and repair, hepatocellular carcinoma, prognosis, HBV, chemotherapy

INTRODUCTION

Liver cancer remains a major contributor to the global cancer burden, and it is estimated that the global incidence cases will exceed 1 million by 2025 (Llovet et al., 2021). Hepatocellular carcinoma (HCC) is the most common form of liver cancer and the fourth-highest cause of cancer mortality (Villanueva, 2019). Hepatitis B and C virus (HBV and HCV) infection, cirrhosis, metabolic diseases, and alcohol-related liver disease are the main risk factors for HCC (Tunissiolli et al., 2018). Although diagnosis and treatment have made rapid progression in HCC, the 5-year survival rates remain very low (Siegel et al., 2013). Because of the different levels of heterogeneity in HCC, particularly interpatient, intertumor, and intratumor (Hoshida et al., 2009), several prognostic biomarkers widely used in clinical practice are still far from satisfying (Liu et al., 2019). Recently, deep mining of public gene expression data tends to be an effective method to identify novel gene prognostic signatures to accurately predict HCC prognosis and guide personalized therapy for patients (Long et al., 2018; Liu et al., 2019; Liu et al., 2020).

Genomic instability has been reported as a fundamental hallmark of cancer (Negrini et al., 2010). Genomic instability refers to the high frequency of harmful changes in the genomic structure due to DNA damage response (Sahin et al., 2016). To maintain genome stability, eukaryotic cells evolve several mechanisms to detect DNA damage, present damage signals, and mediate cellular responses to eliminate the damage (Ciccia and Elledge, 2010; Pandita et al., 2013; Su et al., 2018). This process is called DNA damage response and repair (DDR). The DDR pathway is an important mechanism that consists of eight major pathways: mismatch repair (MMR), base excision repair (BER), nucleotide excision repair (NER), homologous recombination repair (HRR), checkpoint factors (CPF), nonhomologous end-joining (NHEJ), Fanconi anemia (FA), and translesion DNA synthesis (TLS) (Scarbrough et al., 2016; Song et al., 2021). Furthermore, studies have revealed that the DDR system plays an important role in tumorigenesis, tumor progression, and response to therapy (Lima et al., 2019). It is currently appreciated that tumor progression requires downregulation of DNA damage response mechanisms and an increase in genetic instability to achieve uncontrolled proliferation and adaptability to invasive tumors (Jeggo et al., 2016). For tumor treatment, genotoxic drugs have been the mainstay of cancer chemotherapy for over 30 years, which cause DNA damage exceeding the repair capacity of DDR systems (Pearl et al., 2015).

DDR pathways are found to be associated with chemotherapy resistance of HCC (Evans et al., 2016; Chen Y. et al., 2021). HCC cells strengthen their DDR ability to frustrate the DNA damage caused by chemotherapy drugs, often leading to chemotherapy resistance (Al-Hrout et al., 2018; Chen et al., 2018). Consequently, the DDR pathway may impact HCC patients' survival by influencing tumor development and therapeutic response. Recently, some studies have successfully constructed prognostic and predictive signatures based on the expression of the DDR gene (Evans et al., 2016; Sharma et al., 2019; Chen J. et al., 2021). Taken together, it is significant to explore a prognostic DDR-related gene signature to predict the outcome and characterize two different DDR pathway activity subtypes of HCC patients.

In this study, a gene-pair strategy was used to improve the robustness of the identification of the predictive signature (Eddy et al., 2010; Li et al., 2017). Univariate and Lasso-Cox regression analysis was conducted to construct a novel prognostic biomarker. We clustered HCC patients into two risk groups according to 23 DDR-related gene pairs and identified two subtypes related to prognosis and chemotherapy response. In addition, the prognostic value of our DDR-related gene pair signature was further validated in GSE14520 datasets, ICGC-LIRI datasets, and a Chinese HCC cohort (LIHC-CN). Collectively, we identified a robust signature to present new evidence into the prognostic value of the expression of DDR-related genes in HCC and explore the underlying mechanisms of DDR patterns and potential therapeutic drugs in HCC treatment.

MATERIALS AND METHODS

Data Collection and Processing

Level 3 mRNA expression, somatic mutation data, and clinicopathological data were obtained from the TCGA website (https://portal.gdc.cancer.gov/repository). A segment of copy number for the TCGA-LIHC cohort was accessed from the GDAC FireBrowse (http://firebrowse.org/). The raw count data were transferred to transcripts per kilobase of exon model per million mapped reads (TPM) data which would represent the expression of mRNA in the TCGA-LIHC cohort. After filtering mRNAs with low median absolute deviation (mad ≤0.5) across all samples and removing the samples without complete survival information, a total of 351 HCC samples were enrolled in this study. RNA-seq data, somatic mutation data, and clinical data with 240 tumor samples were downloaded from the International Cancer Genome Consortium (ICGC) portal (https://dcc.icgc.org/projects/LIRI-JP). Raw read count values were transformed into TPM values for subsequent analysis. The expression data and detailed clinical information of GSE14520 (including 219 HCC samples based on the GPL3921 platform) were downloaded from the Gene Expression Omnibus (GEO) (http://www.ncbi.nlm.nih.

gov/geo/). Additionally, a LICH-CN cohort with 159 Chinese HCC patients was downloaded for somatic mutation, clinical outcome, and transcriptome expression FPKM value from the literature (Gao et al., 2019).

Construction and Validation of the DDR-Related Gene Pair Signature

DDR-gene list including 557 genes was assembled from relevant gene lists, including MSigDB from the Broad Institute (http://www.broad.mit.edu/gsea/msigdb/) or literature (Pearl et al., 2015; Knijnenburg et al., 2018; Chen J. et al., 2021). Finally, 384 DDR genes detected in all datasets were analyzed in this study (**Supplementary Table S1**). Then, each gene pair was calculated *via* their gene expression level in each HCC sample. According to the pairwise comparison, the calculated score was 0 when the first expression level of the DDR gene was higher than that of the following DDR gene; otherwise, the calculated score was 1. DRGP scoring 0 or 1 in more than 90% of the samples were removed because they could not provide discriminative patients with different survival. The remaining DRGPs were considered as initial candidate DRGPs.

Patients were randomly divided into training and testing sets at cut-of 7:3 in the TCGC cohort. Then, a univariate Cox regression analysis was performed to identify the significant DRGPs related to overall survival (OS) if the FDR *p*-value was less than 0.05. Next, candidate DRGPs were submitted to LASSO-penalized Cox regression analysis based on package "glmnet" in R to construct an optimal prognostic signature in TCGA training datasets (Friedman et al., 2010). A DDR-related gene pair riskscore of each sample was calculated based on the lasso Cox regression model coefficients (β) multiplied with its DRGP score, as follows:

$$Riskscore = \sum_{i=1}^{n} (\beta_i \times Score_i)$$

where $Score_i$ is the relative expression of DRGPs for patient j in each cohort and β_i is the LASSO Cox coefficient of the DRGPs$_i$. Then, all patients were separated into low- (LRisk) or high-risk (HRisk) groups at the median cut-off. Kaplan–Meier survival curves were plotted for prediction of the clinical outcomes in the two groups *via* the "survival" package in R. The differences in survival were evaluated *via* the log-rank test. Time-dependent receiver operating characteristic (ROC) analysis curves were built, and the area under the curves (AUCs) for 1-, 3-, and 5-year overall survival (OS) were calculated utilizing the "survivalROC" package in R (Heagerty et al., 2000). The same method was further investigated in the TCGA testing cohort, TCGA whole cohort, GSE14520 cohort, and ICGC-LIRI cohort.

Subgroup Kaplan-Meier Survival Analysis

To explore the diagnostic capability of the DRGP prognostic signature in different levels of other clinical prognostic parameters, HCC samples in TCGA sets were stratified into different subgroups based on age (≥60 and <60), gender (female and male), TNM stage (I and II + III + IV), grade (G1+G2 and G3+G4), and *TP53* (mutation and wild). Then, cancer samples in each subgroup were clustered into HRisk and LRisk groups. The differences in prognosis between the two groups were assessed *via* Kaplan–Meier OS analysis, followed by a log-rank test.

Correlations Between the DRGP Model and Clinical Properties

To elucidate whether the prognostic model for OS is independent of other prognostic factors, we presented univariate Cox regression analysis and multivariate Cox regression survival analysis to predict the clinical outcomes of HCC patients, which was visualized *via* package "forestplot" in R. Hazard ratio (HR), 95% confidence interval (CI), and *p*-value were calculated, respectively.

Construction and Validation of Gene Prognostic Nomogram

A nomogram was constructed based on all independent prognostic parameters screened by univariate and multivariate Cox proportional hazards regression analysis to predict the probability of 1-, 3-, and 5-year OS using the "rms" package of R software. Then, we used a calibration curve to visualize the performance of the nomogram with the observed rates of the TCGA whole set at corresponding time points by a bootstrap method with 1000 resamples. Furthermore, decision curve analysis (DCA) and calibration curves were detected to check the reliability of our nomogram (Kerr et al., 2016).

Functional Enrichment Analysis

To investigate the difference in biological process between HRisk and LRisk, we performed some enrichment analysis using "GSVA" and "clusterprofiler" R packages (Yu et al., 2012; Hänzelmann et al., 2013). The infiltrating score of 24 microenvironment cell types was calculated with single-sample gene set enrichment analysis (ssGSEA) in the "GSVA" R package. Gene set enrichment analysis (GSEA) was conducted between HRisk and LRisk by using the R "clusterProfiler" package. A signature of eleven oncogenic pathways and a DDR gene list, which include eight core DDR pathways, were obtained from the literature (Pearl et al., 2015; Sanchez-Vega et al., 2018; Lu et al., 2021). Then, we used the gene set variation analysis (GSVA) method to generate enrichment scores for each cohort using the R package "GSVA". The KEGG gene sets (c2.cp.kegg.v7.4.symbols.gmt) was selected as the reference datasets, which was obtained from the MSigDB database.

Prediction of Immunotherapeutic and Chemotherapeutic Response

For immunotherapy, the tumor immune dysfunction and exclusion (TIDE) algorithm (http://tide.dfci.harvard.edu/) was applied to predict potential clinical response to immune checkpoint inhibitors (Jiang et al., 2018). Based on Genomics of Drug Sensitivity 2016 (GDSC 2016; https://www.cancerrxgene.

TABLE 1 | Coefficients of four HBV oncoproteins to the first and second principal components.

Principal components	HBV oncoproteins			
	HBVgp2_S	HBVgp3_X	HBVgp4_c	HBVgp2_pre-S1/S2
Componment1	0.62	0.57	0.34	0.41
Componment2	0.29	0.43	−0.74	−0.42

org/), the R package "pRRophetic" was applied to estimate the chemotherapeutic sensitivity by the half-maximal inhibitory concentration (IC_{50}) of each HCC sample in four cohorts. Therefore, we could investigate the different sensitivity of common liver cancer chemotherapy drugs between HRisk and LRisk. In addition, in order to identify potential drugs in HCC samples, we performed a two-step analysis to find candidate compounds as described previously (Yang et al., 2021). First, differential drug response analysis between top decile riskscore samples and bottom decile riskscore samples was conducted to verify drugs with significantly different estimated IC_{50} in two riskgroups (|log2FC| > 0.2). Next, Spearman correlation analysis was utilized to calculate the correlation coefficients between riskscore and IC_{50} of each candidate drug (|Spearman correlation coefficient| > 0.4).

HBV_{pca} Quantifies the Expression Level of HBV Virus

HBV oncoproteins were quantified for expression according to the previous study: HBVgp2_S, HBVgp3_X, HBVgp4_c, and HBVgp2_pre-S1/S2 (Xue et al., 2021). The four HBV oncoprotein expressions were identified and presented as FPKM values. To comprehensively explain the original expression level of HBV oncoproteins, we established a variable that was calculated by principal component analysis (PCA) as the previous study described (Lu et al., 2019). HBV_{pca} was derived from the first and second principal components that represented 76.73 and 17.10% of the variation in the original data, respectively. The coefficients of four HBV oncoproteins to the first and second principal components are shown in **Table 1**.

Mathematically, let E_{ij} denotes the $\log_2$(FPKM +1) value of specific oncoprotein j in sample i, and C_{jk} represents the corresponding coefficient of HBV oncoprotein (HBV_j; $j \in \{1,2,3,4\}$) for principal component k ($k \in \{1,2\}$). The HBV_{pca} can be calculated as follows:

$$HBV_{pca} = \begin{bmatrix} E_{11} & \cdots & E_{1j} \\ \vdots & \ddots & \vdots \\ E_{i1} & \cdots & E_{ij} \end{bmatrix} \begin{bmatrix} C_{11} & \cdots & E_{1k} \\ \vdots & \ddots & \vdots \\ C_{j1} & \cdots & E_{jk} \end{bmatrix} \begin{bmatrix} 0.7673 \\ 0.1710 \end{bmatrix}$$

Comprehensive Analysis of Genomic Variation Between Different DRGP Subgroups

We then investigated the genomic variation between HRisk and LRisk groups. The mutation landscape was analyzed by the R package "maftools" with the initial removal of 100 FLAGS (Mayakonda et al., 2018). The data CNV segments were detected by Genomic Identification of Significant Targets In Cancer 2.0 (GISTIC 2.0) analysis. In the process of GISTIC 2.0 analysis, except for the refgene file which was "Human_Hg19.mat", parameters were set to the default parameters. The individual fraction of genome altered (FGA), fraction of genome lost (FGL) and fraction of genome gained (FGG) for the HCC in the TCGA cohort were calculated as the study described (Lu et al., 2021). We also obtained GISTIC calls comprising −2 (deletion), −1 (loss), 0 (diploid), 1 (gain), and 2 (amplification) from GISTIC2.0 (Wu et al., 2020).

Statistical Analyses

All statistical analyses were performed with R software (version 4.1.1: http://www.r-project.org) and R Bioconductor packages in this study. Kaplan–Meier analysis with the log-rank test was used to detect differences of OS between different groups through the package "survminer" in R. Time-dependent ROC was utilized to evaluate the predictive accuracy of the DRGP riskscore through package "survivalROC" in R. Cox proportional hazards regression for estimating the hazard ratios (HRs) and 95% confidence interval (CI). Comparison of a continuous variable in two groups was performed using Wilcoxon rank-sum test. Correlation between two continuous variables was measured by Spearman's rank-order correlation. Differences in proportions were compared by the Chi-squared test or Fisher's exact test.

RESULTS

Construction and Validation of the Prognostic DDR-Related Gene Pair Signature

The clinical features of HCC samples in the training and validation sets are listed in **Supplementary Table S2**. In the training datasets of 246 patients, 85 patients died during the follow-up. As tested by the univariate Cox regression OS analysis, 459 DRGPs had significant associations with OS of HCC in the training set (all FDR p-value < 0.05). Based on LASSO-Cox regression analysis, 23 DRGPs were independently related to the prognosis of HCC (**Figures 1A,B**). Among them, 11 gene pairs were risk factors for HCC prognosis (HR > 1). **Supplementary Table S3** lists the 23 selected gene pairs and their coefficients. The regression coefficients and DRGP score of these 23 gene pairs in each sample were used to calculate the riskscore in each HCC cohort.

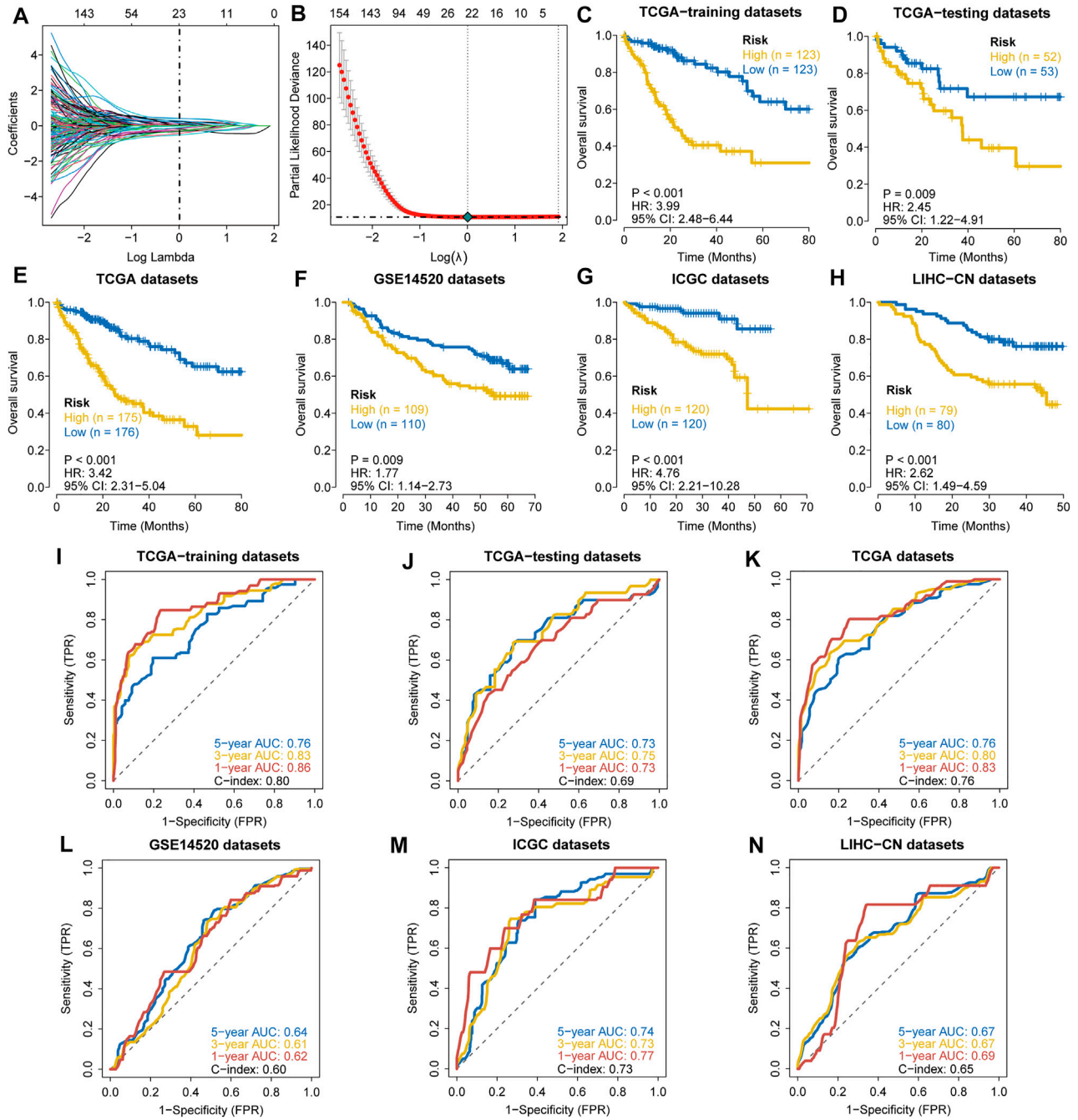

FIGURE 1 | Construction and validation of a prognostic DDR-related gene pair signature. **(A,B)** LASSO regression identified 23 DRGPs. **(C–H)** The Kaplan–Meier overall survival (OS) curves in the TCGA training datasets **(C)**, TCGA testing datasets **(D)**, TCGA datasets **(E)**, GSE14520 datasets **(F)**, ICGC datasets **(G)**, and LIHC-CN datasets **(H)** show that patients in the HRisk group have a poorer prognosis. **(I–N)** ROC curves show the predictive efficiency of the signature for patients in the TCGA training datasets **(I)**, TCGA testing datasets **(J)**, TCGA datasets **(K)**, GSE14520 datasets **(L)**, ICGC datasets **(M)**, and LIHC-CN datasets **(N)** on the survival rate.

The patients in the training datasets were divided into HRisk or LRisk groups at median cut-off. Kaplan-Meier survival analysis indicated that the HRisk group have a poorer OS than the LRisk group (hazard ratio (HR) = 3.99, 95% CI = 2.48–6.44, *p*-value < 0.001, **Figure 1C**). The values of AUC are 0.76, 0.83, and 0.86 at 1-, 3-, and 5-year follow-up, respectively (**Figure 1I**), showing that the signature displays good sensitivity and specificity. The C-index of the DRGP model is 0.80. To determine the predictive ability of this prognostic model, we calculated individual riskscore with the aforementioned method and classified the patients in TCGA-testing set, TCGA whole set and other validation sets into HRisk and LRisk groups. Similarly, we

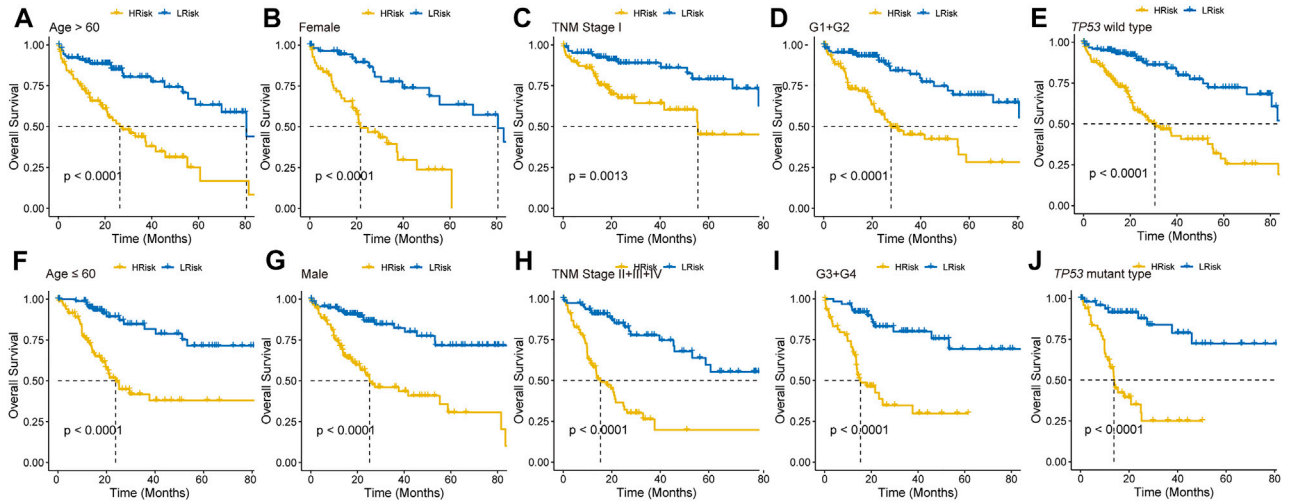

FIGURE 2 | Kaplan–Meier curves analyses of different clinical subgroups in TCGA cohort. Patients were classified into **(A)** Age >60 years, **(B)** Gender: Female, **(C)** TNM stage: I, **(D)** Grade: G1+G2, **(E)** *TP53* wild type, **(F)** Age ≤60 years, **(G)** Gender: Male, **(H)** TNM stage: II + III + IV, **(I)** Grade: G3+G4, and **(J)** *TP53* mutant type.

validated the prediction of signature in these datasets. Consistent with the above findings, the HRisk patients in all cohorts have a markedly shorter OS than those in the LRisk group (**Figures 1D–H**). The AUCs of ROC curves for 1-,3-, and 5- year OS are shown in **Figures 1J–N**.

Independent Prognostic Role of the DRGP Signature

To further explore the clinical potentiality of the prognosis model in HCC, stratified analysis based on these clinical characteristics was conducted. As shown in **Figures 2A–J** and **Supplementary Figure S1**, Kaplan–Meier OS curves also showed that HRisk patients had considerably worse OS than LRisk patients, which further indicated the excellent prediction of the DRGP model. We further analyzed whether the riskscore was an independent prognostic predictor for OS. In univariate Cox regression analyses, high riskscore was significantly associated with shorter OS in TCGA cohort (HR = 3.22, 95% CI = 2.53–4.13, p-value < 0.001, **Figure 3A**) According to the multivariate Cox regression analysis results, we considered the TNM stage (HR = 1.27, 95% CI = 1.00–1.61, p-value = 0.0515) and riskscore (HR = 2.96, 95% CI = 2.29–3.83, p-value < 0.001] are both independent prognosis factors for TCGA (**Figure 3A**). The independence of the DRGP signature for HCC prognosis was also confirmed in GSE14520, ICGC, and LIHC-CN cohorts (**Figures 3A,B**). Collectively, the signature was an independent prognostic factor for HCC.

Construction and Verification of a Prognostic Prediction Nomogram for HCC

We constructed a nomogram based on multivariate Cox regression analysis for prediction of the 1-, 3-, and 5-year survival probability in TCGA datasets (**Figure 3C**). As shown in the calibration chart (**Figure 3D**), the nomogram could robustly predict OS for HCC patients. Moreover, the DCA curve suggested that riskscore was more beneficial when compared with the TNM stage alone (**Figure 3E**). The DCA curve demonstrated that the net benefit of the combined model was comparable to the riskscore. These results showed that the nomogram built with the combined model might help clinical management.

LRisk Group Associated With Higher HBV Virus Expression and Higher Proportion of TIDE-Predicted Responders

A previous study indicated that the high expression of HBV16 E6/E7 was significantly linked to a favorable prognosis because the inflammatory/immune response of the host may be stimulated (Lu et al., 2019). To investigate whether HBV oncoproteins were differentially expressed between two risk groups in HCC, we calculated the HBV_{pca} by principal component analysis (PCA) based on the FPKM value of four HBV oncoproteins in the TCGA cohort. In our study, 96 HVB-infected HCC patients were identified, the first and second principal components were used since they covered almost the variations (93.83%; **Figure 4A**). We found a significant difference in HBV virus expression between HRisk and LRisk (Wilcoxon test, p = 0.018, **Figure 4B**), and HBV_{pca} has also observed a mildly negative correlation with riskscore (R = −0.280, p = 0.006, **Figure 4C**). It means a high level of HBV_{pca} corresponds to low risk in HCC patients.

To evaluate the tumor immune microenvironment in different groups, a ssGSEA method was used to estimate the infiltration levels of the 24 types of immune cells. The ssGSEA score and immune cell types which were differentially infiltrated between LRisk and HRisk groups in the TCGA set are presented in **Figure 4D**. The proportion of 24

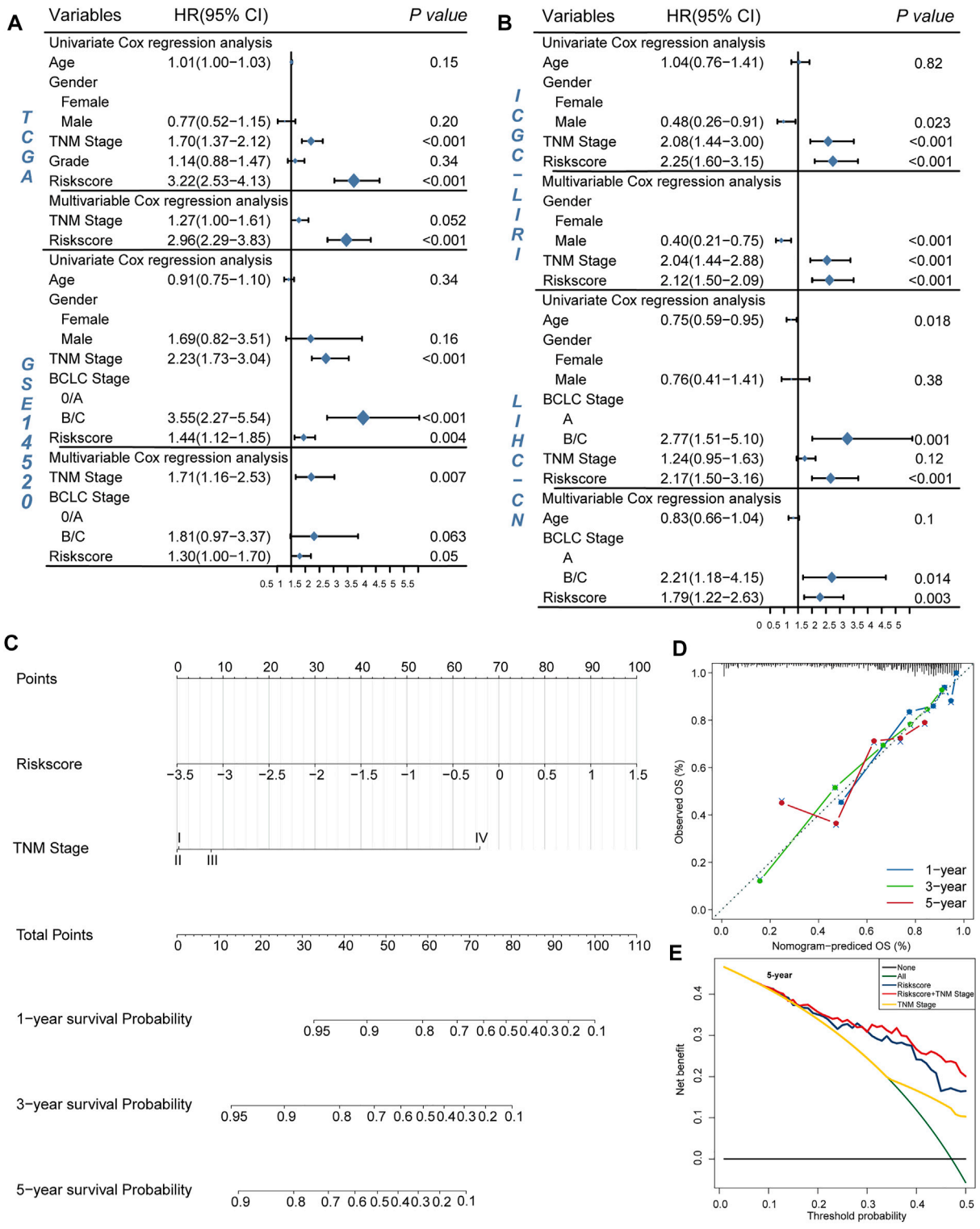

FIGURE 3 | Validation of the independency of the riskscore for prediction of HCC prognosis. **(A,B)** Univariate and multivariate cox regression survival analysis validated riskscore was an independent prognosis factor for HCC patients in TCGA datasets **(A)**, GSE14520 datasets **(A)**, ICGC datasets **(B)**, LIHC-CN datasets **(B)**. The *p*-value, hazard ratio (HR), and 95% confidence interval (CI) were indicated in the forest plots. The blue circle represents the value of HR each parameter scored. **(C,E)** Construct nomogram for survival prediction. **(C)** which integrated with two independent prognosis factors for predicting the probability of patient mortality at 1-, 3-, or 5-year OS. **(D)** The calibration plots for predicting patient 1-, 3-, or 5-year OS. **(E)** DCA curves for two independent prognostic factors or a combination of them in OS prediction.

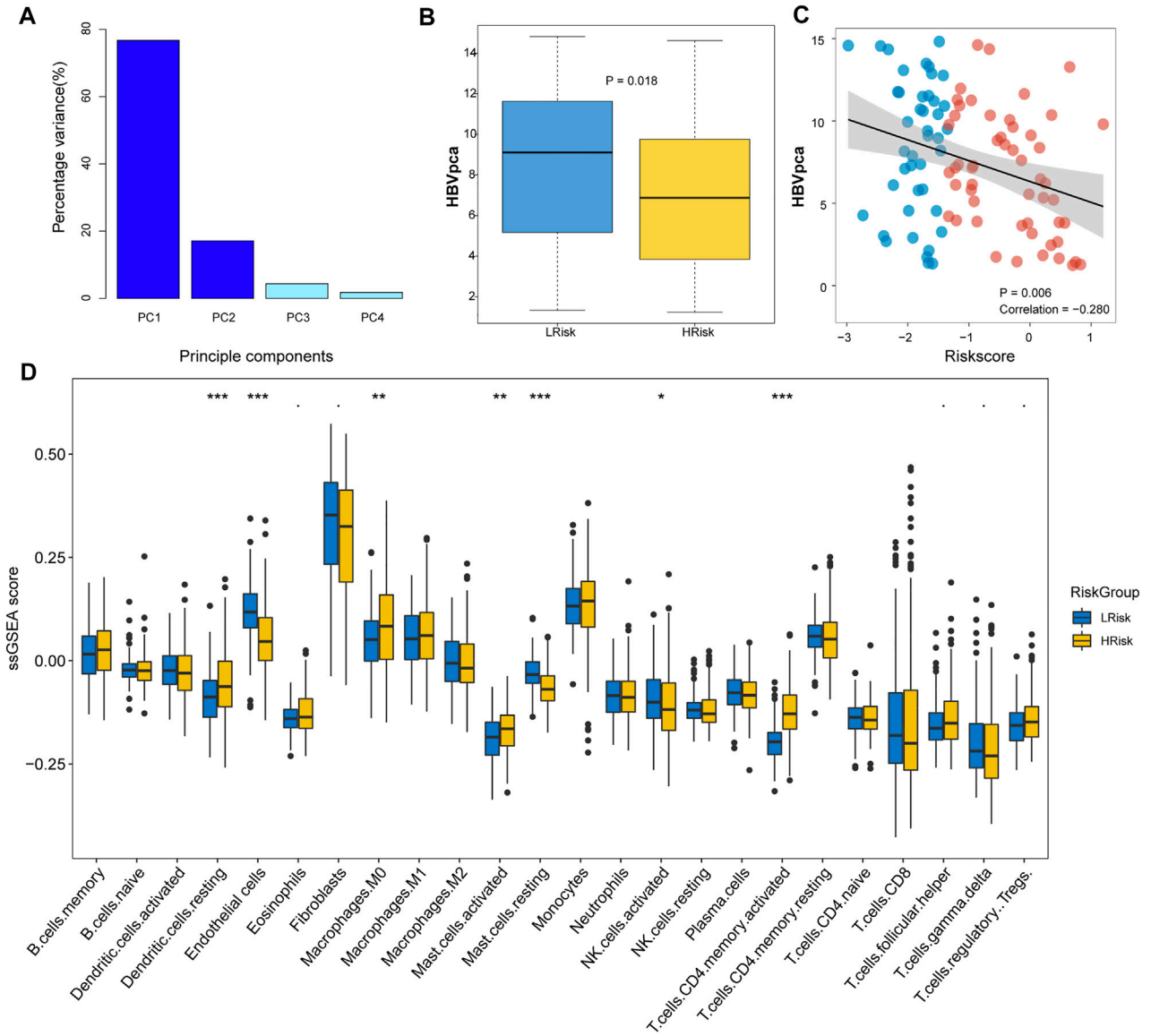

FIGURE 4 | Immune infiltration and HBV_{pca} score between HRisk and LRisk group in TCGA cohort. **(A)** Barplots showing that the first and second principal components present almost all the variations with a summing percentage of 93.83%. **(B)** Boxplot showing HBV_{pca} difference in the HRisk and LRisk groups (Wilcoxon test, $p = 0.018$). **(C)** Spearman correlation analysis between HBV_{pca} and riskscore ($R = -0.280$, $p = 0.006$). **(D)** Boxplot for TCGA cohort showing the enrichment level of 24 microenvironment cell types between HRisk (yellow) and LRisk (blue) groups. Statistical p values were calculated by the Wilcoxon test and represented by. < 0.1, * <0.05, ** <0.01, and *** <0.001.

immune cells in each group is shown in a bar plot. The results revealed that the level of infiltration of dendritic.cells.resting, macrophages.M0, mast.cells.activated, and T.cells.CD4.memory.activated in the HRisk group was significantly higher than that in the LRisk group, while the level of endothelial cells, mast.cells.resting, and NK cells.activated in the LRisk were higher than that in the HRisk group. For further investigating the immune landscape of different risk groups reflected by the DRGP signature, validation cohorts GSE14520, ICGC, and LIHC-CN were also calculated by ssGSEA to verify the differences in risk groups at the immune level (**Supplementary Figure S2**).

We also detected and compared the expression levels of several immune checkpoints between the LRisk and HRisk groups. Results showed that the mRNA expression levels of CTLA4, PDCD1, and TIGIT were consistently overexpressed in the HRisk in TCGA and ICGC datasets (**Figure 5A**), but we could not observe a significant difference in GSE14520 and LIHC-CN cohorts (both, $p > 0.05$, not shown). These results suggested that the HRisk group may contribute to tumor immune dysfunction and immune exclusion in HCC. To investigate whether LRisk

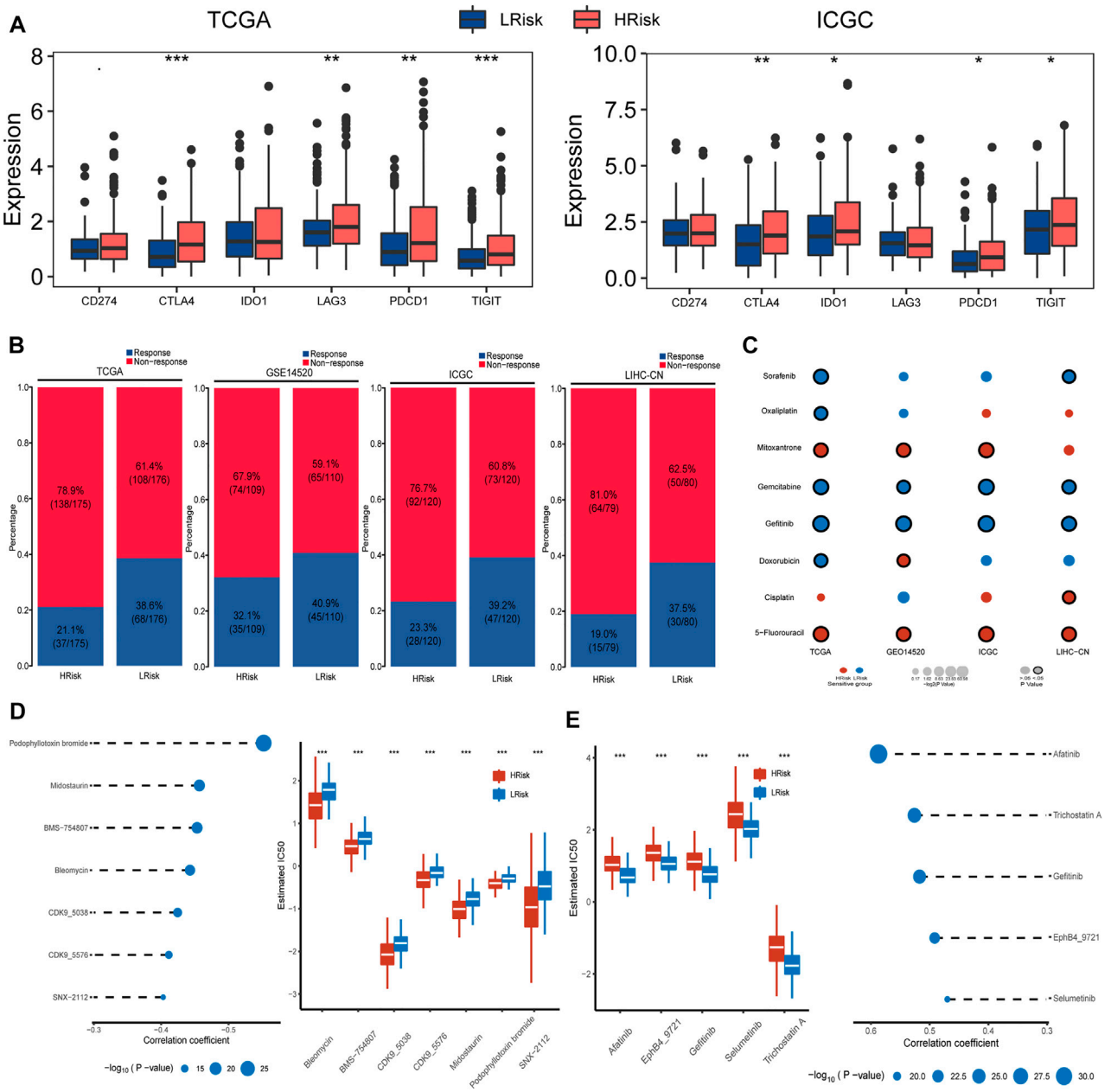

FIGURE 5 | Differential sensitivity to immunotherapy and chemotherapies between HRisk and LRisk. **(A)** Boxplot for TCGA and ICGC cohort showing the different expression levels of six immune checkpoint genes between riskgroups. Statistical *p* values were calculated by the Wilcoxon test and represented by. < 0.1, * <0.05, ** <0.01, and *** <0.001. **(B)** Barplots revealed that LRisk might be more likely to response to immunotherapy than HRisk in TCGA (Chi-square test, $p < 0.001$), GSE14520 (Chi-square test, $p = 0.23$), ICGC (Chi-square test, $p = 0.012$), and LIHC-CN (Chi-square test, $p = 0.016$) cohorts, respectively. **(C)** Bubble plot showing the drug sensitivity for eight commonly used chemotherapeutic drugs in liver cancer between HRisk and LRisk across four cohorts, where red and blue bubbles show that either HRisk or LRisk group is more sensitive to a drug according to the corresponding mean value of predicted IC_{50}; and a black circle wrapped around the bubble presents whether a statistically significant difference is achieved. Statistical *p* values were calculated by the Wilcoxon test. **(D)** The results of Spearman's correlation analysis and boxplots for the distribution of seven HRisk sensitivity drugs response analyses in TCGA datasets. **(E)** The results of Spearman's correlation analysis and boxplots for the distribution of five LRisk sensitivity drugs response analyses in TCGA datasets.

responds to immune checkpoint inhibits, we harnessed the TIDE algorithm to predict the potential response to immunotherapy in different groups. The higher TIDE score represented less promising treatment for response to immunotherapy. In our results, the HRisk group contained lower proportion of TIDE-predicted responders than LRisk group in all four cohorts (TCGA ($p < 0.001$), GSE14520 ($p = 0.23$), ICGC ($p = 0.012$), and LIHC-CN ($p = 0.016$); **Figure 5B**). These results suggest that HCC patients in LRisk might be more beneficial from immune checkpoint inhibitors.

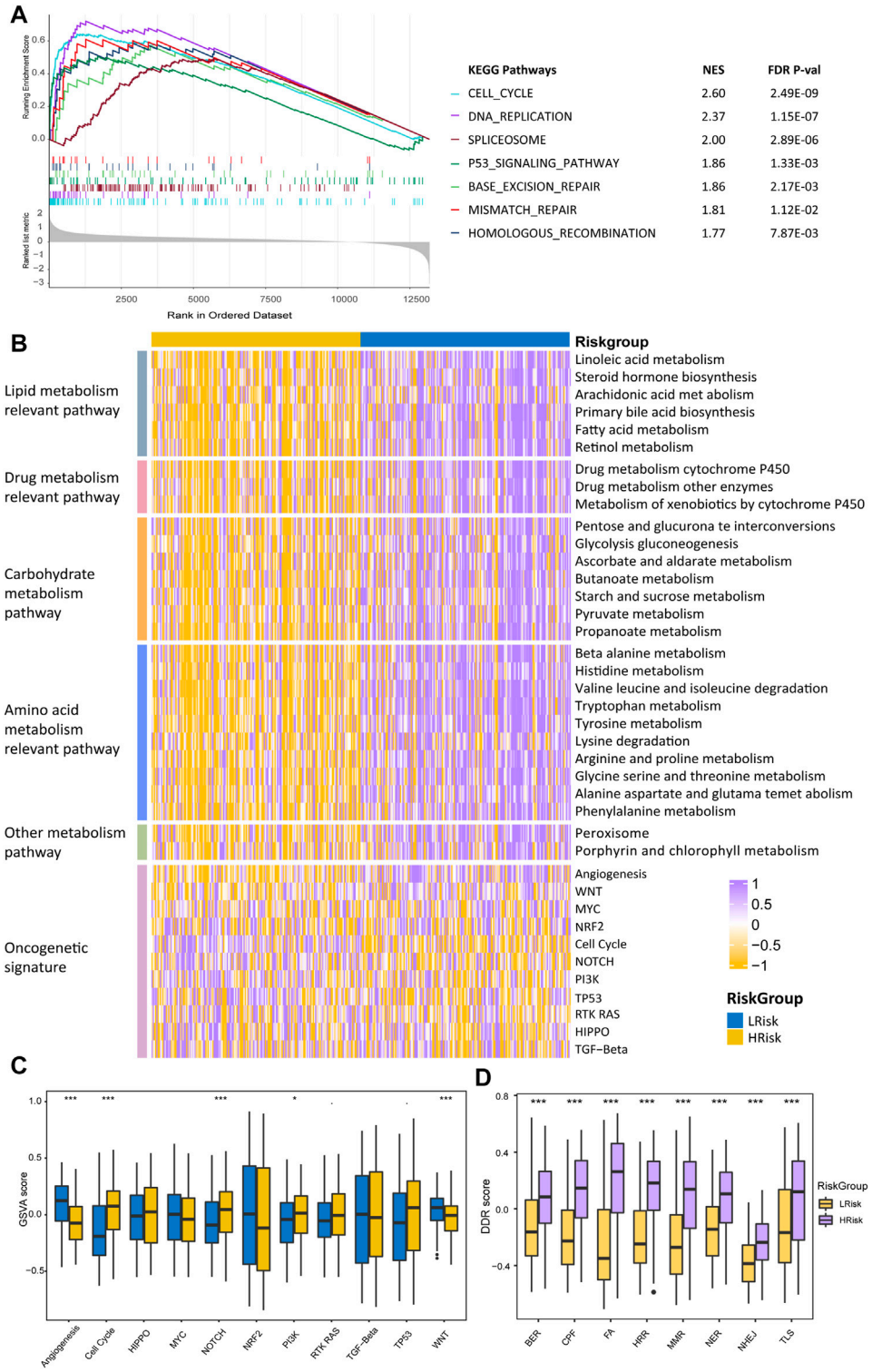

FIGURE 6 | Differentially functional pathways between the HRisk and LRisk group in TCGA. **(A)** GSEA identified upregulated pathways in HRisk. **(B)** Heatmap of enrichment level calculated by GSVA for metabolism-related pathways derived from GSEA and oncogenic pathways. **(C,D)** Boxplot of oncogenic pathways **(C)** and DDR pathways **(D)** from GSVA of two riskgroups. Statistical *p* values were calculated by the Wilcoxon test and represented by. < 0.1, * <0.05, ** <0.01, and *** <0.001.

Prediction the Sensitivity and Chemotherapy

Considering that chemotherapy is a common way to treat liver cancer, we first verify whether the DDR patterns groups may affect the sensitivity of chemotherapeutic drugs commonly used for treating liver cancer (including cisplatin, 5-fluorouracil, gemcitabine, oxaliplatin, doxorubicin, mitoxantrone, gefitinib, and sorafenib). We found that HRisk groups of all four HCC cohorts were highly sensitive to 5-fluorouracil (all, $p < 0.05$; **Figure 5C**, **Supplementary Figure S3**), and four LRisk groups presented with a significantly higher response to gefitinib and gemcitabine (all, $p < 0.05$; **Figure 5C**, **Supplementary Figure S3**). Next, we performed a two-step analysis to find potential therapeutic compounds. Eventually, the analysis obtained seven compounds (including CDK9_5576, CDK9_5038, bleomycin, midostaurin, SNX-2112, BMS-754807, and podophyllotoxin bromide) that had lower IC_{50} in HRisk and a negative correlation with riskscore (**Figure 5D**, **Supplementary Figure S4**) across four datasets and five compounds (including trichostatin A, gefitinib, afatinib, selumetinib, and EphB4_9721) were observed to present a significant response to LRisk and a positive correlation with riskscore (**Figure 5E**, **Supplementary Figure S4**).

Characterization of the HCC Riskgroups Regarding Different Functional Pathways

To better characterize the two HCC riskgroups, differential analyses were performed. Gene set enrichment analysis (GSEA) was conducted using the "clusterProfiler" package, and enrichment differences of pathways were significant if the FDR p-value < 0.15 and |NES| >1 in all four cohorts. The results indicated that 28 metabolism-relevant pathways were significantly upregulated in LRisk, while HRisk enriched in cell cycle, DNA replication, spliceosome, and DDR-relevant pathways (**Figure 6A**). Thus, the HRisk group presents upregulated cell cycle procession and DDR pathways which might contribute to the hyperproliferation and development of tumor cells. Pathway with significant differences in enrichment in all four cohorts was considered subclass specific pathway. GSVA was conducted to quantify and visualize the enrichment of 28 metabolism-related pathways which were classified into four specific metabolism signatures, including lipid metabolism relevant pathway, drug metabolism relevant pathway, carbohydrate metabolism relevant pathway, and amino acids metabolism relevant pathway (**Figure 6A**). Results confirmed that the LRisk group has significant upregulation of metabolism signatures, consistent with the results from GSEA.

To further investigate the activation of oncogenic pathways among HRisk and LRisk (**Figure 6C**), We found that the cell cycle oncogenic pathway was significantly activated in HRisk, while LRisk had a higher score of angiogenesis and Wnt activation-relevant pathways than HRisk (**Figure 6D**). Considering that the risk groups were divided based on DDR-relevant genes signature, we then decided to further explore whether different characteristics exist in distinct DDR pathways. Eight DDR core pathways were quantified using the GSVA algorithm. HRisk group exhibited higher expression for all eight pathways than LRisk. The same results were demonstrated in cohorts GSE14520, ICGC, and LIHC-CN (**Supplementary Figures S5–S7**).

Relationship Between Riskscore and Somatic Mutation and Copy Number Variation

We finally investigated the genomic variations between two different risk groups in the TCGA cohort. To analyze whether differences exist in the somatic variations (10%) of HCC between two riskgroups, R package "maftools" was used (**Figure 7A**). The results showed that the HRisk group had significantly high *TP53* mutations and less *CTNNB1* mutations than the LRisk group (*TP53*: 46.3 *vs.* 12.5%, $p < 0.001$; *CTNNB1*: 17.7 *vs.* 31.8%, $p = 0.007$; **Figure 7B**), and we obtained consistent results in ICGC cohort (*TP53*: 51.7 *vs.* 18.8%, $p < 0.001$; *CTNNB1*:35.0 *vs.* 41.9%, $p = 0.2883$; **Figure 7B**) and LIHC-CN cohort (*TP53*: 73.4 *vs.* 43.8%, $p < 0.001$; *CTNNB1*: 17.7 *vs.* 21.2%, $p = 0.5439$; **Figure 7B**), respectively. Mutation in *TP53* is the most common genetic change in HCC, and patients with mutated *TP53* have shorter OS than those with wild-type *TP53*. Therefore, we conducted special subgroup analyses stratifying samples according to the combination of *TP53* mutation status and riskgroups. We found that some patients with mutant type *TP53* in the HRisk group had significantly shorter OS than those with mutant wild *TP53* in the HRisk group ($p = 0.89$ in TCGA, $p = 0.58$ in ICGC, $p = 0.34$ in LIHC-CN; **Figure 7C**), while patients with mutant type in the LRisk group had longer OS than those with wild type in the HRisk group ($p = 0.0028$ in TCGA; **Figure 7C**), but no significance could be calculated in ICGC and LIHC-CN datasets ($p = 0.58$ in ICGC, $p = 0.40$ in LIHC-CN; **Figure 7C**). These results confirm again that the prognosis model is robust and superior. Unfortunately, we could not find the mutation data of GSE14520.

Copy number variations were a common form of genomic structural change, and an amount of research has demonstrated chromosomal abnormalities play key roles in HCC. GISTIC 2.0 was used to analyze the copy number of HRisk and LRisk in TCGA-HCC samples. We first calculate the FGA, FGL, and FGG scores to evaluate differences in chromosomal instability between the two risk groups. We found the LRisk group had significantly lower copy number loss or gain than HRisk, so it was obvious that LRisk had better chromosomal stability than HRisk (all, $p < 0.001$; **Figure 8B**). Next, we analyzed the copy number in different specific regions in LRisk and HRisk groups. The most frequent arm-level aberrations in the HRisk group identified were 13q, 11q, 4q, etc., for copy number loss, and significantly amplified regions in the HRisk were 1q, 8q, 3q, etc. (**Figure 8A**). Therefore, we decided to further explore the relationship between the copy number variations of specific DDR genes. The relationship between genes in eight core DDR pathways and their copy number alterations were calculated by Spearman analyses. The GISTIC calls of 38 DDR genes ($R < -0.2$ or $R > 0.2$) are shown in **Figure 8C**, and the corresponding expression of DDR genes are shown in **Figure 8D**. These results suggest that HRisk existed

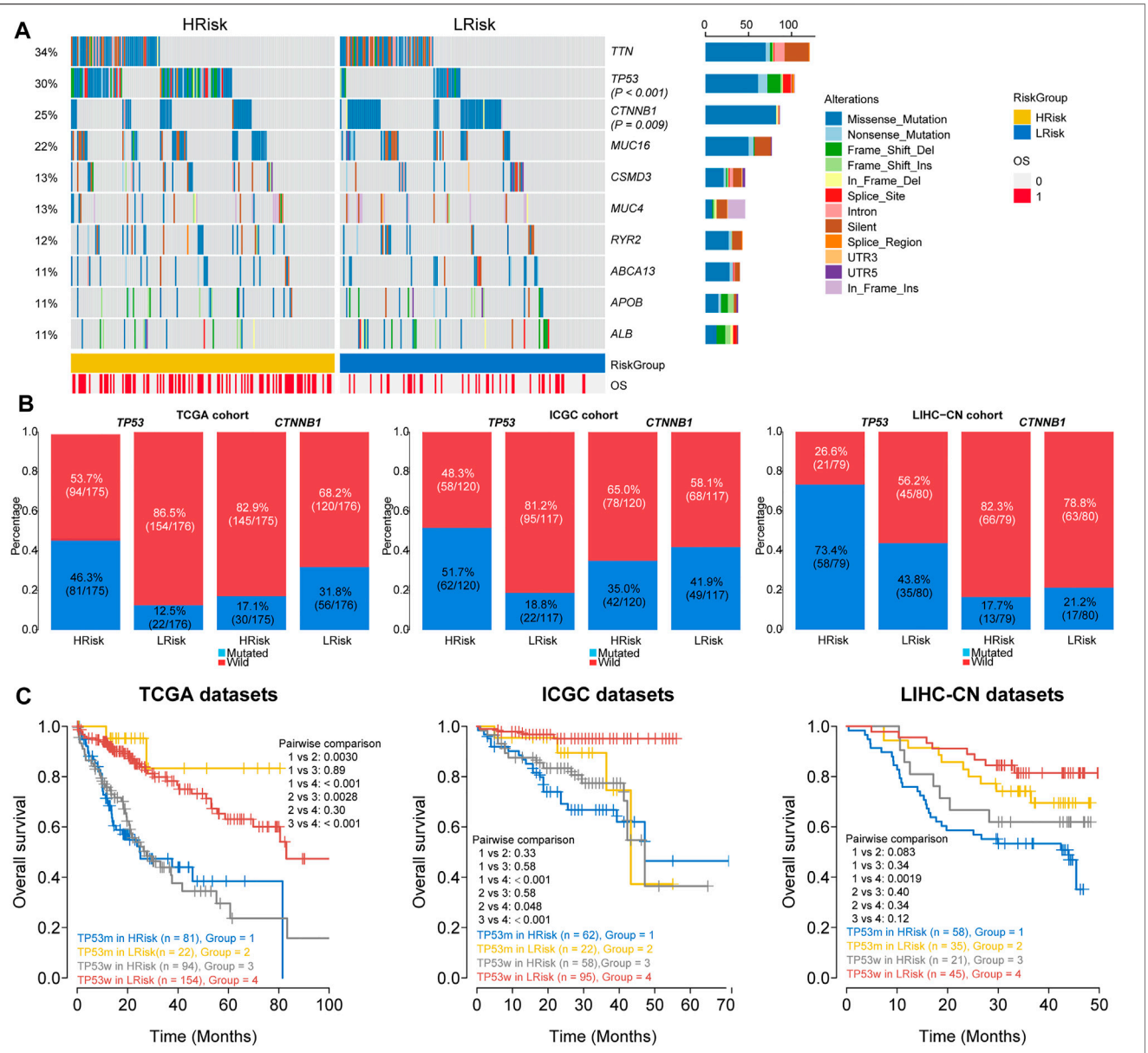

FIGURE 7 | Analysis of mutation characteristics in HRisk and LRisk. **(A)** Oncoprint showing the mutational landscape of mutations with mutated greater than 10% in TCGA-HCC. Mutations of *TP53* and *CTNNB1* were significantly mutated in HRisk (Fisher's exact test, $p < 0.001$) and LRisk (Fisher's exact test, $p = 0.009$) groups, respectively. **(B)** Barplots showing the similar distribution of *TP53* and *CTNNB1* mutation between two riskgroups in TCGA cohort (*TP53*: 46.3 *vs*. 12.5%, $p < 0.001$; *CTNNB1*: 17.7 *vs*. 31.8%, $p = 0.007$), ICGC cohort (*TP53*: 51.7 *vs*. 18.8%, $p < 0.001$; *CTNNB1*:35.0 *vs*. 41.9%, $p = 0.2883$), and LIHC-CN cohort (*TP53*: 73.4 *vs*. 43.8%, $p < 0.001$; *CTNNB1*: 17.7 *vs*. 21.2%, $p = 0.5439$), respectively. **(C)** Kaplan–Meier curve analysis of overall survival is shown for patients classified according to *TP53* mutation status and the riskgroup in three cohorts. TP53w, *TP53*-sequence wild type; TP53m, *TP53*-sequence mutant type.

higher levels of copy number alterations, and both were associated with overexpression of DDR genes.

DISCUSSION

HCC remains a major public health concern in the world. Although continuous achievements in early detection, multimodal therapy, and surgery resection, the mortality is still high (Siegel et al., 2013). Additionally, an effective prognostic signature is very important for the prediction and individualized treatment of HCC. The DDR process is often exaggerated in HCC and affects the tumor development and therapeutic response of HCC patients. As a previous study, Li et al. has developed a seven-gene signature related to the DNA repair process to predict the prognosis of HCC (Li et al., 2019). Hence, it is of significance to construct a prediction model based on the expression profiles of DDR-related gene expression.

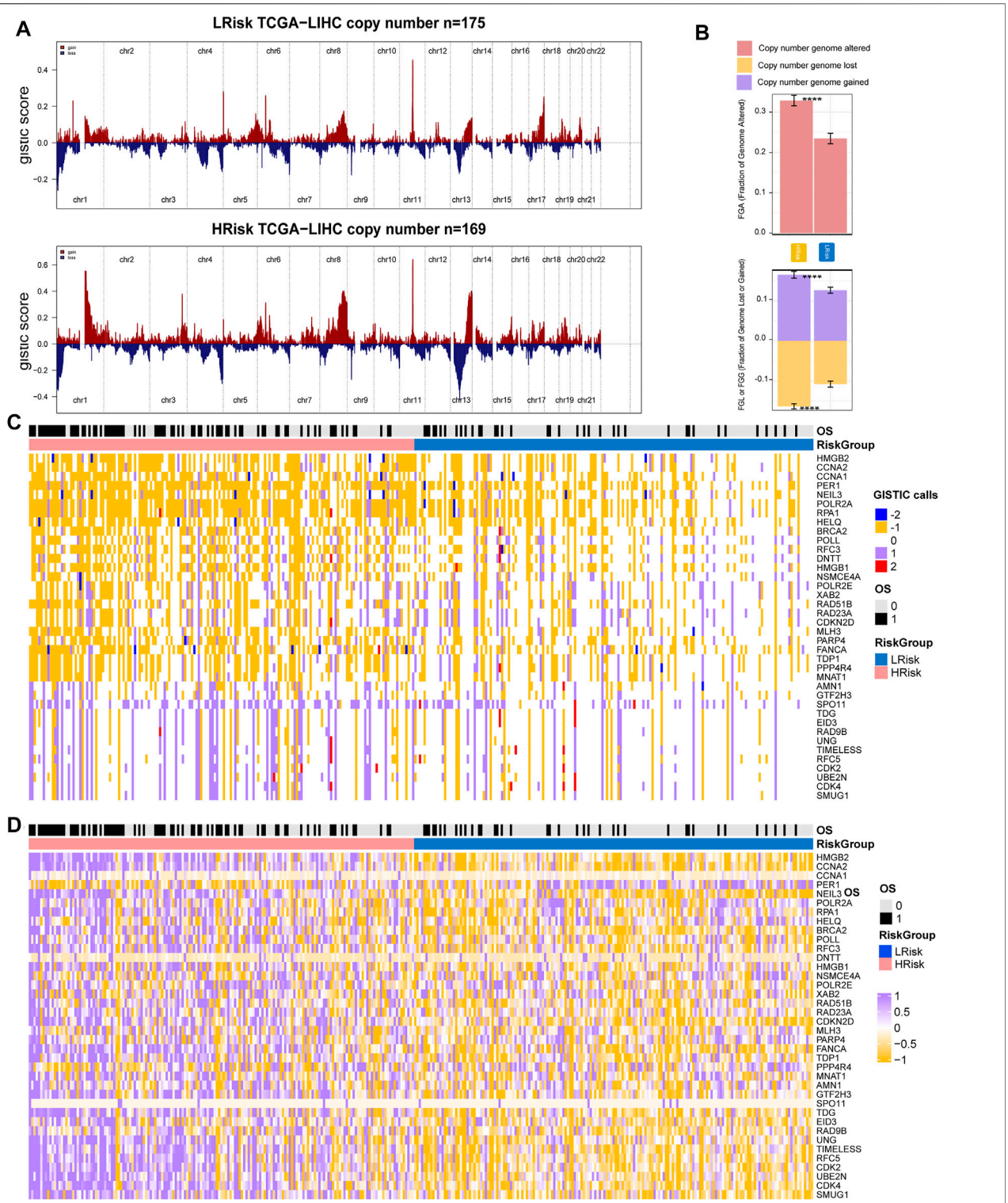

FIGURE 8 | Integrative analysis of copy number alteration and gene expression profiling. **(A)** Copy number gains and deletions identified by GISTIC2.0 in HRisk and LRisk. **(B)** Distribution of fraction genome altered (FGA) and fraction genome loss/gain (FGG/FGL). Bar charts are presented as the mean ± standard error of the mean. **(C)** Heatmap of GISTIC calls of 38 DDR genes. **(D)** Heatmap showing the overexpression pattern of 38 DDR genes.

In this study, we built and validated a robust 23 DDR-related gene pair signature for HCC patients' prognosis and precise treatment. The prognostic model was validated in the dependent TCGA, GSE14520, ICGC-JP, and LIHC-CN cohorts. We divided the HCC patients in each cohort into HRisk and LRisk according to the median cutoff of riskscore. Patients in the LRisk group had significantly longer OS than that in the HRisk group. The signature also demonstrated to be an independent risk factor for OS in HCC patients in four cohorts. Furthermore, subgroup analyses showed that the prognostic model could predict the outcomes of patients in different subgroups. The nomogram-integrated TNM stage and riskscore was established, which proved to be a better predictor than the TNM stage alone. These advantages could be helpful to make clinical decisions and make nomograms a superior tool for predicting prognosis.

Hepatitis B virus (HBV) is associated with the rapid progression of HCC, and its viral load has an adverse effect on overall survival (Yu and Kim, 2014). Studies have found that high HBV viral expression may stimulate the immune response in cervical cancer and favored the patient clinical outcome (Lu et al., 2019). In our study, we compressed the expression of four HBV oncoproteins into a comprehensive PCA-based score, HBV_{pca}. 96 HBV-associated HCC patients in the TCGA cohort, while 43 patients in the LRisk group had a higher HBV viral load than those in the HRisk group. These results indicated that high HBV viral expression is significantly associated with a better prognosis, which is similar to the previous study. Then, we used the ssGSEA algorithm to analyze the immune infiltration between HRisk and LRisk. Although analysis of ssGSEA did not suggest significant greater levels of immune cell infiltrates in the LRisk group, we found that the LRisk group might be more beneficial from checkpoint blockade. The HBV genome can encode the four proteins, which include S, X, C, and P (Yang et al., 1995). There are extensive interactions between the HBV genome and the DDR pathway (Lee et al., 1995). Several findings suggest that HBV viral expression could disrupt the DNA repair pathways of infected hepatocytes (Ko and Ren, 2011; Ricardo-Lax et al., 2015; Schreiner and Nassal, 2017). For example, the hepatitis B virus X protein (HBx) is known to be a multifunctional protein encoded by HBV, playing a pivotal role in the development of viral-induced liver cancer (Becker et al., 1998). HBx might disturb several key cellular processes such as cell cycle, DNA repair, oxidative stress, transcription, protein degradation, signal transduction, and apoptosis. In some cases, components of the DDR network may be antiviral and have detrimental impacts on viral replication (Luftig, 2014; Weitzman and Fradet-Turcotte, 2018). In this study, HCC patients in the TCGA cohort were differentiated into two groups based on DDR-related gene expression profiles which showed different DDR patterns. HRisk group presented upregulated DDR-relevant pathway and cell cycle process, so we speculate DDR pathway might have interrupted the replication cycle of HBV proteins in HRisk so that the LRisk group have a higher HBV expression level was observed.

GSEA showed core DDR-related pathways (base excision repair, mismatch repair, homologous recombination), cell cycle, DNA replication, spliceosome, and p53 signaling pathway were distinctly enriched in HRisk. Patients in the DDR-activated subgroup were significantly related to the inferior prognosis. We also found several significant alterations of molecular characteristics between HRisk and LRisk groups. Common somatic changes include mutations p53 and beta-catenin are frequently detected repeatedly in HCC, resulting in activation of the Wnt signaling pathway and dysregulation of the cell cycle, respectively (Jacobs and Norton, 2021). *TP53* is the most frequently mutated in HCC, and patients with *TP53* mutations had a poorer prognosis compared with patients with wild-type *TP53* (Villanueva and Hoshida, 2011). We observed that the *TP53* gene was more frequently mutated in the HRisk. In contrast to the *TP53* gene, a larger proportion of LRisk carried *CTNNB1* mutations. *CTNNB1* mutations in HCC were mutually exclusive with *TP53* (Calderaro et al., 2017), and mutation-induced activation of *CTNNB1* expression is the dominant cause of Wnt activation (Takagi et al., 2008). In addition, LRisk had a significantly higher score of Wnt activation-relevant signature, which may be activated by mutated *CTNNB1*. LRisk group was significantly involved in many metabolism pathways, including lipid metabolism, drug metabolism, carbohydrate metabolism, and amino acid metabolism relevant pathways, indicating that patients in the LRisk group hold a normal metabolic process (e.g., fatty acid, gluconeogenesis, and histidine) of liver and the activation of metabolism relevant signatures is associated with a favorable prognosis in patients. These findings are in keeping with a previous proteogenomics study, which proved that *CTNNB1*-mutated tumor was concentrated with various metabolic processes, including amino acid metabolism, glycolysis/gluconeogenesis, and drug metabolism (Gao et al., 2019). Along with mutations, chromosomal abnormalities are frequent genetic events in HCC (Schulze et al., 2016). In particular, broad genomic deletions have been noted for 1p, 4q, 6q, 8p, 13q, 16p, and 17q and gains for 1q, 6p, 8q, 17q, and 20q (Jacobs and Norton, 2021). We found that HRisk had significantly higher copy number alterations than LRisk, suggesting that HRisk existed a deeper degree of chromosomal instability. Somatic copy alterations (SCNAs) are widespread in human cancers that promote tumor initiation and progression (Beroukhim et al., 2010). Higher levels of SCNAs are associated with an increased expression level of the cell cycle (Davoli et al., 2017). Our results indicated that the HRisk group with a significantly higher cell proliferation signature is related to higher SCNA levels of DDR genes and expression. Altogether, our study provides a comprehensive overview of molecular characteristics between HRisk and LRisk.

Although there are several therapeutic options for HCC, chemotherapy is one of the most important treatment modalities for advanced HCC. However, the efficacy of chemotherapy remains unsatisfactory, so it is necessary to identify a signature to better predict chemotherapy responses of HCC patients. Interestingly, the two groups had different sensitivity to common chemotherapy for treating HCC. Potential drugs for HRisk and LRisk patients were then investigated. Cyclin-dependent kinases provided by a family of

serine kinases primarily control the eukaryotic cell cycle (Aprelikova et al., 1995). Both CDK9_5038 and CDK9_5576 are CDK9 inhibitors. Bleomycin is classified as an "antitumor antibiotic" drug, and the drug works by binding to DNA that could generate lesions on both strands of DNA (Chen and Stubbe, 2005). The epidermal growth factor receptor (EGFR) plays a central role in the development and progression of different cancers. Afatinib and gefitinib are the currently available EGFR-tyrosine kinase inhibitors (EGFR-TKIs), which have been approved so far for non-small cell lung patients. In this study, patients in HRisk may be more sensitive to CDK9 inhibitors and Bleomycin, while patients in LRisk may be more sensitive to EGFR-TKIs, which should be validated in future clinical trials.

There are several limitations to our study. First, although our research was validated by other independent cohorts, they were all retrospective data. Second, highly heterogeneous, intratumoral heterogeneity in HCC might have an impact on the DRGP riskscore in each tumor, so its significance for clinical translation therapy needs to be further confirmed. Moreover, we determined several drugs that have different sensitivity in HCC patients. However, investigations about the antitumor effects of some drugs are lacking.

CONCLUSION

A signature based on the 23 DDR-related gene pairs was successfully constructed, which stratifies HCC patients into two riskgroups with different survival outcomes. Enrichment analysis, CNV, gene mutation, and tumor immune environmental analyses were conducted between HRisk and LRisk. The prediction of therapy sensitivity may be helpful to clinicians in selecting patients that could benefit from further treatments. These findings may provide a novel prognostic signature for HCC from a DDR perspective and enhance biological understanding and clinical strategies in HCC.

DATA AVAILABILITY STATEMENT

The datasets presented in this study can be found in online repositories. The names of the repository/repositories and accession number(s) can be found in the article/ **Supplementary Material**.

AUTHOR CONTRIBUTIONS

Conception and design: FY and XL. Collection and assembly of data: YC and MH. Analysis of data and statistical analysis: YC, JZ, and LX. Drafting the manuscript: YC, MH, and WC. Revision of the manuscript: FY and XL. All the authors provided critical advice for the final manuscript.

FUNDING

This work was supported by the Key R&D Program of Jiangsu Province (Social Development) (BE2020694) and the National Natural Science Foundation of China (81973145).

ACKNOWLEDGMENTS

We greatly appreciate the patients and investigators who participated in the corresponding medical project and for providing these valuable public datasets.

SUPPLEMENTARY MATERIAL

The Supplementary Material for this article can be found online at: https://www.frontiersin.org/articles/10.3389/fphar.2022.857060/full#supplementary-material

REFERENCES

Al-Hrout, A., Chaiboonchoe, A., Khraiwesh, B., Murali, C., Baig, B., El-Awady, R., et al. (2018). Safranal Induces DNA Double-Strand Breakage and Er-Stress-Mediated Cell Death in Hepatocellular Carcinoma Cells. *Sci. Rep.* 8, 16951. doi:10.1038/s41598-018-34855-0

Aprelikova, O., Xiong, Y., and Liu, E. T. (1995). Both p16 and P21 Families of Cyclin-dependent Kinase (CDK) Inhibitors Block the Phosphorylation of Cyclin-dependent Kinases by the CDK-Activating Kinase. *J. Biol. Chem.* 270, 18195–18197. doi:10.1074/jbc.270.31.18195

Becker, S. A., Lee, T. H., Butel, J. S., and Slagle, B. L. (1998). Hepatitis B Virus X Protein Interferes with Cellular DNA Repair. *J. Virol.* 72, 266–272. doi:10.1128/JVI.72.1.266-272.1998

Beroukhim, R., Mermel, C. H., Porter, D., Wei, G., Raychaudhuri, S., Donovan, J., et al. (2010). The Landscape of Somatic Copy-Number Alteration across Human Cancers. *Nature* 463, 899–905. doi:10.1038/nature08822

Calderaro, J., Couchy, G., Imbeaud, S., Amaddeo, G., Letouzé, E., Blanc, J. F., et al. (2017). Histological Subtypes of Hepatocellular Carcinoma Are Related to Gene Mutations and Molecular Tumour Classification. *J. Hepatol.* 67, 727–738. doi:10.1016/j.jhep.2017.05.014

Chen, C. C., Chen, C. Y., Ueng, S. H., Hsueh, C., Yeh, C. T., Ho, J. Y., et al. (2018). Corylin Increases the Sensitivity of Hepatocellular Carcinoma Cells to Chemotherapy through Long Noncoding RNA RAD51-AS1-Mediated Inhibition of DNA Repair. *Cell Death Dis.* 9, 543. doi:10.1038/s41419-018-0575-0

Chen, J., Qian, X., He, Y., Han, X., and Pan, Y. (2021a). An Artificial Neural Network Model Based on DNA Damage Response Genes to Predict Outcomes of Lower-Grade Glioma Patients. *Brief. Bioinform.* 22, bbab190. doi:10.1093/bib/bbab190

Chen, J., and Stubbe, J. (2005). Bleomycins: Towards Better Therapeutics. *Nat. Rev. Cancer* 5, 102–112. doi:10.1038/nrc1547

Chen, Y., Wang, X., Deng, X., Zhang, Y., Liao, R., Li, Y., et al. (2021b). DNA Damage Repair Status Predicts Opposite Clinical Prognosis Immunotherapy and Non-immunotherapy in Hepatocellular Carcinoma. *Front. Immunol.* 12, 2882. doi:10.3389/fimmu.2021.676922

Ciccia, A., and Elledge, S. J. (2010). The DNA Damage Response: Making it Safe to Play with Knives. *Mol. Cel.* 40, 179–204. doi:10.1016/j.molcel.2010.09.019

Davoli, T., Uno, H., Wooten, E. C., and Elledge, S. J. (2017). Tumor Aneuploidy Correlates with Markers of Immune Evasion and with Reduced Response to Immunotherapy. *Science* 355, eaaf8399. doi:10.1126/science.aaf8399

Eddy, J. A., Sung, J., Geman, D., and Price, N. D. (2010). Relative Expression Analysis for Molecular Cancer Diagnosis and Prognosis. *Technol. Cancer Res. Treat.* 9, 149–159. doi:10.1177/153303461000900204

Evans, J. R., Zhao, S. G., Chang, S. L., Tomlins, S. A., Erho, N., Sboner, A., et al. (2016). Patient-Level DNA Damage and Repair Pathway Profiles and Prognosis after Prostatectomy for High-Risk Prostate Cancer. *JAMA Oncol.* 2, 471–480. doi:10.1001/jamaoncol.2015.4955

Friedman, J., Hastie, T., and Tibshirani, R. (2010). Regularization Paths for Generalized Linear Models *via* Coordinate Descent. *J. Stat. Softw.* 33, 1–22. doi:10.18637/jss.v033.i01

Gao, Q., Zhu, H., Dong, L., Shi, W., Chen, R., Song, Z., et al. (2019). Integrated Proteogenomic Characterization of HBV-Related Hepatocellular Carcinoma. *Cell* 179, 1240–1577. doi:10.1016/j.cell.2019.08.05210.1016/j.cell.2019.10.038

Hänzelmann, S., Castelo, R., and Guinney, J. (2013). Gsva: Gene Set Variation Analysis for Microarray and RNA-Seq Data. *BMC Bioinformatics* 14, 7. doi:10.1186/1471-2105-14-7

Heagerty, P. J., Lumley, T., and Pepe, M. S. (2000). Time-Dependent Roc Curves for Censored Survival Data and a Diagnostic Marker. *Biometrics* 56, 337–344. doi:10.1111/j.0006-341x.2000.00337.x

Hoshida, Y., Nijman, S. M., Kobayashi, M., Chan, J. A., Brunet, J. P., Chiang, D. Y., et al. (2009). Integrative Transcriptome Analysis Reveals Common Molecular Subclasses of Human Hepatocellular Carcinoma. *Cancer Res.* 69, 7385–7392. doi:10.1158/0008-5472.CAN-09-1089

Jacobs, N. R., and Norton, P. A. (2021). Role of Chromosome 1q Copy Number Variation in Hepatocellular Carcinoma. *World J. Hepatol.* 13, 662–672. doi:10.4254/wjh.v13.i6.662

Jeggo, P. A., Pearl, L. H., and Carr, A. M. (2016). DNA Repair, Genome Stability and Cancer: A Historical Perspective. *Nat. Rev. Cancer* 16, 35–42. doi:10.1038/nrc.2015.4

Jiang, P., Gu, S., Pan, D., Fu, J., Sahu, A., Hu, X., et al. (2018). Signatures of T Cell Dysfunction and Exclusion Predict Cancer Immunotherapy Response. *Nat. Med.* 24, 1550–1558. doi:10.1038/s41591-018-0136-1

Kerr, K. F., Brown, M. D., Zhu, K., and Janes, H. (2016). Assessing the Clinical Impact of Risk Prediction Models with Decision Curves: Guidance for Correct Interpretation and Appropriate Use. *J. Clin. Oncol.* 34, 2534–2540. doi:10.1200/JCO.2015.65.5654

Knijnenburg, T. A., Wang, L., Zimmermann, M. T., Chambwe, N., Gao, G. F., Cherniack, A. D., et al. (2018). Genomic and Molecular Landscape of DNA Damage Repair Deficiency across the Cancer Genome Atlas. *Cell Rep.* 23, 239–e6. doi:10.1016/j.celrep.2018.03.076

Ko, H. L., and Ren, E. C. (2011). Novel Poly (Adp-Ribose) Polymerase 1 Binding Motif in Hepatitis B Virus Core Promoter Impairs DNA Damage Repair. *Hepatology* 54, 1190–1198. doi:10.1002/hep.24502

Kumar, R., Horikoshi, N., Singh, M., Gupta, A., Misra, H. S., Albuquerque, K., et al. (2013). Chromatin Modifications and the DNA Damage Response to Ionizing Radiation. *Front. Oncol.* 2, 214. doi:10.3389/fonc.2012.00214

Lee, T. H., Elledge, S. J., and Butel, J. S. (1995). Hepatitis B Virus X Protein Interacts with a Probable Cellular DNA Repair Protein. *J. Virol.* 69, 1107–1114. doi:10.1128/JVI.69.2.1107-1114.1995

Li, B., Cui, Y., Diehn, M., and Li, R. (2017). Development and Validation of an Individualized Immune Prognostic Signature in Early-Stage Nonsquamous Non-small Cell Lung Cancer. *JAMA Oncol.* 3, 1529–1537. doi:10.1001/jamaoncol.2017.1609

Li, N., Zhao, L., Guo, C., Liu, C., and Liu, Y. (2019). Identification of a Novel DNA Repair-Related Prognostic Signature Predicting Survival of Patients with Hepatocellular Carcinoma. *Cancer Manag. Res.* 11, 7473–7484. doi:10.2147/CMAR.S204864

Lima, Z. S., Ghadamzadeh, M., Arashloo, F. T., Amjad, G., Ebadi, M. R., and Younesi, L. (2019). Recent Advances of Therapeutic Targets Based on the Molecular Signature in Breast Cancer: Genetic Mutations and Implications for Current Treatment Paradigms. *J. Hematol. Oncol.* 12, 38. doi:10.1186/s13045-019-0725-6

Liu, G.-M., Zeng, H.-D., Zhang, C.-Y., and Xu, J.-W. (2019). Identification of a Six-Gene Signature Predicting Overall Survival for Hepatocellular Carcinoma. *Cancer Cel. Int.* 19, 138. doi:10.1186/s12935-019-0858-2

Liu, G. M., Xie, W. X., Zhang, C. Y., and Xu, J. W. (2020). Identification of a Four-Gene Metabolic Signature Predicting Overall Survival for Hepatocellular Carcinoma. *J. Cel. Physiol.* 235, 1624–1636. doi:10.1002/jcp.29081

Llovet, J. M., Kelley, R. K., Villanueva, A., Singal, A. G., Pikarsky, E., Roayaie, S., et al. (2021). Hepatocellular Carcinoma. *Nat. Rev. Dis. Primers* 7, 6–34. doi:10.1038/s41572-020-00240-3

Long, J., Zhang, L., Wan, X., Lin, J., Bai, Y., Xu, W., et al. (2018). A Four-Gene-Based Prognostic Model Predicts Overall Survival in Patients with Hepatocellular Carcinoma. *J. Cel. Mol. Med.* 22, 5928–5938. doi:10.1111/jcmm.13863

Lu, X., Jiang, L., Zhang, L., Zhu, Y., Hu, W., Wang, J., et al. (2019). Immune Signature-Based Subtypes of Cervical Squamous Cell Carcinoma Tightly Associated with Human Papillomavirus Type 16 Expression, Molecular Features, and Clinical Outcome. *Neoplasia* 21, 591–601. doi:10.1016/j.neo.2019.04.003

Lu, X., Meng, J., Su, L., Jiang, L., Wang, H., Zhu, J., et al. (2021). Multi-omics Consensus Ensemble Refines the Classification of Muscle-invasive Bladder Cancer with Stratified Prognosis, Tumour Microenvironment and Distinct Sensitivity to Frontline Therapies. *Clin. Translational Med.* 11, e601. doi:10.1002/ctm2.601

Luftig, M. A. (2014). Viruses and the DNA Damage Response: Activation and Antagonism. *Annu. Rev. Virol.* 1, 605–625. doi:10.1146/annurev-virology-031413-085548

Mayakonda, A., Lin, D. C., Assenov, Y., Plass, C., and Koeffler, H. P. (2018). Maftools: Efficient and Comprehensive Analysis of Somatic Variants in Cancer. *Genome Res.* 28, 1747–1756. doi:10.1101/gr.239244.118

Negrini, S., Gorgoulis, V. G., and Halazonetis, T. D. (2010). Genomic Instability-Aan Evolving Hallmark of Cancer. *Nat. Rev. Mol. Cel. Biol.* 11, 220–228. doi:10.1038/nrm2858

Pearl, L. H., Schierz, A. C., Ward, S. E., Al-Lazikani, B., and Pearl, F. M. (2015). Therapeutic Opportunities within the DNA Damage Response. *Nat. Rev. Cancer* 15, 166–180. doi:10.1038/nrc3891

Ricardo-Lax, I., Ramanan, V., Michailidis, E., Shamia, T., Reuven, N., Rice, C. M., et al. (2015). Hepatitis B Virus Induces Rnr-R2 Expression *via* DNA Damage Response Activation. *J. Hepatol.* 63, 789–796. doi:10.1016/j.jhep.2015.05.017

Sahin, I. H., Lowery, M. A., Stadler, Z. K., Salo-Mullen, E., Iacobuzio-Donahue, C. A., Kelsen, D. P., et al. (2016). Genomic Instability in Pancreatic Adenocarcinoma: A New Step towards Precision Medicine and Novel Therapeutic Approaches. *Expert Rev. Gastroenterol. Hepatol.* 10, 893–905. doi:10.1586/17474124.2016.1153424

Sanchez-Vega, F., Mina, M., Armenia, J., Chatila, W. K., Luna, A., La, K. C., et al. (2018). Oncogenic Signaling Pathways in the Cancer Genome Atlas. *Cell* 173, 321–e10. doi:10.1016/j.cell.2018.03.035

Scarbrough, P. M., Weber, R. P., Iversen, E. S., Brhane, Y., Amos, C. I., Kraft, P., et al. (2016). A Cross-Cancer Genetic Association Analysis of the DNA Repair and DNA Damage Signaling Pathways for Lung, Ovary, Prostate, Breast, and Colorectal Cancer. *Cancer Epidemiol. Biomarkers Prev.* 25, 193–200. doi:10.1158/1055-9965.EPI-15-0649

Schreiner, S., and Nassal, M. (2017). A Role for the Host DNA Damage Response in Hepatitis B Virus cccDNA Formation-and Beyond? *Viruses* 9, 125. doi:10.3390/v9050125

Schulze, K., Nault, J. C., and Villanueva, A. (2016). Genetic Profiling of Hepatocellular Carcinoma Using Next-Generation Sequencing. *J. Hepatol.* 65, 1031–1042. doi:10.1016/j.jhep.2016.05.035

Sharma, P., Barlow, W. E., Godwin, A. K., Parkes, E. E., Knight, L. A., Walker, S. M., et al. (2019). Validation of the DNA Damage Immune Response Signature in Patients with Triple-Negative Breast Cancer from the Swog 9313c Trial. *J. Clin. Oncol.* 37, 3484–3492. doi:10.1200/jco.19.00693

Siegel, R., Naishadham, D., and Jemal, A. (2013). Cancer Statistics, 2013. *CA Cancer J. Clin.* 63, 11–30. doi:10.3322/caac.21166

Song, Y., Huang, J., Liang, D., Hu, Y., Mao, B., Li, Q., et al. (2021). DNA Damage Repair Gene Mutations Are Indicative of a Favorable Prognosis in Colorectal Cancer Treated with Immune Checkpoint Inhibitors. *Front. Oncol.* 10, 3349. doi:10.3389/fonc.2020.549777

Su, M., Wang, H., Wang, W., Wang, Y., Ouyang, L., Pan, C., et al. (2018). lncRNAs in DNA Damage Response and Repair in Cancer Cells. *Acta Biochim. Biophys. Sin (Shanghai)* 50, 433–439. doi:10.1093/abbs/gmy022

Takagi, H., Sasaki, S., Suzuki, H., Toyota, M., Maruyama, R., Nojima, M., et al. (2008). Frequent Epigenetic Inactivation of SFRP Genes in Hepatocellular Carcinoma. *J. Gastroenterol.* 43, 378–389. doi:10.1007/s00535-008-2170-0

Tunissiolli, N. M., Castanhole-Nunes, M. M. U., Pavarino, É. C., da Silva, R. F., da Silva, R. C. M. A., and Maria Goloni-Bertollo, E. (2018). Clinical,

Epidemiological and Histopathological Aspects in Patients with Hepatocellular Carcinoma Undergoing Liver Transplantation. *Asian Pac. J. Cancer Prev.* 19, 2795–2802. doi:10.22034/apjcp.2018.19.10.2795

Villanueva, A. (2019). Hepatocellular Carcinoma. *N. Engl. J. Med.* 380, 1450–1462. doi:10.1056/NEJMra1713263

Villanueva, A., and Hoshida, Y. (2011). Depicting the Role of TP53 in Hepatocellular Carcinoma Progression. *J. Hepatol.* 55, 724–725. doi:10.1016/j.jhep.2011.03.018

Weitzman, M. D., and Fradet-Turcotte, A. (2018). Virus DNA Replication and the Host DNA Damage Response. *Annu. Rev. Virol.* 5, 141–164. doi:10.1146/annurev-virology-092917-043534

Wu, Z., Li, S., Tang, X., Wang, Y., Guo, W., Cao, G., et al. (2020). Copy Number Amplification of DNA Damage Repair Pathways Potentiates Therapeutic Resistance in Cancer. *Theranostics* 10, 3939–3951. doi:10.7150/thno.39341

Xue, C., Gu, X., and Li, L. (2021). Immune Classifier-Based Signatures Provide Good Prognostic Stratification and Predict the Clinical Benefits of Immune-Based Therapies for Hepatocellular Carcinoma. *Cancer Cel. Int.* 21, 471. doi:10.1186/s12935-021-02183-5

Yang, C., Huang, X., Li, Y., Chen, J., Lv, Y., and Dai, S. (2021). Prognosis and Personalized Treatment Prediction in TP53-Mutant Hepatocellular Carcinoma: An In Silico Strategy towards Precision Oncology. *Brief. Bioinform.* 22, bbaa164. doi:10.1093/bib/bbaa164

Yang, Z., Lauder, I. J., and Lin, H. J. (1995). Molecular Evolution of the Hepatitis B Virus Genome. *J. Mol. Evol.* 41, 587–596. doi:10.1007/BF00175817

Yu, G., Wang, L. G., Han, Y., and He, Q. Y. (2012). Clusterprofiler: An R Package for Comparing Biological Themes Among Gene Clusters. *OMICS* 16, 284–287. doi:10.1089/omi.2011.0118

Yu, S. J., and Kim, Y. J. (2014). Hepatitis B Viral Load Affects Prognosis of Hepatocellular Carcinoma. *World J. Gastroenterol.* 20, 12039–12044. doi:10.3748/wjg.v20.i34.12039

Conflict of Interest: The authors declare that the research was conducted in the absence of any commercial or financial relationships that could be construed as a potential conflict of interest.

Publisher's Note: All claims expressed in this article are solely those of the authors and do not necessarily represent those of their affiliated organizations, or those of the publisher, the editors, and the reviewers. Any product that may be evaluated in this article, or claim that may be made by its manufacturer, is not guaranteed or endorsed by the publisher.

frontiers | Frontiers in Pharmacology

ORIGINAL RESEARCH
published: 08 April 2022
doi: 10.3389/fphar.2022.879751

Transcriptomics and Metabolomics Identify Drug Resistance of Dormant Cell in Colorectal Cancer

Lang Xie[1†], *Renli Huang*[1†], *Hongyun Huang*[1†], *Xiaoxia Liu*[2*] *and Jinlong Yu*[1*]

[1]*Department of General Surgery, Zhujiang Hospital, Southern Medical University, Guangzhou, China,* [2]*Guangdong Provincial Key Laboratory of Colorectal and Pelvic Floor Disease, The Sixth Affiliated Hospital (Guangdong Gastrointestinal and Anal Hospital), Sun Yat-sen University, Guangzhou, China*

Background: Tumor dormancy is an important way to develop drug resistance. This study aimed to identify the characteristics of colorectal cancer (CRC) cell dormancy.

Methods: Based on the CRC cohorts, a total of 1,044 CRC patients were included in this study, and divided into a dormant subgroup and proliferous subgroup. Non-negative matrix factorization (NMF) was used to distinguish the dormant subgroup of CRC *via* transcriptome data of cancer tissues. Gene Set Enrichment Analysis (GSEA) was used to explore the characteristics of dormant CRC. The characteristics were verified in the cell model, which was used to predict key factors driving CRC dormancy. Potential treatments for CRC dormancy were also examined.

Results: The dormant subgroup had a poor prognosis and was more likely to relapse. GSEA analysis showed two defining characteristics of the dormant subgroup, a difference in energy metabolism and synergistic effects of cancer-associated fibroblasts (CAFs), which were verified in a dormant cell model. Transcriptome and clinical data identified *LMOD1, MAB21L2*, and *ASPN* as important factors associated with cell dormancy and verified that erlotinib, and CB-839 were potential treatment options.

Conclusion: Dormant CRC is associated with high glutamine metabolism and synergizes with CAFs in 5-FU resistance, and the key effectors are LMOD1, MAB21L2, and ASPN. Austocystin D, erlotinib, and CB-839 may be useful for dormant CRC.

Keywords: tumor dormancy, metabolomics, cancer-associated fibroblasts, colorectal cancer, transcriptomics

OPEN ACCESS

Edited by:
Clare Y. Slaney,
Peter MacCallum Cancer Centre, Australia

Reviewed by:
Purvi Patel,
Columbia University, United States
Yibing Ji,
University at Buffalo, United States

***Correspondence:**
Xiaoxia Liu
liuxx37@mail.sysu.edu.cn
Jinlong Yu
yujinlong640506@163.com

[†]*These authors have contributed equally to this work and share first authorship*

Specialty section:
This article was submitted to Pharmacology of Anti-Cancer Drugs, a section of the journal Frontiers in Pharmacology

Received: *20 February 2022*
Accepted: *14 March 2022*
Published: *08 April 2022*

Citation:
Xie L, Huang R, Huang H, Liu X and Yu J (2022) Transcriptomics and Metabolomics Identify Drug Resistance of Dormant Cell in Colorectal Cancer. Front. Pharmacol. 13:879751. doi: 10.3389/fphar.2022.879751

INTRODUCTION

Colorectal cancer (CRC) is one of the most common malignant tumors worldwide (Siegel et al., 2020), and recurrence after surgery and chemotherapy is a leading factor of CRC-related deaths (Katona and Weiss, 2020). Recent studies have shown that CRC cells can enter a reversible dormant state leading to chemotherapy resistance (Rehman et al., 2021). In the dormant state, cancer cells regulate their cell cycle to enter a slow cycle mode (Basu et al., 2022). This allows the cells to survive in hostile environments such as hypoxia, effects of the immune system, and the effects of chemotherapy (Ju et al., 2020; Manjili et al., 2022).

In this study, we identified a dormant subgroup of CRC cells based on the transcriptome data of CRC patients. We then clarified two characteristics in the dormant subgroup of CRC cells, energy metabolism reprogramming and synergized with CAFs, and verified the results *in vitro*. Furthermore, we identified

dormancy-related genes that regulated drug resistance of dormant CRC cells and predicated three drugs that may be effective against dormant CRC cells.

MATERIALS AND METHODS

Patients and Samples

In this study, we included 459 patients identified in The Cancer Genome Atlas-Colon Adenocarcinoma (TCGA-COAD) population (https://portal.gdc.cancer.gov/) and 585 patients in GSE39582 (Marisa et al., 2013) of the Gene Expression Omnibus (GEO, http://www.ncbi.nlm.nih.gov/geo/). Raw RNA-sequencing data counts (level 3) of patients in the TCGA-COAD cohort were downloaded from the TCGA database as recommended by guidelines and converted into transcripts per kilobase million for analysis. Raw CEL files (Affymetrix DNA microarray image analysis) of patients in GSE39582 were downloaded from the website mentioned above, and processed by "affy" and "simpleaffy" R packages (Irizarry et al., 2003).

Identification of CRC Subgroups

The Gene Set Enrichment Analysis (GSEA) website (https://www.gsea-msigdb.org/gsea/msigdb/cards/GOBP_CELL_CYCLE_ARREST.html) was searched for gene sets associated with cell cycle regulation, and the intersections between these gene sets and the genes in the TCGA-COAD and GSE39582 were identified and selected for subsequent analysis. Genes of low median absolute deviation value (≤0.5) across all datasets were excluded.

A total of 223 genes associated with cell cycle arrest genes were identified. These genes were processed by non-negative matrix factorization (NMF) clustering (Possemato et al., 2011) using the R software NMF package (version 0.23.0). The maximum number of clusters for consistency analysis was 6, and the matrix was drawn 50 times. The consensus map function (CMF) of the NMF package was used for producing clustered heatmaps. Rank values where the magnitude of the cophenetic correlation coefficient began to fall were chosen as the optimal number of clusters (Brunet et al., 2004).

Characterization of CRC Subgroups and Identification of Dormancy-Related Genes

The Limma package (version: 3.40.2) of R software was used to study the differential expression of mRNAs. The Log (fold-change) of all genes in datasets were used to perform GSEA analysis in webgestalt (http://www.webgestalt.org/) (Liao et al., 2019) for identification and characterization of CRC subgroups. An adjusted p value <0.05 and Log (fold-change) > 1 or Log (fold-change) < −1 were defined as the thresholds for identifying differentially expressed genes (DEGs) among CRC subgroups. The intersections of DEGs between the TCGA-COAD and GSE39582 were selected for prognostic analysis. The Kaplan-Meier method and log-rank test was used to compare survival between groups, and data were reported as p value, hazard ratio (HR), and 95% confidence interval (CI). Univariate Cox proportional hazards regression analysis was performed using the R survival and survminer packages (version 4.0.3). DEGs with a value of $p < 0.05$ were considered dormancy-related genes. Gene Set Cancer Analysis (GSCA, http://bioinfo.life.hust.edu.cn/GSCA/) (Liu et al., 2018) was used to examine correlations between dormancy-related genes and cell cycle pathway activity.

Cell Culture and Dormant Cell Model Construction

The CRC cells lines LoVo and RKO were donated by Dr Xiaoxia Liu (Affiliated Sixth Hospital, Sun Yat-sen University, Guangzhou, China). The CRC cell lines HCT116 and DLD1 were obtained from the American Type Culture Collection (ATCC, United States). Cells were cultured in DMEM medium (Code: C11875500BT, Gibco, United States) with 10% fetal bovine serum (FBS) (Code: 10270-106, Gibco), 100 μg/ml streptomycin and 100 U/mL penicillin in a 5% CO2 atmosphere at 37°C. 5-Fluorouracil (5-FU) (Code: HY-90006, MCE, United States) (200 μM) was added to the cultures as a proxy for more than 4 months to select drug-resistant persister cells.

Cell Cycle Analysis

LoVo persister cells (LoVo-P) and RKO persister cells (RKO-P) were collected on day 1 and day 10 after the adding 5-FU. Cells in each group (1×10^6) were pelleted, harvested after being starved for 24 h, fixed with 75% cold ethanol overnight, and stained with propidium iodide (PI) using a PI kit (Beyotime Biotechnology, Shanghai, China). Flow cytometry and the cell cycle module of FlowJo™ software (version 7.0) detected the distributions of cell cycle phases.

Primary Human Cancer-Associated Fibroblasts Line Generation

Specimens of high-grade CRC (T4Nx) were obtained from chemotherapy naïve patients (age range 18–70 years) undergoing surgery at the Sixth Affiliated Hospital of Sun Yat-sen University (SYSU), China. The study was approved by the Human Medical Ethics Committee of the Sixth Affiliated Hospital of Sun Yat-sen University, and informed consent was obtained from all patients before surgery.

Primary CAFs were isolated from tumor specimens as previously described (Ligorio et al., 2019; Peng et al., 2021). Briefly, tumor tissue was chopped with a sterile scalpel and then digested for 3 h at 37°C using collagenase Digestion Medium (DMEM, penicillin 100 U/mL, streptomycin 100 μg/ml, collagenase digestion 125 units/mg). Following tissue digestion, cells were plated under adherent conditions in Growth Medium (DMEM, PenStrep 1X, 10% FBS) and passaged regularly. CAFs grew by adherence with fibroblast-like morphology and had a strong capacity for proliferation.

Metabolon-Based Energy Metabolism Detection

LoVo-P or LoVo-nP cells were collected, and metabolites were extracted and detected. Briefly, cells (5×10^6) were pelleted,

washed with cold PBS, and snap-frozen in liquid nitrogen. Cells were then ultrasonicated at 4°C for 20 min, the supernatant was collected (20 min at 14,000×*g*, 4°C), and then sent for Metabolon-Associated Energy Metabolism analysis (Applied Protein Technology, Shanghai, China).

The supernatants were dried in a vacuum centrifuge. The dried samples were dissolved in 100 μL acetonitrile/water (1:1, v/v), adequately vortexed, and centrifuged (14,000 rpm, 4°C, 15 min). The supernatants were collected for liquid chromatography-tandem mass spectrometry (LC-MS/MS) analysis.

U-^{13}C Glucose Labeling

The indicated cells (LoVo-P/nP and RKO-P/nP) cells were grown to 80-90% confluence in 10 cm cell culture dishes and then cultured in glucose-free DMEM (Thermo Fisher Scientific) supplemented with 4.5 g/L U-^{13}C-glucose (Cambridge Isotope Laboratories, Andover, MA) and 10% FBS for 24 h. The medium was removed, and the cells were washed twice in the culture dish with 2 ml saline without disturbing cell attachment. Next, 500 μl of methanol was added to the cells to quench metabolic reactions, followed by an equal volume of water. The cells were then collected by scraping and placed in 2 ml Eppendorf tubes, and 500 μl chloroform was added to each tube. The cell extracts were vortexed at 4°C for 30 min. The samples were centrifuged at 14,000×*g* for 5 min at room temperature. For analysis of polar metabolites, the upper layer of the aqueous phase (700 μl) was transferred to a new tube for evaporation under airflow (N2 gas or vacuum concentrator, 3 h, 45°C). The dried metabolites were stored at −80°C until LC-MS/MS analysis. The LC/MS was performed at the Metabolic Innovation Center (MIC) of Sun Yat-Sen University.

Cell Survival and Proliferation Analysis

The cell survival rate was assessed using a Cell Counting Kit-8 (CCK-8) (Dojindo Lab, Japan) assay according to the manufacturer's instructions. CAFs were isolated from primary tumor samples, and then we collected conditioned medium (CAF-co CM) from each of the CRC cells/CAFs co-culture. Briefly, a total of 5×10^4 persister or parental cells were placed into the upper chamber in 0.2 ml of complete DMEM, and 2×10^5 CAF cells in 1 ml of complete DMEM was placed in the lower chamber, and then the cells were incubated for 24 h. The medium in the lower chamber was collected and defined as CM/co-P and CM/co-nP, respectively. The CM was filtered with a 0.8 mm filter to remove cell debris and then used. After that, a total of 5,000 cells/well were seeded into 96-well plates overnight, then cultured in DMEM containing 10% FBS with 25% CAF-co CM or control medium and treated with the indicated concentrations of 5-FU for 72 h. The absorbance at 450 nm was measured using a Thermo Scientific Varioskan Flash instrument after incubation with 10 μl CCK-8 solution for 2 h at 37°C, and the proliferation index was calculated.

Cell proliferation was also assessed via IncuCyte ZOOM (Essen BioScience). A total of 5,000 cells/well were cultured as described above 96-well plates and were automatically monitored and data recorded every 2 h by IncuCyte ZOOM for 72 h.

Drug Sensitivity Analysis

Gene Set Cancer Analysis (GSCA, http://bioinfo.life.hust.edu.cn/GSCA/) was used for analyzing correlations between the expressions of dormancy-related genes and drug sensitivity of cell lines in the Cancer Therapeutics Response Portal database (CTRP, http://portals.broadinstitute.org/ctrp/). DMEM medium with CB-839 (Code: S7655, Selleck, United States)] and erlotinib (Code: HY-50896, MCE, United States) (2 μM) was used for evaluating drug sensitivity rescue.

Statistical Analysis

Statistical analysis was performed using R (version 4.0.2) and GraphPad Primer 8.0 (GraphPad Prism, GraphPad Software, La Jolla, CA). All p values were 2-tailed, and values <0.05 were considered to indicate statistical significance.

RESULTS

Definition of CRC Dormancy or Proliferation

To define dormancy or proliferation in CRC, we first selected gene sets in cell cycle arrest (GO: 0007050) and used their expression data for clustering by NMF. As shown in **Figures 1A,C**, following the rules of NMF, the optimum number of the cluster was two in both GSE39582 and TCGA-COAD gene sets. After defining the two groups, GSEA analysis was performed, and the normalized enrichment score (NES) and false discover rate (FDR) were determined; an FDR <0.25 was considered significant. Only the top and bottom categories (according to NES) are shown in **Figure 1E**. The results showed that hypoactive Kyoto Encyclopedia of Genes and Genomes (KEGG) pathways in the two datasets reflected processes of cell proliferation such as ribosome generation, DNA replication, and RNA synthesis. As shown in **Figure 1**, the proliferation ability of CRC in group 1 was weaker than that of group 2; thus, group 1 was considered the dormant subgroup and the other the proliferous subgroup.

Increasing evidence has shown that dormant cells can evade the effects of chemotherapy and cause cancer relapse. Thus, we examined prognostic data of the two groups. The dormant subgroup showed an unfavorable prognosis concerning overall survival (OS) and recurrence-free survival (RFS) in the GSE39582 dataset and an unfavorable prognosis for progression-free survival (PFS) in the TCGA-COAD dataset (**Figures 1B,D**). In addition, the GSEA results also indicated an enhanced interaction between cells and matrix in the dormant group of both datasets and obvious differences in energy metabolism in the TCGA-COAD dataset.

Metabolic Reprogramming in Dormant Subgroup

In order to verify the characteristics of the dormant subgroup and clarify the differences between the two subgroups, we constructed a model of the dormant subgroup *in vitro* (Cho et al., 2021). CRC

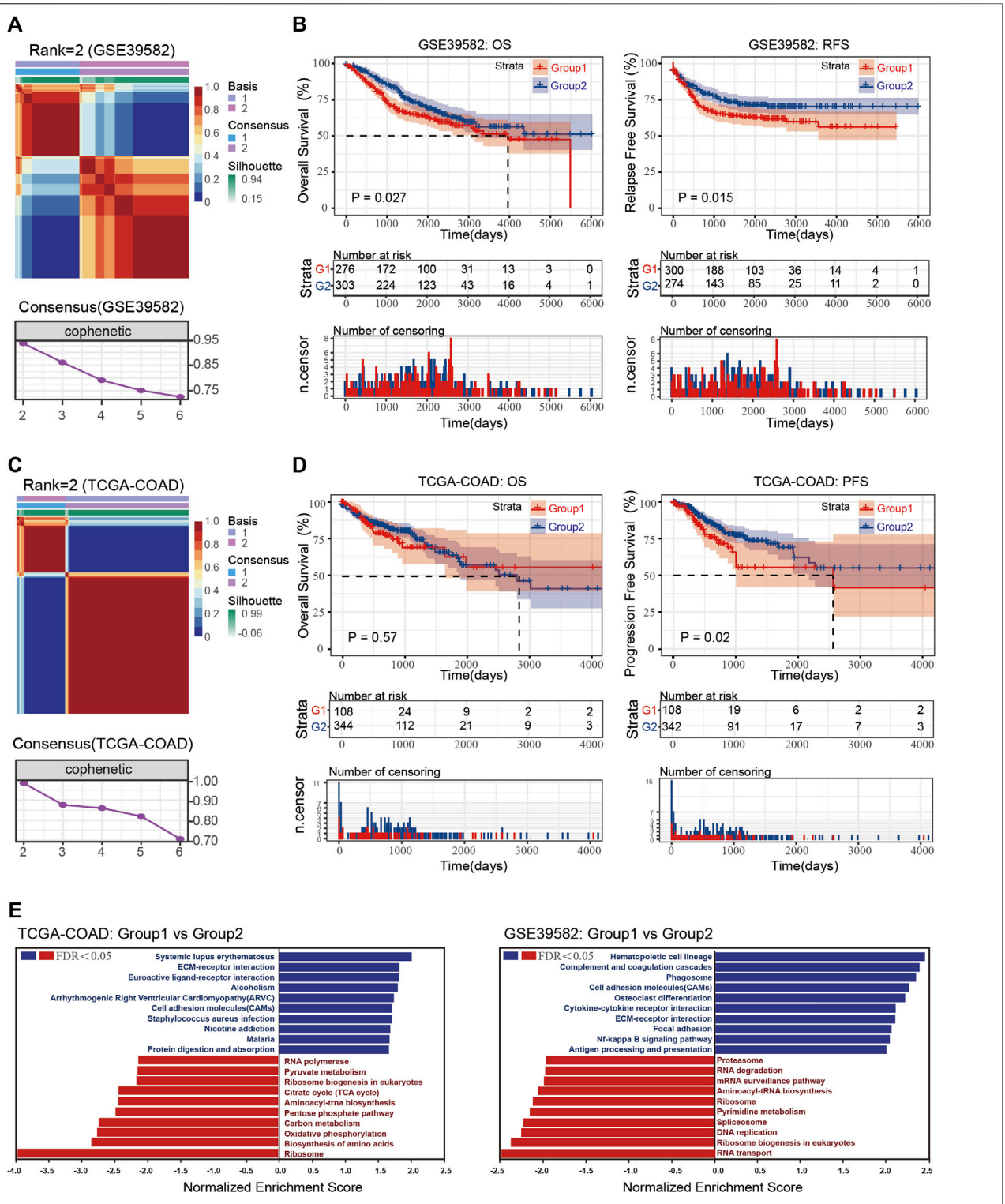

FIGURE 1 | (A) Consensus map and consensus results of GSE39582 with rank = 2. **(B)** Overall survival (OS) and recurrence-free survival (RFS) of the dormant and proliferous subgroups in GSE39582. **(C)** Consensus map and consensus results of TCGA-COAD with rank = 2. **(D)** OS and RFA of the dormant and proliferous subgroups in TCGA-COAD. **(E)** GSEA results of Group 1 vs. Group 2 in TCGA-COAD and GSE39582.

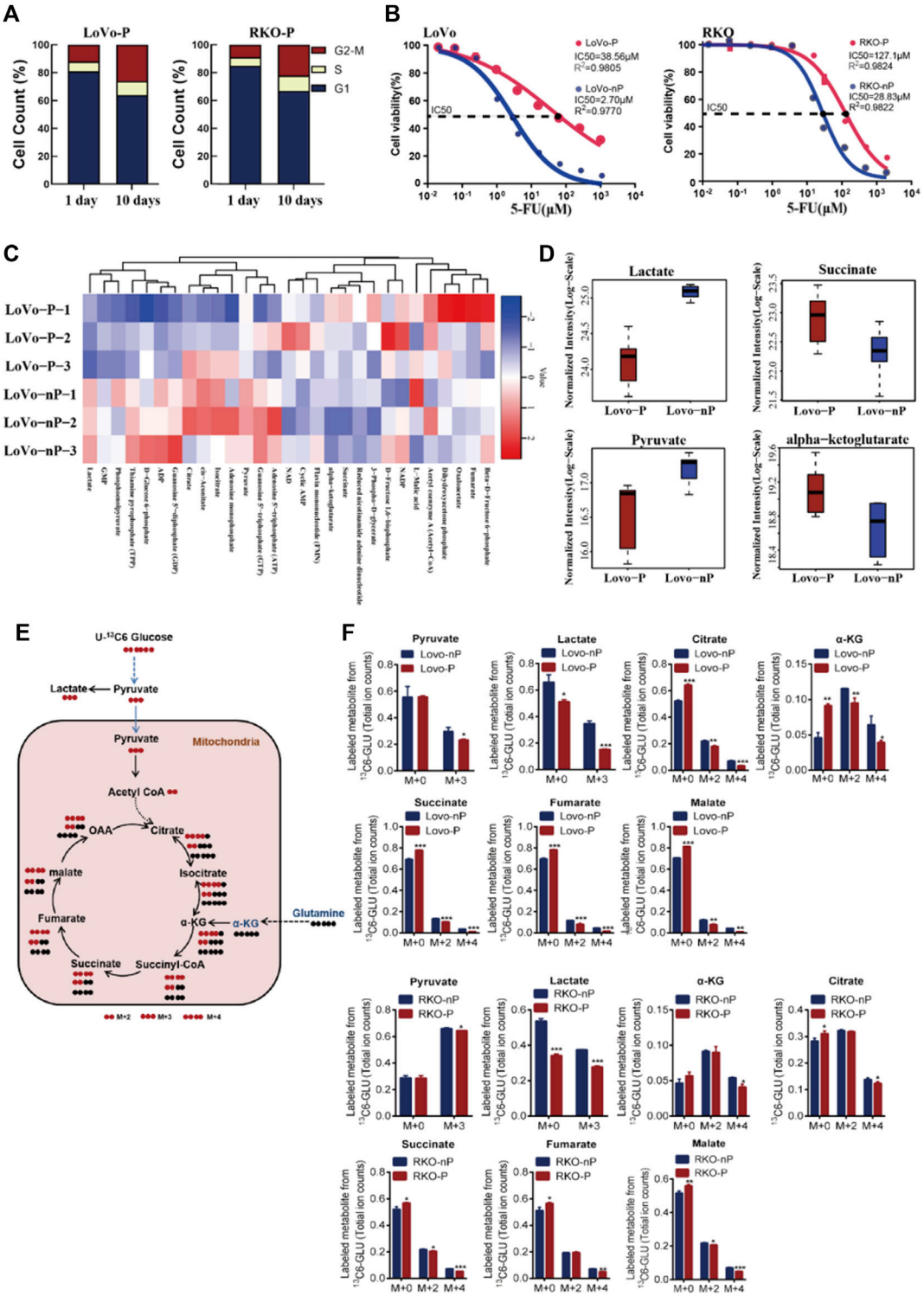

FIGURE 2 | (A) Distribution of cell cycle phases in LoVo-P and RKO-P cells on day 1 and 10 after treatment with 5-FU. **(B)** Half maximal inhibitory concentration (IC50) of 5-FU between DTP cells (LoVo-P and RKO-P) and parental cells (LoVo-nP and RKO-nP). **(C)** Heatmap of metabolites in the energy pathway determined by metabolomics in LoVo-P and LoVo-nP cells. The levels of energy metabolites are shown in **Supplementary Table S1. (D)** Compared to LoVo-nP cells, the main discriminant metabolite levels in LoVo-P cells. **(E)** Schematic illustration of glucose recycling using U-^{13}C-glucose. **(F)** U-^{13}C-glucose tracing analysis of LoVo and RKO DTP cells and parental cells. Cells were cultured in U-^{13}C-glucose and DMEM for 24 h to synthesize U-^{13}C metabolites ($n = 3$). Bars, mean ± SD. $^{*}p < 0.05$; $^{**}p < 0.01$; $^{***}p < 0.001$.

cell lines LoVo and RKO were used to construct persister cells by treatment with 5-FU. After the 5-FU induction period, the proliferation rates of persister cells (LoVo-P and RKO-P) were significantly reduced compared with the parental LoVo and RKO (LoVo-nP and RKO-nP) cells (**Figure 2A**), and they exhibited more resistance to 5-FU (**Figure 2B**). We then examined the cell cycles of persister cells at different times after removing 5-FU, and the results showed that LoVo-P and RKO-P cells could return to a proliferative state.

To better understand the metabolic changes associated with the dormant status, energy metabolism-related metabolites were examined by LC-MS/MS-based metabolomics (**Figure 2C**). A total of 29 out of 31 metabolites were identified to be energy metabolism-related, and there were significant differences in the levels between the two subgroups (**Supplementary Table S1**). A total of 12 different metabolites were significantly altered in persister cells. Compared with the parental group, five metabolites (α-KG, succinate, cyclic AMP, FMN, 3-phospho-D-glycerate) were increased, and seven metabolites (lactate, cis-aconitate, NAD, isocitrate, citrate, pyruvate, GTP) were decreased in the persister group. Overall, the results showed that the metabolite levels involved in glycolysis (lactate and pyruvate) were drastically reduced, whereas persister cells had increased levels of metabolites involved in glutaminolysis (such as α-KG and succinate). The results suggest that drug-tolerant persister (DTP) cells may have altered their metabolic requirements in response to the cytotoxic stress (**Figure 2D**).

Altered metabolism to sustain rapid growth is one of the hallmarks of cancer (Vander Heiden and DeBerardinis, 2017). Next, we further examined the metabolic changes in DTP cells by U-^{13}C-glucose tracing and metabolomics analysis (**Figure 2E**). Consistent with our previous data, DTP cells showed a significantly lower enrichment in glycolytic ^{13}C labeled lactate than did non-persister cells, indicative of the Warburg effect. By contrast, DTP cells had significantly higher fractions of α-KG (M+0), succinate (M+0), fumarate (M+0), malate (M+0), and citrate (M+0), indicating enhanced Krebs cycle and glutamine metabolism (**Figure 2F**). These data, along with the LC-MS/MS-based metabolomics data, indicate that DTP cells require glutamine metabolism to meet increased energy demands.

Drivers of Dormant State: Dormancy-Related Genes and Synergistic Effect of Cancer-Associated Fibroblasts

After confirming metabolic reprogramming in the dormant subgroup, we examined the enhanced interaction between cells and the extracellular matrix in the dormant subgroup. In order to clarify which stromal cells play critical roles, we first used TCGA-COAD and GSE39582 transcriptome data to determine DEGs between the two subgroups according to the pre-set conditions. As shown in **Figures 3A,B**, 44 up-regulated DEGs were identified as overlapping dormancy-related genes between TCGA-COAD and GSE39582 datasets. *RGS2* has been confirmed to regulate a dormant state in non-small cell lung cancer (NSCLC). Specifically, *RGS2* caused prolonged translational arrest in dormant cells through persistent eukaryotic initiation factor 2 phosphorylation *via* proteasome-mediated degradation of activating transcription factors (Cho et al., 2021). In addition, a cancer cell in a dormant state is always associated with chemotherapy resistance and tumor relapse; thus, we used Cox proportional hazards regression analyses to identify prognosis-related genes associated with RFS or PFS. The results showed that in both datasets, *APOD, ASPN, FNDC1, GPX3, LMOD1, MAB21L2, SCG2, SLIT2*, and *TAGLN* were potential genes causing or maintaining a dormant state of CRC (**Figure 3C**). Next, we used the GCSA database to explore the effects of these nine genes on common cancer-related pathways, and the results showed that they possibly negatively regulate the cell cycle and slow down cell metabolism (**Figure 3D**).

Next, we used the single-cell database GSE146771 (Zhang et al., 2020) and Characterizing Tumor Subpopulations (TISCH, https://http://tisch.comp-genomics.org//) (Sun et al., 2021) to ascertain the expressions of these nine genes in various stromal cells. The result showed that these nine genes are primarily highly expressed in fibroblasts (**Figures 3E,F**). While there is little evidence to show a direct correlation between fibroblasts and cancer dormancy, CAFs are the major subpopulation of fibroblasts in tumor stroma, and CAFs are also related to dormancy-related factors such as transforming growth factor-beta (TGF-β), interferon (IFN), insulin-like growth factor (IGF), fibroblast growth factor (FGF), macrophage-stimulating factor (M-SCF), and interleukin (IL) (Dai et al., 2021). This may indicate that CAFs can influence the state of cancer cells through remodeling the ECM, producing exosomes, mediating the balance of angiogenesis, or recruiting immune cells.

CAFs Maintain the Drug-Tolerant Persister State of CRC Cells

We speculated a synergistic effect between CAFs and CRC cells in maintaining the dormant state and enhancing drug resistance. In order to verify our hypothesis, the regular medium was replaced with CM/co-P or CM/co-nP and then treated with different concentrations of 5-FU for 72 h. The result showed that CM/co-P conferred more resistance to 5-FU in RKO and LoVo parental cells than CM/co-nP and control medium (**Figure 4A**). To further verify the efficacy of CM/co-P in other CRC cell lines, we used HCT116 and DLD1 cells. Consistently, the CCK-8 assay for cell survival showed that the CM/co-P also could induce 5-FU resistance in HCT116 and DLD1 cells even under a high concentration of 5-FU (40 μM) (**Figure 4B**). As shown in **Figure 4C**, Phase Object Confluence (%) detected by IncuCyte ZOOM further confirmed the chemotherapy-resistant in HCT116 and DLD1 cells after incubation with CM/co-P for up to 96 h treatment with 40 μM 5-FU. These data suggest that CM collected from CAFs following co-culture with DTP cells can protect against cytotoxic stress in CRC cells.

Potential Treatment: Focus on *ASPN*, *LMOD1*, and MAB21L2 and Reverse the Drug-Tolerant Persister State of CRC

It has been shown that if tumor cells remain in a dormant state, they have developed significantly increased resistance to available

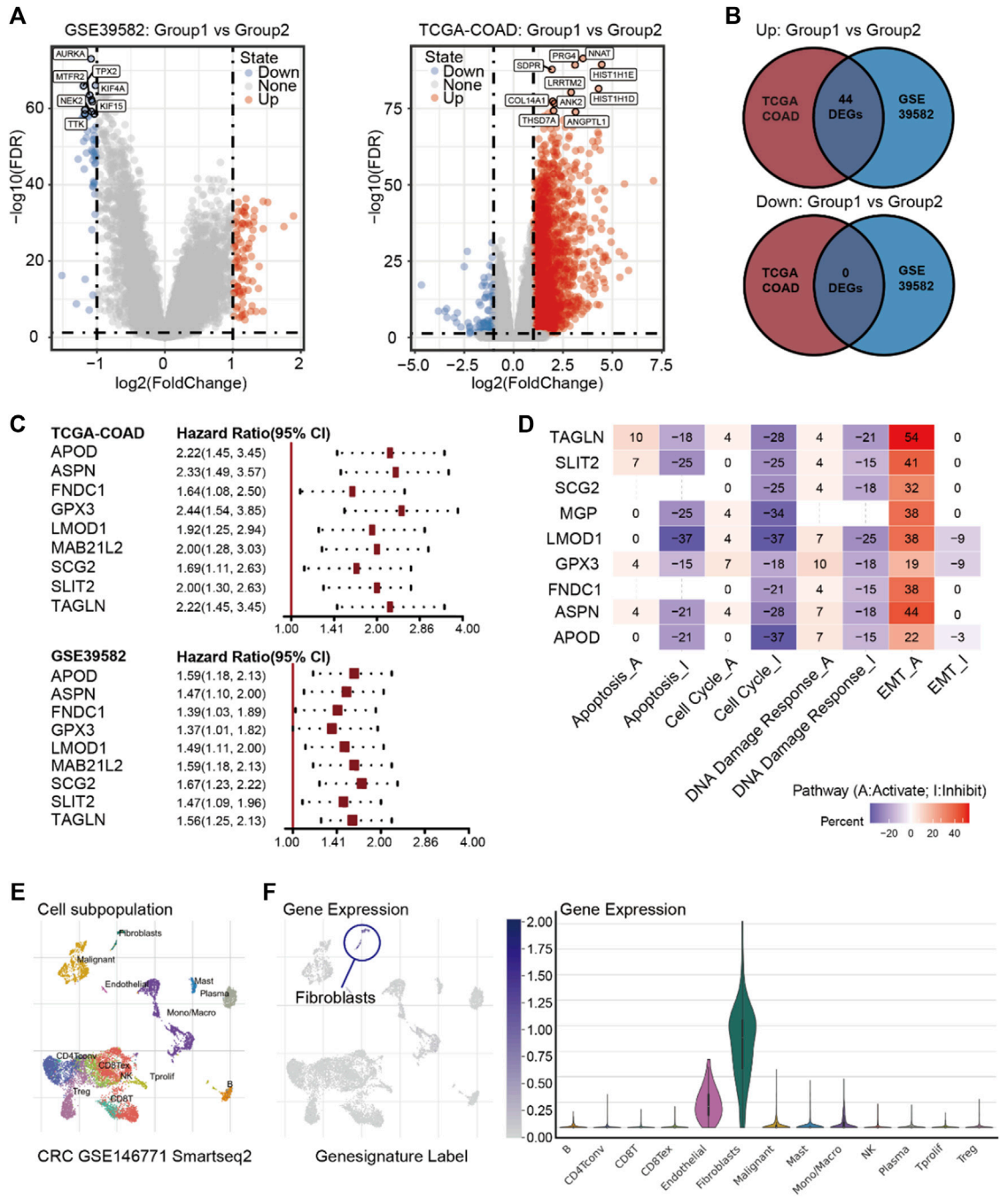

FIGURE 3 | (A) Volcano plot of DEGs between Group 1 and Group 2 in GSE39582 and TCGA-COAD. **(B)** Intersections of DEGs between TCGA-COAD and GSE39582. **(C)** Cox proportional hazards regression analyses of nine prognosis-related genes in GSE39582 and TCGA-COAD. **(D)** Pathway activity of the nine prognosis-related genes. **(E)** Annotations of cell subpopulations in GSE146771. **(F)** Expressions of nine prognosis-related genes among cell subpopulations in GSE146771.

chemotherapy drugs (Sosa et al., 2014). Following chemotherapy, residual DTP cells might re-enter the cell cycle and thus regain the ability to proliferate, causing a recurrence (Lin and Zhu, 2021). Therefore, it is critical to find new compounds to restore chemotherapy drug sensitivity that can kill DTP cells effectively. We used the CTRP drug database via GCSA (Liu et al., 2018) to analyze the correlations between expressions of the nine dormancy-related genes and drug sensitivity. All of the genes are up-regulated in the dormant subgroup, and the gene expression levels of *LMOD1, MAB21L2*, and *ASPN* increased significantly with drug resistance (**Figure 5A**). This result suggests that ASPN, LMOD1, and MAB21L2 are key proteins that drive chemotherapy resistance

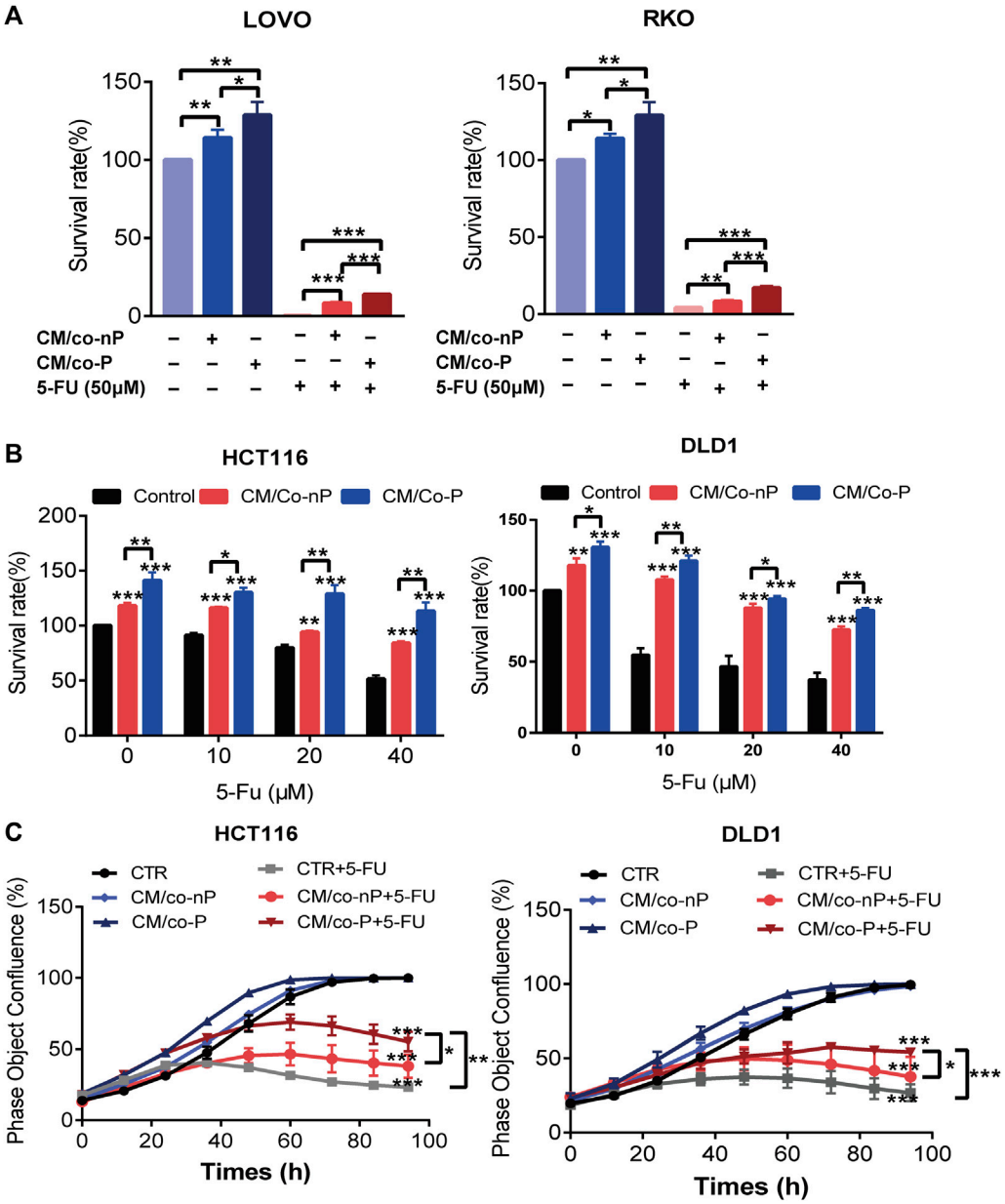

FIGURE 4 | (A) Comparison of the sensitivity of LoVo (left panel) and RKO (right panel) cells to 5-FU after 72 h incubation with different CMs. Cell viability was measured by a CCK-8 assay. $n = 3$. **(B)** HCT116 (left panel) and DLD1 (right panel) cells incubation with indicated CM were treated with different concentrations of 5-FU for 72 h, and cell viability was measured by CCK-8 assay. $n = 3$. **(C)** Growth curves of HCT116 (left panel) and DLD1 (right panel) cells were cultured under the indicated conditions for 72 h. The image data for phase object confluence were processed by IncuCyte Zoom software. $n = 3$. Bars, mean ± SD. $^{*}p < 0.05$; $^{**}p < 0.01$; $^{***}p < 0.001$.

and tumor recurrence in the dormant subgroup, and CRC patients with high expression of *LMOD1, MAB21L2*, and *ASPN* are at high risk of recurrence (**Figures 5B–G**). In addition, using the CTRP drug database, we found that sensitivity to austocystin D and erlotinib increased as *LMOD1, MAB21L2*, and *ASPN* expression increased (**Figure 5H**).

Interestingly, the EGFR signaling pathway is related to tumor dormancy and drug resistance (Luo et al., 2018). Besides, The transport of glutamine is also related to the drug sensitivity of cetuximab (Ma et al., 2018). Therefore, we speculated that they might contribute to the death of DTP cells in CRC. Thus, we verified our hypothesis using DTP cells (LoVo-P, RKO-P), and the results suggested that erlotinib can restore chemotherapy drug sensitivity and kill DTP cells (**Figure 5I**).

Austocystin D is a newly developed anti-cancer drug and is reported to overcome chemoresistance (Marks et al., 2011).

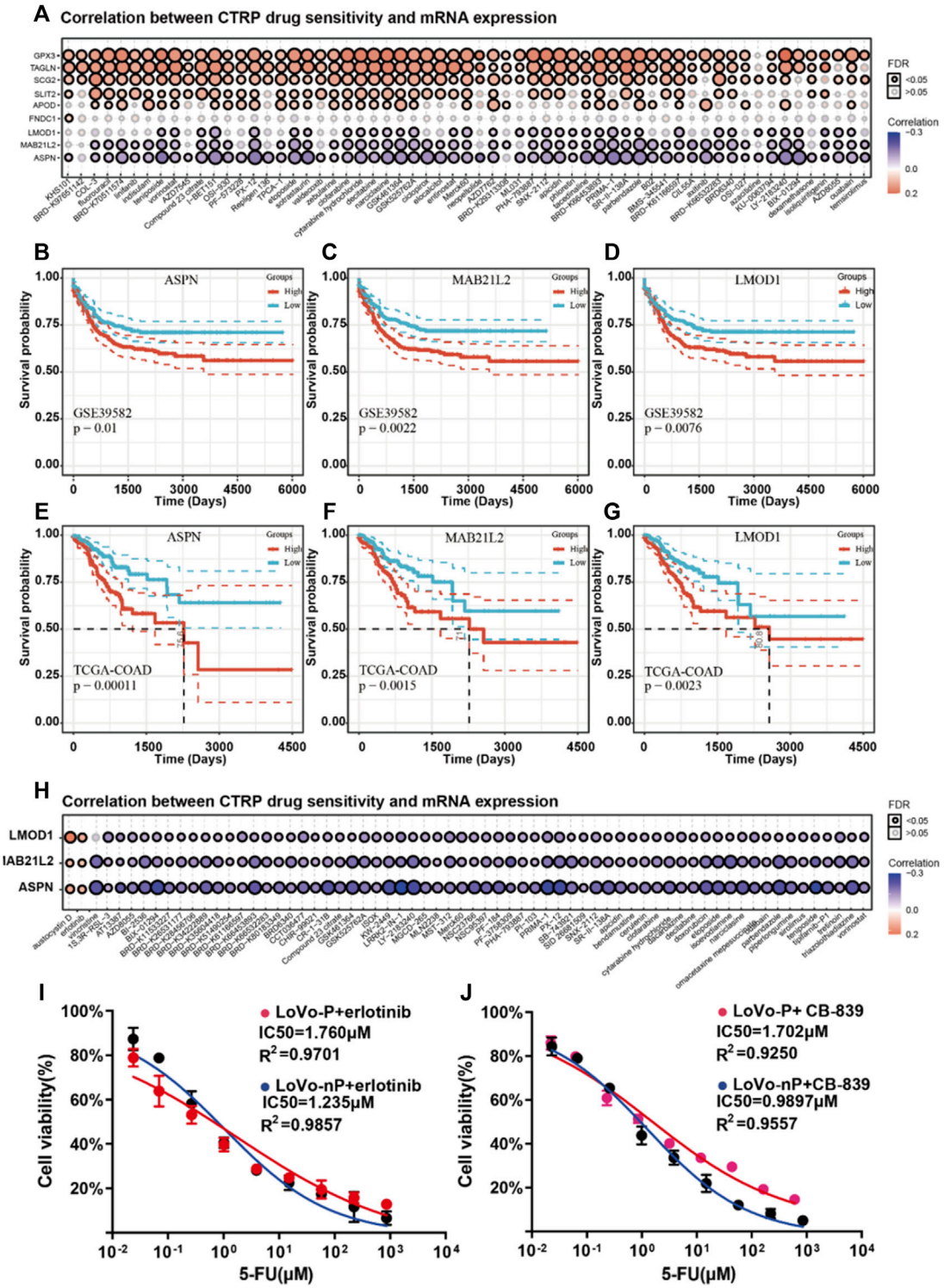

FIGURE 5 | (A) Correlation analysis between mRNA expression of nine prognosis-related genes and CTRP drug sensitivity. **(B–D)** Recurrence-free survival (RFS) of *ASPN*, *LMOD1*, and *MAB21L2* in GSE39582. **(E–G)** Progression-free survival (PFS) of *ASPN*, *LMOD1*, and *MAB21L2* in GSE39582. **(H)** Correlation analysis between mRNA expression of *ASPN*, *LMOD1*, and *MAB21L2* and CTRP drug sensitivity. **(I-J)** IC50 of 5-FU between DTP cells (LoVo-P and RKO-P) and parental cells (LoVo-nP and RKO-nP) cultured with erlotinib (2 μM) and CB-839 (2 μM).

However, it was not available to determine its effect on DTP cells. What is more, we used CB-839 to inhibit cells' glutamine metabolism and found that targeted GLS/GLS2 were the other strategies for overcoming chemoresistance of DTP cells (**Figure 5J**). Therefore, erlotinib, CB-839 may be potential treatments for overcoming resistance to chemotherapy in CRC patients.

DISCUSSION

Tumor dormancy is a significant factor in chemoresistance and cancer relapse. Identifying and characterizing tumor dormancy can help develop appropriate strategies for reversing the dormant state to overcome chemoresistance. However, nearly all of the research regarding the dormant state of cancer is based on cell and animal models. Our research began with transcriptome data from two large cohorts of patients with CRC and divided the patients into those with dormant and proliferous subgroups. GSEA analysis indicated that the two cohorts have strong consistency. It is generally believed that increased tumor proliferative activity in cancer patients often predicts poor outcomes, such as rapid progression and a poor prognosis, while weak proliferative activity is associated with a low degree of invasiveness and a good prognosis. In this study, patients in the dormant group were at high risk of cancer recurrence. Furthermore, based on the GSEA analysis, we identified two major characteristics of the dormant subgroup; metabolic changes and enhanced interactions with the cell matrix. At present, there are no other studies that have examined metabolic changes in dormant CRC cells. In this study, we found that indicators of cell energy metabolism such as pyruvate metabolism, the TCA cycle, and oxidative phosphorylation in the dormant subgroup were significantly different from that of the proliferous group, and we found that lactic acid and pyruvate in dormant cells were significantly reduced, which indicated the reversal of the Warburg effect (Vander Heiden et al., 2009).

Studies have shown that tumor cells can switch between aerobic glycolysis and oxidative phosphorylation to survive in a high-stress environment (Wangpaichitr et al., 2017). This adaptability is achieved by changing the method of energy metabolism, called metabolic reprogramming (Faubert et al., 2020). Metabolic reprogramming is a dominant evolutionary choice in tumor cells' malignant transformation, which aids in survival (Herst et al., 2018). During chemotherapy, drug-resistant cells usually exhibit higher mitochondrial activity (Daniel et al., 2021). Drug-resistant cells may also rely on fatty acid metabolism or glutaminolysis to sustain their energy needs. Our results showed that the synthesis of lactic acid and pyruvate in dormant cancer cells were decreased compared with that of parent cells. We also found increased metabolites of the TCA cycle, such as α-KG and succinate, which indicates that energy reprogramming may be present, and there are alternate synthetic pathways of these metabolites in DTP cells. This phenomenon illustrates the importance of glutamine metabolism (Altman et al., 2016; Martinez-Outschoorn et al., 2017), which can synthesize α-ketoglutarate into the TCA cycle to produce ATP from glutamine *via* glutaminase and glutamate. Therefore, we detected the flow of carbon sources in dormant CRC cells and confirmed our hypothesis that dormant cells significantly increased the effect of glutamine metabolism. This finding indicates that glutamine is an energy source of dormant CRC cells. Interestingly, a recent study revealed that CRC cells exhibited the highest glutamine uptake in the tumor microenvironment, whereas myeloid cells had the greatest capacity to take up intra-tumoral glucose (cell-programmed nutrient partitioning) in the tumor microenvironment.

In addition, other GSEA analysis results suggested that the interaction between cells and matrix was enhanced in the dormant subgroup. Further analysis using the single-cell database indicated that fibroblasts play a critical role in the interaction. No prior studies examine the interaction between dormant CRC cells and cancer-associated fibroblasts; however, studies have shown that CAFs are closely related to tumor cell proliferation and survival. They can release lactate and glutamine to create a nutrient-rich microenvironment that assists tumor cell survival (Whitaker-Menezes et al., 2011; Kim et al., 2013). The most critical regulatory factor is hypoxia-inducible factor 1α (HIF-1α), as HIF-1α can regulate the expression of microcystin 1 (Cav-1) to affect the autophagy level of CAFs (Kannan et al., 2014). Studies have also shown that fibroblasts lacking Cav-1 secrete more glutamine into the microenvironment (Sotgia et al., 2012; Zhao et al., 2016). This mechanism is consistent with the metabolic characteristics of dormant CRC cells. i.e., increased demand for glutamine.

CAFs consume more glucose in most solid tumors and secretes more lactic acid than normal fibroblasts (Zhao et al., 2016). Our co-culture results showed that CAFs could enhance the drug resistance of DTP cells. The founding suggests that dormant CRC cells interact with CAFs to promote glutamine metabolism and resist the effects of chemotherapy. In order to determine the key drivers of this effect, we identified 44 DEGs in the two cohorts. Prior study has shown that *RGS2* is a driver of dormant cells in NSCLC (Cho et al., 2021). Subsequently, nine prognosis-related genes were identified through univariate analysis, and finally, *LMOD1, MAB21L2*, and *ASPN* were established as potential genes resulting in drug resistance in CRC dormancy via the CTPR database. We also predicted that erlotinib, CB-839, and austocystin D could potentially kill dormant CRC cells and verified the impact of erlotinib and CB-839 with DTP cells. According to the Human Protein Atlas (HPA, https://www.proteinatlas.org/), ASPN and MAB21L2 is located in the nucleus. In addition, studies have shown that ASPN is enriched in CAFs (Hesterberg et al., 2021) and can promote cancer cell metastasis via regulating cell metabolism (Sasaki et al., 2021).

Further studies of how these predicted driver genes regulate the dormant state of CRC are warranted. In subsequent research, we will focus on ASPN and regulating CRC dormancy. Establishing the mechanism of drug resistance in CRC dormant cells may assist in the development of new types of chemotherapy that can improve the survival of patients with CRC.

DATA AVAILABILITY STATEMENT

The datasets presented in this study can be found in online repositories. The names of the repository/repositories and accession number(s) can be found in the article/ **Supplementary Material**.

ETHICS STATEMENT

The study was approved by the Human Medical Ethics Committee of the Sixth Affiliated Hospital of Sun Yat-sen University, and informed consent was obtained from all patients before surgery.

AUTHOR CONTRIBUTIONS

JY and LX contributed to the conception and design of the study. XL, RH, and HH performed research, analyzed data, and wrote the manuscript. All authors discussed the results and revised the manuscript. XL, RH, and HH contributed equally to this work and should be considered co-first authors.

FUNDING

This work was supported by the Natural Science Foundation of Guangdong Province (grant numbers 2021A1515010639 and 2020A151501613) and the Science and Technology Planning Project of Guangdong Province (grant numbers 2019B030316011).

SUPPLEMENTARY MATERIAL

The Supplementary Material for this article can be found online at: https://www.frontiersin.org/articles/10.3389/fphar.2022.879751/full#supplementary-material

REFERENCES

Altman, B. J., Stine, Z. E., and Dang, C. V. (2016). From Krebs to Clinic: Glutamine Metabolism to Cancer Therapy. *Nat. Rev. Cancer* 16, 619–634. doi:10.1038/nrc.2016.71

Basu, S., Dong, Y., Kumar, R., Jeter, C., and Tang, D. G. (2022). Slow-cycling (Dormant) Cancer Cells in Therapy Resistance, Cancer Relapse and Metastasis. *Semin. Cancer Biol.* 78 (21), 90–103. doi:10.1016/j.semcancer.2021.04.021

Brunet, J. P., Tamayo, P., Golub, T. R., and Mesirov, J. P. (2004). Metagenes and Molecular Pattern Discovery Using Matrix Factorization. *Proc. Natl. Acad. Sci. U S A.* 101, 4164–4169. doi:10.1073/pnas.0308531101

Cho, J., Min, H.-Y., Lee, H. J., Hyun, S. Y., Sim, J. Y., Noh, M., et al. (2021). RGS2-mediated Translational Control Mediates Cancer Cell Dormancy and Tumor Relapse. *J. Clin. Invest.* 131, e136779. doi:10.1172/JCI136779

Dai, L., Li, M., Zhang, W. L., Tang, Y. J., Tangling, Y. L., and Liang, X. H. (2021). Fibroblasts in Cancer Dormancy: Foe or Friend? *Cancer Cell Int* 21, 184. doi:10.1186/s12935-021-01883-2

Daniel, Y., Lelou, E., Aninat, C., Corlu, A., and Cabillic, F. (2021). Interplay between Metabolism Reprogramming and Epithelial-To-Mesenchymal Transition in Cancer Stem Cells. *Cancers (Basel)* 13, 1973. doi:10.3390/cancers13081973

Faubert, B., Solmonson, A., and DeBerardinis, R. J. (2020). Metabolic Reprogramming and Cancer Progression. *Science* 368, eaaw5473. doi:10.1126/science.aaw5473

Herst, P. M., Grasso, C., and Berridge, M. V. (2018). Metabolic Reprogramming of Mitochondrial Respiration in Metastatic Cancer. *Cancer Metastasis Rev.* 37, 643–653. doi:10.1007/s10555-018-9769-2

Hesterberg, A. B., Rios, B. L., Wolf, E. M., Tubbs, C., Wong, H. Y., Schaffer, K. R., et al. (2021). A Distinct Repertoire of Cancer-Associated Fibroblasts Is Enriched in Cribriform Prostate Cancer. *J. Pathol. Clin. Res.* 7, 271–286. doi:10.1002/cjp2.205

Irizarry, R. A., Hobbs, B., Collin, F., Beazer-Barclay, Y. D., Antonellis, K. J., Scherf, U., et al. (2003). Exploration, Normalization, and Summaries of High Density Oligonucleotide Array Probe Level Data. *Biostatistics* 4, 249–264. doi:10.1093/biostatistics/4.2.249

Ju, S., Wang, F., Wang, Y., and Ju, S. (2020). CSN8 Is a Key Regulator in Hypoxia-Induced Epithelial-Mesenchymal Transition and Dormancy of Colorectal Cancer Cells. *Mol. Cancer* 19, 168. doi:10.1186/s12943-020-01285-4

Kannan, A., Krishnan, A., Ali, M., Subramaniam, S., Halagowder, D., and Sivasithamparam, N. D. (2014). Caveolin-1 Promotes Gastric Cancer Progression by Up-Regulating Epithelial to Mesenchymal Transition by Crosstalk of Signalling Mechanisms under Hypoxic Condition. *Eur. J. Cancer* 50, 204–215. doi:10.1016/j.ejca.2013.08.016

Katona, B. W., and Weiss, J. M. (2020). Chemoprevention of Colorectal Cancer. *Gastroenterology* 158, 368–388. doi:10.1053/j.gastro.2019.06.047

Kim, S., Kim, D. H., Jung, W. H., and Koo, J. S. (2013). Expression of Glutamine Metabolism-Related Proteins According to Molecular Subtype of Breast Cancer. *Endocr. Relat. Cancer* 20, 339–348. doi:10.1530/ERC-12-0398

Liao, Y., Wang, J., Jaehnig, E. J., Shi, Z., and Zhang, B. (2019). WebGestalt 2019: Gene Set Analysis Toolkit with Revamped UIs and APIs. *Nucleic Acids Res.* 47, W199–W205. doi:10.1093/nar/gkz401

Ligorio, M., Sil, S., Malagon-Lopez, J., Nieman, L. T., Misale, S., Di Pilato, M., et al. (2019). Stromal Microenvironment Shapes the Intratumoral Architecture of Pancreatic Cancer. *Cell* 178, 160. e27. doi:10.1016/j.cell.2019.05.012

Lin, Y. H., and Zhu, H. (2021). A Malignant Case of Arrested Development: Cancer Cell Dormancy Mimics Embryonic Diapause. *Cancer Cell* 39, 142–144. doi:10.1016/j.ccell.2021.01.013

Liu, C. J., Hu, F. F., Xia, M. X., Han, L., Zhang, Q., and Guo, A. Y. (2018). GSCALite: A Web Server for Gene Set Cancer Analysis. *Bioinformatics* 34, 3771–3772. doi:10.1093/bioinformatics/bty411

Luo, X. L., Deng, C. C., Su, X. D., Wang, F., Chen, Z., Wu, X. P., et al. (2018). Loss of MED12 Induces Tumor Dormancy in Human Epithelial Ovarian Cancer via Downregulation of EGFR. *Cancer Res.* 78, 3532–3543. doi:10.1158/0008-5472.CAN-18-0134

Ma, H., Wu, Z., Peng, J., Li, Y., Huang, H., Liao, Y., et al. (2018). Inhibition of SLC1A5 Sensitizes Colorectal Cancer to Cetuximab. *Int. J. Cancer* 142, 2578–2588. doi:10.1002/ijc.31274

Manjili, S. H., Isbell, M., Ghochaghi, N., Perkinson, T., and Manjili, M. H. (2022). Multifaceted Functions of Chronic Inflammation in Regulating Tumor Dormancy and Relapse. *Semin. Cancer Biol.* 78 (21), 17–22. doi:10.1016/j.semcancer.2021.03.023

Marisa, L., de Reyniès, A., Duval, A., Selves, J., Gaub, M. P., Vescovo, L., et al. (2013). Gene Expression Classification of Colon Cancer into Molecular Subtypes: Characterization, Validation, and Prognostic Value. *Plos Med.* 10, e1001453. doi:10.1371/journal.pmed.1001453

Marks, K. M., Park, E. S., Arefolov, A., Russo, K., Ishihara, K., Ring, J. E., et al. (2011). The Selectivity of Austocystin D Arises from Cell-line-specific Drug Activation by Cytochrome P450 Enzymes. *J. Nat. Prod.* 74, 567–573. doi:10.1021/np100429s

Martinez-Outschoorn, U. E., Peiris-Pagés, M., Pestell, R. G., Sotgia, F., and Lisanti, M. P. (2017). Cancer Metabolism: A Therapeutic Perspective. *Nat. Rev. Clin. Oncol.* 14, 11–31. doi:10.1038/nrclinonc.2016.60

Peng, S., Chen, D., Cai, J., Yuan, Z., Huang, B., Li, Y., et al. (2021). Enhancing Cancer-Associated Fibroblast Fatty Acid Catabolism within a Metabolically

Challenging Tumor Microenvironment Drives colon Cancer Peritoneal Metastasis. *Mol. Oncol.* 15, 1391–1411. doi:10.1002/1878-0261.12917

Possemato, R., Marks, K. M., Shaul, Y. D., Pacold, M. E., Kim, D., Birsoy, K., et al. (2011). Functional Genomics Reveal that the Serine Synthesis Pathway Is Essential in Breast Cancer. *Nature* 476, 346–350. doi:10.1038/nature10350

Rehman, S. K., Haynes, J., Collignon, E., Brown, K. R., Wang, Y., Nixon, A. M. L., et al. (2021). Colorectal Cancer Cells Enter a Diapause-like DTP State to Survive Chemotherapy. *Cell* 184, 226. e21. doi:10.1016/j.cell.2020.11.018

Sasaki, Y., Takagane, K., Konno, T., Itoh, G., Kuriyama, S., Yanagihara, K., et al. (2021). Expression of Asporin Reprograms Cancer Cells to Acquire Resistance to Oxidative Stress. *Cancer Sci.* 112, 1251–1261. doi:10.1111/cas.14794

Siegel, R. L., Miller, K. D., Goding Sauer, A., Fedewa, S. A., Butterly, L. F., Anderson, J. C., et al. (2020). Colorectal Cancer Statistics, 2020. *CA Cancer J. Clin.* 70, 145–164. doi:10.3322/caac.21601

Sosa, M. S., Bragado, P., and Aguirre-Ghiso, J. A. (2014). Mechanisms of Disseminated Cancer Cell Dormancy: An Awakening Field. *Nat. Rev. Cancer* 14, 611–622. doi:10.1038/nrc3793

Sotgia, F., Martinez-Outschoorn, U. E., Howell, A., Pestell, R. G., Pavlides, S., and Lisanti, M. P. (2012). Caveolin-1 and Cancer Metabolism in the Tumor Microenvironment: Markers, Models, and Mechanisms. *Annu. Rev. Pathol.* 7, 423–467. doi:10.1146/annurev-pathol-011811-120856

Sun, D., Wang, J., Han, Y., Dong, X., Ge, J., Zheng, R., et al. (2021). TISCH: A Comprehensive Web Resource Enabling Interactive Single-Cell Transcriptome Visualization of Tumor Microenvironment. *Nucleic Acids Res.* 49, D1420–D1430. doi:10.1093/nar/gkaa1020

Vander Heiden, M. G., Cantley, L. C., and Thompson, C. B. (2009). Understanding the Warburg Effect: The Metabolic Requirements of Cell Proliferation. *Science* 80-324, 1029–1033. doi:10.1126/science.1160809

Vander Heiden, M. G., and DeBerardinis, R. J. (2017). Understanding the Intersections between Metabolism and Cancer Biology. *Cell* 168, 657–669. doi:10.1016/j.cell.2016.12.039

Wangpaichitr, M., Wu, C., Li, Y. Y., Nguyen, D. J. M., Kandemir, H., Shah, S., et al. (2017). Exploiting ROS and Metabolic Differences to Kill Cisplatin Resistant Lung Cancer. *Oncotarget* 8, 49275–49292. doi:10.18632/oncotarget.17568

Whitaker-Menezes, D., Martinez-Outschoorn, U. E., Lin, Z., Ertel, A., Flomenberg, N., Witkiewicz, A. K., et al. (2011). Evidence for a Stromal-Epithelial "lactate Shuttle" in Human Tumors: MCT4 Is a Marker of Oxidative Stress in Cancer-Associated Fibroblasts. *Cell Cycle* 10, 1772–1783. doi:10.4161/cc.10.11.15659

Zhang, L., Li, Z., Skrzypczynska, K. M., Fang, Q., Zhang, W., O'Brien, S. A., et al. (2020). Single-Cell Analyses Inform Mechanisms of Myeloid-Targeted Therapies in Colon Cancer. *Cell* 181, 442. e29. doi:10.1016/j.cell.2020.03.048

Zhao, H., Yang, L., Baddour, J., Achreja, A., Bernard, V., Moss, T., et al. (2016). Tumor Microenvironment Derived Exosomes Pleiotropically Modulate Cancer Cell Metabolism. *Elife* 5, e10250. doi:10.7554/eLife.10250

Conflict of Interest: The authors declare that the research was conducted in the absence of any commercial or financial relationships that could be construed as a potential conflict of interest.

Publisher's Note: All claims expressed in this article are solely those of the authors and do not necessarily represent those of their affiliated organizations, or those of the publisher, the editors and the reviewers. Any product that may be evaluated in this article, or claim that may be made by its manufacturer, is not guaranteed or endorsed by the publisher.

GLOSSARY

α-KG alpha ketoglutarate
APOD apolipoprotein D
ASPN asporin
ATP adenosine triphosphate
CAFs cancer-associated fibroblasts
CM conditioned media
Cav-1 microcystin 1
CHARTS characterizing tumor subpopulations
CRC colorectal cancer
CTRP Cancer Therapeutics Response Portal database
DEGs differentially expressed genes
DTP drug-tolerant persister
EGFR epidermal growth factor receptor
FMN1 formin 1
FNDC1 fibronectin type III domain containing 1
FGF fibroblast growth factor
GSCA Gene Set Cancer Analysis
GTP guanosine triphosphate
GPX3 glutathione peroxidase 3
HIF-1α hypoxia-inducible factor 1 alpha
HR hazard ratio
IFN interferon
IGF insulin-like growth factor
IL interleukin
LC-MS/MS liquid chromatography-tandem mass spectrometry
LMOD1 leiomodin 1
MAB21L2 Mab-21 like 2
M-SCF macrophage-stimulating factor
NAD nicotinamide adenine dinucleotide
NES Normalized Enrichment Score
NMF non-negative matrix factorization
OS overall survival
PFS progression-free survival
RGS2 regulator of G protein signaling 2
RFS recurrence-free survival
SCG2 secretogranin II
SLIT2 slit guidance ligand 2
TAGLN transgelin
TCA cycle tricarboxylic acid cycle
TCGA The Cancer Genome Atlas
TGF-β transforming growth factor beta

frontiers | Frontiers in Pharmacology

ORIGINAL RESEARCH
published: 04 May 2022
doi: 10.3389/fphar.2022.875149

TCR Coexpression Signature Predicts Immunotherapy Resistance in NSCLC

Yuntao Wang[1†], Yi Liu[2†], Xiaohua Li[3†], Weiming Li[3†], Zhihong Xue[1], Xiaoqian He[1], Weijie Xiong[1], Lang He[1] and Yifeng Bai[4]**

[1]Department of Oncology, The Fifth People's Hospital Affiliated to Chengdu University of Traditional Chinese Medicine the Second Clinical Medical College, Chengdu, China, [2]Wenjiang District People's Hospital of Chengdu City, Chengdu, China, [3]Department of Respiratory and Critical Care Medicine, Sixth People's Hospital of Chengdu, Chengdu, China, [4]Department of Oncology, Sichuan Provincial People's Hospital, University of Electronic Science and Technology of China, Chengdu, China

Background: Lung cancer has the highest morbidity and mortality rate among types of malignant tumors, and as such, research into prolonging the survival time of patients is vital. The emergence of immune checkpoint inhibitors (ICIs) has greatly improved the survival of patients with non-small cell lung cancer (NSCLC), however, the lack of effective biomarkers to predict the prognosis of immunotherapy has made it difficult to maximize the benefits. T cell receptor (TCR) is one of the most important components for recognizing tumor cells, and with this study we aim to clarify the relationship between TCR coexpression and the prognosis of NSCLC patients receiving immunotherapy.

Methods: Univariate COX regression, logistics regression, and KM survival analysis were used to evaluate the relationship between TCR coexpression and the prognosis of immunotherapy. Additionally, CIBERSORT, Gene Set Enrichment Analysis (GSEA), and single-sample GSEA (ssGSEA) algorithms were used to evaluate the tumor immune microenvironment (TIME) of NSCLC patients.

Results: Univariate Cox regression analysis showed that the TCR coexpression signature can be used as a clinical prognostic indicator for NSCLC patients receiving immunotherapy (p = 0.0205). In addition, those in the NSCLC group with a high TCR coexpression signature had significantly improved progression-free survival (PFS) (p = 0.014). In the ICI treatment cohort (GSE35640). In addition, there was a high infiltration of CD8+T cells, activated memory CD4+T cells, and M1 macrophages in the TIME of those with a high TCR coexpression signature. The results of pathway enrichment analysis showed that patients with a high TCR coexpression signature had significantly activated signal pathways such as lymphocyte proliferation and activation, chemokine binding, and inflammatory cytokine production. Also, we found that patients with a high TCR coexpression signature had an elevated T cell inflammation gene expression profile (GEP).

Conclusion: We show that the TCR coexpression signature may be useful as a new biomarker for the prognosis of NSCLC patients undergoing immunotherapy, with high signatures indicating better treatment response. Additionally, we found that patients with a high TCR coexpression signature had tumor immune microenvironments with beneficial anti-tumor characteristics.

Keywords: ICIs, tumor immune microenvironment, NSCLC, biomarker, TCR—T cell receptor

OPEN ACCESS

Edited by:
Clare Y. Slaney,
Peter MacCallum Cancer Centre, Australia

Reviewed by:
Chaozheng Zhou,
Southern Medical University, China
Wenjie Shi,
Pius-Hospital Oldenburg, Germany

****Correspondence:***
Lang He
helang729@163.com
Yifeng Bai
baiyifeng@med.uestc.edu.cn

†These authors have contributed equally to this work and share first authorship

Specialty section:
This article was submitted to Pharmacology of Anti-Cancer Drugs, a section of the journal Frontiers in Pharmacology

Received: *13 February 2022*
Accepted: *21 March 2022*
Published: *04 May 2022*

Citation:
Wang Y, Liu Y, Li X, Li W, Xue Z, He X, Xiong W, He L and Bai Y (2022) TCR Coexpression Signature Predicts Immunotherapy Resistance in NSCLC. Front. Pharmacol. 13:875149. doi: 10.3389/fphar.2022.875149

INTRODUCTION

Lung cancer currently has the highest morbidity (11.6%) and mortality (18.4%) among all tumors (Bray et al., 2018). About 75% are advanced (stage III–IV) at the time of diagnosis, and the 5-years survival rate is less than 20%. Non-small cell lung cancer (NSCLC) is the most common, accounting for 80–85% of all lung cancers, and about 57% of patients with advanced NSCLC have distant metastasis at the time of diagnosis (Zappa and Mousa, 2016; Guan et al., 2019). Chemotherapy, targeted therapy, and anti-angiogenic drugs have become the cornerstone of treatment for these patients, but in recent years, the emergence of immune checkpoint inhibitors (ICIs) has changed the approach to NSCLC treatment. According to the literature, the 5-years survival rate of NSCLC patients receiving multi-line therapy that includes immunotherapy treatment can reach 16% (Gettinger et al., 2018). For a non-selective population, the objective response rate (ORR) of ICIs administered without other drugs has been measured at 19–22%. In order to further optimize the benefits of immunotherapy, it is necessary to find biomarkers suitable for predicting the curative effect.

With the rapid development of research in this field, many prognostic markers relating to immune checkpoint blockade (ICB) therapy have been found (Lin et al., 2021). The existing markers for predicting the efficacy of immunotherapy, however, have their limitations. The application of PD-L1 is limited by the variations of time, tumor heterogeneity, and differences in detection method thresholds (Velcheti et al., 2014; McLaughlin et al., 2016; Hui et al., 2017; Mok et al., 2019) The use of tumor mutational burden (TMB) is limited due to the complexity and high cost of whole exon sequencing (WES) (Luo et al., 2019), with the biggest obstacle being the complicated threshold standard, which is difficult to determine (Gandara et al., 2018). Additionally, in regard to NSCLC, although some studies have shown that high microsatellite instability (MSI-H) is related to the efficacy of ICB (Le et al., 2015; Goodman et al., 2017; Prelaj et al., 2019; Niu et al., 2020; Huang et al., 2021; Zhang et al., 2021), MSI-H is very rare in lung cancer. Whether MSI-H can be used as an effective immunotherapy marker for NSCLC patients remains unverified. Therefore, there is still a need to investigate biomarkers and establish models that predict the curative effect to further screen for the patients who would benefit most from the treatment.

Immune repertoire is defined as the total number of T cells and B cells with functional diversity within an individual's circulatory system at any given time, and is a measure of the diversity and specificity of the individual's immune state (Looney et al., 2019). T lymphocytes recognize new tumor antigens and proliferate via the T cell antigen receptor (TCR), which is the key process in activating the host immune response against cancer cells. As these T cells carry TCR to recognize and eliminate tumor cells, TCR expression plays an important role in immunotherapy (Looney et al., 2019; Morita et al., 2020). Many studies have confirmed that the characteristics of the baseline TCR repertoire are related to the curative effect of therapy (Manuel et al., 2012; Robins, 2013; Robert et al., 2014; Postow et al., 2015). For example, low baseline T-cell diversity in the peripheral blood of breast cancer patients undergoing chemotherapy has been linked with poor prognosis (Manuel et al., 2012). According to Postow's research, after CTLA-4 was used, the increased TCR diversity at baseline was related to an increase in efficacy and benefits (Postow et al., 2015). In addition, studies have shown that patients with low T cell diversity in peripheral blood can receive great benefit from anti-PD-1 treatment (Hogan et al., 2019). Currently, there is no research in the literature on the relationship between TCR coexpression signature and the efficacy of NSCLC after receiving ICB. Therefore, in this study we explore and verify the role of TCR (specifically the TCR coexpression signature) in predicting the prognosis of NSCLC patients after immunotherapy at the level of the TIME. With these results, we aim to better identify the population who may benefit most from ICB therapy.

METHODS

Collection of Immunotherapy Cohort and TCGA Cohort Data

We downloaded an NSCLC cohort published by Hwang and colleagues on anti-PD-1 from the GEO database, which we named ICI-NSCLC (GSE136961) (Hwang et al., 2020). This cohort includes clinical prognosis and expression data for patients who received immunotherapy. In addition, we downloaded the expression and clinical data of TCGA-LUAD and TCGA-LUSC cohorts from the GDC database using the R package named TCGAbiolinks (Colaprico et al., 2016). In order to better study the population of NSCLC, we combined the TCGA-LUAD and TCGA-LUSC cohorts and named it the TCGA-NSCLC cohort. Because there were very few NSCLC cohorts with both ICI treatment data and expression data, we collected a melanoma cohort with ICI treatment from the GEO database and named it ICI-Melanoma (GSE35640) (Ulloa-Montoya et al., 2013). We also obtained an open-source bladder cancer cohort treated with ICIs from a published article by Mariathasan and his colleagues, which we designated ICI-BLCA (Mariathasan et al.) (Mariathasan et al., 2018; Zhou et al., 2021).

Calculation and Grouping of TCR Coexpression Signatures

According to the gene set definition in the expression data published by Hwang and his colleagues, we used the ssGSEA algorithm (Reas et al., 2007) and the R package named Gene Set Variation Analysis (GSVA) (Hänzelmann et al., 2013) to analyze each patient in the ICI-NSCLC (GSE136961), ICI-Melanoma (GSE35640), ICI-BLCA (Mariathan et al.), and TCGA-NSCLC cohorts. For each cohort, we divided the patients into high and low groups according to the median value of TCR coexpression signatures of all patients in each cohort. The gene set of TCR coexpression signature was detailed in **Supplementary Table S1**.

Tumor Immune Microenvironment Analysis

First, we uploaded the expression data of each cohort to the CIBERSORT webtool (Chen et al., 2018), selected LM22, set the number of iterations to 1,000, and analyzed the results. From this, we

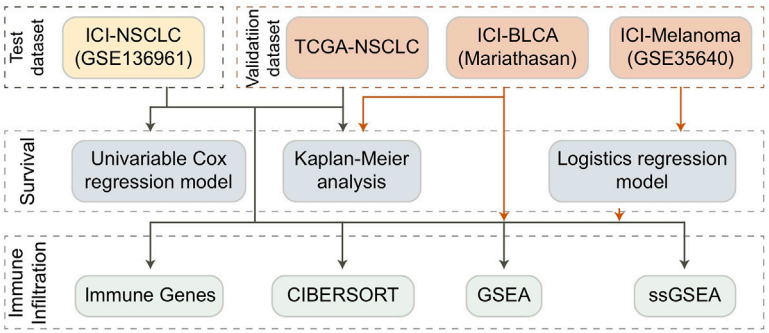

FIGURE 1 | Flowchart of data processing for the TCGA dataset and ICI-treated cohort.

were able to measure the prevalence of 22 types of immune cells for each patient in each cohort. Secondly, as one of the important targets of ICIs, data on immune checkpoint molecules were obtained from a published study for comparison (Rooney et al., 2015). Data on the genes and molecules that play a very important role in TIME was also obtained from published studies (Rooney et al., 2015; Thorsson et al., 2018). Using this data, we were able to compare the abundance of immune cells, the expression of immune checkpoint molecules, and the expression of immune-related genes among the high and low groups to determine which elements played a vital role.

Pathway Activity Analysis

We performed a difference analysis on the expression data for each cohort using the R package named Limma (Ritchie et al., 2015), and we used the results as the input file for gene set enrichment analysis (GSEA). We then used the R package named ClusterProfiler to analyze the enrichment of gene sets in the GO-BP, GO-CC, GO-MF, KEGG, and REACTOME databases according to the ranked list (including ENTREZID and logFC) (Subramanian et al., 2005). In addition, we used the R package named GSVA to analyze the ssGSEA of gene sets from the Molecular Signatures Database (MSigDB) (https://www.gsea-msigdb.org/gsea/msigdb/genesets.jsp). By obtaining the ssGSEA score for each patient, we were able to further compare the activity differences between the high and low groups on the same pathway.

Statistical Analysis

For continuous variables such as the abundance of immune cells, the expression of genes, and ssGSEA score, we used the Mann-Whitney U test to compare differences between the high and low groups. To study the predictive effect of TCR coexpression on the prognosis of immunotherapy, we used univariate COX regression, Kaplan-Meier (KM) regression, and logistics regression analysis. For the KM analysis, log-rank P was used to evaluate statistical significance. All the analyses in this study were conducted on R software (Version. 3.7). Statistical significance was evaluated by p value, with $p < 0.05$ regarded as having statistical difference and being bilateral.

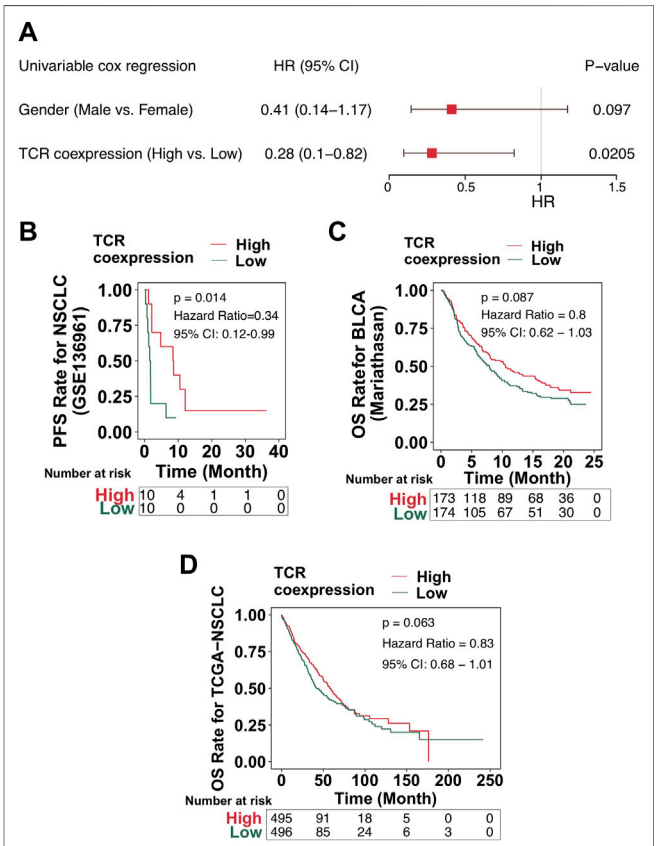

FIGURE 2 | High TCR coexpression signature was associated with improved prognosis of patients receiving immunotherapy. **(A)** The results of the univariate regression analyses displayed as a forest map (GSE136961). The main part of the forest map is used to show the HR and 95% confidence intervals. Factors associated with improved prognosis are log10(HR) < 1, and those associated with poor prognosis are log10(HR) > 1. **(B)** KM survival curves of PFS for NSCLC patients from the ICI cohort (GSE136961). **(C)** KM survival curves of OS for patients in the ICI-BLCA cohort (Mariathasan et al.). **(D)** KM survival curves of OS for patients in the TCGA-NSCLC cohort.

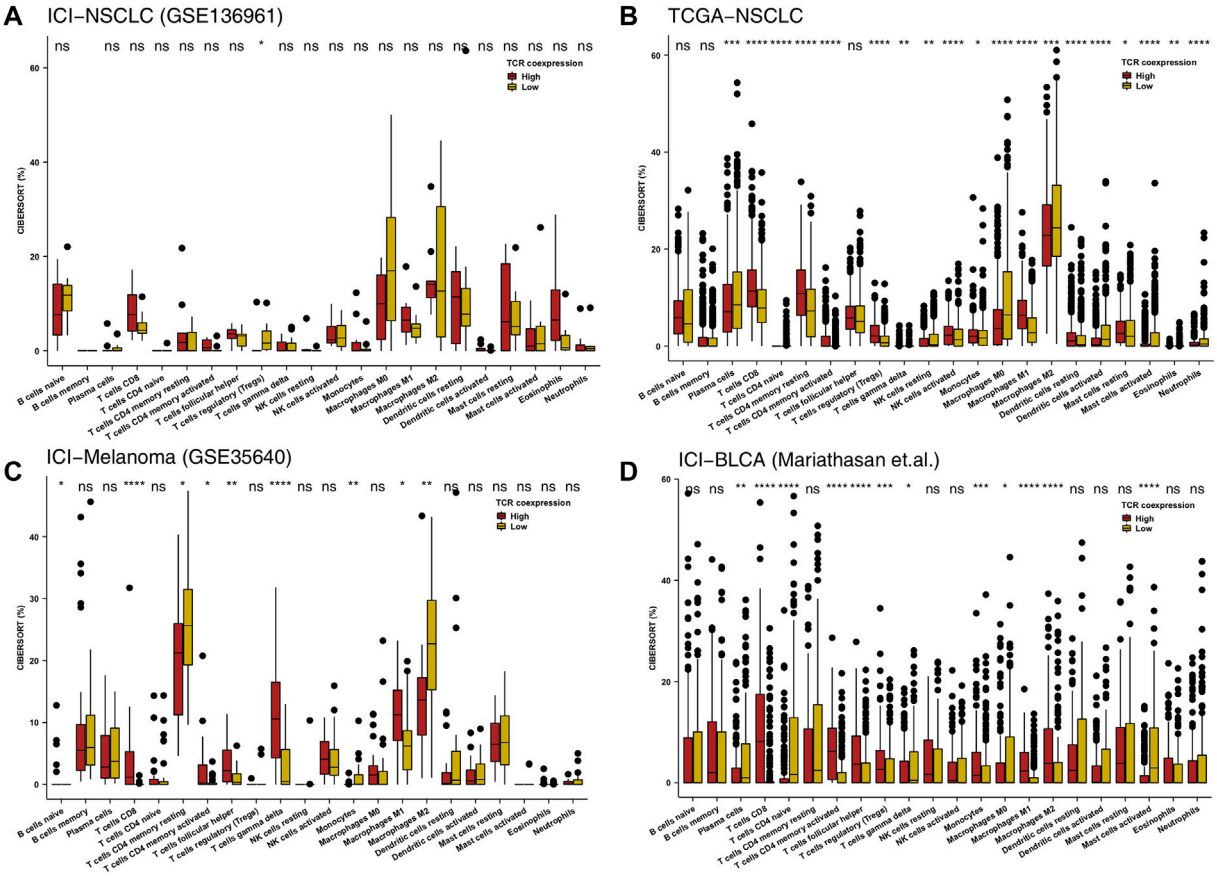

FIGURE 3 | High TCR coexpression signature was associated with a high proportion of activated immune cells. The 22 immune cell types estimated by CIBERSORT methods between the high- and low- TCR coexpression signature groups of the ICI-NSCLC **(A)**, TCGA-NSCLC **(B)**, ICI-Melanoma (GSE35640) **(C)**, and ICI-BLCA (Mariathasan et al.) **(D)** cohorts. The range of *p*-values is presented by the asterisks above each box plot (*$p < 0.05$; **$p < 0.01$; ***$p < 0.001$; ****$p < 0.0001$; Mann-Whitney U test).

RESULTS

High TCR Coexpression Signature Indicated Better Prognosis and Response to Immunotherapy

Our results showed a positive relationship between the TCR coexpression signature and the survival benefit and immune response of NSCLC patients treated with ICB. The process used to analyze our data is shown in detail in **Figure 1**. Firstly, we collected from a public database the expression data for an NSCLC cohort that had received immunotherapy and used it to calculate the TCR coexpression signature of each patient. For the ICI-NSCLC cohort, univariate Cox regression analysis showed that the TCR coxpression signature can be used as a predictor of clinical prognosis for NSCLC patients receiving immunotherapy [**Figure 2A**; $p = 0.0205$; Hazard ratio (HR) = 0.41]. Further analysis showed that the gender of patients was not related to the prognosis of NSCLC patients receiving immunotherapy (**Figure 2A**). No other clinical features of this cohort were available for analysis. The results of a survival rate analysis showed that the NSCLC group with a high TCR coexpression signature had significantly improved progression-free survival (PFS) (log-rank $p = 0.014$; HR = 0.34; 95%Cl: 0.12–0.99; **Figure 2B**). In the ICI-BLCA (Mariathasan et al.), we found that patients with a high TCR coexpression signature tended towards a prolonged PFS, although the results were not statistically significant ($p = 0.087$; HR = 0.8; **Figure 2C**). It should be noted that, although $p > 0.05$, the sample size of this cohort was small and thus may not be representative. To clarify the relationship between the TCR coexpression signature and clinical prognosis of NSCLC patients receiving routine treatment, the TCGA-NSCLC cohort was used for subsequent analysis. In the TCGA-NSCLC cohort (**Figure 2D**), the TCR coexpression signature did not show a significant relationship with the survival time of patients undergoing routine treatment (log-rank $p > 0.05$). The above results suggest that TCR coexpression signatures may be a suitable biomarker for predicting the treatment response of NSCLC patients receiving ICB therapy.

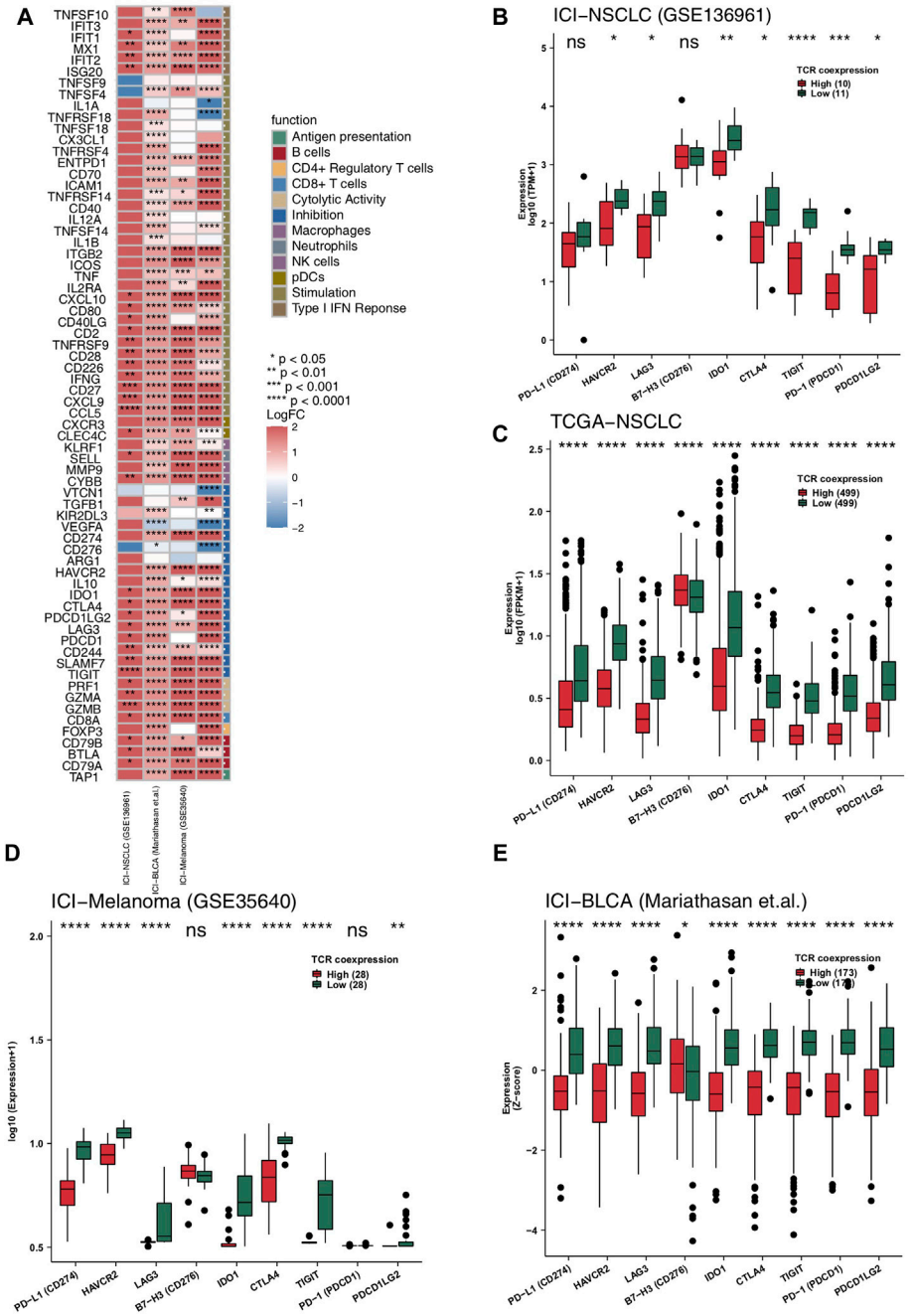

FIGURE 4 | High TCR coexpression signature was associated with high expression levels of immune-related genes. **(A)** Comparison of the expression levels of immune-related genes between the high- and low- TCR coexpression signature groups. Heat map depicting the mean differences in immune-related gene mRNA expression between high- and low- TCR coexpression signature groups across different cohorts. The *x*-axis of the heat map indicates different cohorts, and the *y*-axis indicates gene names. Each square represents the fold change or difference of each indicated immune-related gene between the high- and low- TCR coexpression signature groups in each cohort. Red indicates up-regulation and blue indicates down-regulation. Box plots comparing the expression levels of immune checkpoint molecules between the high- and low- TCR coexpression signature groups from the ICI-NSCLC **(B)**, TCGA-NSCLC **(C)**, ICI-Melanoma (GSE35640) **(D)**, and ICI-BLCA (Mariathasan et al.) **(E)** cohorts. The range of p-values is presented by the asterisks above each box plot (*$p < 0.05$; **$p < 0.01$; ***$p < 0.001$; ****$p < 0.0001$; Mann-Whitney U test).

High TCR Coexpression Signatures Were Related to a High Infiltration of Activated Immune Cells

Immune cells play an important role in detecting and killing tumor cells in the TIME. To clarify the relationship between a high TCR coexpression signature and the prognosis of immunotherapy, we used the CIBERSORT algorithm and evaluated the abundance of immune cell infiltration in the TIME. In the ICI-NSCLC cohort, we found that the TIME of the high TCR coexpression signature group had significantly less regulatory T lymphocytes when compared to low TCR coexpression signature group ($p < 0.05$; **Figure 3A**). In the TCGA-NSCLC cohort, we found that the high TCR coexpression signature group had a high infiltration of CD8+T cells, activated memory CD4+T cells, activated NK cells, and m1-type macrophages in the TIME. Additionally, the degree of infiltration for some immune cells with suppressed or static function in the high group was significantly lower than that in the low group. This included naive CD4+T cells, gamma delta T cells (γδ T cells), resting NK cells, and resting mast cells ($p < 0.05$; **Figure 3B**). In the ICI cohort (GSE35640), CD8+T cells, activated memory CD4+T cells, follicular helper T cells (TFH), γ δ T cells, and M1-type macrophages were significantly more frequent in patients with a high TCR coexpression signature. We also found that the relative abundance of CD4+T cells and M2-type macrophages in the high group was significantly lower than that in the low group ($p < 0.05$; **Figure 3C**). For the second ICI cohort (Mariathasan et al.), the high TCR coexpression signature group showed increased CD8+T cells, activated memory CD4+T cells, TFH, and M1-type macrophages in the TIME. Accordingly, the high group had a lower proportion of resting memory $CD4^+$ T cells and M0-type macrophages in the TIME ($p < 0.05$; **Figure 3D**). The above results suggest that a high TCR coexpression signature is related to a high infiltration of activated immune cells.

High TCR Coexpression Signatures Were Related to High Expression Levels of Anti-Tumor Related Immune Genes

Anti-tumor related immune genes include those relating to cytotoxic T lymphocytes, antigen processing and presentation, and immune stimulation. We put together a list of relevant anti-tumor immunity genes and analyzed them on-by-one in the four data sets of this study (**Figure 4A**). The heatmap in **Figure 4A** shows multiple changes in expression level for these genes in both the high and the low TCR coexpression groups. It can be seen from this figure that the expression levels of many cytotoxicity related genes (CD8A, GZMB, GZMA, and PRF1), chemokines (CXCR3, CCL5, CXCL9, and CXCL10), inflammatory cytokines (INFG, IL1, TNFSF4, and TNFSF9), and antigen processing and presentation related genes (TAP1) in the high TCR coexpression group were significantly higher than those in low group. We then analyzed the differences in common immune checkpoint molecules between the two groups. In the ICI-NSCLC cohort (GSE136961), compared with the low TCR coexpression group, the high group shows a significantly lower expression of immune checkpoint molecules, such as HAVCR2, LAG3, IDO1, CTLA4, TIGIT,PD-1, and PDCD1LG2 (**Figure 4B**). In the TCGA-NSCLC cohort, except for B7-H3, the expression of remaining checkpoint molecules in the high group was also significantly lower than that in low group ($p < 0.05$; **Figure 4C**). The other two cohorts undergoing immunotherapy showed similar results, with the expression of most checkpoint genes in the low TCR coexpression groups being significantly higher than in the high groups (**Figures 4D, E**).

High TCR Coexpression Signature is Related to High Activity of Anti-Tumor Related Signal Pathways

Signaling pathways also play an important role in anti-tumor activity, so we evaluated them in our patient cohorts using GSEA and ssGSEA. We found significant up-regulation of anti-tumor immune-related signal pathway activity [Enrichment score (ES) > 0; $p < 0.05$] in the high TCR coexpression signature group (**Figures 5A–D**). This included the B cell receptor signaling pathway, adaptive immune response, B cell activation, immune response-activating cell surface receptor signaling pathway, positive regulation of immune response, lymphocyte activation, positive regulation of leukocyte mediated immunity, and immunoregulatory interactions between lymphoid and a non-lymphoid cells. We utilized the ssGSEA algorithm to evaluate the activity of each pathway for every patient and found, in all four cohorts (**Figure 5E**), activation of $CD8^+$ T cells, proliferation of B cells, and lymphocytes, binding of chemokines including CXCR3, and production of cytokines (such as IL-10,IL-1). Also, the cytokine-mediated inflammatory response pathway showed significantly more activation in the high TCR coexpression group when compared to the low group. At the same time, activation of cell cycle checkpoint and DNA damage repair signal pathways were significantly lower in the high group.

DISCUSSION

In this study, we found that the TCR coexpression signature may be used as a biomarker to predict the prognosis of immunotherapy for NSCLC, with a high signature indicating a better prognosis. In addition, our results revealed that patients with a high TCR coexpression signature have a TIME with anti-tumor characteristics, such as a higher proportion of functional activated immune cells, lower proportion of functional depleted immune cells, and high expression of cytotoxicity, antigen treatment and presentation, genes related to immunostimulation, and a highly activated anti-tumor related immune response pathway.

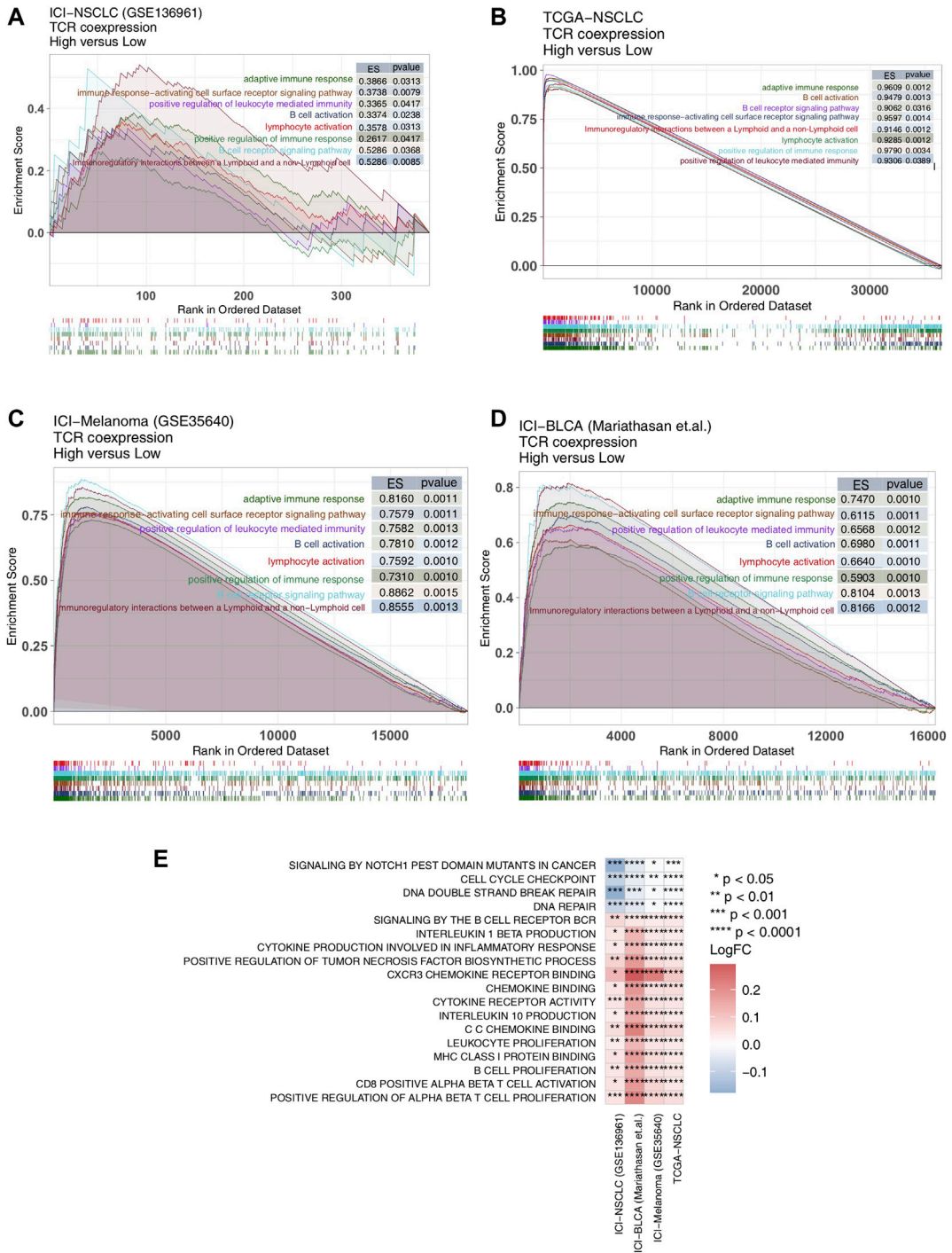

FIGURE 5 | High TCR coexpression signature was associated with a high degree of activated immune-related signaling pathways. Results of the GSEA for the ICI-NSCLC **(A)**, TCGA-NSCLC **(B)**, ICI-Melanoma (GSE35640) **(C)**, and ICI-BLCA (Mariathasan et al.) **(D)** cohorts. The low TCR coexpression signature group served as the control group. Enrichment score (ES) > 0 indicates that the corresponding pathways were significantly enriched in the experimental groups (high TCR coexpression signature group). The color of the curves corresponds to the font colors of the pathway names. **(E)** Heat map depicting the mean differences in the ssGSEA score of signaling pathways between high- and low- TCR coexpression signature groups across different cohorts. The *x*-axis of the heat map indicates different cohorts, and the *y*-axis indicates signaling pathways. Each square represents the fold change or difference of each indicated ssGSEA score of signaling pathways between high- and low-TCR coexpression signature groups in each cohort. Red indicates up-regulation; blue indicates down-regulation.

As patients with a high TCR coexpression signature had a consistently higher proportion of functional activated immune cells, we suggest the metric as one way to significantly improve the prognosis of immunotherapy. The immune system response to tumors is extremely complex, and the new antigen polypeptides formed by tumor mutations need to be both effectively presented by HLA-I and recognized by T lymphocytes carrying specific TCR. This is the key to immune activation. Previous studies have shown, in tissue samples of patients with advanced melanoma, that the degree of $CD8^+$ T cell infiltration can adequately predict the efficacy of PD-1/PD-L1 monoclonal antibody treatment (Tumeh et al., 2014). Antigen treatment and presentation are also very important components of the anti-tumor immune response (Wang et al., 2019; Yi et al., 2022), with previous studies showing that antigen treatment and signature presentation are related to a better prognosis for patients undergoing immunotherapy (Wang et al., 2019). In the process of antigen presentation, TAP-mediated peptides are transported into the endoplasmic reticulum cavity, where they combine with MHC-I complex, finally resulting in T cells which recognize new cell surface antigens (Schumacher and Schreiber, 2015). It has been found that M1 macrophages are able to use two different mechanisms simultaneously to destroy tumor cells once they have been recognized (Hu et al., 2016; Liang et al., 2020). One is that M1 macrophages directly mediate cytotoxicity in order to kill tumor cells. The other is that, stimulated by IFN-γ, macrophages can increase the secretion of inducible nitric oxide synthase, cell adhesion molecules, and other substances which enhance their tumor killing effect (Garrido-Martin et al., 2020). M2 macrophages are able to promote the proliferation of tumor cells through the arginase pathway, and can also participate in tumor angiogenesis (Garrido-Martin et al., 2020). For example, they can produce urokinase-type plasminogen activator and induce the formation of capillary networks via the release of various matrix metalloproteinases (Jayasingam et al., 2019). Additionally, M2 macrophages destroy the basement membrane of endothelial cells by secreting serine protease, metalloprotease, and cathepsin, and are able to decompose a series of collagen and other components of the extracellular matrix. In this way, M2 macrophages help the migration of tumor interstitial cells and tumor cells (Jayasingam et al., 2019; Ham et al., 2020). Using CIBERSORT, a calculation method for inferring leukocyte subtypes from tumor expression data, we found that M2 type macrophages were more predominant than M1 type macrophages in patients with low TCR coexpression signature (M2 type TAM predominant). According to the above results, we determined that patients with a low TCR coexpression signature were more likely to show TIME factors that promote the polarization of macrophages from M1 to M2 type, while in those with high TCR coexpression signatures, factors that maintain the polarization of M1 macrophages and encourage $CD8^+$ T cell infiltration were more dominant. In addition, the results of the GSEA and ssGSEA showed that the activity of signal pathways such as lymphocyte activation and proliferation were significantly up-regulated in patients with a higher TCR coexpression signature.

Besides immune cells, high levels of inflammatory cytokine expression and highly activated inflammatory cytokine signaling pathways have also been suggested as mechanisms by which the high TCR coexpression signature group significantly improves the prognosis of immunotherapy. Cytokines, such as interleukins, also play an important role in the TIME. Interleukins are the lymphatic factor of interaction between leukocytes or immune cells, and are essential for transmitting cellular information. They activate and regulate immune cells, mediate the activation, proliferation, and differentiation of T and B cells, and also play an important role in the inflammatory reaction. Ayers and his colleagues (Cristescu et al., 2018) defined a GEP of T cell inflammation as containing IFN-γ response genes, antigen presentation, chemokine expression, cytotoxicity, and adaptive immune resistance. They found that patients with higher GEP scores of T cells were more likely to benefit from immunotherapy. In addition, Cristescu et al. found that patients with high TMB and GEP expression undergoing treatment with pabrizumab had significantly improved PFS compared to patients with low TMB or GEP expression. In our study, we found that genes related to cytotoxicity (CD8A, GZMB, GZMA, and PRF1), chemokines (CXCR3, CCL5, CXCL9, and CXCL10), inflammatory cytokines (INFG, IL1, TNFSF4, and TNFSF9), and antigen processing and presentation related genes (TAP1) were significantly up-regulated in patients with a high TCR coexpression signature. In addition, the results of our GSEA and ssGSEA showed that the high TCR coexpression signature group had a higher degree of chemokine binding, CXCR3 chemokine binding, cytokine (such as IL-10, IL-1) production, cytokine-mediated inflammatory response, and other signal pathways.

Although our results are promising, some limitations in this study exist. Firstly, NSCLC cohorts with both immunotherapy prognosis data and expression data are very rare, which resulted in the use of only one NSCLC cohort collected from the public database, and the use of other cancer immunotherapy cohorts (such as melanoma and urinary system tumors) for the follow-up verification of TCR coexpression. Therefore, for future research we will continue to collect data for NSCLC patients receiving immunotherapy, to further verify the relationship between TCR coexpression and predicted prognosis. Secondly, only ssGSEA was used to estimate TCR coexpression. Moreover, the relationship between TCR diversity (such as the number of clonal species) and the TCR coexpression signature is still not well established. Considering these limitations, we were not able to comprehensively explore the potential mechanism between TCR coexpression signatures and the prognosis of NSCLC patients receiving immunotherapy.

CONCLUSION

In this study, we found that a high TCR coexpression signature is a potential biomarker for the prognosis of NSCLC in patients treated with ICB. With regard to the TIME, we found that patients with a high TCR coexpression signature have an immune microenvironment which promotes anti-tumor activity.

DATA AVAILABILITY STATEMENT

The original contributions presented in the study are included in the article/**Supplementary Material**, further inquiries can be directed to the corresponding authors.

AUTHOR CONTRIBUTIONS

Conceptualization, LH and YB; Formal analysis, YW; Visualization, YW; Writing–original draft, YL, XL, ZX, XH, and WX.; Writing–review and editing, YW, YL, XL, ZX, XH, WL, WX, LH, and YB. All authors read and approved the final manuscript.

FUNDING

This work was supported by Key Research and Development Projects of Sichuan Science and Technology (2021YFS0128); Medical Science and Technology Project of Sichuan Provincial Health Commission (21PJ153); Construction of a neoadjuvant radiotherapy niche screening platform for esophageal cancer based on imagingomics technology (2022YFS0378); Regulation of angiogenesis and immune microenvironment in non-small cell lung cancer by DLL4-NOTCH signaling pathway (2022YFS0156); A multidimensional deep learning model based on imagingomics predicts superior population screening for EGFR-mutated non-small cell lung cancer immunotherapy (2022YFS0221), 2020 Beijing CSCO Clinical Oncology Research Foundation Project (Y-MSD2020-0406). Thanks to the guidance of the Cancer Psychology and Health Managment Committee of Sichuan Cancer Society (S.C.S.), and the Chengdu High-level Key Clinical Specialty Construction Project.

SUPPLEMENTARY MATERIAL

The Supplementary Material for this article can be found online at: https://www.frontiersin.org/articles/10.3389/fphar.2022.875149/full#supplementary-material

REFERENCES

Bray, F., Ferlay, J., Soerjomataram, I., Siegel, R. L., Torre, L. A., and Jemal, A. (2018). Global Cancer Statistics 2018: GLOBOCAN Estimates of Incidence and Mortality Worldwide for 36 Cancers in 185 Countries. *CA Cancer J. Clin.* 68, 394–424. doi:10.3322/caac.21492

Chen, B., Khodadoust, M. S., Liu, C. L., Newman, A. M., and Alizadeh, A. A. (2018). Profiling Tumor Infiltrating Immune Cells with CIBERSORT. *Methods Mol. Biol.* 1711, 243–259. doi:10.1007/978-1-4939-7493-1_12

Colaprico, A., Silva, T. C., Olsen, C., Garofano, L., Cava, C., Garolini, D., et al. (2016). TCGAbiolinks: An R/Bioconductor Package for Integrative Analysis of TCGA Data. *Nucleic Acids Res.* 44, e71. doi:10.1093/nar/gkv1507

Cristescu, R., Mogg, R., Ayers, M., Albright, A., Murphy, E., Yearley, J., et al. (2018). Pan-Tumor Genomic Biomarkers for PD-1 Checkpoint Blockade-Based Immunotherapy. *Science* 362, 362. doi:10.1126/science.aar3593

Gandara, D. R., Paul, S. M., Kowanetz, M., Schleifman, E., Zou, W., Li, Y., et al. (2018). Blood-Based Tumor Mutational Burden as a Predictor of Clinical Benefit in Non-Small-Cell Lung Cancer Patients Treated with Atezolizumab. *Nat. Med.* 24, 1441–1448. doi:10.1038/s41591-018-0134-3

Garrido-Martin, E. M., Mellows, T. W. P., Clarke, J., Ganesan, A. P., Wood, O., Cazaly, A., et al. (2020). M1hot Tumor-Associated Macrophages Boost Tissue-Resident Memory T Cells Infiltration and Survival in Human Lung Cancer. *J. Immunother. Cancer* 8, 8. doi:10.1136/jitc-2020-000778

Gettinger, S., Horn, L., Jackman, D., Spigel, D., Antonia, S., Hellmann, M., et al. (2018). Five-Year Follow-Up of Nivolumab in Previously Treated Advanced Non-Small-Cell Lung Cancer: Results from the CA209-003 Study. *J. Clin. Oncol.* 36, 1675–1684. doi:10.1200/JCO.2017.77.0412

Goodman, A. M., Kato, S., Bazhenova, L., Patel, S. P., Frampton, G. M., Miller, V., et al. (2017). Tumor Mutational Burden as an Independent Predictor of Response to Immunotherapy in Diverse Cancers. *Mol. Cancer Ther.* 16, 2598–2608. doi:10.1158/1535-7163.MCT-17-0386

Guan, R., Lin, A., Luo, P., and Zhang, J. (2019). Association Between Circulating Inflammatory Proteins and Clinical Prognosis in Chinese Patients with EGFR Mutation-Positive Non-Small Cell Lung Cancer. *J. Thorac. Oncol.* 14, e222. doi:10.1016/j.jtho.2019.05.027

Ham, S., Lima, L. G., Lek, E., and Möller, A. (2020). The Impact of the Cancer Microenvironment on Macrophage Phenotypes. *Front. Immunol.* 11, 1308. doi:10.3389/fimmu.2020.01308

Hänzelmann, S., Castelo, R., and Guinney, J. (2013). GSVA: Gene Set Variation Analysis for Microarray and RNA-Seq Data. *BMC Bioinformatics* 14, 7. doi:10.1186/1471-2105-14-7

Hogan, S. A., Courtier, A., Cheng, P. F., Jaberg-Bentele, N. F., Goldinger, S. M., Manuel, M., et al. (2019). Peripheral Blood TCR Repertoire Profiling May Facilitate Patient Stratification for Immunotherapy Against Melanoma. *Cancer Immunol. Res.* 7, 77–85. doi:10.1158/2326-6066.CIR-18-0136

Hu, W., Li, X., Zhang, C., Yang, Y., Jiang, J., and Wu, C. (2016). Tumor-Associated Macrophages in Cancers. *Clin. Transl. Oncol.* 18, 251–258. doi:10.1007/s12094-015-1373-0

Huang, W., Lin, A., Luo, P., Liu, Y., Xu, W., Zhu, W., et al. (2021). EPHA5 Mutation Predicts the Durable Clinical Benefit of Immune Checkpoint Inhibitors in Patients with Lung Adenocarcinoma. *Cancer Gene Ther.* 28, 864–874. doi:10.1038/s41417-020-0207-6

Hui, R., Garon, E. B., Goldman, J. W., Leighl, N. B., Hellmann, M. D., Patnaik, A., et al. (2017). Pembrolizumab as First-Line Therapy for Patients with PD-L1-Positive Advanced Non-Small Cell Lung Cancer: A Phase 1 Trial. *Ann. Oncol.* 28, 874–881. doi:10.1093/annonc/mdx008

Hwang, S., Kwon, A. Y., Jeong, J. Y., Kim, S., Kang, H., Park, J., et al. (2020). Immune Gene Signatures for Predicting Durable Clinical Benefit of Anti-PD-1 Immunotherapy in Patients with Non-Small Cell Lung Cancer. *Sci. Rep.* 10, 643. doi:10.1038/s41598-019-57218-9

Jayasingam, S. D., Citartan, M., Thang, T. H., Mat Zin, A. A., Ang, K. C., and Ch'ng, E. S. (2019). Evaluating the Polarization of Tumor-Associated Macrophages into M1 and M2 Phenotypes in Human Cancer Tissue: Technicalities and Challenges in Routine Clinical Practice. *Front. Oncol.* 9, 1512. doi:10.3389/fonc.2019.01512

Le, D. T., Uram, J. N., Wang, H., Bartlett, B. R., Kemberling, H., Eyring, A. D., et al. (2015). PD-1 Blockade in Tumors with Mismatch-Repair Deficiency. *N. Engl. J. Med.* 372, 2509–2520. doi:10.1056/NEJMc151035310.1056/NEJMoa1500596

Liang, W., Huang, X., Carlos, C. J. J., and Lu, X. (2020). Research Progress of Tumor Microenvironment and Tumor-Associated Macrophages. *Clin. Transl. Oncol.* 22, 2141–2152. doi:10.1007/s12094-020-02367-x

Lin, A., Qiu, Z., Zhang, J., and Luo, P. (2021). Effect of NCOR1 Mutations on Immune Microenvironment and Efficacy of Immune Checkpoint Inhibitors in Patient with Bladder Cancer. *Front. Immunol.* 12, 630773. doi:10.3389/fimmu.2021.630773

Looney, T. J., Topacio-Hall, D., Lowman, G., Conroy, J., Morrison, C., Oh, D., et al. (2019). TCR Convergence in Individuals Treated with Immune Checkpoint Inhibition for Cancer. *Front. Immunol.* 10, 2985. doi:10.3389/fimmu.2019.02985

Luo, P., Lin, A., Li, K., Wei, T., and Zhang, J. (2019). DDR Pathway Alteration, Tumor Mutation Burden, and Cisplatin Sensitivity in Small Cell Lung Cancer: Difference Detected by Whole Exome and Targeted Gene Sequencing. *J. Thorac. Oncol.* 14, e276–e279. doi:10.1016/j.jtho.2019.08.2509

Manuel, M., Tredan, O., Bachelot, T., Clapisson, G., Courtier, A., Parmentier, G., et al. (2012). Lymphopenia Combined with Low TCR Diversity (Divpenia) Predicts Poor Overall Survival in Metastatic Breast Cancer Patients. *Oncoimmunology* 1, 432–440. doi:10.4161/onci.19545

Mariathasan, S., Turley, S. J., Nickles, D., Castiglioni, A., Yuen, K., Wang, Y., et al. (2018). TGFβ Attenuates Tumour Response to PD-L1 Blockade by Contributing to Exclusion of T Cells. *Nature* 554, 544–548. doi:10.1038/nature25501

McLaughlin, J., Han, G., Schalper, K. A., Carvajal-Hausdorf, D., Pelekanou, V., Rehman, J., et al. (2016). Quantitative Assessment of the Heterogeneity of PD-L1 Expression in Non-Small-Cell Lung Cancer. *JAMA Oncol.* 2, 46–54. doi:10.1001/jamaoncol.2015.3638

Mok, T. S. K., Wu, Y. L., Kudaba, I., Kowalski, D. M., Cho, B. C., Turna, H. Z., et al. (2019). Pembrolizumab versus Chemotherapy for Previously Untreated, PD-L1-Expressing, Locally Advanced or Metastatic Non-Small-Cell Lung Cancer (KEYNOTE-042): A Randomised, Open-Label, Controlled, Phase 3 Trial. *Lancet* 393, 1819–1830. doi:10.1016/S0140-6736(18)32409-7

Morita, K., Tsuda, S., Kobayashi, E., Hamana, H., Tsuda, K., Shima, T., et al. (2020). Analysis of TCR Repertoire and PD-1 Expression in Decidual and Peripheral CD8+ T Cells Reveals Distinct Immune Mechanisms in Miscarriage and Preeclampsia. *Front. Immunol.* 11, 1082. doi:10.3389/fimmu.2020.01082

Niu, Y., Lin, A., Luo, P., Zhu, W., Wei, T., Tang, R., et al. (2020). Prognosis of Lung Adenocarcinoma Patients with NTRK3 Mutations to Immune Checkpoint Inhibitors. *Front. Pharmacol.* 11, 1213. doi:10.3389/fphar.2020.01213

Postow, M. A., Manuel, M., Wong, P., Yuan, J., Dong, Z., Liu, C., et al. (2015). Peripheral T Cell Receptor Diversity Is Associated with Clinical Outcomes Following Ipilimumab Treatment in Metastatic Melanoma. *J. Immunother. Cancer* 3, 23. doi:10.1186/s40425-015-0070-4

Prelaj, A., Tay, R., Ferrara, R., Chaput, N., Besse, B., and Califano, R. (2019). Predictive Biomarkers of Response for Immune Checkpoint Inhibitors in Non-Small-Cell Lung Cancer. *Eur. J. Cancer* 106, 144–159. doi:10.1016/j.ejca.2018.11.002

Reas, C., Fry, B., and Maeda, J. (2007). *Processing: A Programming Handbook for Visual Designers*, 1. MA: MIT Press Cambridge, 49–54.

Ritchie, M. E., Phipson, B., Wu, D., Hu, Y., Law, C. W., Shi, W., et al. (2015). Limma Powers Differential Expression Analyses for RNA-Sequencing and Microarray Studies. *Nucleic Acids Res.* 43, e47. doi:10.1093/nar/gkv007

Robert, L., Tsoi, J., Wang, X., Emerson, R., Homet, B., Chodon, T., et al. (2014). CTLA4 Blockade Broadens the Peripheral T-Cell Receptor Repertoire. *Clin. Cancer Res.* 20, 2424–2432. doi:10.1158/1078-0432.CCR-13-2648

Robins, H. (2013). Immunosequencing: Applications of Immune Repertoire Deep Sequencing. *Curr. Opin. Immunol.* 25, 646–652. doi:10.1016/j.coi.2013.09.017

Rooney, M. S., Shukla, S. A., Wu, C. J., Getz, G., and Hacohen, N. (2015). Molecular and Genetic Properties of Tumors Associated with Local Immune Cytolytic Activity. *Cell* 160, 48–61. doi:10.1016/j.cell.2014.12.033

Schumacher, T. N., and Schreiber, R. D. (2015). Neoantigens in Cancer Immunotherapy. *Science* 348, 69–74. doi:10.1126/science.aaa4971

Subramanian, A., Tamayo, P., Mootha, V. K., Mukherjee, S., Ebert, B. L., Gillette, M. A., et al. (2005). Gene Set Enrichment Analysis: A Knowledge-Based Approach for Interpreting Genome-Wide Expression Profiles. *Proc. Natl. Acad. Sci. U S A.* 102, 15545–15550. doi:10.1073/pnas.0506580102

Thorsson, V., Gibbs, D. L., Brown, S. D., Wolf, D., Bortone, D. S., Ou Yang, T. H., et al. (2018). The Immune Landscape of Cancer. *Immunity* 48, 812–e14. doi:10.1016/j.immuni.2018.03.023

Tumeh, P. C., Harview, C. L., Yearley, J. H., Shintaku, I. P., Taylor, E. J., Robert, L., et al. (2014). PD-1 Blockade Induces Responses by Inhibiting Adaptive Immune Resistance. *Nature* 515, 568–571. doi:10.1038/nature13954

Ulloa-Montoya, F., Louahed, J., Dizier, B., Gruselle, O., Spiessens, B., Lehmann, F. F., et al. (2013). Predictive Gene Signature in MAGE-A3 Antigen-Specific Cancer Immunotherapy. *J. Clin. Oncol.* 31, 2388–2395. doi:10.1200/JCO.2012.44.3762

Velcheti, V., Schalper, K. A., Carvajal, D. E., Anagnostou, V. K., Syrigos, K. N., Sznol, M., et al. (2014). Programmed Death Ligand-1 Expression in Non-Small Cell Lung Cancer. *Lab. Invest.* 94, 107–116. doi:10.1038/labinvest.2013.130

Wang, S., He, Z., Wang, X., Li, H., and Liu, X. S. (2019). Antigen Presentation and Tumor Immunogenicity in Cancer Immunotherapy Response Prediction. *Elife* 8, 8. doi:10.7554/eLife.49020

Yi, R., Hong, S., Zhang, Y., Lin, A., Ying, H., Zou, W., et al. (2022). MHC-II Signature Correlates with Anti-Tumor Immunity and Predicts Anti-PD-L1 Response of Bladder Cancer. *Front. Cell Dev. Biol.* 10, 757137. doi:10.3389/fcell.2022.757137

Zappa, C., and Mousa, S. A. (2016). Non-Small Cell Lung Cancer: Current Treatment and Future Advances. *Transl. Lung Cancer Res.* 5, 288–300. doi:10.21037/tlcr.2016.06.07

Zhang, J., Zhou, N., Lin, A., Luo, P., Chen, X., Deng, H., et al. (2021). ZFHX3 Mutation as a Protective Biomarker for Immune Checkpoint Blockade in Non-Small Cell Lung Cancer. *Cancer Immunol. Immunother.* 70, 137–151. doi:10.1007/s00262-020-02668-8

Zhou, C., Lin, A., Cao, M., Ding, W., Mou, W., Guo, N., et al. (2021). Activation of the DDR Pathway Leads to the Down-Regulation of the TGFβ Pathway and a Better Response to ICIs in Patients with Metastatic Urothelial Carcinoma. *Front. Immunol.* 12, 634741. doi:10.3389/fimmu.2021.634741

Conflict of Interest: The authors declare that the research was conducted in the absence of any commercial or financial relationships that could be construed as a potential conflict of interest.

Publisher's Note: All claims expressed in this article are solely those of the authors and do not necessarily represent those of their affiliated organizations, or those of the publisher, the editors and the reviewers. Any product that may be evaluated in this article, or claim that may be made by its manufacturer, is not guaranteed or endorsed by the publisher.

frontiers | Frontiers in Pharmacology

ORIGINAL RESEARCH
published: 05 May 2022
doi: 10.3389/fphar.2022.868830

Crosstalk of Histone and RNA Modifications Identified a Stromal-Activated Subtype with Poor Survival and Resistance to Immunotherapy in Gastric Cancer

Cheng Yuan[1,2†], Junchang Zhang[1,3†], Cuncan Deng[1,2†], Yujian Xia[4], Bo Li[2,5], Sijun Meng[1,2], Xinghan Jin[1,3], Lvjia Cheng[6], Huafu Li[7], Changhua Zhang[1,2,5] and Yulong He[1,2,3,5]**

[1]Digestive Diseases Center, The Seventh Affiliated Hospital of Sun Yat-sen University, Shenzhen, China, [2]Guangdong Provincial Key Laboratory of Digestive Cancer Research, The Seventh Affiliated Hospital of Sun Yat-sen University, Shenzhen, China, [3]Department of Gastrointestinal Surgery, The First Affiliated Hospital of Sun Yat-sen University, Guangzhou, China, [4]Department of Thyroid Surgery, The Second Affiliated Hospital, College of Medicine, Zhejiang University, Hangzhou, China, [5]Scientific Research Center, The Seventh Affiliated Hospital of Sun Yat-sen University, Shenzhen, China, [6]Gastrointestinal Surgery, The First Affiliated Hospital of Jinan University, Guangzhou, China, [7]The Institute of Cancer Research, London, United Kingdom

Emerging evidence has revealed the pivotal role of epigenetic modifications in shaping the tumor microenvironment (TME). However, crosstalk between different modification types and their clinical relevance in cancers remain largely unexplored. In this study, using ChIP/MeRIP-seq data of seven human gastric cell lines, we systematically characterized the crosstalk of four epigenetic modification types including H3K4me1, H3K4me3, H3K27ac, and N6-methyladenosine (m6A) and identified a recurrent subtype with high FTO expression and low HDAC1 expression across three independent gastric cancer (GC) cohorts, which we named the epigenetic-modification-dysregulated (EMD) subtype. Patients of the EMD subtype were featured with poor survival, stromal activation, and immune suppression. Extensive relevance to clinical characteristics was observed in the EMD subtype, including the Lauren classification, MSI status, histological grade, TNM stage, the Asian Cancer Research Group classification, and the immune/fibrotic classification. An EMD score was then constructed using WGCNA and ssGSEA algorithms, to precisely recognize the EMD subtype and indicate prognosis and response to immunotherapy in multiple independent GC cohorts. Correlations of the EMD score with tumor mutation burden, tumor purity, aneuploidy score, tumorigenic pathways, TME characteristics, and FTO/HDAC1 ratio were measured. *In vitro* experiments were performed to demonstrate the correlation between FTO and the epithelial–mesenchymal transition pathway, which suggested FTO as a targetable vulnerability for GC patients with a high EMD score. Altogether, by comprehensively analyzing the epigenetic modification patterns of 1518 GC patients, we identified a novel stromal-activated subtype with poor survival and resistance to immunotherapy, which might benefit from the combined immune checkpoint inhibition therapy with FTO inhibition.

Keywords: gastric cancer, histone modification, m6A, tumor microenvironment, prognosis, immunotherapy

OPEN ACCESS

Edited by:
Haitao Wang,
National Cancer Institute (NIH), United States

Reviewed by:
Guangchun Han,
University of Texas MD Anderson Cancer Center, United States
Chang Gu,
Tongji University, China
Yaqiang Cao,
National Institutes of Health (NIH), United States
Lu Ji,
Stanford University, United States
Xin Qin,
Shandong University, China

****Correspondence:***
Changhua Zhang
zhchangh@mail.sysu.edu.cn
Yulong He
heyulong@mail.sysu.edu.cn

[†]These authors have contributed equally to this work and share first authorship

Specialty section:
This article was submitted to Pharmacology of Anti-Cancer Drugs, a section of the journal Frontiers in Pharmacology

Received: *03 February 2022*
Accepted: *07 March 2022*
Published: *05 May 2022*

Citation:
Yuan C, Zhang J, Deng C, Xia Y, Li B, Meng S, Jin X, Cheng L, Li H, Zhang C and He Y (2022) Crosstalk of Histone and RNA Modifications Identified a Stromal-Activated Subtype with Poor Survival and Resistance to Immunotherapy in Gastric Cancer. Front. Pharmacol. 13:868830. doi: 10.3389/fphar.2022.868830

1 INTRODUCTION

Gastric cancer (GC), the fifth most common cancer and the third most common cause of cancer deaths in the world, remains a non-negligible health problem and social burden globally (Smyth et al., 2020). Patients with early-stage GC featured a 5-year overall survival (OS) rate of more than 60%, for whom surgical resection is the best option (Thrift and El-Serag, 2020). For patients with advanced GC, chemotherapy represented by fluoropyrimidines and platinum significantly improves survival and the quality of life. Unfortunately, due to the high frequency of advanced stage at diagnosis and chemotherapy resistance, the 5-year overall survival rate of advanced GC is still less than 5% (Yuan et al., 2020). As a complex disease with molecular and clinical heterogeneity, GC shows versatile phenotypes in initiation, progression, and even the response to treatment among different patients. Thus, more effective individualized strategies both in diagnosis and therapy for GC are urgently needed to be explored.

Epigenetic modification, mainly including DNA methylation, histone modification, and RNA modification, is a significant regulatory mechanism of diverse physiological or pathological processes (Zhao et al., 2021a). Histone modification mainly refers to the post-translational modifications (PTMs) that occur in the N-terminal tails of histone proteins of nucleosomes, including but not limited to methylation, acetylation, and ubiquitination (Zhao and Shilatifard, 2019). Generally, histone modifications (such as H3K4me1, H3K4me3, and H3K27ac) enriched at the enhancer or promoter region presumably facilitate the transcription process of the targeted genes (Bannister and Kouzarides, 2011). N6-methyladenosine (m6A), defined as methylation of adenosine at the N6 position, is one of the most abundant RNA modification types in eukaryotic species including mammals, plants, insects, yeast, and certain viruses (Gu et al., 2020). Recently, accumulating evidence has suggested the extensive interactions between histone and m6A modifications, which trigger epigenetic remodeling and cause profound impacts on various aspects of cancer progression, including the resistance to medical treatment. (Huang et al., 2019; Li et al., 2020a; Yang et al., 2021a; Li et al., 2021). For example, Li et al. uncovered a SOX4/EZH2/METTL3 axis in TMZ-resistant glioblastoma (GBM), in which EZH2 regulates the METTL3 expression *via* an H3K27me3 modification-independent manner, and METTL3 leads to nonsense-mediated mRNA decay of EZH2 reversely (Li et al., 2021). Moreover, Li et al. found that the m6A reader YTHDC1 physically interacts with and recruits KDM3B to m6A-associated chromatin regions, promoting H3K9me2 demethylation and gene expression, establishing a direct link between m6A and histone modification (Li et al., 2020a). Similar interactions have also been observed in GC. Yang et al.'s study suggested that HDAC3 regulates the FTO (fat-mass and obesity-associated protein) expression in a FOXA2-dependent manner, thus promoting the proliferation, migration, and invasion of GC cells (Yang et al., 2021a).

The tumor microenvironment (TME), known as the soil of the tumor seed, which plays a pivotal role in tumorigenesis and anti-tumor immunity, has been recently reported to be shaped by various epigenetic modifications (Huang et al., 2012; Gu et al., 2021). For instance, Yin et al. reported that EZH2 depletion increased generation of the IL-15 receptor (IL-15R), CD122 (+) NK precursors, and mature NK progeny from both mouse and human hematopoietic stem and progenitor cells, demonstrating the impact of histone modification H3K27me3 on early NK cell differentiation (Yin et al., 2015). Wang et al. found that METTL3/14-deficient tumors increased cytotoxic tumor-infiltrating $CD8^+$ T cells and elevated secretion of IFN-γ, CXCL9, and CXCL10 in the TME *in vivo*, and inhibition of METTL3/14 enhanced response to anti-PD-1 treatment in pMMR-MSI-L CRC and melanoma (Wang et al., 2020). However, the epigenetic modification patterns and their association with TME, prognosis, and therapeutic response in GC remain poorly investigated.

In this study, we aimed to characterize the extensive crosstalk between histone and m6A modifications in GC, trying to explain the molecular and clinical heterogeneity of GC from the perspective of epigenetic dysregulations.

2 MATERIALS AND METHODS

2.1 Data Acquisition and Processing

As shown in the flowchart of this study (**Figure 1**), we obtained ChIP-seq data of three histone modification types (H3K4me1, H3K4me3, and H3K27ac) in four gastric cell lines (GES-1, SNU719, NCC24, and YCC10), and MeRIP-seq data of m6A in three GC cell lines (AGS, BGC823, and SGC7901) from previously published literature reports with the access number of GSE135175 (Okabe et al., 2020), GSE166972 (Chen et al., 2021a), GSE133132 (Yue et al., 2019), and PRJNA595769 in the Gene Expression Omnibus (or the European Nucleotide Archive), respectively (**Supplementary Table S1**). For ChIP-seq, raw sequencing reads were aligned using Hisat2 (Kim et al., 2019) with default parameters to the hg19. Sambamba (Tarasov et al., 2015) was used to remove PCR duplicates and obtain the uniquely mapped reads. For MeRIP-seq, raw sequencing reads were aligned using Hisat2 with default parameters to the hg38. Samtools (Li et al., 2009) was used to remove the reads with a mapping quality below 30.

Totally 1518 GC patients from eight independent cohorts with complete transcriptomic data and clinical information were obtained from The Cancer Genome Atlas TCGA-STAD (stomach adenocarcinoma, https://portal.gdc.cancer.gov), Gene Expression Omnibus [GSE62254 (Cristescu et al., 2015), GSE15459 (Ooi et al., 2009), GSE13861 (Cho et al., 2011), GSE26899 (Oh et al., 2018), GSE26901 (Oh et al., 2018), GSE84437, https://www.ncbi.nlm.nih.gov/gds], and European Nucleotide Archive (PRJEB25780, https://www.ebi.ac.uk) (**Supplementary Table S1**). Cohorts were divided into exploring set (TCGA-STAD, GSE15459, and GSE62254) and validation set (GSE13861, GSE26899, GSE26901, GSE84437, and PRJEB25780) (**Figure 1**). Patients with prior or synchronous malignancy diagnoses or patients who survived less than 30 days were excluded from this study. Sva (Jeffrey, 2020) was used to correct the non-biological batch effects among different cohorts.

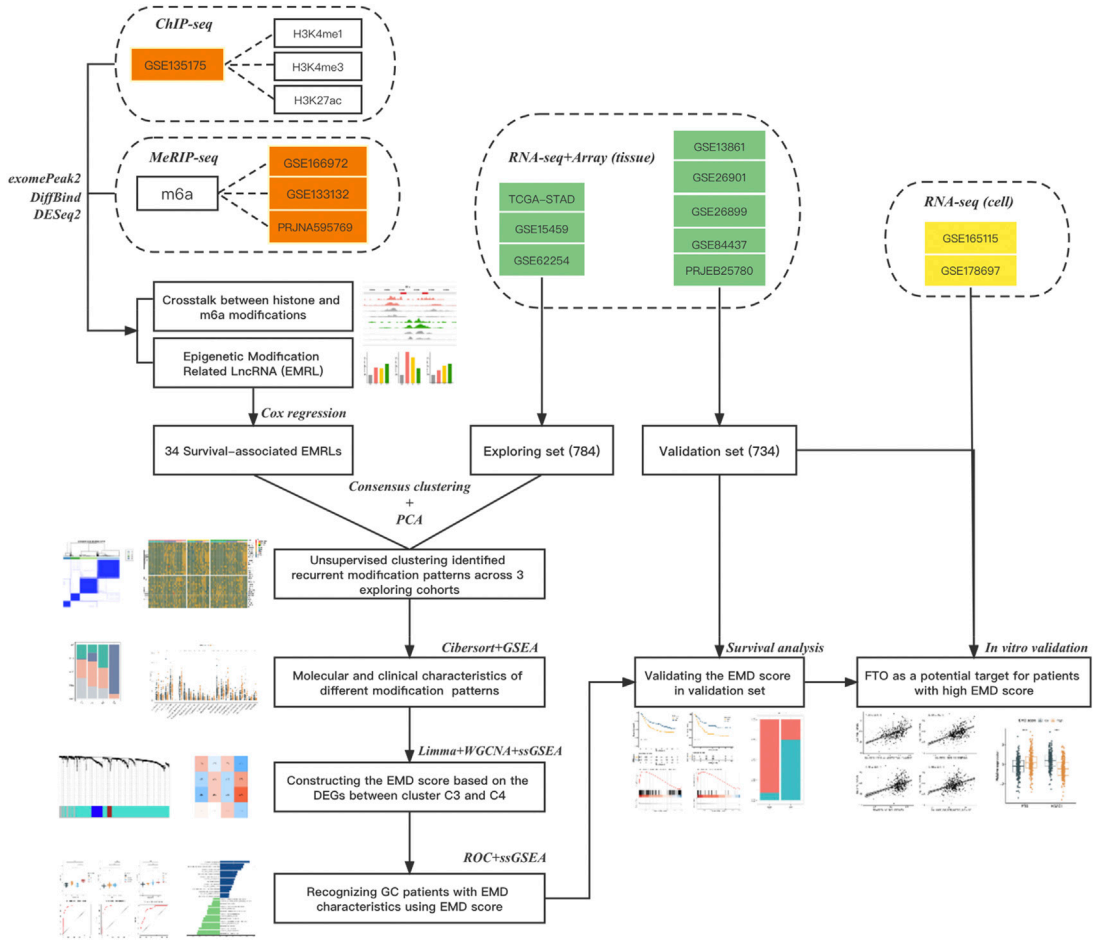

FIGURE 1 | Flow chart of this study. Three types of data from 14 datasets were used in this study: datasets in red refer to the epigenetic data (ChIPseq or MeRIPseq) targeting on histone or m6A modifications, datasets in green refer to the RNAseq or array data with complete clinical information (survival or ICI response), and datasets in yellow refer to the RNAseq data of cell lines with or without FTO depletion. The main method used in each step was also listed.

2.2 Collection of Epigenetic Regulators

Epigenetic regulators, defined as the key genes that play crucial roles in the regulation or function of epigenetic modifications, mainly include the methyltransferases/demethylases of histone methylation (H3K4me1 and K3K4me3), acetylases/deacetylases of histone acetylation (H3K27ac), and writers/readers/erasers of m6A modification. In our study, totally 43 epigenetic regulators (**Supplementary Table S1**), including histone methyltransferases (SETD1A, SETD1B, KMT2A, KMT2B, KMT2C, and KMT2D), histone demethylases (KDM1A, KDM1B, KDM2A, KDM2B, KDM5A, KDM5B, KDM5C, and KDM5D), histone acetylases (CREBBP and EP300), histone deacetylases (HDAC1, HDAC2, HDAC3, HDAC8, and HDAC11), m6A writers (METTL14, METTL3, METTL16, RBM15, RBM15B, ZC3H13, ZCCHC4, WTAP, CBLL1, and VIRMA), m6A readers (YTHDC1, YTHDC2, YTHDF1, YTHDF2, YTHDF3, IGF2BP1, IGF2BP2, IGF2BP3, HNRNPA2B1, and HNRNPC), and m6A erasers (ALKBH5 and FTO), were collected from the published literature (Zhao and Shilatifard, 2019; Zhao et al., 2021a; Deng et al., 2021) for our study. All the included regulators have been experimentally demonstrated to regulate one or more modification types, most of which were reported to participate in tumorigenesis or progression of GC (Yue et al., 2019; Wu et al., 2021a). Maftools (Mayakonda et al., 2018) was used to identify the mutation (**Figure 6F**) or co-mutation (**Figure 2A**) events of epigenetic regulators in the TCGA-STAD cohort. Co-occurrence events with p values less than 0.05 were defined as the co-mutation events (**Supplementary Table S2**).

2.3 Identification of the Epigenetic Modification-Related Gene

For histone modifications (H3K4me1, H3K4me3, and H3K27ac), DiffBind (Stark and Brown, 2011) was used to identify the differentially-histone-modfied site (DHMS) between GC cell lines and GES-1 according to the criteria of |fold-change| >1 and $p < 0.05$. BigWig data were downloaded from the GEO with the access number GSE135175. DESeq2 (Love et al., 2014) was used to identify the differentially expressed gene (DEG) between GC cell lines and GES-1 with the criteria of $|\log_2 FC| > 1$ and $p <$

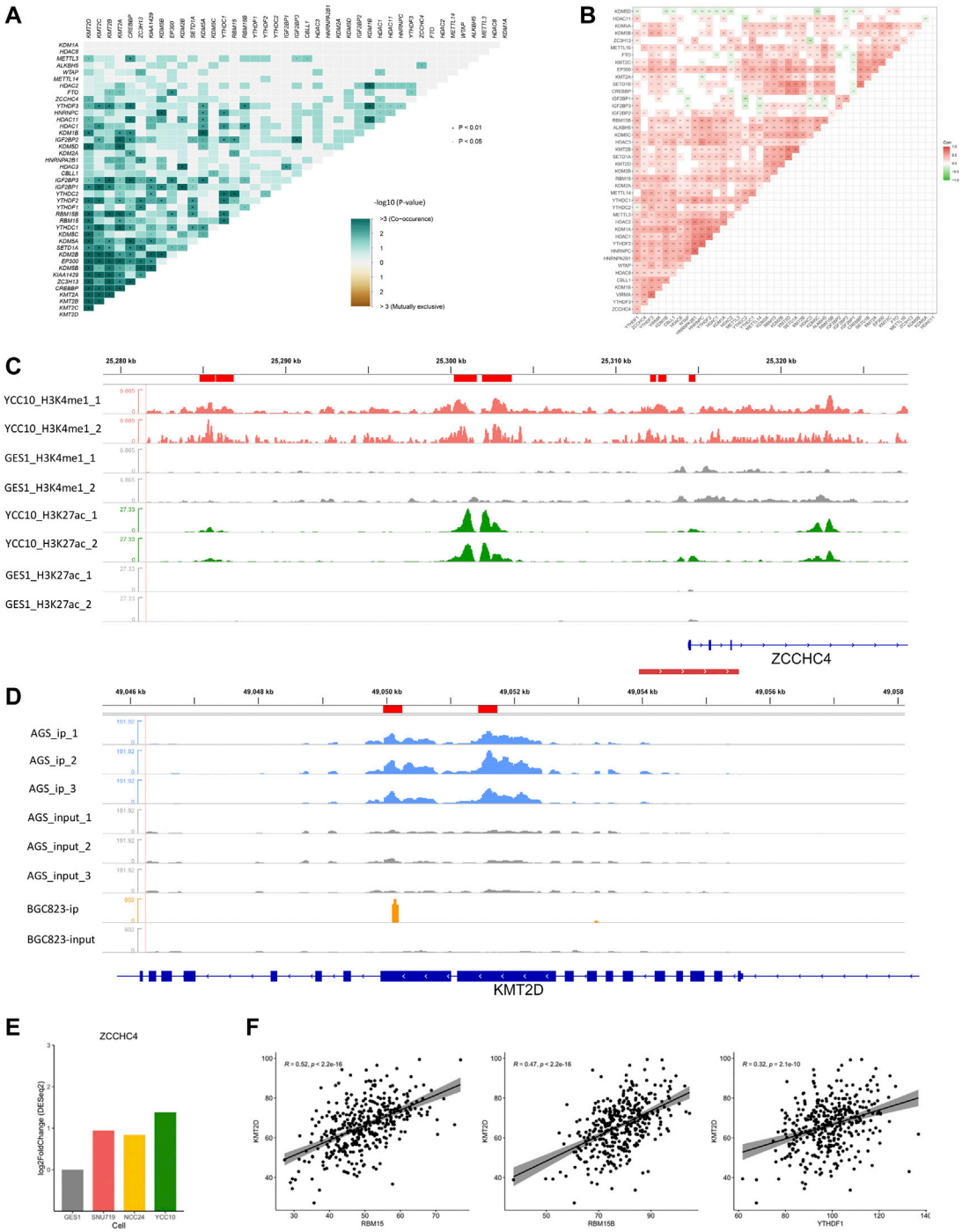

FIGURE 2 | Crosstalk between regulators of histone and m6A modifications. **(A)** Co-mutation heatmap of epigenetic regulators in the TCGA-STAD cohort. **(B)** Co-expression heatmap of epigenetic regulators in the TCGA-STAD cohort. **(C)** Differential H3K4me1 and H3K27ac modifications in the m6A regulator ZCCHC4. Peaks in red and green refer to the H3K4me1 and H3K27ac modifications in GC cell lines, respectively, and gray refers to the corresponding modification in GES-1 as control. The red line at the bottom refers to the promoter region. **(D)** Differential m6A modification in the histone modification regulator KMT2D. Peaks in blue and orange refer to the immunoprecipitation (IP) signals of AGS and BGC823 cell lines, respectively. Peaks in gray refer to the corresponding input signals. **(E)** Differential expression of ZCCHC4 between GC cell lines and GES-1 ($p < 0.05$). **(F)** Correlations of KMT2D with the m6A regulators including RBM15, RBM15B, and YTHDF1 (Spearman, $p < 0.05$).

0.05. For m6A modification, exomePeak2 (Wei, 2020) was used to identify the m6A-modified site (MMS) in each GC cell line, according to the criteria of |fold-change|>1 and $p < 0.05$. The Wilcoxon test was used to identify the correlatively expressed gene (CEG) of the 22 m6A regulators using the criteria of |r|>0.3 and adjusted $p < 0.05$.

Generally, histone methylations/acetylations (such as H3K4me1, H3K4me3, and H3K27ac) enriched at enhancers or promoters, as well as m6A modifications enriched at coding sequence (CDS) or the 3′ untranslated region (3′ UTR) region, presumably facilitate the expression of target genes (Bannister and Kouzarides, 2011; Shi et al., 2019). Thus, those genes which satisfy one of the following criteria were defined as the epigenetic-modification-related gene (EMRG):

1) At least one DHMS was located in the promoter of the DEG, and the expression of the DEG changed in the same direction as the DHMS in at least one GC cell line (SNU719, NCC24, and YCC10);
2) At least one MMS was located in the CEG in at least one GC cell line (AGS, BGC823, and SGC7901), and the CEG positively correlated (r > 0.3, Wilcoxon test) with at least one of the m6A writers/readers, or negatively correlated (r < −0.3, Wilcoxon test) with at least one of the m6A erasers.

The promoter region was defined as 3 kb upstream and downstream of the transcriptional start site (TSS) in each gene. The correlations between the CEG and m6A regulators were calculated in the TCGA-STAD cohort. Long non-coding RNAs (LncRNAs) of the epigenetic modification-related Gene were defined as the epigenetic-modification-related LncRNA (EMRL), according to the GENCODE annotations (Yang et al., 2021b).

2.4 Unsupervised Clustering in the Exploring Set

By performing univariate Cox hazard analysis in the TCGA-STAD cohort, we selected 34 survival-associated EMRLs ($p < 0.01$) for further study. Based on the 34 survival-associated EMRLs, ConsensusClusterPlus (Wilkerson and Hayes, 2010) was applied to perform unsupervised clustering in the exploring set with the following parameters: maxK = 7, cluster algorithm = km, and correlation method = Euclidean.

2.5 Construction of the EMD Score

We first identified 1,674 DEGs between the epigenetic-modification-dysregulated (EMD) subtype (C4) and cluster C3 using limma (Ritchie et al., 2015). (**Supplementary Table S7**) Weighted gene co-expression network analysis (WGCNA) (Langfelder and Horvath, 2008) was then performed based on the DEGs to recognize the most positively correlated (Meturquois, Spearman-r = 0.75) and negatively correlated (MEblue, Spearman-r = −0.61) gene modules relating to cluster C4 (**Figures 6A–C**). We further chose 147 (set1) and 64 (set2) genes from the turquoise and blue modules, respectively, according to their correlation coefficients with the EMD subtype and corresponding modules (**Figure 6D**; **Supplementary Table S8**). The single sample gene set enrichment analysis (ssGSEA) algorithm in R package GSVA (Hänzelmann et al., 2013) was used to estimate the relative abundance (ssGSEA value) of set1 and set2, respectively, for each patient in the GC cohorts. The EMD score was defined as the ratio of the two ssGSEA values. Log transition of the ratio was also performed to make the score less discrete. For each GC patient, the EMD score was calculated as follows:

$$EMD\ score = \log_2\{ssGSEA\ score\ (set1) / ssGSEA\ score\ (set2)\}.$$

2.6 TME Characterization and Function Enrichment Analysis

CIBERSORT (Chen et al., 2018) and ESTIMATE (Yoshihara et al., 2013) were used to evaluate the relative abundance of immune infiltration and stromal components in tumor samples, respectively. Deconvolution results of CIBERSORT were evaluated by a derived p-value ($p < 0.05$) to filter out the samples with less significant accuracy. The tumor immune dysfunction and exclusion (TIDE) algorithm (Jiang et al., 2018) was used to measure the antitumor immunity features of each patient. ClusterProfiler (Yu et al., 2012) was used to perform gene set enrichment analysis (GSEA), using the hallmark gene sets downloaded from the molecular signatures database (MSigDB).

2.7 Cell Culture and Treatment

Human GC cell lines (SNU719 and SGC7901) were purchased from American Type Culture Collection (Manassas, United States). SNU719 and SGC7901 cells were cultured in RPMI-1640 medium (Gibco) with 10% fetal bovine serum (Gibco). Cells were maintained at 37°C and 5% CO_2. SNU719 and SGC7901 cells were plated onto 6-well plates and reached 70–80% cell confluence on the day of treatment. Cells were divided into the BS group and the control group. The BS group was treated with the FTO inhibitor (Brequinar sodium, V17016, 5 umol/l, InvivoChem), and the DMSO group was treated with an equivalent DMSO concentration as control for 48 h.

2.8 Western Blot

48 h after treatment, the EMT markers in SNU719 and SGC7901 were analyzed by Western blot. In brief, whole protein samples of all groups were extracted, and the concentration was detected by using the Pierce BCA Protein Assay Kit (Thermo 23225). Equal amounts of protein (20 ug per well) were loaded, and the samples were separated by 10% sodium dodecyl sulfate–polyacrylamide gel electrophoresis. Then, the proteins were transferred to 0.45 μm polyvinylidene fluoride (PVDF) membranes. The membranes were blocked with 5% nonfat milk and incubated with primary antibodies at 4°C overnight. Later, the membranes were washed with TBST three times and incubated with the secondary HRP antibody at room temperature for 2 h. The primary antibodies used in this research were as follows: E-cadherin (20874-1-AP, 1:2000, Proteintech), N-cadherin (22018-1-AP, 1:2000, Proteintech), Vimentin (10366-1-AP, 1:5,000, Proteintech), and TWIST1 (25465-1-AP, 1:1,000, Proteintech). β-actin (3700T, 1:5,000, CST) was used as a loading control.

2.9 Statistical Analysis

All statistical analyses were performed using R (v4.0.2) (Team, R. C 2020) and its appropriate packages. p-values <0.05 were regarded as statistically significant.

3 RESULTS

3.1 Crosstalk between Regulators of Histone and m6A Modifications

First, we examined the interactions of the four modification types in the TCGA-STAD cohort. Totally, 211 co-mutation events ($p < 0.05$) and 266 co-expression events ($|r|>0.3$, $p < 0.05$) were observed in the 43 epigenetic regulators (**Figures 2A, B**; **Supplementary Table S2**). These correlations were further illustrated by the ChIP/MeRIP-seq data from GC cell lines. Specifically, m6A regulators including ZCCHC4, IGF2BP3, and VIRMA were differentially expressed between the GC cell lines and GES-1, which were accompanied by differential histone modifications in their TSS regions (**Figure 2**; **Supplementary Figure S1**). Similarly, the histone modification regulators, SETD1A and KMT2D, which showed positive correlations with the m6A regulators (RBM15, RMM15B, and YTHDF1), had differential m6A modification in their exons (**Figure 2**; **Supplementary Figure S1**; **Supplementary Table S2**). These findings revealed the active crosstalk between histone and m6A modifications, both in genome and transcriptome levels.

3.2 Identification of the EMRG and EMRL

To generally characterize the transcriptome landscape altered by the four epigenetic modification types, we then identified the dysregulated genes associated with each of the modification types. Using the criteria described earlier, we finally identified 4,999 EMRGs of H3K4me1, 3,693 EMRGs of H3K4me3, 4,095 EMRGs of H3K27ac, and 6,117 EMRGs of m6A. Previous studies suggested that some histone modifications (such as H3K4me1, H3K4me3, and H3K27ac) enriched at the enhancer or promoter region presumably facilitate the transcription of targeted genes (Bannister and Kouzarides, 2011). Similarly, unbalanced distribution was also observed in the m6A modification, with more than 40% of all modification sites in mRNA being present in 3′ UTRs) (Ke et al., 2015; Kan et al., 2022). Consistent with the previous studies, most of MMSs were located at the 3′UTR, followed by exons, and then the promoter region (**Figure 3A**). Meanwhile, for the three histone modification types, most of DHMSs were located within the promoter (<1 kb), followed by the promoter (1–2 kb) and promoter (2–3 kb) (**Figure 3A**). Among the EMRGs, nearly 50% of genes were simultaneously regulated by more than one modification type, which was another evidence for the crosstalk between different modification types. Specifically, about 360 protein-coding genes (PCGs) were co-regulated by the four modification types (**Figure 3B**).

As another key member of epigenetic regulation, LncRNA was demonstrated to participate in various tumorigenic processes due to their extensive biological functions in the transcriptome level (Sempere et al., 2021; Kan et al., 2021). To further characterize the epigenetic modification patterns with clinical relevance in GC, we also identified 370 EMRLs (**Supplementary Table S3**) from the EMRG. Interestingly, three EMRLs (PAXIP1-AS2, MNX1-AS1, and PVT1) were co-regulated by the four modification types (**Figure 3B**). LINC00511, previously reported as an oncogene in several solid tumors (Wu et al., 2020; Peng et al., 2021; Dong et al., 2021), was significantly modified with H3K4me1 (**Supplementary Figure S2**) and simultaneously overexpressed in the three GC cell lines (**Figure 3F**). Similarly, concomitant histone modification and overexpression were observed in LINC01091 (**Supplementary Figure S2**). Moreover, we found MNX1-AS1, another oncogene in multiple cancers (Wu et al., 2019; Li et al., 2020b; Li et al., 2020c; Wu et al., 2021b), was simultaneously regulated by both histone and m6A modifications, with differential expression across three GC cell lines and positive correlations to multiple m6A regulators (**Figures 3C–F**). The aforementioned findings shed light on the close connections inside epigenetic regulators including epigenetic modifications and LncRNA, offering a new perspective for exploring the complicated regulation network of the epigenome.

3.3 Unsupervised Clustering Based on EMRL Identified an EMD Subtype of GC

Next, we set out to characterize the modification patterns in the exploring set. Through univariate Cox regression analysis, we selected 34 EMRLs with a significant prognosis value ($p < 0.01$) for further study (**Supplementary Table S4**). Unsupervised clustering was then performed based on the 34 survival-associated EMRLs, which divided the exploring set into four distinct clusters (**Figures 4A, B**; **Supplementary Figure S3A**; **Supplementary Table S5**). Surprisingly, extremely similar expression patterns were observed across the three independent GC cohorts (TCGA-STAD, GSE15459, and GSE62254), especially in cluster C4. Specifically, the C4 population of each cohort was characterized by strikingly elevated EMRLs including ZEB1-AS1, NR2F1-AS1, MIR100HG, ZFHX4-AS1, and PART1 and the suppression of EMRLs including HOTTIP, HOXA11-AS, CASC2, and LINC00467. Moreover, a significant difference in prognosis was observed among the four clusters, with cluster C4 having the worst survival and cluster C3 the best (**Figure 4C**).

Consistently, unbalanced modification patterns both of histone and m6A modifications were observed in cluster C4. Specifically, cluster C4 was characterized by the high expression of multiple histone modification writers (SETD1B, KMT2A, and CREBBP) and the low expression of histone modification erasers (KDM1A, KDM1B, HDAC1, and HDAC2). While in the m6A modification, high-expressed erasers (FTO and ALKBH5) and low-expressed readers (YTHDF2, YTHDF3, IGF2BP2, IGF2BP3, and HNRNPC) were observed in cluster C4 (**Figure 4D**). Then, we further explored the mutation profiling of cluster C4. Interestingly, cluster C4 was also featured with a distinctive mutation pattern, with rarely detected mutations of the

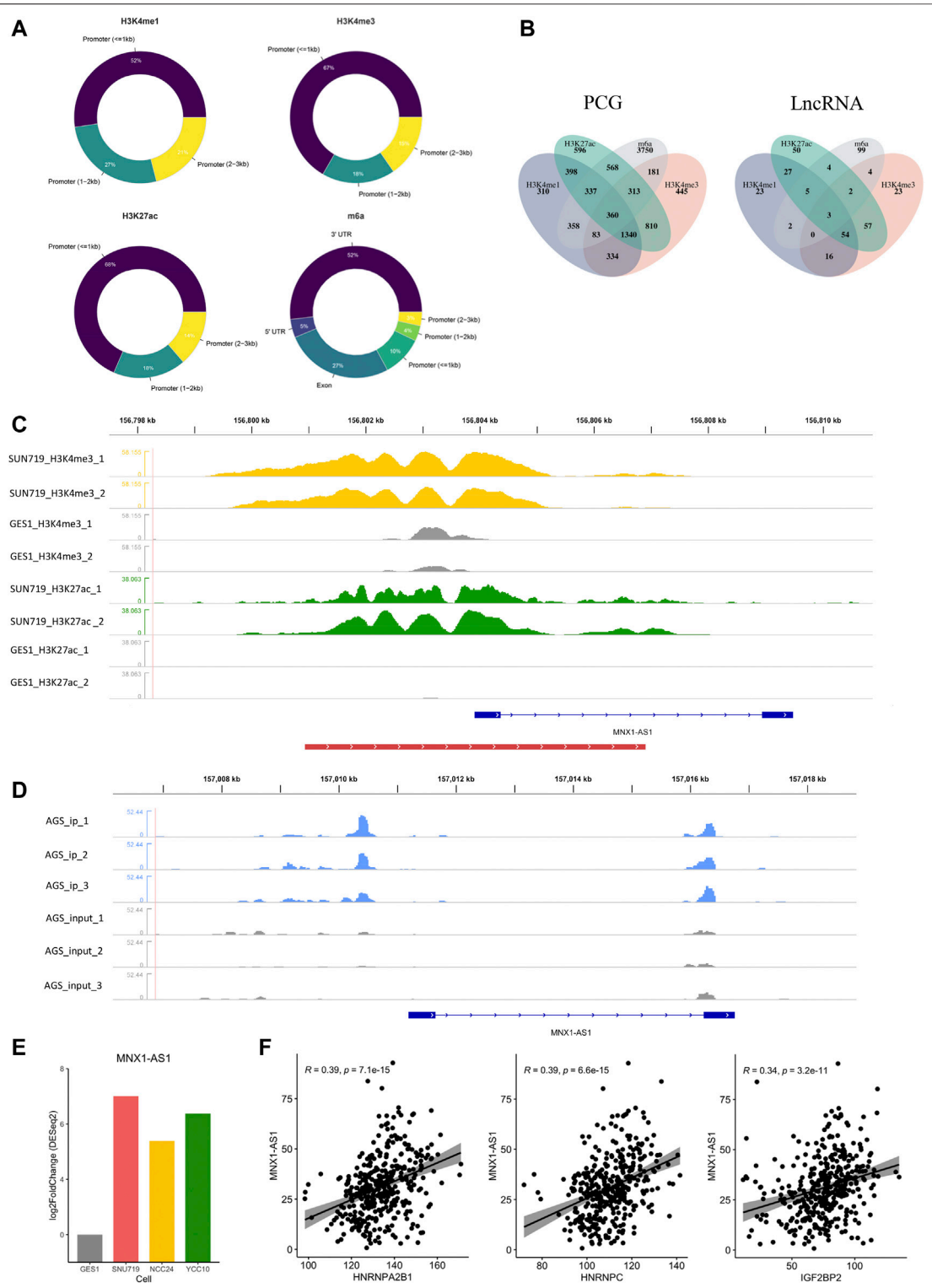

FIGURE 3 | Identification of epigenetic modification-related LncRNA (EMRL). **(A)** Doughnut charts showed the distribution of DHMS or MMS in each modification type. **(B)**Venn diagram showed the overlaps of EMRG (or EMRL) regulated by different modification types. PCG refers to the protein-coding genes, and LncRNA refers to the long non-coding RNAs. **(C)** MNX1-AS1 was potentially regulated by H3K4me3 and H3K27ac in GC cell lines. Peaks in yellow and green refer to H3K4me3 and H3K27ac, respectively, while gray ones refer to the corresponding modification in GES-1 as control. The red line at the bottom refers to the promoter region. **(D)** m6A modification regions of MNX1-AS1 in the AGS cell line. Peaks in blue refer to the immunoprecipitation (IP) signals. Peaks in gray refer to the input signals. **(E)** Differential expression of MNX1-AS1 in GC cell lines and GES-1 ($p < 0.05$). **(F)** Correlations of MNX1-AS1 with the m6A regulators including HNRNPC, HNRNPA2B1, and IGF2BP2 (Spearman, $p < 0.05$).

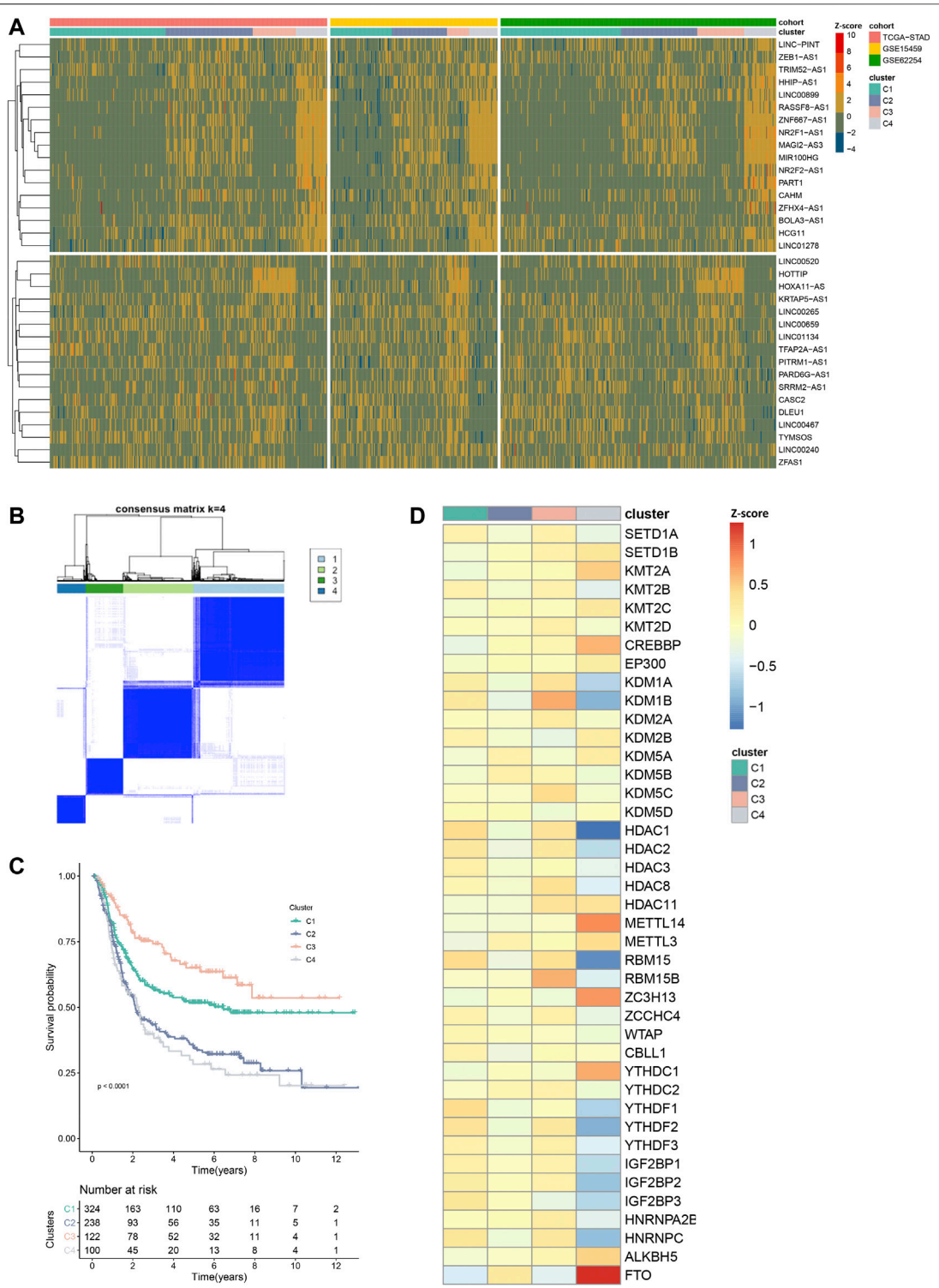

FIGURE 4 | Distinctive epigenetic modification patterns across three GC cohorts recognized by EMRL. **(A)** Heatmap showed the highly concordant expression patterns of the three GC cohorts in the exploring set. **(B)** Consensus unsupervised clustering divided the exploring set into four distinct clusters. **(C)** Kaplan–Meier curves showed the different overall survival of the four clusters. **(D)** Heatmap showed the distinct expression patterns of the epigenetic regulators in the exploring set. VIRMA and METTL16 were excluded in this section due to lack of expression information in the GSE15459 or GSE62254 cohort.

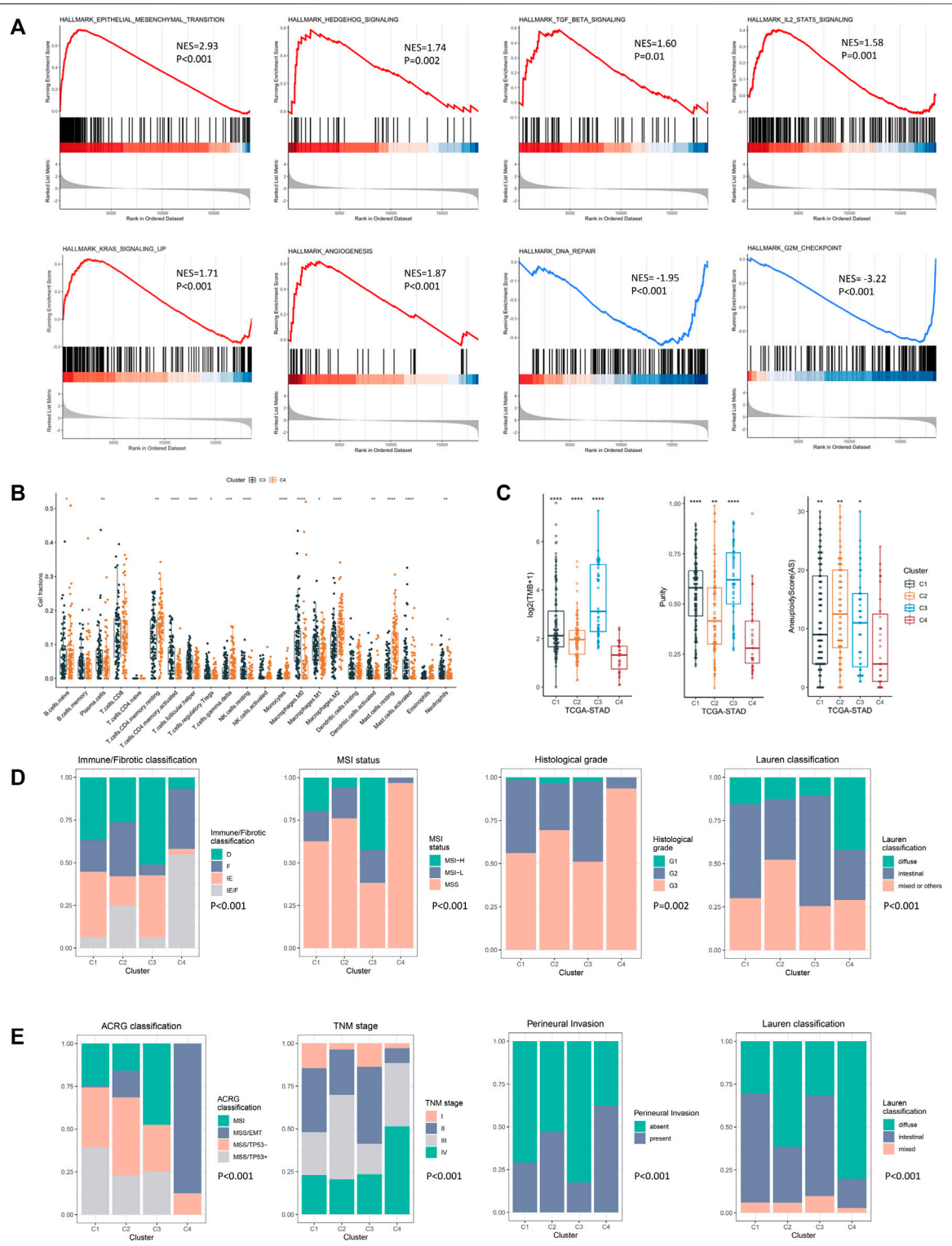

FIGURE 5 | Molecular and clinical characteristics of four epigenetic modification patterns. **(A)** GSEA analysis identified the differentially activated pathways of cluster C4 compared with cluster C3. **(B)** CIBERSORT analysis estimated the relative ratio of tumor-infiltrating cells in clusters C3 and C4. Each value was defined as the relative ratio compared to the 22 human hematopoietic cell types contained in CIBERSORT. **(C)** Different TMB, tumor purity, and aneuploidy score among four clusters in the TCGA-STAD cohort. **(D)** Clinical relevance of the EMD subtype in the TCGA-STAD cohort. **(E)** Clinical relevance of the EMD subtype in the GSE62254 cohort (*p < 0.05, **p < 0.01, ***p < 0.001, and ****p < 0.0001).

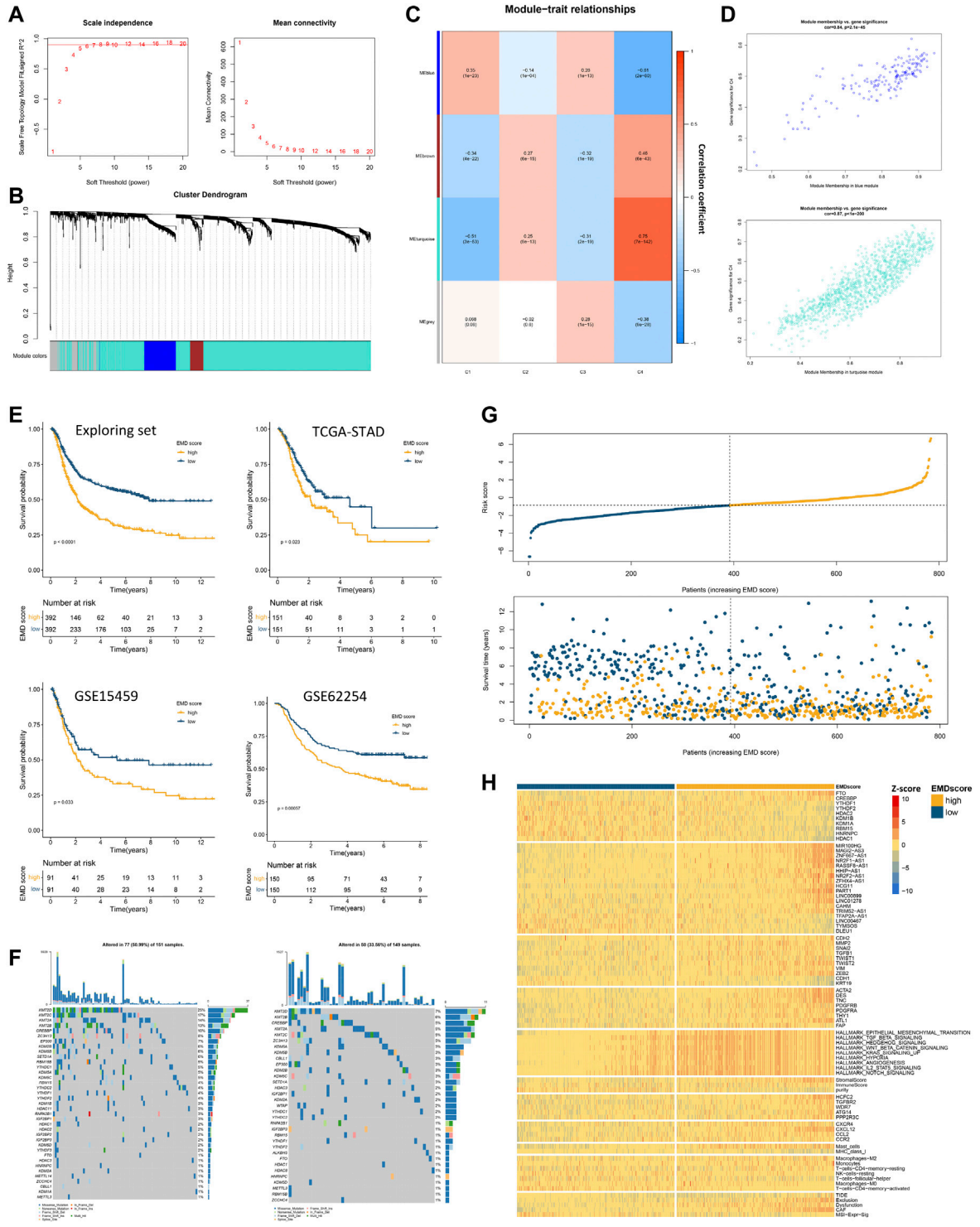

FIGURE 6 | Construction of the EMD score in the exploring set. **(A–D)** WGCNA analysis based on 1674 DEGs in the exploring set. **(E)** Kaplan–Meier curves showed the different overall survival between the high- and low-EMD score groups in the exploring set. Patients were separated into the high and low groups according to the median EMD score of each cohort. **(F)** Mutation landscape of epigenetic regulators in high- and low-EMD score groups in the TCGA-STAD cohort. **(G)** Risk curves showed more frequent death events with the increasing EMD score in the exploring set. Dots in yellow referred to death events observed in the cohorts. **(H)** Heatmap showed the close correlations of the EMD score with various molecular characteristics including epigenetic regulators, EMRLs, TME markers, oncogenes, and tumorigenic pathways. All the values were scaled using the Z-score.

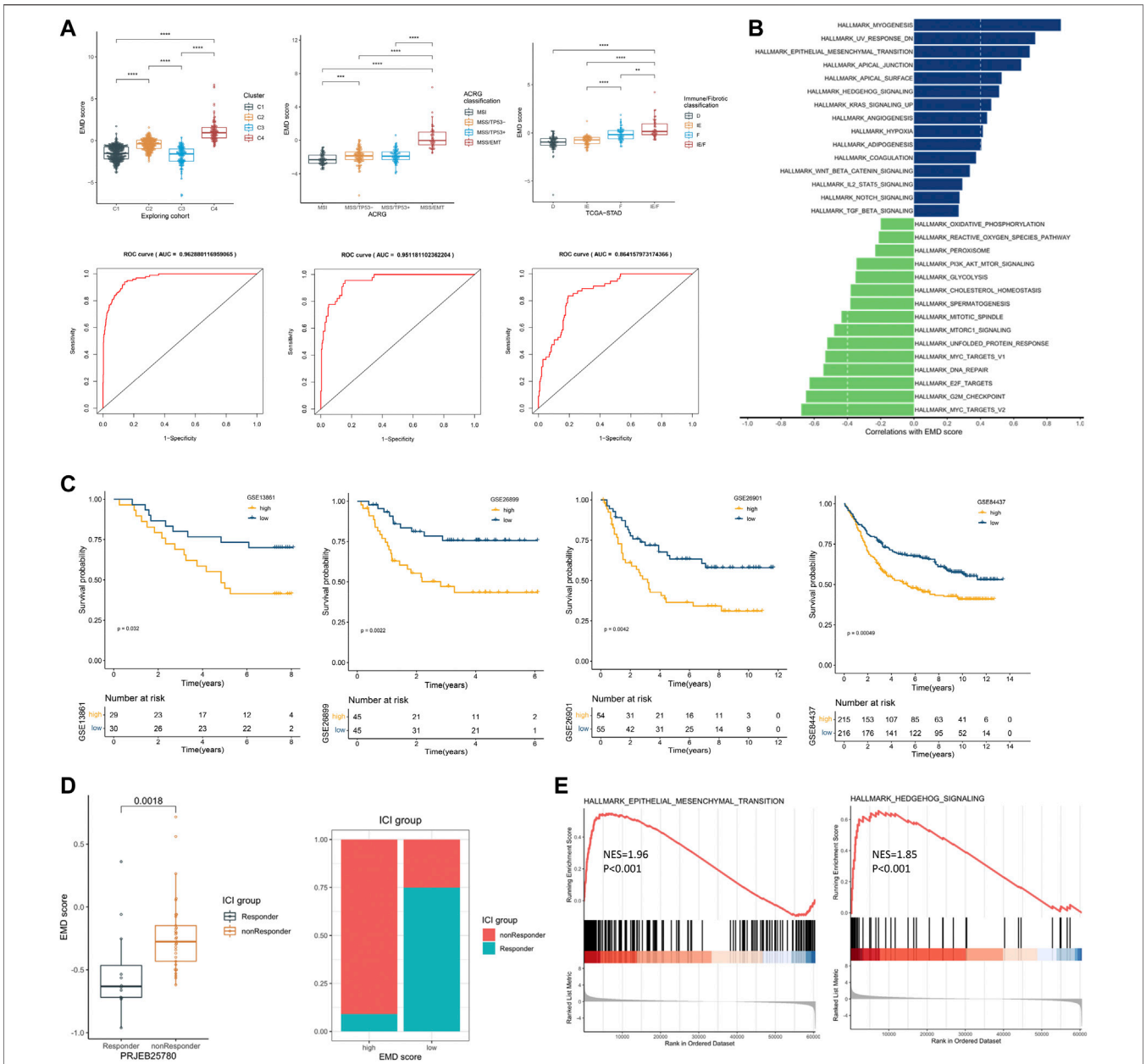

FIGURE 7 | Recognizing patients with EMD characteristics using the EMD score. **(A)** Differential EMD score of subtypes in three classification proposals. The ROC below showed the performance of the EMD score in recognizing the EMD, MSS/EMT, and IE/F subtype in the corresponding cohort. **(B)** Hallmark pathways correlated with the EMD score in the validation set. **(C)** Kaplan–Meier curves showed the different overall survival between the high and low EMD groups in the validation set. Patients were separated into high and low groups according to the median EMD score of each cohort. **(D)** Correlations of the EMD score with the ICI outcome in the cohort PRJEB25780. Patients were divided into high or low groups according to the lower quartile (Q1) of the EMD scores (right panel). **(E)** GSEA analysis suggested significant activated EMT and Hedgehog pathways in non-responders compared with the responder.

epigenetic regulators (**Supplementary Figure S3B**). Given the distinctive modification patterns in transcriptome and genome levels and the poor prognosis of cluster C4, we named it the epigenetic-modification-dysregulated (EMD) subtype in further study. In this section, using survival-associated EMRLs, we identified a conserved EMD subtype with distinctive modification patterns in GC.

3.4 Molecular and Clinical Characterization of the EMD Subtype

To figure out the mechanism underlying the poor prognosis of the EMD subtype, we comprehensively explored the molecular and clinical characteristics of the EMD subtype by comparing it with cluster C3 (cluster with the best prognosis) in the exploring set. In the GSEA analysis, multiple tumorigenic pathways including the

epithelial–mesenchymal transition (EMT, $p < 0.001$), Hedgehog ($p = 0.002$), TGF-β ($p = 0.01$), IL2-STAT5 ($p = 0.001$), KRAS ($p < 0.001$), and angiogenesis ($p < 0.001$) were significantly activated in the EMD subtype (**Figure 5A**), whereas pathways including DNA repair ($p < 0.001$) and G2M checkpoint ($p < 0.001$) were observed to be significantly suppressed in the EMD subtype (**Figure 5A**).

Then, we performed CIBERSORT analysis to explore the TME characteristic of the EMD subtype. Compared with cluster C3, the EMD subtype showed a significantly higher ratio of macrophages M2 ($p < 0.001$) and resting $CD4^+$ T cell ($p < 0.01$) and a significantly lower ratio of macrophages M1 ($p < 0.05$) and activated $CD4^+$ T cell ($p < 0.001$) (**Figure 5B**). Moreover, a relatively lower $CD4^+/CD8^+$ T cell ratio was observed in the EMD subtype ($p < 0.05$, **Supplementary Figure S4A**), which usually indicates more advanced tumors or immune deficiency in cancer patients. In the TCGA-STAD cohort, we also observed a significant decrease of tumor mutation burden (TMB, $p < 0.001$), tumor purity ($p < 0.001$), and aneuploidy score (AS, $p < 0.05$) in the EMD subtype (**Figure 5C**).

In addition to the distinctive molecular characteristics, the EMD subtype also showed extensive correlations to various clinical characteristics of GC (**Supplementary Table S6**). In the TCGA-STAD cohort (**Figure 5D**), we found the EMD subtype as a good indicator for the IE/F subtype of the newly reported immune/fibrotic classification (Bagaev et al., 2021) ($p < 0.001$). Besides, more patients with MSS subtype ($p < 0.001$), poor differentiation ($p = 0.002$), or diffuse histotype ($p < 0.001$) were observed in the EMD subtype. While in the GSE62254 cohort (**Figure 5E**), the EMD subtype mostly overlapped with the MSS/EMT subtype of ACRG classification (Cristescu et al., 2015) ($p < 0.001$). Similarly, more patients with advanced TNM stage ($p < 0.001$), perineural invasion ($p < 0.001$), or diffuse histotype ($p < 0.001$) were observed in the EMD subtype.

These findings suggested distinctive stromal-activated and immune-suppressed characteristics of the EMD subtype, which may account for the poor prognosis of this subtype.

3.5 Construction of the EMD Score in the Exploring Set

Since clusters C3 and C4 showed marked differences in prognosis and molecular characteristics, we chose clusters C3 and C4 for further study. To expand the applicability of the EMD subtype, an EMD score was then constructed based on the DEGs between the EMD subtype (C4) and cluster C3 using WGCNA (**Figures 6A–D**) and ssGSEA algorithms. Strikingly, the EMD score was closely related to the prognosis in the exploring set, where the increasing EMD score was accompanied by more death events (**Figure 6G**) and worse survival (**Figure 6E**).

Consistent with the EMD subtype, extensive correlations of the EMD score with stromal-activated and immune-suppressed TME characteristics could be observed in the exploring set (**Figure 6H**; **Supplementary Tables S9, S10**). Specifically, patients with a high EMD score showed activation of multiple pathways (EMT, TGF-β, and Hedgehog), elevated stromal scores, high abundance of cancer-associated fibroblast (CAF) and mast cells, whereas those with a low EMD score showed low MHC-I expression, low infiltration of activated $CD4^+$ T cells, and low M1/M2 ratio. These were further evidenced by upregulated markers of EMT activation (ZEB2, TWIST1, SNAI2, MMP2, CDH2, VIM, etc.), CAF (ACAT2, DES, TNC, PDGFRB, etc.), and immune-suppressed chemokine axis (CXCR4, CXCL12, CCL2, and CCR2) with the increasing EMD score. Moreover, we also observed the overexpression of multiple immune evasion-related genes (CREBBP, HCFC2, TGFBR2, WDR7, ATG14, and PPP2R3C), which were experimentally demonstrated (Lawson et al., 2020), in the patients with a high EMD score. Additionally, in the TIDE analysis, we found the EMD score significantly correlated with the exclusion, dysfunction, CAF, and MSI signature, which implied the potential of the EMD score in predicting the ICI efficacy. Similar to the EMD subtype, a high EMD score indicated a lower frequency of regulator mutation (34%, 51%, **Figure 6F**). These findings suggested the EMD score as a good indicator for recognizing the EMD subtype in GC.

3.6 Recognizing Patients with EMD Characteristics in the Validation Set Using the EMD Score

We first tested the correlations of the EMD score with the four clusters we identified earlier, ACRG classification, and immune/fibrotic classification. Strikingly, the EMD score showed an excellent performance in recognizing the EMD subtype (AUC = 0.96, **Figure 7A**) in the exploring set, as well as the MMS/EMT subtype (AUC = 0.95, **Figure 7A**) of ACRG classification and the IE/F subtype of the immune/fibrotic classification (AUC = 0.86, **Figure 7A**).

To further validate the ability of the EMD score in predicting prognosis and response to ICI treatment, we calculated the EMD score for patients in four independent GC cohorts. As we expected, a high EMD score was closely related to a worse OS ($p < 0.05$, **Figure 7C**) in each cohort of the validation set. Strong correlations between the EMD score and multiple pathways (EMT, TGF-β, Hedgehog, etc. **Figure 7B**; **Supplementary Table S11**) could also be observed in the validation set. In the cohort PRJEB25780, we also observed a distinct difference in the response rate to immune checkpoint inhibitor (ICI) treatment between high and low EMD score groups (10 *vs.* 75%, $p = 0.0018$, **Figure 7D**). Moreover, non-responders were featured with significant activated EMT (NES = 1.96, $p < 0.001$) and Hedgehog (NES = 1.85, $p < 0.001$) pathways compared with the responders (**Figure 7E**). These findings successfully validated the ability of the EMD score in recognizing the patients with EMD characteristics and the potential of recognizing patients sensitive to ICI treatment in GC.

3.7 FTO as a Potential Target for Patients with High EMD Score

Fat mass- and obesity-associated protein (FTO) was recently reported to participate in multiple tumorigenic processes including immune evasion in several malignant tumors (Li et al., 2017; Zhao et al., 2020; Tao et al., 2021; Zhou et al., 2021), implying the therapeutic potential of FTO inhibition in treating multiple cancers. In this study, high FTO expression and low HDAC1 expression were both observed in patients with high EMD score (**Figure 8A**). Moreover, FTO and HDAC1 were the most positively correlated (Spearman-r = 0.48, $p < 0.001$) and negatively correlated

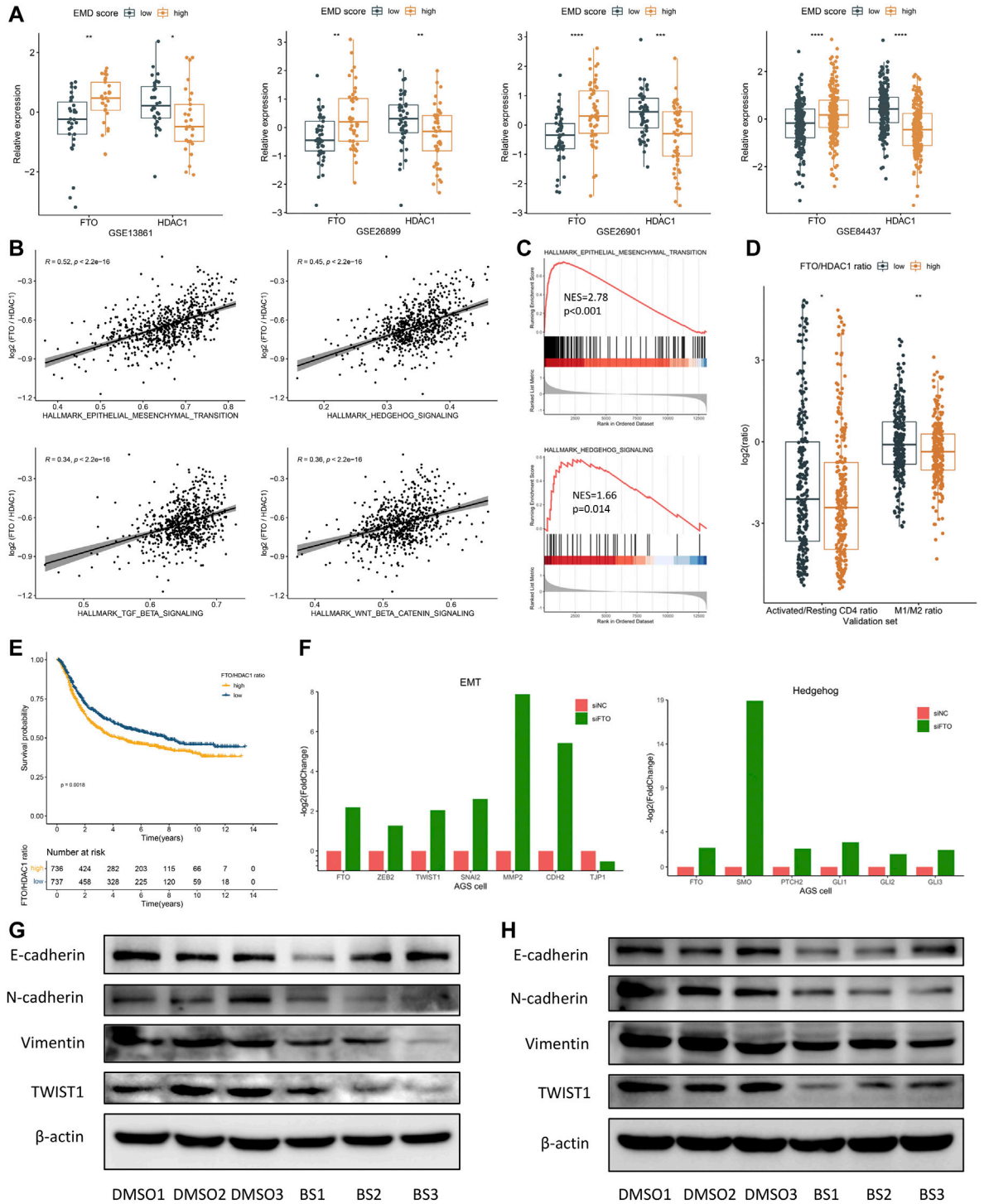

FIGURE 8 | FTO may serve as a potential target for patients with a high EMD score. **(A)** Correlations of the EMD score with FTO and HDAC1 in each cohort of the validation set. **(B)** Correlations of the FTO/HDAC1 ratio with multiple pathways in the validation set. **(C)** GSEA analysis confirmed the activation of EMT and Hedgehog pathways in patients with a high FTO/HDAC1 ratio. **(D)** Correlations of the FTO/HDAC1 ratio with the activated/resting $CD4^+$ T cell ratio and M1/M2 ratio in the validation set. Activated/resting $CD4^+$ T cell ratio refers to the ratio of activated $CD4^+$ T cells and resting $CD4^+$ T cells. The M1/M2 ratio refers to the ratio of macrophage M1 and macrophage M2. **(E)** Kaplan–Meier curves showed the different overall survival between the high and low FTO/HDAC1 ratio group in the whole cohort of this study. Patients were separated into high and low groups according to the median EMD score of the whole cohort. **(F)** Barplots showed the fold change of EMT and Hedgehog markers under FTO depletion in the AGS cell line (GSE178697). **(G)** Western blot showed the suppression of the EMT pathway under FTO inhibition in the SNU719 cell line. **(H)** Western blot showed the suppression of the EMT pathway under FTO inhibition in the SGC7901 cell line (*$p < 0.05$, **$p < 0.01$, ***$p < 0.001$, and ****$p < 0.0001$).

(Spearman-r = −0.45, $p < 0.001$) regulators relating to the EMD score, which also represented the m6A and histone modifications, respectively. To characterize the EMD subtype with both histone and m6A modification features, we measured the FTO/HDAC1 ratio for each GC patient. Interestingly, we found the FTO/HDAC1 ratio closely correlated with the EMD subtype (**Supplementary Figure S4B**), as well as the EMT (r = 0.52, $p < 0.001$, **Figures 8B, C**) and TGF-β (r = 0.34, $p < 0.001$, **Figures 8B, C**) pathway activation, which indicated stromal-activated TME characteristics. Also, a high FTO/HDAC1 ratio was accompanied by a low $CD4^+$ T cell activation rate and a low M1/M2 ratio (**Figure 8D**), which indicated immune-suppressed TME characteristics. Moreover, a high FTO/HDAC1 ratio was related to a worse OS in the whole cohort of this study (**Figure 8E**). These findings revealed the close links of FTO with GC prognosis and multiple tumorigenic pathways.

These links were further evidenced by the significant downregulation of activated EMT markers (ZEB2, TWIST1, SNAI2, MMP2, and CDH2) in a GC cell line with FTO knockdown (FTO^{-KD}) (**Figure 8F**; **Supplementary Table S12**). Consistently, EMT ($p < 0.001$) and TGF-β ($p = 0.007$) suppressions were also observed in an FTO^{-KD} colon cancer (CC) cell line (**Supplementary Figures S3C–E**; **Supplementary Table S12**). Targeting FTO, as we assumed, might help to improve the immune-suppressed TME caused by the activated EMT and TGF-β pathway.

Brequinar sodium (BS) was reported to bind tightly with FTO protein and inhibit the demethylase activity of FTO (Su et al., 2020). To confirm the FTO's function of regulating the EMT pathway, we conducted *in vitro* experiments using two GC cell lines, SNU719 and SGC7901. Strikingly, when treated with BS, markers of EMT activation including N-cadherin, Vimentin, and TWIST1 were downregulated in both cell lines (**Figures 8G, H**). Although no significant upregulation of E-cadherin (the epithelial marker) was observed in the BS-treated cell lines, we still noticed a remarkable increase of the E-cadherin/N-cadherin ratio after BS treatment, especially in SGC7901 cell line ($p < 0.05$, not presented). These findings suggested FTO as a promising target for inhibiting the EMT pathway in GC, especially for patients with high EMD score.

4 DISCUSSION

Extensive interactions between epigenetic modification types in shaping the TME of cancers have drawn increasing attention recently. Chen et al. systematically characterized the interactions of four RNA modification types (m6A, N1-methyladenosine, alternative polyadenylation, and adenosine-to-inosine RNA editing) and demonstrated that multilayer alterations of RNA modification "writer" are associated with patient survival and TME cell-infiltrating characteristics (Chen et al., 2021b). Zhao et al. focused on the relationship between LncRNAs and histone/DNA modifications and identified key LncRNA regulators as a prognostic biomarker for breast cancer subtypes (Zhao et al., 2021b). Similarly, regarding GC, Meng et al. (2021) elucidated the interactions between DNA methylation regulators and generated a DMS score for separating GC patients with distinctive prognosis and treatment efficacy (Meng et al., 2021). These studies provided insights into the active interaction networks of epigenetic modifications, suggesting their pivotal roles in shaping the TME across multiple tumors. However, the interactions between histone and RNA modifications and their impact on the TME in GC had not been fully explored yet.

In this study, for the first time, we comprehensively depicted the epigenetic regulation network including histone modification, RNA modification, and LncRNA in GC. Both in genome and transcriptome levels, we characterized the crosstalk between regulators of these four modification types. Zhan et al. found that several important histone regulator genes, including KMT2D, KMT2C, CREBBP, and EP300, are frequently altered in esophageal squamous cell carcinoma (Song et al., 2014). In our study, we further observed frequent co-mutations of these regulators, such as KMT2D-CREBBP, KMT2C-EP300, and CREBBP-EP300 in GC, which implied potential vulnerabilities based on epigenetic-related synthetic lethality in GC (Yang et al., 2019). Moreover, by identifying EMRLs using ChIP/MeRIP-seq data, our study added new evidence to the crosstalk between epigenetic modifications and LncRNA, which is also one of the key members of epigenetic regulation (Kan et al., 2021). Meng et al. defined a DMS score based on specific DNA methylation patterns to recognize GC patients with immune activation status and enhanced efficacy of immunotherapy (Meng et al., 2021). Consistent with Meng's study, strong links between epigenetic modification patterns and the tumor environment were observed in GC, which in combination suggested epigenetic modification as a promising resource for developing new vulnerabilities for TME-targeting therapy.

With strong complexity and heterogeneity, GC presented disappointing results in most of the clinical trials on novel agents during the last decade (Serra et al., 2019). Thus, increasing molecular classification proposals were developed to characterize the molecular and clinical features of GC so as to optimize individualized diagnosis and treatment. ACRG classification is a globally accepted classification system of GC reported by the Asian Cancer Research Group in 2015, which divides GC into four subtypes: MSI, MSS/EMT, MSS/TM53 (+), and MSS/TP53 (−) (Cristescu et al., 2015). According to the GSE62254 cohort, the MSI subtype had the best prognosis with more than 60% patients of intestinal histotype, while the MSS/EMT subtype had the worst prognosis, over 80% of which were the diffuse histotype. However, the epigenetic modification patterns underlying the MSS/EMT subtype remain largely unexplored. In this study, we surprisingly found the EMD subtype we defined mostly overlapped with the MSS/EMT subtype (91.4%, **Supplementary Table S6**) in the GSE62254 cohort. Consistently, the EMD subtype had the worst overall survival and mostly consisted of diffuse histotype (80%, **Supplementary Table S6**). Our findings revealed the distinctive epigenetic modification patterns existing in the MSS/EMT subtype. By identifying the EMD subtype, our study provided not only new strategies for recognizing patients with poor prognosis in GC but also new sights into the epigenetic characterization of the widely used ACRG subtype.

Though with the rapid progress of ICI therapy in recent years, there were still limited GC patients benefiting from the ICI treatment. According to a meta-analysis based on 2003 patients from nine clinical trials, the objective response rate and disease control ratio were 9.9 and 33.3%, respectively, for

advanced gastric or gastroesophageal junction (G/GEJ) cancer treated with ICI therapy (Chen et al., 2019). Mechanistically, the immune-suppressed TME may be one of the main causes of the resistance to ICI treatment. Hegde et al. proposed three distinct immunophenotypes (inflamed, immune-excluded, and immune-desert) based on the spatial distribution of $CD8^+$ T cells in the TME (Hegde et al., 2016). Immune-excluded tumors were featured with an immune-suppressed TME, represented by T cells clearly embedded in the tumor stromal microenvironment with the presence of low MHC-I expression, TGF-β activation, myeloid inflammation, and angiogenesis (Hegde et al., 2016). Consistent with immune-excluded tumors, the EMD subtype we defined was characterized by the immune-suppressed TME with a low MHC-I expression, TGF-β activation, and angiogenesis activation, which also presented a low response rate to ICI treatment. Moreover, the EMD score we developed showed promising ability in recognizing GC patients with poor prognosis and resistance to ICI therapy. Desbois et al. reported that TGF-β-activated fibroblasts contribute to an immune-suppressed environment by cytokine production in ovarian cancer (Desbois et al., 2020; Desbois and Wang, 2021). In our study, TGF-β activation and high abundance of CAF were both observed in patients with a high EMD score, strongly implying the close links between TGF-β-activated fibroblasts and resistance to ICI treatment in GC.

Recently, combined therapy of ICI with radiotherapy, chemotherapy, or targeted therapy became a prospective strategy for improving the efficacy of cancer treatment. Results from CheckMate 649 showed that nivolumab with chemotherapy improved OS [hazard ratio (HR) 0.71 (98.4% CI 0.59–0.86); $p < 0.0001$] and PFS [HR 0.68 (98% CI 0.56–0.81); $p < 0.0001$] in GC patients with a PD-L1 CPS (combined positive score) of five or more when compared with chemotherapy alone (Janjigian et al., 2021). As one of the pivotal roles contributing to the immune-suppressed TME, the EMT pathway provided multiple therapeutic targets for combined therapy of ICI (Dongre et al., 2017; Jiang and Zhan, 2020). Combined ICI therapy with anti-EMT therapy would be a promising strategy, especially for patients with significant EMT activation. In our study, close correlations of the FTO overexpression with a high EMD score and activation of multiple tumorigenic pathways including EMT, TGF-β, and Hedgehog were observed. Moreover, a significant downregulation of the EMT pathway was observed in two FTO^{-KD} cell lines (**Figure 8F**, S1C-E), implying the potential links between FTO and the immune-suppressed TME. Su et al. demonstrated that FTO inhibition sensitizes leukemia cells to T cell cytotoxicity and overcomes hypomethylating agent-induced immune evasion (Su et al., 2020). Liu et al. developed a novel FTO inhibitor, Dac51, which can block FTO-mediated immune evasion and synergize with the checkpoint blockade for better tumor control (Liu et al., 2021). In this study, through the *in vitro* experiments of FTO inhibition conducted in two GC cell lines, we demonstrated that pharmacological inhibition of FTO significantly suppressed the EMT pathway. Our findings provided new clues of FTO's participation in immune evasion and also suggested FTO as a potential target of combined ICI therapy with anti-EMT therapy in GC.

This study also has some limitations. First, the ability of the EMD score in predicting ICI efficacy needs to be further validated using more GC cohorts in the future. Besides, it remains unclear how FTO regulates the EMT pathway. Further studies are urgently needed to explore the underlying mechanism and verify the efficacy of combined ICI therapy with FTO inhibition in GC.

5 CONCLUSION

Collectively, we comprehensively characterized the crosstalk between histone and RNA modifications and identified the EMD subtype of GC with poor survival and distinctive TME characteristics. EMD score is a good indicator for prognosis and TME characteristics in GC and also might be a promising tool for recognizing patients suitable for combination ICI therapy.

DATA AVAILABILITY STATEMENT

The datasets presented in this study can be found in online repositories. The names of the repository/repositories and accession number(s) can be found in the article/**Supplementary Material**.

AUTHOR CONTRIBUTIONS

CY, YH, and CZ conceived and designed the whole project. CY and JZ collected, processed, and analyzed the data. CD conducted the cell experiments. CY and CD wrote the manuscript. LC and HL reviewed and revised the manuscript. YX, BL, SM, and XJ provided material or technical support for this study. All authors contributed to the article and approved the submitted version.

FUNDING

This study was supported by Sanming Project of Medicine in Shenzhen (No. SZSM201911010).

ACKNOWLEDGMENTS

We would like to thank Zhijun Zhou (MD) from the University of Oklahoma Health Sciences Center, and Luyu Xie (PhD) from National Cancer Center Singapore for providing professional suggestions for this study.

SUPPLEMENTARY MATERIAL

The Supplementary Material for this article can be found online at: https://www.frontiersin.org/articles/10.3389/fphar.2022.868830/full#supplementary-material

REFERENCES

Bagaev, A., Kotlov, N., Nomie, K., Svekolkin, V., Gafurov, A., Isaeva, O., et al. (2021). Conserved Pan-Cancer Microenvironment Subtypes Predict Response to Immunotherapy. *Cancer Cell* 39 (6), 845–e7. doi:10.1016/j.ccell.2021.04.014

Bannister, A. J., and Kouzarides, T. (2011). Regulation of Chromatin by Histone Modifications. *Cell Res* 21 (3), 381–395. doi:10.1038/cr.2011.22

Chen, B., Khodadoust, M. S., Liu, C. L., Newman, A. M., and Alizadeh, A. A. (2018). Profiling Tumor Infiltrating Immune Cells with CIBERSORT. *Methods Mol. Biol.* 1711, 243–259. doi:10.1007/978-1-4939-7493-1_12

Chen, C., Zhang, F., Zhou, N., Gu, Y. M., Zhang, Y. T., He, Y. D., et al. (2019). Efficacy and Safety of Immune Checkpoint Inhibitors in Advanced Gastric or Gastroesophageal junction Cancer: a Systematic Review and Meta-Analysis. *Oncoimmunology* 8 (5), e1581547. doi:10.1080/2162402X.2019.1581547

Chen, H., Yao, J., Bao, R., Dong, Y., Zhang, T., Du, Y., et al. (2021). Cross-talk of Four Types of RNA Modification Writers Defines Tumor Microenvironment and Pharmacogenomic Landscape in Colorectal Cancer. *Mol. Cancer* 20 (1), 29. doi:10.1186/s12943-021-01322-w

Chen, X. Y., Liang, R., Yi, Y. C., Fan, H. N., Chen, M., Zhang, J., et al. (2021). The m6A Reader YTHDF1 Facilitates the Tumorigenesis and Metastasis of Gastric Cancer via USP14 Translation in an m6A-dependent Manner. *Front Cel Dev Biol* 9, 647702. doi:10.3389/fcell.2021.647702

Cho, J. Y., Lim, J. Y., Cheong, J. H., Park, Y. Y., Yoon, S. L., Kim, S. M., et al. (2011). Gene Expression Signature-Based Prognostic Risk Score in Gastric Cancer. *Clin. Cancer Res.* 17 (7), 1850–1857. doi:10.1158/1078-0432.CCR-10-2180

Cristescu, R., Lee, J., Nebozhyn, M., Kim, K. M., Ting, J. C., Wong, S. S., et al. (2015). Molecular Analysis of Gastric Cancer Identifies Subtypes Associated with Distinct Clinical Outcomes. *Nat. Med.* 21 (5), 449–456. doi:10.1038/nm.3850

Deng, S., Zhang, H., Zhu, K., Li, X., Ye, Y., Li, R., et al. (2021). M6A2Target: a Comprehensive Database for Targets of m6A Writers, Erasers and Readers. *Brief Bioinform* 22 (3), bbaa055. doi:10.1093/bib/bbaa055

Desbois, M., Udyavar, A. R., Ryner, L., Kozlowski, C., Guan, Y., Durrbaum, M., et al. (2020). Integrated Digital Pathology and Transcriptome Analysis Identifies Molecular Mediators of T-Cell Exclusion in Ovarian Cancer. *Nat. Commun.* 11 (1), 5583. doi:10.1038/s41467-020-19408-2

Desbois, M., and Wang, Y. (2021). Cancer-associated Fibroblasts: Key Players in Shaping the Tumor Immune Microenvironment. *Immunol. Rev.* 302 (1), 241–258. doi:10.1111/imr.12982

Dong, L. M., Zhang, X. L., Mao, M. H., Li, Y. P., Zhang, X. Y., Xue, D. W., et al. (2021). LINC00511/miRNA-143-3p Modulates Apoptosis and Malignant Phenotype of Bladder Carcinoma Cells via PCMT1. *Front. Cel Dev Biol* 9, 650999. doi:10.3389/fcell.2021.650999

Dongre, A., Rashidian, M., Reinhardt, F., Bagnato, A., Keckesova, Z., Ploegh, H. L., et al. (2017). Epithelial-to-Mesenchymal Transition Contributes to Immunosuppression in Breast Carcinomas. *Cancer Res.* 77 (15), 3982–3989. doi:10.1158/0008-5472.CAN-16-3292

Gu, C., Shi, X., Dai, C., Shen, F., Rocco, G., Chen, J., et al. (2020). RNA m6A Modification in Cancers: Molecular Mechanisms and Potential Clinical Applications. *Innov.*. 1 (3), 100066. doi:10.1016/j.xinn.2020.100066

Gu, Y., Wu, X., Zhang, J., Fang, Y., Pan, Y., Shu, Y., et al. (2021). The Evolving Landscape of N6-Methyladenosine Modification in the Tumor Microenvironment. *Mol. Ther.* 29 (5), 1703–1715. doi:10.1016/j.ymthe.2021.04.009

Hänzelmann, S., Castelo, R., and Guinney, J. (2013). GSVA: Gene Set Variation Analysis for Microarray and RNA-Seq Data. *BMC Bioinformatics* 14, 7. doi:10.1186/1471-2105-14-7

Hegde, P. S., Karanikas, V., and Evers, S. (2016). The where, the when, and the How of Immune Monitoring for Cancer Immunotherapies in the Era of Checkpoint Inhibition. *Clin. Cancer Res.* 22 (8), 1865–1874. doi:10.1158/1078-0432.CCR-15-1507

Huang, H., Weng, H., Zhou, K., Wu, T., Zhao, B. S., Sun, M., et al. (2019). Histone H3 Trimethylation at Lysine 36 Guides m6A RNA Modification Co-transcriptionally. *Nature* 567, 414–419. doi:10.1038/s41586-019-1016-7

Huang, Y., Min, S., Lui, Y., Sun, J., Su, X., Liu, Y., et al. (2012). Global Mapping of H3K4me3 and H3K27me3 Reveals Chromatin State-Based Regulation of Human Monocyte-Derived Dendritic Cells in Different Environments. *Genes Immun.* 13 (4), 311–320. doi:10.1038/gene.2011.87

Janjigian, Y. Y., Shitara, K., Moehler, M., Garrido, M., Salman, P., Shen, L., et al. (2021). First-line Nivolumab Plus Chemotherapy versus Chemotherapy Alone for Advanced Gastric, Gastro-Oesophageal junction, and Oesophageal Adenocarcinoma (CheckMate 649): a Randomised, Open-Label, Phase 3 Trial. *Lancet* 398 (10294), 27–40. doi:10.1016/S0140-6736(21)00797-2

Jeffrey, T. L. (2020). Surrogate Variable Analysis. Biostatistics.

Jiang, P., Gu, S., Pan, D., Fu, J., Sahu, A., Hu, X., et al. (2018). Signatures of T Cell Dysfunction and Exclusion Predict Cancer Immunotherapy Response. *Nat. Med.* 24 (10), 1550–1558. doi:10.1038/s41591-018-0136-1

Jiang, Y., and Zhan, H. (2020). Communication between EMT and PD-L1 Signaling: New Insights into Tumor Immune Evasion. *Cancer Lett.* 468, 72–81. doi:10.1016/j.canlet.2019.10.013

Kan, R. L., Chen, J., and Sallam, T. (2022). Crosstalk between Epitranscriptomic and Epigenetic Mechanisms in Gene Regulation. *Trends Genet.* 38 (2), 182–193. doi:10.1016/j.tig.2021.06.014

Kan, R. L., Chen, J., and Sallam, T. (2021). Crosstalk between Epitranscriptomic and Epigenetic Mechanisms in Gene Regulation. *Trends Genet.* 38, 182–193. doi:10.1016/j.tig.2021.06.01

Ke, S., Alemu, E. A., Mertens, C., Gantman, E. C., Fak, J. J., Mele, A., et al. (2015). A Majority of m6A Residues Are in the Last Exons, Allowing the Potential for 3' UTR Regulation. *Genes Dev.* 29 (19), 2037–2053. doi:10.1101/gad.269415.115

Kim, D., Paggi, J. M., Park, C., Bennett, C., and Salzberg, S. L. (2019). Graph-based Genome Alignment and Genotyping with HISAT2 and HISAT-Genotype. *Nat. Biotechnol.* 37 (8), 907–915. doi:10.1038/s41587-019-0201-4

Langfelder, P., and Horvath, S. (2008). WGCNA: an R Package for Weighted Correlation Network Analysis. *BMC Bioinformatics* 9, 559. doi:10.1186/1471-2105-9-559

Lawson, K. A., Sousa, C. M., Zhang, X., Kim, E., Akthar, R., Caumanns, J. J., et al. (2020). Functional Genomic Landscape of Cancer-Intrinsic Evasion of Killing by T Cells. *Nature* 586 (7827), 120–126. doi:10.1038/s41586-020-2746-2

Li, F., Chen, Q., Xue, H., Zhang, L., Wang, K., and Shen, F. (2020). LncRNA MNX1-AS1 Promotes Progression of Intrahepatic Cholangiocarcinoma through the MNX1/Hippo axis. *Cell Death Dis* 11 (10), 894. doi:10.1038/s41419-020-03029-0

Li, F., Chen, S., Yu, J., Gao, Z., Sun, Z., Yi, Y., et al. (2021). Interplay of M6 A and Histone Modifications Contributes to Temozolomide Resistance in Glioblastoma. *Clin. Transl Med.* 11 (9), e553. doi:10.1002/ctm2.553

Li, H., Handsaker, B., Wysoker, A., Fennell, T., Ruan, J., Homer, N., et al. (2009). The Sequence Alignment/Map Format and SAMtools. *Bioinformatics* 25 (16), 2078–2079. doi:10.1093/bioinformatics/btp352

Li, J., Li, Q., Li, D., Shen, Z., Zhang, K., Bi, Z., et al. (2020). Long Non-coding RNA MNX1-AS1 Promotes Progression of Triple Negative Breast Cancer by Enhancing Phosphorylation of Stat3. *Front. Oncol.* 10, 1108. doi:10.3389/fonc.2020.01108

Li, Y., Xia, L., Tan, K., Ye, X., Zuo, Z., Li, M., et al. (2020). N6-Methyladenosine Co-transcriptionally Directs the Demethylation of Histone H3K9me2. *Nat. Genet.* 52 (9), 870–877. doi:10.1038/s41588-020-0677-3

Li, Z., Weng, H., Su, R., Weng, X., Zuo, Z., Li, C., et al. (2017). FTO Plays an Oncogenic Role in Acute Myeloid Leukemia as a N6-Methyladenosine RNA Demethylase. *Cancer Cell* 31 (1), 127–141. doi:10.1016/j.ccell.2016.11.017

Liu, Y., Liang, G., Xu, H., Dong, W., Dong, Z., Qiu, Z., et al. (2021). Tumors Exploit FTO-Mediated Regulation of Glycolytic Metabolism to Evade Immune Surveillance. *Cell Metab* 33 (6), 1221–e11. doi:10.1016/j.cmet.2021.04.001

Love, M. I., Huber, W., and Anders, S. (2014). Moderated Estimation of Fold Change and Dispersion for RNA-Seq Data with DESeq2. *Genome Biol.* 15 (12), 550. doi:10.1186/s13059-014-0550-8

Mayakonda, A., Lin, D. C., Assenov, Y., Plass, C., and Koeffler, H. P. (2018). Maftools: Efficient and Comprehensive Analysis of Somatic Variants in Cancer. *Genome Res.* 28 (11), 1747–1756. doi:10.1101/gr.239244.118

Meng, Q., Lu, Y. X., Ruan, D. Y., Yu, K., Chen, Y. X., Xiao, M., et al. (2021). DNA Methylation Regulator-Mediated Modification Patterns and Tumor Microenvironment Characterization in Gastric Cancer. *Mol. Ther. Nucleic Acids* 24, 695–710. doi:10.1016/j.omtn.2021.03.023

Oh, S. C., Sohn, B. H., Cheong, J. H., Kim, S. B., Lee, J. E., Park, K. C., et al. (2018). Clinical and Genomic Landscape of Gastric Cancer with a Mesenchymal Phenotype. *Nat. Commun.* 9 (1), 1777. doi:10.1038/s41467-018-04179-8

Okabe, A., Huang, K. K., Matsusaka, K., Fukuyo, M., Xing, M., Ong, X., et al. (2020). Cross-species Chromatin Interactions Drive Transcriptional Rewiring in Epstein-Barr Virus-Positive Gastric Adenocarcinoma. *Nat. Genet.* 52 (9), 919–930. doi:10.1038/s41588-020-0665-7

Ooi, C. H., Ivanova, T., Wu, J., Lee, M., Tan, I. B., Tao, J., et al. (2009). Oncogenic Pathway Combinations Predict Clinical Prognosis in Gastric Cancer. *Plos Genet.* 5 (10), e1000676. doi:10.1371/journal.pgen.1000676

Peng, X., Li, X., Yang, S., Huang, M., Wei, S., Ma, Y., et al. (2021). LINC00511 Drives Invasive Behavior in Hepatocellular Carcinoma by Regulating Exosome Secretion and Invadopodia Formation. *J. Exp. Clin. Cancer Res.* 40 (1), 183. doi:10.1186/s13046-021-01990-y

Ritchie, M. E., Phipson, B., Wu, D., Hu, Y., Law, C. W., Shi, W., et al. (2015). Limma powers Differential Expression Analyses for RNA-Sequencing and Microarray Studies. *Nucleic Acids Res.* 43 (7), e47. doi:10.1093/nar/gkv007

Sempere, L. F., Powell, K., Rana, J., Brock, A. A., and Schmittgen, T. D. (2021). Role of Non-coding RNAs in Tumor Progression and Metastasis in Pancreatic Cancer. *Cancer Metastasis Rev.* 40 (3), 761–776. doi:10.1007/s10555-021-09995-x

Serra, O., Galán, M., Ginesta, M. M., Calvo, M., Sala, N., and Salazar, R. (2019). Comparison and Applicability of Molecular Classifications for Gastric Cancer. *Cancer Treat. Rev.* 77, 29–34. doi:10.1016/j.ctrv.2019.05.005

Shi, H., Wei, J., and He, C. (2019). Where, when, and How: Context-dependent Functions of RNA Methylation Writers, Readers, and Erasers. *Mol. Cel* 74 (4), 640–650. doi:10.1016/j.molcel.2019.04.025

Smyth, E. C., Nilsson, M., Grabsch, H. I., van Grieken, N. C., and Lordick, F. (2020). Gastric Cancer. *Lancet* 396 (10251), 635–648. doi:10.1016/S0140-6736(20)31288-5

Song, Y., Li, L., Ou, Y., Gao, Z., Li, E., Li, X., et al. (2014). Identification of Genomic Alterations in Oesophageal Squamous Cell Cancer. *Nature* 509 (7498), 91–95. doi:10.1038/nature13176

Stark, R., and Brown, G. (2011). DiffBind: Differential Binding Analysis of ChIP-Seq Peak Data. *Bioconductor*.

Su, R., Dong, L., Li, Y., Gao, M., Han, L., Wunderlich, M., et al. (2020). Targeting FTO Suppresses Cancer Stem Cell Maintenance and Immune Evasion. *Cancer Cell* 38 (1), 79–e11. doi:10.1016/j.ccell.2020.04.017

Tao, L., Mu, X., Chen, H., Jin, D., Zhang, R., Zhao, Y., et al. (2021). FTO Modifies the m6A Level of MALAT and Promotes Bladder Cancer Progression. *Clin. Transl Med.* 11 (2), e310. doi:10.1002/ctm2.310

Tarasov, A., Vilella, A. J., Cuppen, E., Nijman, I. J., and Prins, P. (2015). Sambamba: Fast Processing of NGS Alignment Formats. *Bioinformatics* 31 (12), 2032–2034. doi:10.1093/bioinformatics/btv098

Team, R.C (2020). A Language and Environment for Statistical Computing. AvaliableAt: https://www.R-project.org

Thrift, A. P., and El-Serag, H. B. (2020). Burden of Gastric Cancer. *Clin. Gastroenterol. Hepatol.* 18 (3), 534–542. doi:10.1016/j.cgh.2019.07.045

Wang, L., Hui, H., Agrawal, K., Kang, Y., Li, N., Tang, R., et al. (2020). m6 A RNA Methyltransferases METTL3/14 Regulate Immune Responses to Anti-PD-1 therapyA RNA Methyltransferases METTL3/14 Regulate Immune Responses to Anti-PD-1 Therapy. *EMBO J.* 39 (20), e104514. doi:10.15252/embj.2020104514

Wei, Z. (2020). exomePeak2: Bias Awared Peak Calling and Quantification for MeRIP-Seq. R package version 1.2.0.

Wilkerson, M. D., and Hayes, D. N. (2010). ConsensusClusterPlus: a Class Discovery Tool with Confidence Assessments and Item Tracking. *Bioinformatics* 26 (12), 1572–1573. doi:10.1093/bioinformatics/btq170

Wu, F., Zhong, Y., Lang, X. B., Tu, Y. L., and Sun, S. F. (2019). MNX1-AS1 Accelerates the Epithelial-Mesenchymal Transition in Osteosarcoma Cells by Activating MNX1 as a Functional Oncogene. *Eur. Rev. Med. Pharmacol. Sci.* 23 (19), 8194–8202. doi:10.26355/eurrev_201910_19126

Wu, J., Chai, H., Shan, H., Pan, C., Xu, X., Dong, W., et al. (2021). Histone Methyltransferase SETD1A Induces Epithelial-Mesenchymal Transition to Promote Invasion and Metastasis through Epigenetic Reprogramming of Snail in Gastric Cancer. *Front. Cel Dev Biol* 9, 657888. doi:10.3389/fcell.2021.657888

Wu, Q. N., Luo, X. J., Liu, J., Lu, Y. X., Wang, Y., Qi, J., et al. (2021). MYC-activated LncRNA MNX1-AS1 Promotes the Progression of Colorectal Cancer by Stabilizing YB1. *Cancer Res.* 81 (10), 2636–2650. doi:10.1158/0008-5472.CAN-20-3747

Wu, Y., Li, L., Wang, Q., Zhang, L., He, C., Wang, X., et al. (2020). LINC00511 Promotes Lung Squamous Cell Carcinoma Proliferation and Migration via Inhibiting miR-150-5p and Activating TADA1. *Transl Lung Cancer Res.* 9 (4), 1138–1148. doi:10.21037/tlcr-19-701

Yang, H., Cui, W., and Wang, L. (2019). Epigenetic Synthetic Lethality Approaches in Cancer Therapy. *Clin. Epigenetics* 11 (1), 136. doi:10.1186/s13148-019-0734-x

Yang, H., Gao, L., Zhang, M., Ning, N., Wang, Y., Wu, D., et al. (2021). Identification and Analysis of an Epigenetically Regulated Five-lncRNA Signature Associated with Outcome and Chemotherapy Response in Ovarian Cancer. *Front. Cel Dev Biol* 9, 644940. doi:10.3389/fcell.2021.644940

Yang, Z., Jiang, X., Zhang, Z., Zhao, Z., Xing, W., Liu, Y., et al. (2021). HDAC3-dependent Transcriptional Repression of FOXA2 Regulates FTO/m6A/MYC Signaling to Contribute to the Development of Gastric Cancer. *Cancer Gene Ther.* 28 (1-2), 141–155. doi:10.1038/s41417-020-0193-8

Yin, J., Leavenworth, J. W., Li, Y., Luo, Q., Xie, H., Liu, X., et al. (2015). Ezh2 Regulates Differentiation and Function of Natural Killer Cells through Histone Methyltransferase Activity. *Proc. Natl. Acad. Sci. U S A.* 112 (52), 15988–15993. doi:10.1073/pnas.1521740112

Yoshihara, K., Shahmoradgoli, M., Martínez, E., Vegesna, R., Kim, H., Torres-Garcia, W., et al. (2013). Inferring Tumour Purity and Stromal and Immune Cell Admixture from Expression Data. *Nat. Commun.* 4, 2612. doi:10.1038/ncomms3612

Yu, G., Wang, L. G., Han, Y., and He, Q. Y. (2012). clusterProfiler: an R Package for Comparing Biological Themes Among Gene Clusters. *OMICS* 16 (5), 284–287. doi:10.1089/omi.2011.0118

Yuan, L., Xu, Z. Y., Ruan, S. M., Mo, S., Qin, J. J., and Cheng, X. D. (2020). Long Non-coding RNAs towards Precision Medicine in Gastric Cancer: Early Diagnosis, Treatment, and Drug Resistance. *Mol. Cancer* 19 (1), 96. doi:10.1186/s12943-020-01219-0

Yue, B., Song, C., Yang, L., Cui, R., Cheng, X., Zhang, Z., et al. (2019). METTL3-mediated N6-Methyladenosine Modification Is Critical for Epithelial-Mesenchymal Transition and Metastasis of Gastric Cancer. *Mol. Cancer* 18 (1), 142. doi:10.1186/s12943-019-1065-4

Zhao, H., Liu, X., Yu, L., Lin, S., Zhang, C., Xu, H., et al. (2021). Comprehensive Landscape of Epigenetic-Dysregulated lncRNAs Reveals a Profound Role of Enhancers in Carcinogenesis in BC Subtypes. *Mol. Ther. Nucleic Acids* 23, 667–681. doi:10.1016/j.omtn.2020.12.024

Zhao, L., Kong, X., Zhong, W., Wang, Y., and Li, P. (2020). FTO Accelerates Ovarian Cancer Cell Growth by Promoting Proliferation, Inhibiting Apoptosis, and Activating Autophagy. *Pathol. Res. Pract.* 216 (9), 153042. doi:10.1016/j.prp.2020.153042

Zhao, Y., Chen, Y., Jin, M., and Wang, J. (2021). The Crosstalk between m6A RNA Methylation and Other Epigenetic Regulators: a Novel Perspective in Epigenetic Remodeling. *Theranostics* 11 (9), 4549–4566. doi:10.7150/thno.54967

Zhao, Z., and Shilatifard, A. (2019). Epigenetic Modifications of Histones in Cancer. *Genome Biol.* 20 (1), 245. doi:10.1186/s13059-019-1870-5

Zhou, G., Yan, K., Liu, J., Gao, L., Jiang, X., and Fan, Y. (2021). FTO Promotes Tumour Proliferation in Bladder Cancer via the FTO/miR-576/CDK6 axis in an m6A-dependent Manner. *Cell Death Discov* 7 (1), 329. doi:10.1038/s41420-021-00724-5

Conflict of Interest: The authors declare that the research was conducted in the absence of any commercial or financial relationships that could be construed as a potential conflict of interest.

Publisher's Note: All claims expressed in this article are solely those of the authors and do not necessarily represent those of their affiliated organizations, or those of the publisher, the editors, and the reviewers. Any product that may be evaluated in this article, or claim that may be made by its manufacturer, is not guaranteed or endorsed by the publisher.

frontiers | Frontiers in Pharmacology

REVIEW
published: 10 May 2022
doi: 10.3389/fphar.2022.900825

Application and Prospect of CRISPR/Cas9 Technology in Reversing Drug Resistance of Non-Small Cell Lung Cancer

Lu Huang[1,2†], Zhi Liao[3†], Zhixi Liu[1,2], Yan Chen[1], Tingwenli Huang[1,2] and Hongtao Xiao[1,2]*

[1]Department of Clinical Pharmacy, Sichuan Cancer Center, School of Medicine, Sichuan Cancer Hospital and Institute, University of Electronic Science and Technology of China, Chengdu, China, [2]Personalized Drug Therapy Key Laboratory of Sichuan Province, Chengdu, China, [3]Department of Gynecology and Obstetrics, Sichuan Academy of Medical Sciences and Sichuan Provincial People's Hospital, Chengdu, China

Cancer drug resistance has always been a major factor affecting the treatment of non-small cell lung cancer, which reduces the quality of life of patients. The clustered regularly interspaced short palindromic repeats/CRISPR associated protein 9 (CRISPR/Cas9) technology, as an efficient and convenient new gene-editing technology, has provided a lot of help to the clinic and accelerated the research of cancer and drug resistance. In this review, we introduce the mechanisms of drug resistance in non-small cell lung cancer (NSCLC), discuss how the CRISPR/Cas9 system can reverse multidrug resistance in NSCLC, and focus on drug resistance gene mutations. To improve the prognosis of NSCLC patients and further improve patients' quality of life, it is necessary to utilize the CRISPR/Cas9 system in systematic research on cancer drug resistance.

Keywords: non-small cell lung cancer, drug resistance, CRISPR/Cas9, gene editing, TKIs

OPEN ACCESS

Edited by:
Jian Zhang,
Zhujiang Hospital, Southern Medical University, China

Reviewed by:
Zhuo-Xun Wu,
St. John's University, United States
Eng Wee Chua,
National University of Malaysia, Malaysia

****Correspondence:***
Hongtao Xiao
xht927@163.com

†These authors have contributed equally to this work and share first authorship

Specialty section:
This article was submitted to Pharmacology of Anti-Cancer Drugs, a section of the journal Frontiers in Pharmacology

Received: *21 March 2022*
Accepted: *25 April 2022*
Published: *10 May 2022*

Citation:
Huang L, Liao Z, Liu Z, Chen Y, Huang T and Xiao H (2022) Application and Prospect of CRISPR/Cas9 Technology in Reversing Drug Resistance of Non-Small Cell Lung Cancer. Front. Pharmacol. 13:900825. doi: 10.3389/fphar.2022.900825

1 INTRODUCTION

Lung cancer is one of the most common cancers and is the leading cause of cancer death, accounting for approximately 18% of cancer deaths (Sung et al., 2021). Non-small cell lung cancer (NSCLC) is the most common type of lung cancer, accounting for more than 85% of total lung cancer cases, and the World Health Organization (WHO) classifies NSCLC into adenocarcinomas, squamous carcinomas, and large cell carcinomas based on differences in immunohistochemical markers (Mengoli et al., 2018). The high lethality of lung cancer is associated with difficulty in diagnosis, treatment, and poor prognosis (Woodard et al., 2016). The mainstay of treatment for NSCLC is surgery and adjuvant cisplatin-based therapy (Duma et al., 2019), Many challenges remain in the screening and treatment of lung cancer, and mortality is difficult to control. Although chemotherapy can prolong survival to some extent in patients with moderately advanced NSCLC, the overall response rate is only about 30%, the median survival is 8–12 months, and the 1-year survival rate is 30–40% (Reck and Rabe, 2017). The advent of targeted agents has led to improvements in the treatment of NSCLC.

However, the treatment failure in NSCLC is closely related to the phenomenon of acquired drug resistance and multidrug resistance (MDR) in prognosis. For example, in NSCLC patients harboring EGFR gene mutations, the EGFR-TKI class of drugs is the standard first-line treatment, showing disease progression after 9–13 months despite some therapeutic efficacy (Kelly et al., 2015). Tumors with EGFR-TKI resistance mechanisms had EGFR secondary mutations, bypass or downstream

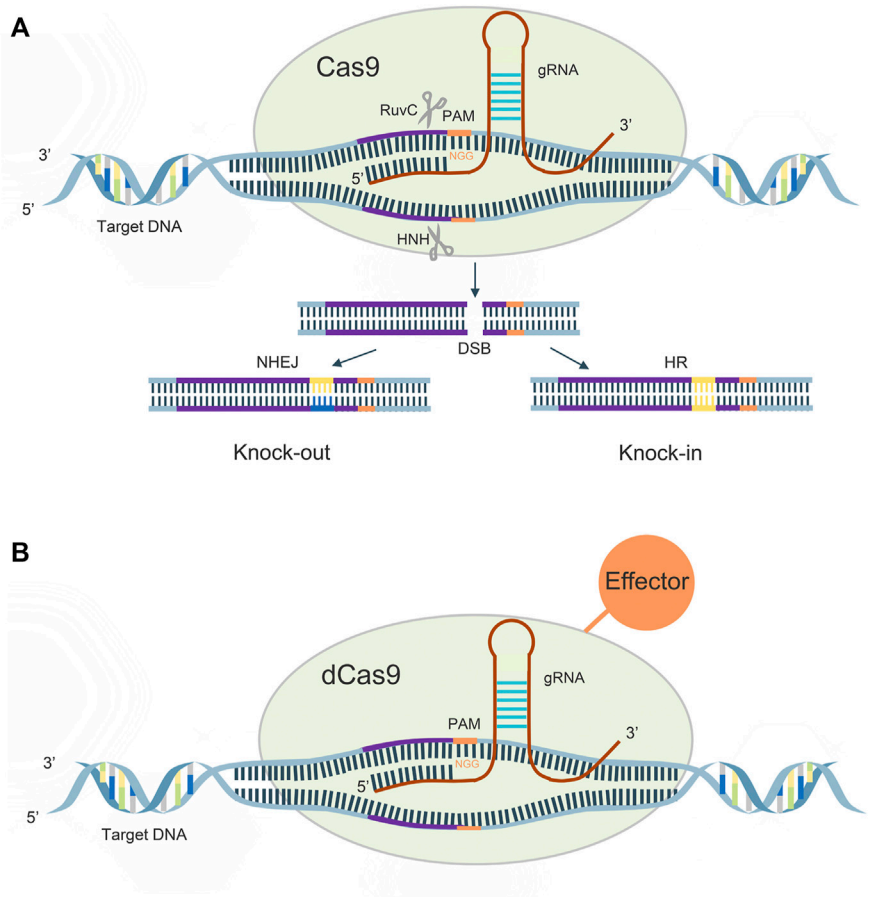

FIGURE 1 | (A): Mechanism of CRISPR/Cas9 system; **(B)**: Mechanism of CRISPR/dCas9 system.

pathway activation: such as HER2 amplification, met amplification, FGFR1 activation, PI3K/Akt pathway activation, BRAF mutation, and loss of PTEN expression (Uchibori et al., 2018; Leonetti et al., 2019).

Clustered regularly interspaced short palindromic repeats/CRISPR associated protein 9 (CRISPR/Cas9) technology is the most powerful gene-editing technology after zinc finger nucleases (ZFNs), transcription activator-like effector nucleases (Talens) (Carroll, 2011; Joung and Sander, 2013), with flexible and convenient features, it is inexpensive and has been widely used in biology, microbiology, agriculture, and animal husbandry.

To further investigate the mechanisms of multidrug resistance in NSCLC and improve the prognosis and quality of life of NSCLC patients, we discuss issues related to NSCLC drug resistance by reversing NSCLC multidrug resistance via CRISPR/Cas9, screening drug-resistant targets, and targeting therapies.

2 MECHANISM OF THE CRISPR/CAS9 SYSTEM

CRISPR/Cas, an acquired immune defense system that evolved during long-term evolution in bacteria and archaea to fight invading viruses and foreign DNA, was first identified in 1987 (Ishino et al., 1987) and was later shown to have powerful gene-editing functions.

CRISPR gene sequences are constituted by multiple short and conserved repeats and non-repetitive sequences called spacers, and CAS proteins are a family of endonucleases. There are three main stages in the mechanism of acquired immune protection by CRISPR/Cas9, which are the acquisition of CRISPR spacer sequences, expression of CRISPR genes, and CRISPR interference (Deveau et al., 2010). When a foreign gene first invades a bacterium, CRISPR/Cas9 recognizes the protospacer adjacent motif (PAM), and cuts the DNA sequence adjacent to the PAM as a candidate protospacer from the foreign DNA, inserts downstream of the leader region of the CRISPR sequence, and repairs. When foreign genes re-invade, CRISPR sequences are transcribed to form pre-CRISPR-derived RNA (pre-crRNA) and trans-acting crRNA (tracrRNA), the former of which is sheared by Cas proteins into mature CRISPR derived RNA (crRNA). Subsequently, a complex consisting of pre-crRNA, tracrRNA and cas9 protein allows recognition of the foreign gene and DNA double-strand cleavage.

A guide RNA (gRNA), consisting of 20–24 bases, recognizes the PAM on both sides of the target DNA for target sequence

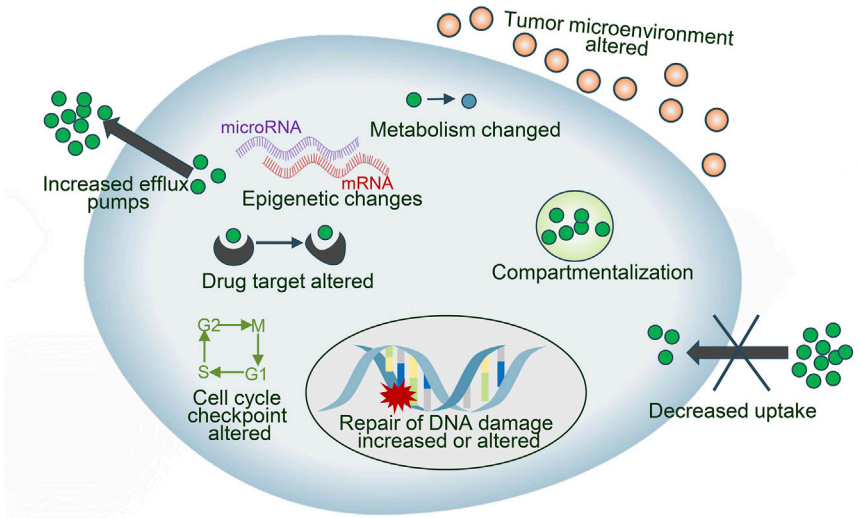

FIGURE 2 | Different mechanisms involved in anticancer drug resistance.

cleavage, its HNH enzyme will shear the crRNA complementary DNA strand, while its RUVC active site will shear the noncomplementary strand, causing double-strand breaks (DSBs), and the cell performs DNA repair by non-homologous end joining (NHEJ) and homologous directed recombination (HDR) pathways, thus creating a permanent mutation (**Figure 1A**).

In 2013, Qi et al. introduced h840a mutations in the HNH domain of the cas9 protein and D10A mutations in the RUVC domain, which rendered the protein activity defective and, although DNA could still be precisely targeted, lost its original function (Qi et al., 2013). The dCas9 can regulate target genes under the guidance of sgRNAs without generating DSBs. The dcas9 protein can carry different effector domains, recruit endogenous transcriptional activators and RNA polymerase to target DNA sequences for target gene activation, and also disrupt transcription factor binding or hinder RNA polymerase binding, thereby silencing target gene expression (McCarty et al., 2020) (**Figure 1B**).

3 PRINCIPLES OF MULTIDRUG RESISTANCE IN NSCLC REVERSED BY CRISPR/CAS9 TECHNOLOGY

Drug resistance is an essential factor leading to treatment failure in many intractable diseases, which limits the application of chemotherapeutics in NSCLC patients, and the reasons why tumor cells develop drug resistance are complex and variable, mainly including drug inactivation, enhanced drug efflux, epigenetic changes, DNA repair ability, apoptosis inhibition, alteration of drug targets Epithelial-mesenchymal transition (EMT), etc. (Gottesman, 2002; Panda and Biswal, 2019) (**Figure 2**). These mechanisms can act independently or in combination and act through various signal transduction pathways. CRISPR/Cas9 has been used for the study of drug sensitization and resistance. We discuss the key reasons for drug failure in NSCLC and the role of CRISPR/Cas9 technology.

3.1 Studies on Drug Resistance Genes

NSCLCs are strongly associated with mutations in related genes that cause alterations in the structure or number of proteins encoded by the genes, leading to changes in the function of their associated genes. In addition to the well-known EGFR and ALK, BRAF mutations, ros1 rearrangements, RET rearrangements, and others are common in NSCLC. There are a variety of targeted drugs acting on the relevant receptors (**Table 1**; **Figure 3**). The CRISPR/Cas9 system can be used to remove the functional regions of drug resistance genes, thereby reversing drug resistance. It can also be used to knock out or overexpress drug resistance genes in cell lines and animals, making it easier to research drug resistance mechanisms in tumors.

3.1.1 EGFR

EGFR is a tyrosine kinase receptor that Homo—or heterodimerizes with ligands to cause autophosphorylation, which in turn regulates downstream signaling pathways leading to tumor proliferation, invasion, metastasis and angiogenesis. Mutations in the EGFR kinase domain are present in approximately 10%–40% of patients with NSCLC. Treatment of EGFR mutant lung cancers with EGFR-TKIs effectively inhibits tumor progression and prolongs progression free survival (PFS) in patients with NSCLC compared with standard chemotherapeutic agents (Schrank et al., 2018). Approximately 90% of EGFR mutations are caused by mutations in exon 19 (exon 19 deletion mutation) and exon 21 (L858R) (Camidge et al., 2014; Robichaux et al., 2018). After administration of TKIs, most patients develop acquired resistance, which is usually caused by a secondary mutation at position 790 in exon 20 (Cross et al., 2014),

TABLE 1 | Summary of targeted therapeutic drugs for non-small cell lung cancer.

Targrt	Mechanism of Action	Drug	Usage	Ref
First generation EGFR-TKIs	Inhibits by binding to the ATP site of the EGFR receptor	Erlotinib	For first-line treatment of locally advanced or metastatic NSCLC with sensitive gene mutations in EGFR.	Zhou et al. (2011)
		Gefitinib	It is used for single drug continuous treatment of locally advanced or metastatic NSCLC with platinum and docetaxel chemotherapy failure	Goss et al. (2013)
Second generation EGFR-TKIs	Blocking the EGFR-HER2 signaling pathway	Afatinib	It can significantly improve the progression free survival, objective response rate (ORR) and 8-weeks disease control rate	Park et al. (2016)
Third generation EGFR-TKIs	Play a role in secondary drug resistance. the binding of ALK	Osimertinib	Targeted treatment of patients with EGFR mutation and T790M drug resistance mutation significantly prolonged PFS in patients with NSCLC.	Cho et al. (2019)
First generation ALK-TKIs	Competitive binding to ATP binding sites blocks. The binding of the ALK enzyme to ATP, hinders the subsequent autophosphorylation process, and leads to the inactivation of the ALK downstream signal pathway	Crizotinib	It can effectively inhibit NSCLC caused by ROS 1 gene rearrangement	Moro-Sibilot et al. (2019)
Second generation ALKK-TKIs		Ceritinib	It is applicable to NSCLC patients who progress after treatment with kezotinib or cannot tolerate its toxic and side effects	Soria et al. (2017)
BRAF inhibitor	The continuous activation of BRAF gene leads to the over activation of MEK/ERK signaling pathway, which leads to tumor production and even tumor metastasis	Dabrafenib	Combined with trimetinib to treat patients with advanced NSCLC with braf-v600e mutation	Planchard et al. (2017)
c-Met inhibitor	c-MET can affect the downstream PI3K/Akt and MAPK pathways, and abnormal c-met activity leads to abnormal metabolism	Tivantinib	Combined with EGFR-TKI can effectively prolong the PFS of EGFR mutant NSCLC.	Yoshioka et al. (2015)

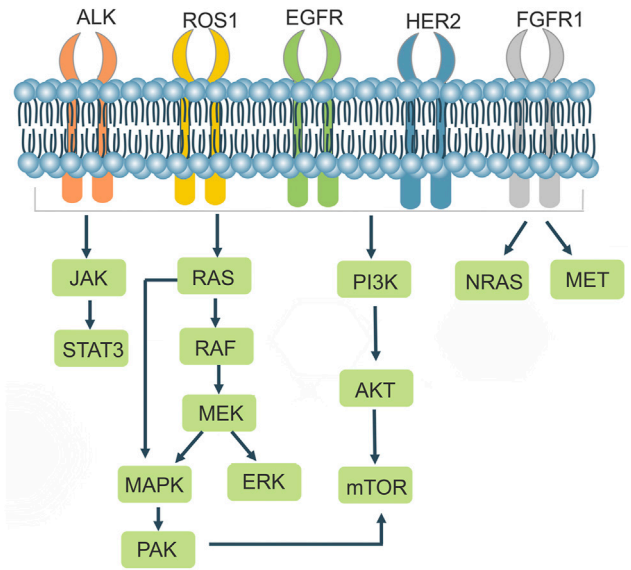

FIGURE 3 | Cell signaling in NSCLC drug resistance.

Targeting the third-generation EFGR-TKI Osimertinib for this resistance occurs where the EGFR c797s mutation blocks efficient binding of Osimertinib to the target EGFR c797 site (Jia et al., 2016). Tang et al. proposed an individualized molecular surgical treatment strategy for EGFR mutant lung cancer using CRISPR/Cas9 technology, which generates breaks at mutation sites or exons. The wild-type sequence containing the exon and the donor DNA with its left and right homology arms would then replace the mutated sequence or exon by HDR, an approach that would eradicate the drug resistance gene and thus prevent cancer progression (Tang and Shrager, 2016). Liu et al. used CRISPR/Cas9 technology to create renal cell carcinoma (RCC) cell lines with EGFR knockout, which significantly inhibited cancer cell proliferation and induced cell arrest in the G2/M phase. However, knocking out EGFR resulted in high ERK expression, but the authors discovered that ERK and Akt could be inhibited by Sunitinib (a multi-targeted TKI) in combination (Liu et al., 2020), suggesting that CRISPR mediated knockout of drug resistance genes may be a promising option for future disease treatment.

3.1.2 ALK

Anaplastic lymphoma kinase (ALK), which belongs to the insulin receptor (IR) superfamily, is a highly conserved receptor tyrosine kinase. ALK rearrangements are found in approximately 3%–7% of NSCLC patients (Devarakonda et al., 2015). ALK is mutated as a fusion with echinoderm microtubule-associated protein like 4 (EML4), encoding the form of an EML4-ALK fusion protein that leads to ALK dimerization, which results in the activation of ALK and its downstream signaling pathways such as JAKs/STAT3 and RAS/MEK/ERK, leading to aberrant cell proliferation and differentiation and promoting tumorigenesis (Soda et al., 2007; Sasaki et al., 2010). In 2014, Blasco et al. designed sgRNAs targeting intron 14 of the EML4 gene and intron 19 of the ALK gene in mice, generated DSBs using Cas9, and generated EML4-ALK rearrangements in non-small cell lung cancer cells, which were able to promote tumor formation in the lungs of mice, demonstrating the importance of the CRISPR/Cas9 system for studying chromosomal rearrangements (Blasco et al., 2014). EML4-ALK exhibits potent oncogenic properties both *in vitro* and *in vivo*, in which tumor development can be rapidly

suppressed using ALK TKIs (Soda et al., 2008). Tumor cells often develop acquired resistance to ALK inhibitors, resulting from secondary mutations in the patient's kinase domain, gene amplification, and activation of alternative signaling pathways (e.g., EGFR, kit, IGF1R, etc.) and epithelial mesenchymal transformation (Spaans and Goss, 2014; Kong et al., 2019). ALK creates secondary mutations that promote an altered spatial conformation of the kinase, weaker binding to the drug, or stronger binding to ATP, leading to the development of drug resistance. The initial ALK mutation was the L1196m mutation, and the leucine residue L1196 in the ALK kinase domain, located at the bottom of the ATP binding pocket, is mutated to methionine. The thioether side chain of methionine would create a steric hindrance to hinder the binding of the ALK-TKI Crizotinib to the ALK kinase, resulting in Crizotinib resistance (Doebele et al., 2012).

3.1.3 ROS1

The receptor tyrosine kinase ROS proto-oncogene 1 (ROS1) belongs to a group of receptor tyrosine kinases in the insulin family of receptors, and ROS1 rearrangements are observed in approximately 1%–2% of patients with NSCLC (Gainor and Shaw, 2013). The kinase domains of ALK and ROS1 share homology, and Crizotinib, an ALK-EML 4 inhibitor, was used to interfere with ROS1 fusion gene-positive and ALK-EML4 fusion gene-positive lung cancer cells, and Crizotinib was found to inhibit the growth of hcc78 cells (ROS1 fusion gene-positive) (Bergethon et al., 2012), Accordingly, some ALK-TKIs have been shown to be effective in patients with ros1 rearrangement (Huber et al., 2014). Choi et al. achieved the first CD74-ROS1 translocation event utilizing CRISPR/Cas9 technology in 2014, suggesting that Cas9-induced DSB can result in chromosome translocation (Choi and Meyerson, 2014). Sato et al. designed gRNAs to target EZR intron 9 and ROS1 intron 33 and successfully generated EZR/ROS1 fusions in HBECp53 lung adenocarcinoma cells, which highly induced the phosphorylation of MEK and ERK, and the MEK/ERK signaling pathway can mediate the primary or acquired resistance to ROS11 TKIs in ROS1 rearranged lung adenocarcinoma patients. Using a combination of Selumetinib and Crizotinib, the authors effectively inhibited the growth of ros1 fusion positive cells *in vitro* and *in vivo* (Sato et al., 2020), providing a therapeutic strategy for NSCLC.

3.1.4 KRAS

Kirsten rat sarcoma viral oncogene (KRAS) belongs to the RAS protein family, and KRAS mutation is a common type of mutation in non-small cell lung cancer. When KRAS is bound to guanosine triphosphate (GTP), it is activated and can activate downstream BRAF/MEK/ERK and PI3K/Akt/mTOR signaling pathways (Friedlaender et al., 2020). The mutation rate of KRAS in NSCLC is 20%–30%, and about 97% of these mutations are point mutations in codon 12 or 13 in exon 2 (Rotow and Bivona, 2017). KRAS is a marker of resistance to EGFR-TKIs drugs, and KRAS mutation is an indicator of poor prognosis in NSCLC. So far, no effective KRAS inhibitors have been developed. Gao et al. used the CRISPR/Cas9 system to knock out KRAS G12S, used dcas9 KRAB to bind to the target. KRAB, a transcription inhibitor, can downregulate mRNA transcription. Cas9-sgG12S suppressed the proliferation of tumor cells by inhibiting the production of the KRAS (G12S) protein in A549 cells, as well as the phosphorylation levels of downstream molecules Akt and ERK. The tumor volume reduced by 46%, the tumor volume decreased by 30%, and the expression of KRAS mutant protein decreased dramatically in A549 mice treated with Adv-Cas9-sgG12S (Gao et al., 2020).

3.1.5 BRAF

V-Raf mouse sarcoma viral oncogene homolog B (BRAF) is a serine/threonine kinase that is downstream of KRAS in the MAPK signaling cascade pathway. BRAF is mutated in 60% of melanomas and drives oncogenes for a variety of malignancies such as colorectal, ovarian, and papillary thyroid cancer. RAS-GTP binding to the receptor-binding domain (RBD) activates RAF, leading to RAF phosphorylation and the induction of MEK and ERK activation, which results in cell proliferation and differentiation (Wan et al., 2004). Ding et al. tested the amplification refractory mutation system in 1680 NSCLC patients and found that the BRAF mutation rate was 1.7%, and was mostly found in lung adenocarcinoma patients and female patients (Ding et al., 2017). The predominant type of mutation in the brae gene in NSCLC is V600E, with a mutation rate of over 50% (Li et al., 2014), and investigators have found two mutations, V458L and K438T, on exon 11 in lung adenocarcinoma (Brose et al., 2002). Resistance to the BRAF inhibitor dabrafenib often develops within 8 months (Flaherty et al., 2010; Chapman et al., 2011). As BRAF mutations are more common in melanoma, studies utilizing CRISPR/Cas9 for chemotherapeutic agents have often revolved around the melanoma. Wu et al. developed a light-inducible CRISPR/Cas9 system to cleave the mutated BRAF gene (BRAF V600E), which promotes melanoma cell apoptosis and effectively inhibits melanoma cell proliferation, invasion, and migration (Wu et al., 2020).

3.1.6 MET

C-MET proto-oncogene, receptor tyrosine kinase (c-MET), a transmembrane receptor encoded by the met gene, belongs to the hepatocyte growth factor (HGF) receptor family, and HGF, in combination with c-MET, undergoes phosphorylation and autophosphorylation and activates downstream PI3 K/Akt and MAPK signaling pathways (Pasquini and Giaccone, 2018), MET amplification accounts for 5%–20% of NSCLC patients and is a poor prognostic factor for EGFR-TKI acquired resistance (Bubendorf et al., 2017). Met exon 14 mutations are common and account for 3% of lung adenocarcinomas (Schrock et al., 2016). Crizotinib acts as a tyrosine kinase receptor inhibitor capable of inhibiting c-MET. Togashi and others used CRISPR/Cas9 system to knock out the exon of MET 14 in HEK293 cell line, MET phosphorylation raised, protein expression increased, cell proliferation was reinforced, and cell sensitivity to Crizotinib was improved (Togashi et al., 2015), demonstrating that targeted therapy for MET exon 14 deleted non-small cell lung cancer holds promise.

3.1.7 Other Genes

Nonspecific conventional chemotherapy drugs, such as cisplatin, paclitaxel, and etoposide, are also commonly used in the treatment of NSCLC. Chen et al. silenced Rsf-1 in NSCLC by CRISPR/Cas9, which inhibited cancer cell inhibition and migration and promoted cancer cell apoptosis, demonstrating that Rsf-1 regulates NF-κ B pathways to influence NSCLC sensitivity to paclitaxel (Chen et al., 2017). Aurora-B is a key factor regulating mitosis and is frequently overexpressed in lung cancer. Yu et al. knocked down Aurora-B in the A549 cell line by CRISPR/Cas9 technology, and demonstrated that Aurora-B could confer NSCLC drug resistance by inhibiting cell proliferation, p53 related DNA damage response and apoptotic pathways, while knocking down Aurora-B was able to restore cell sensitivity to cisplatin and paclitaxel (Yu et al., 2018). Zhang et al. found that transducing-like (β) receptor 1 (tbl1xr1) was overexpressed in NSCLC and promoted cancer progression by regulating the MEK and Akt signaling pathways through its master regulator c-MET, knockdown of tbl1xr1 by CRISPR/Cas9 in A549 and H460 cell lines resulted in an increase in the number of cells in G0/G1 phase, inhibited cell proliferation and migration, and promoted apoptosis with a concomitant increase in sensitivity to cisplatin (Zhang T. et al., 2020).

3.2 Application of CRISPR/Cas9 in Screening Drug Resistance Genes

CRISPR/Cas9 technology is also being used for genetic screening of potential drug resistance in NSCLC. Previously, RNA interference (RNAi) - based genetic screens, the mainstay of genome-wide loss of function screens, have been effective in identifying genes in tumor cells that can respond to chemotherapeutic agents and in studying signaling pathways. However, there are a series of challenges in the application of RNAi. For example, the high specificity of RNAi is relative, in some cases siRNAs produce the off-target phenomenon. RNAi cannot wholly block the expression of genes in mammalian cells, especially those that are abnormally highly expressed (Jackson et al., 2006; Mullenders and Bernards, 2009). CRISPR/Cas9 technology can activate or repress gene expression and can label functional regions at specific genomic loci, resulting in accurate genome editing with the advantages of fewer false positives and lower off-target effects (Evers et al., 2016), which has now been applied to screen drug resistance genes in a variety of tumors.

Zeng et al., through genome-wide CRISPR/Cas9 gene screening, found that inactivation of GPCR related effectors produced obvious synergistic effects with EGFR inhibition in EGFR mutated NSCLC cells, deficiency of GPCR related effector - RIC8A could improve cell sensitivity to chemotherapeutic drugs, and targeting RIC8A is promising as a new approach to preventing EGFR-TKI resistance in NSCLC (Zeng et al., 2019). Lee et al. used CRISPR/Cas9 libraries to screen human lung cancer cell lines (NCI-H820) and knockdown of the genes MDM4, PSMA6, PSMB6, ANAPC5, and CDK1 increased the sensitivity of lung cancer cells to the EGFR-TKI Erlotinib, the MDM4 inhibitor nutlin-3 synergized with PSMA6, and the PSMB6 inhibitor Carfilzomib synergized with Erlotinib *in vitro* cell lines and *in vivo* patient-derived xenograft experiments, can promote tumor cell death, target cell cycle or protein ubiquitination pathways, and may inhibit Erlotinib resistance progression (Lee et al., 2021).

3.3 Modification of Cellular Transport Pathways

Cancer cells often efflux chemotherapeutic agents out of the cell to lower intracellular drug concentrations by up regulating one or more adenosine triphosphate binding cassette (ABC) membrane transporters (Mollazadeh et al., 2018). Three transporters multidrug resistance protein 1 (MDR1), multidrug resistance-associated protein 1 (MRP1), and breast cancer resistance protein (BCRP) - have been implicated in cancer resistance (Sakaeda et al., 2002; Cole, 2014; Mao and Unadkat, 2015). P-glycoprotein (P-gp), a member of the ABC superfamily of structural transporters that have been extensively studied, is encoded by MDR1 (Panczyk et al., 2007), is widely distributed in tissues such as the brain, lung, liver, kidney and gastrointestinal tract (Gupta et al., 2015), and is highly expressed within tumor cells, which confers drug resistance (Ambudkar, 1995; Li et al., 2016). Studies in many different types of cancer have shown that increased expression of any one of these transporters in cancer cells leads to suboptimal clinical outcomes. Jia et al. showed that the expression level of P-gp in ovarian cancer tissues was significantly higher than that in adjacent normal tissues, and increased with higher clinical stage of ovarian cancer (Jia et al., 2018). EL-Masry et al. demonstrated that in adult acute myeloid leukemia (AML) patients, BCRP was highly expressed in 34 out of 50 adult AML patients (68%) (El-Masry et al., 2018). In chronic myeloid leukemia (CML), tumor sensitivity can be increased using febuxostat, a BCRP inhibitor (Ito et al., 2021).

Using the CRISPR/Cas9 system to target the MDR1 gene in the MDR cell lines KBV 200 and HCT-8/V, Yang et al. were able to improve vincristine and doxorubicin sensitivity in MDR cancer cells (Yang et al., 2016a). The PI3K inhibitor BAY-1082439 was able to down regulate P-gp and BCRP expression, and nonviral transgenic vector-mediated CRISPR/Cas9 knockdown of PI3K in non-small cell lung cancer H460 cell line and its resistant subline H460/MX20 110 α And 110.0 β Subunit, leading to downregulation of P-gp and BCRP and reversing P-gp-mediated drug resistance (Zhang L. et al., 2020).

3.5 CRISPR/Cas9 for Epigenetic Regulation

Epigenetic regulation of cancer cells has an important role in the process of drug resistance. Epigenetics refers to the regulatory mechanisms of gene expression that result in an altered phenotype through the modification of DNA bases. Many of the genes that play a key role in the process of cancer drug resistance often have abnormal alterations in epigenetics to escape the body's immune surveillance. Many of the sites that are mutated at high frequency on the drug-resistant genomes of tumors are genes encoding enzymes associated with epigenetic regulation (Yu et al., 2011; Azad et al., 2013). Common epigenetic regulations include DNA methylation, histone modification,

noncoding RNA regulation, and chromatin remodeling, among others (Dawson and Kouzarides, 2012). DNA methylation is the addition of a methyl group to the cytosine of certain specific regions (i.e., the Cp G Islands) where methylation occurs, leading to the expression of the gene being affected. Transcriptional inactivation, silencing of tumor suppressor genes when aberrantly methylated, or activation of oncogenes due to DNA hypomethylation may underlie tumorigenesis and chemotherapeutic resistance (Liu B. et al., 2016). Terai et al. showed that gefitinib-resistant lung cancer cells had significantly increased methylation relative to parental cells (Terai et al., 2015). Protein modification refers to the process by which histones undergo methylation, acetylation, phosphorylation, ubiquitination and other modifications under the action of related enzymes (Audia and Campbell, 2016). In hepatocellular carcinoma (HCC), G9a, a histone methyltransferase, promotes HCC proliferation and metastasis by regulating the dimethylation level of rarres3 histone (Wei et al., 2017). In 2016, Okano et al. initially demonstrated the essential role of the dCas9-Tet1 and dCas9-Dnmt3a systems for epigenetic regulation by using Tet1 and Dnmt3a catalytically inactive cas9 fusion proteins to target the brain-derived neurotrophic factor (BDNF) promoter Ⅳ and distal enhancer of myogenic determination factor (MyoD) (Liu X. S. et al., 2016). In terms of histone deacetylation modification, Liu et al. fused dCas9 to HDAC1 and achieved deacetylation of histones at the KRAS promoter and effectively silenced the oncogene KRAS, providing a novel approach for cancer therapy (Liu et al., 2021).

Rakshit et al. used CRISPR/Cas9 to knock down BRCA1 in human CD4 + T helper cells and demonstrated that the expression of the BRCA1 gene in the VEGFA and aimp1 loci was suppressed in NSCLC, and aberrant expression of multiple DNA damage/repair factors was found in the aimp1 and VEGFA loci. However, knockdown of BRCA1 results in high levels of R-loop formation at the VEGFA and AIMP1 loci, and the R-loop structure is one of the major intracellular causes of genomic instability (Rakshit et al., 2021). Choudhury et al. used the CRISPR/dCas9 system at the promoter region of BRCA1 to reduce DNA methylation and reactivate gene expression to restore function to BRCA1 for the purpose of cancer suppression (Choudhury et al., 2016). Kang et al. used CRISPR/Cas9 to change the CpG dinucleotides in the promoter region to unmethylated dinucleotides and achieved selective DNA demethylation by targeting methylated CpG sites using the CRISPR/dCas9-Tet1 system (Kang et al., 2019).

Studies on miRNA Expression

MicroRNAs (miRNAs), a class of endogenous non-coding RNAs with 19–24 nucleotides in length, play key roles in regulating tumor cell proliferation, differentiation, migration, invasion, and miRNAs and their mediated signaling pathways are directly involved in the regulation of multiple cell biological pathways and cisplatin response in non-small cell lung cancer (Zang et al., 2017; Santos and Almeida, 2020). Yang et al. demonstrated that miR-26a could inhibit the HMGA2 mediated E2F1-Akt signaling pathway by down regulating intracellular high mobility group a 2 (HMGA2) expression, which in turn enhanced cisplatin resistance (Yang et al., 2016b). MiRNAs can regulate non-small cell lung cancer apoptosis, and then regulate the drug resistance of cells. Qiu et al. found that miR-503 specifically targeted anti-apoptotic protein Bcl-2, and then reversed cisplatin resistance in non-small cell lung cancer (Qiu et al., 2013).

Overexpression of miR-421 in NSCLC promoted lung cancer cell migration and invasion and increased the resistance of lung cancer cells to paclitaxel. CRISPR/Cas9 knockout β- Catenin downregulates miR-421 levels in A549 cells (Duan et al., 2019). Knockdown of LHX6 in HCC827/ER cells by CRISPR/Cas9 system reversed the reduced cell invasion and Erlotinib resistance caused by downregulation of miR-214 (Liao et al., 2017). Overexpression of miR-1304 significantly decreased the number of NSCLC cells and promoted apoptosis. Li et al. showed that the expression of HO-1 was significantly increased by knockdown of endogenous miR-1304 by CRISPR/Cas9, and miR-1304 inhibited NSCLC cell growth by targeting HO-1, demonstrating that modulation of miR-1304/HO-1 may be a novel therapeutic avenue (Li et al., 2017).

3.6 Studies on Epithelial Mesenchymal Transition

Epithelial to mesenchymal transition (EMT) refers to the process in which, under certain conditions, cells of the epithelial phenotype appear to have downregulated expression of characteristic proteins of the epithelial phenotype, whereas cells of the mesenchymal phenotype are upregulated, that is, epithelial cells undergo a morphological transition to a fibroblastic or mesenchymal phenotype, and cells undergo loss of cell polarity, which enables increased motility (Tsai and Yang, 2013). Key signaling pathways involved in EMT include TGF-β, Wnt, Notch and Hedgehog et al. (Gonzalez and Medici, 2014; David et al., 2016; De Francesco et al., 2018; Teeuwssen and Fodde, 2019). Several methodologies have been utilized to investigate the role of various genes in the EMT process in various diseases. RNAi is often used in EMT research, but because its low specificity is inevitable, CRISPR/Cas9 is now being widely used to help us identify potential therapeutic targets for EMT-associated diseases. For example, Survivin, one of the main members of the inhibitor of apoptosis (IAP), was highly expressed in a variety of tumor tissues and cells and promoted EMT, which was associated with proliferation, migration and chemoresistance in various cancers, such as breast cancer, non-small cell lung cancer, and prostate cancer. Using the CRISPR/Cas9 system, Zhao et al. showed that TGF-β could be attenuated by knockdown of BIRC5, the gene encoding Survivin, in ovarian cancer cells SKOV3 and OVCAR3 signaling that inhibits cancer cell proliferation and migration and restores sensitivity to paclitaxel (Zhao et al., 2017).

Using CRISPR/Cas9 mediated silencing of Smad3/Smad4, Tong et al. showed decreased mRNA expression of Myocardin (MYOCD) and downregulation of TGF-β Induced invasion and epithelial-mesenchymal transition of non-small cell lung cancer cells (Tong et al., 2020). Perumal et al. used the CRISPR/Cas9 system to knock out the phosphatase and tensin homolog (PTEN) in the non-small cell lung cancer cell lines A549 and NCI-H460

by Nuclear translocation of β-catenin and Snail/Slug in lung cancer cells promotes EMT, which leads to metastasis (Perumal et al., 2019). Mesenchymal cells are poorly sensitive to EGFR inhibitors. Raoof et al. identified FGFR1 as the highest genomic target to re-sensitize cells to EGF816 using a genome-wide CRISPR screen, and EGFR inhibitors synergize with FGFR1 inhibitors to overcome chemoresistance in NSCLC with mesenchymal features (Raoof et al., 2019).

4 DELIVERY METHOD OF CRISPR/CAS9 SYSTEM

4.1 Physical Methods

In *in vitro* experiments, physical methods are often used to deliver the CRISPR system, which is a simple and efficient way, mainly including electroporation and microinjection. Cas9-sgRNA complex encoded by plasmid is delivered through the cell membrane. Microinjection has high costs and low efficiency. Chen et al. used electroporation to efficiently deliver cas9/sgRNA ribonucleoprotein to mouse fertilized eggs to realize mouse genome editing (Chen et al., 2016).

4.2 Nonviral Vector

Nonviral vectors are less immunogenic, have larger capacities, and can deliver large genes but less efficiently. Lipid nanoparticles (LNPS) are one of the most commonly used nucleic acid delivery systems. Negatively charged nucleic acids complex with positively charged lipids via electrostatic interactions to form lipid nanoparticles, which can protect nucleic acids from destruction by nucleases and enter target cells via endocytosis (Chen et al., 2020). The method is safe, cost-effective and straightforward, but has low delivery efficiency. Cationic liposomes, zwitterionic liposomes, and liposome-like materials have been used in CRISPR delivery systems. Zhang et al. constructed a novel delivery system based on polyethene glycol phospholipid modified cationic lipid nanoparticles (PLNP), which significantly downregulated Polo-like kinase 1 (PLK-1) protein and inhibited melanoma growth *in vivo* and *in vitro* (Zhang et al., 2017).

Polymeric carriers are widely used for gene-drug delivery with the advantages of easy synthesis, safety and no immunogenicity. Kang et al., using polymer derived Cas9 complexed with sgRNA targeting antibiotic resistance by covalently modifying the protein with a cationic polymer to induce DNA double-strand breaks, demonstrated potential applications compared to liposomes for enhanced delivery efficiency (Kang et al., 2017).

Inorganic nanoparticles can also be used to deliver nucleic acids with the advantages of low toxicity, high stability, flexibility and easy regulation (Duncan et al., 2010). Mout et al. used arginine functionalized gold nanoparticles (ArgNPs) to cotransport cas9 protein and sgRNA, and ArgNPs delivered RNP to both the cytoplasm and nucleus and achieved 90–95% delivery efficiency (Mout and Rotello, 2017).

4.3 Viral Vectors

Lentiviral (LVs) vectors, based on the HIV-1 virus and consisting of a spherical structure composed of single-stranded RNA, have been widely used to deliver CRISPR/cas9. The major advantage of lentiviral vectors is that they can reach 7 kb in load and accommodate the SpCas9 gene and one or more sgRNAs. Holmgaard et al. delivered CRISPR/Cas9 system based on lentiviral vectors. Knockdown of the vascular endothelial growth factor A (Vegfa) gene has led to new treatments for ocular diseases (Holmgaard et al., 2017).

Adenoviruses (ADVs) are non enveloped linear double-stranded DNA viruses with a wide host range, genetic stability, high transduction efficiency and large loading capacity. Jin et al. used Gateway cloning technology to develop an integrated adenoviral vector without traditional enzymatic digestion and ligation, improving transduction efficiency (Jin et al., 2019).

Adeno associated virus (AAVs) is extremely low immunogenic relative to other viral vectors and has safety and therapeutic potential. AAV sequences are long-lived in non-dividing cells, provide stable transgene expression, and are the most widely used viral vector to deliver CRISPR/Cas9 systems.

In 2021, Zhang Feng's team developed a new delivery vector-selective endogenous encapsidation for cellular delivery (SEND), which is composed of a retrovirus-like protein, PEG10, that binds to its mRNA and forms vesicles around it. The research team modified and designed it to package and deliver specific RNAs (Segel et al., 2021).

5 DEFICIENCIES AND CHALLENGES

The CRISPR/Cas9 system can well break through the limitations of traditional diagnosis and combat tumor resistance, and is a promising therapy, but some problems still need to be solved.

The off-target effect of CRISPR/Cas9 system is a widespread phenomenon, and the serious consequences caused by off-target limited CRISPR/Cas9 system from basic research to clinic, mainly due to the local matching between the recognition sequence of sgRNA and non-target DNA, the structure of sgRNA, PAM sequence The cas9 protein, along with regulatory small molecules of the DSB pathway, among others, all contribute to targeting efficiency (Zhang et al., 2015). When the concentration of the cas9 sgRNA complex is increased, the specificity of cas9 cleavage is reduced and the RNA polymerase II transcription system can be used to express sgRNA and control the amount of sgRNA expressed (Kiani et al., 2014). In addition to guiding cas9 to bind to specific targets, sgRNAs can also affect the specificity of targets (Pattanayak et al., 2013). Increasing the guide sequence length of the sgRNA did not improve target specificity, which was found to be increased when the sgRNA contained 17–18 nucleotides (Fu et al., 2014). To improve the specificity of DNA cleavage, investigators have used mutant dCas9 that forms a dimer with the nuclease Fok I (FOK I-dCas9) to reduce off-target effects, which is more than 140 fold more specific than wild-type cas9 (Guilinger et al., 2014). Meanwhile, direct delivery of purified recombinant cas9 protein and sgRNA into cells can also reduce off-target effects (Kim et al., 2014).

Recent studies have found that the CRISPR/Cas system may adversely affect cell growth, and Leibowitz et al. found that

CRISPR/Cas9 genome editing induces structural changes in the nucleus, micronuclei, and chromosomal bridges, leading to the occurrence of chromosomal rearrangement processes (Leibowitz et al., 2021). Delivery vectors for CRISPR/Cas9 are closely related to gene editing efficiency, and it is crucial to find safe, efficient, and specific vectors. The loading capacity of vectors is limited, and it is challenging to load Cas9 and gRNA into a certain size carrier and improve the delivery efficiency *in vivo*. Currently, the most widely used *in vivo* experiments are viral vectors, but some nonviral vectors still need to be developed for more safe and effective delivery tools (Chen et al., 2020). The intein-mediated split-Cas9 system, which reconstitutes a full-length SpCas9 protein by fusing the segmented two segments of SpCas9 with the N-terminus of intein fused to the C-terminus, respectively, and mediates CIS splicing when both fusion proteins are coexpressed, has been shown to be effective in addressing the challenge of insufficient AAV loading capacity (Truong et al., 2015). Carlson-Stevermer et al. used short RNA and streptavidin to assemble and deliver a CRISPR repair kit to DNA cleavage sites, greatly improving the precision of gene editing, which resulted in an 18 fold increase in accuracy compared with conventional CRISPR Technology (Carlson-Stevermer et al., 2017). At the same time, there is a certain risk of pathogenicity associated with viral vectors, and safety concerns are also issues to consider when viral vectors are used in animal experiments.

At the same time, gene knockout causes permanent changes in genetic material and there are hidden dangers of mutation. Therefore, it is necessary to find new methods to solve this problem. Prime editor is a more accurate gene-editing method. Its protease is fused by cas9 notch enzyme (h840a) and reverse transcriptase. It can accurately insert and delete the target site without introducing DSB and donor DNA templates. Compared with HDR, it has higher efficiency, fewer by-products and a lower off-target rate (Anzalone et al., 2019).

P53 is a tumor suppressor gene, and CRISPR/Cas9 can induce p53 mediated DNA damage response, resulting in cell cycle arrest and other phenomena and reducing the efficiency of genome editing. Whereas inhibition of p53 predisposes cells to the effects of other oncogenic mutations (Haapaniemi et al., 2018; Jiang et al., 2022). Therefore, it is necessary to monitor the function of p53 when CRISPR/Cas9 is used clinically.

There was a study that detected antibodies against Sacas9 and Spcas9 in 78% and 58% of donor sera, respectively. Anti-Sacas9 T cells and anti-Spcas9 T cells were found in 78% and 67% of donors, indicating that there is human immunity to cas9 protein (Charlesworth et al., 2019). In the future, we need more research to determine the safety and effectiveness of CRISPR/Cas9 system.

6 CONCLUSION

CRISPR/Cas9 gene-editing technology has developed rapidly since its inception. Compared with ZFNs and TALENs, CRISPR/Cas9 gene-editing technology is more straightforward and efficient. It is suitable for ordinary laboratories and greatly promotes the progress of life science and basic medical research. Now there is a genome-wide targeted CRISPR/Cas9 system, which contains all genes of mouse embryonic stem cells and human cells (Wang et al., 2014). Lu et al. carried out the world's first human clinical trial based on CRISPR/Cas9 gene-editing technology. Immune cells were extracted from the blood of a patient with metastatic non-small cell lung cancer. The PD-1 gene that inhibits immune function was knocked out *in vitro* by CRISPR technology, and then amplified and reinfused into the patient's body to achieve the effect of anti-tumor. The safety and feasibility of this therapy in NSCLC were proved for the first time (Lu et al., 2020). In addition, several laboratories are also competing to plan clinical trials. Researchers at the University of Pennsylvania have launched trials on myeloma, sarcoma and melanoma.

The use of CRISPR/Cas9 gene-editing technology has also caused ethical and social problems. Due to the disadvantages such as being off-target, CRISPR/Cas9 gene-editing technology may cause some additional harm to patients, and the potential high risk does not allow CRISPR/Cas9 gene-editing technology to be used in the treatment of germline genes, Gene editing for reproductive purposes may irreversibly change the human genome and bring incalculable impact to mankind. In the future, more evidence should be collected from animal experiments to ensure the safety and feasibility of CRISPR/Cas9 gene-editing technology in clinical practice.

The genetic complexity of non-small cell lung cancer is one of the main causes of chemotherapeutic drug resistance. Unfortunately, no effective gene-targeted drugs have been developed. We reviewed and summarized the progress of CRISPR/Cas9, which provides a reference for further research on the application of CRISPR/Cas9 gene-editing technology in the treatment and drug resistance of non-small cell lung cancer. We believe that further systematic and in-depth research is necessary. We need to make full use of the advantages of CRISPR/Cas9 gene-editing technology, explore its potential in the study of drug resistance mechanisms, promote the rapid development of cancer research and bring new hope to cancer patients.

AUTHOR CONTRIBUTIONS

LH and ZxL were responsible for writing the manuscript; TH and LH prepared the figures; ZL and YC were responsible for supervising the writing of the manuscript; HX aided in conceptualization and the supporting funding.

FUNDING

This work was supported by Sichuan Cancer Hospital (Grant No. YB2019001), Chengdu City Science and Technology Project (Grant No.11PPYB010SF-289), and the Young Scholars Foundation of Sichuan Provincial People's Hospital (Grant No. 30305030606 and 30305030859).

ACKNOWLEDGMENTS

Authors thank all the participants enrolled in the study and the staff.

REFERENCES

Ambudkar, S. V. (1995). Purification and Reconstitution of Functional Human P-Glycoprotein. *J. Bioenerg. Biomembr.* 27 (1), 23–29. doi:10.1007/bf02110327

Anzalone, A. V., Randolph, P. B., Davis, J. R., Sousa, A. A., Koblan, L. W., Levy, J. M., et al. (2019). Search-and-replace Genome Editing without Double-Strand Breaks or Donor DNA. *Nature* 576 (7785), 149–157. doi:10.1038/s41586-019-1711-4

Audia, J. E., and Campbell, R. M. (2016). Histone Modifications and Cancer. *Cold Spring Harb. Perspect. Biol.* 8 (4), a019521. doi:10.1101/cshperspect.a019521

Azad, N., Zahnow, C. A., Rudin, C. M., and Baylin, S. B. (2013). The Future of Epigenetic Therapy in Solid Tumours-Llessons from the Past. *Nat. Rev. Clin. Oncol.* 10 (5), 256–266. doi:10.1038/nrclinonc.2013.42

Bergethon, K., Shaw, A. T., Ou, S. H., Katayama, R., Lovly, C. M., McDonald, N. T., et al. (2012). ROS1 Rearrangements Define a Unique Molecular Class of Lung Cancers. *J. Clin. Oncol.* 30 (8), 863–870. doi:10.1200/jco.2011.35.6345

Blasco, R. B., Karaca, E., Ambrogio, C., Cheong, T. C., Karayol, E., Minero, V. G., et al. (2014). Simple and Rapid *In Vivo* Generation of Chromosomal Rearrangements Using CRISPR/Cas9 Technology. *Cell Rep.* 9 (4), 1219–1227. doi:10.1016/j.celrep.2014.10.051

Brose, M. S., Volpe, P., Feldman, M., Kumar, M., Rishi, I., Gerrero, R., et al. (2002). BRAF and RAS Mutations in Human Lung Cancer and Melanoma. *Cancer Res.* 62 (23), 6997–7000. Available at: https://pubmed.ncbi.nlm.nih.gov/12460918/.

Bubendorf, L., Dafni, U., Schöbel, M., Finn, S. P., Tischler, V., Sejda, A., et al. (2017). Prevalence and Clinical Association of MET Gene Overexpression and Amplification in Patients with NSCLC: Results from the European Thoracic Oncology Platform (ETOP) Lungscape Project. *Lung Cancer* 111, 143–149. doi:10.1016/j.lungcan.2017.07.021

Camidge, D. R., Pao, W., and Sequist, L. V. (2014). Acquired Resistance to TKIs in Solid Tumours: Learning from Lung Cancer. *Nat. Rev. Clin. Oncol.* 11 (8), 473–481. doi:10.1038/nrclinonc.2014.104

Carlson-Stevermer, J., Abdeen, A. A., Kohlenberg, L., Goedland, M., Molugu, K., Lou, M., et al. (2017). Assembly of CRISPR Ribonucleoproteins with Biotinylated Oligonucleotides via an RNA Aptamer for Precise Gene Editing. *Nat. Commun.* 8 (1), 1711. doi:10.1038/s41467-017-01875-9

Carroll, D. (2011). Genome Engineering with Zinc-Finger Nucleases. *Genetics* 188 (4), 773–782. doi:10.1534/genetics.111.131433

Chapman, P. B., Hauschild, A., Robert, C., Haanen, J. B., Ascierto, P., Larkin, J., et al. (2011). Improved Survival with Vemurafenib in Melanoma with BRAF V600E Mutation. *N. Engl. J. Med.* 364 (26), 2507–2516. doi:10.1056/NEJMoa1103782

Charlesworth, C. T., Deshpande, P. S., Dever, D. P., Camarena, J., Lemgart, V. T., Cromer, M. K., et al. (2019). Identification of Preexisting Adaptive Immunity to Cas9 Proteins in Humans. *Nat. Med.* 25 (2), 249–254. doi:10.1038/s41591-018-0326-x

Chen, S., Lee, B., Lee, A. Y., Modzelewski, A. J., and He, L. (2016). Highly Efficient Mouse Genome Editing by CRISPR Ribonucleoprotein Electroporation of Zygotes. *J. Biol. Chem.* 291 (28), 14457–14467. doi:10.1074/jbc.M116.733154

Chen, X., Sun, X., Guan, J., Gai, J., Xing, J., Fu, L., et al. (2017). Rsf-1 Influences the Sensitivity of Non-small Cell Lung Cancer to Paclitaxel by Regulating NF-κB Pathway and its Downstream Proteins. *Cell Physiol. Biochem.* 44 (6), 2322–2336. doi:10.1159/000486116

Chen, F., Alphonse, M., and Liu, Q. (2020). Strategies for Nonviral Nanoparticle-Based Delivery of CRISPR/Cas9 Therapeutics. *Wiley Interdiscip. Rev. Nanomed. Nanobiotechnol.* 12 (3), e1609. doi:10.1002/wnan.1609

Cho, B. C., Chewaskulyong, B., Lee, K. H., Dechaphunkul, A., Sriuranpong, V., Imamura, F., et al. (2019). Osimertinib versus Standard of Care EGFR TKI as First-Line Treatment in Patients with EGFRm Advanced NSCLC: FLAURA Asian Subset. *J. Thorac. Oncol.* 14 (1), 99–106. doi:10.1016/j.jtho.2018.09.004

Choi, P. S., and Meyerson, M. (2014). Targeted Genomic Rearrangements Using CRISPR/Cas Technology. *Nat. Commun.* 5, 3728. doi:10.1038/ncomms4728

Choudhury, S. R., Cui, Y., Lubecka, K., Stefanska, B., and Irudayaraj, J. (2016). CRISPR-dCas9 Mediated TET1 Targeting for Selective DNA Demethylation at BRCA1 Promoter. *Oncotarget* 7 (29), 46545–46556. doi:10.18632/oncotarget.10234

Cole, S. P. (2014). Multidrug Resistance Protein 1 (MRP1, ABCC1), a "multitasking" ATP-Binding Cassette (ABC) Transporter. *J. Biol. Chem.* 289 (45), 30880–30888. doi:10.1074/jbc.R114.609248

Cross, D. A., Ashton, S. E., Ghiorghiu, S., Eberlein, C., Nebhan, C. A., Spitzler, P. J., et al. (2014). AZD9291, an Irreversible EGFR TKI, Overcomes T790M-Mediated Resistance to EGFR Inhibitors in Lung Cancer. *Cancer Discov.* 4 (9), 1046–1061. doi:10.1158/2159-8290.cd-14-0337

David, C. J., Huang, Y. H., Chen, M., Su, J., Zou, Y., Bardeesy, N., et al. (2016). TGF-β Tumor Suppression through a Lethal EMT. *Cell* 164 (5), 1015–1030. doi:10.1016/j.cell.2016.01.009

Dawson, M. A., and Kouzarides, T. (2012). Cancer Epigenetics: From Mechanism to Therapy. *Cell* 150 (1), 12–27. doi:10.1016/j.cell.2012.06.013

De Francesco, E. M., Maggiolini, M., and Musti, A. M. (2018). Crosstalk between Notch, HIF-1α and GPER in Breast Cancer EMT. *Int. J. Mol. Sci.* 19 (7), 2011. doi:10.3390/ijms19072011

Devarakonda, S., Morgensztern, D., and Govindan, R. (2015). Genomic Alterations in Lung Adenocarcinoma. *Lancet Oncol.* 16 (7), e342–51. doi:10.1016/s1470-2045(15)00077-7

Deveau, H., Garneau, J. E., and Moineau, S. (2010). CRISPR/Cas System and its Role in Phage-Bacteria Interactions. *Annu. Rev. Microbiol.* 64, 475–493. doi:10.1146/annurev.micro.112408.134123

Ding, X., Zhang, Z., Jiang, T., Li, X., Zhao, C., Su, B., et al. (2017). Clinicopathologic Characteristics and Outcomes of Chinese Patients with Non-small-cell Lung Cancer and BRAF Mutation. *Cancer Med.* 6 (3), 555–562. doi:10.1002/cam4.1014

Doebele, R. C., Pilling, A. B., Aisner, D. L., Kutateladze, T. G., Le, A. T., Weickhardt, A. J., et al. (2012). Mechanisms of Resistance to Crizotinib in Patients with ALK Gene Rearranged Non-small Cell Lung Cancer. *Clin. Cancer Res.* 18 (5), 1472–1482. doi:10.1158/1078-0432.ccr-11-2906

Duan, F. G., Wang, M. F., Cao, Y. B., Dan Li, L., Li, R. Z., Fan, X. X., et al. (2019). MicroRNA-421 Confers Paclitaxel Resistance by Binding to the KEAP1 3'UTR and Predicts Poor Survival in Non-small Cell Lung Cancer. *Cell Death Dis.* 10 (11), 821. doi:10.1038/s41419-019-2031-1

Duma, N., Santana-Davila, R., and Molina, J. R. (2019). Non-Small Cell Lung Cancer: Epidemiology, Screening, Diagnosis, and Treatment. *Mayo Clin. Proc.* 94 (8), 1623–1640. doi:10.1016/j.mayocp.2019.01.013

Duncan, B., Kim, C., and Rotello, V. M. (2010). Gold Nanoparticle Platforms as Drug and Biomacromolecule Delivery Systems. *J. Control Release* 148 (1), 122–127. doi:10.1016/j.jconrel.2010.06.004

El-Masry, M. W., Gouda, H. M., Shaheen, I. A., Edesa, W., Hassan, N. M., and Ramzy, R. (2018). Breast Cancer Resistance Protein (BCRP) Gene Expression in a Cohort of Adult Egyptian Patients with Acute Myeloid Leukemia. *Afr. Health Sci.* 18 (4), 958–964. doi:10.4314/ahs.v18i4.15

Evers, B., Jastrzebski, K., Heijmans, J. P., Grernrum, W., Beijersbergen, R. L., and Bernards, R. (2016). CRISPR Knockout Screening Outperforms shRNA and CRISPRi in Identifying Essential Genes. *Nat. Biotechnol.* 34 (6), 631–633. doi:10.1038/nbt.3536

Flaherty, K. T., Puzanov, I., Kim, K. B., Ribas, A., McArthur, G. A., Sosman, J. A., et al. (2010). Inhibition of Mutated, Activated BRAF in Metastatic Melanoma. *N. Engl. J. Med.* 363 (9), 809–819. doi:10.1056/NEJMoa1002011

Friedlaender, A., Drilon, A., Weiss, G. J., Banna, G. L., and Addeo, A. (2020). KRAS as a Druggable Target in NSCLC: Rising like a Phoenix after Decades of Development Failures. *Cancer Treat. Rev.* 85, 101978. doi:10.1016/j.ctrv.2020.101978

Fu, Y., Sander, J. D., Reyon, D., Cascio, V. M., and Joung, J. K. (2014). Improving CRISPR-Cas Nuclease Specificity Using Truncated Guide RNAs. *Nat. Biotechnol.* 32 (3), 279–284. doi:10.1038/nbt.2808

Gainor, J. F., and Shaw, A. T. (2013). Novel Targets in Non-small Cell Lung Cancer: ROS1 and RET Fusions. *Oncologist* 18 (7), 865–875. doi:10.1634/theoncologist.2013-0095

Gao, Q., Ouyang, W., Kang, B., Han, X., Xiong, Y., Ding, R., et al. (2020). Selective Targeting of the Oncogenic KRAS G12S Mutant Allele by CRISPR/Cas9 Induces Efficient Tumor Regression. *Theranostics* 10 (11), 5137–5153. doi:10.7150/thno.42325

Gonzalez, D. M., and Medici, D. (2014). Signaling Mechanisms of the Epithelial-Mesenchymal Transition. *Sci. Signal* 7 (344), re8. doi:10.1126/scisignal.2005189

Goss, G. D., O'Callaghan, C., Lorimer, I., Tsao, M. S., Masters, G. A., Jett, J., et al. (2013). Gefitinib versus Placebo in Completely Resected Non-small-cell Lung

Cancer: Results of the NCIC CTG BR19 Study. *J. Clin. Oncol.* 31 (27), 3320–3326. doi:10.1200/jco.2013.51.1816

Gottesman, M. M. (2002). Mechanisms of Cancer Drug Resistance. *Annu. Rev. Med.* 53, 615–627. doi:10.1146/annurev.med.53.082901.103929

Guilinger, J. P., Thompson, D. B., and Liu, D. R. (2014). Fusion of Catalytically Inactive Cas9 to FokI Nuclease Improves the Specificity of Genome Modification. *Nat. Biotechnol.* 32 (6), 577–582. doi:10.1038/nbt.2909

Gupta, P., Garg, T., Tanmay, M., and Arora, S. (2015). Polymeric Drug-Delivery Systems: Role in P-Gp Efflux System Inhibition. *Crit. Rev. Ther. Drug Carr. Syst.* 32 (3), 247–275. doi:10.1615/critrevtherdrugcarriersyst.2015011592

Haapaniemi, E., Botla, S., Persson, J., Schmierer, B., and Taipale, J. (2018). CRISPR-Cas9 Genome Editing Induces a P53-Mediated DNA Damage Response. *Nat. Med.* 24 (7), 927–930. doi:10.1038/s41591-018-0049-z

Holmgaard, A., Askou, A. L., Benckendorff, J. N. E., Thomsen, E. A., Cai, Y., Bek, T., et al. (2017). *In Vivo* Knockout of the Vegfa Gene by Lentiviral Delivery of CRISPR/Cas9 in Mouse Retinal Pigment Epithelium Cells. *Mol. Ther. Nucleic Acids* 9, 89–99. doi:10.1016/j.omtn.2017.08.016

Huber, K. V., Salah, E., Radic, B., Gridling, M., Elkins, J. M., Stukalov, A., et al. (2014). Stereospecific Targeting of MTH1 by (S)-crizotinib as an Anticancer Strategy. *Nature* 508 (7495), 222–227. doi:10.1038/nature13194

Ishino, Y., Shinagawa, H., Makino, K., Amemura, M., and Nakata, A. (1987). Nucleotide Sequence of the Iap Gene, Responsible for Alkaline Phosphatase Isozyme Conversion in *Escherichia coli*, and Identification of the Gene Product. *J. Bacteriol.* 169 (12), 5429–5433. doi:10.1128/jb.169.12.5429-5433.1987

Ito, F., Miura, M., Fujioka, Y., Abumiya, M., Kobayashi, T., Takahashi, S., et al. (2021). The BCRP Inhibitor Febuxostat Enhances the Effect of Nilotinib by Regulation of Intracellular Concentration. *Int. J. Hematol.* 113 (1), 100–105. doi:10.1007/s12185-020-03000-x

Jackson, A. L., Burchard, J., Schelter, J., Chau, B. N., Cleary, M., Lim, L., et al. (2006). Widespread siRNA "Off-Target" Transcript Silencing Mediated by Seed Region Sequence Complementarity. *RNA* 12 (7), 1179–1187. doi:10.1261/rna.25706

Jia, Y., Yun, C. H., Park, E., Ercan, D., Manuia, M., Juarez, J., et al. (2016). Overcoming EGFR(T790M) and EGFR(C797S) Resistance with Mutant-Selective Allosteric Inhibitors. *Nature* 534 (7605), 129–132. doi:10.1038/nature17960

Jia, Y., Sun, S., Gao, X., and Cui, X. (2018). Expression Levels of TUBB3, ERCC1 and P-Gp in Ovarian Cancer Tissues and Adjacent Normal Tissues and Their Clinical Significance. *J. Buon* 23 (5), 1390–1395. Available at: https://pubmed.ncbi.nlm.nih.gov/30570863/.

Jiang, L., Ingelshed, K., Shen, Y., Boddul, S. V., Iyer, V. S., Kasza, Z., et al. (2022). CRISPR/Cas9-Induced DNA Damage Enriches for Mutations in a P53-Linked Interactome: Implications for CRISPR-Based Therapies. *Cancer Res.* 82 (1), 36–45. doi:10.1158/0008-5472.can-21-1692

Jin, Y. H., Joo, H., Lee, K., Kim, H., Didier, R., Yang, Y., et al. (2019). Streamlined Procedure for Gene Knockouts Using All-In-One Adenoviral CRISPR-Cas9. *Sci. Rep.* 9 (1), 277. doi:10.1038/s41598-018-36736-y

Joung, J. K., and Sander, J. D. (2013). TALENs: A Widely Applicable Technology for Targeted Genome Editing. *Nat. Rev. Mol. Cell Biol.* 14 (1), 49–55. doi:10.1038/nrm3486

Kang, Y. K., Kwon, K., Ryu, J. S., Lee, H. N., Park, C., and Chung, H. J. (2017). Nonviral Genome Editing Based on a Polymer-Derivatized CRISPR Nanocomplex for Targeting Bacterial Pathogens and Antibiotic Resistance. *Bioconjug Chem.* 28 (4), 957–967. doi:10.1021/acs.bioconjchem.6b00676

Kang, J. G., Park, J. S., Ko, J. H., and Kim, Y. S. (2019). Regulation of Gene Expression by Altered Promoter Methylation Using a CRISPR/Cas9-mediated Epigenetic Editing System. *Sci. Rep.* 9 (1), 11960. doi:10.1038/s41598-019-48130-3

Kelly, K., Altorki, N. K., Eberhardt, W. E., O'Brien, M. E., Spigel, D. R., Crinò, L., et al. (2015). Adjuvant Erlotinib versus Placebo in Patients with Stage IB-IIIA Non-small-cell Lung Cancer (RADIANT): A Randomized, Double-Blind, Phase III Trial. *J. Clin. Oncol.* 33 (34), 4007–4014. doi:10.1200/jco.2015.61.8918

Kiani, S., Beal, J., Ebrahimkhani, M. R., Huh, J., Hall, R. N., Xie, Z., et al. (2014). CRISPR Transcriptional Repression Devices and Layered Circuits in Mammalian Cells. *Nat. Methods* 11 (7), 723–726. doi:10.1038/nmeth.2969

Kim, S., Kim, D., Cho, S. W., Kim, J., and Kim, J. S. (2014). Highly Efficient RNA-Guided Genome Editing in Human Cells via Delivery of Purified Cas9 Ribonucleoproteins. *Genome Res.* 24 (6), 1012–1019. doi:10.1101/gr.171322.113

Kong, X., Pan, P., Sun, H., Xia, H., Wang, X., Li, Y., et al. (2019). Drug Discovery Targeting Anaplastic Lymphoma Kinase (ALK). *J. Med. Chem.* 62 (24), 10927–10954. doi:10.1021/acs.jmedchem.9b00446

Lee, J., Choi, A., Cho, S. Y., Jun, Y., Na, D., Lee, A., et al. (2021). Genome-scale CRISPR Screening Identifies Cell Cycle and Protein Ubiquitination Processes as Druggable Targets for Erlotinib-Resistant Lung Cancer. *Mol. Oncol.* 15 (2), 487–502. doi:10.1002/1878-0261.12853

Leibowitz, M. L., Papathanasiou, S., Doerfler, P. A., Blaine, L. J., Sun, L., Yao, Y., et al. (2021). Chromothripsis as an On-Target Consequence of CRISPR-Cas9 Genome Editing. *Nat. Genet.* 53 (6), 895–905. doi:10.1038/s41588-021-00838-7

Leonetti, A., Sharma, S., Minari, R., Perego, P., Giovannetti, E., and Tiseo, M. (2019). Resistance Mechanisms to Osimertinib in EGFR-Mutated Non-small Cell Lung Cancer. *Br. J. Cancer* 121 (9), 725–737. doi:10.1038/s41416-019-0573-8

Li, S., Li, L., Zhu, Y., Huang, C., Qin, Y., Liu, H., et al. (2014). Coexistence of EGFR with KRAS, or BRAF, or PIK3CA Somatic Mutations in Lung Cancer: A Comprehensive Mutation Profiling from 5125 Chinese Cohorts. *Br. J. Cancer* 110 (11), 2812–2820. doi:10.1038/bjc.2014.210

Li, W., Zhang, H., Assaraf, Y. G., Zhao, K., Xu, X., Xie, J., et al. (2016). Overcoming ABC Transporter-Mediated Multidrug Resistance: Molecular Mechanisms and Novel Therapeutic Drug Strategies. *Drug Resist. Updat.* 27, 14–29. doi:10.1016/j.drup.2016.05.001

Li, C. G., Pu, M. F., Li, C. Z., Gao, M., Liu, M. X., Yu, C. Z., et al. (2017). MicroRNA-1304 Suppresses Human Non-small Cell Lung Cancer Cell Growth *In Vitro* by Targeting Heme Oxygenase-1. *Acta Pharmacol. Sin.* 38 (1), 110–119. doi:10.1038/aps.2016.92

Liao, J., Lin, J., Lin, D., Zou, C., Kurata, J., Lin, R., et al. (2017). Down-regulation of miR-214 Reverses Erlotinib Resistance in Non-small-cell Lung Cancer through Up-Regulating LHX6 Expression. *Sci. Rep.* 7 (1), 781. doi:10.1038/s41598-017-00901-6

Liu, B., Song, J., Luan, J., Sun, X., Bai, J., Wang, H., et al. (2016a). Promoter Methylation Status of Tumor Suppressor Genes and Inhibition of Expression of DNA Methyltransferase 1 in Non-small Cell Lung Cancer. *Exp. Biol. Med. (Maywood)* 241 (14), 1531–1539. doi:10.1177/1535370216645211

Liu, X. S., Wu, H., Ji, X., Stelzer, Y., Wu, X., Czauderna, S., et al. (2016b). Editing DNA Methylation in the Mammalian Genome. *Cell* 167 (1), 233. doi:10.1016/j.cell.2016.08.056

Liu, B., Diaz Arguello, O. A., Chen, D., Chen, S., Saber, A., and Haisma, H. J. (2020). CRISPR-mediated Ablation of Overexpressed EGFR in Combination with Sunitinib Significantly Suppresses Renal Cell Carcinoma Proliferation. *PLoS One* 15 (5), e0232985. doi:10.1371/journal.pone.0232985

Liu, J., Sun, M., Cho, K. B., Gao, X., and Guo, B. (2021). A CRISPR-Cas9 Repressor for Epigenetic Silencing of KRAS. *Pharmacol. Res.* 164, 105304. doi:10.1016/j.phrs.2020.105304

Lu, Y., Xue, J., Deng, T., Zhou, X., Yu, K., Deng, L., et al. (2020). Safety and Feasibility of CRISPR-Edited T Cells in Patients with Refractory Non-small-cell Lung Cancer. *Nat. Med.* 26 (5), 732–740. doi:10.1038/s41591-020-0840-5

Mao, Q., and Unadkat, J. D. (2015). Role of the Breast Cancer Resistance Protein (BCRP/ABCG2) in Drug Transport-Aan Update. *AAPS J.* 17 (1), 65–82. doi:10.1208/s12248-014-9668-6

McCarty, N. S., Graham, A. E., Studená, L., and Ledesma-Amaro, R. (2020). Multiplexed CRISPR Technologies for Gene Editing and Transcriptional Regulation. *Nat. Commun.* 11 (1), 1281. doi:10.1038/s41467-020-15053-x

Mengoli, M. C., Longo, F. R., Fraggetta, F., Cavazza, A., Dubini, A., Alì, G., et al. (2018). The 2015 World Health Organization Classification of Lung Tumors: New Entities since the 2004 Classification. *Pathologica* 110 (1), 39–67. Available at: https://pubmed.ncbi.nlm.nih.gov/30259912/.

Mollazadeh, S., Sahebkar, A., Hadizadeh, F., Behravan, J., and Arabzadeh, S. (2018). Structural and Functional Aspects of P-Glycoprotein and its Inhibitors. *Life Sci.* 214, 118–123. doi:10.1016/j.lfs.2018.10.048

Moro-Sibilot, D., Cozic, N., Pérol, M., Mazières, J., Otto, J., Souquet, P. J., et al. (2019). Crizotinib in C-MET- or ROS1-Positive NSCLC: Results of the AcSé Phase II Trial. *Ann. Oncol.* 30 (12), 1985–1991. doi:10.1093/annonc/mdz407

Mout, R., and Rotello, V. M. (2017). Cytosolic and Nuclear Delivery of CRISPR/Cas9-ribonucleoprotein for Gene Editing Using Arginine Functionalized Gold Nanoparticles. *Bio Protoc.* 7 (20), e2586. doi:10.21769/BioProtoc.2586

Mullenders, J., and Bernards, R. (2009). Loss-of-function Genetic Screens as a Tool to Improve the Diagnosis and Treatment of Cancer. *Oncogene* 28 (50), 4409–4420. doi:10.1038/onc.2009.295

Panczyk, M., Sałagacka, A., and Mirowski, M. (2007). MDR1 (ABCB1) Gene Encoding Glycoprotein P (P-Gp), a Member of ABC Transporter Superfamily: Consequences for Therapy and Progression of Neoplastic Diseases. *Postepy Biochem.* 53 (4), 361–373. Available at: https://pubmed.ncbi.nlm.nih.gov/19024901/.

Panda, M., and Biswal, B. K. (2019). Cell Signaling and Cancer: A Mechanistic Insight into Drug Resistance. *Mol. Biol. Rep.* 46 (5), 5645–5659. doi:10.1007/s11033-019-04958-6

Park, K., Tan, E. H., O'Byrne, K., Zhang, L., Boyer, M., Mok, T., et al. (2016). Afatinib versus Gefitinib as First-Line Treatment of Patients with EGFR Mutation-Positive Non-small-cell Lung Cancer (LUX-Lung 7): A Phase 2B, Open-Label, Randomised Controlled Trial. *Lancet Oncol.* 17 (5), 577–589. doi:10.1016/s1470-2045(16)30033-x

Pasquini, G., and Giaccone, G. (2018). C-MET Inhibitors for Advanced Non-small Cell Lung Cancer. *Expert Opin. Investig. Drugs* 27 (4), 363–375. doi:10.1080/13543784.2018.1462336

Pattanayak, V., Lin, S., Guilinger, J. P., Ma, E., Doudna, J. A., and Liu, D. R. (2013). High-throughput Profiling of Off-Target DNA Cleavage Reveals RNA-Programmed Cas9 Nuclease Specificity. *Nat. Biotechnol.* 31 (9), 839–843. doi:10.1038/nbt.2673

Perumal, E., So Youn, K., Sun, S., Seung-Hyun, J., Suji, M., Jieying, L., et al. (2019). PTEN Inactivation Induces Epithelial-Mesenchymal Transition and Metastasis by Intranuclear Translocation of β-catenin and Snail/slug in Non-small Cell Lung Carcinoma Cells. *Lung Cancer* 130, 25–34. doi:10.1016/j.lungcan.2019.01.013

Planchard, D., Smit, E. F., Groen, H. J. M., Mazieres, J., Besse, B., Helland, Å., et al. (2017). Dabrafenib Plus Trametinib in Patients with Previously Untreated BRAFV600E-Mutant Metastatic Non-small-cell Lung Cancer: an Open-Label, Phase 2 Trial. *Lancet Oncol.* 18 (10), 1307–1316. doi:10.1016/s1470-2045(17)30679-4

Qi, L. S., Larson, M. H., Gilbert, L. A., Doudna, J. A., Weissman, J. S., Arkin, A. P., et al. (2013). Repurposing CRISPR as an RNA-Guided Platform for Sequence-specific Control of Gene Expression. *Cell* 152 (5), 1173–1183. doi:10.1016/j.cell.2013.02.022

Qiu, T., Zhou, L., Wang, T., Xu, J., Wang, J., Chen, W., et al. (2013). miR-503 Regulates the Resistance of Non-small Cell Lung Cancer Cells to Cisplatin by Targeting Bcl-2. *Int. J. Mol. Med.* 32 (3), 593–598. doi:10.3892/ijmm.2013.1439

Rakshit, S., Sunny, J. S., George, M., Hanna, L. E., and Sarkar, K. (2021). R-loop Modulated Epigenetic Regulation in T Helper Cells Mechanistically Associates Coronary Artery Disease and Non-small Cell Lung Cancer. *Transl. Oncol.* 14 (10), 101189. doi:10.1016/j.tranon.2021.101189

Raoof, S., Mulford, I. J., Frisco-Cabanos, H., Nangia, V., Timonina, D., Labrot, E., et al. (2019). Targeting FGFR Overcomes EMT-Mediated Resistance in EGFR Mutant Non-small Cell Lung Cancer. *Oncogene* 38 (37), 6399–6413. doi:10.1038/s41388-019-0887-2

Reck, M., and Rabe, K. F. (2017). Precision Diagnosis and Treatment for Advanced Non-small-cell Lung Cancer. *N. Engl. J. Med.* 377 (9), 849–861. doi:10.1056/NEJMra1703413

Robichaux, J. P., Elamin, Y. Y., Tan, Z., Carter, B. W., Zhang, S., Liu, S., et al. (2018). Mechanisms and Clinical Activity of an EGFR and HER2 Exon 20-selective Kinase Inhibitor in Non-small Cell Lung Cancer. *Nat. Med.* 24 (5), 638–646. doi:10.1038/s41591-018-0007-9

Rotow, J., and Bivona, T. G. (2017). Understanding and Targeting Resistance Mechanisms in NSCLC. *Nat. Rev. Cancer* 17 (11), 637–658. doi:10.1038/nrc.2017.84

Sakaeda, T., Nakamura, T., and Okumura, K. (2002). MDR1 Genotype-Related Pharmacokinetics and Pharmacodynamics. *Biol. Pharm. Bull.* 25 (11), 1391–1400. doi:10.1248/bpb.25.1391

Santos, P., and Almeida, F. (2020). Role of Exosomal miRNAs and the Tumor Microenvironment in Drug Resistance. *Cells* 9 (6), 1450. doi:10.3390/cells9061450

Sasaki, T., Rodig, S. J., Chirieac, L. R., and Jänne, P. A. (2010). The Biology and Treatment of EML4-ALK Non-small Cell Lung Cancer. *Eur. J. Cancer* 46 (10), 1773–1780. doi:10.1016/j.ejca.2010.04.002

Sato, H., Schoenfeld, A. J., Siau, E., Lu, Y. C., Tai, H., Suzawa, K., et al. (2020). MAPK Pathway Alterations Correlate with Poor Survival and Drive Resistance to Therapy in Patients with Lung Cancers Driven by ROS1 Fusions. *Clin. Cancer Res.* 26 (12), 2932–2945. doi:10.1158/1078-0432.ccr-19-3321

Schrank, Z., Chhabra, G., Lin, L., Iderzorig, T., Osude, C., Khan, N., et al. (2018). Current Molecular-Targeted Therapies in NSCLC and Their Mechanism of Resistance. *Cancers (Basel)* 10 (7), 224. doi:10.3390/cancers10070224

Schrock, A. B., Frampton, G. M., Suh, J., Chalmers, Z. R., Rosenzweig, M., Erlich, R. L., et al. (2016). Characterization of 298 Patients with Lung Cancer Harboring MET Exon 14 Skipping Alterations. *J. Thorac. Oncol.* 11 (9), 1493–1502. doi:10.1016/j.jtho.2016.06.004

Segel, M., Lash, B., Song, J., Ladha, A., Liu, C. C., Jin, X., et al. (2021). Mammalian Retrovirus-like Protein PEG10 Packages its Own mRNA and can Be Pseudotyped for mRNA Delivery. *Science* 373 (6557), 882–889. doi:10.1126/science.abg6155

Soda, M., Choi, Y. L., Enomoto, M., Takada, S., Yamashita, Y., Ishikawa, S., et al. (2007). Identification of the Transforming EML4-ALK Fusion Gene in Non-small-cell Lung Cancer. *Nature* 448 (7153), 561–566. doi:10.1038/nature05945

Soda, M., Takada, S., Takeuchi, K., Choi, Y. L., Enomoto, M., Ueno, T., et al. (2008). A Mouse Model for EML4-ALK-Positive Lung Cancer. *Proc. Natl. Acad. Sci. U. S. A.* 105 (50), 19893–19897. doi:10.1073/pnas.0805381105

Soria, J. C., Tan, D. S. W., Chiari, R., Wu, Y. L., Paz-Ares, L., Wolf, J., et al. (2017). First-line Ceritinib versus Platinum-Based Chemotherapy in Advanced ALK-Rearranged Non-small-cell Lung Cancer (ASCEND-4): A Randomised, Open-Label, Phase 3 Study. *Lancet* 389 (10072), 917–929. doi:10.1016/s0140-6736(17)30123-x

Spaans, J. N., and Goss, G. D. (2014). Trials to Overcome Drug Resistance to EGFR and ALK Targeted Therapies - Past, Present, and Future. *Front. Oncol.* 4, 233. doi:10.3389/fonc.2014.00233

Sung, H., Ferlay, J., Siegel, R. L., Laversanne, M., Soerjomataram, I., Jemal, A., et al. (2021). Global Cancer Statistics 2020: GLOBOCAN Estimates of Incidence and Mortality Worldwide for 36 Cancers in 185 Countries. *CA Cancer J. Clin.* 71 (3), 209–249. doi:10.3322/caac.21660

Tang, H., and Shrager, J. B. (2016). CRISPR/Cas-mediated Genome Editing to Treat EGFR-Mutant Lung Cancer: A Personalized Molecular Surgical Therapy. *EMBO Mol. Med.* 8 (2), 83–85. doi:10.15252/emmm.201506006

Teeuwssen, M., and Fodde, R. (2019). Wnt Signaling in Ovarian Cancer Stemness, EMT, and Therapy Resistance. *J. Clin. Med.* 8 (10), 1658. doi:10.3390/jcm8101658

Terai, H., Soejima, K., Yasuda, H., Sato, T., Naoki, K., Ikemura, S., et al. (2015). Long-term Exposure to Gefitinib Induces Acquired Resistance through DNA Methylation Changes in the EGFR-mutant PC9 Lung Cancer Cell Line. *Int. J. Oncol.* 46 (1), 430–436. doi:10.3892/ijo.2014.2733

Togashi, Y., Mizuuchi, H., Tomida, S., Terashima, M., Hayashi, H., Nishio, K., et al. (2015). MET Gene Exon 14 Deletion Created Using the CRISPR/Cas9 System Enhances Cellular Growth and Sensitivity to a MET Inhibitor. *Lung Cancer* 90 (3), 590–597. doi:10.1016/j.lungcan.2015.10.020

Tong, X., Wang, S., Lei, Z., Li, C., Zhang, C., Su, Z., et al. (2020). MYOCD and SMAD3/SMAD4 Form a Positive Feedback Loop and Drive TGF-β-Induced Epithelial-Mesenchymal Transition in Non-small Cell Lung Cancer. *Oncogene* 39 (14), 2890–2904. doi:10.1038/s41388-020-1189-4

Truong, D. J., Kühner, K., Kühn, R., Werfel, S., Engelhardt, S., Wurst, W., et al. (2015). Development of an Intein-Mediated Split-Cas9 System for Gene Therapy. *Nucleic Acids Res.* 43 (13), 6450–6458. doi:10.1093/nar/gkv601

Tsai, J. H., and Yang, J. (2013). Epithelial-mesenchymal Plasticity in Carcinoma Metastasis. *Genes Dev.* 27 (20), 2192–2206. doi:10.1101/gad.225334.113

Uchibori, K., Inase, N., Nishio, M., Fujita, N., and Katayama, R. (2018). Identification of Mutation Accumulation as Resistance Mechanism Emerging in First-Line Osimertinib Treatment. *J. Thorac. Oncol.* 13 (7), 915–925. doi:10.1016/j.jtho.2018.04.005

Wan, P. T., Garnett, M. J., Roe, S. M., Lee, S., Niculescu-Duvaz, D., Good, V. M., et al. (2004). Mechanism of Activation of the RAF-ERK Signaling Pathway by Oncogenic Mutations of B-RAF. *Cell* 116 (6), 855–867. doi:10.1016/s0092-8674(04)00215-6

Wang, T., Wei, J. J., Sabatini, D. M., and Lander, E. S. (2014). Genetic Screens in Human Cells Using the CRISPR-Cas9 System. *Science* 343 (6166), 80–84. doi:10.1126/science.1246981

Wei, L., Chiu, D. K., Tsang, F. H., Law, C. T., Cheng, C. L., Au, S. L., et al. (2017). Histone Methyltransferase G9a Promotes Liver Cancer Development by Epigenetic Silencing of Tumor Suppressor Gene RARRES3. *J. Hepatol.* 67 (4), 758–769. doi:10.1016/j.jhep.2017.05.015

Woodard, G. A., Jones, K. D., and Jablons, D. M. (2016). Lung Cancer Staging and Prognosis. *Cancer Treat. Res.* 170, 47–75. doi:10.1007/978-3-319-40389-2_3

Wu, X., Huang, H., Yu, B., and Zhang, J. (2020). A Blue Light-Inducible CRISPR-Cas9 System for Inhibiting Progression of Melanoma Cells. *Front. Mol. Biosci.* 7, 606593. doi:10.3389/fmolb.2020.606593

Yang, Y., Qiu, J. G., Li, Y., Di, J. M., Zhang, W. J., Jiang, Q. W., et al. (2016a). Targeting ABCB1-Mediated Tumor Multidrug Resistance by CRISPR/Cas9-based Genome Editing. *Am. J. Transl. Res.* 8 (9), 3986–3994.

Yang, Y., Zhang, P., Zhao, Y., Yang, J., Jiang, G., and Fan, J. (2016b). Decreased MicroRNA-26a Expression Causes Cisplatin Resistance in Human Non-small Cell Lung Cancer. *Cancer Biol. Ther.* 17 (5), 515–525. doi:10.1080/15384047.2015.1095405

Yoshioka, H., Azuma, K., Yamamoto, N., Takahashi, T., Nishio, M., Katakami, N., et al. (2015). A Randomized, Double-Blind, Placebo-Controlled, Phase III Trial of Erlotinib with or without a C-Met Inhibitor Tivantinib (ARQ 197) in Asian Patients with Previously Treated Stage IIIB/IV Nonsquamous Nonsmall-Cell Lung Cancer Harboring Wild-type Epidermal Growth Factor Receptor (ATTENTION Study). *Ann. Oncol.* 26 (10), 2066–2072. doi:10.1093/annonc/mdv288

Yu, W., Jin, C., Lou, X., Han, X., Li, L., He, Y., et al. (2011). Global Analysis of DNA Methylation by Methyl-Capture Sequencing Reveals Epigenetic Control of Cisplatin Resistance in Ovarian Cancer Cell. *PLoS One* 6 (12), e29450. doi:10.1371/journal.pone.0029450

Yu, J., Zhou, J., Xu, F., Bai, W., and Zhang, W. (2018). High Expression of Aurora-B is Correlated with Poor Prognosis and Drug Resistance in Non-small Cell Lung Cancer. *Int. J. Biol. Markers* 33 (2), 215–221. doi:10.1177/1724600817753098

Zang, H., Wang, W., and Fan, S. (2017). The Role of microRNAs in Resistance to Targeted Treatments of Non-small Cell Lung Cancer. *Cancer Chemother. Pharmacol.* 79 (2), 227–231. doi:10.1007/s00280-016-3130-7

Zeng, H., Castillo-Cabrera, J., Manser, M., Lu, B., Yang, Z., Strande, V., et al. (2019). Genome-wide CRISPR Screening Reveals Genetic Modifiers of Mutant EGFR Dependence in Human NSCLC. *Elife* 8, e50223. doi:10.7554/eLife.50223

Zhang, X. H., Tee, L. Y., Wang, X. G., Huang, Q. S., and Yang, S. H. (2015). Off-target Effects in CRISPR/Cas9-mediated Genome Engineering. *Mol. Ther. Nucleic Acids* 4 (11), e264. doi:10.1038/mtna.2015.37

Zhang, L., Wang, P., Feng, Q., Wang, N., Chen, Z., Huang, Y., et al. (2017). Lipid Nanoparticle-Mediated Efficient Delivery of CRISPR/Cas9 for Tumor Therapy. *NPG Asia Mater* 9 (10), e441. doi:10.1038/am.2017.185

Zhang, L., Li, Y., Wang, Q., Chen, Z., Li, X., Wu, Z., et al. (2020a). The PI3K Subunits, P110α and P110β Are Potential Targets for Overcoming P-Gp and BCRP-Mediated MDR in Cancer. *Mol. Cancer* 19 (1), 10. doi:10.1186/s12943-019-1112-1

Zhang, T., Liu, C., Yu, Y., Geng, J., Meng, Q., Xu, S., et al. (2020b). TBL1XR1 is Involved in C-Met-Mediated Tumorigenesis of Human Nonsmall Cell Lung Cancer. *Cancer Gene Ther.* 27 (3-4), 136–146. doi:10.1038/s41417-019-0111-0

Zhao, G., Wang, Q., Gu, Q., Qiang, W., Wei, J. J., Dong, P., et al. (2017). Lentiviral CRISPR/Cas9 Nickase Vector Mediated BIRC5 Editing Inhibits Epithelial to Mesenchymal Transition in Ovarian Cancer Cells. *Oncotarget* 8 (55), 94666–94680. doi:10.18632/oncotarget.21863

Zhou, C., Wu, Y. L., Chen, G., Feng, J., Liu, X. Q., Wang, C., et al. (2011). Erlotinib versus Chemotherapy as First-Line Treatment for Patients with Advanced EGFR Mutation-Positive Non-small-cell Lung Cancer (OPTIMAL, CTONG-0802): A Multicentre, Open-Label, Randomised, Phase 3 Study. *Lancet Oncol.* 12 (8), 735–742. doi:10.1016/s1470-2045(11)70184-x

Conflict of Interest: The authors declare that the research was conducted in the absence of any commercial or financial relationships that could be construed as a potential conflict of interest.

Publisher's Note: All claims expressed in this article are solely those of the authors and do not necessarily represent those of their affiliated organizations, or those of the publisher, the editors and the reviewers. Any product that may be evaluated in this article, or claim that may be made by its manufacturer, is not guaranteed or endorsed by the publisher.

frontiers | Frontiers in Pharmacology

SYSTEMATIC REVIEW
published: 11 May 2022
doi: 10.3389/fphar.2022.881493

Impact of Smoking on Response to the First-Line Treatment of Advanced ALK-Positive Non-Small Cell Lung Cancer: A Bayesian Network Meta-Analysis

Kehai Lin[1,2†], Jie Lin[2†], Zhong Huang[2], Jiding Fu[3], Qi Yi[2], Jiazuo Cai[2], Muhammad Khan[2], Yawei Yuan[1,2] and Junguo Bu[1*]*

[1]Department of Oncology, Guangdong Second Provincial General Hospital, Guangzhou, China, [2]Department of Radiation Oncology, Affiliated Cancer Hospital & Institute of Guangzhou Medical University, State Key Laboratory of Respiratory Diseases, Guangzhou Institute of Respiratory Disease, Guangzhou, China, [3]Department of Intensive Care Unit, Affiliated Cancer Hospital & Institute of Guangzhou Medical University, Guangzhou, China

OPEN ACCESS

Edited by:
Jian Zhang,
Southern Medical University, China

Reviewed by:
Umberto Malapelle,
University of Naples Federico II, Italy
Lian Liu,
Shandong University, China

***Correspondence:**
Junguo Bu
bujg@gd2h.org.cn
Yawei Yuan
yuanyawei@gzhmu.edu.cn

[†]These authors have contributed equally to this work and share first authorship

Specialty section:
This article was submitted to Pharmacology of Anti-Cancer Drugs, a section of the journal Frontiers in Pharmacology

Received: 22 February 2022
Accepted: 08 April 2022
Published: 11 May 2022

Citation:
Lin K, Lin J, Huang Z, Fu J, Yi Q, Cai J, Khan M, Yuan Y and Bu J (2022) Impact of Smoking on Response to the First-Line Treatment of Advanced ALK-Positive Non-Small Cell Lung Cancer: A Bayesian Network Meta-Analysis. Front. Pharmacol. 13:881493. doi: 10.3389/fphar.2022.881493

Background: The impact of smoking on the efficacy of anaplastic lymphoma kinase (ALK)-positive non-small cell lung cancer (NSCLC) treatment is controversial and has not been systematically explored in the first-line setting. We performed a systematic review based on a pairwise meta-analysis and a Bayesian network meta-analysis (NMA) to address this issue.

Methods: PubMed, Embase, Web of Science, Cochrane Library, Clinical-Trials.gov, and other resources were searched until 5 January 2022. Progression-free survival (PFS) was considered the main outcome of interest. Randomized controlled trials with smoking status analysis were included. Cochrane Risk of Bias Tool was performed to assess the risk of bias. Random effects models were adopted conservatively in meta-analysis. The NMA was performed in a Bayesian framework using the "gemtc" version 1.0–1 package of R-4.1.2 software.

Results: A total of 2,484 patients from nine studies were eligible for this study, with 1,547 never-smokers (62.3%) and 937 smokers (37.7%). In a pairwise meta-analysis, in the overall population, no significant difference was found between never-smokers and smokers. However, in the subgroup analyses based on crizotinib-controlled studies, anaplastic lymphoma kinase tyrosine kinase inhibitors (ALK-TKIs) derived better PFS in the smoking group over the never-smoking group in the Asian population (HR = 0.17, 95% CI = 0.09–0.31 in the smoking group, HR = 0.39, 95%CI = 0.24–0.65 in the never-smoking group, $p = 0.04$, low quality of evidence). In NMA, among never-smokers, lorlatinib ranked the highest for PFS (SUCRA = 96.2%), but no significant superiority was found among the new-generation ALK-TKIs except for ceritinib. In smokers, low-dose alectinib performed best (SUCRA = 95.5%) and also demonstrated a significant superiority over ensartinib (HR = 0.23, 95%CI = 0.08–0.68, very low quality of evidence), brigatinib (HR = 0.38, 95%CI = 0.14–0.99, low quality of evidence), ceritinib (HR = 0.24, 95%CI = 0.09–0.66, low quality of

evidence), crizotinib (HR = 0.18, 95%CI = 0.08–0.41, moderate quality of evidence), and chemotherapy (HR = 0.11, 95%CI = 0.05–0.28, low quality of evidence).

Conclusion: In general, smoking may not affect the treatment efficacy of advanced ALK-positive NSCLC in the first-line setting. However, alectinib may perform better in the smoking Asian population. Moreover, lorlatinib in never-smokers and low-dose alectinib in smokers could be considered optimal first-line therapy for advanced ALK-positive NSCLC. Acceptable limitations of evidence, such as study risk of bias, inconsistency, and imprecision, were present in this NMA.

Keywords: non-small cell lung cancer, anaplastic lymphoma kinase, tyrosine kinase inhibitors, smoking, progression-free survival, network meta-analysis

1 INTRODUCTION

Lung cancer, one of the most malignant tumors in both sexes, ranked first in cancer-related deaths and second in newly diagnosed cancer cases worldwide, with percentages of 18.2% and 12.2%, respectively (Cancer today, 2022). Non-small cell lung cancer (NSCLC) accounts for approximately 85% of lung cancer cases (Thai et al., 2021). Oncogenic alterations gradually play an increasingly important role in the development. It is well-known that smoking rates are high, and the role of different smoking statuses varies significantly in carcinogenesis (Bossé and Amos, 2017; Li et al., 2017; Singal et al., 2019; Wang et al., 2021a; Thai et al., 2021), among which EGFR mutations are the most common oncogenic alterations, ranging from 15% in Europe to 62% in Asia in NSCLC of adenocarcinoma histology. EGFR tyrosine kinase inhibitors have performed well in the targeted treatments, extending patients' median overall survival to more than 38 months by gefitinib or osimertinib alone, and even to more than 50 months when combined with chemotherapy. Interestingly, more and more oncogenic alterations have also been developed into useful treatment strategies in NSCLC, such as ALK, RET, NTRK, and ROS1 (Thai et al., 2021).

Anaplastic lymphoma kinase (ALK) gene translocation, leading to abnormal expression of constitutively active ALK fusion proteins, is a key mechanism for inducing lung tumorigenesis of ALK-positive NSCLC (3%–5% of NSCLCs). It is more common in never- or light-smokers and younger age and is associated with adenocarcinoma histology (Shaw and Engelman, 2013; Thai et al., 2021). During the past decade, ALK tyrosine kinase inhibitors (ALK-TKIs) have demonstrated remarkable efficacy in the treatment of advanced or metastatic NSCLC and now are the standard options in the first-line treatment of advanced ALK-positive NSCLCs instead of chemotherapy. Compared with cytotoxic chemotherapy, the first-generation ALK-TKI crizotinib significantly has extended median progression-free survival (PFS) of advanced NSCLC (around 11 *vs.* 7 months) (Solomon et al., 2014; Wu et al., 2018). Moreover, the PFS has been remarkably prolonged by the next-generation ALK-TKIs, such as ceritinib, alectinib, brigatinib, ensartinib, and lorlatinib (Soria et al., 2017; Zhou et al., 2019; Mok et al., 2020; Nakagawa et al., 2020; Shaw et al., 2020; Camidge et al., 2021; Horn et al., 2021). Undoubtedly, targeted therapy is the preferred treatment of oncogene-driven advanced NSCLC. Although never- or light-smokers account for a much higher proportion of ALK-positive NSCLC, it is of great interests and necessitous to figure out the effect of smoking on ALK-positive NSCLCs treatment efficacy in the first-line therapy.

To date, previous meta-analyses have investigated the correlation between smoking status and the efficacy of advanced NSCLC treatments (Breadner et al., 2020; Li et al., 2020). However, conflict occurs in the benefit of never-smoking, as one previous meta-analysis found that never-smokers tended to benefit from ALK-TKIs compared with cytotoxic chemotherapy, whereas another denoted that there were similar benefits regardless of the smoking status. Meanwhile, a network meta-analysis focusing on the relative efficacy of first-line targeted therapies in advanced ALK-positive NSCLCs has simply highlighted the role of smoking in the subgroup analysis (Wang et al., 2021b). These previous works could be systematically expanded to determine the correlation between smoking status and efficacy of ALK-targeted agents in the first-line treatment of advanced ALK-positive NSCLC.

Therefore, our study attempted to compare the impact of smoking on the efficacy of advanced ALK-positive NSCLC with high-quality first-line setting randomized controlled trials. Furthermore, a comprehensive NMA of the relative efficacy of first-line treatments according to different smoking statuses was also performed.

2 MATERIALS AND METHODS

This study was carried out following the guidelines of the 2020 Preferred Reporting Items for Systematic Reviews and Meta-Analysis (PRISMA) (Page et al., 2021) and the extension statement of NMA (Hutton et al., 2015). It was registered on the INPLASY website (registration number: INPLASY202180009, https://inplasy.com/inplasy-2021-8-0009/, accessed on 03 August 2021).

2.1 Literature Search and Study Selection

We searched PubMed, Embase, Web of Science, Cochrane Library, and Clinical-Trials.gov up to 19 August 2021 without

language limitations for eligible studies, which was finally updated on 05 January 2022. In addition, abstracts were searched from the main oncology congresses databases, including the American Society of Clinical Oncology (ASCO), the European Society for Medical Oncology (ESMO), and the World Conference on Lung Cancer (WCLC). The search strategy is presented in **Supplementary Table S2**. The following search terms were used: non-small cell lung cancer (NSCLC), anaplastic lymphoma kinase (ALK), ALK tyrosine kinase inhibitors, crizotinib, ceritinib, alectinib, brigatinib, ensartinib, lorlatinib, entrectinib, and their medical subject headings (MeSH) terms. The inclusion criteria were as follows: 1) randomized controlled trials with clinical outcomes, such as PFS and OS; 2) patients with pathologically confirmed locally advanced or metastatic NSCLC; 3) studies with clear baseline characteristics of patients and ALK mutation status; and 4) studies including data of smoking status analysis required for meta-analysis. The relevant titles and abstracts were screened to remove duplicated and irrelevant publications. Then, the full texts and relevant reference lists of the other articles were browsed thoroughly for the final inclusion.

2.2 Data Extraction and Quality Assessment

The following information was extracted: the trial name, publication year, design, interventions, sample size, race, patients age and gender, baseline brain metastases, adverse effects, previous treatments, number of smokers (defined as current and/or former smokers) and never-smokers, and hazard ratio (HR) with 95% confidence intervals (CIs) for PFS of whole group and subgroup. Quality assessment was performed using the Cochrane Risk of Bias Tool (Higgins et al., 2011). It includes seven domains (random sequence generation, allocation concealment, blinding of participants and personnel, blinding of outcome assessment, incomplete outcome data, selective outcome reporting, and other bias), for which a judgment (low, high, or unclear risk) was assessed respectively. Study selection, data extraction, and risk of bias assessment were independently executed by two reviewers (KL, JL). For any unresolved discrepancies, a third reviewer (ZH) was concerned.

2.3 Data Synthesis and Statistical Analysis

PFS was defined as the time from randomization to RECIST-defined disease progression or death from any cause. The HR was regarded as a measure of effect size for PFS. Because overall survival (OS) is immature for most trials and there is a lack of smoking subgroup analysis results, this part of the analysis was not performed.

2.3.1 Pairwise Meta-Analysis

PFS-HR of current smokers and former smokers was combined as the smoker group when smoking statuses were multiply categorized. The HR of current smokers in some studies was ignored because it was not applicable due to a small population. Heterogeneity across studies was assessed by I^2 statistics, with $I^2 < 25\%$, $25\% \leq I^2 \leq 50\%$, and $I^2 > 50\%$ being interpreted as signifying low-level, intermediate-level, and high-level heterogeneity, respectively. If necessary, subgroup analysis would be performed. Any heterogeneity between the smoker subgroup and never-smoker subgroup was detected by the Cochran Q test. A p-value (two-sided) of less than 0.05 was considered statistically significant. The analysis process was carried out by RevMan 5.4.1, applying the random-effect model conservatively.

2.3.2 Network Meta-Analysis

With the model of the lower deviance information criterion (DIC), which is more feasible (Oravecz and Muth, 2017), a network meta-analysis of different therapeutic drugs in both never smokers and smokers based on a Bayesian framework was performed using the "gemtc 1.0–1" package of R software (version 4.1.2) (Neupane et al., 2014; Tonin et al., 2017). This method integrated both direct and indirect comparisons for any given pair of managements and certain endpoints. The function mtc.run was applied to generate samples, and we set 10000 simulations for each chain as the "burn-in" period, yielding 50,000 iterations to obtain the HR of model parameters when four Markov chains run simultaneously. The Brooks–Gelman–Rubin diagnosis plots method, trace plot, and density plot were used to access the model convergence (Wu et al., 2013). Rank probabilities were calculated to obtain the hierarchy of each treatment, and a plot of rank probabilities was created by the "gemtc" package (Gelman and Rubin, 1992). The probability of the competing treatments was ranked by the surface under the cumulative ranking curve (SUCRA), the highest and lowest values of which mean the highest probability of ranking the best and worst, respectively (Salanti et al., 2011; Tonin et al., 2017).

Stata/SE 15.1 and RevMan 5.4.1 were used to generate network and funnel plots for a visual illustration of relationships among each treatment and evaluation of the studies' publication bias. The mtc.anohe command of the "gemtc" package was used to evaluate global heterogeneity. A sensitivity analysis was performed by removing the trials deemed to be heterogeneous to ensure reliability.

2.4 Quality of Evidence

The quality of evidence was assessed in accordance with the GRADE working group approach (Guyatt et al., 2008; Puhan et al., 2014). In this method, the quality of evidence was categorized into four levels (high, moderate, low, and very low), and the starting point of quality of direct evidence based on RCTs would be high, which could be downrated to moderate, low, or very low according to five domains (risk of bias, indirectness, imprecision, inconsistency, and publication bias). We used the GRADEpro Guideline Development Tool (www.gradepro.org) to rate the quality of evidence in a pairwise meta-analysis. In network meta-analysis (Puhan et al., 2014), the quality of indirect evidence was consistent with the lower confidence rating of two direct comparisons that contribute as first-order loops to the indirect estimates. As there are no closed loops in this NMA, the direct or indirect estimates constituted the final outcome.

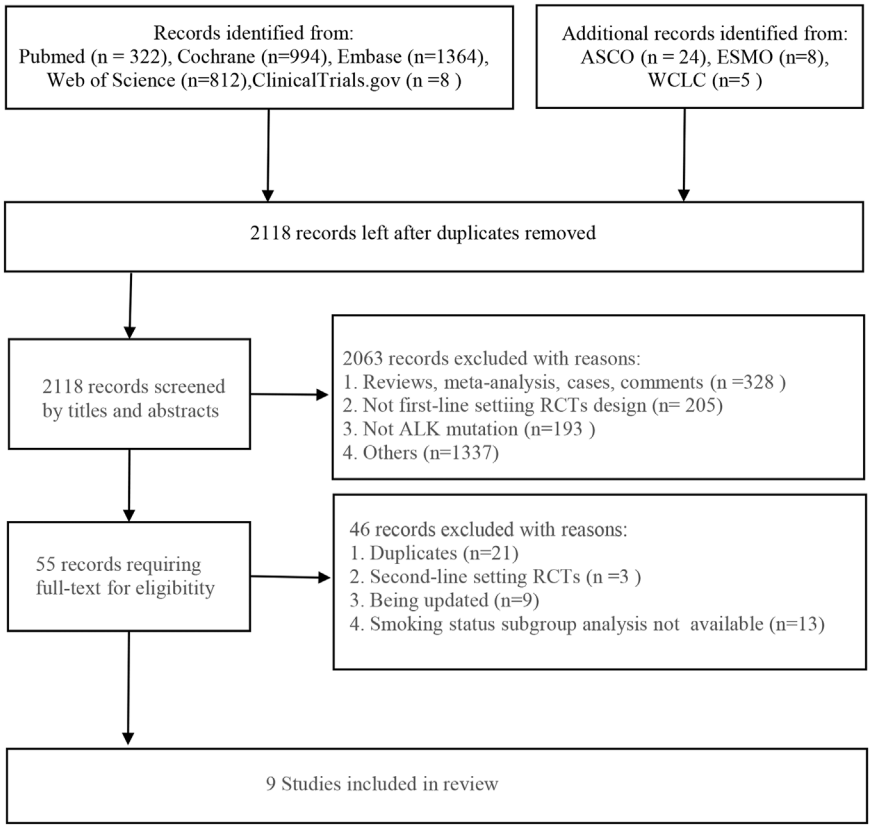

FIGURE 1 | Flowchart of the literature screening. ASCO, the American Society of Clinical Oncology; ESMO, the European Society for Medical Oncology; WCLC, the World Conference on Lung Cancer; RCTs, randomized controlled trials; ALK, anaplastic lymphoma kinase.

3 RESULTS

3.1 Literature Search

Initially, 3,537 eligible studies were yielded from the searching strategies, including 322 studies from PubMed, 1,364 studies from Embase, 812 from Web of Science, 994 studies from Cochrane Library, and 8 studies from Clinical-Trials.gov. In addition, 37 studies were found from other sources. After removing 1,419 duplicates, additional 2,063 studies were excluded by screening the title and abstract. Eventually, nine studies were included in our analysis according to the inclusion criteria. The flowchart of the literature screening is presented in **Figure 1**.

3.2 Study Characteristics

Table 1 presents the detailed characteristics of included studies. All of the included nine studies were phase 3 randomized controlled trials, enrolling 2,484 participants totally, with 1,547 never-smokers (62.3%) and 937 smokers (37.7%). Among them, three were cytotoxic chemotherapy-controlled studies, with PROFILE1014 and PROFILE1029 investigating crizotinib and ASCEND-4 investigating ceritinib and six were crizotinib-controlled studies, with eXalt3 investigating ensartinib, ALTA-1L investigating brigatinib, CROWN investigating lorlatinib, and J-ALEX, ALEX, and ALESIA investigating alectinib). For race differences, three studies were Asian-only trials (PROFILE 1029, J-ALEX, and ALESIA), and six were multi-race trials (Crown, ALEX, ALTA-1L, PROFILE 1014, eXalt3, and ASCEND-4).

3.3 Quality Evaluation

All nine studies were open-label studies prone to a high risk of performance bias. However, a low risk of detection bias was observed in all included studies due to the blinding of outcome assessment completed by a blinded independent review committee. Unclear risk occurred in selection bias, attrition bias, reporting bias, and other bias due to the lack of detailed information. Detailed quality assessment is illustrated in **Supplementary Figure S1**.

Both the trace and density plot (**Supplementary Figure S2** for never-smoker, **Supplementary Figure S3** for smoker) and Brooks–Gelman–Rubin diagnosis plot (**Supplementary Figure S2** for never-smoker, **Supplementary Figure S3** for smoker), showing no single chain fluctuation and normal distribution of density map, illustrated an excellent convergence of the models performed in NMA. As seen in **Supplementary Figure S4**, there was no significant publication bias in the pooled analyses. In terms of inconsistency analyses, the global analysis showed low heterogeneity in nonsmokers and moderate heterogeneity in the

TABLE 1 | Characteristics of the included studies of first-line ALK-TKI treatment for advanced ALK-positive NSCLC.

Study, year	Design	Drug	Sample size	Nonsmoker	Only Asian	PC (%)	Age (median)	Male (%)	BM (%)	G3AE (%)	PFS (months)	HR (95%CI)
PROFILE1014 Solomon et al. (2014)	Phase III, open-	Criz	172	106	No	0	52	40	26	NA	10.9 (8.3–13.9)	0.45
2014	label, RCT	Chem	171	112		0	54	37	27	NA	7.0 (6.8–8.2)	(0.35–0.60)
PROFILE1029 Wu et al. (2018)	Phase III, open-	Criz	104	78	Yes	0	48	48.1	20.2	NA	11.1 (8.3–12.6)	0.402
2018	label, RCT	Chem	103	72		0	50	41.7	31.1	NA	6.8 (5.7–7.0)	(0.286–0.565)
ASCEND-4 Soria et al. (2017)	Phase III, open-	Ceri	189	108	No	0	55	46	31	NA	16·6 (12·6–27·2)	0·55
2017	label, RCT	Chem	187	122		0	54	39	33	NA	8·1 (5·8–11·1)	(0·42–0·73)
J-ALEX Nakagawa et al. (2020)	Phase III, open-	Alec_L	103	56	Yes	36	61	40	14	36.9	34.1 (22.1–NR)	0·37
2020	label, RCT	Criz	104	61		36	59.5	39	28	60.6	10·2 (8·3–12·0)	(0.26–0.52)
ALESIA Zhou et al. (2019)	Phase III, open-	Alec_H	125	84	Yes	0	51	51	35	29	NR (20·3–NR)	0·22
2019	label, RCT	Criz	62	45		0	49	55	37	48	11·1 (9·1–13·0)	(0·13–0·38)
ALEX Mok et al. (2020)	Phase III, open-	Alec_H	152	92	No	0	58	45	42	52	34.8 (17.7–NR)	0.43
2020	label, RCT	Criz	151	98		0	54	42	38	56.3	10.9 (9.1–12.9)	(0.32–0.58)
ALTA-1L Camidge et al. (2021)	Phase III, open-	Brig	137	84	No	26	58	50	29	78	24.0 (18.5–43.2)	0.48
2021	label, RCT	Criz	138	75		27	60	41	30	64	11.1 (9.1–13)	(0.35–0.66)
CROWN Shaw et al. (2020)	Phase III, open-	Lorl	149	81	No	0	61	44	26	77.2	NR (NR–NR)	0.28
2020	label, RCT	Criz	147	94		0	56	38	27	60.6	9.3 (7.6–11.1)	(0.19–0.41)
eXalt3 Horn et al. (2021)	Phase III, open-	Ensa	143	85	No	23.8	54	50.3	32.9	50.4	25.8 (21.8-NR)	0.51
2021	label, RCT	Criz	147	94		28.6	53	52.4	38.8	42.4	12.7 (9.2–16.6)	(0.35–0.72)

ALK, anaplastic lymphoma kinase; TKI, tyrosine kinase inhibitor; NSCLC, non-small cell lung cancer; RCT, randomized controlled trial; Chem, chemotherapy (cisplatin [75 mg/m2], or carboplatin [target area under the curve of 5–6] plus pemetrexed [500 mg/m2]) given every 21 days; Criz, crizotinib (250 mg twice daily); Brig, brigatinib (90 mg once daily for 7 days, then 180 mg once daily); Ceri, ceritinib (750 mg once daily); Ensa, ensartinib (225 mg once daily); Alec_L, low-dose alectinib (300 mg twice daily); Alec_H, high-dose alectinib (600 mg twice daily); Lorl, lorlatinib (100 mg once daily); PC, previous chemotherapy; BM, brain metastasis; G3AE, adverse event ≥ grade 3; HR, hazard ratio; CI, confidence interval; NA, not available; NR, not reached.

smokers (I^2 = 4%, I^2 = 26%, respectively). As no closed loop exits in this NMA, local inconsistency analysis was not performed. Thus, a satisfactory consistency among the studies was obtained. The transitivity across the included studies was well balanced by strictly including RCTs according to the selection criteria in this NMA.

3.4 Pooled Efficacy for Never-Smokers *Versus* Smokers

We compared the pooled efficacy for never-smokers against smokers in the chemotherapy-controlled studies and crizotinib-controlled studies, respectively. In chemotherapy-controlled studies (**Figure 2**, **Supplementary Table S3**), the pooled PFS-HR for never-smokers was 0.42 (95%CI = 0.31–0.57, moderate quality of evidence), while 0.58 (95%CI = 0.44–0.76, moderate quality of evidence) for smokers. Compared with chemotherapy, treatment with ALK-TKIs exhibited no statistically significant difference between smokers and never-smokers (p = 0.14).

In crizotinib-controlled studies (**Figure 3**, **Supplementary Table S4**), the pooled PFS-HR analysis yielded 0.37 (95%CI = 0.31–0.46, moderate quality of evidence) for never-smokers and 0.40 (95%CI = 0.26–0.60, very low quality of evidence) for smokers. Compared with crizotinib, treatment with both the second- and third-generation (2/3G) ALK-TKIs presented similar benefits between smokers and never-smokers (p =

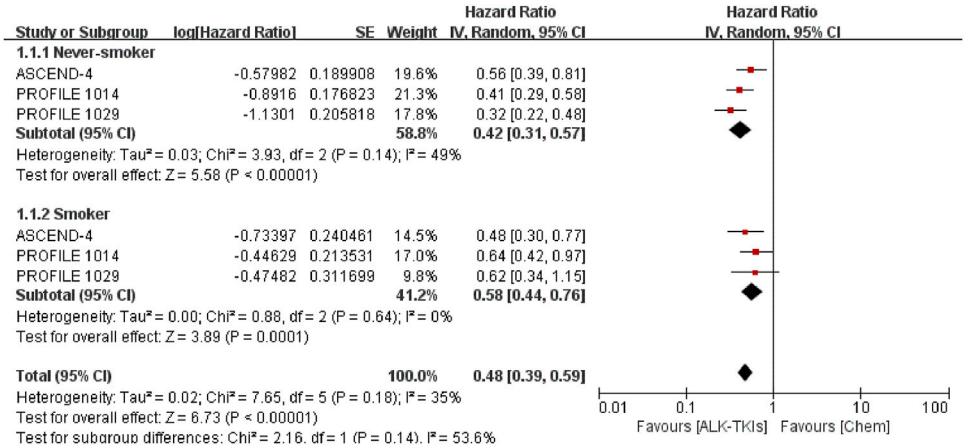

FIGURE 2 | Comparison between smoking status subgroups in chemotherapy-controlled studies. ALK-TKIs, anaplastic lymphoma kinase tyrosine kinase inhibitors; Chem, chemotherapy.

0.80). The smoker subgroup exhibited significant heterogeneity (I^2 = 59%). As such, we conducted subgroup analysis by race. In Asian-only studies, pooled PFS-HR was 0.39 (95%CI = 0.24–0.65, moderate quality of evidence) for never smokers and 0.17 (95%CI = 0.09–0.31, low quality of evidence) for smokers, with significant difference (p = 0.04). In others, pooled PFS-HR 0.37 (95%CI = 0.29–0.47, moderate quality of evidence) for never smokers and 0.50 (95%CI = 0.36–0.69, moderate quality of evidence) for smokers had no significant difference (p = 0.15). Moreover, no significant heterogeneity was found in both subgroup analysis (Asian-only subgroup: I^2 = 29% in never-smoker subgroup, 0% in smoker subgroup; multirace subgroup: I^2 = 9% in never-smoker subgroup, 25% in smoker subgroup).

3.5 Network Meta-Analysis for Efficacy

Figure 4 presents the network plot of each treatment. Eight treatments were involved in this NMA, with low-dose alectinib (ld-alectinib, 300 mg twice daily) and high-dose alectinib (hd-alectinib, 600 mg twice daily) being regarded as separate treatments.

3.5.1 Network Meta-Analysis for Efficacy in the Never-Smoker Group

In the never-smoker group, as presented in **Figure 5**, all ALK-TKIs were significantly superior to chemotherapy; significant superiority was observed for all next-generation ALK-TKIs other than ceritinib when compared to crizotinib (HR = 0.24, 95%CI = 0.14–0.41, moderate quality of evidence for lorlatinib; HR = 0.37, 95%CI = 0.26–0.51, moderate quality of evidence for hd-alectinib; HR = 0.39, 95%CI = 0.23–0.66, moderate quality of evidence for ensartinib; HR = 0.43, 95%CI = 0.28–0.65, moderate quality of evidence for brigatinib; HR = 0.5, 95%CI = 0.28–0.89, low quality of evidence for ld-alectinib; HR = 1.51, 95%CI = 0.96–2.38, low quality of evidence for ceritinib); and no significant difference was noticed between hd- and ld-alectinib (HR = 0.74, 95%CI = 0.38–1.43, low quality of evidence), with the former showing relatively better efficacy. Additionally, lorlatinib, presenting highest SUCRA and Prbest values (SUCRA = 96.2%, Prbest = 82.2%) (**Supplementary Tables S5, S6**, **Supplementary Figure S5**), performed best, followed by hd-alectinib (SUCRA = 74.1%), ensartinib (SUCRA = 69.7%), brigatinib (SUCRA = 62.5%), ld-alectinib (SUCRA = 54.5%), crizotinib (SUCRA = 28.2%), ceritinib (SUCRA = 14.8%), and chemotherapy (SUCRA = 0.00%).

For assessment of between-study heterogeneity (**Supplementary Figure S6**), we found no significant difference either in the crizotinib-chemotherapy comparison in both PROFILE1014 and PROFILE1029 or the comparison between crizotinib and hd-alectinib in both ALEX and ALESIA, with both showing no heterogeneity (I^2 = 0.0%). Because three trials (J-ALEX, eXalt3, and ALTA-1L) had also enrolled patients with history of previous chemotherapy, a sensitivity analysis was performed by excluding these trials. Then, rank probabilities by SUCRA values were generated in the remaining studies. **Figure 5** and **Supplementary Table S6** reveal the same results for the relative ranking of the five remaining treatment groups. Based on these results, we may conclude that a history of previous treatment may not affect the outcomes of our NMA.

3.5.2 Network Meta-Analysis for Efficacy in the Smoker Group

In the smoker group, as presented in **Figure 6**, ld-alectinib showed significantly better PFS than other ALK-TKIs except for hd-alectinib and lorlatinib (HR = 0.18, 95%CI = 0.08–0.41, moderate quality of evidence for crizotinib; HR = 0.23, 95%CI = 0.08–0.68, very low quality of evidence for ensartinib; HR = 0.24, 95%CI = 0.09–0.66, low quality of evidence for ceritinib; HR = 0.38, 95%CI = 0.14–0.99, low quality of evidence for brigatinib; HR = 0.5, 95%CI = 0.18–1.37, moderate quality of evidence for lorlatinib; HR = 0.62, 95%CI = 0.21–1.83, very low quality of evidence for hd-alectinib). Though lorlatinib has demonstrated a greater effect in the never-smoker group, it was not superior to both ld- and hd-alcetinib in PFS for the smoker group (HR = 0.5, 95%CI = 0.18–1.37, moderate quality of evidence for ld-alectinib; HR = 0.81, 95%CI = 0.33–1.97, very low quality of evidence for

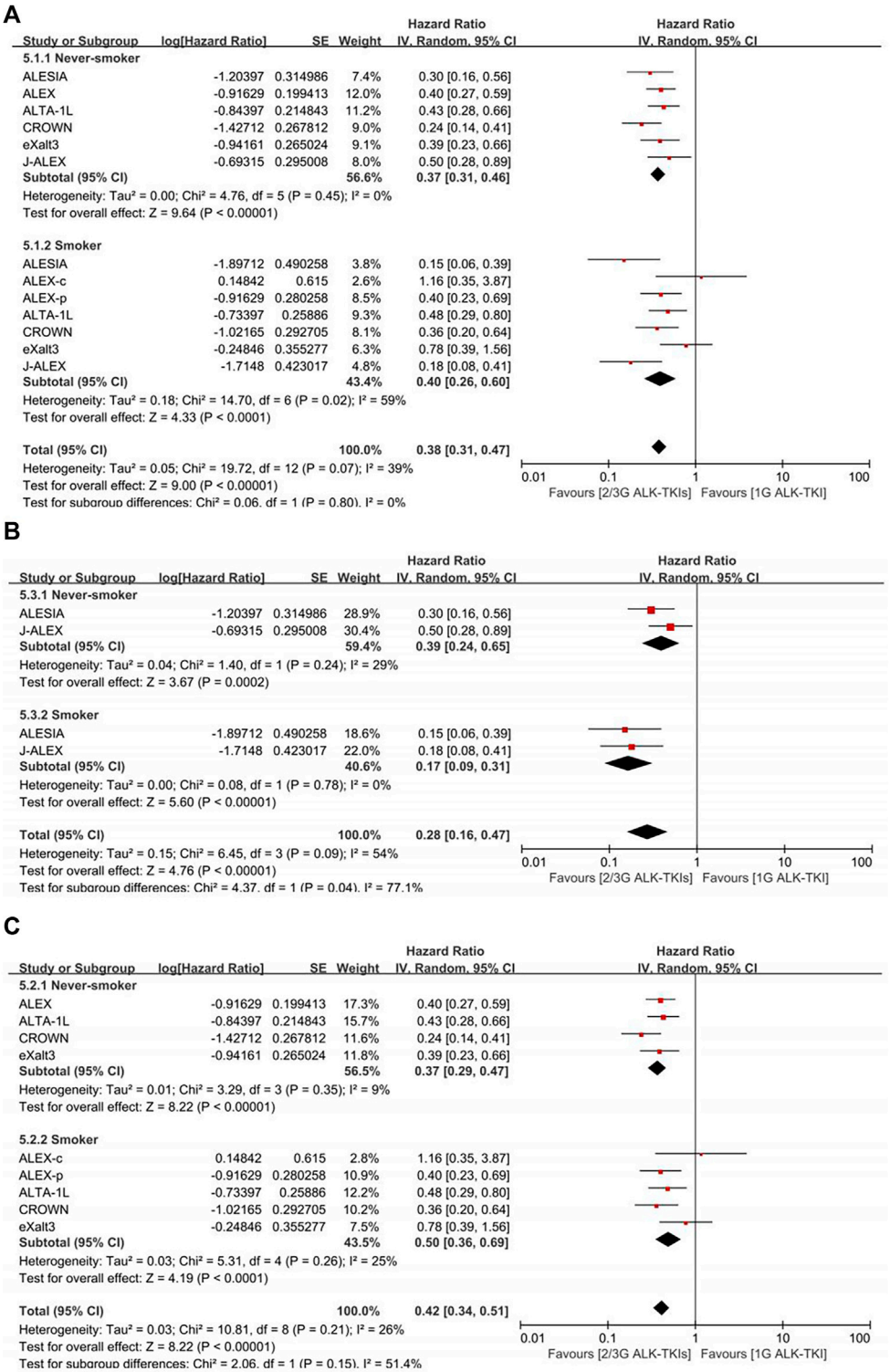

FIGURE 3 | Comparison between smoking status subgroups in crizotinib-controlled studies. **(A)** Initial analysis. **(B)** Asian-only subgroup analysis. **(C)** Multiracial subgroup analysis. ALEX-c, current smoker subgroup of ALEX; ALEX-p, previous smoker subgroup of ALEX; 2/3G ALK-TKIs, both second- and third-generation anaplastic lymphoma kinase tyrosine kinase inhibitors; 1G ALK-TKI, first-generation anaplastic lymphoma kinase tyrosine kinase inhibitor.

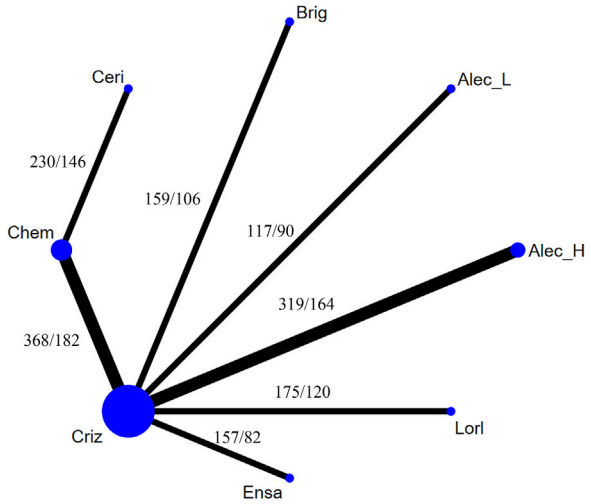

FIGURE 4 | Network constructions for comparisons in progression-free survival of the never-smoker group or smoker group. Chem, chemotherapy; Criz, crizotinib; Brig, brigatinib; Ceri, ceritinib; Ensa, ensartinib; Alec_L, low-dose alectinib; Alec_H, high-dose alectinib; Lorl, lorlatinib. The "number 1/number 2" listed in the upper left of each comparison means that number 1 is the number of never-smokers and number 2 is the number of smokers in each comparison.

hd-alectinib). Additionally, ld-alectinib (SUCRA = 95.5%, Prbest = 76.9%) (**Supplementary Tables S6, S7, Supplementary Figure S7**) was considered to rank first with greatest probability, followed by hd-alectinib (SUCRA = 81.6%), lorlatinib (SUCRA = 72.8%), brigatinib (SUCRA = 58.8%), ceritinib (SUCRA = 36.2%), ensartinib (SUCRA = 34.3%), crizotinib (SUCRA = 20.2%), and chemotherapy (SUCRA = 0.01%).

For assessment of between-study heterogeneity (**Supplementary Figure S8**), a significant difference was found in the crizotinib-hd-alectinib comparison in both ALEX and ALESIA (I^2 = 73.5%) but not in the crizotinib-chemotherapy group in both PROFILE1014 and PROFILE1029 (I^2 = 0). High heterogeneity between ALEX and ALESIA was considered to result from a small number of smokers in the crizotinib arm (only 14) in the ALESIA study. Under such circumstances, we performed a sensitivity analysis by excluding ALESIA. The results (**Figure 6** and **Supplementary Table S6**) showed that ld-alectinib still performed better, and the relative ranking of other treatments was consistent with the result from the initial NMA except for hd-alectinib, which was not better than lorlatinib and brigatinib. More sensitivity analyses by excluding studies enrolling patients with a history of previous chemotherapy are

Lorl	1.53 (0.83, 2.85)	-	-	-	**4.17 (2.46, 7.03)**	**6.3 (3.14, 12.66)**	**11.24 (6.23,20.24)**
0.65 (0.35,1.21)	**Alec_H**	-	-	-	**2.71 (1.95, 3.78)**	**4.1 (2.33, 7.22)**	**7.33 (4.8, 11.18)**
0.62 (0.29,1.28)	0.95 (0.51,1.75)	**Ensa**	-	-	-	-	-
0.56 (0.29,1.1)	0.86 (0.5,1.46)	0.91 (0.46,1.77)	**Brig**	-	-	-	-
0.48 (0.22,1.05)	0.74 (0.38,1.43)	0.78 (0.36,1.7)	0.86 (0.42,1.76)	**Alec_L**	-	-	-
0.24 (0.14,0.41)	**0.37 (0.26,0.51)**	**0.39 (0.23,0.66)**	**0.43 (0.28,0.66)**	**0.5 (0.28,0.89)**	**Criz**	1.51 (0.96, 2.39)	**2.7 (2.07, 3.51)**
0.16 (0.08,0.32)	**0.24 (0.14,0.43)**	**0.26 (0.13,0.51)**	**0.28 (0.15,0.53)**	**0.33 (0.16,0.69)**	0.66 (0.42,1.04)	**Ceri**	**1.78 (1.23, 2.59)**
0.09 (0.05,0.16)	**0.14 (0.09,0.21)**	**0.14 (0.08,0.26)**	**0.16 (0.1,0.26)**	**0.19 (0.1,0.35)**	**0.37 (0.28,0.48)**	**0.56 (0.39,0.81)**	**Chem**

Lorl Alec_H Ensa Brig Alec_L Criz Ceri Chem
Best Initial analysis **worst**

Lorl Alec_H Criz Ceri Chem
Best Sensitivity analysis **worst**

FIGURE 5 | NMA results of never-smoker on progression-free survival (lower left) and sensitivity analysis (upper right), followed by the ranking distribution according to SUCRA values (lower arrow shape). NMA, network meta-analysis; SUCRA, the surface under the cumulative ranking curve; Chem, chemotherapy; Criz, crizotinib; Ceri, ceritinib; Alec_L, low-dose alectinib; Alec_H, high-dose alectinib; Brig, brigatinib; Lorl, lorlatinib; Ensa, ensartinib. Values in bold mean statistically significant.

Alec_L	3.28 (0.89,11.99)	2 (0.73,5.47)	**2.66 (1.01,7.06)**	**4.2 (1.52,11.58)**	**4.33 (1.47,12.75)**	**5.55 (2.42,12.73)**	**8.75 (3.55,21.54)**
0.62 (0.21,1.83)	**Alec_H**	0.61 (0.19,1.93)	0.81 (0.26,2.49)	1.28 (0.4,4.07)	1.32 (0.39,4.46)	1.7 (0.62,4.59)	2.67 (0.93,7.68)
0.5 (0.18,1.37)	0.81 (0.33,1.97)	**Lorl**	1.33 (0.62,2.87)	2.1 (0.93,4.76)	2.16 (0.88,5.33)	**2.78 (1.56,4.92)**	**4.38 (2.24,8.55)**
0.38 (0.14,0.99)	0.6 (0.26,1.42)	0.75 (0.35,1.61)	**Brig**	1.58 (0.73,3.42)	1.63 (0.69,3.85)	**2.08 (1.26,3.46)**	**3.29 (1.78,6.06)**
0.24 (0.09,0.66)	**0.38 (0.15,0.95)**	0.48 (0.21,1.08)	0.64 (0.29,1.38)	**Ceri**	1.03 (0.41,2.55)	1.32 (0.74,2.37)	**2.08 (1.3,3.34)**
0.23 (0.08,0.68)	**0.37 (0.14,0.99)**	0.46 (0.19,1.14)	0.61 (0.26,1.45)	0.97 (0.39,2.41)	**Ensa**	1.28 (0.64,2.57)	2.02 (0.93,4.42)
0.18 (0.08,0.41)	**0.29 (0.14,0.58)**	**0.36 (0.2,0.64)**	**0.48 (0.29,0.8)**	0.76 (0.42,1.36)	0.78 (0.39,1.56)	**Criz**	**1.58 (1.12,2.23)**
0.11 (0.05,0.28)	**0.18 (0.08,0.4)**	**0.23 (0.12,0.45)**	**0.3 (0.17,0.56)**	**0.48 (0.3,0.77)**	0.49 (0.23,1.08)	**0.63 (0.45,0.9)**	**Chem**

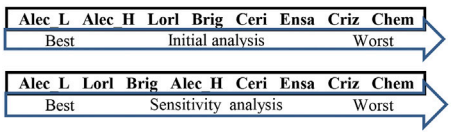

FIGURE 6 | NMA results of smokers on progression-free survival (lower left) and sensitivity analysis (upper right), followed by the ranking distribution according to SUCRA values (lower arrow shape). NMA, network meta-analysis; SUCRA, the surface under the cumulative ranking curve; Chem, chemotherapy; Criz, crizotinib; Ceri, ceritinib; Alec_L, low-dose alectinib; Alec_H, high-dose alectinib; Brig, brigatinib; Lorl, lorlatinib; Ensa, ensartinib. Values in bold mean statistically significant.

shown in **Supplementary Table S6**. It is concluded that the similar outcomes, to a certain extent, symbolized the inherent robustness of the NMA, which confirms the ultimate results.

4 DISCUSSION

On the one hand, it is well-known that smoking is of great importance in the morbidity and mortality of lung cancer (Loeb et al., 1984; Jung et al., 2016). On the other hand, the impact of smoking on treatment decisions is controversial and is recently being widely investigated (Lin et al., 2018; Li et al., 2020; Xiao et al., 2020; Chen et al., 2021; Zhao et al., 2021). To our knowledge, the comprehensive and systematic analysis of the relationship between smoking status and first-line treatment efficacy of advanced ALK-positive NSCLC has not been reported yet. Our present work may contribute to resolving this discrepancy and provide useful advice for clinical strategy.

As ALK-TKIs have replaced traditional chemotherapies as the upfront treatments with great advantages in efficacy and safety (Guidelines Detail, 2022), we classified the included studies into two groups: the chemotherapy-controlled and crizotinib-controlled groups. Although we found no difference between the smoking group and the never-smoking group in both chemotherapy- and crizotinib-controlled groups, the subgroup analysis by race in the crizotinib-controlled group indicated that ALK-TKIs in Asian-only derived better outcomes in the smoking group compared to the never-smoking group. In contrast to our outcomes, Breadner's meta-analysis found a greater degree of benefit with ALK-TKIs in the never-smoker group (Breadner et al., 2020). Nonetheless, their study included second-line setting studies in the chemotherapy-controlled group. Moreover, it is possible that the advancement of lung cancer may have constrained the smoking factor from being detected. In real-world data, smoking history has been regarded as an independent negative prognostic factor for survival benefits (Jin et al., 2018; Britschgi et al., 2020). Tobacco use impairs the treatment efficacy of lung cancer and shortens patients' survival as smoking tobacco directly influences response to anti-tumor drugs by affecting drugs metabolism (Gemine and Lewis, 2016). On the contrary, immunotherapy performs better in NSCLC patients with a smoking history (Li et al., 2020; Nie et al., 2020; Zhao et al., 2021). Notably, both studies in the Asian-only subgroup used alectinib, despite dosage differences, which may suggest the excellent efficacy of alectinib in smokers, while the experimental ALK-TKIs in another group dramatically varied in multiracial studies.

Recently, network meta-analyses have demonstrated the great advantage of both lorlatinib and alectinib on PFS, with the former being the best (Ando et al., 2021; Chuang et al., 2021). Our NMA of the never-smoking group also supports the advantageous effect of lorlatinib on PFS with significant superiority over crizotinib and ceritinib. As it was designed to easily penetrate the blood–brain barrier and against resistance to all known ALK mutants (Johnson et al., 2014; Zou et al., 2015; Solomon et al., 2018; El Darsa et al., 2020), lorlatinib had an extraordinarily good performance on PFS, not only in the frontline therapy but also in subsequent therapy owing to the failure of first- or second-generation ALK inhibitors (Shaw et al., 2020; Kuang and Leighl, 2021). Nevertheless, interestingly, consistent with Chuang's finding of ld-alectinib ranking first in the patients with baseline brain metastasis (Chuang et al., 2021), the efficacy of ld-alectinib surpassed that of lorlatinib in the NMA of the smoking group, although there were no significant differences. Moreover, ld-alectinib administration resulted in significantly superior PFS to that of ensartinib, ceritinib, crizotinib, and chemotherapy. It is a feature of ld-alectinib, but not hd-alectinib, to show relatively high activity in the smoking

subgroup of advanced ALK-positive NSCLC. However, there is little direct evidence to explain the potent mechanism of this discrepancy. To our knowledge, smokers suffer far more mutations than never-smokers, among which TP53 mutation deserves more attention in lung cancer (Le Calvez et al., 2005; Ding et al., 2008). It is noted that there is a high rate of TP53 co-mutation in ALK-positive NSCLC, which has shown a significantly worse prognosis (Aisner et al., 2017; Kron et al., 2018). In Yoda's research, TP53 mutation coexisted in half of the lorlatinib-resistant samples (Yoda et al., 2018). In the ALTA-1L study (Camidge et al., 2021), patients with TP53 mutant derived apparently shorter PFS not only in the crizotinib treatment group but also in the brigatinib group. However, there was no more information concerning TP53 mutation and efficacy of other ALK-TKIs and relevant correlation with smoking. Probably, the abundant mutations in smokers complicate the drug efficacy. Therefore, additional studies are required to clarify the potential optimal treatment for smokers and never-smokers with elucidation on mechanistic details.

Importantly, adverse effects (AEs) play an indispensable role in clinical treatment decision-making. A lower dose of alectinib, 300 mg twice daily, is a legally experimental dose resulting from Japanese authority due to Japan's historical maximum intake level of sodium lauryl sulfate, one of the capsule excipients for alectinib (Seto et al., 2013; Zhou et al., 2019). Inconsistent with theoretical assumptions, compared with hd-alectinib, 600 mg twice daily, dose reduction of alectinib did not obviously show a better safety profile in J-ALEX (≥ grade 3 AEs in J-ALEX = 36.9%; ALESIA = 29%; and ALEX = 52%). However, median follow-ups varied in these trials, which may have an impact on the safety profile. Median follow-up was 42.4 months for ld-alectinib in J-ALEX and 48.2 months for hd-alectinib in ALEX, which were much longer than 16.2 months for hd-alectinib in ALESIA (Zhou et al., 2019; Mok et al., 2020; Nakagawa et al., 2020). Also, 36% of participants had received previous chemotherapy in J-ALEX, which may have escalated their adverse effects. Accordingly, the safety profile of ld-alectinib is not worse than that of hd-alectinib, which means ld-alectinib is well tolerated. Lorlatinib (Shaw et al., 2020) is also well tolerated. Although the rate of adverse events (≥ grade 3) was as high as 77%, most of them were hyperlipidemia, weight gain, and hypertension. Moreover, cognitive effects and peripheral neuropathy were common but generally mild, all of which could be well managed.

Lastly, several limitations in our NMA are inevitable. First, in these RCTs, smoking history was not a stratification factor in randomization and small sample sizes existed, probably resulting in heterogeneity in patients selection for our meta-analysis and imprecision of evidence. Second, the direct comparisons were all based on chemotherapy- and crizotinib-controlled studies, which means a lack of direct comparison between next-generation ALK-TKIs and closed loops in the analysis, so the direct evidence among each comparison is insufficient. Third, there is only one trial for each of the next-generation ALK-TKI other than alectinib, and insufficient data may result in instability of the outcome. Fourth, the overall survival of most next-generation ALK-TKIs studies is immature, and subgroup outcome of smoking status is rarely presented. Consequently, extrapolation of long-term outcomes is prevented. Even with the inherent limitations of this NMA, we strictly follow the guidelines of PRISMA and the extension statement of NMA, which improves the quality of our analyses.

5 CONCLUSION

In summary, this systematic review compared the impact of smoking status on treatment efficacy and the relative efficacy of each frontline choice in the first-line setting of advanced ALK-positive NSCLC in terms of PFS. Although, in the overall population, there were no significant differences between smoking statuses, we found in the subgroup analyses that ALK-TKIs derived better PFS in the smoking group over the never-smoking group in the Asian population. Among never-smokers, lorlatinib ranks the highest for PFS, but no significant superiority was found among new-generation ALK-TKIs except for comparison with ceritinib. However, ld-alectinib performed better than lorlatinib among smokers, with ld-alectinib ranking first, followed by lorlatinib, brigatinib, hd-alectinib, ceritinib, ensartinib, crizotinib, and chemotherapy. Moreover, ld-alectinib was significantly superior to ensartinib, brigatinib, ceritinib, crizotinib, and chemotherapy. Given the limitations of this meta-analysis, further research focusing on the smoking status is needed to verify these conclusions.

DATA AVAILABILITY STATEMENT

The original contributions presented in the study are included in the article/**Supplementary Material**, further inquiries can be directed to the corresponding authors.

AUTHOR CONTRIBUTIONS

KL, JL, and ZH: study design. KL and JL: literature searching and extraction of data. ZH, QY, and JC: rechecking data. KL, JL, and JF: data analysis. KL and MK: writing-original draft. JB and YY: writing-review and editing, and study supervision. All authors contributed to the article and approved the submitted version.

FUNDING

This work was supported by the Key Clinical Technology of Guangzhou (Grant no. 2019ZD17).

ACKNOWLEDGMENTS

We sincerely thank the support from all participants.

SUPPLEMENTARY MATERIAL

The Supplementary Material for this article can be found online at: https://www.frontiersin.org/articles/10.3389/fphar.2022.881493/full#supplementary-material

REFERENCES

Aisner, D. L., Sholl, L. M., Berry, L. D., Rossi, M. R., Chen, H., Fujimoto, J., et al. (2017). The Impact of Smoking and TP_{53} Mutations in Lung Adenocarcinoma Patients with Targetable Mutations-The Lung Cancer Mutation Consortium ($LCMC_2$). *Clin. Cancer Res.* 24, 1038–1047. doi:10.1158/1078-0432.ccr-17-2289

Ando, K., Manabe, R., Kishino, Y., Kusumoto, S., Yamaoka, T., Tanaka, A., et al. (2021). Comparative Efficacy and Safety of Lorlatinib and Alectinib for ALK-Rearrangement Positive Advanced Non-small Cell Lung Cancer in Asian and Non-asian Patients: A Systematic Review and Network Meta-Analysis. *Cancers (Basel)* 13, 3704. doi:10.3390/cancers13153704

Bossé, Y., and Amos, C. I. (2017). A Decade of GWAS Results in Lung Cancer. *Cancer Epidemiol. Biomarkers Prev.* 27, 363–379. doi:10.1158/1055-9965.epi-16-0794

Breadner, D., Blanchette, P., Shanmuganathan, S., Boldt, R. G., and Raphael, J. (2020). Efficacy and Safety of ALK Inhibitors in ALK-Rearranged Non-small Cell Lung Cancer: A Systematic Review and Meta-Analysis. *Lung Cancer* 144, 57–63. doi:10.1016/j.lungcan.2020.04.011

Britschgi, C., Addeo, A., Rechsteiner, M., Delaloye, R., Früh, M., Metro, G., et al. (2020). Real-World Treatment Patterns and Survival Outcome in Advanced Anaplastic Lymphoma Kinase (ALK) Rearranged Non-small-cell Lung Cancer Patients. *Front. Oncol.* 10, 1299. doi:10.3389/fonc.2020.01299

Camidge, D. R., Kim, H. R., Ahn, M. J., Yang, J. C. H., Han, J. Y., Hochmair, M. J., et al. (2021). Brigatinib versus Crizotinib in ALK Inhibitor-Naive Advanced ALK-Positive NSCLC: Final Results of Phase 3 ALTA-1L Trial. *J. Thorac. Oncol.* 16, 2091–2108. doi:10.1016/j.jtho.2021.07.035

Cancer today (2022). Global Cancer Observatory. Available at: https://gco.iarc.fr/today/home (Accessed February 17, 2022).

Chen, D. L., Li, Q. Y., and Tan, Q. Y. (2021). Smoking History and the Efficacy of Immune Checkpoint Inhibitors in Patients with Advanced Non-small Cell Lung Cancer: a Systematic Review and Meta-Analysis. *J. Thorac. Dis.* 13, 220–231. doi:10.21037/jtd-20-1953

Chuang, C. H., Chen, H. L., Chang, H. M., Tsai, Y. C., Wu, K. L., Chen, I. H., et al. (2021). Systematic Review and Network Meta-Analysis of Anaplastic Lymphoma Kinase (ALK) Inhibitors for Treatment-Naïve ALK-Positive Lung Cancer. *Cancers (Basel)* 13, 1966. doi:10.3390/cancers13081966

Ding, L., Getz, G., Wheeler, D. A., Mardis, E. R., McLellan, M. D., Cibulskis, K., et al. (2008). Somatic Mutations Affect Key Pathways in Lung Adenocarcinoma. *Nature* 455, 1069–1075. doi:10.1038/nature07423

El Darsa, H., Abdel-Rahman, O., and Sangha, R. (2020). Pharmacological and Clinical Properties of Lorlatinib in the Treatment of ALK-Rearranged Advanced Non-small Cell Lung Cancer. *Expert Opin. Pharmacother.* 21, 1547–1554. doi:10.1080/14656566.2020.1774552

Gelman, A., and Rubin, D. B. (1992). Inference from Iterative Simulation Using Multiple Sequences. *Statist. Sci.* 7. doi:10.1214/ss/1177011136

Gemine, R., and Lewis, K. (2016). Smoking Cessation With Lung Cancer: not Too Little, Never Too Late. *EMJ Respir.* 4, 86

Guidelines Detail (2022). National Comprehensive Cancer Network. Available at: https://www.nccn.org/guidelines/guidelines-detail?category=1&id=1450 (Accessed February 17, 2022).

Guyatt, G. H., Oxman, A. D., Vist, G. E., Kunz, R., Falck-Ytter, Y., Alonso-Coello, P., et al. (2008). GRADE: an Emerging Consensus on Rating Quality of Evidence and Strength of Recommendations. *BMJ* 336, 924–926. doi:10.1136/bmj.39489.470347.ad

Higgins, J. P., Altman, D. G., Gøtzsche, P. C., Jüni, P., Moher, D., Oxman, A. D., et al. (2011). The Cochrane Collaboration's Tool for Assessing Risk of Bias in Randomised Trials. *BMJ* 343, d5928. doi:10.1136/bmj.d5928

Horn, L., Wang, Z., Wu, G., Poddubskaya, E., Mok, T., Reck, M., et al. (2021). Ensartinib vs Crizotinib for Patients with Anaplastic Lymphoma Kinase-Positive Non-small Cell Lung Cancer: A Randomized Clinical Trial. *JAMA Oncol.* 7, 1617–1625. doi:10.1001/jamaoncol.2021.3523

Hutton, B., Salanti, G., Caldwell, D. M., Chaimani, A., Schmid, C. H., Cameron, C., et al. (2015). The PRISMA Extension Statement for Reporting of Systematic Reviews Incorporating Network Meta-Analyses of Health Care Interventions: Checklist and Explanations. *Ann. Intern. Med.* 162, 777–784. doi:10.7326/m14-2385

Jin, Y., Chen, Y., Yu, X., and Shi, X. (2018). A Real-World Study of Treatment Patterns and Survival Outcome in Advanced Anaplastic Lymphoma Kinase-Positive Non-small-cell Lung Cancer. *Oncol. Lett.* 15, 8703–8710. doi:10.3892/ol.2018.8444

Johnson, T. W., Richardson, P. F., Bailey, S., Brooun, A., Burke, B. J., Collins, M. R., et al. (2014). Discovery of (10R)-7-Amino-12-Fluoro-2,10,16-Trimethyl-15-Oxo-10,15,16,17-Tetrahydro-2h-8,4-(metheno)pyrazolo[4,3-H][2,5,11]-Benzoxadiazacyclotetradecine-3-Carbonitrile (PF-06463922), a Macrocyclic Inhibitor of Anaplastic Lymphoma Kinase (ALK) and C-Ros Oncogene 1 (ROS1) with Preclinical Brain Exposure and Broad-Spectrum Potency against ALK-Resistant Mutations. *J. Med. Chem.* 57, 4720–4744. doi:10.1021/jm500261q

Jung, K. J., Jeon, C., and Jee, S. H. (2016). Smoking Effect on Lung Cancer: Ethnic Difference and Smoking Paradox. *Epidemiol. Health* 38, e2016060. doi:10.4178/epih.e2016060

Kron, A., Alidousty, C., Scheffler, M., Merkelbach-Bruse, S., Seidel, D., Riedel, R., et al. (2018). Impact of TP53 Mutation Status on Systemic Treatment Outcome in ALK-Rearranged Non-small-cell Lung Cancer. *Ann. Oncol.* 29, 2068–2075. doi:10.1093/annonc/mdy333

Kuang, S., and Leighl, N. B. (2021). Lorlatinib in ALK-Rearranged Lung Cancer. *Cancer Cell* 39, 25–27. doi:10.1016/j.ccell.2020.12.017

Le Calvez, F., Mukeria, A., Hunt, J. D., Kelm, O., Hung, R. J., Tanière, P., et al. (2005). TP53 and KRAS Mutation Load and Types in Lung Cancers in Relation to Tobacco Smoke: Distinct Patterns in Never, Former, and Current Smokers. *Cancer Res.* 65, 5076–5083. doi:10.1158/0008-5472.can-05-0551

Li, X., Huang, C., Xie, X., Wu, Z., Tian, X., Wu, Y., et al. (2020). The Impact of Smoking Status on the Progression-free Survival of Non-small Cell Lung Cancer Patients Receiving Molecularly Target Therapy or Immunotherapy versus Chemotherapy: A Meta-Analysis. *J. Clin. Pharm. Ther.* 46, 256–266. doi:10.1111/jcpt.13309

Li, Y., Xiao, X., Han, Y., Gorlova, O., Qian, D., Leighl, N., et al. (2017). Genome-wide Interaction Study of Smoking Behavior and Non-small Cell Lung Cancer Risk in Caucasian Population. *Carcinogenesis* 39, 336–346. doi:10.1093/carcin/bgx113

Lin, L., Zhao, J., Hu, J., Zou, G., Huang, F., Han, J., et al. (2018). Current Smoking Has a Detrimental Effect on Survival for Epidermal Growth Factor Receptor (EGFR) and Anaplastic Lymphoma Kinase (ALK) Negative Advanced Non-squamous Non-small Cell Lung Cancer (NSCLC) Patients Treated with Pemetrexed Continuation Maintenance. *J. Cancer* 9, 2140–2146. doi:10.7150/jca.24872

Loeb, L. A., Ernster, V. L., Warner, K. E., Abbotts, J., and Laszlo, J. (1984). Smoking and Lung Cancer: an Overview. *Cancer Res.* 44, 5940

Mok, T., Camidge, D. R., Gadgeel, S. M., Rosell, R., Dziadziuszko, R., Kim, D. W., et al. (2020). Updated Overall Survival and Final Progression-free Survival Data for Patients with Treatment-Naive Advanced ALK-Positive Non-small-cell Lung Cancer in the ALEX Study. *Ann. Oncol.* 31, 1056–1064. doi:10.1016/j.annonc.2020.04.478

Nakagawa, K., Hida, T., Nokihara, H., Morise, M., Azuma, K., Kim, Y. H., et al. (2020). Final Progression-free Survival Results from the J-ALEX Study of Alectinib versus Crizotinib in ALK-Positive Non-small-cell Lung Cancer. *Lung Cancer* 139, 195–199. doi:10.1016/j.lungcan.2019.11.025

Neupane, B., Richer, D., Bonner, A. J., Kibret, T., and Beyene, J. (2014). Network Meta-Analysis Using R: A Review of Currently Available Automated Packages. *PLoS ONE* 9, e115065. doi:10.1371/journal.pone.0115065

Nie, R. C., Duan, J. L., Liang, Y., Chen, X. J., Chen, Y. M., Luo, T. Q., et al. (2020). Smoking Status-Based Efficacy Difference in Anti-PD-1/pd-L1 Immunotherapy: a Systematic Review and Meta-Analysis. *Immunotherapy* 12, 1313–1324. doi:10.2217/imt-2020-0007

Oravecz, Z., and Muth, C. (2017). Fitting Growth Curve Models in the Bayesian Framework. *Psychon. Bull. Rev.* 25, 235–255. doi:10.3758/s13423-017-1281-0

Page, M. J., McKenzie, J. E., Bossuyt, P. M., Boutron, I., Hoffmann, T. C., Mulrow, C. D., et al. (2021). The PRISMA 2020 Statement: an Updated Guideline for Reporting Systematic Reviews. *BMJ* 372, n71. doi:10.1136/bmj.n71

Puhan, M. A., Schünemann, H. J., Murad, M. H., Li, T., Brignardello-Petersen, R., Singh, J. A., et al. (2014). A GRADE Working Group Approach for Rating the Quality of Treatment Effect Estimates from Network Meta-Analysis. *BMJ* 349, g5630. doi:10.1136/bmj.g5630

Salanti, G., Ades, A. E., and Ioannidis, J. P. (2011). Graphical Methods and Numerical Summaries for Presenting Results from Multiple-Treatment

Meta-Analysis: an Overview and Tutorial. *J. Clin. Epidemiol.* 64, 163–171. doi:10.1016/j.jclinepi.2010.03.016

Seto, T., Kiura, K., Nishio, M., Nakagawa, K., Maemondo, M., Inoue, A., et al. (2013). CH5424802 (RO5424802) for Patients with ALK-Rearranged Advanced Non-small-cell Lung Cancer (AF-001JP Study): a Single-Arm, Open-Label, Phase 1-2 Study. *Lancet Oncol.* 14, 590–598. doi:10.1016/s1470-2045(13)70142-6

Shaw, A. T., Bauer, T. M., de Marinis, F., Felip, E., Goto, Y., Liu, G., et al. (2020). First-Line Lorlatinib or Crizotinib in Advanced ALK-Positive Lung Cancer. *N. Engl. J. Med.* 383, 2018–2029. doi:10.1056/nejmoa2027187

Shaw, A. T., and Engelman, J. A. (2013). ALK in Lung Cancer: Past, Present, and Future. *J. Clin. Oncol.* 31, 1105–1111. doi:10.1200/jco.2012.44.5353

Singal, G., Miller, P. G., Agarwala, V., Li, G., Kaushik, G., Backenroth, D., et al. (2019). Association of Patient Characteristics and Tumor Genomics with Clinical Outcomes Among Patients with Non-small Cell Lung Cancer Using a Clinicogenomic Database. *JAMA* 321, 1391–1399. doi:10.1001/jama.2019.3241

Solomon, B. J., Besse, B., Bauer, T. M., Felip, E., Soo, R. A., Camidge, D. R., et al. (2018). Lorlatinib in Patients with ALK-Positive Non-small-cell Lung Cancer: Results from a Global Phase 2 Study. *Lancet Oncol.* 19, 1654–1667. doi:10.1016/s1470-2045(18)30649-1

Solomon, B. J., Mok, T., Kim, D.-W., Wu, Y.-L., Nakagawa, K., Mekhail, T., et al. (2014). First-Line Crizotinib versus Chemotherapy in ALK-Positive Lung Cancer. *N. Engl. J. Med.* 371, 2167–2177. doi:10.1056/nejmoa1408440

Soria, J. C., Tan, D. S. W., Chiari, R., Wu, Y. L., Paz-Ares, L., Wolf, J., et al. (2017). First-line Ceritinib versus Platinum-Based Chemotherapy in Advanced ALK-Rearranged Non-small-cell Lung Cancer (ASCEND-4): a Randomised, Open-Label, Phase 3 Study. *Lancet* 389, 917–929. doi:10.1016/s0140-6736(17)30123-x

Thai, A. A., Solomon, B. J., Sequist, L. V., Gainor, J. F., and Heist, R. S. (2021). Lung Cancer. *The Lancet* 398, 535–554. doi:10.1016/s0140-6736(21)00312-3

Tonin, F. S., Rotta, I., Mendes, A. M., and Pontarolo, R. (2017). Network Meta-Analysis: a Technique to Gather Evidence from Direct and Indirect Comparisons. *Pharm. Pract. (Granada)* 15, 943. doi:10.18549/pharmpract.2017.01.943

Wang, L., Sheng, Z., Zhang, J., Song, J., Teng, L., Liu, L., et al. (2021). Comparison of Lorlatinib, Alectinib and Brigatinib in ALK Inhibitor-Naive/untreated ALK-Positive Advanced Non-small-cell Lung Cancer: a Systematic Review and Network Meta-Analysis. *J. Chemother.* 34, 1–10. doi:10.1080/1120009x.2021.1937782

Wang, Y., Ji, M., Zhu, M., Fan, J., Xie, J., Huang, Y., et al. (2021). Genome-wide Gene-Smoking Interaction Study Identified Novel Susceptibility Loci for Non-small Cell Lung Cancer in Chinese Populations. *Carcinogenesis* 42, 1154–1161. doi:10.1093/carcin/bgab064

Wu, H. Y., Huang, J. W., Lin, H. J., Liao, W. C., Peng, Y. S., Hung, K. Y., et al. (2013). Comparative Effectiveness of Renin-Angiotensin System Blockers and Other Antihypertensive Drugs in Patients with Diabetes: Systematic Review and Bayesian Network Meta-Analysis. *BMJ* 347, f6008. doi:10.1136/bmj.f6008

Wu, Y. L., Lu, S., Lu, Y., Zhou, J., Shi, Y. K., Sriuranpong, V., et al. (2018). Results of PROFILE 1029, a Phase III Comparison of First-Line Crizotinib versus Chemotherapy in East Asian Patients with ALK-Positive Advanced Non-small Cell Lung Cancer. *J. Thorac. Oncol.* 13, 1539–1548. doi:10.1016/j.jtho.2018.06.012

Xiao, J., Zhou, L., He, B., and Chen, Q. (2020). Impact of Sex and Smoking on the Efficacy of EGFR-TKIs in Terms of Overall Survival in Non-small-cell Lung Cancer: A Meta-Analysis. *Front. Oncol.* 10, 1531. doi:10.3389/fonc.2020.01531

Yoda, S., Lin, J. J., Lawrence, M. S., Burke, B. J., Friboulet, L., Langenbucher, A., et al. (2018). Sequential ALK Inhibitors Can Select for Lorlatinib-Resistant Compound ALK Mutations in ALK-Positive Lung Cancer. *Cancer Discov.* 8, 714–729. doi:10.1158/2159-8290.cd-17-1256

Zhao, W., Jiang, W., Wang, H., He, J., Su, C., and Yu, Q. (2021). Impact of Smoking History on Response to Immunotherapy in Non-small-cell Lung Cancer: A Systematic Review and Meta-Analysis. *Front. Oncol.* 11, 703143. doi:10.3389/fonc.2021.703143

Zhou, C., Kim, S. W., Reungwetwattana, T., Zhou, J., Zhang, Y., He, J., et al. (2019). Alectinib versus Crizotinib in Untreated Asian Patients with Anaplastic Lymphoma Kinase-Positive Non-small-cell Lung Cancer (ALESIA): a Randomised Phase 3 Study. *Lancet Respir. Med.* 7, 437–446. doi:10.1016/s2213-2600(19)30053-0

Zou, H. Y., Friboulet, L., Kodack, D. P., Engstrom, L. D., Li, Q., West, M., et al. (2015). PF-06463922, an ALK/ROS1 Inhibitor, Overcomes Resistance to First and Second Generation ALK Inhibitors in Preclinical Models. *Cancer Cell* 28, 70–81. doi:10.1016/j.ccell.2015.05.010

Conflict of Interest: The authors declare that the research was conducted in the absence of any commercial or financial relationships that could be construed as a potential conflict of interest.

frontiers | Frontiers in Pharmacology

ORIGINAL RESEARCH
published: 20 May 2022
doi: 10.3389/fphar.2022.900699

Integrative Pan-Cancer Analysis Confirmed that FCGR3A is a Candidate Biomarker Associated With Tumor Immunity

*Lilin Li[1†], Zijian Huang[1†], Kunpeng Du[2], Xiang Liu[1], Chunhui Li[1], Duanyu Wang[1], Yangfeng Zhang[1], Changqian Wang[1] and Jiqiang Li[1,2]**

[1]Department of Radiation Oncology, Oncology Center, Zhujiang Hospital of Southern Medical University, Guangzhou, China, [2]Department of Oncology, The First Affiliated Hospital of Guangdong Pharmaceutical University, Guangzhou, China

OPEN ACCESS

Edited by:
Clare Y. Slaney,
Peter MacCallum Cancer Centre, Australia

Reviewed by:
Qiushi Feng,
China Pharmaceutical University, China
Yuting Hua,
Wuxi Huishan District People's Hospital, China

***Correspondence:**
Jiqiang Li
ljq821028@126.com
orcid.org/0000-0002-585-5911

[†]These authors have contributed equally to this work

Specialty section:
This article was submitted to Pharmacology of Anti-Cancer Drugs, a section of the journal Frontiers in Pharmacology

Received: 21 March 2022
Accepted: 18 April 2022
Published: 20 May 2022

Citation:
Li L, Huang Z, Du K, Liu X, Li C, Wang D, Zhang Y, Wang C and Li J (2022) Integrative Pan-Cancer Analysis Confirmed that FCGR3A is a Candidate Biomarker Associated With Tumor Immunity. Front. Pharmacol. 13:900699. doi: 10.3389/fphar.2022.900699

Background: Fc gamma receptor 3A (FCGR3A) encodes a receptor for the Fc portion of immunoglobulin G, which plays a significant role in the immune response. However, the role of FCGR3A in cancers remains unclear. This study aimed to visualize the prognostic landscape of FCGR3A in pan-cancer and investigate the relationship between FCGR3A expression and tumor microenvironment.

Method: Based on the TCGA database, GTEx database, and GDSC database, we analyzed the expression of FCGR3A in pan-cancers and adjacent normal tissues and its relationship with prognosis, immune cells infiltration, immune-related genes, DNA mismatch repair (MMR) genes, DNA methylation, and drugs sensitivity. The gene alteration frequency of FCGR3A was acquired on the cBioportal website. Moreover, we constructed PPI networks, performed GO and KEGG analysis to illustrate the function, and signaling pathways of FCGR3A-related genes, and conducted gene set enrichment analysis (GSEA) of FCGR3A to further explore its potential biological functions.

Result: The differential analysis results of the publicly available databases showed that FCGR3A was generally highly expressed in pan-cancer. Survival analysis revealed that FCGR3A predominated as a risk prognostic factor in most cancers. Additionally, the expression of FCGR3A was confirmed to be associated with several immune cells infiltration, multiple immune checkpoint genes, and DNA mismatch repair genes expression in generalized carcinoma. We also identified a negative correlation between FCGR3A and DNA methylation levels. Through GO/KEGG and GESA, we found that FCGR3A was involved in many pathologic and physiological processes, and was most closely related to tumor immune-related pathways. Drug sensitivity analysis showed that higher FCGR3A expression predicts a low IC50 value for the vast majority of drugs.

Conclusions: FCGR3A may be an immune-oncogenic molecule that correlates with tumor immune infiltration levels and affects drug sensitivity, thus it can be served as a promising biomarker for cancer detection, prognosis, therapeutic design, and follow-up.

Keywords: pan-cancer analysis, FCGR3A, tumor biomarker, immune infiltration, tumor microenvironment, prognosis, drug sensitivity

INTRODUCTION

Malignant tumor is one of the main causes of death in the world and a major obstacle affecting the quality of human life. So far, there is no absolute cure for cancer (Bray et al., 2018). Tumor biomarkers can be used for early detection, diagnosis, therapeutic targets, response prediction, treatment monitoring, prognosis determination, and personalized combination therapy. More and more tumor biomarkers, such as PD-L1, BRCA1/2, BRAF, HER2, etc., have been discovered, which become an indispensable tool in current tumor treatment due to its ability to assist various clinical decisions (Zhou et al., 2015). However, most targeted or immunotherapy has limited efficacy, so it is necessary to discover more tumor markers and study their role and value in generalized cancer, evaluate their correlation with clinical prognosis and related signaling pathways, in order to accurately predict prognosis and provide options for tumor treatment.

There are two FcγRIII genes in the human genome, one encodes FcγRIIIa and the other encodes FcγRIIIb. These two proteins share 97% homology at the amino acid level (Gessner et al., 1995). FCGR3A gene encodes the FcγRIIIa receptor in most effector cells such as macrophages, NK, and γδ T cells, and possesses a low affinity for IgG-containing immune complexes (IC). Human FcγRIIIa (CD16a), a type I transmembrane protein, is an extensively glycosylated heterogeneous protein, the Fc-fragment is recognized through loops of the C-terminal receptor domain of the FcγRIII, transmitting activating signals in effector cells (Sondermann et al., 2001). Mutations in the FCGR3A gene are linked to recurrent viral infections, susceptibility to systemic lupus erythematosus, and alloimmune neonatal neutropenia (Cartron et al., 1991; Patel et al., 2020).

FCGR3A is involved in the removal of antigen-antibody complexes from the circulation, as well as other antibody-dependent responses (Vance et al., 1993; Hargreaves et al., 2015). Activation of FcγRIIIa on NK cells plays a key role in mediating antibody-dependent cell-mediated cytotoxicity (ADCC), while activation of FcγRIIIa on macrophages is important in mediating antibody-dependent cellular phagocytosis (ADCP) (Morvan and Lanier, 2016), which are the innate immune mechanism that eliminates cancer cells. They can be used to treat a variety of cancers that overexpress unique antigens, such as neuroblastoma, breast cancer, B cell lymphoma, etc. (Pandey and Namboodiri, 2014; Ziakas et al., 2016; Musolino et al., 2022)

In addition, there is a G559T polymorphism in the FCGR3A gene, whose two common alleles encode two variants that differ at position 158, one Val (V158) or one Phe (F158). The binding affinity of FcγRIIIa to IgG varies with allele variants. Specifically, FcγRIIIa-V158 has a higher affinity to human IgG1 and IgG3 than does FcγRIIIa-158F, this stronger binding affinity results in more potent *in vitro* ADCC and tumor cell death (Koene et al., 1997). ADCC is a key effector mechanism of NK cells mediated by therapeutic monoclonal antibody (mAb). Better clinical outcomes have been observed in patients expressing high-affinity FcγRIIIa variant (V158) when they were treated with anti-CD20 or anti-EGFR antibodies (Veeramani et al., 2011). An over-representation of the FcγRIIIa-158F allele has been reported as a major risk factor for patients with systemic lupus erythematosus (SLE) (Edberg et al., 2002). In addition, FcγRIIIa polymorphisms influence clinical outcomes in colorectal cancer, squamous cell head and neck cancer, and ERBB2/HER2-positive breast cancer patients treated with anti-epidermal growth factor receptor (EGFR) antibodies such as rituximab, cetuximab, and trastuzumab: Patients with FCGR3A-157V/V genotypes had significantly longer survival (Calemma et al., 2012; Gavin et al., 2017; Magnes et al., 2018).

Although the FCGR3A-158 V-F polymorphism impacts multiple autoimmune and infectious diseases and affects the response of monoclonal therapy (mAb) in some tumor patients, there is insufficient scientific evidence regarding the pathogenic role of FCGR3A in diverse cancers and whether FCGR3A functions in the immune microenvironment of different tumors through certain common molecular mechanisms.

It is well known that cancer is a genetic disease, and even when patients are affected by apparently the same type of cancer, the mutant signature of the cancer type can vary from patient to patient. These genetic changes may affect the efficacy of anticancer drugs and affect the clinical response in tumor patients. For example, Venetoclax is effective in small cell lung cancer with high bcl-2 expression (Lochmann et al., 2018). However, for the vast majority of tumor types and available therapeutic agents, the genotype-phenotypic association between gene expression differences and anticancer drug responses is not simple (Vuong et al., 2014). Therefore, in this study, we used multiple databases to analyze FCGR3A gene expression, prognosis, immune infiltration correlation, and epigenetic status in pan-cancer, and to explore the underlying molecular mechanisms and its relationship with drug sensitivity, so as to evaluate the impact of FCGR3A on the tumor microenvironment.

MATERIALS AND METHODS

Expression Analysis of FCGR3A in Pan-Cancer

The expression difference of the FCGR3A gene in pan-cancer and their adjacent normal tissues were analyzed using the Sangerbox website (http://sangerbox.com/). Sangerbox is an open network containing tumor and normal samples data from The Cancer Genome Atlas (TCGA) (https://portal.gdc.cancer.gov/) and the Genotype-Tissue Expression (GTEx) database (https://gtexportal.org/). To further evaluate FCGR3A expression in pan-cancer, we also using Tumor Immune Estimate Resources (TIMER2.0) (http://timer.cistrome.org/) and Gene Expression Profiling Interactive Analysis (GEPIA2) (http://gepia2.cancer-pku.cn/#analysis) web server to obtain the FCGR3A expression prospect in TCGA datasets. In order to identify the tumor cell types in which FCGR3A is predominantly expressed, we downloaded the FCGR3A gene

expression data in 886 tumor cell lines from the Genomics of Drug Sensitivity in Cancer (GDSC) database (https://www.cancerrxgene.org/). The R packages "ggplot2" and "ggpubr" were used to analyze and compare the expression of FCGR3A in different tumor cell lines. FCGR3A gene expression levels in pan-cancer single-cell samples were also obtained through the cancerSCEM website (https://ngdc.cncb.ac.cn/cancerscem/). In addition, the expression of FCGR3A at the protein level in different tumors was analyzed in the Clinical Proteomic Tumor Analysis Consortium (CPTAC) (https://pdc.cancer.gov/pdc/browse) and the Human Protein Atlas (HPA) database (http://www.proteinatlas.org/). The criterion for classifying tumor samples into high and low expression was the median FCGR3A expression. Kruskal-Wallis rank-sum test was applied to statistical analysis, with $p < 0.05$ being deemed statistically significant.

Survival Prognosis Analysis

Expression data of various genes in pan-cancer were obtained from TCGA database and the GTEx database by UCSC Xena (http://xenabrowser.net/datapages/). Extraction of FCGR3A single-gene expression data with Strawberry Perl (http://strawberryperl.com/). Survival data also downloaded from UCSC Xena. To determine the relationship between expression of FCGR3A and survival prognosis, R package "survival" was performed to determine the correlation between FCGR3A mRNA expression with overall survival (OS), disease specific survival (DSS) and progression-free survival (PFS), and univariate Cox regression analysis was used as statistical method. It was described as forest plots using the R package "forestplot". Furthermore, we used the "Stage Plot " module of the GEPIA2 website to obtain violin plots of FCGR3A expression in all TCGA tumors at different pathological stages.

Immunological Correlation Analysis

Using the TIMER2.0 web server (http://timer.cistrome.org/) to acquire the correlation data of FCGR3A expression with infiltrating immune cells and the abundance of immune cell markers from the TCGA pan-cancer. The expression status of immune-related genes (including immunosuppressive genes and chemokines) in 33 cancers was obtained from the UCSC Xena website (http://xenabrowser.net/datapages/). R package "limma" was utilized for the purpose of investigating the relationship between FCGR3A expression and the expression level of immune-related genes, and the correlation coefficient was determined by Spearman's correlation analysis. Visualization was carried out through the R "reshape2" and "RColorBreyer" packages.

Genetic Alteration and DNA Mis-Match Repair Genes Correlation Analysis

In the cBioPortal website (https://www.cbioportal.org/), select the "TCGA Pan Cancer Atlas Studies" in the "Quick select" module, FCGR3A was input to query the characteristics of genetic change and obtain the change frequency, mutation type, and CNA (copy number alteration) results of all TCGA tumors. In addition, R package "limma" was used to estimate the correlation between the FCGR3A gene and the expression of four MMRs (MLH1, MSH2, MSH6, and PMS2), and the results were visualized as correlation heat map by R packages "reshape2" and "RColorBreyer". The MMRs gene expression profiles of various tumors were derived from the TCGA database.

DNA Methylation Correlation Analysis

Based on the TCGA database, methylation levels of different tumors and their corresponding normal tissues were analyzed using the "methylation" module of the UALCAN website (http://ualcan.path.uab.edu/), and boxplots of difference analysis were downloaded. Tumor samples were divided into high- and low-expression groups based on median FCGR3A expression. On the vertical axis, beta value ranging from 0 (unmethylated) to 1 (fully methylated) represent DNA methylation levels. A beta value of 0.7–0.5 is generally considered to be hypermethylation, while a beta value of 0.3–0.25 is hypomethylation (Men et al., 2017).

FCGR3A-Related Gene Analysis

We used the STRING website (https://cn.string-db.org/) to obtain the available experimentally determined FCGR3A-binding proteins according to the following criteria: network type ("full STRING networks"), meaning of network edges ("evidence"), active interaction sources ("experiments, text mining, databases"), minimum required interaction score ["medium confidence (0.400)"], max number of interactors to show ("no more than 30 interactors" in 1st shell) and active interaction sources ("experiments"). Protein-protein interaction (PPI) networks were visualized using Cytoscape (version 3.8.2). Next, we conducted Gene Ontology (GO) and Kyoto Encyclopedia of Genes and Genomes (KEGG) enrichment analysis for the above FCGR3A-related genes using the R package "Cluster Profiler", and visualized using the "ggplot2" package.

Gene Set Enrichment Analysis of FCGR3A in Pan-Cancer

With the help of the R software package "clusterProfiler", we performed GSEA based on the GO dataset to explore the biological function of FCGR3A in tumor progression. We selected eight types of cancer whose prognosis is associated with FCGR3A expression, and use the "enrichplot" package to show the top five signaling pathways most significantly enrichment enriched in the database.

Drug Sensitivity Analysis

The data of gene expression level in pan-cancer cell lines and the drug sensitivity (IC50) of 265 compounds in these cell lines were downloaded from the Genomics of Drug Sensitivity in Cancer (GDSC) database (https://www.cancerrxgene.org/). Spearman's-correlation analysis was used to explore the correlation between drug sensitivity and FCGR3A gene

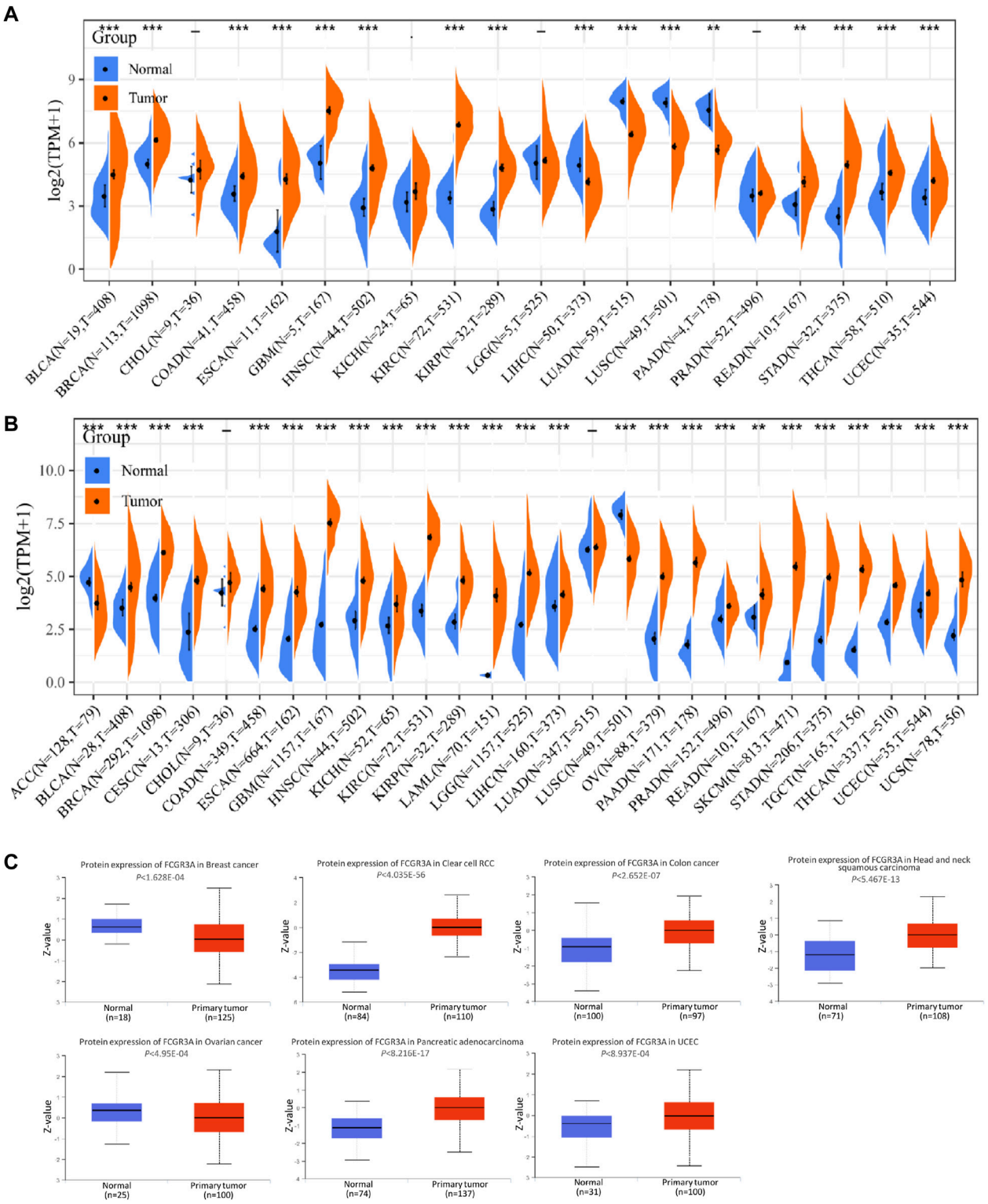

FIGURE 1 | Expression level of FCGR3A gene in pan-cancer. **(A)** FCGR3A expression levels in tumors containing 20 TCGA tissues and paired adjacent non-cancerous tissues; **(B)** FCGR3A expression difference in 27 tumors integrating data of normal tissues in GTEx database and data of tumor tissues in TCGA database; **(C)** Based on the CPTAC dataset, the expression level of FCGR3A protein in normal and primary tumor tissues was analyzed. *$p < 0.05$; **$p < 0.01$; ***$p < 0.001$.

expression in 962 cancer cell lines. Then, all cell lines were divided into low expression and high expression groups according to the median FCGR3A expression level. Kruskal-Wallis rank-sum test was used to analyze the drug sensitivity (IC50) difference of six commonly used anticancer drugs, $p < 0.05$ was considered statistically significant.

RESULTS

Expression Levels of FCGR3A in Pan-Cancer

FCGR3A mRNA expression levels were analyzed by using different databases to detect FCGR3A expression across a wide range of cancers. The differential expression profile of FCGR3A in tumor and adjacent tumor tissues was retrieved from the TCGA database, as shown in **Figure 1A**. Considering the small number of normal samples in TCGA, we integrated data from the TCGA and GTEx database to conducted FCGR3A expression differential analysis in 27 tumors (**Figure 1B**), compared with the corresponding normal group, FCGR3A was generally overexpressed in the cancer group, including bladder urothelial carcinoma (BLCA), breast invasive carcinoma (BRCA), cervical squamous cell carcinoma and endocervical adenocarcinoma (CESC), colon adenocarcinoma (COAD), esophageal carcinoma (ESCA), glioblastoma multiforme (GBM), head and neck squamous cell carcinoma (HNSC), kidney chromophobe (KICH), kidney renal clear cell carcinoma (KIRC), kidney renal papillary cell carcinoma (KIRP), acute myeloid leukemia (LAML), brain lower grade glioma (LGG), liver hepatocellular carcinoma (LIHC), ovarian serous cystadenocarcinoma (OV), pancreatic adenocarcinoma (PAAD), Prostate adenocarcinoma (PRAD), rectum adenocarcinoma (READ), skin cutaneous melanoma (SKCM), stomach adenocarcinoma (STAD), testicular germ cell tumors (TGCT), thyroid carcinoma (THCA), and uterine corpus endometrial carcinoma (UCEC) and uterine carcinosarcoma (UCS). Meanwhile, a lower expression of FCGR3A was found in adrenocortical carcinoma (ACC) and lung squamous cell carcinoma (LUSC) dataset. To further verify the above results, we applied the TIMER and GEPIA2 website to obtain the expression status of FCGR3A across various cancer types of TCGA, and both showed that FCGR3A was highly expressed in most tumor tissues (**Supplementary Figure S1**). Furthermore, to identify tumor cell types that predominantly express FCGR3A, we analyzed FCGR3A gene expression levels in pan-cancer single cell lines using the GDSC database (**Supplementary Figure S1A**) and the CancerSCEM website (**Supplementary Figure S1B**), and the results showed that FCGR3A was highly expressed in most tumor cell lines. The top 5 FCG3A-expressing tumor cell lines in the GDSC database are chronic lymphocytic leukemia (CLL), TGCT, lymphoid neoplasm diffuse large B-cell lymphoma (DLBC), LAML, and mesothelioma (MESO), while the top 5 FCG3A-expressing tumor cell lines in the CancerSCEM database are GBM, lung cancer, PRAD, LAML, and coloretal cancer (CRC). Lastly, results from the CPTAC dataset showed that FCGR3A total protein expression was higher in primary tissues of breast cancer, clear cell renal cell carcinoma, colon cancer, head and neck squamous cell carcinoma, ovarian cancer, pancreatic adenocarcinoma, and uterine corpus endometrial carcinoma than in normal tissues. (**Figure 1C**).

Moreover, to assess FCGR3A expression at the protein level, we acquired immunohistonchemistry (IHC) results from the HPA database and compared the results with FCGR3A gene expression data from TCGA. As shown in **Figures 2A–C**, the data analysis results of the two databases were consistent. Normal skin and testis tissues showed not detected staining with FCGR3A IHC, while tumor tissues showed medium staining. In contrast, normal lung tissue showed strong FCGR3A staining and lung cancer showed weak FCGR3A staining.

Prognostic Value of FCGR3A in Pan-Cancer

To evaluate the effect of FCGR3A expression on prognosis, we conducted univariate Cox regression analysis to analyze the relationship between FCGR3A expression and OS, DSS and PFS in TCGA pan-cancer. The results are presented in **Figures 3A–C**, in terms of overall survival (OS), FCGR3A was an independent risk prognostic factor in KIRC ($p = 0.026$, HR = 1.163), LGG ($p < 0.001$, HR = 1.317), thymoma (THYM) ($p = 0.026$, HR = 1.649) and uveal melanoma (UVM) ($p = 0.011$, HR = 1.326), but was a protective prognostic factor in SKCM ($p < 0.001$, HR = 0.814). Then, the analysis of disease-specific survival (DSS) revealed that FCGR3A had a detrimental role in KIRC ($p = 0.020$, HR = 1.224), LGG ($p < 0.001$, HR = 1.322) and UVM ($p = 0.019$, HR = 1.311). Meanwhile, FCGR3A played a protective role in SKCM ($p < 0.001$, HR = 0.807) and THCA ($p = 0.013$, HR = 0.320). In the analysis of progression-free survival (PFS), FCGR3A was an independent risk prognostic factor in GBM ($p = 0.023$, HR = 1.199), KIRC ($p = 0.022$, HR = 1.173), LGG ($p < 0.001$, HR = 1.274), PRAD ($p < 0.001$, HR = 1. 593) and UVM ($p = 0.016$, HR = 1.289), while was a protective prognostic factor in SKCM ($p = 0.010$, HR = 0.912). It was suggested that FCGR3A is mainly a poor prognostic indicator in KIRC, LGG and UVM, on the contrary, it is also a favorable prognostic factor in SKCM.

We also examined the differential expression of FCGR3A in patients with different tumor types based on the main pathological stage and found that FCGR3A expression was only related to tumor stage in 5 cancers, including ACC, ESCA, KICH, SKCM, and STAD (**Figure 3D**). Notably, differences in FCGR3A expression mainly occurred between stages I-II or II-III. However, we did not obtain significant differences in other tumor types.

Correlation Analysis of FCGR3A Expression and Tumor Immune Microenvironment

Tumor infiltrating immune cells are essential components of the tumor microenvironment and play a crucial role in the modulation of tumor initiate development and immune checkpoint response (Fridman et al., 2011). Here, we first analyzed the relationship between FCGR3A expression and the infiltration levels of six common immune cells (B cells, CD4+T cells, CD8+T cells, DC

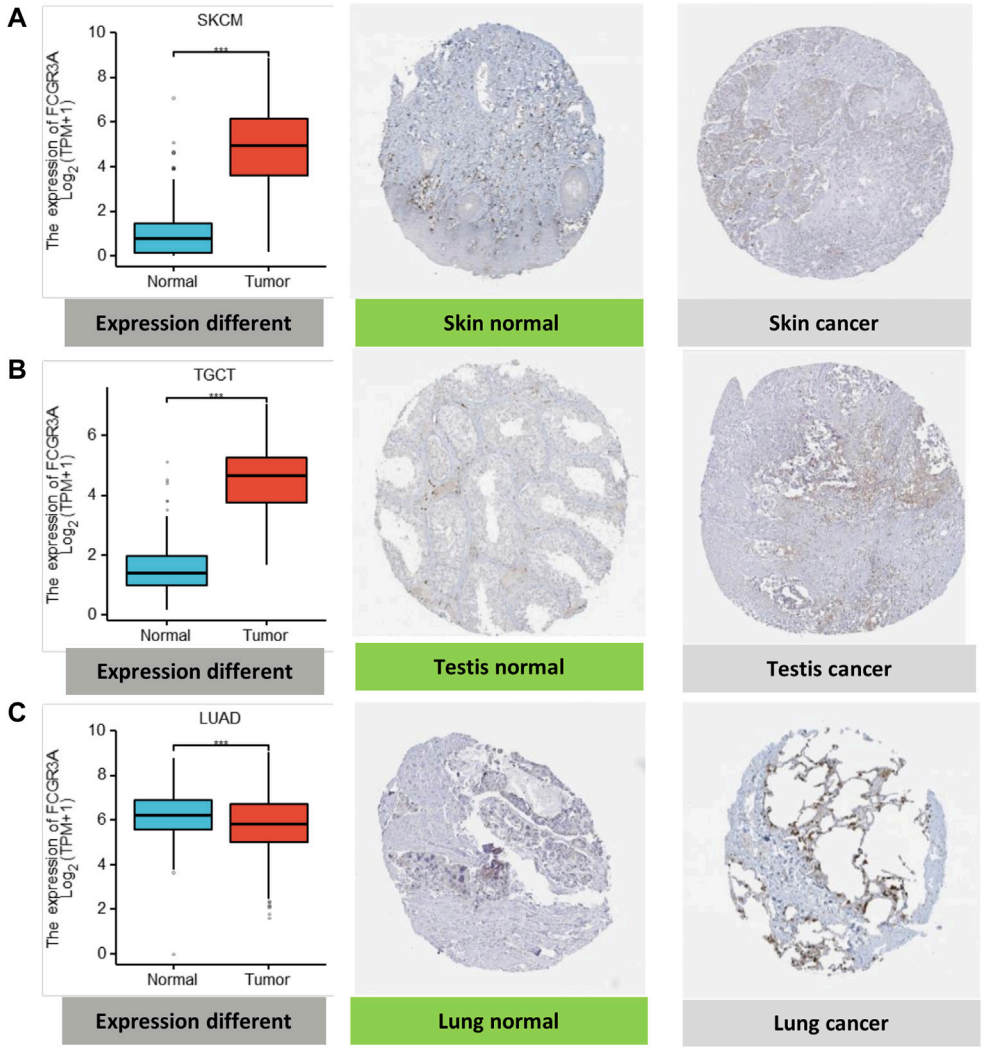

FIGURE 2 | Comparison of FCGR3A gene expression between normal and tumor tissues (left) and immunohistochemistry images in normal (middle) and tumor (right) tissues. **(A)** Skin; **(B)** Testis; **(C)** Lung. *$p < 0.05$; **$p < 0.01$; ***$p < 0.001$.

cells, macrophages, and neutrophils), and observed a positive correlation in the vast majority of tumor types. The scatter diagram of correlation analysis between FCGR3A and immune infiltrating cells of each tumor can be obtained directly through the TIMER algorithm. The four highest correlation coefficients, including CESC, COAD, KIRP, and UCEC, are illustrated in **Figure 4A**. Moreover, we also analyzed the correlation between FCGR3A expression and 25 immune cell markers to identify potential subtypes of infiltrating immune cells. As shown in **Figure 4B**, FCGR3A expression level was significantly positively correlated with most of the immune cell markers, among which macrophages, monocytes, and myeloid dendritic cells were the three immune cell types most closely related to FCGR3A expression.

Gene co-expression analysis was performed to explore the relationship between FCGR3A and the expression levels of immunosuppressive genes and chemokines in 33 TCGA-cancers. As shown in **Figure 5**, FCGR3A expression showed significant positive correlation with almost all immunosuppressive genes (**Figure 5A**) and chemokine genes (**Figure 5B**) in pan-cancer. Therefore, these results demonstrated that FCGR3A expression affects tumor immunity in different ways.

Analysis of Genetic Alteration Status of FCGR3A and the Relationship Between FCGR3A and DNA Mismatch Repair Genes

The genetic alteration status of FCGR3A in various tumor samples in the TCGA cohort is shown in **Figure 6A**. It was not difficult for us to find that "amplification" was the main mutation type in most tumors. The alteration frequency of FCGR3A was the highest in bladder urothelial carcinoma (>15%), with "amplification" accounting for >90%. All cholangiocarcinoma, liver hepatocellular carcinoma,

pancreatic adenocarcinoma pheochromocytoma and paraganglioma, diffuse large B-cell lymphoma, ovarian serous cystadenocarcinoma, thymoma, and mesothelioma cases with genetic alteration had FCGR3A amplification. The "mutation" type of FCGR3A was the dominant type in skin cutaneous melanoma, with a frequency of approximately 3%. It was noteworthy that there was a certain proportion of FCGR3A copy number deletion in stomach adenocarcinoma, prostate adenocarcinoma, and kidney renal papillary cell carcinoma.

Mismatch repair (MMR) is a post-replicative repair mechanism, which is critical for maintaining genomic fidelity (Loeb, 2001). As shown in **Figure 6B**, FCGR3A was positively correlated with the expression of four MMR genes (MLH1, MSH2, MSH6, and PMS2) in most tumor types, while FCGR3A showed negative correlation with MMR gene expression in CESC, GBM, LAML, sarcoma (SARC), mesothelioma (MESO), THCA and THYM. In addition, no statistical difference was observed in ACC, ESCA, KIRP, and pheochromocytoma and paraganglioma (PCPG) ($p > 0.05$).

Association of FCGR3A Expression With DNA Methylation

A large number of studies have demonstrated that promoter methylation leads to the inactivation of tumor suppressor genes, which is an important mechanism of tumor occurrence and development (Qureshi et al., 2010). Therefore, we used the UALCAN dataset to analyze the methylation levels of the FCGR3A promoter in different tumors and normal tissues, which determined that the methylation levels of the FCGR3A promoter in 12 tumors including BLCA, BRCA, CHOL, COAD, ESCA, HNSC, KIRC, LIHC, lung adenocarcinoma (LUAD), LUSC, PAAD, and PRAD were significantly lower than those in normal tissues (**Figures 7A–L**).

PPI Network and KEGG/GO Enrichment Analysis of FCGR3A Related Genes

In order to further explore the molecular mechanism of FCGR3A gene in tumorigenesis, we obtained a total of 30 FCGR3A targeted binding proteins by using the STRING tool.

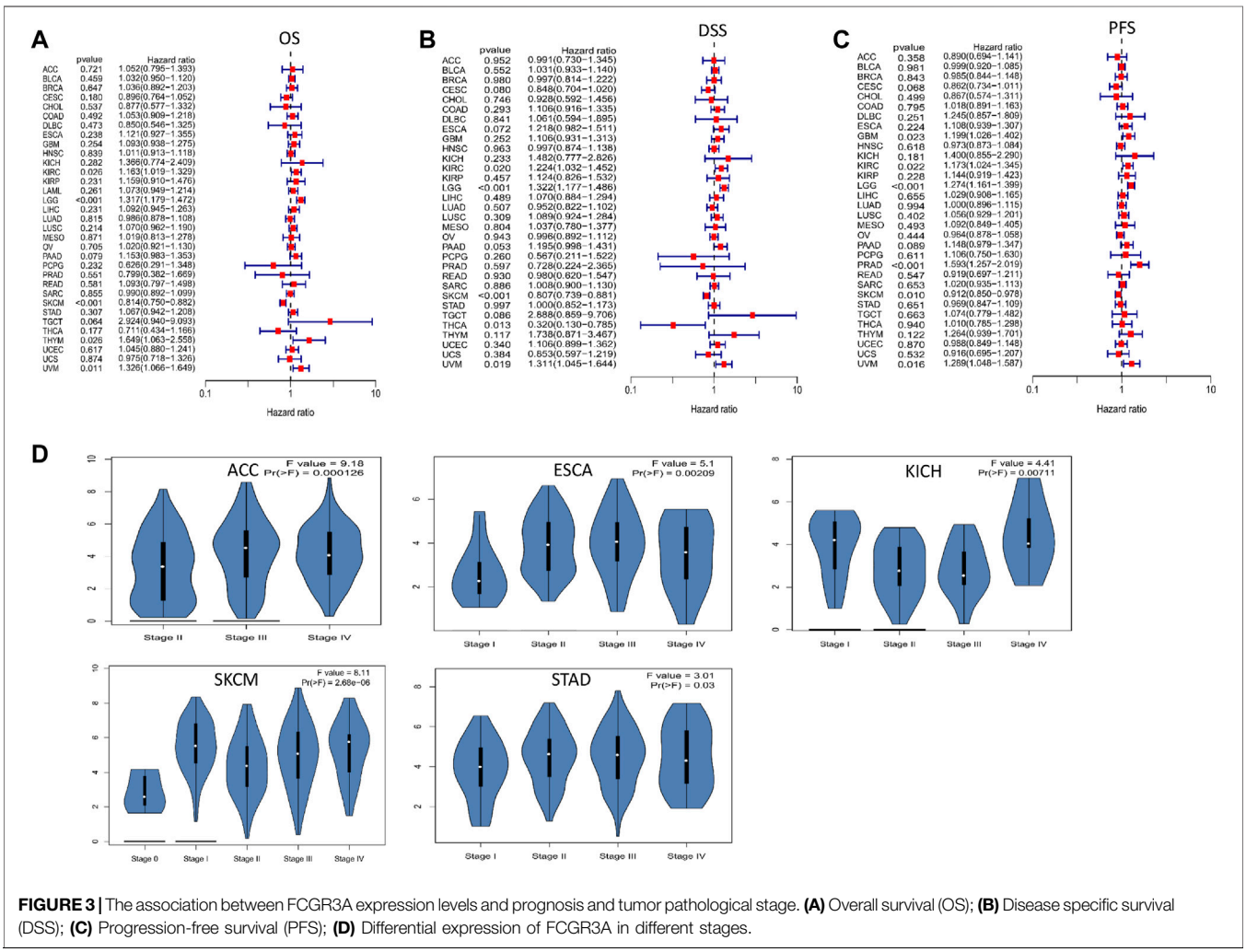

FIGURE 3 | The association between FCGR3A expression levels and prognosis and tumor pathological stage. **(A)** Overall survival (OS); **(B)** Disease specific survival (DSS); **(C)** Progression-free survival (PFS); **(D)** Differential expression of FCGR3A in different stages.

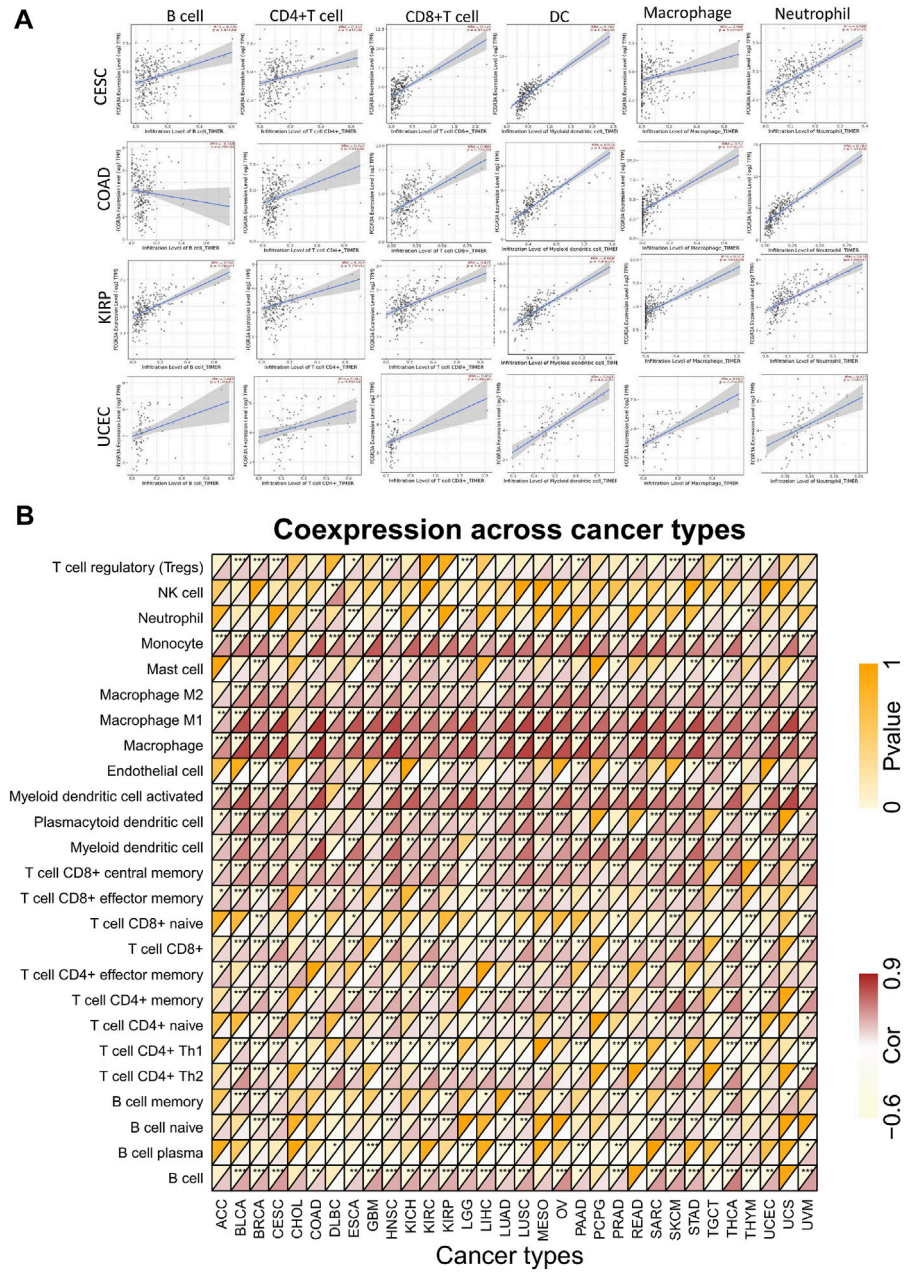

FIGURE 4 | Correlation analysis of FCGR3A expression with immune cells infiltration. **(A)** The scatter plot showed a correlation between FCGR3A and the levels of infiltration of six major immune cells in CESC, COAD, KIRP, and UCEC; **(B)** Heat map showed the relationship between FCGR3A expression and 25 immune cell markers. CESC, cervical squamous cell carcinoma and endocervical adenocarcinoma; COAD, colon adenocarcinoma; KIRP, kidney renal papillary cell carcinoma; UCEC, uterine corpus endometrial carcinoma. *$p < 0.05$; **$p < 0.01$; ***$p < 0.001$.

Figure 8A shows the interaction network of these proteins. Cytoscape software was utilized to further visualized the PPI network (**Figure 8B**). The results of GO and KEGG pathway analysis are presented in **Figures 8C,D**. The GO enrichment analysis consisted of three parts: biological process (BP), cellular component (CC), and molecular function (MF). The BP primarily included the Fc receptor signaling pathway, Fc receptor mediated stimulatory signaling pathway, Fc-gamma receptor signaling pathway, Fc-gamma receptor signaling pathway involved in phagocytosis, and immune response-regulating cell surface receptor signaling pathway involved in phagocytosis. The CC was mainly covered with cell leading edge, actin filament, site of DNA damage, site of double-strand break and Arp2/3 protein complex. The MF was primarily enriched in actin binding, actin filament binding, protein tyrosine kinase activity, phosphoprotein binding, and non-

membrane spanning protein tyrosine kinase activity. The KEGG pathway was associated with Fc gamma mediated phagocytosis, pathogenic *Escherichia coli* infection, regulation of actin cytoskeleton, *Yersinia* infection, and bacterial invasion of epithelial cells.

Correlation Between FCGR3A and Cancer Pathway

In order to observe the expression and enrichment status of FCGR3A in GO pathway sets, we divided the human tumor

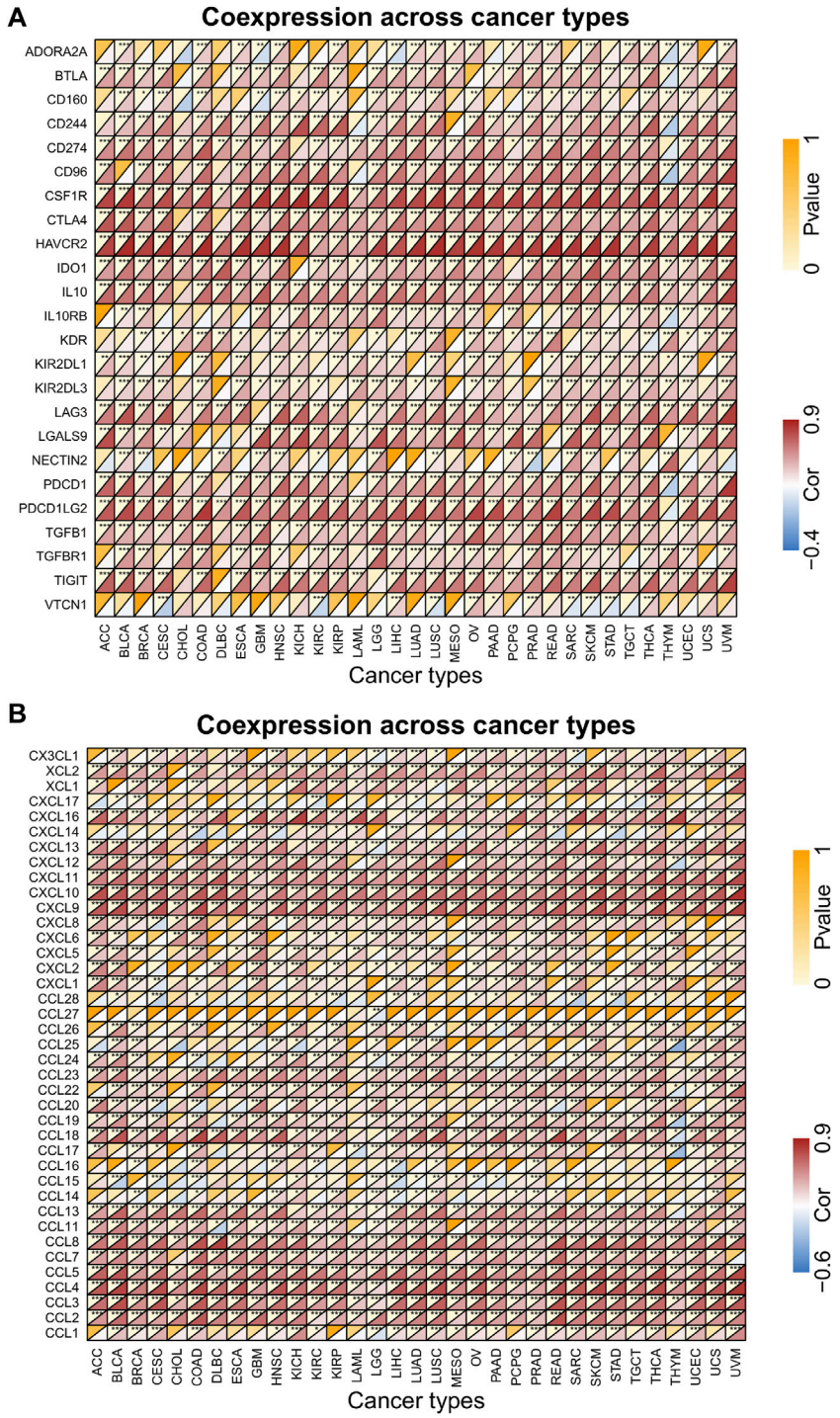

FIGURE 5 | Correlation analysis of FCGR3A expression with immune-related genes. **(A)** immunosuppressive related genes; **(B)** chemokine genes. *$p < 0.05$; **$p < 0.01$; ***$p < 0.001$.

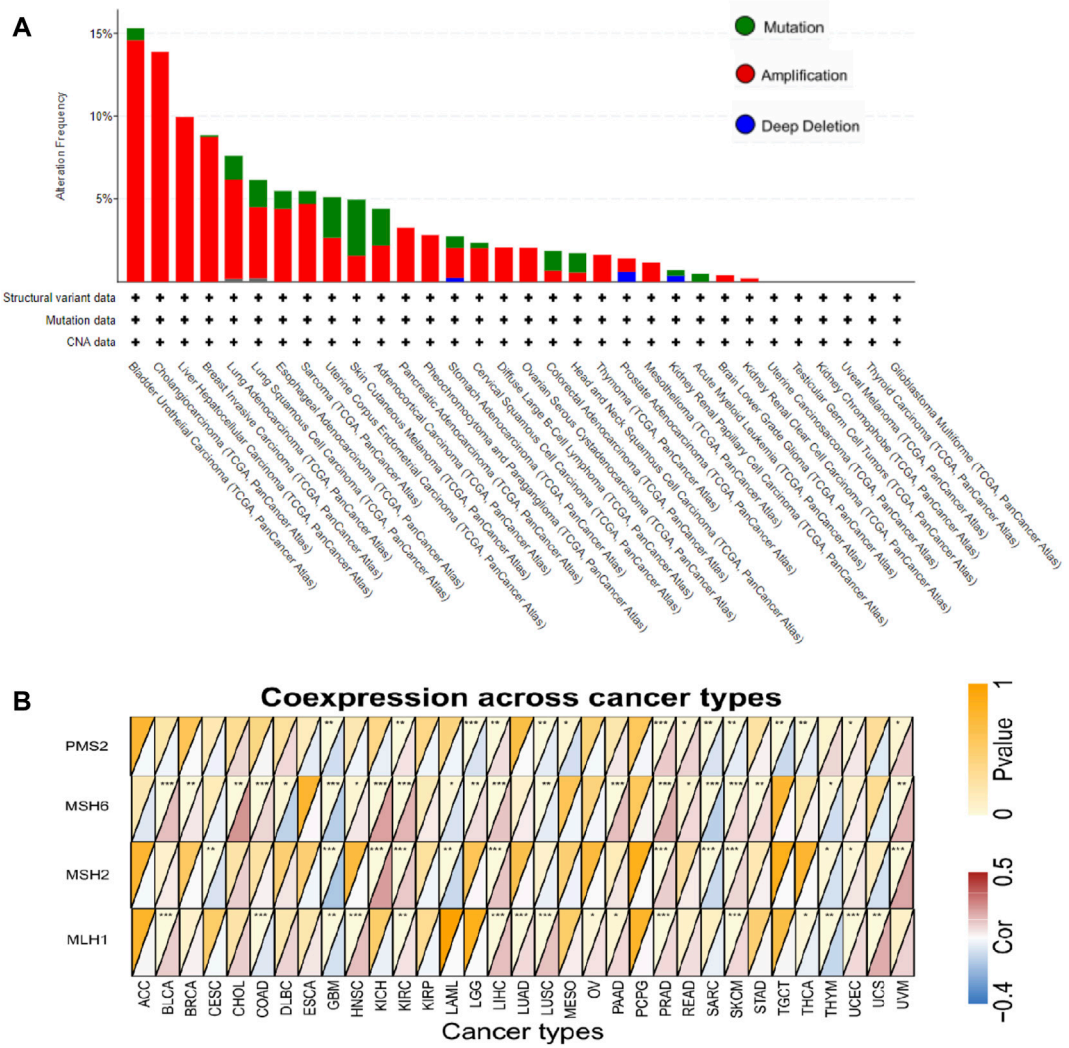

FIGURE 6 | Mutation characteristics of FCGR3A in different TCGA tumors and its relationship with DNA mismatch repair genes (MMRs). **(A)** Alteration frequency of FCGR3A mutation types in different tumors; **(B)** Heat maps showed the association of APOC1 expression with expression levels of four MMRs genes in various cancers. $^{*}p < 0.05$; $^{**}p < 0.01$; $^{***}p < 0.001$.

samples into high expression and low expression group according to the median FCGR3A expression and analyzed the enrichment of the GO signaling pathway in the two groups by GSEA. The top 5 signaling pathways with the most significant enrichment in the eight tumors (including GBM, KIRC, LGG, PRAD, SKCM, THCA, THYM, and UVM) are listed in **Figures 9A–H**. It was found that negative regulation of blood vessel endothelial cell migration, epidermal cell differentiation, immune response regulating cell surface receptor signaling pathway, adaptive immune response based on somatic recombination, immune receptors built from, humoral immune response, immune response regulating cell surface receptor signal pathway, negative regulation of immune system process, positive regulation of cytokine production, chronic inflammatory response, erection of external biotic stimulus and adaptive immune response based on somatic were described as the most abundant GO pathways in eight tumors whose prognosis was associated with APOC1 expression. This suggested that FCGR3A is extensively implicated in the negative regulation of tumor angiogenesis and the regulation of cancer immune signaling pathways.

Relationship Between FCGR3A Expression and Drug Sensitivity

Genetic alterations affect the drug sensitivity of cancer to clinical treatment and therefore are potential biomarkers for drug screening. Therefore, we question the association between mRNA expression levels of FCGR3A and patient sensitivity to antitumor drugs. Based on the GDSC database, we performed a correlation analysis between gene expression level and drug sensitivity of 265 drugs across 963

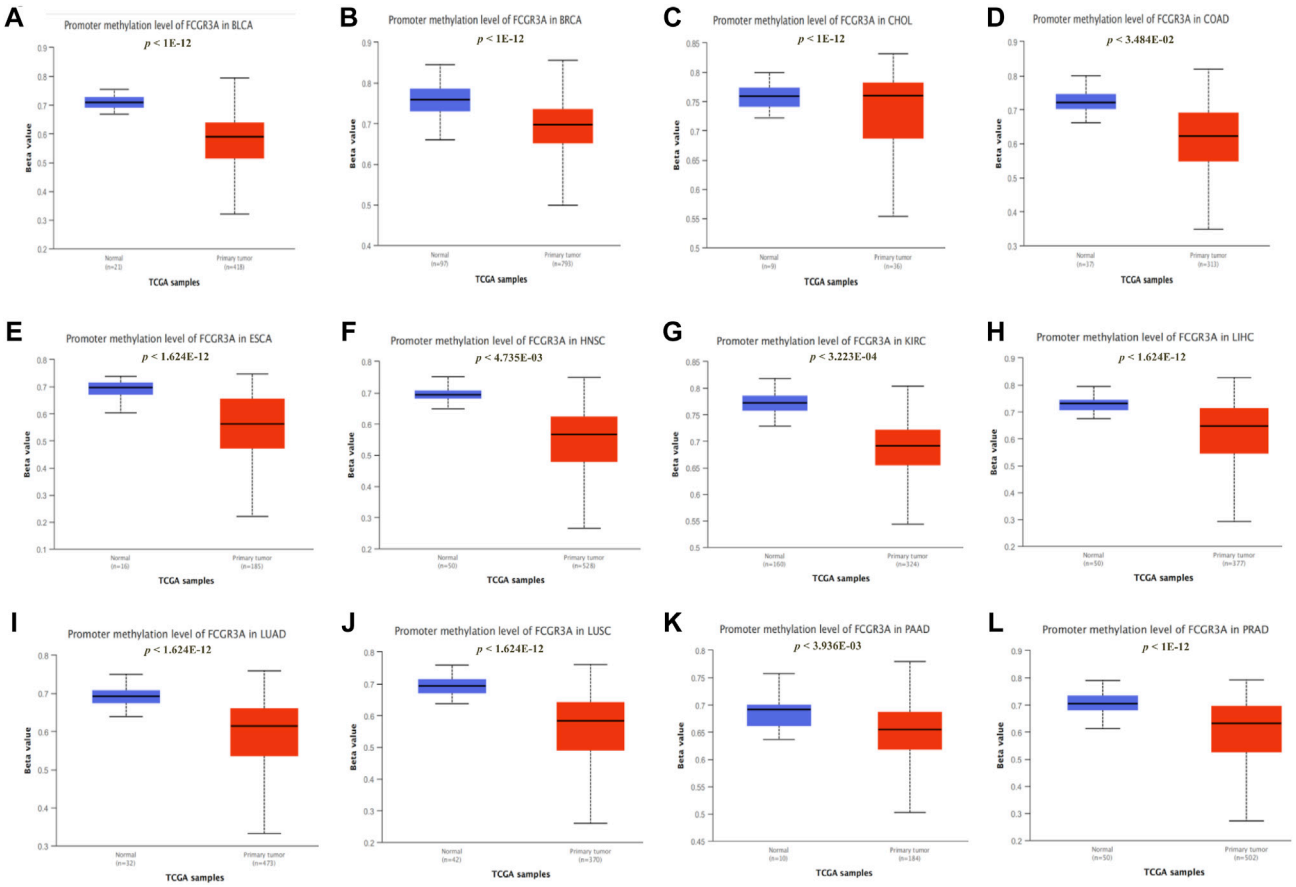

FIGURE 7 | Correlation between FCGR3A expression and gene promoter methylation. **(A)** Bladder urothelial carcinoma (BLCA); **(B)** Breast invasive carcinoma (BRCA); **(C)** Cholangiocarcinoma (CHOL); **(D)** Colon adenocarcinoma (COAD); **(E)** Esophageal carcinoma (ESCA); **(F)** Head and neck squamous cell carcinoma (HNSC); **(G)** Kidney renal clear cell carcinoma (KIRC); **(H)** liver hepatocellular carcinoma (LIHC); **(I)** Lung adenocarcinoma (LUAD); **(J)** Lung squamous cell carcinoma (LUSC); **(K)** Pancreatic adenocarcinoma (PAAD); **(L)** Prostate adenocarcinoma (PRAD).

cell lines, and a total of 158 drugs were identified to be associated with FCGR3A expression. **Figures 10A,B** exhibites the six drugs with the strongest negative correlation and the six drugs with the strongest positive correlation respectively. The IC50s of BYA 61-3606 ($r = -0.190$, $p < 0.001$), KIN001-236 ($r = -0.184$, $p < 0.001$), XDM8-85 ($r = -0.180$, $p < 0.001$), IPA-3 ($r = -0.177$, $p < 0.001$), PAC-1 ($r = -0.170$, $p < 0.001$) and XMD14-99 ($r = -0.173$, $p < 0.001$) were negatively correlated with FCGR3A expression (**Figure 10A**). Additionally, the IC50s of six drugs (only 6), including Bicalutamide ($r = 0.083$, $p = 0.014$), Trametinib ($r = 0.090$, $p = 0.007$), PD-0325901 ($r = 0.076$, $p < 0.020$), Doxetaxel ($r = 0.073$, $p = 0.034$), AZD6244 ($r = 0.072$ $p = 0.030$) and READ119 ($r = 0.072$, $p = 0.030$), were positively correlated with FCGR3A expression (**Figure 10B**). Complete drug sensitivity analysis results are shown in **Supplementary Table S1**. As shown in **Figure 10C**, six commonly used anticancer drugs, such as 5-fluorouracil, Camptothecin, Etoposide, Doxorubicin, Gemcitabine, and Methotrexate have lower IC50 values (better efficacy) in patients with high FCGR3A expression. These results confirmed our hypothesis that the expression level of FCGR3A interacts with the sensitivity of antitumor drugs.

DISCUSSION

FCGR3A is the encoding gene of CD16a, and the up-regulation of FCGR3A results in high expression of CD16a. Almost all NK cells express the low-affinity Fc γ receptor (FCγR) IIIA/CD16a. The activated receptor CD16a on the NK cell surface promotes antibot-dependent cell-mediated cytotoxicity (ADCC), which is a key effect of NK cells and tumor antigen-targeting mechanism (Nimmerjahn and Ravetch, 2008).

Many but not all studies have reported significant associations between functional polymorphisms of Fcγ RIIIA-activated receptors and antitumor mAb immunotherapy outcomes (Cartron et al., 2002; Weng and Levy, 2003; Treon et al., 2005; Calemma et al., 2012; Seidel et al., 2013; Gavin et al., 2017; Magnes et al., 2018). Unfortunately, whether FCGR3A works in different tumors through some common molecular mechanism remains to be answered. A literature search revealed limited and

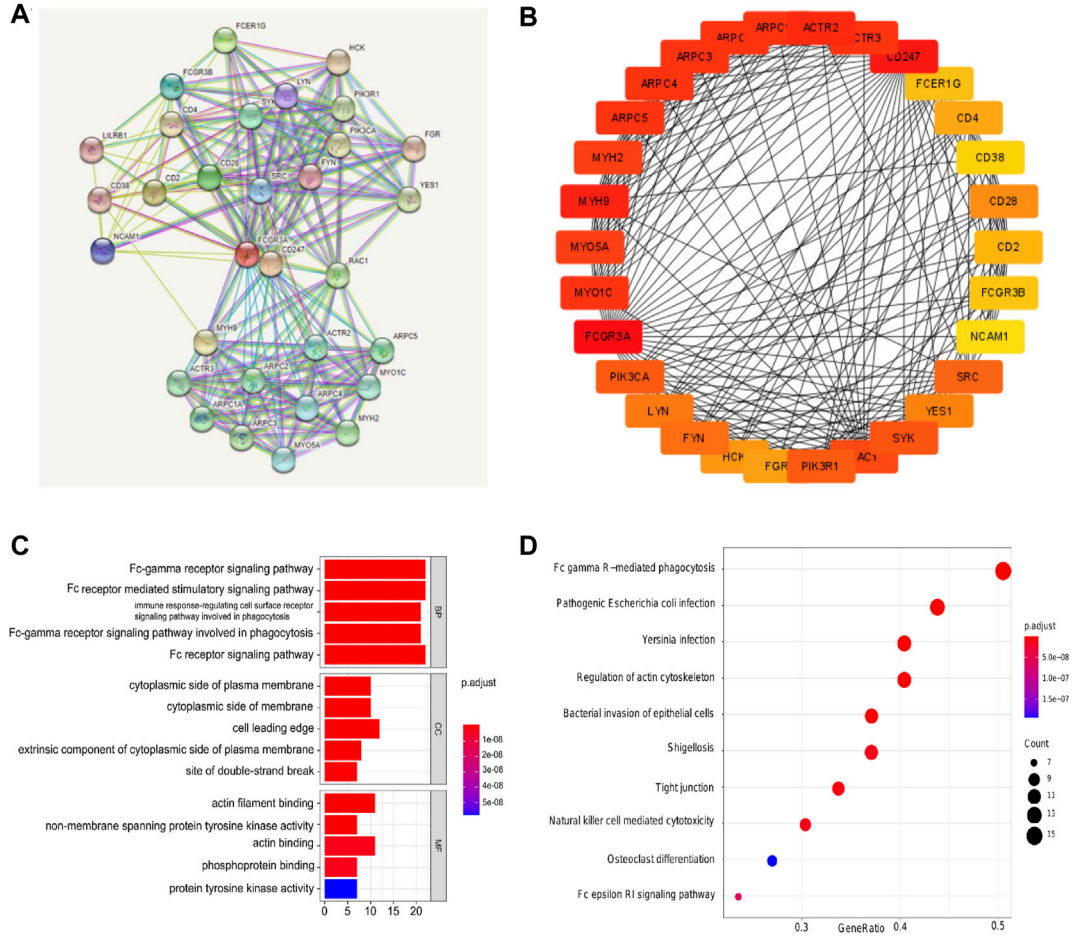

FIGURE 8 | Protein-protein interaction (PPI) network, gene ontology (GO) analysis, and Kyoto Encyclopedia of Genes and Genomes (KEGG) analysis of FCGR3A-related genes. **(A,B)** PPI network; **(C)** GO analyses; **(D)** KEGG analysis.

weak data available for a pan-cancer analysis of FCGR3A from a whole-tumor perspective. Therefore, we comprehensively examined FCGR3A in pan-cancer based on data from TCGA and GTEx databases.

We found that FCGR3A was overexpressed in 23 cancers, and IHC analysis confirmed this trend at the protein level. COX regression analysis showed that the prognosis analysis data of the FCGR3A gene proposed different conclusions for different tumors, but these correlations were only seen in a small number of tumors. High FCGR3A expression was mainly associated with poor prognoses of six cancer types (KIRC, LGG, THYM, PRAD, and UVM), while it was associated with good prognoses of SKCM and THCA. This difference may be due to discrepancies in tumor samples, so larger sample sizes may be needed to verify the above conclusions. Combined with the above results, FCGR3A is regarded as a potential biomarker or therapeutic target.

With the clinical success of cancer immunotherapy, there is an increasing need for a comprehensive understanding of tumor-immune interactions. Understanding the tumor microenvironment, including immune cell infiltration, may help decipher the mechanisms behind tumor development. The Fc receptor (FcR) plays a major role in normal immunity and anti-infection and provides the humoral immune system with cellular effectors. Previous studies have suggested that the G-protein-coupled receptors (GPCR) of chemokines can detect chemical attractants produced by bacteria in inflammatory responses and activate signaling pathways that regulate actin polymerization and allow cells to migrate to bacteria. Various receptors, such as Fcγ and C3a receptors, then bind to targets and activate signaling pathways, resulting in actin aggregation around the bacteria, forming phagocytic rings (Pan et al., 2016). An effective mechanism of tumor cell phagocytosis is mediated by the uptake of Fc receptors (FcR) by antibody-coated tumor cells. Depending on the nature of the FcR and Fc parts of the antibody, binding of the cell-associated antigen-antibody complex to FcR can trigger complement, ADCC, or phagocytosis and induce DC maturation, thereby stimulating T cell responses against the captured antigens and antitumor immunity (Rafiq et al., 2002; Schuurhuis et al., 2006; Dilillo and Ravetch, 2015).

CD8+T cells are known to regulate specific expression of tumor antigens, so they are considered as key mediators of tumor destruction and play an indispensable role in

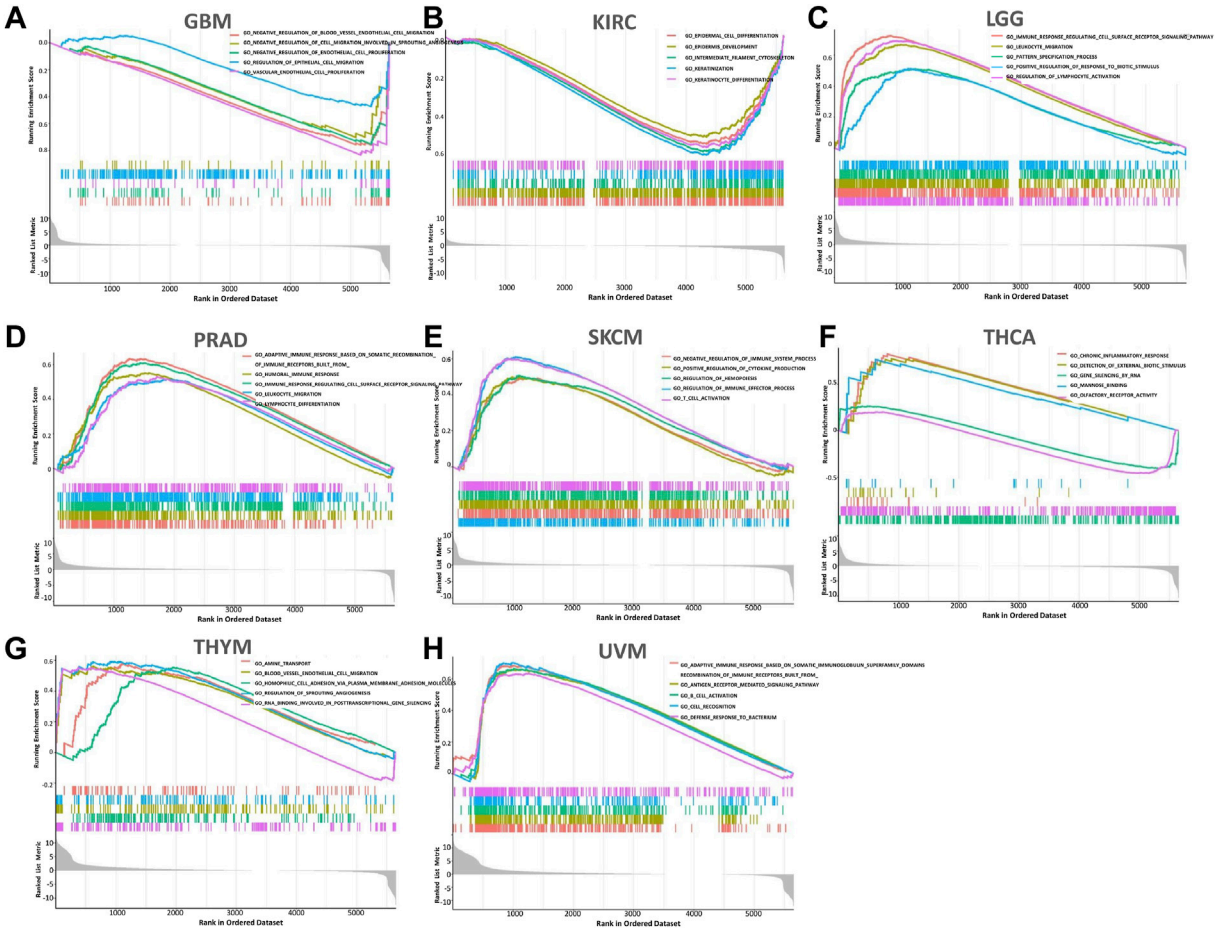

FIGURE 9 | The 5 most relevant signaling pathways of FCGR3A's GSEA in the GO dataset. **(A)** Glioblastoma multiforme (GBM); **(B)** Kidney renal clear cell carcinoma (KIRC); **(C)** brain lower grade glioma (LGG); **(D)** Prostate adenocarcinoma (PRAD); **(E)** Skin cutaneous melanoma (SKCM); **(F)** Thyroid carcinoma (THCA); **(G)** Thymoma (THYM); **(H)** Uveal melanoma (UVM).

immunotherapy (Kishton et al., 2017). Clinical studies on tumor-infiltrating immune cells have identified the role of cytotoxic T cells (CTL) and tumor-associated macrophages (TAM) in some diseases (Bingle et al., 2002; Fridman et al., 2012). In addition to focusing on CD8+T cells, this study also observed a significant association between tumor FCGR3A expression and other immune cells such as $CD4^+$ T cells, B cells, DC cells, macrophages, and neutrophil infiltration, although the current study was unable to establish a causal relationship. Interestingly, the relationship between FCGR3A expression and certain immune cell markers (such as Th1, Th2, M1/M2 macrophages, mast cells, monocytes, Tregs, and so on) does not always follow the general trend (**Figure 6C**), suggesting specific interactions between FCGR3A and certain immune cell subtypes. In addition, our study also revealed the co-expression of FCGR3A and immunosuppression-related genes and chemokine genes. These results indicate that the expression level of FCGR3A can affect the tumor immune microenvironment, which will provide a new reference for the prognosis of immune checkpoint inhibitors (ICIs) treatment.

Mismatch repair (MMR) genes are efficient guardians of genomic integrity and stability, and the presence of MMR gene mutations can predict tumor patients' sensitivity to immune checkpoint blocking therapy (Le et al., 2017). According to our results, the expression of FCGR3A was positively correlated with the expression of MMRs genes in most tumors, suggesting that FCGR3A may maintain the viability of tumor cells by up-regulating DNA mis-match repair-related genes.

The mutation analysis found that the alteration frequency of FCGR3A in bladder urothelial carcinoma was the highest, and the main type is the amplification mutation. This enriched our understanding of the functionality of FCGR3A. Furthermore, disruption of DNA methylation patterns is a relatively common feature in cancer and is associated with various developmental defects and tumorigenesis (Fernandez et al., 2012). Feinberg, A.P et al. also reported significant hypommethylation in cancer genes compared with normal corresponding cells (Feinberg and Vogelstein, 1983). Similarly, our study reached the same conclusion, suggesting that FCGR3A may influence DNA

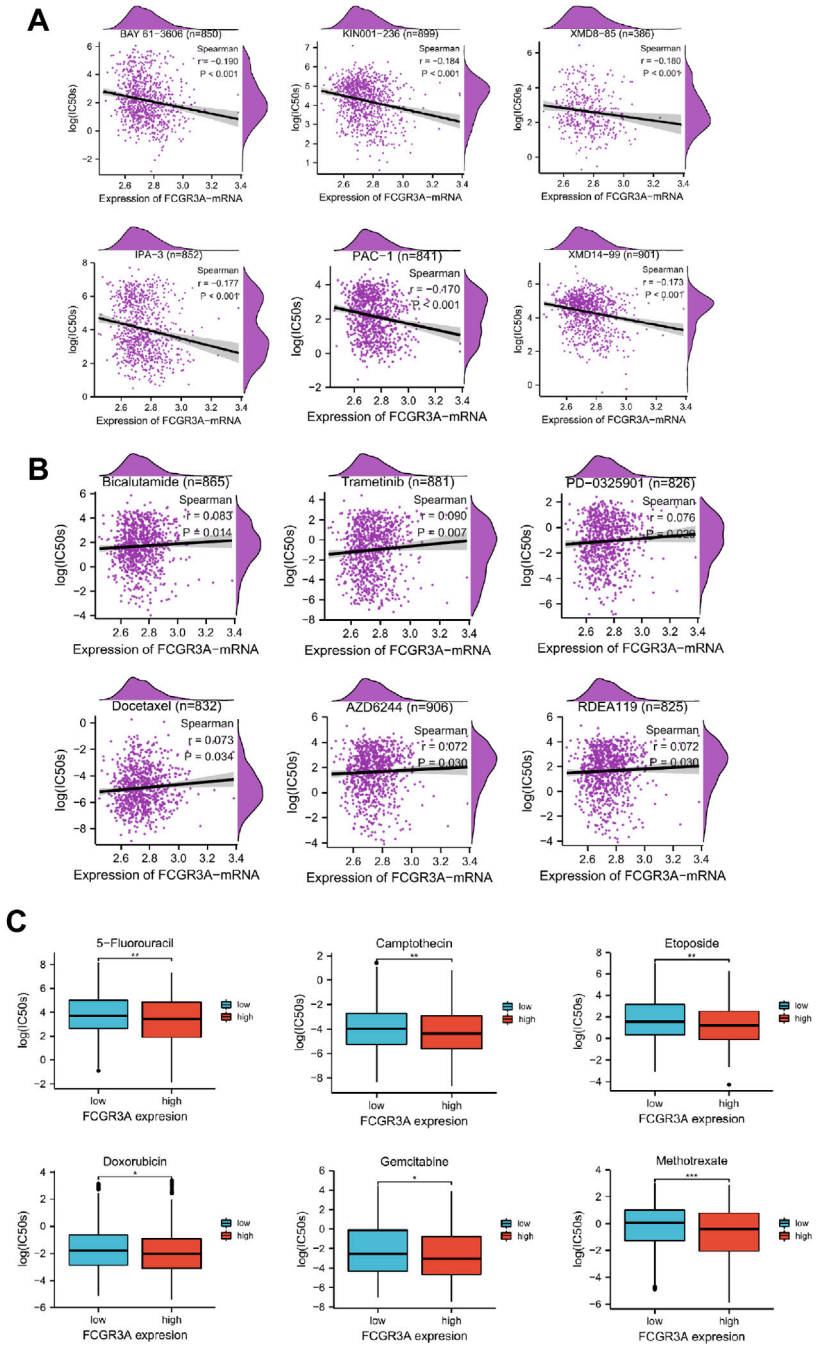

FIGURE 10 | Relationship between FCGR3A expression and drug sensitivity. **(A)** The top six negatively correlated. **(B)** The only six positively correlated. **(C)** The difference of drug sensitivity of six commonly used anticancer drugs (5-fluorouracil, Camptothecin, Etoposide, Doxorubicin, Gemcitabine, and Methotrexate) in high and low FCGR3A expression groups was shown in the forms of boxplot charts. *$p < 0.05$; **$p < 0.01$; ***$p < 0.001$.

methylation and promote tumor development, although the detailed mechanism is still unknown.

Through GO and KEGG pathway analysis, we further clarified FCGR3A's involvement in a variety of biological processes, molecular functions, and cellular components, mainly including the Fc receptor signaling pathway, immune response-regulating cell surface receptor signaling pathway involved in phagocytosis, humoral immunity, and pathogen infection. Using GSEA enrichment analysis, it was found that FCGR3A was mainly enriched in pathways related to negative regulation of angiogenesis, epidermal cell differentiation, chronic inflammation, and adaptive immune response.

The analysis of basic gene expression can reveal the relationship between cell's resting physiological state and drug

sensitivity, which is valuable for the analysis of drug action mechanism. Through drug sensitivity analysis, we found that high FCGR3A expression was negatively correlated with IC50 values of most anticancer drugs (i.e., drug response was well). This is consistent with previous findings (Vuong et al., 2014; Salvadores et al., 2020) that the level of gene expression is a predictor of drug response. It is indicated that the measurement of FCGR3A expression level can be used as a reliable indicator of clinical treatment, highlighting the potential of FCGR3A as an anticancer drug target. Even if it is not a direct target of a compound, it may play a crucial role in the processes before and after the compound binds to its target, and variations in its expression may underlie individual differences in drug responses (Vuong et al., 2014). These results will help us better understand how drug-target interactions can benefit cancer treatment, and have important implications for guiding the combination therapy in patients with advanced or recurrent tumor, and guiding the drug selection in patients with multiline treatment resistance.

In searchable articles reports, most of studies on FCGR3A (CD16a) have focused on the pathogenesis, diagnosis, and treatment of inflammatory diseases such as IgG immune complexes (including rheumatoid arthritis and systemic lupus erythematosus), and little attention has been paid to cancer. In 2020, Hofmann L et al. confirmed that CD16-positive exosomes could be used as an indicator of immunosuppressive grade of HNSC: the later the tumor stage or the more aggressive the tumor, the higher the CD16 level of total exosomes in patients (Hofmann et al., 2020). Sconocchia G et al. found that tumor invasion of FcγRIII (CD16) + bone marrow cells is associated with improved survival in colorectal cancer patients (Sconocchia et al., 2011). And Zhang W et al. indicated that relatively increased CD16 + monocytes contribute to the pro-tumor microenvironment of T cell non-Hodgkin lymphoma (Zhang et al., 2020). This provides an idea for our study. The significance of our work is to prospectively reveal the interaction of FCGR3A in the tumor microenvironment and provide insights based on bioinformatics and computational biology for further understanding the role of FCGR3A in tumor metabolism and immune regulation.

However, there are still had several limitations in our study. First, the results of this study were acquired solely from bioinformatics analysis, lacking actual experimental or clinical data. Second, tumor tissue information is mainly derived from the collection of large amounts of microarray and sequencing data from public databases, and cell-level analysis of immune cell markers may introduce systematic bias. Third, although we identified that FCGR3A expression was associated with survival in some tumor patients and affected immune cell infiltration, we were unable to prove a clear causal relationship between FCGR3A altering immune infiltration and affecting patient survival. The role of FCGR3A in cancer needs to be further explored and verified through biological experiments in the future.

In conclusion, FCGR3A not only affects the prognosis of cancer patients and regulates the immune microenvironment, but also is a strong predictor for anticancer drug response, suggesting that FCGR3A may be an immunocarcinogenic molecule and can be used as a promising biomarker to provide a direction for immune-based anti-tumor strategies.

DATA AVAILABILITY STATEMENT

The original contributions presented in the study are included in the article/**Supplementary Material**, further inquiries can be directed to the corresponding author.

AUTHOR CONTRIBUTIONS

LL, ZH made the bioinformatic analysis, wrote, discussed, and revised the manuscript of this article. KD made literature search and draft the manuscript of this article. XL and CL edited the manuscript, DW, YZ, and CW revised the design of the image. All authors contributed to the submitted version.

FUNDING

This project is supported by the National Natural Science Foundation of China (No.: 81503526) and the Natural Science Foundation of Guangdong Province (No.: 2015a030310448).

SUPPLEMENTARY MATERIAL

The Supplementary Material for this article can be found online at: https://www.frontiersin.org/articles/10.3389/fphar.2022.900699/full#supplementary-material

Supplementary Figure S1 | The expression of FCGR3A in different TCGA cancer types was analyzed using TIMER **(A)** and GEPIA2 **(B)** respectively.

Supplementary Figure S2 | The expression of FCGR3A in pan-cancer single cell lines was analyzed using GDSC database **(A)** and the cancerSCEM website **(B)** respectively.

Supplementary Table S1 | Spearman correlation analysis between FCGR3A expression and all the 265 drugs IC50 in the GDSC database.

REFERENCES

Bingle, L., Brown, N. J., and Lewis, C. E. (2002). The Role of Tumour-Associated Macrophages in Tumour Progression: Implications for New Anticancer Therapies. *J. Pathol.* 196 (3), 254–265. doi:10.1002/path.1027

Bray, F., Ferlay, J., Soerjomataram, I., Siegel, R. L., Torre, L. A., and Jemal, A. (2018). Global Cancer Statistics 2018: GLOBOCAN Estimates of Incidence and Mortality Worldwide for 36 Cancers in 185 Countries. *CA Cancer J. Clin.* 68 (6), 394–424. doi:10.3322/caac.21492

Calemma, R., Ottaiano, A., Trotta, A. M., Nasti, G., Romano, C., Napolitano, M., et al. (2012). Fc Gamma Receptor IIIa Polymorphisms in Advanced Colorectal Cancer Patients Correlated with Response to Anti-EGFR Antibodies and Clinical Outcome. *J. Transl. Med.* 10, 232. doi:10.1186/1479-5876-10-232

Cartron, J., Tchernia, G., Celton, J. L., Damay, M., Cheron, G., Farrokhi, P., et al. (1991). Alloimmune Neonatal Neutropenia. *Am. J. Pediatr.*

Hematol. Oncol. 13 (1), 21–25. doi:10.1097/00043426-199121000-00005

Cartron, G., Dacheux, L., Salles, G., Solal-Celigny, P., Bardos, P., Colombat, P., et al. (2002). Therapeutic Activity of Humanized Anti-CD20 Monoclonal Antibody and Polymorphism in IgG Fc Receptor FcgammaRIIIa Gene. *Blood* 99 (3), 754–758. doi:10.1182/blood.v99.3.754

Dilillo, D. J., and Ravetch, J. V. (2015). Fc-Receptor Interactions Regulate Both Cytotoxic and Immunomodulatory Therapeutic Antibody Effector Functions. *Cancer Immunol. Res.* 3 (7), 704–713. doi:10.1158/2326-6066.CIR-15-0120

Edberg, J. C., Langefeld, C. D., Wu, J., Moser, K. L., Kaufman, K. M., Kelly, J., et al. (2002). Genetic Linkage and Association of Fcgamma Receptor IIIA (CD16A) on Chromosome 1q23 with Human Systemic Lupus Erythematosus. *Arthritis Rheum.* 46 (8), 2132–2140. doi:10.1002/art.10438

Feinberg, A. P., and Vogelstein, B. (1983). Hypomethylation Distinguishes Genes of Some Human Cancers from Their normal Counterparts. *Nature* 301 (5895), 89–92. doi:10.1038/301089a0

Fernandez, A. F., Assenov, Y., Martin-Subero, J. I., Balint, B., Siebert, R., Taniguchi, H., et al. (2012). A DNA Methylation Fingerprint of 1628 Human Samples. *Genome Res.* 22 (2), 407–419. doi:10.1101/gr.119867.110

Fridman, W. H., Galon, J., Dieu-Nosjean, M. C., Cremer, I., Fisson, S., Damotte, D., et al. (2011). Immune Infiltration in Human Cancer: Prognostic Significance and Disease Control. *Curr. Top. Microbiol. Immunol.* 344, 1–24. doi:10.1007/82_2010_46

Fridman, W. H., Pagès, F., Sautès-Fridman, C., and Galon, J. (2012). The Immune Contexture in Human Tumours: Impact on Clinical Outcome. *Nat. Rev. Cancer* 12 (4), 298–306. doi:10.1038/nrc3245

Gavin, P. G., Song, N., Kim, S. R., Lipchik, C., Johnson, N. L., Bandos, H., et al. (2017). Association of Polymorphisms in FCGR2A and FCGR3A with Degree of Trastuzumab Benefit in the Adjuvant Treatment of ERBB2/HER2-Positive Breast Cancer: Analysis of the NSABP B-31 Trial. *JAMA Oncol.* 3 (3), 335–341. doi:10.1001/jamaoncol.2016.4884

Gessner, J. E., Grussenmeyer, T., Kolanus, W., and Schmidt, R. E. (1995). The Human Low Affinity Immunoglobulin G Fc Receptor III-A and III-B Genes. Molecular Characterization of the Promoter Regions. *J. Biol. Chem.* 270 (3), 1350–1361. doi:10.1074/jbc.270.3.1350

Hargreaves, C. E., Rose-Zerilli, M. J., Machado, L. R., Iriyama, C., Hollox, E. J., Cragg, M. S., et al. (2015). Fcγ Receptors: Genetic Variation, Function, and Disease. *Immunol. Rev.* 268 (1), 6–24. doi:10.1111/imr.12341

Hofmann, L., Ludwig, S., Schuler, P. J., Hoffmann, T. K., Brunner, C., and Theodoraki, M. N. (2020). The Potential of CD16 on Plasma-Derived Exosomes as a Liquid Biomarker in Head and Neck Cancer. *Int. J. Mol. Sci.* 21 (11), 3739. doi:10.3390/ijms21113739

Kishton, R. J., Sukumar, M., and Restifo, N. P. (2017). Metabolic Regulation of T Cell Longevity and Function in Tumor Immunotherapy. *Cell Metab.* 26 (1), 94–109. doi:10.1016/j.cmet.2017.06.016

Koene, H. R., Kleijer, M., Algra, J., Roos, D., von dem Borne, A. E., and de Haas, M. (1997). Fc gammaRIIIa-158V/F Polymorphism Influences the Binding of IgG by Natural Killer Cell Fc gammaRIIIa, Independently of the Fc gammaRIIIa-48L/R/H Phenotype. *Blood* 90 (3), 1109–1114. doi:10.1182/blood.v90.3.1109.1109_1109_1114

Le, D. T., Durham, J. N., Smith, K. N., Wang, H., Bartlett, B. R., Aulakh, L. K., et al. (2017). Mismatch Repair Deficiency Predicts Response of Solid Tumors to PD-1 Blockade. *Science* 357 (6349), 409–413. doi:10.1126/science.aan6733

Lochmann, T. L., Floros, K. V., Naseri, M., Powell, K. M., Cook, W., March, R. J., et al. (2018). Venetoclax is Effective in Small-Cell Lung Cancers with High BCL-2 Expression. *Clin. Cancer Res.* 24 (2), 360–369. doi:10.1158/1078-0432.CCR-17-1606

Loeb, L. A. (2001). A Mutator Phenotype in Cancer. *Cancer Res.* 61 (8), 3230–3239.

Magnes, T., Melchardt, T., Hufnagl, C., Weiss, L., Mittermair, C., Neureiter, D., et al. (2018). The Influence of FCGR2A and FCGR3A Polymorphisms on the Survival of Patients with Recurrent or Metastatic Squamous Cell Head and Neck Cancer Treated with Cetuximab. *Pharmacogenomics J.* 18 (3), 474–479. doi:10.1038/tpj.2017.37

Men, C., Chai, H., Song, X., Li, Y., Du, H., and Ren, Q. (2017). Identification of DNA Methylation Associated Gene Signatures in Endometrial Cancer via Integrated Analysis of DNA Methylation and Gene Expression Systematically. *J. Gynecol. Oncol.* 28 (6), e83. doi:10.3802/jgo.2017.28.e83

Morvan, M. G., and Lanier, L. L. (2016). NK Cells and Cancer: You Can Teach Innate Cells New Tricks. *Nat. Rev. Cancer* 16 (1), 7–19. doi:10.1038/nrc.2015.5

Musolino, A., Gradishar, W. J., Rugo, H. S., Nordstrom, J. L., Rock, E. P., Arnaldez, F., et al. (2022). Role of Fcγ Receptors in HER2-Targeted Breast Cancer Therapy. *J. Immunother. Cancer* 10 (1). doi:10.1136/jitc-2021-003171

Nimmerjahn, F., and Ravetch, J. V. (2008). Fcgamma Receptors as Regulators of Immune Responses. *Nat. Rev. Immunol.* 8 (1), 34–47. doi:10.1038/nri2206

Pan, M., Xu, X., Chen, Y., and Jin, T. (2016). Identification of a Chemoattractant G-Protein-Coupled Receptor for Folic Acid that Controls Both Chemotaxis and Phagocytosis. *Dev. Cel.* 36 (4), 428–439. doi:10.1016/j.devcel.2016.01.012

Pandey, J. P., and Namboodiri, A. M. (2014). Immunoglobulin GM and FcγRIIIa Genotypes Influence Cytotoxicity of Neuroblastoma Cells. *J. Neuroimmunol.* 270 (1-2), 95–97. doi:10.1016/j.jneuroim.2014.03.003

Patel, K. R., Roberts, J. T., and Barb, A. W. (2020). Allotype-specific Processing of the CD16a N45-Glycan from Primary Human Natural Killer Cells and Monocytes. *Glycobiology* 30 (7), 427–432. doi:10.1093/glycob/cwaa002

Qureshi, S. A., Bashir, M. U., and Yaqinuddin, A. (2010). Utility of DNA Methylation Markers for Diagnosing Cancer. *Int. J. Surg.* 8 (3), 194–198. doi:10.1016/j.ijsu.2010.02.001

Rafiq, K., Bergtold, A., and Clynes, R. (2002). Immune Complex-Mediated Antigen Presentation Induces Tumor Immunity. *J. Clin. Invest.* 110 (1), 71–79. doi:10.1172/JCI15640

Salvadores, M., Fuster-Tormo, F., and Supek, F. (2020). Matching Cell Lines with Cancer Type and Subtype of Origin via Mutational, Epigenomic, and Transcriptomic Patterns. *Sci. Adv.* 6 (27), eaba1862. doi:10.1126/sciadv.aba1862

Schuurhuis, D. H., van Montfoort, N., Ioan-Facsinay, A., Jiawan, R., Camps, M., Nouta, J., et al. (2006). Immune Complex-Loaded Dendritic Cells Are superior to Soluble Immune Complexes as Antitumor Vaccine. *J. Immunol.* 176 (8), 4573–4580. doi:10.4049/jimmunol.176.8.4573

Sconocchia, G., Zlobec, I., Lugli, A., Calabrese, D., Iezzi, G., Karamitopoulou, E., et al. (2011). Tumor Infiltration by FcγRIII (CD16)+ Myeloid Cells is Associated with Improved Survival in Patients with Colorectal Carcinoma. *Int. J. Cancer* 128 (11), 2663–2672. doi:10.1002/ijc.25609

Seidel, U. J., Schlegel, P., and Lang, P. (2013). Natural Killer Cell Mediated Antibody-dependent Cellular Cytotoxicity in Tumor Immunotherapy with Therapeutic Antibodies. *Front. Immunol.* 4, 76. doi:10.3389/fimmu.2013.00076

Sondermann, P., Kaiser, J., and Jacob, U. (2001). Molecular Basis for Immune Complex Recognition: A Comparison of Fc-Receptor Structures. *J. Mol. Biol.* 309 (3), 737–749. doi:10.1006/jmbi.2001.4670

Treon, S. P., Hansen, M., Branagan, A. R., Verselis, S., Emmanouilides, C., Kimby, E., et al. (2005). Polymorphisms in FcgammaRIIIA (CD16) Receptor Expression Are Associated with Clinical Response to Rituximab in Waldenström's Macroglobulinemia. *J. Clin. Oncol.* 23 (3), 474–481. doi:10.1200/JCO.2005.06.059

Vance, B. A., Huizinga, T. W., Wardwell, K., and Guyre, P. M. (1993). Binding of Monomeric Human IgG Defines an Expression Polymorphism of Fc Gamma RIII on Large Granular Lymphocyte/natural Killer Cells. *J. Immunol.* 151 (11), 6429–6439.

Veeramani, S., Wang, S. Y., Dahle, C., Blackwell, S., Jacobus, L., Knutson, T., et al. (2011). Rituximab Infusion Induces NK Activation in Lymphoma Patients with the High-Affinity CD16 Polymorphism. *Blood* 118 (12), 3347–3349. doi:10.1182/blood-2011-05-351411

Vuong, H., Cheng, F., Lin, C. C., and Zhao, Z. (2014). Functional Consequences of Somatic Mutations in Cancer Using Protein Pocket-Based Prioritization Approach. *Genome Med.* 6 (10), 81. doi:10.1186/s13073-014-0081-7

Weng, W. K., and Levy, R. (2003). Two Immunoglobulin G Fragment C Receptor Polymorphisms Independently Predict Response to Rituximab in Patients with Follicular Lymphoma. *J. Clin. Oncol.* 21 (21), 3940–3947. doi:10.1200/JCO.2003.05.013

Zhang, W., Ruan, J., Zhou, D., Han, X., Zhang, Y., Wang, W., et al. (2020). Predicting Worse Survival for Newly Diagnosed T Cell Lymphoma Based

on the Decreased Baseline CD16-/CD16 + Monocyte Ratio. *Sci. Rep.* 10 (1), 7757. doi:10.1038/s41598-020-64579-z

Zhou, Q., Hu, H. G., and Hou, L. (2015). Discover, Develop & Validate--Advance and Prospect of Tumor Biomarkers. *Clin. Lab.* 61 (11), 1589–1599. doi:10.7754/clin.lab.2015.150332

Ziakas, P. D., Poulou, L. S., and Zintzaras, E. (2016). FcγRIIa-H131R Variant is Associated with Inferior Response in Diffuse Large B Cell Lymphoma: A Meta-Analysis of Genetic Risk. *J. BUON.* 21 (6), 1454–1458.

Conflict of Interest: The authors declare that the research was conducted in the absence of any commercial or financial relationships that could be construed as a potential conflict of interest.

Publisher's Note: All claims expressed in this article are solely those of the authors and do not necessarily represent those of their affiliated organizations, or those of the publisher, the editors and the reviewers. Any product that may be evaluated in this article, or claim that may be made by its manufacturer, is not guaranteed or endorsed by the publisher.

GLOSSARY

ACC adrenocortical carcinoma
ADCC antibot-dependent cell-mediated cytotoxicity
ADCP antibody-dependent cellular phagocytosis
BP biological process
BLCA bladder urothelial carcinoma
BRCA breast invasive carcinoma
CAN copy number alteration
CC cellular component
CESC cervical squamous cell carcinoma and endocervical adenocarcinoma
CHOL cholangiocarcinoma
COAD colon adenocarcinoma
CLL chronic lymphocytic leukemia
CRC coloretal cancer
CPTAC Clinical Proteomic Tumor Analysis Consortium
CI confidence interval
CTL cytotoxic T cells
DC dendritic cell
DLBC lymphoid neoplasm diffuse large B-cell lymphoma
DSS disease-specific survival
ESCA esophageal carcinoma
FCGR3A Fc gamma receptors 3A
GBM glioblastoma multiforme
GDSC Genomics of Drug Sensitivity in Cancer
GEPIA Gene Expression Profiling Interactive Analysis
GTEx Genotype-Tissue Expression
GO Gene Ontology
GPCR G-protein-coupled receptors
HER2 human epidermalgrowth factor receptor-2
HNSC head and neck squamous cell carcinoma
HPA Human Protein Atlas
HR hazard ratio
ICI Immune checkpoint inhibitor
IC50 half maximal inhibitory concentration
IHC immunohistonchemistry
KEGG Kyoto Encyclopedia of Genes and Genomes
KICH kidney chromophobe
KIRC kidney renal clear cell carcinoma
KIRP kidney renal papillary cell carcinoma
LAML acute myeloid leukemia
LGG brain lower grade glioma
LIHC liver hepatocellular carcinoma
LUAD lung adenocarcinoma
LUSC lung squamous cell carcinoma
MESO mesothelioma
MMR DNA mis-match repair genes
MF molecular function
OV ovarian serous cystadenocarcinoma
OS overall survival
PAAD pancreatic adenocarcinoma
PCPG pheochromocytoma and paraganglioma
PD-L1 programmed cell death-Ligand 1
PFI progression-free interval
PFS progression-free survival
PRAD prostate adenocarcinoma
PPI protein–protein interaction
READ rectum adenocarcinoma
SARC sarcoma
SKCM skin cutaneous melanoma
STAD stomach adenocarcinoma
TAM tumor-associated macrophages
TCGA The Cancer Genome Atlas
TGCT testicular germ cell tumors
THCA thyroid carcinoma
THYM thymoma
TIMER Tumor Immune Estimate Resources
UCEC uterine corpus endometrial carcinoma
UCS uterine carcinosarcoma
UVM uveal melanoma

frontiers | Frontiers in Pharmacology

ORIGINAL RESEARCH
published: 06 June 2022
doi: 10.3389/fphar.2022.920939

Homologous Recombination Pathway Alternation Predicts Prognosis of Colorectal Cancer With Chemotherapy

Yan Lin[1†], Xiaoli Liao[1†], Yumei Zhang[1], Guobin Wu[2], Jiazhou Ye[2], Shanshan Luo[3], Xinxin He[3], Min Luo[1], Mingzhi Xie[1], Jinyan Zhang[1], Qian Li[1], Yu Huang[1], Sina Liao[1], Yongqiang Li[1] and Rong Liang[1]**

[1]Department of Medical Oncology, Guangxi Medical University Cancer Hospital, Nanning, China, [2]Department of Hepatobiliary Surgery, Guangxi Medical University Cancer Hospital, Nanning, China, [3]Department of Gastrointestinal Surgery, Guangxi Medical University Cancer Hospital, Nanning, China

OPEN ACCESS

Edited by:
Clare Y. Slaney,
Peter MacCallum Cancer Centre, Australia

Reviewed by:
Xinwei Han,
Zhengzhou University, China
Xiaohua Li,
Sixth People's Hospital of Chengdu, China

***Correspondence:**
Rong Liang
liangrong@gxmu.edu.cn
Yongqiang Li
liyongqiang@gxmu.edu.cn

[†]These authors have contributed equally to this work and share first authorship

Specialty section:
This article was submitted to Pharmacology of Anti-Cancer Drugs, a section of the journal Frontiers in Pharmacology

Received: 15 April 2022
Accepted: 23 May 2022
Published: 06 June 2022

Citation:
Lin Y, Liao X, Zhang Y, Wu G, Ye J, Luo S, He X, Luo M, Xie M, Zhang J, Li Q, Huang Y, Liao S, Li Y and Liang R (2022) Homologous Recombination Pathway Alternation Predicts Prognosis of Colorectal Cancer With Chemotherapy. Front. Pharmacol. 13:920939. doi: 10.3389/fphar.2022.920939

Background: Chemotherapy is the basic treatment for colorectal cancer (CRC). However, colorectal cancer cells often develop resistance to chemotherapy drugs, leading to recurrence and poor prognosis. More and more studies have shown that the Homologous recombination (HR) pathway plays an important role in chemotherapy treatment for tumors. However, the relationship between HR pathway, chemotherapy sensitivity, and the prognosis of CRC patients is still unclear.

Methods: We collected 35 samples of CRC patients after chemotherapy treatment from Guangxi Medical University Cancer Hospital, then collected mutation data and clinical prognosis data from the group. We also downloaded Mondaca-CRC, TCGA-CRC cohorts for chemotherapy treatment.

Result: We found that HR mutant-type (HR-MUT) patients are less likely to experience tumor metastasis after receiving chemotherapy. Additionally, our univariate and multivariate cox regression models showed that HR-MUT can be used as an independent predictor of the prognosis of chemotherapy for CRC patients. The KM curve showed that patients with HR-MUT CRC had significantly prolonged overall survival (OS) time (log-rank $p = 0.017$; hazard ratio (HR) = 0.69). Compared to HR mutant-type (HR-WT), HR-MUT has a significantly lower IC50 value with several chemotherapeutic drugs. Pathway enrichment analysis further revealed that the HR-MUT displayed a significantly lower rate of DNA damage repair ability, tumor growth, metastasis activity, and tumor fatty acid metabolism activity than HR-WT, though its immune response activity was notably higher.

Abbreviation: CRC, colorectal cancer; ECOG, Eastern Cooperative Oncology Group Performance Status; GSEA, gene set enrichment analysis; HR, Homologous recombination; HR-MUT, HR mutant-type; HR-WT, HR wild-type; IC50, half maximal inhibitory concentration; HRD, homologous recombination defect; LD, lipid droplets; IFN-γ, interferon-γ; MSI: Microsatellite instability; NER, Nucleotide excision repair; OS, overall survival; TMB, Tumor mutational burden, ssGSEA, single sample gene set enrichment analysis.

Conclusion: These findings indicate that HR-MUT may be a relevant marker for CRC patients receiving chemotherapy, as it is closely related to improving OS time and reducing chemotherapy resistance.

Keywords: colorectal cancer, chemotherapy, biomarker, prognosis, homologous recombination

INTRODUCTION

Colorectal cancer, or colon cancer, is one of the most common types of malignant tumors found in the human digestive tract and is a seriously threat to human health. Its incidence rate ranks third amongst that of all malignant tumors worldwide, and its mortality rate ranks second (Miller et al., 2020; Liu et al., 2022a; Liu et al., 2022b). At present, besides surgery, chemotherapy is the main treatment for colon cancer. However, due to the high heterogeneity of colon cancer, the benefits of these treatments for difference patients may vary greatly. Moreover, the occurrence of chemotherapy resistance can result in failure of the final treatment of colon cancer patients (Bian et al., 2016; Fu et al., 2016). Therefore, it is of the utmost importance to investigate the specific mechanism of the occurrence and development of colon cancer and any accompanying chemotherapy resistance in order to develop new therapeutic targets, reverse chemotherapy resistance, and ultimately improve the prognosis of colon cancer patients.

Recent studies have shown that the molecular mechanisms of chemotherapy resistance mainly involve: 1) The reduction of the activation of drug precursors and the concentration of drugs in cells through drug efflux and inactivation; 2) Changes in drug action targets; 3) Disturbance of cell survival and apoptosis; 4) Hypoxia in the tumor microenvironment; 5) Changes in the extracellular mechanism; 5) Cytokines and other growth factors that maintain the activation of tumor survival-related pathways (Li et al., 2017).

Homologous recombination (HR) is a stable and error-free repair process that uses homologous sister chromatids as a template. HR determines the survival and fate of cells (Gonzalez and Stenzinger, 2021; Liu et al., 2021). Still, despite its reliability, the main cause of DNA damage in the S/G2 cell cycle is HR (Lisby and Rothstein, 2015). HR plays an important role in repairing cisplatin adducts, a DNA repair process that plays an important role in the chemotherapy resistance of tumor cells (Zdraveski et al., 2000). For example, HR-deficient Escherichia coli strains are known to show higher sensitivity to chemotherapeutic drugs than Nucleotide excision repair (NER)-deficient Escherichia coli strains (Zdraveski et al., 2000), while homologous recombination defect (HRD) is known to be related to chemotherapy resistance in ovarian cancer patients (Xiao et al., 2017). However, at present, the relationship between the mutation state of the HR pathway and the chemotherapy efficacy, prognosis, and chemotherapy sensitivity of CRC patients is unclear.

In this study, we use data collected from a sample of CRC patients who have been treated with chemotherapy from Guangxi Medical University Cancer Hospital to explore the relationship between the mutation state of HR pathway and the prognosis of the chemotherapy efficacy of CRC patients through curative effect analysis, prognosis analysis, and drug sensitivity analysis. Through this process, we found that HR-MUT CRC patients had significantly prolonged survival time and higher sensitivity to chemotherapy drugs. Therefore, HR-MUT may be a useful predictive marker for CRC patients receiving chemotherapy in future treatments.

MATERIALS AND METHODS

CRC Cohort Collection

This study includes samples of primary CRC patients that underwent colon cancer resection and chemotherapy in Guangxi Medical University Cancer Hospital between 2015 to 2021. The sample patients were divided into patients with tumor metastasis and without tumor metastasis. We obtained the mutation data by targeted sequencing. We also collected the clinical data of the 35 patients, including their level of metastasis, sex, TNM stage, Eastern Cooperative Oncology Group Performance Status (ECOG), age, height, and weight. All participants signed a written informed consent agreement, and the work was approved by the Research Ethics Committee of Guangxi Medical University Cancer Hospital.

To expand our data, we downloaded a CRC cohort for chemotherapy (Mondaca-CRC; https://www.cbioportal.org/study/clinicalData?id=crc_apc_impact_2020) from the cbioportal web tool (Mondaca et al., 2020), as well as the entirety of the exon sequencing data and clinical data (including Tumor mutational burden (TMB), Microsatellite instability (MSI) scores, MSI status, gender, TNM stage, ECOG and age). We downloaded the RNA sequencing data, mutation data, and clinical prognosis data of TCGA-COAD and TCGA-READ from TCGA database (https://portal.gdc.cancer.gov/) using TCGAbiolinks R package (Colaprico et al., 2016). We then combined TCGA-COAD cohort and TCGA-READ cohort into TCGA-CRC cohort, which was used for our subsequent analysis. The TMB of TCGA-CRC was downloaded from the previous literature (Lin et al., 2020). Clinical basic information about Local-CRC, Mondaca-CRC and TCGA-CRC are defined in **Supplementary Table S1–S3**, respectively.

Definition of the Abrupt State of HR Pathway

We downloaded the gene list of KEGG_HOMOLOGOUS_RECOMBINATION (**Supplementary Table S4**) from MsigDB database (Liberzon et al., 2011). Firstly, the synonymous mutations in the mutation data from Local-CRC, Mondaca-CRC and TCGA-CRC were deleted, retaining only the mutation data of non-synonymous mutation types. According to the gene list of KEGG_homologus_recombination (HR), we counted the

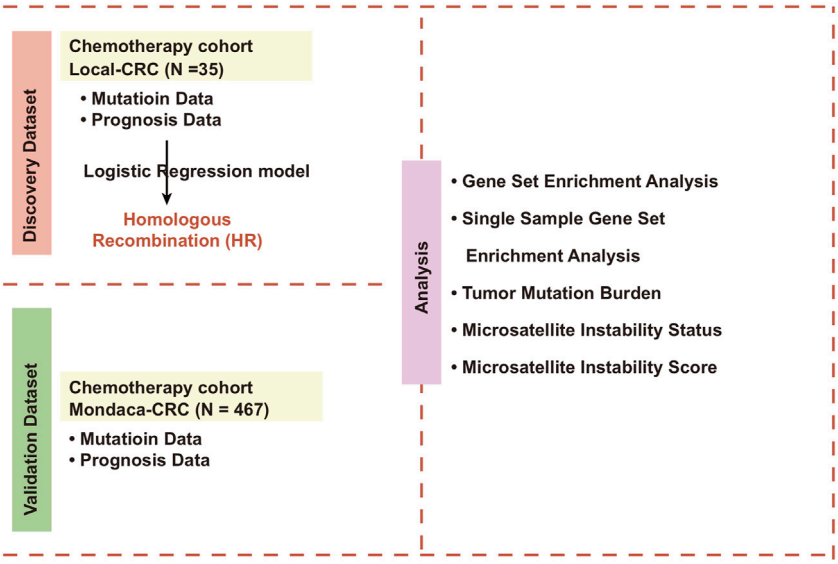

FIGURE 1 | Overall design of the study.

mutation number of the HR pathway in each patient. When the number of gene mutations in a patient's HR pathway was zero, we labeled it the HR wild-type (WT). Otherwise, they were referred to as the HR mutant-type (MUT).

Relationship Between HR Pathway Mutation and Prognosis or Curative Effect of CRC Patients

We used logistic regression analysis to explore the relationship between the mutation status of HR pathway and whether Local-CRC patients had metastasis after receiving chemotherapy. In Mondaca-CRC cohort, univariable and multivariate Cox regression analysis, as well as Kaplan-Meier analysis, were used to evaluate the influence of HR pathway mutation on the survival time of CRC patients after receiving chemotherapy.

Path Enrichment Analysis

Using clusterProfiler R package and gene set enrichment analysis (GSEA) (Yu et al., 2012), we analyzed the expression profile data of the HR-MUT and HR-WT groups and compared the enrichment scores and p values of the HR-MUT and HR-WT groups to those of GO-BP, GO-CC, GO-MF, KEGG, and REACTOME. We also used single sample GSEA (ssGSEA) to analyze the pathway score of each CRC patient (Lin et al., 2022).

Statistical Analysis

The Mann-Whitney U test was used to compare the differences between the continuity variables of the HR-MUT and HR-WT groups, while Fisher' exact test was used to compare the differences in the classification variables of the HR-MUT and HR-WT groups. The log-rank test in combination with Kaplan-Meier analysis was used to calculate the p value. All statistical analysis and visual analysis in this study were based on R language. Here, the p value was bilateral and any p value of less than 0.05 was regarded as statistically significant.

RESULTS

HR-MUT is Related to a Better Curative Effect and Prognosis in CRC Patients Receiving Chemotherapy

In order to explore the relationship between the mutation state of HR pathway and the chemotherapy efficacy and prognosis of CRC patients (**Figure 1**), we first analyzed whether HR-MUT can influence the presence of tumor metastasis in CRC patients after chemotherapy (**Figure 2A**). The results showed that HR-MUT might indeed cause less tumor metastasis in CRC patients after chemotherapy (OR < 0; $p < 0.05$). The results displayed in **Figure 2B** demonstrate how HR-WT was often found in CRC patients without tumor metastasis after chemotherapy ($p < 0.05$). Meanwhile, as shown in **Figure 2C**, CRC patients with HR-MUT often did not display any tumor metastasis after receiving chemotherapy ($p < 0.05$). For Mondaca-CRC patients, our univariable and multivariate Cox regression analysis showed that HR-MUT could be used as an independent predictor of chemotherapy prognosis for CRC patients (**Figure 2D**). Notably, the Kaplan-Meier curve showed that HR-MUT had significantly longer OS time than HR-WT (log-rank $p = 0.017$; HR = 0.69; **Figure 2E**).

In order to further verify the relationship between HR-MUT and the sensitivity of chemotherapeutic drugs, we evaluated the IC50 value of several chemotherapeutic drugs using pRRophetic algorithm combined with the CRC patient expression data. From this analysis, we found that HR-MUT group displayed a

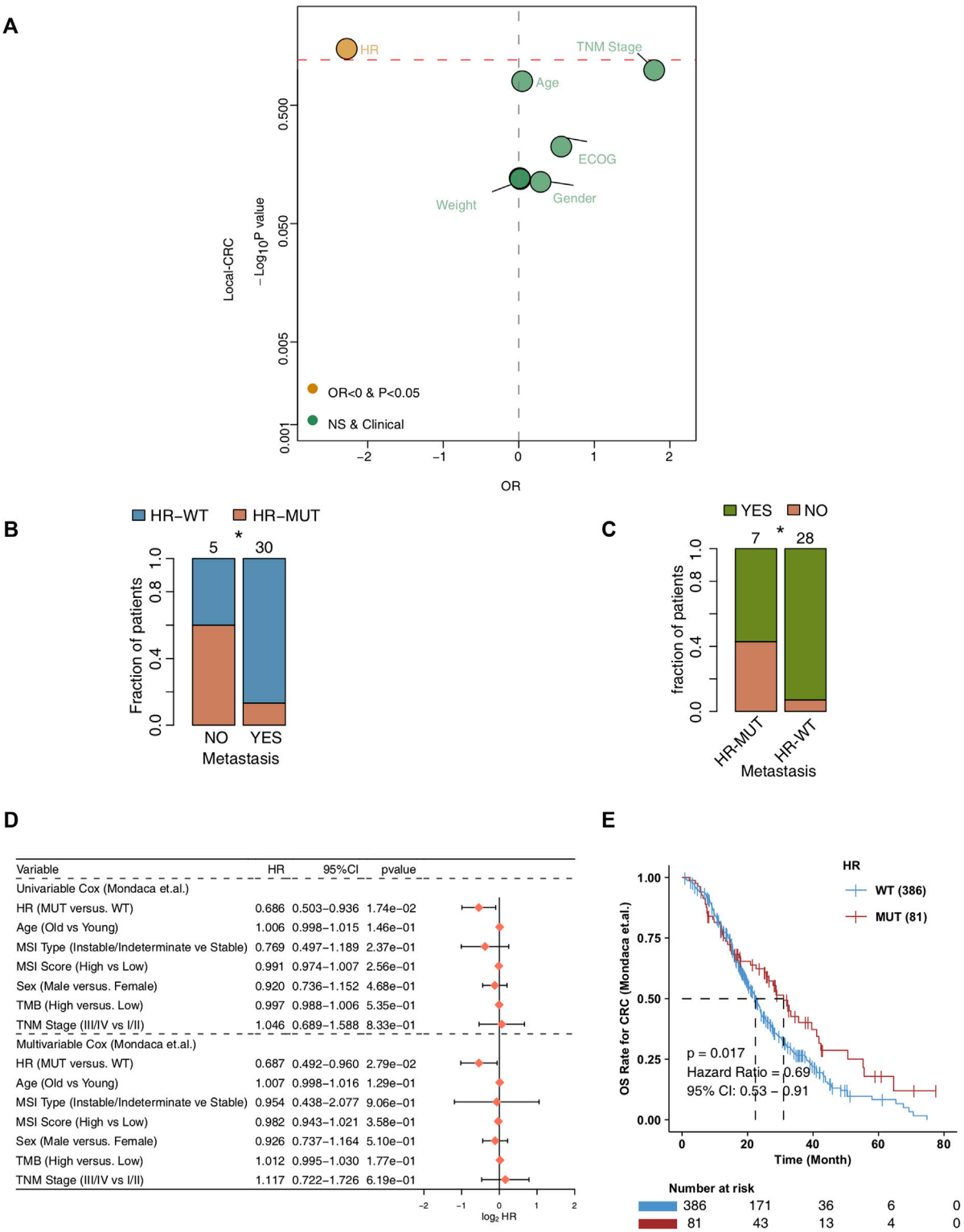

FIGURE 2 | The prognosis value of the HR-MUT group **(A)**. Logistic regression model of the HR-MUT group and clinical characteristics in the Local-CRC cohort **(B)**. A comparison between the HR mutation statuses of the metastasis-yes group and metastasis-no group **(C)**. A comparison between the tumor metastasis statuses of the HR-MUT and HR-WT groups **(D)**. The univariable and multivariable cox regression model of the HR-MUT group and clinical characteristics in the Mondaca-CRC cohort **(E)**. KM curve showed the HR-MUT CRC patients displayed a significant improvement in OS time compared with the HR-WT CRC patients in the Mondaca-CRC cohort (*$p < 0.05$).

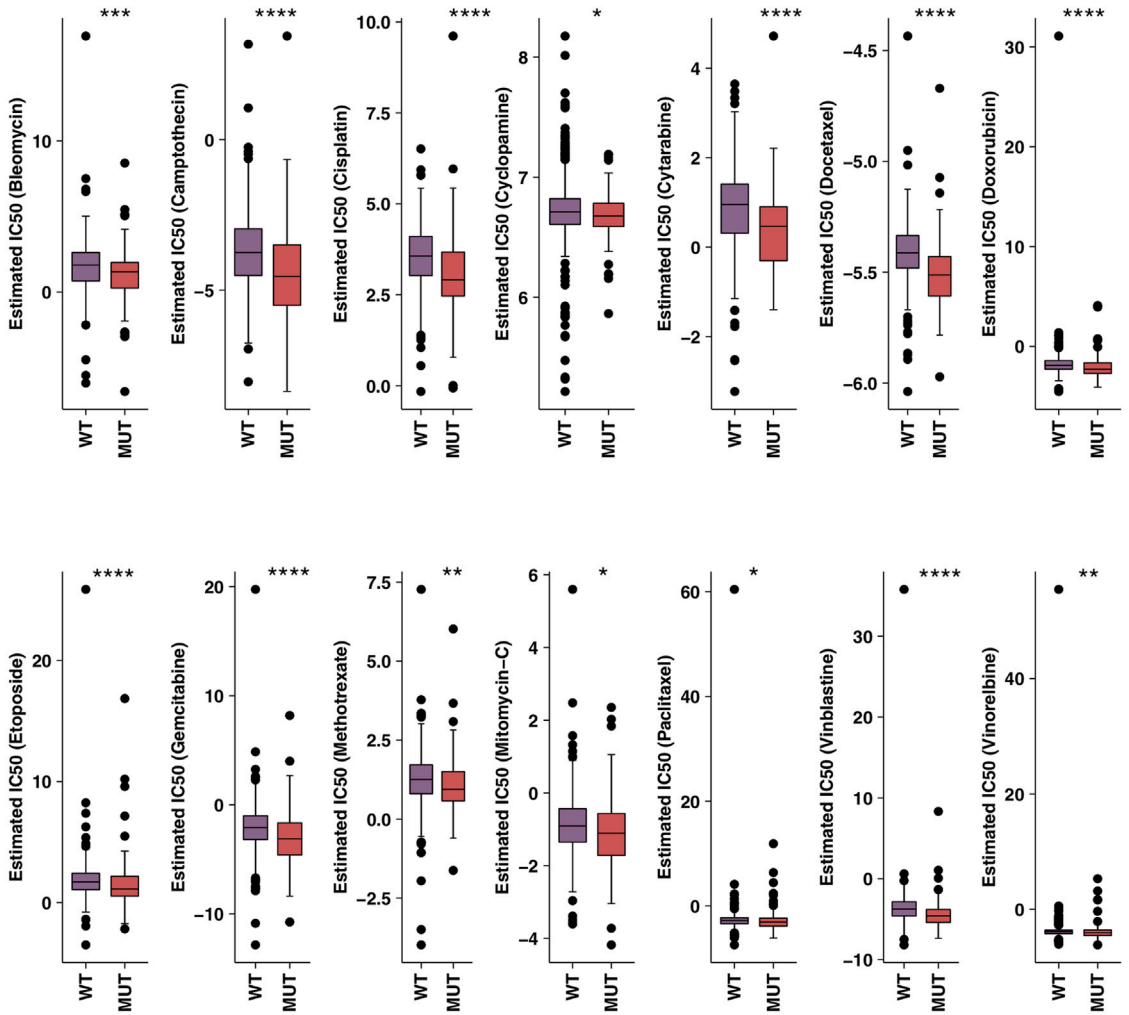

FIGURE 3 | A comparison between the IC50 values of common chemotherapy drugs used on HR-MUT and the HR-WT CRC patients (*$p < 0.05$; **$p < 0.01$; ***$p < 0.001$; ****$p < 0.0001$).

significantly lower IC50 value with the chemotherapeutic drugs than the HR-WT group (**Figure 3**).

HR-MUT is Associated With Higher Mutation Frequency, TMB, and MSIscore

Next, we compare the gene mutation frequencies of the HR-MUT and HR-WT groups to the top 20 mutation frequencies found in the other CRC cohorts. For Local-CRC, the HR-MUT group had significantly higher mutation frequency than the HR-WT group in *Gli3* (42.9% vs. 3.6%), *BRCA2* (42.9% vs. 0.0%), and *ITGB2* (42.9% vs. 0.0%) (all $p < 0.05$; **Figure 4A**). In Mondaca-CRC, the HR-MUT group was notably higher than the HR-WT group in *RNF43* (17.3% vs. 6.2%), *ARID1A* (21.0% vs. 4.9%), *KMT2D* (22.2% vs. 4.7%), *PTPRS* (18.5% vs. 4.7%), *ERBB4* (12.3% vs. 4.1%), *PTPRT* (11.1% vs. 4.1%), *NF1* (9.9% vs. 4.1%), and *PTEN* (11.1% vs. 3.6%), all of which had significantly increased mutation frequency (all $p < 0.05$; **Figure 4B**). **Supplementary Figures S1A,B** shows the mutual exclusion and co-occurrence of the top 20 gene mutations in the Local-CRC and Mondaca-CRC cohorts, respectively, while **Supplementary Figures S2A,B** show the gene mutation of HR-MUT patients in the Local-CRC Cohort and Mondaca-CRC Cohort, respectively.

Compared with HR-WT, HR-MUT displayed a significantly higher level of TMB in Local-CRC and Mondaca-CRC ($p = 2.55e-04$, **Figure 4C**; P = 5e-05, **Figure 4D**). We also found that HR-MUT had a higher MSI score than HR-WT ($p = 2.66e-02$; **Figure 4E**). Similarly, HR-MUT had a higher prevelence of instable MSI status ($p < 0.0001$; **Figure 4F**).

HR-MUT is Related to the Less Active DNA Repair Ability of CRC Patients and Promoting Tumor Metastasis and Metabolism

In order to further explore the difference between HR-MUT and HR-WT in pathway activity, we utilized GSEA and

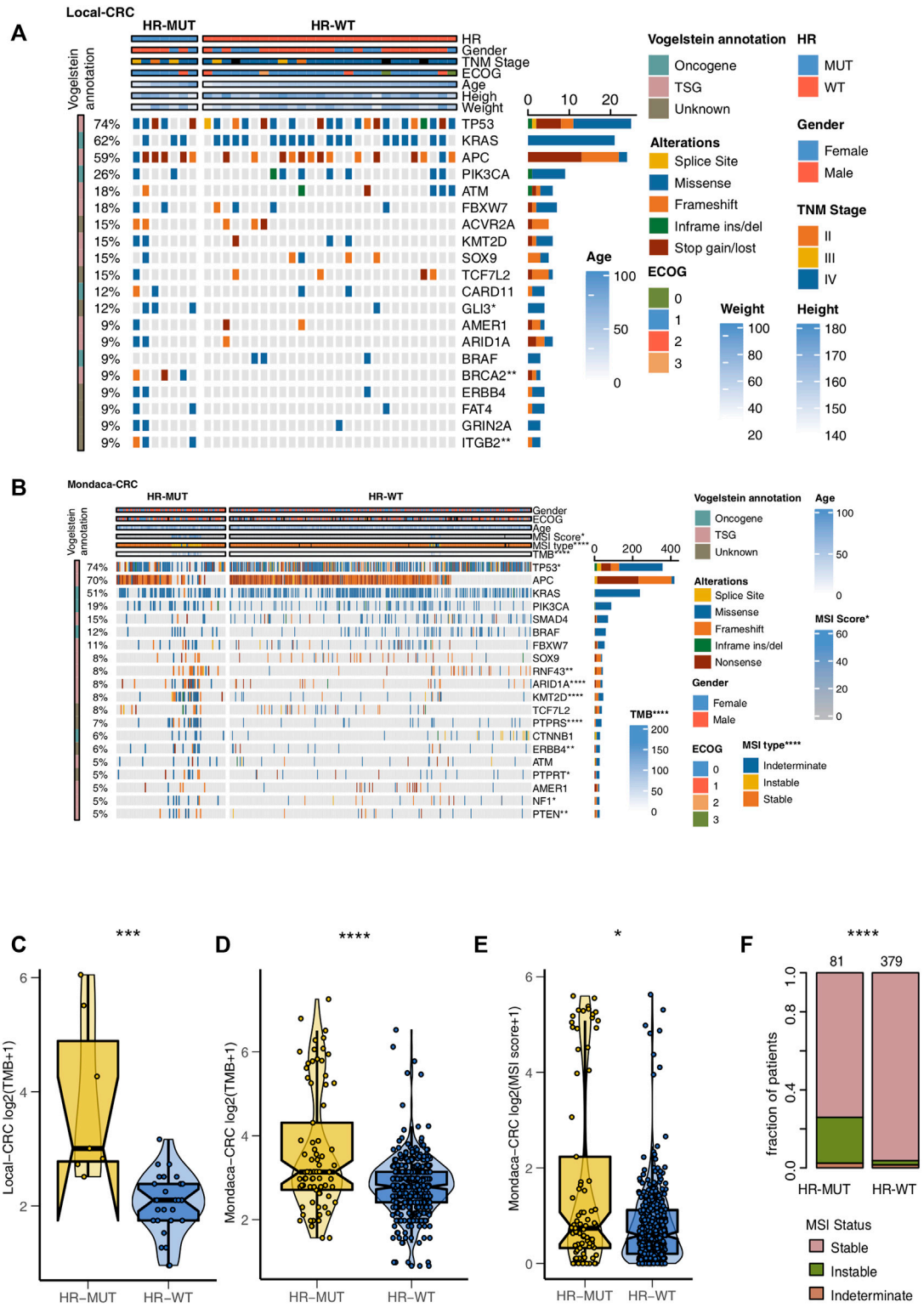

FIGURE 4 | The mutation profiles of the HR-MUT and HR-WT CRC patients. The mutational landscape of the top mutated gene mutations in the Local-CRC cohort **(A)** and Mondaca-CRC cohort **(B)**. A comparison of the TMB levels of the HR-MUT group and HR-WT group in the Local-CRC cohort **(C)** and Mondaca-CRC cohort **(D)**. A comparison between the MSI scores **(E)** and MSI statuses **(F)** the HR-MUT and HR-WT groups in the Mondaca-CRC cohort (*$p < 0.05$; **$p < 0.01$; ***$p < 0.001$; ****$p < 0.0001$).

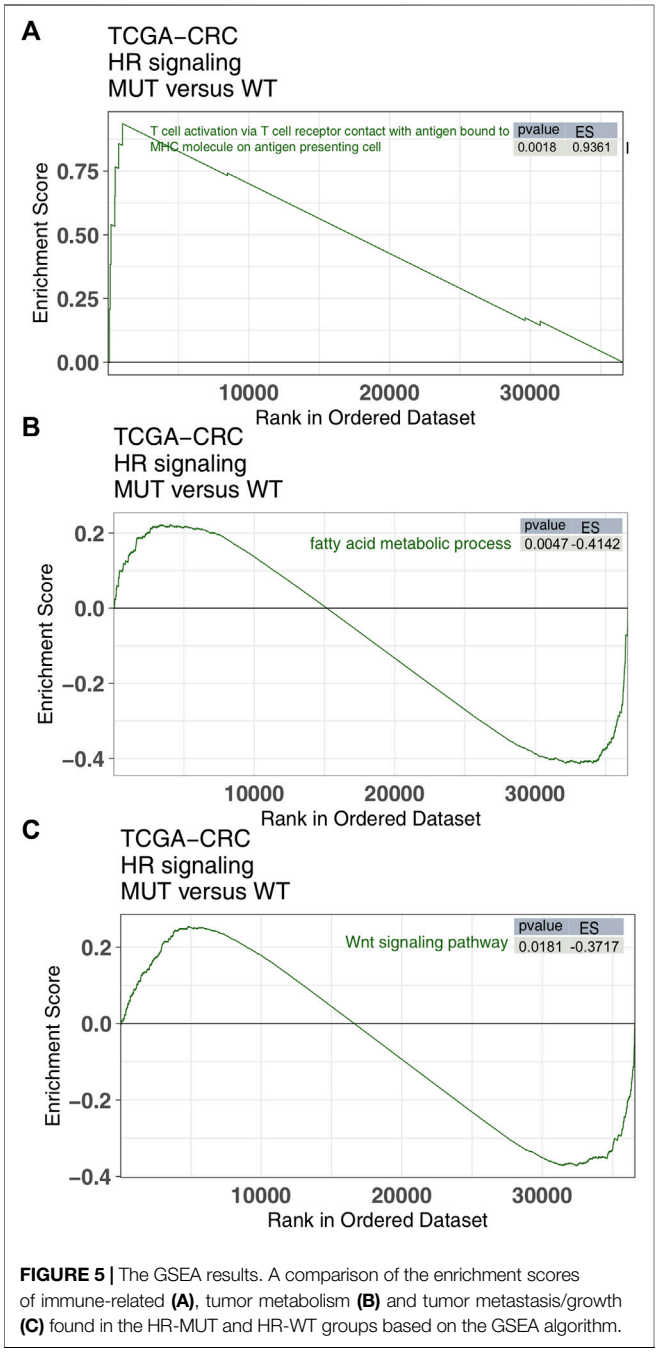

FIGURE 5 | The GSEA results. A comparison of the enrichment scores of immune-related **(A)**, tumor metabolism **(B)** and tumor metastasis/growth **(C)** found in the HR-MUT and HR-WT groups based on the GSEA algorithm.

ssGSEA. Compared with HR-WT, HR-MUT displayed a significant increase in immune activity, which is manifested by an increase in antigen presenting ability, infiltration and recruitment of $CD4^+$ T cells, and production of INF-gamma (ES > 0, $p < 0.05$, **Figure 5A**; **Supplementary Table S5**). Additionally, HR-MUT had significantly reduced tumor metabolic activity, as well as fatty acid metabolic activity (ES < 0, $p < 0.05$; **Figure 5B**; **Supplementary Table S5**). Compared with HR-WT, HR-MUT also had significantly reduced WNT pathway activity (ES < 0, $p < 0.05$; **Figure 5C**; **Supplementary Table S5**).

In order to further verify the channel activity, we used the ssGSEA algorithm and obtained similar results (**Figures 6A–D**). From this, we found that HR-MUT had significantly higher immune response ability than HR-WT (**Figure 6A**), while HR-MUT had significantly lower DNA repair ability, tumor metabolism ability, and tumor metastasis ability (**Figures 6B–D**).

DISCUSSION

In this study, we found that HR-MUT is related to the reduced occurrence of tumor metastasis in CRC patients who have received chemotherapy. Additionally, HR-MUT was related to a significantly longer OS time than HR-WT for CRC patients receiving chemotherapy. More importantly, univariate and multivariate cox regression models showed that HR-MUT acts as an independent prognostic marker for CRC patients receiving chemotherapy. From the data derived from the genome level analysis, we found that HR-MUT CRC patients had significantly increased TMB and MSI scores, as well as MSI-Instable status, in comparison to HR-WT CRC patients. Based on the pathway enrichment analysis, HR-MUT patients displayed a significant reduction in their DNA repair ability, tumor survival or metastasis related activity, and tumor metabolic activity. Conversely, HR-MUT patients displayed a much higher level of immune response activity. We also found that HR-MUT CRC patients had a longer survival time after receiving immunotherapy than HR-WT CRC patients. Therefore, we speculate that HR-MUT may be a valuable prognostic marker for CRC patients receiving chemotherapy.

The stronger immune response in the tumor microenvironment may be one of the potential mechanisms behind the better prognosis found in HR-MUT patients receiving chemotherapy. In the HR-MUT group, the activity of the interferon gamma production pathway was significantly higher than that of the HR-WT group. In this vein, studies have shown that although chemotherapeutic drugs can directly clear divided endothelial cells by inhibiting enzymes involved in DNA replication or microtubule metabolism, most of the vascular injuries may be caused by chemotherapy-induced inflammation (Kerbel and Kamen, 2004; Lee and Wu, 2015). This is due to the fact that in the process of tumor rejection induced by cyclopamine, immune downregulation is activated to produce interferon-γ (IFN-γ), thus inhibiting angiogenesis (Ibe et al., 2001). IFNγ-γ-mediated vascular inhibition is one of the important anti-tumor mechanisms of T cells (Qin and Blankenstein, 2000; Kammertoens et al., 2017), as it can reduce the expression of Dll4 signaling pathway in endothelial cells, destroy the connection between endothelial cells, and resist angiogenesis in tumor tissue (Deng et al., 2014). However, in a study on early treatment of tumors that combined IFNγ with chemotherapy, it was found that IFNγ could in fact increase the mortality rate (Alberts et al., 2008; Zarogoulidis et al., 2013). As for the activity of IL-6 production, the rates in HR-MUT were significantly lower than that in HR-WT. Further research on this topic has revealed that IL-6 activates the STAT3 signaling

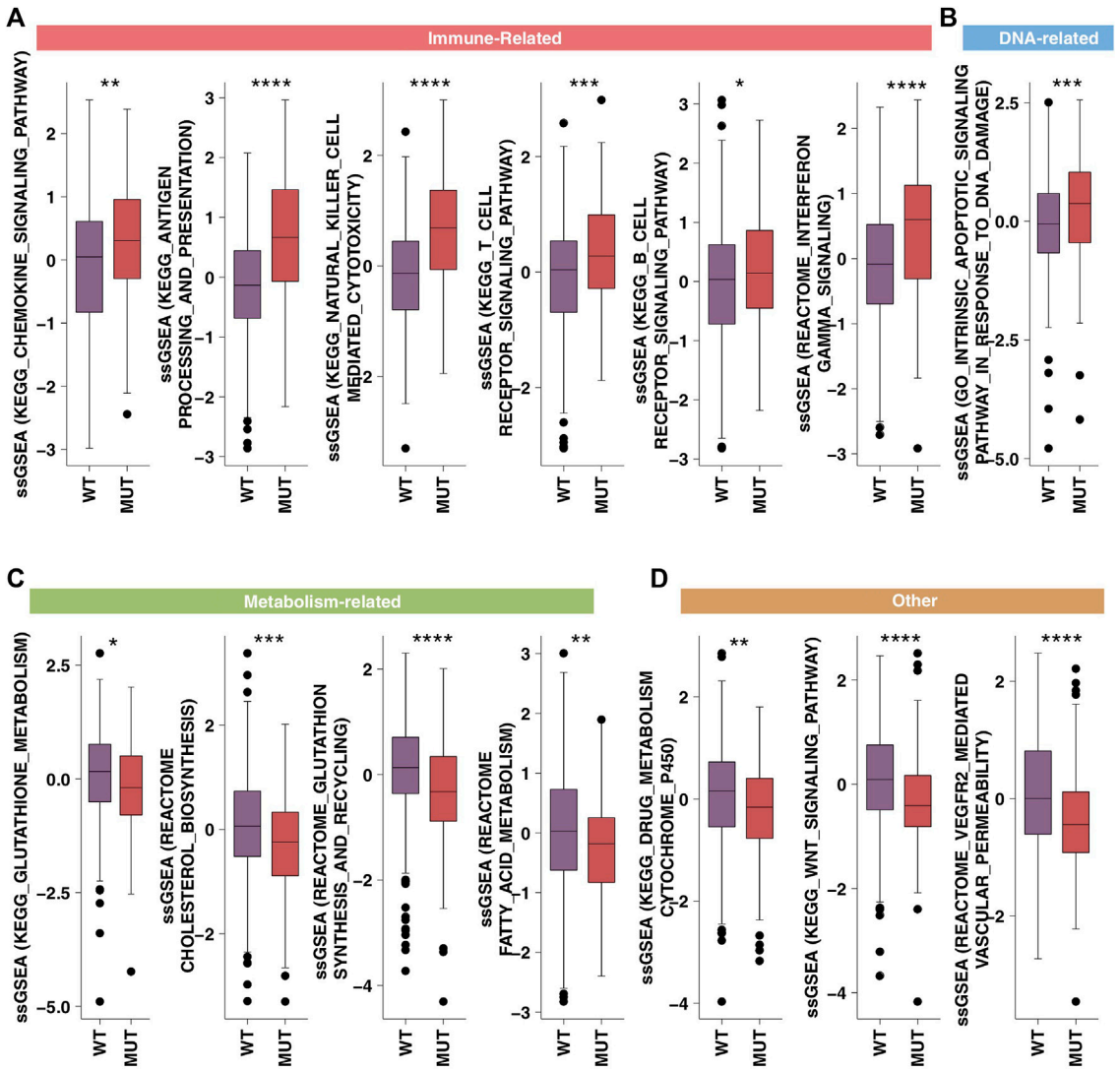

FIGURE 6 | The ssGSEA results. A comparison between the ssGSEA scores in the category of immune-related **(A)**, DNA-related **(B)**, metabolism-related **(C)** and tumor metastasis/growth related **(D)** of the HR-MUT and HR-WT based on the ssGSEA algorithm (*$p < 0.05$; **$p < 0.01$; ***$p < 0.001$; ****$p < 0.0001$).

pathway of tumor cells and promotes the expression of VEGF, thereby inducing angiogenesis (Wei et al., 2003). We also found that the activation of macrophages in the HR-MUT group was significantly lower than that in the HR-WT group. Earlier research on this shows that macrophages are one of the main cell types in the tumor microenvironment, and they can promote cell survival and chemotherapy resistance by releasing interleukin -17 (Guo et al., 2017). Similarly, according to an earlier study by Ruffell. et al., it was found that M2 macrophage inhibited the production of IL-12 by dendritic cells through the over-secretion of IL-10, therefore blocking the immune response of CD8+T cells (Ruffell et al., 2014).

Tumor metabolic reprogramming may also be one of the important mechanisms involved in CRC chemotherapy resistance. In our study, we found that lipid metabolism was significantly down-regulated in HR-MUT. Beyond our own results, other studies have confirmed that lipid metabolism rearrangement is involved in the regulation of the CRC cell chemotherapy resistance mechanism (Fiucci et al., 2000; Cotte et al., 2018), plays a role in the occurrence and development of CRC (Hwang et al., 2014; Liu et al., 2016; Mihajlovic et al., 2019; Liu et al., 2020), and has an impact on the prognosis (de Figueiredo Junior et al., 2018). Research has also found that lipid droplets (LD) levels in CRC cells are significantly higher than in those of normal cells, indicating that it may play a key role in the development of CRC (Accioly et al., 2008). Many studies have confirmed that lipid metabolism-related enzymes participate in the occurrence and development of CRC (Liu et al., 2020), regulate cell proliferation and invasion (Sánchez-Martínez et al., 2015; Nath and Chan, 2016), and participate in drug resistance (Fiucci et al., 2000; Cotte et al., 2018). Because of this, fatty acids, phospholipids, and cholesterol are synthesized actively, and their concentrations are significantly increased in tumor tissues (Janardhan

et al., 2006; Lupu and Menendez, 2006). With this in mind, some anti-tumor drugs have been developed to significantly reduce cell cholesterol levels by blocking different steps of cholesterol biosynthesis (Eliassen et al., 2005; Gorin et al., 2012; Luu et al., 2013). Except for lipid metabolism, we found that the activity of glutathione synthesis in HR-MUT group was significantly lower than that in HR-WT group. Glutamine metabolism can also promote drug resistance in tumors by influencing the post-translational modification of proteins. Treatment with glutamine analogue DON can increase the sensitivity of pancreatic cancer to gemcitabine. In past studies, researchers have found that DON can inhibit hexosamine pathways, which leads to a change in the glycosylation level of protein groups in the cell as while. This ultimately affects the sensitivity of tumors to chemotherapy (Chen et al., 2017). Additionally, glutamine metabolism can affect the drug resistance of tumors epigenetically. In *KRAS* mutant colon cancer cells, *SLC25A22* promotes the accumulation of succinic acid, a metabolite of glutamine in the tricarboxylic acid cycle, which further increases the local methylation degree of DNA and then promotes the activation of Wnt signaling pathway. This sequence of events leads to tolerance of colon cancer cells to chemotherapeutic drugs (Wong et al., 2020).

In addition to immune response and tumor metabolism reprogramming, pathways related to tumor growth and metastasis may also be involved in CRC chemotherapy resistance. Based on GSEA and ssGSEA, we found that the WNT pathway activity was significantly upregulated in HR-WT. According to Nagaraj et al., the expression levels of β-catenin and survivin in A549 sensitive and drug-resistant cells were higher than those in sensitive cells after cisplatin treatment (Nagaraj et al., 2015). Furthermore, Novetsky et al.'s research indicated that inhibiting the activity of GSK-3β in cells can activate the WNT pathway, which mediates chemotherapy resistance (Novetsky et al., 2013). Zhang et al. found that interfering with β-catenin using siRNA can improve the sensitivity of tumor cells to chemotherapeutic drugs, further proving that the WNT pathway plays an important role in chemotherapeutic drug resistance (Zhang et al., 2015). In our own research, we found that VEGFR2 pathway was significantly activated in HR-WT. Similarly, Mann et al. inhibited the phosphorylation of VEGFR2 in tumor cells and observed that while blood vessels in the tumor remained normal, the sensitivity of the tumor cells to chemotherapeutic drugs such as cyclophosphamide and cisplatin was enhanced (Stockmann et al., 2008).

CONCLUSION

In summary, our research shows that HR-MUT is associated with less tumor metastasis in CRC patients after receiving chemotherapy. The HR-MUT CRC patients had significantly improved OS time and, as such, HR-MUT could be used as a predictor of chemotherapy prognosis in the future treatment plan. Additionally, HR-MUT patients had higher TMB levels, MSI scores, and immune response activity, while they also had lower tumor survival, metastasis pathway activity, and tumor metabolic reprogramming activity. The activity of these pathways may greatly increase the sensitivity of HR-MUT patients to chemotherapy drugs. Therefore, HR-MUT may be used as a new predictive marker for CRC patients who are receiving chemotherapy treatment.

DATA AVAILABILITY STATEMENT

The original contributions presented in the study are included in the article/**Supplementary Material**, further inquiries can be directed to the corresponding authors.

ETHICS STATEMENT

The studies involving human participants were reviewed and approved by Guangxi Medical University Cancer Hospital. The patients/participants provided their written informed consent to participate in this study.

AUTHOR CONTRIBUTIONS

Conceptualization, YL and RL; Formal analysis, YL and XL; Visualization, YL and XL; Writing–original draft, YZ, GW, JY, SL, XH, ML, MX, JZ, QL, YH, SL, YL, and RL; Writing–review and editing, YL, XL, YZ, GW, JY, SL, XH, ML, MX, JZ, QL, YH, SL, YL, and RL. All authors read and approved the final manuscript.

SUPPLEMENTARY MATERIAL

The Supplementary Material for this article can be found online at: https://www.frontiersin.org/articles/10.3389/fphar.2022.920939/full#supplementary-material

Supplementary Figure S1 | The co-occurrence and mutually exclusive occurrence of the top 20 mutated genes in the Local-CRC **(A)** and the Mondaca-CRC **(B)** cohorts.

Supplementary Figure S2 | The mutation landscape of the HR mutations of the HR-MUT CRC patients in the Local-CRC **(A)** and the Mondaca-CRC **(B)** cohorts.

Supplementary Table S1 | The clinical characteristics of the Local-CRC cohort.

Supplementary Table S2 | The clinical characteristics of the Mondaca-CRC cohort.

Supplementary Table S3 | The clinical characteristics of the TCGA-CRC cohort.

Supplementary Table S4 | The gene set of the HR signaling used in this study.

Supplementary Table S5 | The GSEA result of the enrichment scores between the HR-MUT and HR-WT groups based on the GSEA algorithm.

REFERENCES

Accioly, M. T., Pacheco, P., Maya-Monteiro, C. M., Carrossini, N., Robbs, B. K., Oliveira, S. S., et al. (2008). Lipid Bodies Are Reservoirs of Cyclooxygenase-2 and Sites of Prostaglandin-E2 Synthesis in Colon Cancer Cells. *Cancer Res.* 68, 1732–1740. doi:10.1158/0008-5472.CAN-07-1999

Alberts, D. S., Marth, C., Alvarez, R. D., Johnson, G., Bidzinski, M., Kardatzke, D. R., et al. (2008). Randomized Phase 3 Trial of Interferon Gamma-1b Plus Standard Carboplatin/Paclitaxel Versus Carboplatin/paclitaxel Alone for First-Line Treatment of Advanced Ovarian and Primary Peritoneal Carcinomas: Results from a Prospectively Designed Analysis of Progression-Free Survival. *Gynecol. Oncol.* 109, 174–181. doi:10.1016/j.ygyno.2008.01.005

Bian, Z., Jin, L., Zhang, J., Yin, Y., Quan, C., Hu, Y., et al. (2016). LncRNA-UCA1 Enhances Cell Proliferation and 5-Fluorouracil Resistance in Colorectal Cancer by Inhibiting miR-204-5p. *Sci. Rep.* 6, 23892. doi:10.1038/srep23892

Chen, R., Lai, L. A., Sullivan, Y., Wong, M., Wang, L., Riddell, J., et al. (2017). Disrupting Glutamine Metabolic Pathways to Sensitize Gemcitabine-Resistant Pancreatic Cancer. *Sci. Rep.* 7, 7950. doi:10.1038/s41598-017-08436-6

Colaprico, A., Silva, T. C., Olsen, C., Garofano, L., Cava, C., Garolini, D., et al. (2016). TCGAbiolinks: An R/Bioconductor Package for Integrative Analysis of TCGA Data. *Nucleic Acids Res.* 44, e71. doi:10.1093/nar/gkv1507

Cotte, A. K., Aires, V., Fredon, M., Limagne, E., Derangère, V., Thibaudin, M., et al. (2018). Lysophosphatidylcholine Acyltransferase 2-Mediated Lipid Droplet Production Supports Colorectal Cancer Chemoresistance. *Nat. Commun.* 9, 322. doi:10.1038/s41467-017-02732-5

de Figueiredo Junior, A. G., Serafim, P. V. P., de Melo, A. A., Felipe, A. V., Lo Turco, E. G., da Silva, I. D. C. G., et al. (2018). Analysis of the Lipid Profile in Patients with Colorectal Cancer in Advanced Stages. *Asian Pac J. Cancer Prev.* 19, 1287–1293. doi:10.22034/APJCP.2018.19.5.1287

Deng, J., Liu, X., Rong, L., Ni, C., Li, X., Yang, W., et al. (2014). Ifnγ-Responsiveness of Endothelial Cells Leads to Efficient Angiostasis in Tumours Involving Down-Regulation of Dll4. *J. Pathol.* 233, 170–182. doi:10.1002/path.4340

Eliassen, A. H., Colditz, G. A., Rosner, B., Willett, W. C., and Hankinson, S. E. (2005). Serum Lipids, Lipid-Lowering Drugs, and the Risk of Breast Cancer. *Arch. Intern Med.* 165, 2264–2271. doi:10.1001/archinte.165.19.2264

Fiucci, G., Czarny, M., Lavie, Y., Zhao, D., Berse, B., Blusztajn, J. K., et al. (2000). Changes in Phospholipase D Isoform Activity and Expression in Multidrug-Resistant Human Cancer Cells. *Int. J. Cancer* 85, 882–888. doi:10.1002/(sici)1097-0215(20000315)85:6<882::aid-ijc24>3.0.co;2-e

Fu, Q., Cheng, J., Zhang, J., Zhang, Y., Chen, X., Xie, J., et al. (2016). Downregulation of YEATS4 by miR-218 Sensitizes Colorectal Cancer Cells to L-OHP-Induced Cell Apoptosis by Inhibiting Cytoprotective Autophagy. *Oncol. Rep.* 36, 3682–3690. doi:10.3892/or.2016.5195

Gonzalez, D., and Stenzinger, A. (2021). Homologous Recombination Repair Deficiency (HRD): From Biology to Clinical Exploitation. *Genes Chromosom. Cancer* 60, 299–302. doi:10.1002/gcc.22939

Gorin, A., Gabitova, L., and Astsaturov, I. (2012). Regulation of Cholesterol Biosynthesis and Cancer Signaling. *Curr. Opin. Pharmacol.* 12, 710–716. doi:10.1016/j.coph.2012.06.011

Guo, B., Li, L., Guo, J., Liu, A., Wu, J., Wang, H., et al. (2017). M2 Tumor-Associated Macrophages Produce Interleukin-17 to Suppress Oxaliplatin-Induced Apoptosis in Hepatocellular Carcinoma. *Oncotarget* 8, 44465–44476. doi:10.18632/oncotarget.17973

Hwang, W. C., Kim, M. K., Song, J. H., Choi, K. Y., and Min, do. S. (2014). Inhibition of Phospholipase D2 Induces Autophagy in Colorectal Cancer Cells. *Exp. Mol. Med.* 46, e124. doi:10.1038/emm.2014.74

Ibe, S., Qin, Z., Schüler, T., Preiss, S., and Blankenstein, T. (2001). Tumor Rejection by Disturbing Tumor Stroma Cell Interactions. *J. Exp. Med.* 194, 1549–1559. doi:10.1084/jem.194.11.1549

Janardhan, S., Srivani, P., and Sastry, G. N. (2006). Choline Kinase: An Important Target for Cancer. *Curr. Med. Chem.* 13, 1169–1186. doi:10.2174/092986706776360923

Kammertoens, T., Friese, C., Arina, A., Idel, C., Briesemeister, D., Rothe, M., et al. (2017). Tumour Ischaemia by Interferon-γ Resembles Physiological Blood Vessel Regression. *Nature* 545, 98–102. doi:10.1038/nature22311

Kerbel, R. S., and Kamen, B. A. (2004). The Anti-Angiogenic Basis of Metronomic Chemotherapy. *Nat. Rev. Cancer* 4, 423–436. doi:10.1038/nrc1369

Lee, J. G., and Wu, R. (2015). Erlotinib-Cisplatin Combination Inhibits Growth and Angiogenesis Through C-MYC and HIF-1α in EGFR-Mutated Lung Cancer *In Vitro* and *In Vivo*. *Neoplasia* 17, 190–200. doi:10.1016/j.neo.2014.12.008

Li, L., Shang, J., Zhang, Y., Liu, S., Peng, Y., Zhou, Z., et al. (2017). MEG3 Is a Prognostic Factor for CRC and Promotes Chemosensitivity by Enhancing Oxaliplatin-Induced Cell Apoptosis. *Oncol. Rep.* 38, 1383–1392. doi:10.3892/or.2017.5828

Liberzon, A., Subramanian, A., Pinchback, R., Thorvaldsdóttir, H., Tamayo, P., and Mesirov, J. P. (2011). Molecular Signatures Database (MSigDB) 3.0. *Bioinformatics* 27, 1739–1740. doi:10.1093/bioinformatics/btr260

Lin, A., Zhang, J., and Luo, P. (2020). Crosstalk between the MSI Status and Tumor Microenvironment in Colorectal Cancer. *Front. Immunol.* 11, e15236–2039. doi:10.1200/JCO.2020.38.15_suppl.e1523610.3389/fimmu.2020.02039

Lin, A., Qi, C., Wei, T., Li, M., Cheng, Q., Liu, Z., et al. (2022). CAMOIP: A Web Server for Comprehensive Analysis on Multi-Omics of Immunotherapy in Pan-Cancer. *Brief. Bioinform* 23. doi:10.1093/bib/bbac129

Lisby, M., and Rothstein, R. (2015). Cell Biology of Mitotic Recombination. *Cold Spring Harb. Perspect. Biol.* 7, a016535. doi:10.1101/cshperspect.a016535

Liu, M., Du, K., Jiang, B., and Wu, X. (2020). High Expression of Phospholipase D2 Induced by Hypoxia Promotes Proliferation of Colon Cancer Cells Through Activating NF-κ Bp65 Signaling Pathway. *Pathol. Oncol. Res.* 26, 281–290. doi:10.1007/s12253-018-0429-1

Liu, M., Fu, Z., Wu, X., Du, K., Zhang, S., and Zeng, L. (2016). Inhibition of Phospholipase D2 Increases Hypoxia-Induced Human Colon Cancer Cell Apoptosis Through Inactivating of the PI3K/AKT Signaling Pathway. *Tumour Biol.* 37, 6155–6168. doi:10.1007/s13277-015-4348-4

Liu, Z., Guo, C., Dang, Q., Wang, L., Liu, L., Weng, S., et al. (2022). Integrative Analysis from Multi-Center Studies Identities a Consensus Machine Learning-Derived lncRNA Signature for Stage II/III Colorectal Cancer. *EBioMedicine* 75, 103750. doi:10.1016/j.ebiom.2021.103750

Liu, Z., Guo, C., Li, J., Xu, H., Lu, T., Wang, L., et al. (2021). Somatic Mutations in Homologous Recombination Pathway Predict Favourable Prognosis After Immunotherapy Across Multiple Cancer Types. *Clin. Transl. Med.* 11, e619. doi:10.1002/ctm2.619

Liu, Z., Liu, L., Weng, S., Guo, C., Dang, Q., Xu, H., et al. (2022). Machine Learning-Based Integration Develops an Immune-Derived lncRNA Signature for Improving Outcomes in Colorectal Cancer. *Nat. Commun.* 13, 816. doi:10.1038/s41467-022-28421-6

Lupu, R., and Menendez, J. A. (2006). Pharmacological Inhibitors of Fatty Acid Synthase (FASN)–Catalyzed Endogenous Fatty Acid Biogenesis: A New Family of Anti-Cancer Agents? *Curr. Pharm. Biotechnol.* 7, 483–493. doi:10.2174/138920106779116928

Luu, W., Sharpe, L. J., Gelissen, I. C., and Brown, A. J. (2013). The Role of Signalling in Cellular Cholesterol Homeostasis. *IUBMB Life* 65, 675–684. doi:10.1002/iub.1182

Mihajlovic, M., Gojkovic, T., Vladimirov, S., Miljkovic, M., Stefanovic, A., Vekic, J., et al. (2019). Changes in Lecithin: Cholesterol Acyltransferase, Cholesteryl Ester Transfer Protein and Paraoxonase-1 Activities in Patients with Colorectal Cancer. *Clin. Biochem.* 63, 32–38. doi:10.1016/j.clinbiochem.2018.11.010

Miller, K. D., Fidler-Benaoudia, M., Keegan, T. H., Hipp, H. S., Jemal, A., and Siegel, R. L. (2020). Cancer Statistics for Adolescents and Young Adults, 2020. *CA Cancer J. Clin.* 70, 443–459. doi:10.3322/caac.2159010.3322/caac.21637

Mondaca, S., Walch, H., Nandakumar, S., Chatila, W. K., Schultz, N., and Yaeger, R. (2020). Specific Mutations in APC, but Not Alterations in DNA Damage Response, Associate with Outcomes of Patients with Metastatic Colorectal Cancer. *Gastroenterology* 159, 1975–1978. doi:10.1053/j.gastro.2020.07.041

Nagaraj, A. B., Joseph, P., Kovalenko, O., Singh, S., Armstrong, A., Redline, R., et al. (2015). Critical Role of Wnt/β-Catenin Signaling in Driving Epithelial Ovarian Cancer Platinum Resistance. *Oncotarget* 6, 23720–23734. doi:10.18632/oncotarget.4690

Nath, A., and Chan, C. (2016). Genetic Alterations in Fatty Acid Transport and Metabolism Genes Are Associated with Metastatic Progression and Poor Prognosis of Human Cancers. *Sci. Rep.* 6, 18669. doi:10.1038/srep18669

Novetsky, A. P., Thompson, D. M., Zighelboim, I., Thaker, P. H., Powell, M. A., Mutch, D. G., et al. (2013). Lithium Chloride and Inhibition of Glycogen Synthase Kinase 3β as a Potential Therapy for Serous Ovarian Cancer. *Int. J. Gynecol. Cancer* 23, 361–366. doi:10.1097/IGC.0b013e31827cfecb

Qin, Z., and Blankenstein, T. (2000). CD4+ T Cell-Mediated Tumor Rejection Involves Inhibition of Angiogenesis that Is Dependent on IFN Gamma Receptor Expression by Nonhematopoietic Cells. *Immunity* 12, 677–686. doi:10.1016/s1074-7613(00)80218-6

Ruffell, B., Chang-Strachan, D., Chan, V., Rosenbusch, A., Ho, C. M., Pryer, N., et al. (2014). Macrophage IL-10 Blocks CD8+ T Cell-Dependent Responses to Chemotherapy by Suppressing IL-12 Expression in Intratumoral Dendritic Cells. *Cancer Cell* 26, 623–637. doi:10.1016/j.ccell.2014.09.006

Sánchez-Martínez, R., Cruz-Gil, S., Gómez de Cedrón, M., Álvarez-Fernández, M., Vargas, T., Molina, S., et al. (2015). A Link Between Lipid Metabolism and Epithelial-Mesenchymal Transition Provides a Target for Colon Cancer Therapy. *Oncotarget* 6, 38719–38736. doi:10.18632/oncotarget.5340

Stockmann, C., Doedens, A., Weidemann, A., Zhang, N., Takeda, N., Greenberg, J. I., et al. (2008). Deletion of Vascular Endothelial Growth Factor in Myeloid Cells Accelerates Tumorigenesis. *Nature* 456, 814–818. doi:10.1038/nature07445

Wei, L. H., Kuo, M. L., Chen, C. A., Chou, C. H., Lai, K. B., Lee, C. N., et al. (2003). Interleukin-6 Promotes Cervical Tumor Growth by VEGF-Dependent Angiogenesis via a STAT3 Pathway. *Oncogene* 22, 1517–1527. doi:10.1038/sj.onc.1206226

Wong, C. C., Xu, J., Bian, X., Wu, J. L., Kang, W., Qian, Y., et al. (2020). In Colorectal Cancer Cells with Mutant KRAS, SLC25A22-Mediated Glutaminolysis Reduces DNA Demethylation to Increase WNT Signaling, Stemness, and Drug Resistance. *Gastroenterology* 159, 2163–e6. doi:10.1053/j.gastro.2020.08.016

Xiao, M., Cai, J., Cai, L., Jia, J., Xie, L., Zhu, Y., et al. (2017). Let-7e Sensitizes Epithelial Ovarian Cancer to Cisplatin Through Repressing DNA Double Strand Break Repair. *J. Ovarian Res.* 10, 24. doi:10.1186/s13048-017-0321-8

Yu, G., Wang, L. G., Han, Y., and He, Q. Y. (2012). clusterProfiler: An R Package for Comparing Biological Themes Among Gene Clusters. *OMICS* 16, 284–287. doi:10.1089/omi.2011.0118

Zarogoulidis, K., Ziogas, E., Boutsikou, E., Zarogoulidis, P., Darwiche, K., Kontakiotis, T., et al. (2013). Immunomodifiers in Combination with Conventional Chemotherapy in Small Cell Lung Cancer: A Phase II, Randomized Study. *Drug Des. Devel. Ther.* 7, 611–617. doi:10.2147/DDDT.S43184

Zdraveski, Z. Z., Mello, J. A., Marinus, M. G., and Essigmann, J. M. (2000). Multiple Pathways of Recombination Define Cellular Responses to Cisplatin. *Chem. Biol.* 7, 39–50. doi:10.1016/s1074-5521(00)00064-8

Zhang, B., Yang, Y., Shi, X., Liao, W., Chen, M., Cheng, A. S., et al. (2015). Proton Pump Inhibitor Pantoprazole Abrogates Adriamycin-Resistant Gastric Cancer Cell Invasiveness via Suppression of Akt/GSK-B/β-Catenin Signaling and Epithelial-Mesenchymal Transition. *Cancer Lett.* 356, 704–712. doi:10.1016/j.canlet.2014.10.016

Conflict of Interest: The authors declare that the research was conducted in the absence of any commercial or financial relationships that could be construed as a potential conflict of interest.

Publisher's Note: All claims expressed in this article are solely those of the authors and do not necessarily represent those of their affiliated organizations, or those of the publisher, the editors and the reviewers. Any product that may be evaluated in this article, or claim that may be made by its manufacturer, is not guaranteed or endorsed by the publisher.

frontiers | Frontiers in Pharmacology

TYPE Original Research
PUBLISHED 15 August 2022
DOI 10.3389/fphar.2022.950156

OPEN ACCESS

EDITED BY
Haitao Wang,
National Cancer Institute (NIH),
United States

REVIEWED BY
Xinwei Wu,
National Institutes of Health (NIH),
United States
Lin Zhang,
Clinical Center (NIH), United States
Zhiyong Liu,
The Rockefeller University,
United States
Kui Zhang,
The University of Chicago, United States
Jiankang Fang,
University of Pennsylvania, United States

*CORRESPONDENCE
Liangyin Wu,
53537972@qq.com

SPECIALTY SECTION
This article was submitted to Pharmacology of Anti-Cancer Drugs, a section of the journal Frontiers in Pharmacology

RECEIVED 22 May 2022
ACCEPTED 21 July 2022
PUBLISHED 15 August 2022

CITATION
Liu J, Li W and Wu L (2022), Pan-cancer analysis suggests histocompatibility minor 13 is an unfavorable prognostic biomarker promoting cell proliferation, migration, and invasion in hepatocellular carcinoma.
Front. Pharmacol. 13:950156.
doi: 10.3389/fphar.2022.950156

Pan-cancer analysis suggests histocompatibility minor 13 is an unfavorable prognostic biomarker promoting cell proliferation, migration, and invasion in hepatocellular carcinoma

Jun Liu[1,2], Wenli Li[3] and Liangyin Wu[1]*

[1]Department of Clinical Laboratory, Yue Bei People's Hospital, Shantou University Medical College, Shaoguan, Guangdong, China, [2]Medical Research Center, Yue Bei People's Hospital, Shantou University Medical College, Shaoguan, Guangdong, China, [3]Reproductive Medicine Center, Yue Bei People's Hospital, Shantou University Medical College, Shaoguan, Guangdong, China

Histocompatibility Minor 13 (HM13) encoding the signal peptide peptidase plays an important role in maintaining protein homeostasis but its role in tumors remains unclear. In this study, 33 tumor RNA-seq datasets were extracted from The Cancer Genome Atlas (TCGA) database, and the pan-cancer expression profile of HM13 was evaluated in combination with The Genotype-Tissue Expression (GTEx) datasets. The prognostic significance of abnormal HM13 pan-cancer expression was evaluated by univariate Cox regression and Kaplan-Meier analyses. Co-expression analysis was performed to examine the correlation between abnormal pan-cancer expression of HM13 and immune cell infiltration, immune checkpoint, molecules related to RNA modification, tumor mutational burden (TMB), microsatellite instability (MSI), and other related molecules. CellMiner database was used to evaluate the relationship between the expression of HM13 and drug sensitivity. The results showed overexpression of HM13 in almost all tumors except kidney chromophobe (KICH). Abnormally high expression of HM13 in adrenocortical carcinoma (ACC), kidney renal papillary cell carcinoma (KIRP), uveal melanoma (UVM), liver hepatocellular carcinoma (LIHC), brain lower grade glioma (LGG), head and neck squamous cell carcinoma (HNSC), and kidney renal clear cell carcinoma (KIRC) was associated with poor prognosis. Expression of HM13 correlated strongly with pan-cancer immune checkpoint gene expression and immune cell infiltration. Drug sensitivity analysis indicated that the expression of HM13 was an excellent predictor of drug sensitivity. We verified that both mRNA and protein levels of HM13 were abnormally upregulated in HCC tissues, and were independent risk factors for poor prognosis. Furthermore, interference with HM13 expression in Huh-7 and HCCLM3 cells significantly inhibited proliferation, migration, and invasion. Therefore, our findings demonstrate that HM13 is a potential pan-cancer

prognostic marker, thus providing a new dimension for understanding tumor development.

KEYWORDS

histocompatibility minor 13, pan-cancer, prognostic biomarker, drug sensitivity, cell proliferation

Introduction

Cancer is a grave threat to public health worldwide owing to the high morbidity and mortality (Wu et al., 2019). In recent years, the overall death rate due to cancer in developed countries such as the United States has decreased owing to advanced medical technology and the concept of precise and individualized medicine, however, the situation remains unfavorable (Golemis et al., 2018). In the United States, daily, 1,700 people die of cancer (Delman, 2020). Incidence and mortality of cancer in developing countries are showing an increasing trend. With the rise in the aging population globally, researchers predict that the incidence of cancer will double by 2070 relative to 2020 (Soerjomataram and Bray, 2021). In recent years, although the application of immunotherapy and individualized targeted therapy has been successful to an extent, the rate of effectiveness is only 20%, and that of survival among patients remains unsatisfactory. Therefore, the identification of new tumor markers is necessary to facilitate early diagnosis and enhance the prognostic assessment of cancer, thereby increasing the overall survival rate.

The signal peptide peptidase encoded by Histocompatibility Minor 13 (HM13) is localized to the endoplasmic reticulum and is mainly implicated in the regulation of the US2 pathway, which in turn is responsible for the cleavage of the pro-protease and catalytic hydrolysis of proteins in the membrane (Loureiro et al., 2006). Previous studies suggest that HM13 is crucial in the regulation of the production of lymphocyte surface (HLA-E) epitopes that generate MHCI-like signal peptides recognized by the immune system (Lemberg et al., 2001). Moreover, accumulating evidence shows that HM13 is involved in cell signaling and intracellular communication (Brown et al., 2000; Urban et al., 2001). Jian Zhou et al. show that HM13 is highly expressed in lung cancer tissues and is a potential marker for early diagnosis of lung cancer (Zhou et al., 2021). Tine Goovaerts et al. demonstrate that methylation at the promoter level in HM13 is abnormally dysregulated in breast cancer, thus leading to its aberrantly high expression and underlies its involvement (Goovaerts et al., 2018). Currently, very little research has disclosed how HM13 plays a role in tumor development. Further, its pan-cancer expression and role in tumorigenesis remain unclear.

In recent years, with advancements in -omics technology and the application of high-throughput sequencing methods, large-omics data have been generated, which are expected to facilitate studies on the occurrence and related mechanisms underlying diseases (Sherman and Salzberg, 2020). Thus, in this study, we analyzed the pan-cancer expression of HM13 in tissues using RNA-seq datasets in The Cancer Genome Atlas (TCGA). Relying on the large clinical follow-up data, we investigated the effects of abnormal HM13 expression on overall and disease-free survival. Moreover, we elucidated the potential mechanism underlying HM13 action in tumor development and genesis and identified the correlation of HM13 expression with tumor mutation load, immune cell invasion, microsatellite instability, and tumor purity in the tumor microenvironment. Additionally, by transcriptomics and proteomics, we verified the expression and prognostic value of HM13 in hepatocellular carcinoma (HCC). Furthermore, the effects of HM13 were examined on cellular migration, proliferation, and invasion in HCC lines. Herein, the pan-cancer expression of HM13 in tissues was described using multi-omics data, thus providing a new dimension for understanding the occurrence of tumors.

Materials and methods

Acquisition of transcriptomic and clinical data

The unified standardized TCGA pan-cancer dataset and RNA-seq data from TCGA and GTEx in TPM format uniformly processed by the toil method were downloaded from the UCSC database (https://xenabrowser.net/). All relevant survival data from clinical follow-up were obtained. Transcriptome data of HCC (ICGC-LIRI-JP) and corresponding clinical data were extracted from the ICGC database (https://dcc.icgc.org/). Protein data of HCC (PDC000198) processed by Z-score standardization and the corresponding follow-up information were obtained from the CPTAC database (https://pdc.cancer.gov/). In addition, we obtained the microarray data and RNA-Seq of HCC from Gene Expression Omnibus (GEO) database, including GSE36376, GSE63898, GSE64041 and GSE202853 cohort. Microsatellite instability scores for 33 tumors were obtained from the literature review (Bonneville et al., 2017). Level 4 Simple Nucleotide Variation dataset for all TCGA samples processed using the MuTect2 software was obtained from TCGA (https://portal.gdc.cancer.gov/), and subsequently, the tumor mutation burden was calculated (Beroukhim et al., 2010). Purity and ploidy data for several tumors were obtained from the literature (Thorsson et al., 2018).

Differential analysis and prognostic significance of HM13 expression

The differential expression of HM13 between normal and tumor tissues was analyzed by the Wilcoxon rank-sum test. The "survminer" and "survival" packages were used for Kaplan-Meier and univariate COX analyses to examine the effects of HM13 expression on the progression-free survival and overall survival; to estimate the statistical significance of the results, the log-rank test was employed.

Correlation and functional enrichment analyses

Tumour Immune Estimation Resource is a website (TIMER, https://cistrome.shinyapps.io/timer/) used for comprehensively evaluating the levels of tumor immune cells infiltration, and was used to obtain information on six types of immune cell invasion in common tumors in TCGA. The corr. test function in the psych package (R software, version 2.1.6) was employed to calculate the Pearson's correlation coefficient between pan-cancer HM13 expression and immune cell infiltration score. Additionally, we also calculated the Pearson's correlation coefficient between HM13 expression and the previously reported immune checkpoint genes, RNA modified genes, TMB, MSI, purity, and ploidy in tumors. The functions of the GSVA package were used to perform ssGSEA analysis to predict the infiltration of 24 types of immune cells in HCC and calculate the association between immune cell infiltration levels and the HM13 expression (Bindea et al., 2013). The clusterProfiler package in R was used for GO annotation and KEGG pathway enrichment analyses. To construct the potential interaction network for HM13, the GeneMANIA database (http://genemania.org/) was used.

Drug sensitivity analysis of HM13

CellMiner database integrates the correlation between drug sensitivity of tumor cells and genome data for tumor treatment (Reinhold et al., 2012). The CellMiner database was used to evaluate HM13 expression and drug sensitivity data. The Genomics of Drug Sensitivity in Cancer (GDSC) database (https://www.cancerrxgene.org/) was used to obtain drug response data for 265 compounds in 1,001 cancer cell lines. Additionally, the cell lines were categorized as high expression and low expression based on the median HM13 expression. The sensitivity of both cell lines to drugs was compared.

Cell culture

Human normal hepatocytes, LO2, and the HCC cell lines, including HCCLM3, Huh7, and HepG2, were obtained from American Type Culture Collection (ATCC, Manassas, VA, United States). Huh7 and HCCLM3 cells were grown in DMEM supplemented with 10% fetal bovine serum (FBS). HepG2 cells were grown in MEM supplemented with 10% FBS. LO2 cells were grown in RPMI-1640 supplemented with 10% FBS. All cells were cultured in an incubator at 37°C with 5% CO_2. Transfection were performed with 70%–80% cell density, according to the instructions of Lipo3000 (L3000015, Invitrogen, United States). ShRNA was expressed in pRNA-H1.1, and the sequences of shRNA-HM13 were as follows: shRNA-1, GCUGGAGAAGAAAGAGAAATTUUUCUCUUUCUUCUCCAGCTT; shRNA-2, GGCUGGAGAAGAAAGAGAATTUUCUCUUUCUUCUCCAGCCTT; shRNA-3, UGACAGAGAUGUUCAGUUATTUAACUGAACAUCUCUGUCATT.

Quantitative reverse transcription-polymerase chain reaction

Total RNA in cells was extracted using the TRIpure reagent (RP1001, BioTeke, Beijing, China). The concentration of RNA in each sample was measured on an ultraviolet spectrophotometer (NANO 2000; Thermo, United States). The RNA was reverse transcribed into cDNA (D7160L, Beyotime, Shanghai, China) and stored at −80°C till further use. The primer sequences of HM13 were 5′-AGCCTGCCCTCCTATACCT-3′ and 3′-TGTTCCCTCTTTGGATTCTG-5′, and the primer sequences of β-actin were 5′-GGCACCCAGCACAATGAA-3′, 3′-TAGAAGCATTTGCGGTGG-5'. Subsequently, a real-time polymerase chain reaction (RT-PCR) quantitative fluorescence analysis was conducted for four replicates. The RT-PCR reaction conditions were as follows: cDNA template 1μL, the primers (10 μM) 0.5 μl, SYBR GREEN mastermix (PC1150, Solarbio, Beijing, China) 10 μl, and the volumes were adjusted to 20 μl with dd H_2O. The results were standardized against the gene expression of β-actin, and the relative levels of expression were estimated by the $2^{-\Delta\Delta}$ Ct method.

Western blot analysis

After the cell confluency reached 90%, protein extraction, protein quantitative analysis, SDS-PAGE (WLA025, wanleibio, China) transferring onto PVDF membrane (IPVH00010, Millipore, United States), blocking with skim milk (Q/NYLB0039S, YiLi, China), incubation with primary antibody (20416-1-AP, Proteintech, China), and subsequently, secondary antibody (WLA023, wanleibio, China) was performed. Finally,

the results were observed by luminescence using the ECL substrate (WLA003, wanleibio, China). The Gel image processing system (Gel-Pro-Analyzer software) (WD-9413B, LIUYI, China) was used to analyze the optical density values of the target bands.

CCK8 assay

When the confluency of Huh7 and HCCLM3 cells reached 90%, these were collected and seeded into 96-well culture plates with 3×10^3 cells in each well. The experiment was classified into three, namely, the no-operation, the empty vector, and the sh-HM13 groups. Each group was designed with five replicates. The CCK-8 assay was performed at 0, 24, 48, 72, and 96 h.

Clone formation assay

Cells in each group were collected and inoculated in Petri dishes at the amount of 400 cells per dish. After 14 days, visible clones formed. The cells were washed 2 times with PBS after fixation of cells with paraformaldehyde (C104188, Aladdin, China). Giemsa R1 solution (D010, Nanjing Jiancheng, China) was added in the plate to stain for 1 min. We then washed the plate three times with water after satisfactory staining with R2 solution.

Wound healing assay

The cells were collected, counted, and inoculated in a six-well plate. After adhering, the cells were transfected; 48 h following transfection, the original medium was replaced with the serum-free medium containing 1 μg/ml mitomycin C, and 1 hour later, the scratch test was performed using a 200 μl pipette tip. Subsequently, cells were photographed at 24 and 48 h.

Transwell migration and invasion assay

The transwell chambers were constructed using Matrigel glue (356,234, Corning, United States). The cells were grown in six-well plates. When the confluency reached 90%, the cells were digested and diluted to a density of 5×10^4 cells/well with serum-free medium. The invasion assay was performed as follows: Cells in the Transwell containing Matrigel glue were seeded in the upper chamber of 24-well plates, and 800 μl of the medium supplemented with 10% FBS was added to the lower chamber. The migration assay was performed as follows: In 24-well plates, the coated lower chambers of Transwell system were placed with medium containing 10% FBS in 800 μl. Upper chambers were filled with a 200 μl cell suspension. PBS washed the Transwell and 4% paraformaldehyde phosphate buffer was applied (20 min at room temperature), and stained with 0.5% crystal violet (5 min). Cells counting were performed 24 h later.

Statistical analyses

GraphPad Prism 7.0 and R software (version 4.1.1) were used for calculations, graph plotting, and statistical analyses of all data in this study. For comparison between two groups of continuous variables, the statistical significance for the normal distribution was calculated by independent Student t-test, while differences between the non-normally distributed variables were estimated by Mann-Whitney *U*-test (Wilcoxon rank-sum test). All statistical *p*-values were two-tailed, with $p < 0.05$ indicating significance.

Results

Pan-cancer expression of HM13

RNA-seq data from TCGA showed that HM13 mRNA expression was up-regulated in several tumor tissues, including uterine corpus endometrial carcinoma (UCEC), cholangio carcinoma (CHOL), glioblastoma multiforme (GBM), breast invasive carcinoma (BRCA), KIRC, HNSC, LIHC, KIRP, lung squamous cell carcinoma (LUSC), lung adenocarcinoma (LUAD), bladder urothelial carcinoma (BLCA), colon adenocarcinoma (COAD), esophageal carcinoma (ESCA), prostate adenocarcinoma (PRAD), stomach adenocarcinoma (STAD), and rectum adenocarcinoma (READ) (Figure 1A). However, its level of expression in tumor tissues from patients with KICH was lower relative to the normal tissues (Figure 1A). Since TCGA database contains fewer normal samples, we combined the standardized GTEx and TCGA data from the UCSC database. Similarly, HM13 expression tended to be high in all tumor types (Figure 1B). Furthermore, paired analysis was performed to determine HM13 expression in tumors, and the results showed high HM13expression in several tumor tissues, including UCEC, CHOL, BRCA, KIRC, HNSC, LIHC, KIRP, LUSC, LUAD, BLCA, COAD, ESCA, PRAD, STAD, and READ (Figure 1C).

Pan-cancer prognostic value of HM13 expression

To examine the effect of abnormal pan-cancer HM13 expression on the overall survival time, a univariate Cox regression analysis was conducted. The results showed that in several tumors, abnormally high HM13 expression

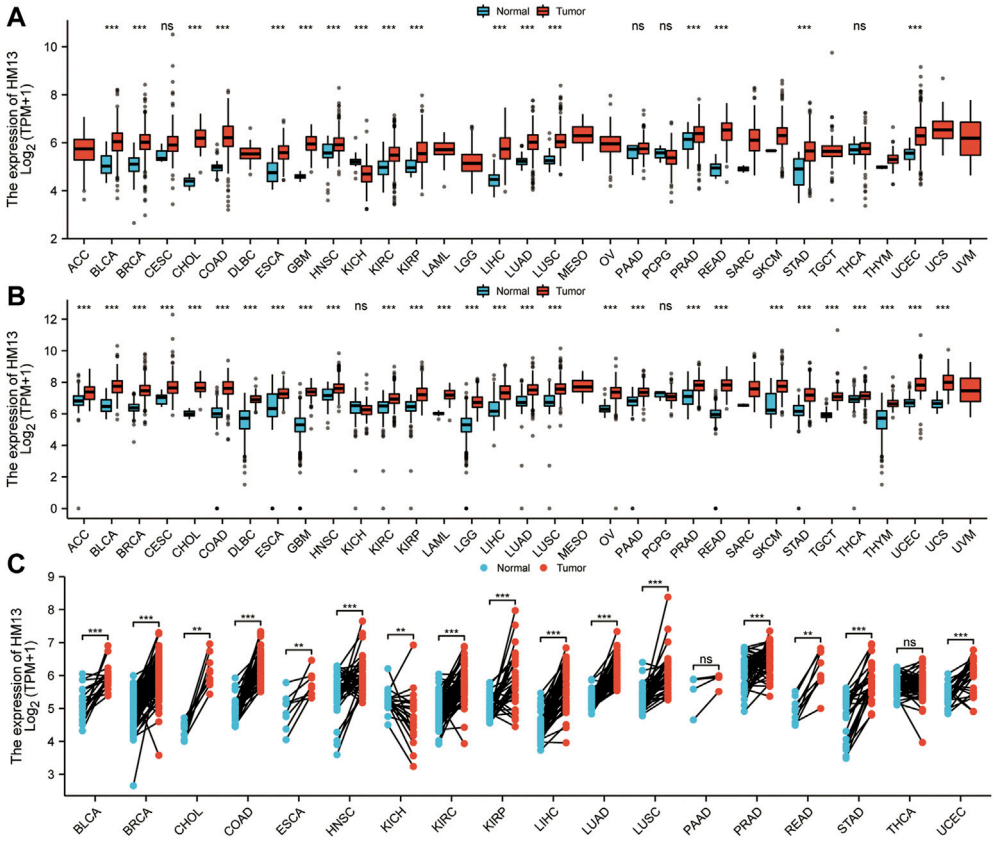

FIGURE 1
Differential expression analysis of HM13. **(A)**. The mRNA Expression level of HM13 from the TCGA database. **(B)**. The mRNA expression of HM13 from TCGA and GTEx databases. **(C)**. The expression differences of HM13 in tumor and corresponding adjacent tissues were compared with paired analysis. Mann-Whitney *U* test was used for this analysis, ns, $p \geq 0.05$; *, $p < 0.05$; **, $p < 0.01$; ***, $p < 0.001$. ACC: Adrenocortical carcinoma, BLCA: Bladder urothelial carcinoma, BRCA: Breast invasive carcinoma, CESC: Cervical and endocervical cancers, CHOL: Cholangiocarcinoma, COAD: Colon adenocarcinoma, DLBC: Lymphoid Neoplasm Diffuse Large B-cell Lymphoma, ESCA: Esophageal carcinoma, GBM: Glioblastoma multiforme, HNSC: Head and Neck squamous cell carcinoma, KICH: Kidney Chromophobe, KIRC: Kidney renal clear cell carcinoma, KIRP: Kidney renal papillary cell carcinoma, LAML: Acute Myeloid Leukemia, LGG: Brain Lower Grade Glioma, LIHC: Liver hepatocellular carcinoma, LUAD: Lung adenocarcinoma, LUSC: Lung squamous cell carcinoma, MESO: Mesothelioma, OV: Ovarian serous cystadenocarcinoma, PAAD: Pancreatic adenocarcinoma, PCPG: Pheochromocytoma and Paraganglioma, PRAD: Prostate adenocarcinoma, READ: Rectum adenocarcinoma, SARC: Sarcoma, SKCM: Skin Cutaneous Melanoma, STAD: Stomach adenocarcinoma, STES: Stomach and Esophageal carcinoma, TGCT: Testicular Germ Cell Tumors, THCA: Thyroid carcinoma, THYM: Thymoma, UCEC: Uterine Corpus Endometrial Carcinoma, UCS: Uterine Carcinosarcoma, UVM: Uveal Melanoma.

predicted worse overall survival time, including the ACC, BRCA, CESC, KIRC, KIRP, LAML, LGG, LIHC, LUAD, READ and UVM (Supplementary Figure S1). Next, Kaplan-Meier survival analysis was performed and the results showed that abnormally high expression of HM13 was associated with shorter overall survival time in ACC, KIRP, UVM, LIHC, LGG, LAML, HNSC and KIRC (Figures 2A–H). Next, the influence of HM13 expression on disease-free survival was investigated, and results of the univariate Cox analysis suggested that patients with ACC, CESC, KIRC, KIRP, LGG, LIHC, TGCG, and UVM showing high expression of HM13 had worse disease-free survival (Supplementary Figure S2). Kaplan-Meier analysis showed that abnormally high expression of HM13 correlated significantly with shorter disease-free survival time in ACC, LGG, HNSC, LIHC, KIRC, LUSC, KIRP, and UVM (Figures 3A–H).

Correlation analysis for HM13 expression with levels of immune infiltration and RNA modification-related molecules

Existing literature confirms that the immune microenvironment is crucial for the development and prognosis of tumors. Previous studies show that HM13 is abnormally high expressed in several tumors, which is related

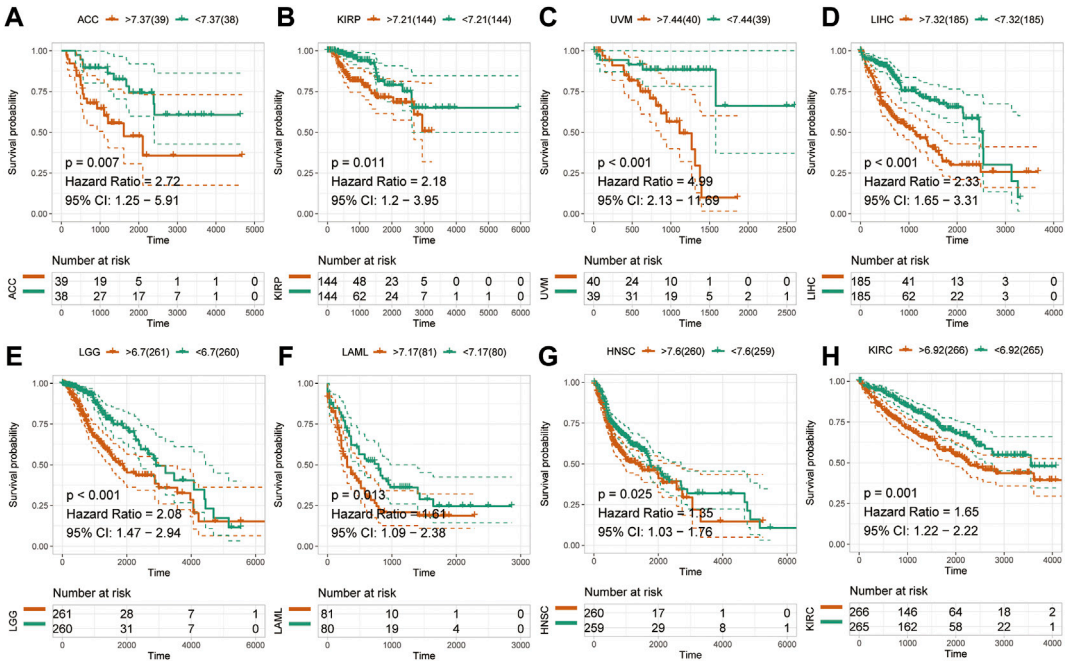

FIGURE 2
Effects of pan-cancer HM13 expression on overall survival. Kaplan-Meier method was used to evaluate the effects of abnormal expression of HM13 on the overall survival rate in ACC **(A)**, KIRP **(B)**, UVM **(C)**, LIHC **(D)**, LGG **(E)**, LAML **(F)**, HNSC **(G)**, and KIRC **(H)**. The *p*-value was calculated using the log-rank test.

to the prognosis of these patients. However, the relationship between HM13 expression and the immune microenvironment remains unclear. The TIMER database provides information on six types of immune cell invasion in 39 tumors. Thus, using the TIMER database, we analyzed the expression of HM13 and the levels of immune cell infiltration. The results suggested that HM13 was correlated significantly with B cells in several tumors, and other immune cells in LGG, KIRC, THYM, GBM, and LIHC (Figure 4A). Next, we obtained 60 immune checkpoint genes (24 inhibitory and 36 stimulatory) from relevant literature and analyzed the correlation between HM13 expression and immunosuppressive points (Thorsson et al., 2018). HM13 expression was correlated significantly with CD276, VEGFB, LAG3, TNFSF9, and TNFRSF18 (Figure 4B). Furthermore, HM13 showed a significant correlation with multiple immunosuppressive point genes implicated in LGG, UVM, LIHC, KIRC, and other tumors (Figure 4B). RNA methylation is reportedly involved in maintaining normal physiology, as well as, pathogenesis and development of diseases. We analyzed the correlation between HM13 expression and RNA modification-related molecules, including m1A, m5C, and m6A. A significant association of HM13 expression with RNA modification-related molecules in OV, KICH, ACC, GBM, LGG, and other tumors was observed (Figure 4C).

Correlation between HM13 expression and genome heterogeneity

Genomic heterogeneity is an important molecular biomarker for several tumor types and has important clinical applicability. Thus, we examined the relationship between HM13 expression and MSI, TMB, purity, and ploidy. MSI analysis showed that HM13 expression correlated significantly with MSI of COAD, DLBC, KICH, LGG, READ, UCEC, and UVM (Figure 5A). TMB analysis showed that a significant correlation was present between HM13 expression with BRCA, COAD, KIRC, LGG, LIHC, LLUAD, PAAD, PCPG, SARC, and UCEC (Figure 5B). Purity analysis showed that HM13 expression also showed a marked association with the tumor purity in SARC, UVM, KIRC, GBM, UCS, and LGG (Figure 5C). Further, ploidy analysis showed that HM13 expression was correlated significantly with polyploidy in COAD, STAD, LIHC, STES, READ, and PAAD (Figure 5D).

Drug sensitivity analysis

Given the developments in precision and individualized medicine, the effects of gene expression patterns on drug sensitivity are increasingly being appreciated. Hence, we

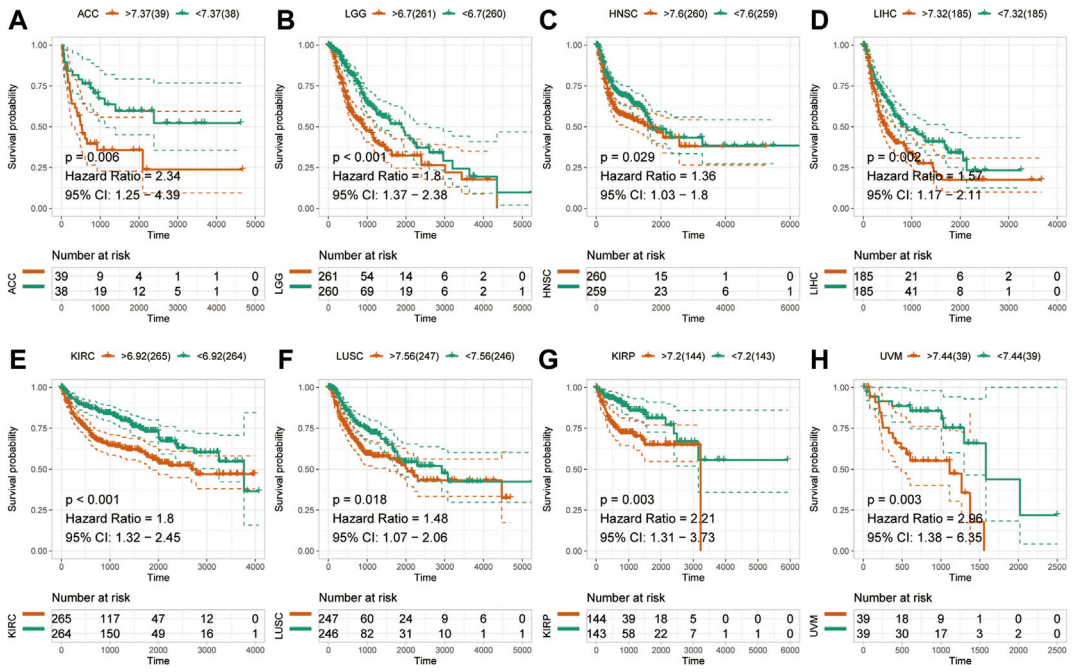

FIGURE 3
Effects of pan-cancer HM13 expression on disease-free survival. Kaplan-Meier method was used to evaluate the effects of abnormal expression of HM13 on the disease-free survival rate in ACC **(A)**, LGG **(B)**, HNSC **(C)**, LIHC **(D)**, KIRC **(E)**, LUSC **(F)**, KIRP **(G)**, and UVM **(H)**. The *p*-value was calculated using the log-rank test.

evaluated the relationship between the mRNA expression of HM13 and drug sensitivity. Based on the CellMiner database, 10 drugs associated with the expression of HM13 were identified. Among them, oxaliplatin (Cor = -0.378, $p = 0.003$), geldanamycin analog (Cor = -0.273, $p = 0.035$), B = by-product of CUDC-305 (Cor = -0.325, $p = 0.011$), amonafide (Cor = -0.306, $p = 0.018$), palbociclib (Cor = -0.296, $p = 0.021$), AT-13387 (Cor = -0.275, $p = 0.033$), pyrazoloacridine (Cor = -0.287, $p = 0.026$), and paclitaxel (Cor = -0.270, $p = 0.037$) showed a significant negative correlation with the expression of HM13 (Figure 6). However, a significant positive correlation was observed between sensitivity to everolimus (Cor = 0.330, $p = 0.010$) and rapamycin (Cor = 0.266, $p = 0.040$) and the expression of HM13 (Figure 6). Additionally, GDSC data showed that low HM13 expression has a lower IC50 value, including AICAR, AKT. Inhibitor, AMG.706, Axitinib, and AZD.0530 (Supplementary Figure S3). These results suggested that the expression of HM13 might affect the sensitivity of antitumor drugs.

Diagnostic and prognostic value of HM13 in HCC

Based on the results of the above analyses, we investigated the role of HM13 in the occurrence and development of HCC. First, we evaluated the diagnostic value of HM13 expression in HCC. ROC analysis showed that the expression of HM13 could differentiate tumor tissues from normal tissues to a certain extent, and the AUC was 0.962 (Figure 7A). Subsequently, we evaluated the predictive efficacy of HM13 expression in the overall survival time of patients with HCC, and the AUCs for 1-, 3-, and 5-years were 0.686, 0.660, and 0.654, respectively (Figure 7B). In addition, we also found that HM13 expression was significantly higher in the high histologic grade and high AFP expression compared with low histologic grade and low AFP expression (Supplementary Figures S4A,B). Methylation analysis showed that significantly higher promoter methylation level of HM13 was observed in normal tissue (Supplementary Figure S4D). Genetic alteration displayed that 1.4% of HCC patients harbor HM13 amplification mutation (Supplementary Figure S4E). Moreover, we also examined the relationship between HM13 expression and the expression of EMT-associated genes (Supplementary Figure S4F). Next, the clinical data were integrated, and by univariate and multivariate Cox regression analyses, we confirmed that HM13 expression was an independent prognostic factor for HCC (Figure 7C). To promote the application of HM13 expression in the assessment of clinical prognosis, we constructed a nomogram in combination with the pathological staging (Figure 7D). Calibration analysis suggested a relatively stable performance

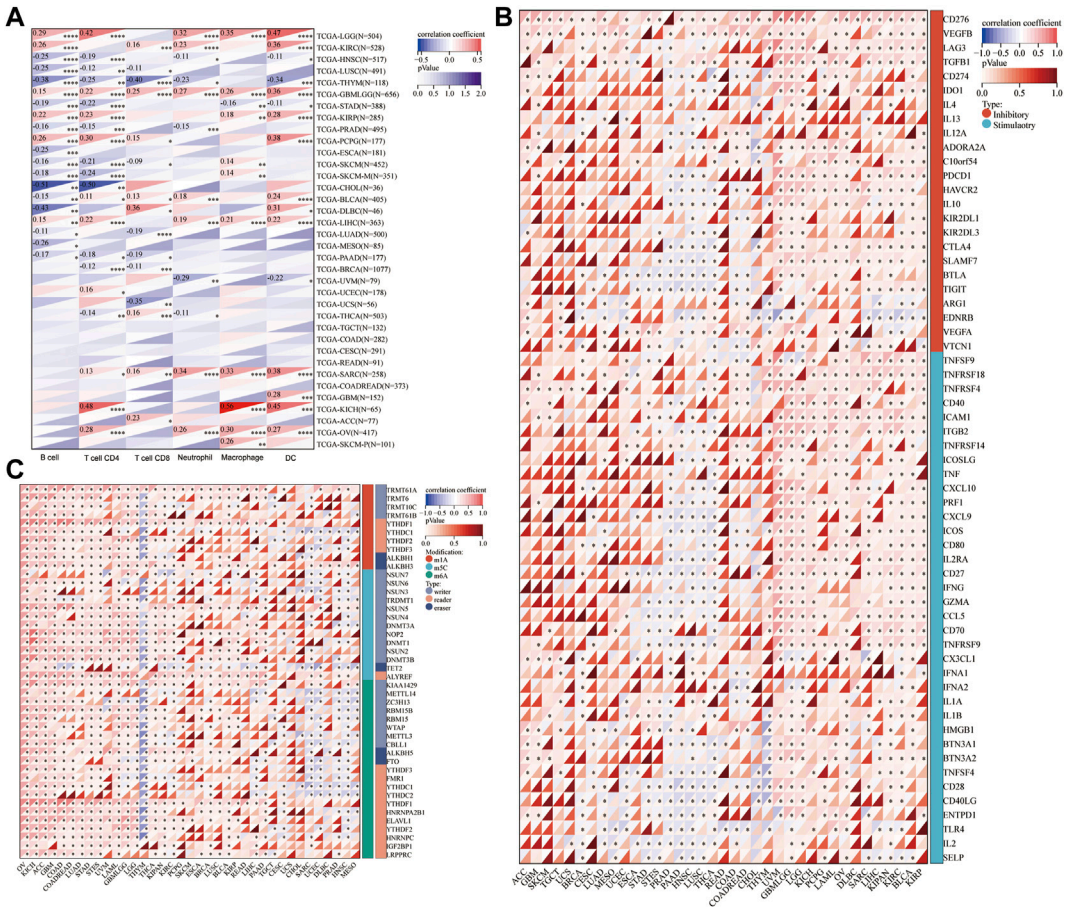

FIGURE 4
Correlation analysis for HM13 expression with immune cell infiltration levels, immune checkpoints, and RNA modification-related molecules. **(A)**. The correlation between HM13 expression and tumor infiltration levels was based on the TIMER database. **(B)**. Pan-cancer co-expression analysis for HM13 and immune checkpoint genes. **(C)**. Co-expression analysis for HM13 and RNA modification-related molecules. *$p < 0.05$, **$p < 0.01$, ***$p < 0.001$, ****$p < 0.0001$.

of the nomogram for predicting the 1-, 3-, and 5-years overall survival rate of patients with HCC (Figure 7E). ROC analysis showed that the nomogram was robust with AUCs of 0.731, 0.739, and 0.702, respectively, for 1-, 3-, and 5-years overall survival rates of patients with HCC (Figure 7F).

To further determine the expression and prognostic value of HM13 in HCC, RNA-seq data were obtained from the ICGC database and standardized processing was performed. Differential analysis indicated significant overexpression of HM13 in HCC tumor tissues (Figure 8A). In addition, the analysis from GEO datasets also indicated that HCC tissues highly expressed HM13, while it was poorly expressed in the non-tumor tissues (Supplementary Figures S5A–D). The Kaplan-Meier survival curve analysis demonstrated that patients with high HM13 expression had worse overall survival (Figure 8B). Results of univariate and multivariate Cox regression indicated that HM13 expression was independent of other clinical factors for HCC prognosis (Figure 8C). Additionally, Z-score normalized HCC protein expression profiles were obtained from the CPTAC database. Subsequently, we analyzed the protein expression of HM13 between normal and HCC tumor tissues, and significant HM13 overexpression was observed in HCC tumor tissues (Figure 8D). As well, a higher expression level of HM13 was observed in high tumor stages compared to low tumor stages (Supplementary Figure S4C). Kaplan-Meier survival curve also demonstrated that high HM13 expression was associated with a poor prognosis (Figure 8E). Furthermore, univariate and multivariate Cox regression analysis also indicated that HM13 expression at the protein level was an independent prognostic factor for HCC (Figure 8F).

Based on TCGA RNA-seq data and the ssGSEA algorithm, we evaluated the infiltration levels of 24 kinds of immune cells in HCC and calculated their correlation with HM13 expression.

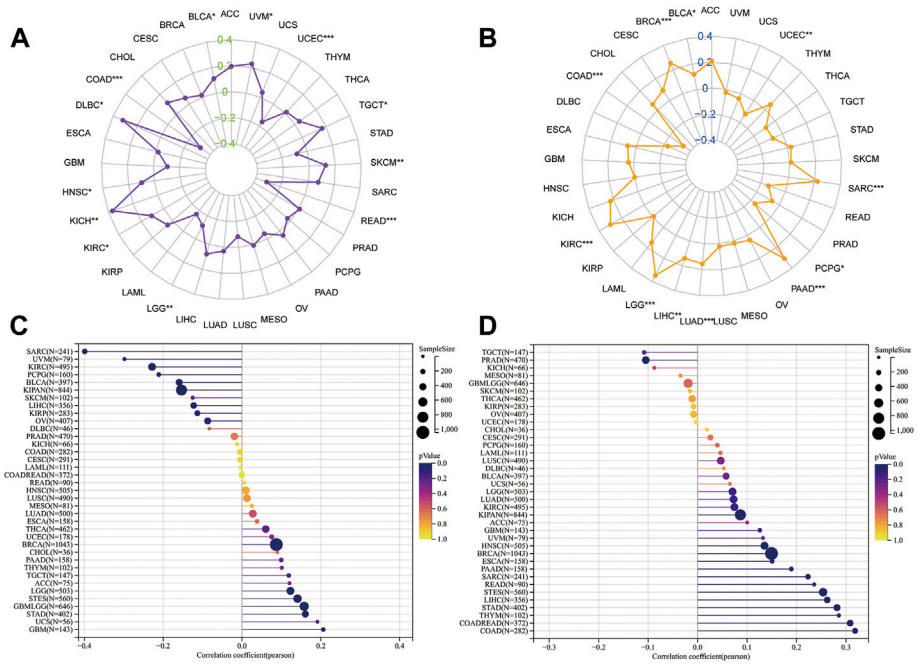

FIGURE 5
Correlation analysis for HM13 expression with MSI **(A)**, TMB **(B)**, purity **(C)**, and ploidy **(D)**. *$p < 0.05$, **$p < 0.01$, ***$p < 0.001$.

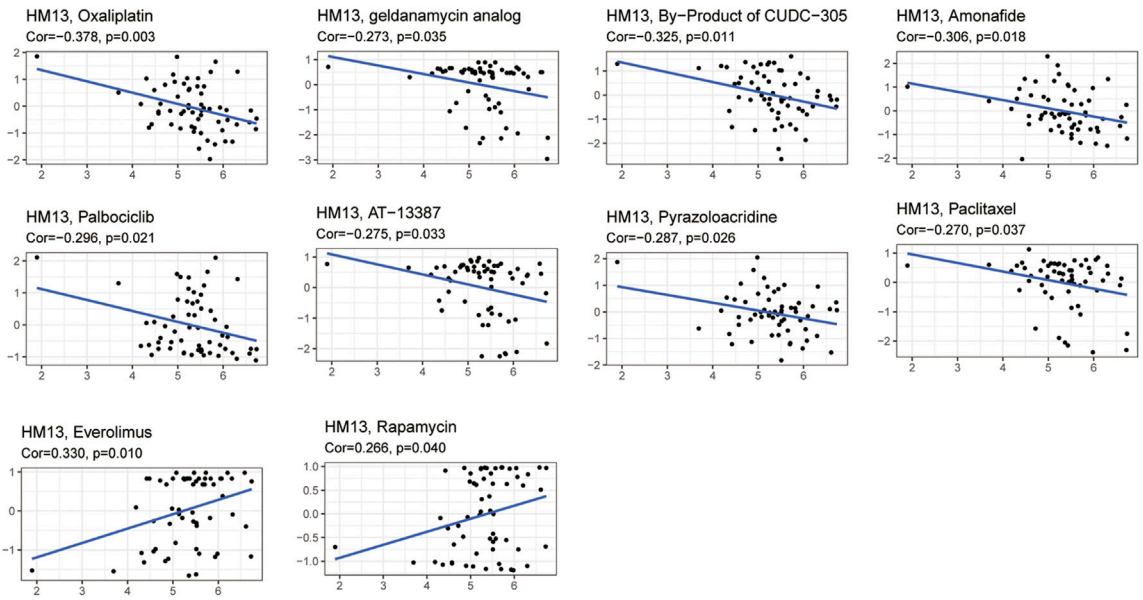

FIGURE 6
Relationship between HM13 expression and drug sensitivity.

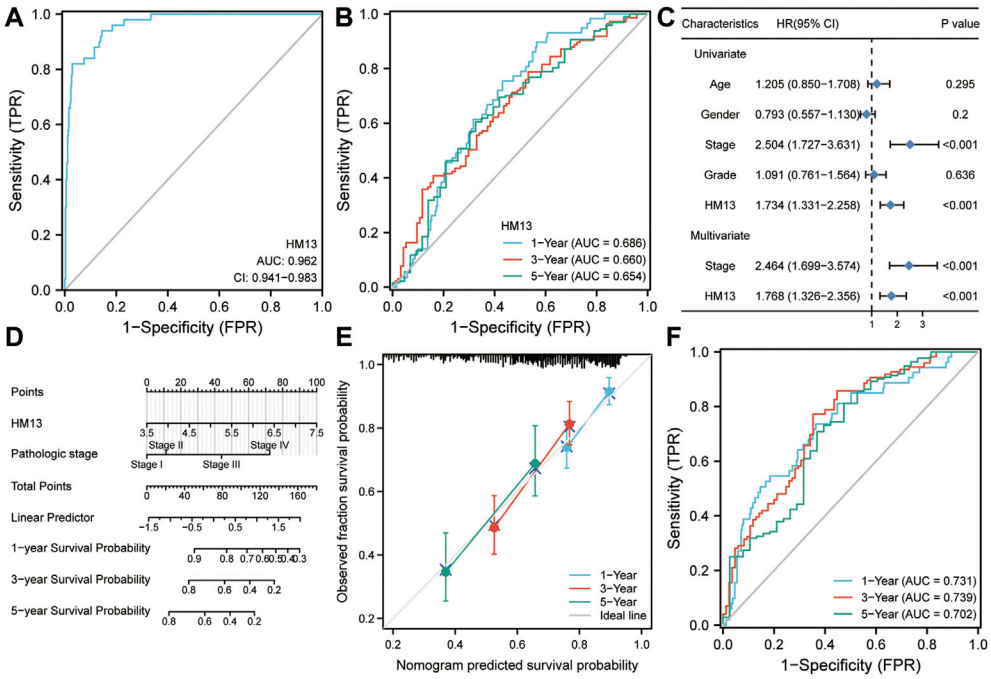

FIGURE 7
Diagnostic and prognostic value of HM13 expression in hepatocellular carcinoma. **(A)**. ROC analysis for HM13 in the diagnosis of hepatocellular carcinoma. **(B)**. ROC analysis for HM13 for predicting 1-, 3-, and 5-years overall survival in patients with hepatocellular carcinoma. **(C)**. Univariate and multivariate Cox regression analyses show that HM13 is an independent predictor of poor prognosis in hepatocellular carcinoma. **(D)**. The nomogram was constructed by combining pathological staging and HM13 expression. **(E)**. Calibration was used to evaluate the validity of the nomogram. **(F)**. ROC analysis was used to evaluate the predictive efficacy of the nomogram.

HM13 expression showed a strong positive correlation with TH2 cells, NK CD56 cells, and TFH cells, while a negative correlation was observed with Tcm and Th17 cells (Figure 9A). To elucidate the potential function of HM13 expression in HCC, we classified the samples into high- and low-risk groups based on the median expression of HM13, the differential genes between the two groups were obtained, and GO and KEGG enrichment analyses were performed. Results of enrichment analysis showed that HM13 was mainly associated with cellular potassium ion transport, glycolysis/gluconeogenesis, IL-17 signaling pathway, and the PPAR signaling pathway (Figures 9B,C). Subsequently, we identified potential interaction of HM13 using GeneMAN. The results suggested the potential interaction of HM13 with SPPL3, SPPL2C, SPPL2A, and SPPL2B (Figure 9D).

HM13 was associated with the proliferation, migration and invasion of HCC cells

The immunohistochemical data for HM13 expression in HCC tissues were extracted from the HPA database (https://www.proteinatlas.org/). The results showed a higher HM13 expression in HCC tumor tissues (Figure 10A). Subsequently, we further investigated the mRNA and protein level expression of HM13 in HCC cell lines. The results showed higher mRNA and protein levels of HM13 expression in HCC lines, including HCCLM3, Huh-7, and HepG2, as compared to the normal liver cell line, LO2 (Figures 10B,C). A total of three shRNA constructs of HM13, namely sh1-HM13, sh2-HM13, and sh3-HM13 were verified for their interference efficiency in Huh-7 cells. The results showed that sh2-HM13 significantly interfered with the mRNA and protein expression of HM13 (Figures 10D,E) and was subsequently selected for further experiments; it was named sh-HM13 (Figure 10F). CCK8 assays proved that interfering HM13 expression could significantly inhibit the proliferation of Huh-7 cells (Figure 11A). Assays of clone formation showed that the knockdown HM13 inhibited the capacity of Huh-7 cells to form colonies (Figure 11B). The results of the scratch assay suggested that interfering with HM13 expression could significantly lead to inhibited cell migration ability (Figures 11C,D). Further, results of the transwell migration and invasion assay confirmed that interfering with HM13 expression could significantly suppress cell migration and invasion abilities (Figure 11E). Moreover, we

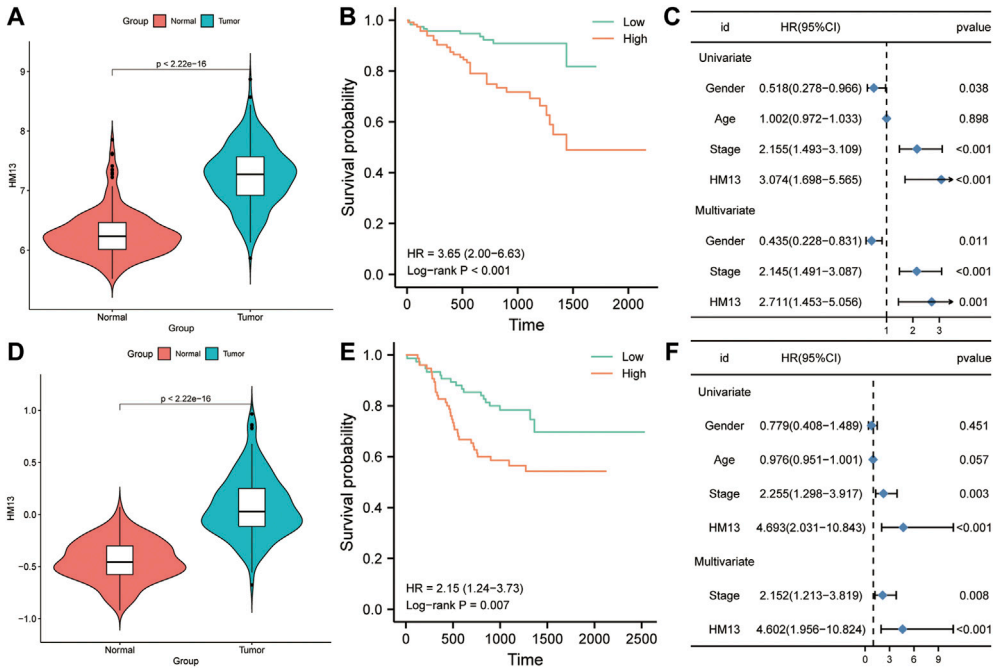

FIGURE 8
The expression level and clinical significance of HM13 in hepatocellular carcinoma (HCC). **(A)**. The mRNA expression of HM13 in ICGC cohort. **(B)**. Based on the ICGC cohort, Kaplan-Meier plot was used to evaluate the relationship between the expression of HM13 and overall survival. **(C)**. Univariate and multivariate COX analyses were carried out to determine the effect of HM13 on overall survival. **(D)**. The protein level of HM13 in CPTAC cohort. **(E)**. Based on the CPTAC cohort, Kaplan-Meier plot was used to evaluate the relationship between the expression of HM13 and overall survival. **(F)**. Univariate and multivariate COX analyses were carried out to determine the effect of HM13 on overall survival.

knocked down HM13 in HCCLM3 cells (Figure 12A). The results of CCK8 assay revealed that suppression of HM13 significantly reduced cell viability (Figure 12B). Additionally, the scratch test and transwell experiments demonstrated that knockdown HM13 inhibited metastasis and invasion of HCCLM3 cells substantially (Figures 12C–E).

Discussion

Cancer is the leading threat to human health because of its complicated pathogenesis, rapid progression, and lack of effective treatment. Understanding high-risk factors for cancer, early detection, and effective treatment are prerequisites to improve the overall survival and prognoses of these patients (Roy et al., 2021). Pan-cancer analysis can help reveal the common basis underlying the development and occurrence of different tumors, and provide new clues for elucidating the mechanism of cancer occurrence and developing personalized precision therapy (Korenjak and Zavadil, 2019). At present, researchers are focusing on pan-cancer genomic analyses and correlating these findings with the results of multi-omics to identify new tumor markers and therapeutic targets (ITP-CAOWG Consortium, 2020). Herein, we comprehensively discussed the expression of HM13 in several tumors for the first time based on RNA-seq data from TCGA. HM13 expression was abnormal and up-regulated in several tumor tissues. Combining pairing analysis with the GETx database, we further confirmed enhanced HM13 expression in UCEC, CHOL, BRCA, KIRC, HNSC, LIHC, KIRP, LUSC, LUAD, BLCA, COAD, ESCA, PRAD, STAD, and READ tumor tissues as compared to those adjacent to the corresponding carcinoma. Through univariate Cox regression and Kaplan-Meier survival analyses, we confirmed high HM13 expression in ACC, KIRP, UVM, LIHC, LGG, HNSC, and KIRC. Abnormal HM13 expression was associated with worse progression-free survival and overall survival.

The role of the tumor immune microenvironment in tumor development and prognosis has attracted increasing attention from researchers (Binnewies et al., 2018). Herein, immune cells can interact with cancer cells to promote/inhibit the growth and metastasis of tumors (Locy et al., 2018). While advances have been made in tumor immunotherapy in clinical settings, due to the complicated relationship between the immune microenvironment and tumor cells, its efficiency needs further improvement (Bader et al., 2020; Zhang and Zhang, 2020). In the present study, HM13 expression correlated negatively with T- and B cell infiltration in a variety of tumors. A positive

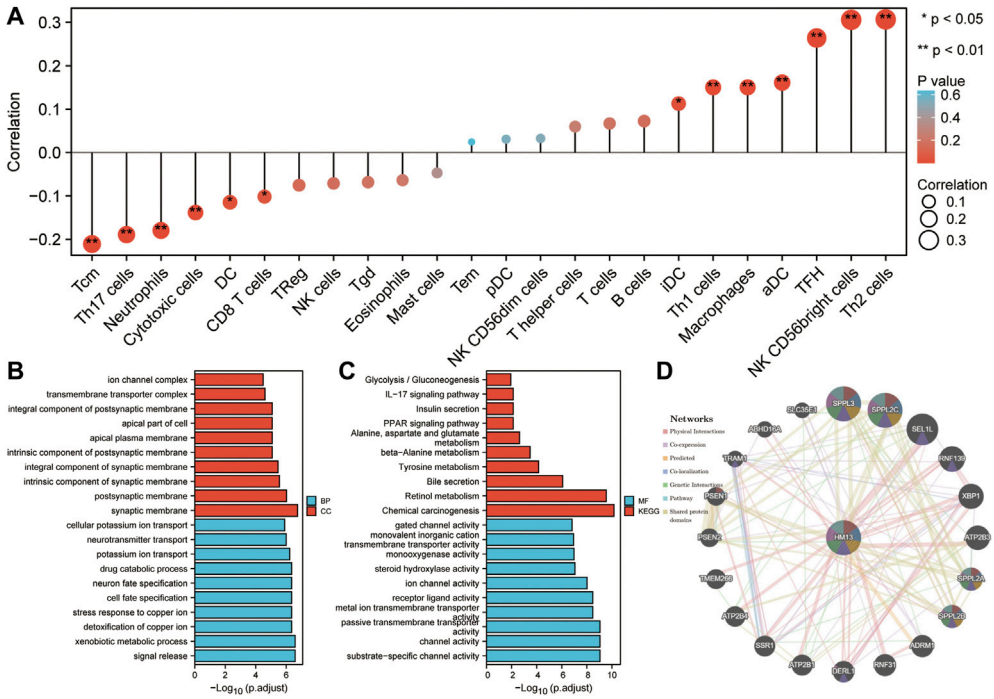

FIGURE 9
Potential function of HM13. **(A)**. Based on ssGSEA method, the relationship between HM13 expression and immune cell infiltration in hepatocellular carcinoma was evaluated. GO and KEGG functional enrichment analysis of the molecules interacted with HM13 **(B,C)**. **(D)**. Protein-protein interaction network of HM13 was constructed based on the comPPI.

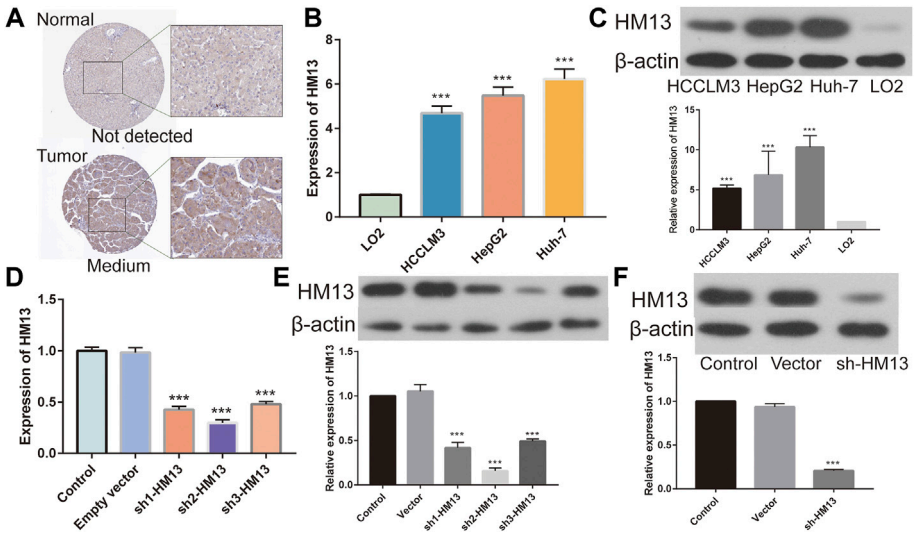

FIGURE 10
Validation of HM13 in HCC cell lines. **(A)**. Based on the human protein atlas (HPA) database, immunohistochemistry validated that the protein level of HM13 in HCC. **(B)**. Real time-qPCR was used to determine the mRNA expression of HM13 in HCC cell lines. **(C)**. Western blot was applied to evaluate the protein level of HM13 in HCC cell lines. The knock down efficiency was determined by real time-qPCR **(D)** and western blot **(E)** in Huh-7 cells. **(F)**. Knock down efficiencies of SH-HM13 was confirmed by western blot in Huh-7 cells. Experiments were repeated three times; $*p < 0.05$, $**p < 0.01$, $***p < 0.001$.

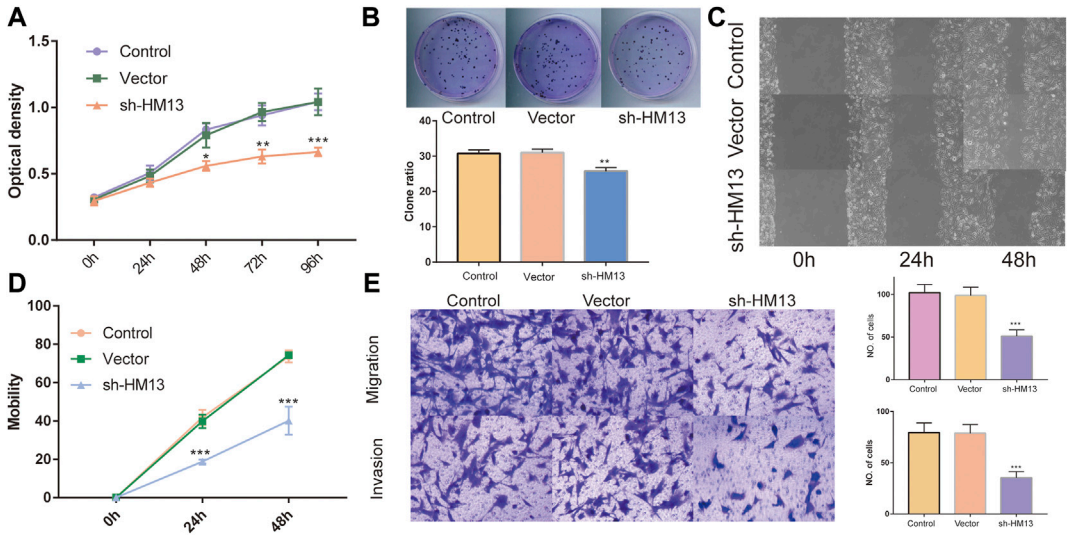

FIGURE 11
The effect of HM13 knockdown on Huh-7 cells functions. Huh-7 cell proliferation was measured by CCK8 assay **(A)** and colony formation **(B)**. **(C,D)**. Cell migration was determined by scratch wound assay. **(E)**. Cell migration and invasion were determined by transwells assay. Experiments were repeated three times; *$p < 0.05$, **$p < 0.01$, ***$p < 0.001$.

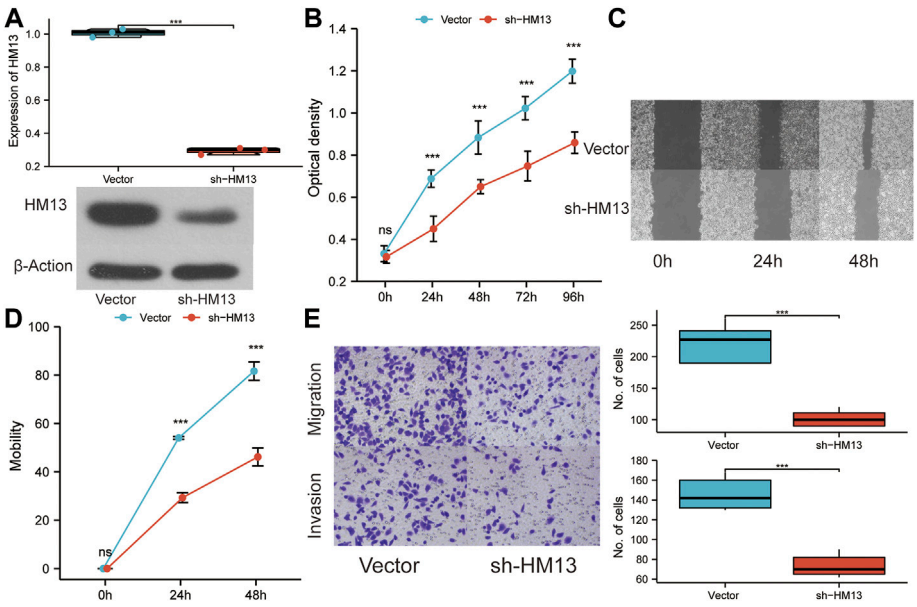

FIGURE 12
The effect of HM13 knockdown on HCCLM3 cell function. **(A)**. RT-PCR and western blot were used to validate the knockdown of HM13 expression. **(B)**. Using the CCK8 assay, HCCLM3 cells were evaluated for their proliferative capacity. **(C)**. **(D)**. Scratch assays were used to examine cell migration abilities. **(E)**. Cell migration and invasion were assessed in HCCLM3 cells using the transwell assay. Experiments were repeated three times; ***$p < 0.001$.

correlation was observed with macrophages in LGG, LIHC, SARC, KICH, OV, and SKCM. Furthermore, the ssGSEA algorithm verified that HM13 expression showed a certain positive correlation with macrophages and a negative correlation with CD8T cells in HCC. Macrophages secrete pro-inflammatory mediators to promote tumor cell proliferation and help tumor cell migration through paracrine routes (Ruffell and Coussens, 2015; Pathria et al., 2019). CD8T cells are important tumor killer cells and can inhibit their growth (Farhood et al., 2019; Raskov et al., 2021). Through immune checkpoint gene expression analysis, the expression of HM13 was found to exhibit a significant correlation with several tumor inhibitory genes, especially VEGFB, LAG3, CD274, and TGFB1. Accumulating evidence suggests that abnormally high expression of these genes is associated with the poor prognosis of cancer patients (Andrews et al., 2017; Lacal and Graziani, 2018; Chen et al., 2019; Cane et al., 2021). These results can explain why HCC patients with high HM13 expression are likely to have a poor prognosis. Therefore, we reasonably speculated that the expression of HM13 could promote the interaction between tumor and immune cells, which provides a new indicator for monitoring immunotherapy or a new adjuvant therapeutic target. Previous studies suggest that gene expression correlates with drug sensitivity (Vuong et al., 2014; Salvadores et al., 2020). In this study, we found that the expression of HM13 correlated negatively with the sensitivity of several drugs. This suggested that HM13 mRNA expression could predict drug responses, thus highlighting the potential of the HM13 as a drug target.

The protein encoded by the HM13 gene is a signal peptide peptidase, which is mainly localized to the endoplasmic reticulum. SPP is mainly involved in protein hydrolysis, especially by mediating the intramembrane cleavage of type 2 transmembrane proteins, which plays an important role in maintaining protein homeostasis (Mentrup et al., 2020). Abnormal expression of HM13 is implicated in several diseases. Hsu FF et al. showed that SPP levels are abnormally high in lung cancer and breast cancer, and it may interact with FKBP8 to regulate the proliferation and migration/invasion ability of lung tumor cells (Hsu et al., 2019). Wei JW et al. show that HM13 is significantly upregulated in high-grade gliomas, and its expression correlates positively with the degree of malignancy (Wei et al., 2017). Knocking out HM13 significantly inhibits tumor cell survival, reduces cytokine secretion in EGFRvIII glioma cells, and affects the biological behavior of surrounding cells by mediating the TGF-β pathway (Delman, 2020). In addition, SPP is associated with the maturation of hepatitis C virus core protein and may play a role in HCC (Moriishi, 2017). In this study, we confirmed the trend of abnormally high HM13 expression in HCC tissues in multiple databases, both at mRNA and protein levels. It was an independent risk factor for poor prognosis in HCC. We also verified the higher expression of HM13 in HCC cell lines. Moreover, to further examine the function of HM13 in the progression of HCC, we constructed shRNA plasmids for HM13. Interfering with HM13 expression significantly inhibited the growth and migration/invasion of HCC cells. These results suggested that HM13 may play an important role in tumor genesis and development, thus making it a promising new marker or therapeutic target. In addition, the enrichment analysis showed that HM13 may act as effective parameters in regulating tumor metabolism. The GeneMANA displayed that HM13 may interact with the SPP-like proteases. Studies have shown that abnormal overexpression of SPP can activate Notch and mTORC signaling pathways and promote tumor proliferation and metastasis (Papadopoulou and Fluhrer, 2020). This suggested that HM13 might involve in the regulation of Notch and mTORC pathways.

However, there were still some limitations to be stated in the present study. We explored the relationship between HM13 expression and immune cell infiltration and the expression of immune checkpoint genes based on bioinformatics analysis. Further *in vivo* and *in vitro* experiments are important to confirm the significance of observations in this study.

In conclusion, we delineated the pan-carcinoma expression profile of HM13 and found that its abnormally upregulated expression correlated with poor prognosis in patients with tumors. The abnormal expression was significantly associated with the levels of immune checkpoint genes and immune cell infiltration. Furthermore, interference with HM13 expression in Huh-7 and HCCLM3 cells significantly suppressed proliferation and migration/invasion of tumor cells. Therefore, our findings suggested that HM13 was crucial for tumor genesis and development, and could be used as a marker for tumor diagnosis and prognostic evaluation.

Data availability statement

The datasets presented in this study can be found in online repositories. The names of the repository/repositories and accession number(s) can be found in the article/Supplementary Material.

Author contributions

JL and WL both involved in drafting the manuscript. JL and LW took part in the design and data collection process of the study and is responsible for the content of the manuscript. All authors read and approved the final manuscript.

Funding

This study is supported by the Science and Technology Bureau of Shaoguan city (grant 210802174538690).

Conflict of interest

The authors declare that the research was conducted in the absence of any commercial or financial relationships that could be construed as a potential conflict of interest.

Publisher's note

All claims expressed in this article are solely those of the authors and do not necessarily represent those of their affiliated organizations, or those of the publisher, the editors and the reviewers. Any product that may be evaluated in this article, or claim that may be made by its manufacturer, is not guaranteed or endorsed by the publisher.

Supplementary material

The Supplementary Material for this article can be found online at: https://www.frontiersin.org/articles/10.3389/fphar.2022.950156/full#supplementary-material

References

Andrews, L. P., Marciscano, A. E., Drake, C. G., and Vignali, D. A. (2017). LAG3 (CD223) as a cancer immunotherapy target. *Immunol. Rev.* 276 (1), 80–96. doi:10.1111/imr.12519

Bader, J. E., Voss, K., and Rathmell, J. C. (2020). Targeting metabolism to improve the tumor microenvironment for cancer immunotherapy. *Mol. Cell.* 78 (6), 1019–1033. doi:10.1016/j.molcel.2020.05.034

Beroukhim, R., Mermel, C. H., Porter, D., Wei, G., Raychaudhuri, S., Donovan, J., et al. (2010). The landscape of somatic copy-number alteration across human cancers. *Nature* 463 (7283), 899–905. doi:10.1038/nature08822

Bindea, G., Mlecnik, B., Tosolini, M., Kirilovsky, A., Waldner, M., Obenauf, A. C., et al. (2013). Spatiotemporal dynamics of intratumoral immune cells reveal the immune landscape in human cancer. *Immunity* 39 (4), 782–795. doi:10.1016/j.immuni.2013.10.003

Binnewies, M., Roberts, E. W., Kersten, K., Chan, V., Fearon, D. F., Merad, M., et al. (2018). Understanding the tumor immune microenvironment (TIME) for effective therapy. *Nat. Med.* 24 (5), 541–550. doi:10.1038/s41591-018-0014-x

Bonneville, R., Krook, M. A., Kautto, E. A., Miya, J., Wing, M. R., Chen, H. Z., et al. (2017). Landscape of microsatellite instability across 39 cancer types. *JCO Precis. Oncol.* 2017, 1–15. doi:10.1200/PO.17.00073

Brown, M. S., Ye, J., Rawson, R. B., and Goldstein, J. L. (2000). Regulated intramembrane proteolysis: A control mechanism conserved from bacteria to humans. *Cell.* 100 (4), 391–398. doi:10.1016/s0092-8674(00)80675-3

Cane, S., Van Snick, J., Uyttenhove, C., Pilotte, L., and Van den Eynde, B. J. (2021). TGFβ1 neutralization displays therapeutic efficacy through both an immunomodulatory and a non-immune tumor-intrinsic mechanism. *J. Immunother. Cancer* 9, e001798. doi:10.1136/jitc-2020-001798

Chen, S., Crabill, G. A., Pritchard, T. S., McMiller, T. L., Wei, P., Pardoll, D. M., et al. (2019). Mechanisms regulating PD-L1 expression on tumor and immune cells. *J. Immunother. Cancer* 7 (1), 305. doi:10.1186/s40425-019-0770-2

Delman, K. A. (2020). Introducing the "virtual tumor board" series in ca: A cancer journal for clinicians. *Ca. Cancer J. Clin.* 70 (2), 77. doi:10.3322/caac.21598

Farhood, B., Najafi, M., and Mortezaee, K. (2019). CD8(+) cytotoxic T lymphocytes in cancer immunotherapy: A review. *J. Cell. Physiol.* 234 (6), 8509–8521. doi:10.1002/jcp.27782

Golemis, E. A., Scheet, P., Beck, T. N., Scolnick, E. M., Hunter, D. J., Hawk, E., et al. (2018). Molecular mechanisms of the preventable causes of cancer in the United States. *Genes Dev.* 32 (13-14), 868–902. doi:10.1101/gad.314849.118

Goovaerts, T., Steyaert, S., Vandenbussche, C. A., Galle, J., Thas, O., Van Criekinge, W., et al. (2018). A comprehensive overview of genomic imprinting in breast and its deregulation in cancer. *Nat. Commun.* 9 (1), 4120. doi:10.1038/s41467-018-06566-7

Hsu, F. F., Chou, Y. T., Chiang, M. T., Li, F. A., Yeh, C. T., Lee, W. H., et al. (2019). Signal peptide peptidase promotes tumor progression via facilitating FKBP8 degradation. *Oncogene* 38 (10), 1688–1701. doi:10.1038/s41388-018-0539-y

ITP-CAOWG Consortium (2020). Pan-cancer analysis of whole genomes. *Nature* 578 (7793), 82–93. doi:10.1038/s41586-020-1969-6

Korenjak, M., and Zavadil, J. (2019). Experimental identification of cancer driver alterations in the era of pan-cancer genomics. *Cancer Sci.* 110 (12), 3622–3629. doi:10.1111/cas.14210

Lacal, P. M., and Graziani, G. (2018). Therapeutic implication of vascular endothelial growth factor receptor-1 (VEGFR-1) targeting in cancer cells and tumor microenvironment by competitive and non-competitive inhibitors. *Pharmacol. Res.* 136, 97–107. doi:10.1016/j.phrs.2018.08.023

Lemberg, M. K., Bland, F. A., Weihofen, A., Braud, V. M., and Martoglio, B. (2001). Intramembrane proteolysis of signal peptides: An essential step in the generation of HLA-E epitopes. *J. Immunol.* 167 (11), 6441–6446. doi:10.4049/jimmunol.167.11.6441

Locy, H., de Mey, S., de Mey, W., De Ridder, M., Thielemans, K., and Maenhout, S. K. (2018). Immunomodulation of the tumor microenvironment: Turn foe into friend. *Front. Immunol.* 9, 2909. doi:10.3389/fimmu.2018.02909

Loureiro, J., Lilley, B. N., Spooner, E., Noriega, V., Tortorella, D., and Ploegh, H. L. (2006). Signal peptide peptidase is required for dislocation from the endoplasmic reticulum. *Nature* 441 (7095), 894–897. doi:10.1038/nature04830

Mentrup, T., Cabrera-Cabrera, F., Fluhrer, R., and Schroder, B. (2020). Physiological functions of SPP/SPPL intramembrane proteases. *Cell. Mol. Life Sci.* 77 (15), 2959–2979. doi:10.1007/s00018-020-03470-6

Moriishi, K. (2017). The potential of signal peptide peptidase as a therapeutic target for hepatitis C. *Expert Opin. Ther. Targets* 21(9), 827–836. doi:10.1080/14728222.2017.1369959

Papadopoulou, A. A., and Fluhrer, R. (2020). Signaling functions of intramembrane aspartyl-proteases. *Front. Cardiovasc. Med.* 7, 591787. doi:10.3389/fcvm.2020.591787

Pathria, P., Louis, T. L., and Varner, J. A. (2019). Targeting tumor-associated macrophages in cancer. *Trends Immunol.* 40 (4), 310–327. doi:10.1016/j.it.2019.02.003

Raskov, H., Orhan, A., Christensen, J. P., and Gogenur, I. (2021). Cytotoxic CD8(+) T cells in cancer and cancer immunotherapy. *Br. J. Cancer* 124 (2), 359–367. doi:10.1038/s41416-020-01048-4

Reinhold, W. C., Sunshine, M., Liu, H., Varma, S., Kohn, K. W., Morris, J., et al. (2012). CellMiner: A web-based suite of genomic and pharmacologic tools to explore transcript and drug patterns in the NCI-60 cell line set. *Cancer Res.* 72 (14), 3499–3511. doi:10.1158/0008-5472.CAN-12-1370

Roy, D., Pascher, A., Juratli, M. A., and Sporn, J. C. (2021). The potential of aptamer-mediated liquid biopsy for early detection of cancer. *Int. J. Mol. Sci.* 22 (11), 5601. doi:10.3390/ijms22115601

Ruffell, B., and Coussens, L. M. (2015). Macrophages and therapeutic resistance in cancer. *Cancer Cell.* 27 (4), 462–472. doi:10.1016/j.ccell.2015.02.015

Salvadores, M., Fuster-Tormo, F., and Supek, F. (2020). Matching cell lines with cancer type and subtype of origin via mutational, epigenomic, and transcriptomic patterns. *Sci. Adv.* 6, eaba1862. doi:10.1126/sciadv.aba1862

Sherman, R. M., and Salzberg, S. L. (2020). Pan-genomics in the human genome era. *Nat. Rev. Genet.* 21 (4), 243–254. doi:10.1038/s41576-020-0210-7

Soerjomataram, I., and Bray, F. (2021). Planning for tomorrow: Global cancer incidence and the role of prevention 2020-2070. *Nat. Rev. Clin. Oncol.* 18 (10), 663–672. doi:10.1038/s41571-021-00514-z

Thorsson, V., Gibbs, D. L., Brown, S. D., Wolf, D., Bortone, D. S., Ou Yang, T. H., et al. (2018). The immune landscape of cancer. *Immunity* 48 (4), 812–830. e14. doi:10.1016/j.immuni.2018.03.023

Urban, S., Lee, J. R., and Freeman, M. (2001). Drosophila rhomboid-1 defines a family of putative intramembrane serine proteases. *Cell.* 107 (2), 173–182. doi:10.1016/s0092-8674(01)00525-6

Vuong, H., Cheng, F., Lin, C. C., and Zhao, Z. (2014). Functional consequences of somatic mutations in cancer using protein pocket-based prioritization approach. *Genome Med.* 6 (10), 81. doi:10.1186/s13073-014-0081-7

Wei, J. W., Cai, J. Q., Fang, C., Tan, Y. L., Huang, K., Yang, C., et al. (2017). Signal peptide peptidase, encoded by HM13, contributes to tumor progression by affecting EGFRvIII secretion profiles in glioblastoma. *CNS Neurosci. Ther.* 23 (3), 257–265. doi:10.1111/cns.12672

Wu, C., Li, M., Meng, H., Liu, Y., Niu, W., Zhou, Y., et al. (2019). Analysis of status and countermeasures of cancer incidence and mortality in China. *Sci. China. Life Sci.* 62 (5), 640–647. doi:10.1007/s11427-018-9461-5

Zhang, Y., and Zhang, Z. (2020). The history and advances in cancer immunotherapy: Understanding the characteristics of tumor-infiltrating immune cells and their therapeutic implications. *Cell. Mol. Immunol.* 17 (8), 807–821. doi:10.1038/s41423-020-0488-6

Zhou, J., Cheng, T., Li, X., Hu, J., Li, E., Ding, M., et al. (2021). Epigenetic imprinting alterations as effective diagnostic biomarkers for early-stage lung cancer and small pulmonary nodules. *Clin. Epigenetics* 13 (1), 220. doi:10.1186/s13148-021-01203-5

frontiers | Frontiers in Pharmacology

TYPE Original Research
PUBLISHED 16 September 2022
DOI 10.3389/fphar.2022.927570

OPEN ACCESS

EDITED BY
Jian Zhang,
Southern Medical University, China

REVIEWED BY
Emine Guven,
Düzce University, Turkey
Budheswar Dehury,
Regional Medical Research Center (ICMR), India

*CORRESPONDENCE
Yasir Waheed,
yasir_waheed_199@hotmail.com
Dong-Qing Wei,
dqwei@sjtu.edu.cn

†These authors have contributed equally to this work

SPECIALTY SECTION
This article was submitted to Pharmacology of Anti-Cancer Drugs, a section of the journal Frontiers in Pharmacology

RECEIVED 24 April 2022
ACCEPTED 25 July 2022
PUBLISHED 16 September 2022

CITATION
Suleman M, Umme-I-Hani S, Salman M, Aljuaid M, Khan A, Iqbal A, Hussain Z, Ali SS, Ali L, Sher H, Waheed Y and Wei D-Q (2022), Sequence-structure functional implications and molecular simulation of high deleterious nonsynonymous substitutions in IDH1 revealed the mechanism of drug resistance in glioma.
Front. Pharmacol. 13:927570.
doi: 10.3389/fphar.2022.927570

Sequence-structure functional implications and molecular simulation of high deleterious nonsynonymous substitutions in *IDH1* revealed the mechanism of drug resistance in glioma

Muhammad Suleman[1†], Syeda Umme-I-Hani[2], Muhammad Salman[3], Mohammed Aljuaid[4], Abbas Khan[5,6†], Arshad Iqbal[1], Zahid Hussain[1], Syed Shujait Ali[1], Liaqat Ali[7], Hassan Sher[8], Yasir Waheed[9]* and Dong-Qing Wei[5,6,10,11]*

[1]Centre for Biotechnology and Microbiology, University of Swat, Swat, Khyber Pakhtunkhwa, Pakistan, [2]Punjab Medical College, Faisalabad, Punjab, Pakistan, [3]Rashid Latif Medical College, Lahore, Punjab, Pakistan, [4]Department of Health Administration, College of Business Administration, King Saud University, Riyadh, Saudi Arabia, [5]Department of Bioinformatics and Biological Statistics, School of Life Sciences and Biotechnology, Shanghai Jiao Tong University, Shanghai, China, [6]Zhongjing Research and Industrialization Institute of Chinese Medicine, Zhongguancun Scientific Park, Meixi, Henan, China, [7]Division of Biology, Kansas State University, Manhattan, KS, United States., [8]Centre for Plant Science and Biodiversity, University of Swat, Charbagh, Pakistan, [9]Office of Research, Innovation and Commercialization, Shaheed Zulfiqar Ali Bhutto Medical University (SZABMU), Islamabad, Pakistan, [10]State Key Laboratory of Microbial Metabolism, Shanghai-Islamabad-Belgrade Joint Innovation Center on Antibacterial Resistances, Joint Laboratory of International Cooperation in Metabolic and Developmental Sciences, Ministry of Education and School of Life Sciences and Biotechnology, Shanghai Jiao Tong University, Shanghai, China, [11]Peng Cheng Laboratory, Shenzhen, Guangdong, China

In the past few years, various somatic point mutations of isocitrate dehydrogenase (IDH) encoding genes (IDH1 and IDH2) have been identified in a broad range of cancers, including glioma. Despite the important function of *IDH1* in tumorigenesis and its very polymorphic nature, it is not yet clear how different nsSNPs affect the structure and function of IDH1. In the present study, we employed different machine learning algorithms to screen nsSNPs in the *IDH1* gene that are highly deleterious. From a total of 207 SNPs, all of the servers classified 80 mutations as deleterious. Among the 80 deleterious mutations, 14 were reported to be highly destabilizing using structure-based prediction methods. Three highly destabilizing mutations G15E, W92G, and I333S were further subjected to molecular docking and simulation validation. The docking

Abbreviations: PredictSNP, predict single nucleotide polymorphism; Polyphen 2, Polymorphism Phenotype version 2; SNAP, Screening of nonacceptable polymorphism; PANTHER, Protein Analysis Through Evolutionary Relationship; MAPP, Multivariate Analysis of Protein Polymorphism; PhD-SNP, predictor of Human Deleterious Single Nucleotide Polymorphism; IDH, isocitrate dehydrogenase (IDH) encoding genes; PCA, principal component analysis; FEL, free energy landscape; RMSD, root mean square deviation; RMSF, root mean square fluctuation; and Rg, radius of gyration.

results and molecular simulation analysis further displayed variation in dynamics features. The results from molecular docking and binding free energy demonstrated reduced binding of the drug in contrast to the wild type. This, consequently, shows the impact of these deleterious substitutions on the binding of the small molecule. PCA (principal component analysis) and FEL (free energy landscape) analysis revealed that these mutations had caused different arrangements to bind small molecules than the wild type where the total internal motion is decreased, thus consequently producing minimal binding effects. This study is the first extensive *in silico* analysis of the *IDH1* gene that can narrow down the candidate mutations for further validation and targeting for therapeutic purposes.

KEYWORDS

nsSNPs, IDH1, molecular docking, simulation, binding free energy, introduction

1 Introduction

In primary brain tumor, glioblastoma, also known as grade IV glioma, is the most common and deadly form of brain tumor (Wirsching and Weller, 2017). In malignant gliomas, the primary GBMs account for 90% while the secondary GBMs that emerge from lower-grade gliomas (LGGs) in younger individuals account for less than 10% of clinical reports (Ohgaki and Kleihues, 2013). After the initial diagnosis, the survival for glioma individuals is from 14 to 16 months. Recent investigations revealed some metabolic features that are shared by virtually all GBMs and help to differentiate tumors from the normal brain (Tan et al., 2020). The GBM metabolic features are the excess generation of lactate in conjunction with the acetate and glucose oxidations to provide macromolecular precursors and energy. In low-grade glioma, secondary glioblastoma, and acute myelogenous leukemia, the oncogenic mutations in the two-isocitrate dehydrogenase (IDH) encoding genes (IDH1 and IDH2) have been identified (Agnihotri et al., 2013; Zhou and Wahl, 2019).

Normally in the Krebs cycle, the isocitrate is converted into a-ketoglutarate (a-KD) by isocitrate dehydrogenases (IDHs) in a NAD(P)-dependent manner. IDH1, IDH2, and IDH3 are three IDH isozymes that function in different subcellular compartments. Various somatic point mutations of IDH1 or IDH2 have been discovered in a variety of malignancies in recent years, such as gliomas and AMLs (acute myeloid leukemias) (Yan et al., 2009; Zhao et al., 2009). Identified mutations such as IDH1 R132H/C/Q, IDH2 R140Q/W/L, and R172K/T/S/G/M adversely affect the normal function of IDH protein and initiate the abnormal activity of protein with IDH mutations that produced oncometabolite 2-hydroxyglutarate from the a-KG (Frezza et al., 2010; Huang, 2019). 2-HG may accumulate to horrifically high levels of 5–35 mmol/g in human glioma samples with IDH1/2 mutations, which is 100-fold higher than its normal level in the brain (Dimitrov et al., 2015).

Single nucleotide polymorphisms (SNPs), which affect both coding and noncoding regions of DNA, are the most common genetic changes. SNPs are found every 200–300 bp in the human genome and account for around 90% of all genetic differences in the human genome. Nonsynonymous SNPs cause genetic alteration in the exonic regions of the protein and disturb their sequence, structure, and normal function by enhancing the abnormal transcription and translation mechanisms. Previously, several *in silico* computational techniques were developed to quickly and precisely assess the functional implications of nonsynonymous variation on protein structure and function (Junaid et al., 2018; Khan et al., 2020a; Khan et al., 2020b; Khan et al., 2021). Until now, a total of 298 SNPs with 207 missense mutations in the human IDH1 gene has been described and deposited to the gnomAD database.

Although IDH1 plays a crucial role in carcinogenesis (gliomas) and has a polymorphism character, it is still unclear how identified nsSNPs alter the protein's structure and biological activity. In this study, we employed a number of computational approaches to find nsSNPs in the IDH1 gene that are extremely detrimental to the structure and function of the IDH1 protein.

2 Materials and methods

2.1 Collection of data

The available data on human IDH1 were obtained from available online databases. The online database gnomAD (https://gnomad.broadinstitute.org/) was used to retrieve all predicted SNPs in the human *IDH1*gene (Karczewski and Francioli, 2017). The amino acid sequence (UniProt: O75874) and previously deposited 3D structure (PDB ID: 6BKX) of the protein that expresses the *IDH1* gene were obtained from the UniProt online database (http://www.uniprot.org/) (Rose et al., 2010; Consortium, 2015). The whole workflow of the work is given in Figure 1.

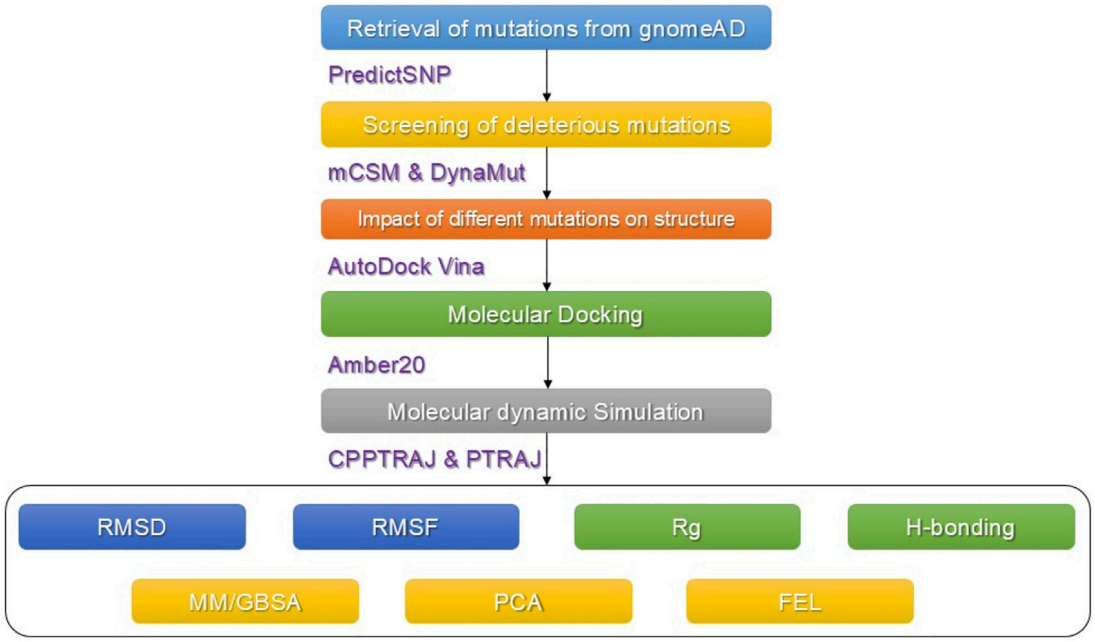

FIGURE 1
Methodological workflow of the work. Each tool used in each step is also given.

2.2 Disease-related single nucleotide polymorphism predictions

2.2.1 Prediction of Functional Consequences of nsSNPs

Different online servers such as PredictSNP (https://loschmidt.chemi.muni.cz/predictsnp1/), Polymorphism Phenotyping version 2 (Polyphen-2) (http://genetics.bwh.harvard.edu/pp2), Sorting Intolerant from Tolerant (SIFT) (http://sift.bii.a-star.edu.sg), Screening of nonacceptable polymorphism (SNAP) (https://rostlab.org/services/snap), Protein Analysis Through Evolutionary Relationship (PANTHER) (http://www.pantherdb.org/tools/csnpScoreForm.jsp, Multivariate Analysis of Protein Polymorphism (MAPP) (http://mendel.stanford.edu/SidowLab/downloads/MAPP/), and predictor of Human Deleterious Single Nucleotide Polymorphism (PhD-SNP) (http://snps.biofold.org/phd-snp/phd-snp.html) were used to predict the functional effect of all nonsynonymous single nucleotide polymorphisms (nsSNPs) (Johnson et al., 2008; Sim et al., 2012; Adzhubei et al., 2013; Landis et al., 2014; Bendl et al., 2015; Capriotti and Fariselli, 2017). All of the nsSNPs that were verified as highly deleterious by all of the aforementioned web servers were selected for further analysis.

2.2.2 Structure-based stability calculation

For structure-based stability prediction, mCSM and DynaMut webservers were used to estimate the impact of each substitution on the structural stability and flexibility (Pires et al., 2014; Rodrigues et al., 2018). The highly deleterious mutations were processed for the prediction of structure-based stability calculation. These servers use graph-based signatures to estimate the impact of each mutation on the protein's structure. The top three mutations were selected based on the mCSM and DynaMut results together for further analysis.

2.2.3 Modeling of mutants of *IDH1* protein

The crystal structure of the *IDH1* protein was extracted from PDB (Entry ID: 6BKX). Both ligands and water molecules were separated from the protein structure, and the Chimera software was used to minimize the wild-type structure of *IDH1* protein. Moreover, the predicted most deleterious mutations such as G15E, W92G, and I333S were modeled in the wild-type structure of *IDH1* protein using the Chimera software.

2.2.4 Molecular docking of DWP with the wild type and mutant *IDH1*

The impact of selected substitutions on the binding of DWP ((6aS,7S,9R, 10aS)-7,10a-dimethyl-8-oxo-2-(phenylamino)-5,6,6a,7,8,9,10,10a-octahydrobenzo[h]quinazoline-9-carbonitrile with the wild type and mutant was also evaluated using the molecular docking approach. For this estimation, a previously described protocol was employed using AutoDock Vina (Eberhardt et al., 2021).

TABLE 1 List of highly deleterious and destabilizing mutations in IDH1. Among the 80 mutations, 14 highly destabilizing ones are shown in bold.

Index	Mutation	ΔΔG mCSM	Outcome
1	**G15E**	**−3.094**	**Highly Destabilizing**
2	D16H	−1.439	Destabilizing
3	**W23C**	**−2.149**	**Highly Destabilizing**
4	Y34C	−1.848	Destabilizing
5	V35A	−1.926	Destabilizing
6	Y42C	−1.287	Destabilizing
7	D43A	−0.396	Destabilizing
8	**R49H**	**−2.437**	**Highly Destabilizing**
9	R49C	−1.957	Destabilizing
10	R49P	−1.427	Destabilizing
11	**I76T**	**−2.36**	**Highly Destabilizing**
12	**R82S**	**−2.362**	**Highly Destabilizing**
13	R82M	−1.294	Destabilizing
14	V83F	−1.491	Destabilizing
15	E85G	−1.128	Destabilizing
16	L88F	−1.714	Destabilizing
17	M91R	−0.476	Destabilizing
18	M91T	−1.317	Destabilizing
19	**W92G**	**−3.644**	**Highly Destabilizing**
20	W92R	−1.562	Destabilizing
21	N96H	−0.752	Destabilizing
22	T98N	−1.142	Destabilizing
23	N101Y	−0.377	Destabilizing
24	T106M	−0.611	Destabilizing
25	**F108V**	**−2.441**	**Highly Destabilizing**
26	R109K	−1.318	Destabilizing
27	I113S	−1.972	Destabilizing
28	G150R	−0.548	Destabilizing
29	**V152G**	**−2.065**	**Highly Destabilizing**
30	I154R	0.027	Stabilizing
31	D160Y	0.05	Stabilizing
32	G177D	−0.073	Destabilizing
33	Y183C	−0.838	Destabilizing
34	A193T	−0.975	Destabilizing
35	L207W	−1.744	Destabilizing
36	**Y208H**	**−2.648**	**Highly Destabilizing**
37	Y208C	−1.847	Destabilizing
38	T214S	−0.522	Destabilizing
39	Y219H	−0.962	Destabilizing
40	Y219C	−0.98	Destabilizing
41	D220G	−1.683	Destabilizing
42	**Y231H**	**−2.007**	**Highly Destabilizing**
43	Y235C	−1.24	Destabilizing
44	**Y246H**	**−2.036**	**Highly Destabilizing**
45	A256V	−0.53	Destabilizing
46	K260N	0.221	Stabilizing
47	G263E	−0.546	Destabilizing
48	D273G	−0.293	Destabilizing
49	G274S	−0.962	Destabilizing
50	V276M	−0.5	Destabilizing
51	S278P	−0.225	Destabilizing
52	S278L	−0.228	Destabilizing
53	D279H	−0.517	Destabilizing
54	M291T	−1.405	Destabilizing
55	T292I	−0.114	Destabilizing
56	S293I	0.169	Stabilizing
57	P298L	−0.358	Destabilizing
58	G300V	−0.604	Destabilizing
59	G300D	−1.749	Destabilizing
60	E306A	0.57	Stabilizing
61	H309R	−0.568	Destabilizing
62	H309Q	0.139	Stabilizing
63	G310R	−0.445	Destabilizing
64	R314C	0.301	Stabilizing
65	H315D	−0.52	Destabilizing
66	R317C	−0.995	Destabilizing
67	R317L	−0.082	Destabilizing
68	T325M	0.467	Stabilizing
69	N328S	−1.25	Destabilizing
70	N328K	−0.122	Destabilizing
71	**I330T**	**−2.449**	**Highly Destabilizing**
72	**I333S**	**−3.298**	**Highly Destabilizing**
73	G339R	−1.576	Destabilizing
74	L346P	−1.191	Destabilizing
75	**I367T**	**−2.845**	**Highly Destabilizing**
76	G370V	−0.276	Destabilizing
77	M372T	−1.565	Destabilizing
78	T373I	−0.732	Destabilizing
79	T373N	−1.561	Destabilizing
80	L401P	-1.626	Destabilizing

2.2.5 Molecular dynamics simulation

The highly destabilizing and functional substitutions were evaluated for the dynamic properties using the AMBER2.0 molecular simulation tool. For this purpose, ff14SB force field was recruited for uniformity with the previous parameters (Salomon Ferrer et al., 2013). A TIP3P water box (cutoff = 10.0 Å) was employed for solvation, while neutralizations were performed by adding sodium ions. Each complex was minimized well in two steps: the first for 6000 steps, while the second was run for 3,000 steps. The further protocol used in the previous study was employed. Lastly, for each

complex, a 100 ns production run under constant pressure was completed. To control the temperature, a Langevin thermostat with 1 atm pressure and 300 K was used (Zwanzig, 1973). The particle mesh Ewald (PME) algorithm was used to compute long-range interactions (Darden et al., 1993; Essmann et al., 1995). The cutoff distances were set to 10 A°. For the covalent bonds involving hydrogen, the SHAKE algorithm was used (Ryckaert et al., 1977). GPU-accelerated simulation (PMEMD.CUDA) was used for all of the processes. Post simulation analyses including dynamic stability calculated as RMSD (root mean square deviation), residual flexibility estimated as RMSF(root mean square fluctuation), hydrogen bonding analysis over the simulation time, and the radius of gyration (Rg) for protein packing assessment were calculated using CPPTRAJ and PTRAJ modules of AMBER1.9 (Roe and Cheatham, 2013).

2.2.6 Binding free energy calculation

For the calculation of binding free energy, a whole trajectory of each complex was subjected to MM/GBSA analysis by utilizing MMPBSA.PY script (Hou et al., 2011). This widely applicable approach, which has been previously used to characterize the binding of various biological complexes, was used for estimation by employing the following equation:

$$\Delta Gbind = \Delta Gcomplex - [\Delta Greceptor + \Delta Gligand] \quad (1)$$

Each term in the binding free energy was estimated using the following equation:

$$G = Gbond + Gele + GvdW + Gpol + Gnpol \quad (2)$$

2.2.7 Clustering of MD trajectories using principal component analysis

To comprehend the motion of MD trajectories, an unsupervised learning method known as principal component analysis (PCA) (Pearson, 1901; Wold et al., 1987) was performed to acquire knowledge regarding the internal motion of the system. For this purpose, an Amber module known as CPPTRAJ was used. The spatial covariance matrix was determined for eigenvector and their atomic co-ordinates. Using an orthogonal coordinate transformation, a diagonal matrix of eigenvalues was generated. Based on the eigenvectors and eigenvalues, the principal components were extracted. Using these PCs, the dominant motions during simulation were plotted (Balsera et al., 1996; Ernst et al., 2015).

3 Results and discussion

3.1 Identification of deleterious nsSNPs

The online public resources were used to retrieve all of the available data on the human *IDH1* gene. According to the information obtained from the online gnomAD database, there were a total of 298 SNPs in the *IDH1* protein. Of these, 207 SNPs were identified as nonsynonymous. These 207 SNPs were submitted to a different online server to identify the deleterious mutations. First, the SNPs were submitted to PredictSNP and MAPP servers, and only 141 and 140 SNPs were found to be deleterious, respectively (Supplementary Table S1). The nsSNPs were then submitted to PhD-SNP and SNAP online tools and found 63 and 55 SNPs as deleterious, respectively (Supplementary Table S2). The other online servers such as PolyPhen-1, PolyPhen-2, SIFT, and PANTHER analyzed the nsSNPs and predicted that out of 119 SNPs only 51, 46, 68, and 80 were deleterious, respectively (Supplementary Tables S3, S4). All of the nsSNPs were selected for further analysis and was predicted as highly deleterious together by all of the abovementioned online servers. Only 80 mutations were selected for the structure-based stability analysis using mCSM as shown in Table 1. mCSM predicted that only 14 mutations (G15E(-3.09), W23C(-2.14), R49H(-2.43), I76T(-2.36), R82S(-2.36), W92G(-3.64), F108V(-2.44), V152G(-2.06), Y208H(-2.64), Y231H(-2.00), Y246H(-2.03), I330T(-2.44), I333S(-3.29), and I367T(-2.84)) out of 80 were highly destabilizing. These 14 mutations were further verified using the DynaMut web server.

The reported 14 highly destabilizing mutations were then processed using the DynaMut server to determine the effect of these 14 mutations on the flexibility of protein structure. Among these 14 mutations, 12 mutations induced higher flexibility while the other two mutations, G15E and V246H, demonstrated structural rigidity. These changes in flexibility shown in red and blue were mapped onto the corresponding protein structure and are presented in Figure 2. Among these 14 mutations, only three mutations were reported to be consistently highly destabilizing, which were then selected for further analysis (Table 2).

3.2 Molecular docking analysis of the wild type and mutants

Molecular docking-based investigation of the binding variations caused by these mutations in contrast to the wild type revealed significant differences. The docking score for the wild type was calculated to be −8.76 kcal/mol. The interaction analysis revealed multiple hydrogen bonds including Ser326, Lys374, and Asp375, while various pi–pi interactions and pi–alkyl interactions were observed. The interaction pattern of the wild type is given in Figure 3A. On the other hand, despite the significant reduction in the number of bonding contacts, the His314 (correspond to His315) hydrogen bond remained conserved, which has been reported to be associated with the inhibitory properties of this drug. With a single hydrogen bond and various other interactions, the docking score for this complex was calculated to be −7.35 kcal/mol. It can be seen that this

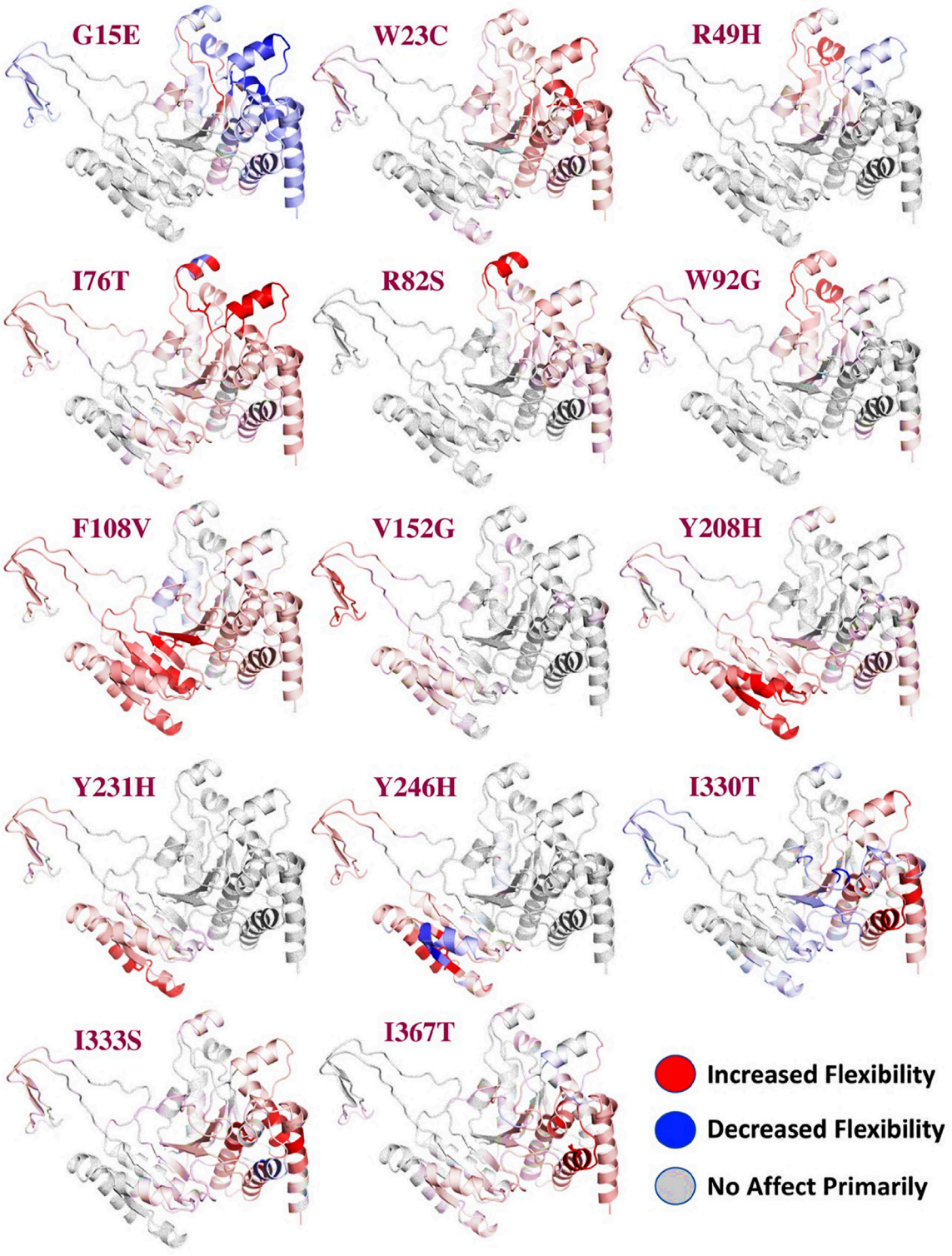

FIGURE 2
Effect of mutations on the flexibility of different residues. Different colors represent different levels of flexibility. The red regions demonstrate that the flexibility is increased, the blue regions show that the flexibility is decreased due to the mutations, and gray represents no change in the flexibility.

TABLE 2 List of highly deleterious and destabilizing mutations in IDH1. Among the 14 mutations, three are highly destabilizing reported by both the servers (mCSM and DynaMut) shown in bold.

Index	Mutation	ΔΔG ENCoM	ΔΔG DynaMut
1	**G15E**	**1.101**	**−3.347**
2	W23C	−0.977	−0.288
3	R49H	−0.348	−1.701
4	I76T	−0.198	−1.926
5	R82S	−0.607	−2.139
6	**W92G**	**−1.741**	**−2.633**
7	F108V	−0.341	−2.520
8	V152G	−0.894	−1.667
9	Y208H	−0.662	−0.591
10	Y231H	−0.369	−0.945
11	Y246H	−0.136	−0.100
12	I330T	−0.171	−0.733
13	**I333S**	**−0.478**	**−3.413**
14	I367T	−0.318	−2.610

complex has lost important hydrogen bonds of essential residues, thus reducing the bonding energy and contributing to resistance to chemotherapy. The interaction pattern of G15E is given in Figure 3B. Moreover, the docking score for W92G was estimated to be −8.62 kcal/mol. This complex retained some important hydrogen contacts, that is, Ser326 and His314 (correspond to His315), which gives comparable results to the wild type. With various hydrogen bonding contacts, many pi–pi, pi–alkyl, and salt bridge contacts were also reported in this complex. The interaction pattern of W92G is given in Figure 3C. I333S lies near the active site and reports a substantial decrease in the bonding pattern. With only one hydrogen bond of His314 (corresponding to His315) and pi–alkyl interaction with Val311, this complex reported a significant decrease in the docking score. The docking score for this complex was calculated to be −6.87 kcal/mol. The interaction pattern of I333S is given in Figure 3D.

3.3 Investigation of the dynamic behavior of the wild-type and mutant complexes

To provide worthy insights into the impact of any particular mutation on the structure and function of a protein comprehension of key dynamic features is essential. For instance, dynamic stability [root mean square deviation (RMSD)] can be used to estimate the stability of a biological complex in a dynamic environment. To assess the structural stability, we herein also calculated RMSD as a function of time. The wild type and the three mutants were compared and are shown in Figures 4A–C. The wild type presented more stable behavior than the three mutants. As shown in Figure 4A, the wild type initially demonstrated a higher RMD for a short period (2–6 ns); thereafter, the complex equilibrated and attained stability at 2.5 Å. The RMSD continued to follow the same trend until 55 ns and then decreased to 2.1 Å until the end of simulation. No significant perturbation was observed during the simulation, and the average RMSD was calculated to be 2.30 Å. Comparatively, the G15E mutant initially demonstrated significant perturbations in the RMSD, particularly between 5 and 20 ns. The RMSD then stabilized for a period between 21 and 55 ns and then continued to increase gradually until the end of the simulation. The complex reported a higher RMSD between 56 and 73 ns, then abruptly decreased, and then increased back with major deviation until the end of simulation. The complex reached the complete stability state after 80 ns. This shows that this mutation, despite its location away from the binding cavity, allosterically affects the binding affinity by compromising the stability of the protein. Since it has been previously reported that mutations that alter the protein stability result in radical function, thus this corroborates with the current findings (Dehury et al., 2020a). The RMSD graph for G15E mutant is given in Figure 4A. Unlike the wild type and G15E, the W92G complex demonstrated significant structural instability from the start of the simulation. The RMSD during the first 60 ns reported minor deviations at different time intervals, thus resulting in continuous destabilization effects of mutation. The RMSD increased to 6.0 Å at 60 ns and then gradually decreased until 100 ns. An average RMSD for W92G was recorded to be 3.60 Å and is shown in Figure 3B. On the other hand, the I333S mutant was reported to be the most destabilizing mutation among the shortlisted top deleterious mutations. First, the complex reported significant deviations until 55 ns and then gradually increased the RMSD and followed the same pattern to demonstrate significant deviations until the end of the simulation. An average RMSD of 3.2 Å was calculated for the I333S complex and is shown in Figure 4C. It has been reported that mutations that increase the stability may also increase the binding while destabilizing mutations decrease the binding. The current findings strongly corroborate with the previous reports where the filtration of mutations to obtain the most deleterious mutations showed that R132C, R132G, R132H, R132L, and R132S decrease the stability of IDH1 (Kumar et al., 2018). The stability feature is also reported to be affected by mutations in other diseases, which results in deleterious effects (Dehury et al., 2020a). Thus, herein, the mutations demonstrated destabilizing effects in contrast to the wild type.

3.4 Protein structure packing analysis

An assessment of protein packing reveals information regarding the binding and unbinding events that occurred during simulation. These events are steered by the bonding of

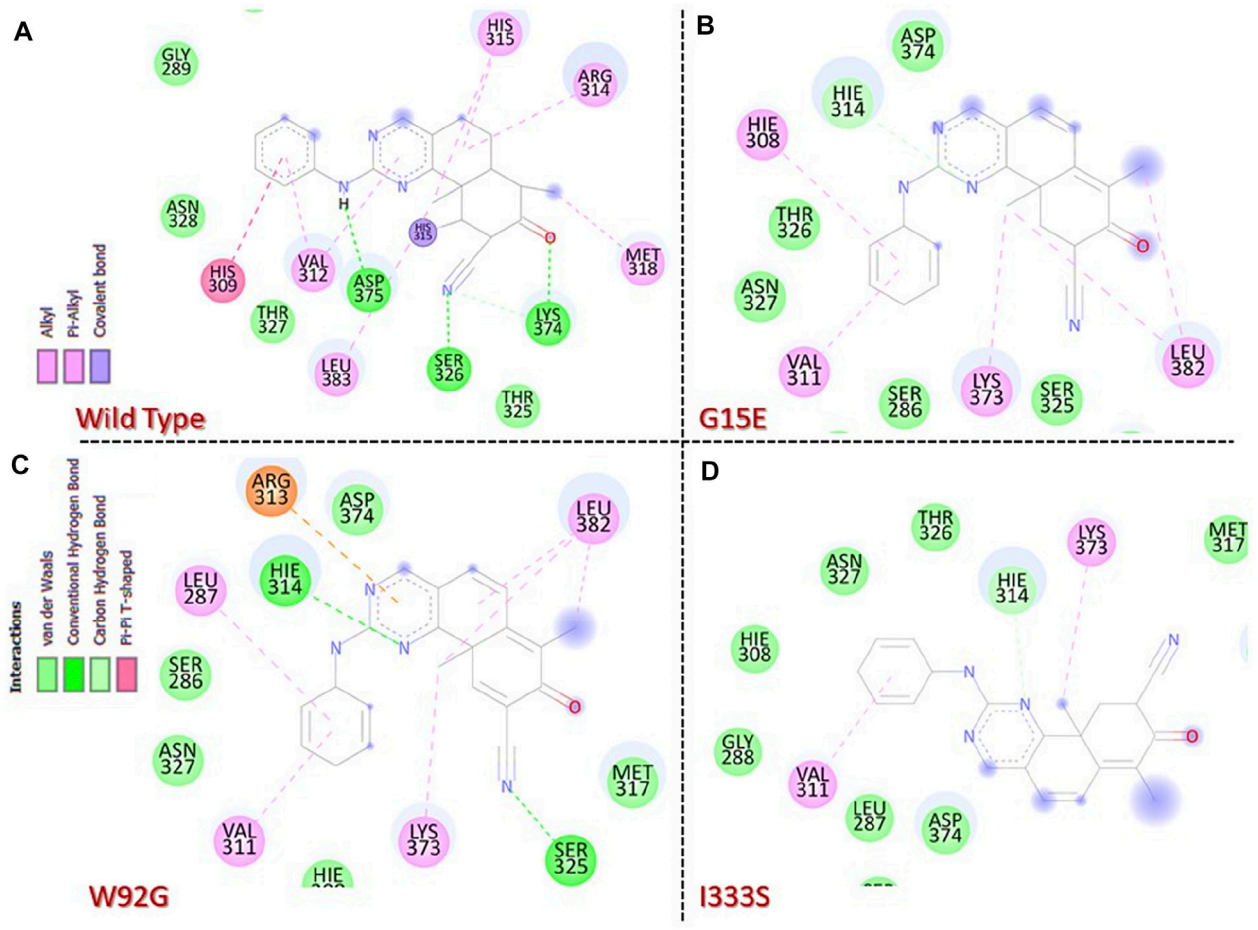

FIGURE 3
Molecular docking analysis of the wild-type and mutant complexes. **(A)** Representation of the interaction pattern of the wild type. **(B)** Representation of the interaction pattern of G15E. **(C)** Representation of the interaction pattern of W92G. **(D)** Representation of the interaction pattern of I333S.

small molecules with the protein cavity. For instance, this approach has been used previously to see the impact of mutations on the structural compactness when IDH1 binds to its homodimer (Yuan et al., 2017). Herein, to understand the structural compactness, radius of gyration (Rg) was calculated as a function of time. Consistent with the RMSD results, the wild-type complex reported a uniform pattern of Rg during the simulation. There was a slight increase in Rg between 40 and 60 ns, but it then stabilized again until the end of the simulation. The average Rg for this complex was calculated to be 22.5 Å. On the other hand, for the G15E mutant, despite its similar Rg value, , wild-type deviations at different time intervals were observed. This trend can be seen for the whole simulation time period (0–100 ns), which shows maximum unbinding events induced by the mutation. The W82G and I333S mutants demonstrated a similar pattern of Rg for the first 40 ns. With slightly higher Rg values, the two complexes reported patterns similar to those of the wild type. However, W92G experienced a continuous increase in the Rg between 41 and 60 ns and then a decreased back effect was observed until 70 ns. The Rg value for the remaining simulation time remained lower; however, major deviations were reported. On the other hand, I333S reported a gradual increase in the Rg value after 45 ns and continued to follow this pattern until 75 ns. The Rg then again decreased and remained consistent until the end of the simulation. The average Rg values for W92G and I333S were calculated to be 22.80 Å and 22.78 Å, respectively. Interestingly the other reported mutations in the interface site, that is, R132C, R132G, R132H, R132L, and R132S, also demonstrated higher radius of gyration values; thus, further validating our findings in terms of protein compactness (Yuan et al., 2017; Bendahou et al., 2020). The Rg graphs for each complex are shown in Figures 5A–C.

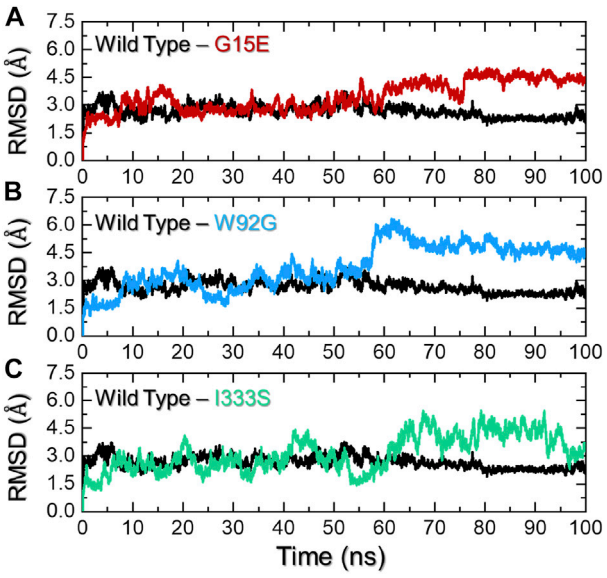

FIGURE 4
Dynamic stability analysis of the wild-type and mutant complexes. **(A)** Representation of the RMSD of the wild type and G15E. **(B)** Representation of the RMSD of the wild type and W92G. **(C)** Representation of the RMSD of the wild type and I333S. The x-axis represents time in nanoseconds while the y-axis represents RMSD in Å.

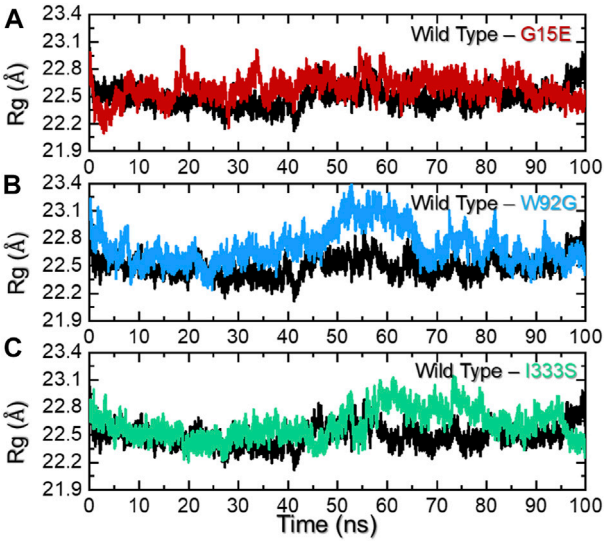

FIGURE 5
Radius of gyration analysis of the wild-type and mutant complexes. **(A)** Representation of the Rg of the wild type and G15E. **(B)** Representation of the Rg of the wild type and W92G. **(C)** Representation of the Rg of the wild type and I333S. The x-axis represent time in nanoseconds while the y-axis represent Rg in Å.

3.5 Residues' flexibility indexing

Residues' flexibility indexing is a key assessment to understand the role of each residue in different biological functions. The flexibility can be applied in different domains, such as molecular recognition, drug binding, cascade signaling, protein coupling, enzyme engineering, and protein designs. To estimate the residual flexibility of each complex, we calculated root mean square fluctuation (RMSF). As shown in Figure 5, all of the complexes demonstrated a more similar pattern of RMSF except for the regions between 125 and175 for all of the complexes. The flexibility at this portion (125–175) revealed a different pattern, which shows the impact of a particular mutation on the protein's internal dynamics. The wild type in this region demonstrates minimal RMSF, while the three mutations reported maximum RMSF. This consequently shows the altered dynamics and residue flexibility by the induced mutations in the structure, thus altering the binding of small molecules and function. This overall higher flexibility with the loss of compactness and intramolecular hydrogen bonds makes these mutations more deleterious than the other mutations. The findings are prevalidated by the previous literature where increased flexibility was observed mediated by different mutations. Moreover, other diseases mutations are reported to decrease the binding either due to increasing the cavity space or affecting the on/off switch, which consequently increases/decreases the distance between essential atoms (Dehury et al., 2020b; Dehury et al., 2020c). The RMSF of each complex is shown in Figure 6.

3.6 Hydrogen bonding analysis

Macromolecular complexes, particularly protein–protein coupling, are primarily driven by numerous factors, among which hydrogen bonding and hydrophobic contacts are essential. The environment of protein interfaces is enriched with water molecules that work with the residues to form hydrogen bonds (Chen et al., 2016). The mechanisms underlying protein–protein interaction as well as the ramifications for hydrogen bonding are unclear (Chodera and Mobley, 2013). Whether hydrogen bonds govern protein–protein docking, in particular, is a long-standing concern, and the mechanism is poorly understood (Patil et al., 2010; Olsson et al., 2011). Therefore, it is important to understand the hydrogen bonding landscape in protein–protein association. For instance, previously, hydrogen bonding was predicted to estimate the strength of the association between two molecules. As shown in Figure 7A, the wild type reported an average of 215 hydrogen bonds, while the G15E complex reported 212 hydrogen bonds over the simulation time. On the other hand, the W92G complex reported 209 average hydrogen bonds in contrast to the wild type. The hydrogen bonds in the wild type and I333S were comparable. In the case of I333S, average hydrogen bonds were calculated to be 215,

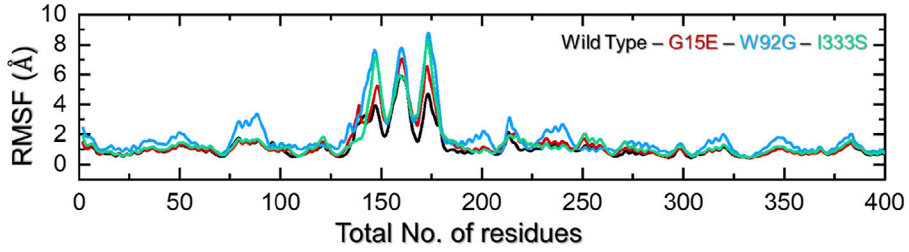

FIGURE 6
Residues' flexibility analysis of the wild-type and mutant complexes. The x-axis represents time in total number of residues while the y-axis represent RMSF in Å.

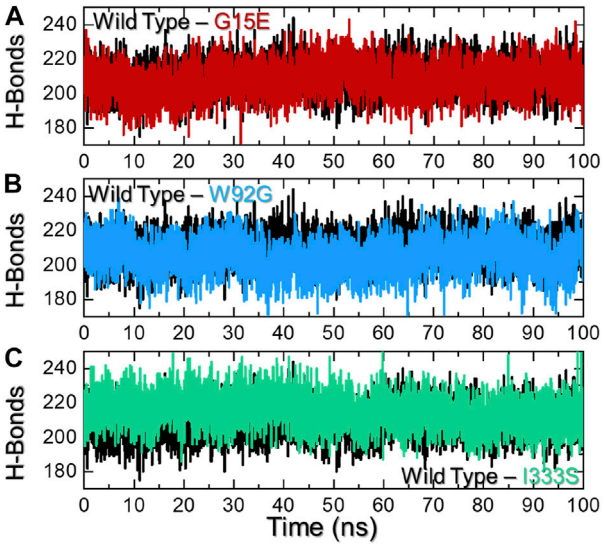

FIGURE 7
Hydrogen bonding analysis of the wild-type and mutant complexes. **(A)** Representation of H-bonds of the wild type and G15E. **(B)** Representation of H-bonds of the wild type and W92G. **(C)** Representation of H-bonds of the wild type and I333S. The x-axis represents time in nanoseconds, while the y-axis represents H-bond population.

same as that of the wild type. This demonstrate that these mutations alter the internal dynamics, consequently altering the hydrogen bonding network and causes resistance to the drug. The hydrogen bonding graphs of all of the complexes are shown in Figures 7A–C.

3.7 Binding free energy calculation

Binding free energy calculation determines the accurate binding strength and conformation of the small molecule. It is an essential estimation to re-evaluate the docking predictions by considering the highest accuracy and reliability than the conventional docking and alchemical methods. It is a widely used approach to explore the interaction strength and reveal the key binding feature, which steers the overall binding. Considering the applicability of the MM/GBSA approach, we also estimated the total binding energy for the wild-type and mutant complex. As shown in Table 3, the vdW for the wild type was estimated to be −40.78 ± 0.045 kcal/mol, while for the mutant it was −35.13 ± 0.054 kcal/mol reported by G15E mutations, −38.07 ± 0.053 kcal/mol reported by W92G, and −36.46 ± 0.06 kcal/mol calculated for the I333S mutant. This shows the loss of important interacting contacts that remained conserved in the wild type. On the other hand, the electrostatic energy determined an inverted trend. In the case of wild type, the electrostatic energy was calculated to be 3.55 ± 0.034 kcal/mol, while for the mutations −1.23 ± 0.057 kcal/mol (G15E) and −2.53 ± 0.052 kcal/mol (W92G), and −0.99 ± 0.06 kcal/mol for I333S mutant was calculated. This shows that due to these mutations the electrostatic contacts are increased, which may consequently alter the binding. Moreover, ΔG total was reported to be −34.77 ± 0.036 kcal/mol for the wild type and −34.07 ± 0.051 kcal/mol for W92G. The total binding energy of the wild type and G15E is comparable. The two mutants, that is, G15E and I333S, demonstrated a significant decrease in the ΔG total. The ΔG total for the G15E mutant was calculated to be −30.90 ± 0.041 kcal/mol, while for I333S, the ΔG total was estimated to be −31.91 ± 0.04 kcal/mol. This consequently shows the impact of these deleterious substitutions on the binding of the small molecule. The other parameters of the total binding free energy are given in Table 3.

3.8 Clustering of protein's motion

We used the principal component analysis (PCA) to cluster the protein motions in the simulation trajectories.

TABLE 3 Total binding free energy for the wild-type, G15E, W92G, and I333S complexes. All of the values are calculated in kcal/mol.

Parameters	Wild type	G15E	W92G	I333S
VDWAALS	−40.78 ± 0.045	−35.13 ± 0.054	−38.07 ± 0.053	−36.46 ± 0.06
EEL	3.55 ± 0.034	−1.23 ± 0.057	−2.53 ± 0.052	−0.99 ± 0.06
EGB	7.22 ± 0.023	9.64 ± 0.040	10.55 ± 0.056	9.73 ± 0.04
ESURF	−4.77 ± 0.003	−4.18 ± 0.007	−4.02 ± 0.005	−4.19 ± 0.008
Delta G Gas	−37.23 ± 0.037	−36.36 ± 0.046	−40.61 ± 0.071	−37.45 ± 0.005
Delta G Solv	2.45 ± 0.023	5.46 ± 0.043	6.53 ± 0.056	5.53 ± 0.005
Delta Total	−34.77 ± 0.036	−30.90 ± 0.041	−34.07 ± 0.051	−31.91 ± 0.04

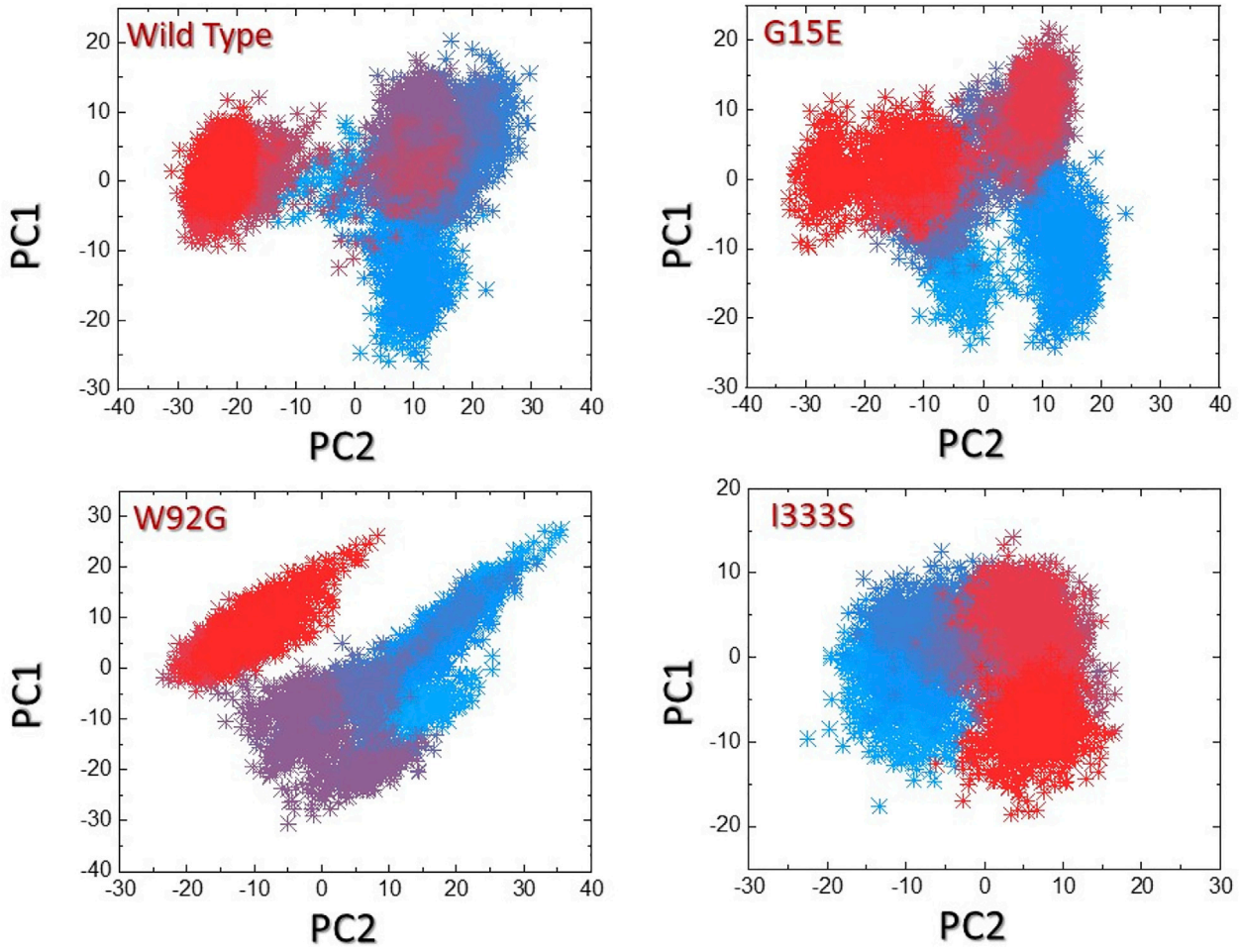

FIGURE 8
Principal component analysis of the wild-type and mutant complexes. **(A)** Representation of PCA of the wild type. **(B)** Representation of PCA of G15E. **(C)** Representation of PCA of W92G. **(D)** Representation of PCA of I333S. The red to sky blue represent the different conformation states, whereas the transition states are represented by dark purple.

The two PCs, that is, PC1 and PC2, reflected these motions in two dimensions. The distributed principal components for each complex are given in Figures 8A–D. The first three eigenvectors contributed 54% of the total motion, while the rest was contributed by the other eigenvectors. In contrast, the three mutants, that is, G15E the first three eigenvectors contributed 49%, W92G reported 48%, and I333S reported 44% of the total motion by the first three eigenvectors. The rest

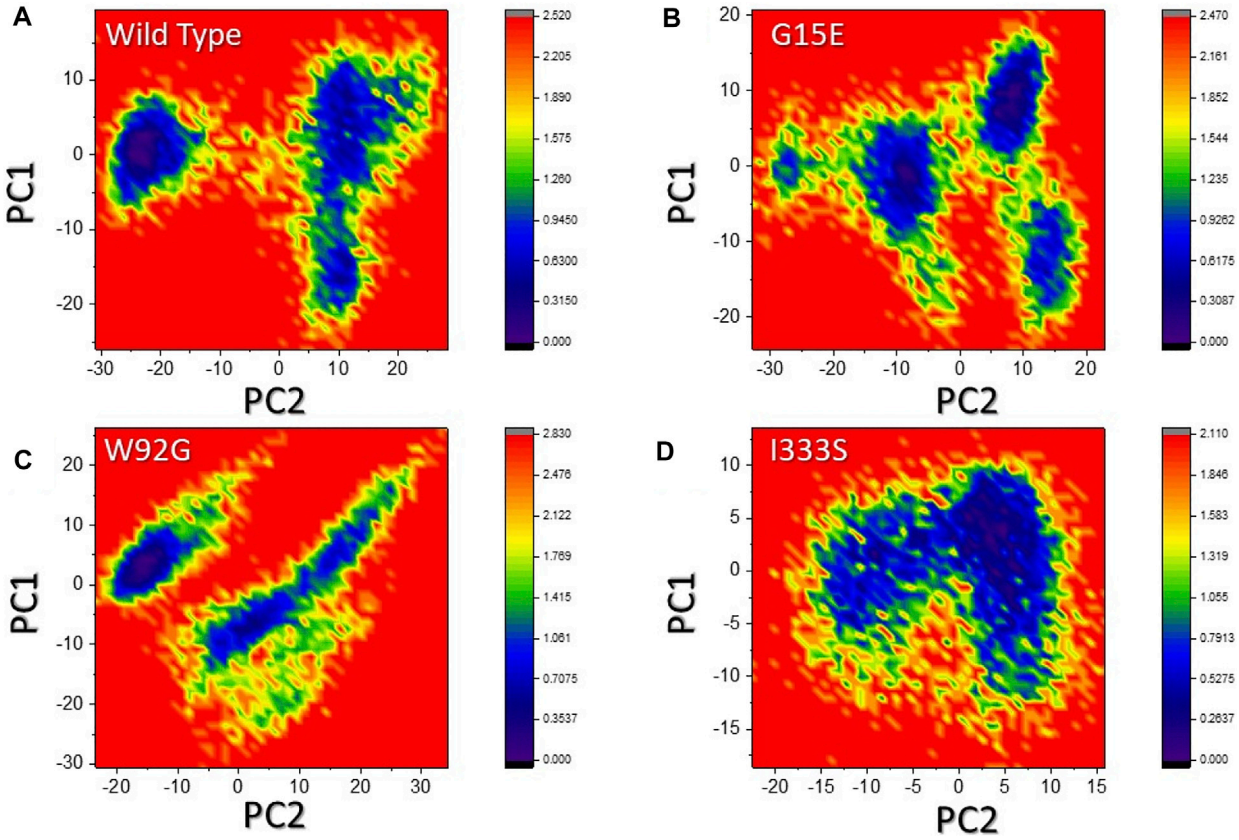

FIGURE 9
Free energy landscape analysis of the wild-type and mutant complexes. **(A)** Representation of DEL of the wild type. **(B)** Representation of FEL of G15E. **(C)** Representation of the FEL of W92G. **(D)** Representation of the FEL of I333S. The dark regions in each show the lowest-energy conformation where the conformational states are separated by subspace in each complex.

demonstrated localized motion by these complexes. The conformational transition can be easily separated from each other by sky blue and red colors. This shows that these mutations had caused different arrangements to bind small molecules compared to the wild type, where the total internal motion is decreased, thus consequently producing minimal binding effects.

3.9 Free energy landscape analysis

The two PCs were then mapped to identify the stable and metastable states for each complex. As shown in Figures 9A–D, the wild type attained one lowest-energy conformation, while G15E and W92G attained two lowest-energy conformations. I333S also attained a single lowest-energy state. The conformational transition in each complex is separated by a subspace. This shows that the mutations had caused a different arrangement to bind small molecules compared to the wild type, thus consequently producing minimal binding effects.

4 Conclusion

The current study used genomic mutation screening and molecular simulation methods to identify the most detrimental mutations in the IDH1 gene. The investigation of a large number of mutations revealed that three mutations, G15E, W92G, and I333S, are the most deleterious and highly destabilizing, which can affect the binding of a drug. These mutations primarily affect the binding of the drug with IDH, thus consequently reducing the efficacy of the already approved drug. Further validations such as molecular docking and dynamics simulation demonstrated that these mutations do not only affect the stability but also alter the bonding network. In addition, the BFE was also observed to have been reduced due to conformational changes mediated by these mutations. In sum, the current mutations contribute to drug resistance in glioma, and the atomic features

explored in this study could be used for structure-based drug designing against resistant glioma.

Data availability statement

The original contributions presented in the study are included in the article/Supplementary Material. Further inquiries can be directed to the corresponding authors.

Author contributions

Conceptualization: MSu, SU-I-H, AK, YW, and D-QW; data curation: MSu, SU-I-H, MSa, MA, and AI; formal analysis: MSu, SU-I-H, AK, and ZH; funding acquisition: YW; investigation: MSa, AI, ZH, and SA; methodology: MS, AK, AI, ZH, and SA; project administration: AK, SA, and YW; resources: MA and YW; software: D-QW; supervision: ZH and D-QW; validation: MA; visualization: SA; writing—original draft: AK, YW, and D-QW; and writing—review and editing: D-QW.

Funding

The author (MA) received a fund from the Researcher Supporting Project number (RSP 2022R481), King Saud University, Riyadh, Saudi Arabia, to support the publication of this article.

Conflict of interest

The authors declare that the research was conducted in the absence of any commercial or financial relationships that could be construed as a potential conflict of interest.

Publisher's note

Supplementary material

The Supplementary Material for this article can be found online at: https://www.frontiersin.org/articles/10.3389/fphar.2022.927570/full#supplementary-material

References

Adzhubei, I., Jordan, D. M., and Sunyaev, S. R. (2013). Predicting functional effect of human missense mutations using PolyPhen-2. *Curr. Protoc. Hum. Genet.* 76, 7. doi:10.1002/0471142905.hg0720s76

Agnihotri, S., Burrell, K. E., Wolf, A., Jalali, S., Hawkins, C., Rutka, J. T., et al. (2013). Glioblastoma, a brief review of history, molecular genetics, animal models and novel therapeutic strategies. *Arch. Immunol. Ther. Exp.* 61, 25–41. doi:10.1007/s00005-012-0203-0

Balsera, M. A., Wriggers, W., Oono, Y., and Schulten, K. (1996). Principal component analysis and long time protein dynamics. *J. Phys. Chem.* 100, 2567–2572. doi:10.1021/jp9536920

Bendahou, M. A., Arrouchi, H., Lakhlili, W., Allam, L., Aanniz, T., Cherradi, N., et al. (2020). Computational Analysis of IDH1, IDH2, and TP53 mutations in low-grade gliomas including oligodendrogliomas and astrocytomas. *Cancer Inf.* 19, 1176935120915839. doi:10.1177/1176935120915839

Bendl, J., Musil, M., Štourač, J., Zendulka, J., Damborský, J., and Brezovský, J. (2015). *PredictSNP2: A Unified Platform for Accurately Evaluating SNP Effects by Exploiting the Different Characteristics of Variants in Distinct Genomic Regions*. Plos computational biology.

Capriotti, E., and Fariselli, P. (2017). PhD-SNPg: A webserver and lightweight tool for scoring single nucleotide variants. *Nucleic Acids Res.* 45, W247–W252. doi:10.1093/nar/gkx369

Chen, D., Oezguen, N., Urvil, P., Ferguson, C., Dann, S., and Savidge, T. (2016). Regulation of protein-ligand binding affinity by hydrogen bond pairing. *Sci. Adv.* 2 (3), e1501240. doi:10.1126/sciadv.1501240

Chodera, J. D., and Mobley, D. L. (2013). Entropy-enthalpy compensation: Role and ramifications in biomolecular ligand recognition and design. *Annu. Rev. Biophys.* 42, 121–142. doi:10.1146/annurev-biophys-083012-130318

Consortium, U. (2015). UniProt: A hub for protein information. *Nucleic Acids Res.* 43, D204–D212. doi:10.1093/nar/gku989

Darden, T., York, D., and Pedersen, L. (1993). Particle mesh Ewald: An N· log (N) method for Ewald sums in large systems. *J. Chem. Phys.* 98, 10089–10092. doi:10.1063/1.464397

Dehury, B., Somavarapu, A. K., and Kepp, K. P. (2020). A computer-simulated mechanism of familial Alzheimer's disease: Mutations enhance thermal dynamics and favor looser substrate-binding to γ-secretase. *J. Struct. Biol.* 212, 107648. doi:10.1016/j.jsb.2020.107648

Dehury, B., Tang, N., and Kepp, K. P. (2020). Insights into membrane-bound presenilin 2 from all-atom molecular dynamics simulations. *J. Biomol. Struct. Dyn.* 38, 3196–3210. doi:10.1080/07391102.2019.1655481

Dehury, B., Tang, N., Mehra, R., Blundell, T. L., and Kepp, K. P. (2020). Side-by-side comparison of Notch- and C83 binding to γ-secretase in a complete membrane model at physiological temperature. *RSC Adv.* 10, 31215–31232. doi:10.1039/d0ra04683c

Dimitrov, L., Hong, C. S., Yang, C., Zhuang, Z., and Heiss, J. D. (2015). New developments in the pathogenesis and therapeutic targeting of the IDH1 mutation in glioma. *Int. J. Med. Sci.* 12, 201–213. doi:10.7150/ijms.11047

Eberhardt, J., Santos-Martins, D., Tillack, A. F., and Forli, S. (2021). AutoDock Vina 1.2. 0: New docking methods, expanded force field, and python bindings. *J. Chem. Inf. Model.* 61, 3891–3898. doi:10.1021/acs.jcim.1c00203

Ernst, M., Sittel, F., and Stock, G. (2015). Contact-and distance-based principal component analysis of protein dynamics. *J. Chem. Phys.* 143, 244114. doi:10.1063/1.4938249

Essmann, U., Perera, L., Berkowitz, M. L., Darden, T., Lee, H., and Pedersen, L. G. (1995). A smooth particle mesh Ewald method. *J. Chem. Phys.* 103, 8577–8593. doi:10.1063/1.470117

Frezza, C., Tennant, D. A., and Gottlieb, E. (2010). IDH1 mutations in gliomas: When an enzyme loses its grip. *Cancer Cell* 17, 7–9. doi:10.1016/j.ccr.2009.12.031

Hou, T., Wang, J., Li, Y., and Wang, W. (2011). Assessing the performance of the MM/PBSA and MM/GBSA methods. 1. The accuracy of binding free energy calculations based on molecular dynamics simulations. *J. Chem. Inf. Model.* 51, 69–82. doi:10.1021/ci100275a

Huang, L. E. (2019). Friend or foe—IDH1 mutations in glioma 10 years on. *Carcinogenesis* 40, 1299–1307. doi:10.1093/carcin/bgz134

Johnson, A. D., Handsaker, R. E., Pulit, S. L., Nizzari, M. M., O'Donnell, C. J., and De Bakker, P. I. (2008). Snap: A web-based tool for identification and annotation of proxy SNPs using HapMap. *Bioinformatics* 24, 2938–2939. doi:10.1093/bioinformatics/btn564

Junaid, M., Shah, M., Khan, A., Li, C.-D., Khan, M. T., Kaushik, A. C., et al. (2018). Structural-dynamic insights into the *H. pylori* cytotoxin-associated gene A (CagA) and its abrogation to interact with the tumor suppressor protein ASPP2 using decoy peptides. *J. Biomol. Struct. Dyn.* 37, 4035–4050. doi:10.1080/07391102.2018.1537895

Karczewski, K., and Francioli, L. (2017). *The genome aggregation database (gnomAD)*. Melbourne: MacArthur Lab.

Khan, A., Junaid, M., Li, C.-D., Saleem, S., Humayun, F., Shamas, S., et al. (2020). Dynamics insights into the gain of flexibility by Helix-12 in ESR1 as a mechanism of resistance to drugs in breast cancer cell lines. *Front. Mol. Biosci.* 6, 159. doi:10.3389/fmolb.2019.00159

Khan, A., Khan, M. T., Saleem, S., Junaid, M., Ali, A., Ali, S. S., et al. (2020). Structural Insights into the mechanism of RNA recognition by the N-terminal RNA-binding domain of the SARS-CoV-2 nucleocapsid phosphoprotein. *Comput. Struct. Biotechnol. J.* 18, 2174–2184. doi:10.1016/j.csbj.2020.08.006

Khan, A., Khan, S., Saleem, S., Nizam-Uddin, N., Mohammad, A., Khan, T., et al. (2021). Immunogenomics guided design of immunomodulatory multi-epitope subunit vaccine against the SARS-CoV-2 new variants, and its validation through *in silico* cloning and immune simulation. *Comput. Biol. Med.* 133, 104420. doi:10.1016/j.compbiomed.2021.104420

Kumar, D. T., Sneha, P., Uppin, J., Usha, S., and Doss, C. G. P. (2018). Investigating the influence of hotspot mutations in protein–protein interaction of IDH1 homodimer protein: A computational approach. *Adv. Protein Chem. Struct. Biol.* 111, 243–261. doi:10.1016/bs.apcsb.2017.08.002

Landis, J. R., Williams, D. A., Lucia, M. S., Clauw, D. J., Naliboff, B. D., Robinson, N. A., et al. (2014). The MAPP research network: Design, patient characterization and operations. *BMC Urol.* 14, 58–17. doi:10.1186/1471-2490-14-58

Ohgaki, H., and Kleihues, P. (2013). The definition of primary and secondary glioblastoma. *Clin. Cancer Res.* 19, 764–772. doi:10.1158/1078-0432.CCR-12-3002

Olsson, T. S., Ladbury, J. E., Pitt, W. R., and Williams, M. A. (2011). Extent of enthalpy–entropy compensation in protein–ligand interactions. *Protein Sci.* 20, 1607–1618. doi:10.1002/pro.692

Patil, R., Das, S., Stanley, A., Yadav, L., Sudhakar, A., and Varma, A. K. (2010). Optimized hydrophobic interactions and hydrogen bonding at the target-ligand interface leads the pathways of drug-designing. *PloS one* 5, e12029. doi:10.1371/journal.pone.0012029

Pearson, K. (1901). LIII. On lines and planes of closest fit to systems of points in space. *Lond. Edinb. Dublin Philosophical Mag. J. Sci.* 2, 559–572. doi:10.1080/14786440109462720

Pires, D. E., Ascher, D. B., and Blundell, T. L. (2014). mCSM: predicting the effects of mutations in proteins using graph-based signatures. *Bioinformatics* 30, 335–342. doi:10.1093/bioinformatics/btt691

Rodrigues, C. H., Pires, D. E., and Ascher, D. B. (2018). DynaMut: Predicting the impact of mutations on protein conformation, flexibility and stability. *Nucleic Acids Res.* 46, W350–W355. doi:10.1093/nar/gky300

Roe, D. R., and Cheatham, T. E., III (2013). PTRAJ and CPPTRAJ: Software for processing and analysis of molecular dynamics trajectory data. *J. Chem. Theory Comput.* 9, 3084–3095. doi:10.1021/ct400341p

Rose, P. W., Beran, B., Bi, C., Bluhm, W. F., Dimitropoulos, D., Goodsell, D. S., et al. (2010). The RCSB protein data bank: Redesigned web site and web services. *Nucleic Acids Res.* 39, D392–D401. doi:10.1093/nar/gkq1021

Ryckaert, J.-P., Ciccotti, G., and Berendsen, H. J. (1977). Numerical integration of the cartesian equations of motion of a system with constraints: Molecular dynamics of n-alkanes. *J. Comput. Phys.* 23, 327–341. doi:10.1016/0021-9991(77)90098-5

Salomon-Ferrer, R., Case, D. A., and Walker, R. C. (2013). An overview of the Amber biomolecular simulation package. *WIREs. Comput. Mol. Sci.* 3, 198–210. doi:10.1002/wcms.1121

Sim, N.-L., Kumar, P., Hu, J., Henikoff, S., Schneider, G., and Ng, P. C. (2012). SIFT web server: Predicting effects of amino acid substitutions on proteins. *Nucleic Acids Res.* 40, W452–W457. doi:10.1093/nar/gks539

Tan, A. C., Ashley, D. M., López, G. Y., Malinzak, M., Friedman, H. S., and Khasraw, M. (2020). Management of glioblastoma: State of the art and future directions. *Ca. Cancer J. Clin.* 70, 299–312. doi:10.3322/caac.21613

Wirsching, H.-G., and Weller, M. (2017). Glioblastoma. *Malignant Brain Tumors*, 265. Handbook of clinical neurology by Elsevier.

Wold, S., Esbensen, K., and Geladi, P. (1987). Principal component analysis. *Chemom. intelligent laboratory Syst.* 2, 37–52. doi:10.1016/0169-7439(87)80084-9

Yan, H., Parsons, D. W., Jin, G., McLendon, R., Rasheed, B. A., Yuan, W., et al. (2009). IDH1 and IDH2 mutations in gliomas. *N. Engl. J. Med.* 360, 765–773. doi:10.1056/NEJMoa0808710

Yuan, S., Chan, H. S., and Hu, Z. (2017). Using PyMOL as a platform for computational drug design. *WIREs Comput. Mol. Sci.* 7, e1298. doi:10.1002/wcms.1298

Zhao, S., Lin, Y., Xu, W., Jiang, W., Zha, Z., Wang, P., et al. (2009). Glioma-derived mutations in IDH1 dominantly inhibit IDH1 catalytic activity and induce HIF-1α. *Science* 324, 261–265. doi:10.1126/science.1170944

Zhou, W., and Wahl, D. R. (2019). Metabolic abnormalities in glioblastoma and metabolic strategies to overcome treatment resistance. *Cancers* 11, 1231. doi:10.3390/cancers11091231

Zwanzig, R. (1973). Nonlinear generalized Langevin equations. *J. Stat. Phys.* 9, 215–220. doi:10.1007/bf01008729

Frontiers in Pharmacology

Explores the interactions between chemicals and living beings

The most cited journal in its field, which advances access to pharmacological discoveries to prevent and treat human disease.

Discover the latest Research Topics

See more →

Frontiers

Avenue du Tribunal-Fédéral 34
1005 Lausanne, Switzerland
frontiersin.org

Contact us

+41 (0)21 510 17 00
frontiersin.org/about/contact